INTEGRATIVE SYSTEMS TOXICOLOGY FOR HUMAN HEALTH

Raju Prasad Sharma

UNIVERSITAT ROVIRA i VIRGILI

VU VRIJE UNIVERSITEIT AMSTERDAM

Integrative Systems Toxicology for Human Health

Raju Prasad Sharma

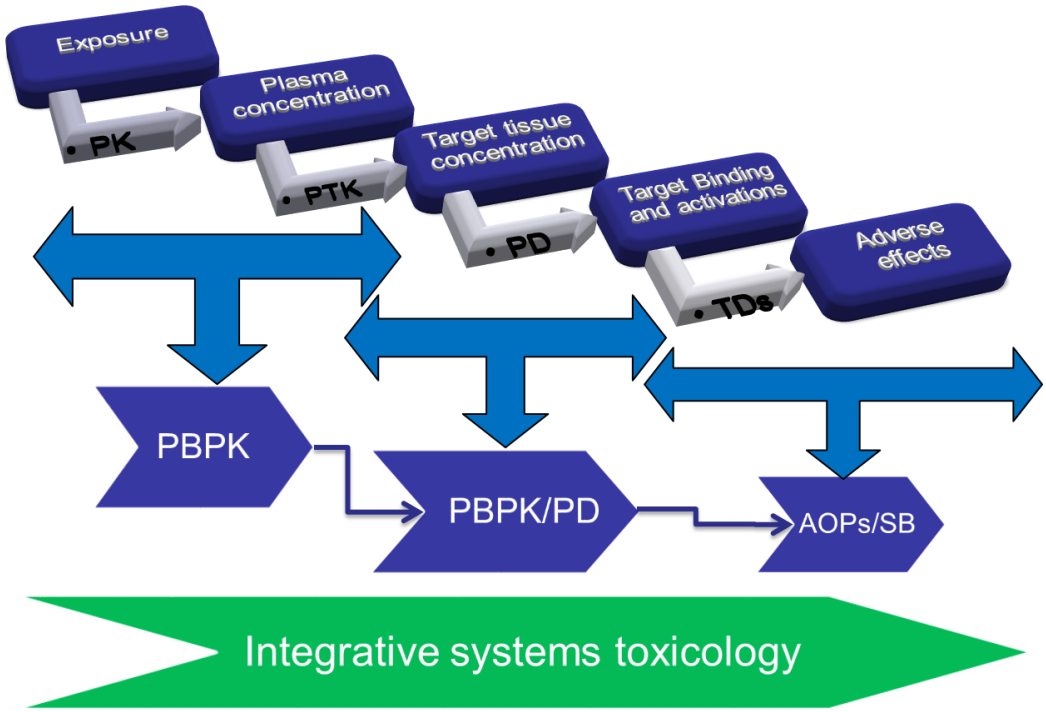

DOCTORAL THESIS
2018

UNIVERSITAT ROVIRA I VIRGILI
INTEGRATIVE SYSTEMS TOXICOLOGY FOR HUMAN HEALTH
Raju Prasad Sharma

Raju Prasad Sharma

Integrative Systems Toxicology for Human Health

DOCTORAL THESIS

Supervised by

Dr. Vikas Kumar

Dr. Marta Schuhmacher Ansuategui

Dr. Alexey Kolodkin

Dr. Hans V. Westerhoff

Department of Chemical Engineering

UNIVERSITAT ROVIRA I VIRGILI

Tarragona, 2018

FAIG CONSTAR que aquest treball, titulat "**Integrative Systems Toxicology for Human Health**", que presenta **Raju Prasad Sharma** per a l'obtenció del títol de Doctor, ha estat realitzat sota la meva direcció al Departament d'Enginyeria Química d'aquesta universitat.

HAGO CONSTAR que el presente trabajo, titulado "**Integrative Systems Toxicology for Human Health**", que presenta **Raju Prasad Sharma** para la obtención del título de Doctor, ha sido realizado bajo mi dirección en el Departamento de Ingeniería Química de esta universidad.

I STATE that the present study, "**Integrative Systems Toxicology for Human Health**", presented by **Raju Prasad Sharma** for the award of the degree of Doctor, has been carried out under my supervision at the Department of Chemical Engineering of this university.

Tarragona, 4nd of July, 2018

El/s director/s de la tesi doctoral
El/los director/es de la tesis doctoral
Doctoral Thesis Supervisor/s

Vikas Kumar

Marta Schuhmacher Ansuategui

Supervisors

Dr. Vikas Kumar
Researcher
Department of Chemical Engineering
Universitat Rovira i Virgili (URV)
Tarragona (Spain)

Dr. Marta Schuhmacher Ansuategui
Director
Department of Chemical Engineering
Universitat Rovira i Virgili (URV)
Tarragona (Spain)

Dr. Alexey Kolodkin
Researcher
Department of Molecular Cell Biology
Faculty of Science
Vrije Universiteit Amsterdam
Amsterdam (The Netherlands)

Dr. Hans V. Westerhoff
Chair
Section of Molecular Cell Physiology
Department of Molecular Cell Biology
Faculty of Science
Vrije Universiteit Amsterdam
Amsterdam (The Netherlands)

VRIJE UNIVERSITEIT

Integrative Systems Toxicology for Human Health

ACADEMISCH PROEFSCHRIFT

ter verkrijging van de graad Doctor aan
de Vrije Universiteit Amsterdam,
op gezag van de rector magnificus
prof.dr. V.Subramaniam,
in het openbaar te verdedigen
ten overstaan van de promotiecommissie
van de Faculteit der Bètawetenschappen
op maandag 3 december 2018 om 9.45 uur
in de aula van de universiteit
De Boelelaan 1105

door

Raju Prasad Sharma

geboren te Barbil, Odisha, India

promotoren: prof.dr. H.V. Westerhoff

prof.dr. M. Schuhmacher Ansuategui

copromotoren: dr. V. Kumar

dr. A. N. Kolodkin

Acknowledgement

It gives me an immense debt of gratitude to express my sincere thanks to my principal advisors: Dr. Vikas Kumar and Professor Marta Schumacher from the URV, Spain; Prof Hans V. Westerhoff and Dr. Alexey Kolodkin from the VUA, The Netherlands for their guidance, encouragement and kind advice throughout my PhD research work. I sincerely appreciate my supervisors for giving me the freedom to plan and conduct my research, at the same time continuing to contribute valuable feedback and advice.

I am grateful to my fellow doctoral students from the URV, Spain Venkat, Fran, Noelia, Nora, Tao, M.Angleles and post-doctoral researchers Quim, Montse Mari, Carmen, and Montse Marques for their support in working time. I am grateful to my fellow doctoral and post-doctoral researchers from the VU, Amsterdam Stefania, Ewlina, Matteo and Thierry. I wish to acknowledge all the excellent staff and financial support of Marti Franques Fellowship, URV. My sincere thanks to the HEALS, EUROMIX and CORBEL -European funding agency for providing funding for research work and conferences and collaboration opportunities.

On my journey I am fortunate to meet great Teachers (Guru). My sincere gratitude to Prof. Sanjay Sing (IIT-BHU), Department of Pharmaceutical engineering, under whom I developed my Master thesis and Dr. Niranjan Patra (Roland institute of Pharmaceutical sciences), Berhampur Odisha, for their support, advice on technical aspects at the beginning of my Professional life.

I am very grateful to Núria Juanpere Mitjana, Jeannet Wijker, and Jacqueline Cransberg for their caring, reminding, arranging, problems solving, and doing many "small" but very important administrative things without which no work would have been possible.

To my family: My special gratitude to my Mother, Brothers and Sisters: Thank you for all the support over the years, and help with real life issues. I wish to acknowledge my beloved joyful nieces Rittika, Laxmi, Anisha and nephews Milan, Sanjay Amish, Bijay and Aayush, and brother in law Neelkunth for their endless love. I would like to thank my parents and my brothers Kamal and Krishna who supported me in all my pursuits. This journey would not have been possible without the support and love of my mother and father. Thank you, all other members of my extended family.

I cherish the friendship I had and take this opportunity to thank my flatmate Venkatanaidu Karri for the wonderful times and all memorable moments. It is pleasure to thank my friends Asmaul, David, Tamal, Bala, Rajesh, Pratap, Rohit, Basudev, Veera, Indrajeet, Sukruth, Anvesh, Sachin, Pankaj, and other Indian crew for their encouragement and love; we have memorable times especially in the weekend cricket time and on the occasions of festivals.

I DEDICATE THIS THESIS TO MY FATHER LATE NARAYAN SHARMA

Abbreviations

AOPs: Adverse outcome pathways

ECHA: The European Chemicals Agency

EDCs: Endocrine disrupting compounds

EFSA: European food safety authority

IATAs: integrated assessment and testing approaches

IST: Integrative systems toxicology

IVIVE: in-vitro in-vivo extrapolation

QIVIVE: Quantitative in-vitro in-vivo extrapolation

PBPK: Physiologically based pharmacokinetics

PD: Pharmacodynamics

PTK: Plasma tissue kinetics

QSAR: Quantitative Structure Activity relationship

SB: Systems biology model

ST: Systems toxicology

BPA: Bisphenol A

FLU: Flutamide

MSP: Microsomal protein

Nrf2: Nuclear factor- erythroid-derived 2

Vmax: Maximum reaction velocity

KM: Concentration at which half maximum reaction occurs

MPPG: Microsomal protein per gram of gut

Contents

UNIVERSITAT ROVIRA I VIRGILI
INTEGRATIVE SYSTEMS TOXICOLOGY FOR HUMAN HEALTH
Raju Prasad Sharma

UNIVERSITAT ROVIRA I VIRGILI
INTEGRATIVE SYSTEMS TOXICOLOGY FOR HUMAN HEALTH
Raju Prasad Sharma

Summary

In industrialised economies large amounts of chemicals are produced and released into the environment. The accumulation of these chemicals in the ecosystem and the consequent exposure of human individuals to them are suspected of causing adverse effects on human health. For the so-called EDCs (Endocrine Disrupting Compounds) these effects include interference with hormonal regulation. REACH (Registration, Evaluation, Authorisation, and Restriction of Chemicals) and 3R (Replacement, Reduction and Refinement) principles have been proposed by the ECHA (European Chemicals Agency) and EFSA (European Food Safety Authority), respectively, in order to regulate the production and use of such chemicals. Both principles address the protection of human health and the environment through a better and earlier identification of the intrinsic properties of chemical substances. Simultaneously they aim to provide an alternative to animal testing by development of in-vitro and in-silico tools, incorporation of integrated assessment and testing approaches (IATAs), etc. The early identification of chemical-induced adverse effects poses several challenges. These include complexities inherent to the biological systems affected, complex mechanisms around structure, stability and solubility of the chemicals themselves, and the complex responses of organisms to exposure at various life stages and time scales. Emerging high-throughput analyses, OMICS and several in-silico tools such as PBPK (Physiologically based pharmacokinetic), PD (Pharmacodynamics), Systems Biology (SB) and AOPs (Adverse outcome pathways) offer opportunities to understand more of the biological complexity and multilevel connectivity. Along with the development of new tools and techniques in toxicological research, it is necessary to have a continuous re-evaluation of existing data, data curation, data integration, and knowledge-based translation of the integral results to implications that might able to solve many current challenges in this field. However, there is a paucity of research that integrates in-vitro, in-vivo, and several in-silico models into platforms that directly tie the results of the new data driven approaches in with predictive adverse outcomes models.

The objective of the current thesis was to develop an Integrative Systems Toxicology Framework enabling to understand the adverse effects of chemicals on a biological system quantitatively. It should comprise exposure, subsequent molecular and physiological alterations, molecular and cellular response as well as the ultimate adverse effect. The platform should be aiming for mechanistic understanding of any chemical's interaction with living systems, more than for the conventional empirical end points and animal based testing. The intended approach should integrate all the approaches that are presently used to address parts of the overall problem, such as chemical exposures, physiology, pharmacokinetics, pharmacodynamics, and biological response.

In chapter I, the literature is reviewed with the aim of identifying proposed mechanisms of action of EDCs, which included the interactions of chemicals with molecular receptors,

Summary

enzymes, proteins, gene-expression regulation and epigenetics thereby affecting the biological system, during and after the window of exposure. This chapter also investigates the normal endogenous pathways pertaining to the relevant hormones as this should aid in understanding the physiology dependent action of the corresponding EDCs. Then, the EDCs classified based on their target organs, the hormones of which they disrupt the action, the targets of those hormones, and the consequent adverse outcomes (response). Finally, a grouping strategy is proposed that is based on similar adverse outcomes. This chapter addresses many complications for the quantitative risk assessment, like multiple mechanisms, delayed response (time lag between exposure to adverse outcomes), dynamic interactions involving crosstalk and common mechanisms (complex mechanisms), and transgenerational effects. Finally, an integrative risk assessment framework is proposed connecting external exposure, internal exposure, and biological effects to the adverse outcomes. This framework includes the use of a PBPK model, a PD (pharmacodynamics) model and the coupling of these two models.

Chapter II includes the development and validation of a PBPK model in adult for Di-2-ethylhexyl phthalate (DEHP) and Flutamide, both categorized as EDCs. The model for DEHP includes four DEHP metabolites namely mono-(2-ethylhexyl) phthalate (MEHP), 5-OH MEHP, 2-ethyl-5-carboxypentyl phthalate (5-cx MEPP) and 5-oxo MEHP. An IVIVE (in-vitro in-vivo extrapolation) tool was successfully used in connection with the PBPK model to derive in-vivo kinetics from in-vitro studies using biologically appropriate scaling. A local parametric sensitivity analysis was performed and the statistical distributions of the most uncertain yet influential parameters were determined by Monte Carlo simulations of model uncertainty. Then the model was evaluated against published independent data on plasma and urine concentrations of DEHP metabolites for different dosing scenarios.

The development of the flutamide PBPK model includes bottom-up, top-down and cross-species extrapolation approaches. First, the model is developed for rat and then it is extrapolated to the human. Evaluated against experimentally observed data addressing 7 compartments, the rat model performed fairly: for most tissues the median values predicted by the model were less than a factor of 10 away from the average experimental values. The extrapolation of the model to predict flutamide kinetics in humans for two different scenarios of dosing (single and multiple) was also in good agreement with the observed data.

Chapter III focuses on the development of a Pregnancy PBPK (P-PBPK) model for Bisphenol-A (BPA) that includes the foetus as a sub compartment into the model structure. First, the adult PBPK model is developed and validated with the human BPA toxicokinetic data. This validated human PBPK model is then extended to become a P-PBPK model which includes the physiological changes during pregnancy and the foetus sub-model. The developed P-PBPK model is in concordance with biomonitoring data and shows that BPA readily transfers to foetal serum and amniotic fluid after maternal

Summary

exposure. De-conjugation of BPA-conjugate (BPAG) in placenta and foetus causes increased BPA exposure in early foetal life. Importantly, free BPA in the foetal compartment are more in steady state and persist even as the maternal level of BPA declines. The mid-gestational period was found to be critical, as during this time the concentration of BPA in the foetus was relatively high. Moreover, this period is also considered as critical for the foetus' body development.

Chapter IV builds an in-silico replica simulation of the biological system's behaviour. It reconstructs the biochemical information on components' communication into mathematical equations. It includes the development and validation of a systems biology model for ROS (reactive active oxygen species). First, we build the models ab initio, starting from the physiology of the response to oxidative stress. Subsequently, we increase the complexity of the network step by step. Adding every new level of complexity in a domino approach enables us to identify design principles of ROS management. It demonstrates that both mitochondrial recovery and mitophagy may avert ROS-induced cell death. The model is validated against several independent in-vitro data sets.

Chapter V includes the integrative systems toxicology approach. This involves two cases: 1) PBPK coupled PD with a mechanistic pathway model (similar to AOP). Perfluoro octane sulfonic acid (PFOS) was selected as a case study to illustrate the ways to incorporate systems biological modeling in the field of toxicology via a Pharmacodynamics-coupled tissue dosimetry model (PBPK/PD). A PBPK and a mechanistic system pathway model are simulated individually in order to generate the component models. Subsequently the integrated PBPK/PD coupled mechanistic model (systems toxicology) was used for simulations. QIVIVE along with PBPK was used to evaluate the performance of the model using in-vitro data.

2) PBPK coupled PD with the detailed ROS systems biology model taking the case study for the flutamide. The previously developed flutamide PBPK (chapter 2) and ROS systems biology models were used to develop integrative systems toxicology. This integral model is used to predict the hepatotoxicity of flutamide, illustrating the wider application of integrative systems toxicology in the field of the Human health risk assessments.

Resum

En una economia industrialitzada, es produeixen i alliberen al medi ambient una gran quantitat de productes químics orgànics. Les acumulacions d'aquestes substàncies químiques en l'ecosistema i la seva posterior exposició per part dels humans es sospita que pot causar efectes adversos sobre la seva salut. Per regular la producció de productes químics i els seus usos per es proposa el principi REACH (Registre, Avaluació, Autorització i Restricció de Productes Químics) i 3R (Substitució, Reducció i Refinament) part de l'ECHA i l'EFSA, respectivament. Ambdós principis tenen per objectiu millorar de la protecció de la salut humana i el medi ambient a través de la identificació primerenca de les propietats intrínseques de les substàncies químiques. Simultàniament, també es proposa una alternativa a les proves amb animals mitjançant el desenvolupament d'eines in vivo i in-silico i la incorporació d'enfocaments integrats d'avaluació i assaig (IATA), etc. Les primeres identificacions d'efectes adversos induïts químicament plantegen diversos reptes com; una complexitat de l'herència dins del sistema biològic i el mecanisme complex del químic o les respostes complexes de l'organisme sobre diferents escales de vida o escales de temps. L'anàlisi d'alta producció emergent, OMIQUES i diverses eines in-silico com PBPK, PD, biologia de sistemes i AOP ofereixen l'oportunitat d'entendre la complexitat biològica i la seva connectivitat multinivell. Juntament amb el desenvolupament de noves eines i tècniques en recerca toxicològica, és necessari tenir una reavaluació contínua de les dades existents, la curació, la integració de dades i la traducció basada en el coneixement que puguin resoldre molts reptes actuals en aquest camp. A més, hi ha una escassa recerca que integra in-vitro, in-vivo i diversos models in-silico en una sola plataforma per lligar directament el resultat a un model predictiu de resultats adversos.

L'objectiu d'aquesta tesi va ser desenvolupar un marc de toxicologia de Sistemes Integrats per comprendre quantitativament els efectes adversos de les substàncies químiques en un sistema biològic, des de la seva exposició a alteracions moleculars i fisiològiques posteriors, mitjançant la integració d'exposició interna-resposta molecular/cel·lular a l'efecte advers. Això es va orientar a la comprensió mecanística de la interacció química amb sistemes vivents versus punts finals empírics convencionals i proves basades en animals. Aquest enfocament integra tot l'esdeveniment, com exposicions químiques, fisiologia, farmacocinètica, farmacodinàmica i resposta biològica.

En el capítol I, es va fer una revisió de la literatura per comprendre els mecanismes d'acció dels En el capítol I, es va fer una revisió de la literatura per comprendre els mecanismes d'acció dels DE que inclouen la interacció de substàncies químiques amb receptors moleculars, enzims, proteïnes, mecanismes reguladors de gens o procés epigenètic que afecten el sistema biològic, incloent l'exposició. Aquest capítol també investiga la via endògena normal de l'hormona per comprendre l'acció dels DE dependent de la fisiologia. A continuació, es va realitzar la classificació dels DE a partir dels seus òrgans diana,

Resum

hormones, biomolècula (objectiu) i resultats adversos (resposta). Finalment, es va proposar una estratègia d'agrupació basada en resultats adversos similars. En aquest capítol es van abordar molts desafiaments, com ara múltiples mecanismes, resposta tardana (retard temporal entre exposició a resultats adversos), interaccions dinàmiques que impliquen interferències i mecanismes comuns (mecanismes complexos), efectes transgeneracionals, etc. en l'avaluació de riscos quantitatius. Finalment, es va proposar un marc d'avaluació de riscos integradors que consisteix en l'exposició exposició interna-efecte biològic als resultats adversos. Això inclou l'ús del model PBPK, PD (model de farmacodinàmica) i l'acoblament d'aquests dos models.

El capítol II inclou el desenvolupament i validació del model PBPK en adults per Di(2-etilhexil) ftalat i quatre metabòlits, és a dir, mono- (2-etilhexil) ftalat (MEHP), 5-OH MEHP, 2-etil-5-carboxpentil ftalat (5-cx MEPP) i 5-oxo MEHP. S'ha utilitzat amb èxit una eina IVIVE en connexió amb un PBPK a cinètica in vivo derivada d'estudis in vitro que utilitzen un escalat biològicament apropiat. Es va realitzar una anàlisi de sensibilitat paramètrica local i es van distribuir estadísticament els paràmetres més incerts però influents per a les simulacions de Monte Carlo per a l'anàlisi de models d'incertesa. A continuació, es va avaluar el model contra les dades independents publicades sobre concentracions plasmàtiques i d'orina de metabòlits DEHP per a diferents escenaris de dosificació.

El capítol II inclou el desenvolupament i validació del model PBPK en adults per Di(2-etilhexil) ftalat i quatre metabòlits, és a dir, mono- (2-etilhexil) ftalat (MEHP), 5-OH MEHP, 2-etil-5-carboxpentil ftalat (5-cx MEPP) i 5-oxo MEHP. S'ha utilitzat amb èxit una eina IVIVE en connexió amb un PBPK a cinètica in vivo derivada d'estudis in vitro que utilitzen un escalat biològicament apropiat. Es va realitzar una anàlisi de sensibilitat paramètrica local i es van distribuir estadísticament els paràmetres més incerts però influents per a les simulacions de Monte Carlo per a l'anàlisi de models d'incertesa. A continuació, es va avaluar el model contra les dades independents publicades sobre concentracions plasmàtiques i d'orina de metabòlits DEHP per a diferents escenaris de dosificació.

El desenvolupament del model PBPK de flutamida inclou un enfocament d'extrapolació de baix datl, de dalt a baix i d'espècies transversals. Primer, el model es va desenvolupar a les rates i després es va extrapolar als humans. El model de rata es va avaluar en comparació amb les dades observades experimentalment en 7 compartiments i el model es va realitzar de manera equitativa: els valors previstos pel model mitjà eren menys d'un factor de 10 fora del valor experimental mitjà per a la majoria dels teixits. L'extrapolació del model per predir la cinètica de la flutamida en humans per a dos escenaris diferents de dosificació (sola i múltiple) també va estar en consens amb les dades observades.

El capítol III es va centrar en el desenvolupament d'un model PBPK per a BPA en dones embarassades que incloïa el cos del fetus com a sub compartiment en l'estructura del

Resum

model. En primer lloc, es va desenvolupar i validar el model PBPK adult amb les dades toxicocinètics BPA humans. Aquest model PBPK humà validat es va estendre per desenvolupar un model P-PBPK que incloïa els canvis fisiològics durant l'embaràs i el submodel del fetus. El model P-PBPK desenvolupat està en concordança amb dades de biomonitorització i va demostrar que BPA es transferia fàcilment al sèrum fetal i al líquid amniòtic després de l'exposició de la mare. Desconjugació en la placenta i el cos del fetus causant una major exposició a BPA en la vida primària fetal. És important destacar que el BPA lliure al compartiment fetal és més estable i continua fins i tot quan el nivell matern de BPA disminueix. Es va trobar que el període de gestació mitjana era molt crític, ja que durant aquest temps, la concentració de BPA al fetus era relativament alta; a més, aquest període també es considera crític per al desenvolupament del fetus.

El capítol IV il·lustra la simulació de la rèplica in-silico del comportament del sistema biològic reconstruint la informació d'emergència biològica i la comunicació dels seus components en equacions matemàtiques. Va incloure el desenvolupament i validació d'un model de biologia de sistemes per a ROS (espècies reactives d'oxigen actiu). En aquest primer hem construït els nostres models ab initio, partint de la fisiologia de la resposta a l'estrès oxidatiu i augmentant la complexitat de la xarxa de manera progressiva. Es va sumar un nou nivell de complexitat en un enfocament de domini el que ens va permetre identificar principis de disseny de la gestió de ROS. Es va demostrar que tant la recuperació mitocondrial com la mitofàgia podrien evitar la mort cel·lular induïda per ROS. El model es va validar amb les dades in-vitro.

El capítol V va incloure l'enfocament integrat de la toxicologia de sistemes. Això implica dos casos:

1) PBPK acoblat PD amb model de via mecànica (similar a AOP); S'ha seleccionat l'àcid perfluoro octano-sulfònic (PFOS) com a estudi de cas per il·lustrar les maneres d'incorporar l'ús del model biològic del sistema en el camp de la toxicologia mitjançant el model de dosimetria tissular unida a la farmacodinàmica (PBPK / PD). Un PBPK i un model de via mecanitzada del sistema simulat individualment per obtenir el model base. Posteriorment es va realitzar la simulació del model mecanicista integrat PBPK / PD (toxicologia dels sistemes). QIVIVE juntament amb PBPK s'utilitza per avaluar el rendiment del model utilitzant dades in-vitro.

2) PBPK acoblat PD amb el model detallat de biologia de sistemes ROS prenent l'estudi de cas per al flutamida. El model de flutamida PBPK desenvolupat prèviament (capítol 2) i ROS es va utilitzar per desenvolupar la toxicologia dels sistemes integradors. Aquest model s'utilitza per predir l'hepatotoxicitat del flutamida, que il·lustra la aplicació més àmplia de la toxicologia dels sistemes integradors en el camp de les avaluacions del risc de salut humana.

Resumen

En las economías industrializadas, se producen y liberan grandes cantidades de sustancias químicas en el medio ambiente. Se sospecha que la acumulación de estos químicos en el ecosistema, y la consiguiente exposición humana a los mismos, causan efectos adversos en la salud. Para los llamados EDC (Compuestos Disruptores Endocrinos) estos efectos se centran en la interferencia con la regulación hormonal. La ECHA (Agencia Europea de Sustancias y Mezclas Químicas) y la EFSA (Autoridad Europea de Seguridad Alimentaria) han propuesto los principios REACH (Reglamento de Registro, Evaluación, Autorización y Restricción de Sustancias Químicas) y 3R (Reemplazo, Reducción y Refinamiento), respectivamente, para regular la producción y uso de tales químicos. Ambos principios abordan la protección de la salud humana y el medio ambiente a través de una identificación mejor y más temprana de las propiedades intrínsecas de las sustancias químicas. Al mismo tiempo, su objetivo es proporcionar una alternativa a las pruebas en animales mediante el desarrollo de herramientas tales como pruebas in-vitro e in-silico, la incorporación de enfoques integrados de evaluación y prueba (IATA), etcétera. La identificación temprana de los efectos adversos inducidos por productos químicos plantea varios desafíos. Estos incluyen complejidades inherentes a los sistemas biológicos afectados, mecanismos complejos alrededor de la estructura, estabilidad y solubilidad de los mismos químicos, y las respuestas complejas de los organismos a la exposición en varias etapas de la vida y escalas de tiempo. Los análisis emergentes de alto rendimiento, OMICS, así como varias herramientas in-silico tales como PBPK, PD, Biología de Sistemas y AOP ofrecen oportunidades para comprender más la complejidad biológica y la conectividad a varios niveles. Junto con el desarrollo de nuevas herramientas y técnicas en investigación toxicológica es necesario realizar una reevaluación, conservación e integración de los datos existentes y su traducción, basada en el conocimiento de los resultados integrales a las implicaciones que podrían resolver muchos desafíos actuales en este campo. Sin embargo, hay pocas investigaciones que integren diferentes modelos in-vitro, in-vivo e in-silico en plataformas que vinculen directamente los resultados de los nuevos enfoques basados en datos con modelos predictivos de resultados adversos.

El objetivo de la tesis actual ha sido desarrollar un Marco de Toxicología de Sistemas Integrados que permitiera comprender cuantitativamente los efectos adversos de los productos químicos en un sistema biológico. Éste debe comprender la exposición, las alteraciones moleculares y fisiológicas posteriores, la respuesta molecular y celular, y el efecto adverso final. La plataforma debe centrarse en la comprensión mecanística de la interacción de cualquier químico con los sistemas vivos, más que en los puntos finales empíricos convencionales y pruebas basadas en animales. El rumbo previsto debe integrar todos los enfoques que se utilizan actualmente para abordar partes del problema general, como la exposición química, fisiología, farmacocinética, farmacodinámica y respuesta biológica.

Resumen

En el capítulo I se revisa la literatura con el objetivo de identificar los mecanismos de acción propuestos de los EDC, incluyendo las interacciones de sustancias químicas con receptores moleculares, enzimas, proteínas y regulación de expresión génica y epigenética, afectando así al sistema biológico, durante y después de la ventana de exposición. Este capítulo también investiga las vías endógenas normales seguidas por las hormonas más relevantes para comprender la acción dependiente de la fisiología de los EDC correspondientes. Luego, los EDC se clasifican en función de sus órganos diana (aquellos cuyas hormonas interrumpen la acción), los objetivos de esas hormonas y los consiguientes resultados adversos (respuesta). Finalmente, se propone una estrategia de agrupación que se basa en resultados adversos similares. Este capítulo aborda muchas complicaciones para la evaluación de riesgos cuantitativos, como mecanismos múltiples, respuesta retrasada (retraso de tiempo entre la exposición a resultados adversos), interacciones dinámicas que involucran interferencias y mecanismos comunes (mecanismos complejos), y efectos transgeneracionales. Finalmente, se propone un marco integrador de evaluación de riesgos que conecta el exposoma, la exposición interna y efectos biológicos a los resultados adversos. Este marco incluye el uso de un modelo PBPK y un modelo PD (farmacodinámico), así como el acoplamiento de ambos.

El Capítulo II incluye el desarrollo y la validación de un modelo de PBPK en adultos para Di-2-etilhexil ftalato (DEHP) y Flutamida, ambos clasificados como EDC. El modelo para DEHP incluye cuatro metabolitos DEHP (mono- (2-etilhexil) ftalato (MEHP), 5-OH MEHP, 2-etil-5-carboxipentil ftalato (5-cx MEPP) y 5-oxo MEHP). A partir de estudios in-vitro utilizando escamas biológicamente apropiadas, se derivó la cinética in-vivo utilizando una herramienta IVIVE en conexión con el modelo PBPK. Se realizó un análisis de sensibilidad paramétrica local y las distribuciones estadísticas de los parámetros influyentes más inciertos se determinaron mediante simulaciones de Monte Carlo. El modelo fue entonces evaluado con datos independientes sobre concentraciones plasmáticas y urinarias de metabolitos de DEHP para diferentes escenarios de dosificación. El desarrollo del modelo de flutamida PBPK incluye enfoques de extrapolación de abajo hacia arriba, de arriba hacia abajo y de especies cruzadas. Primero, el modelo se desarrolló para ratas y luego se extrapoló a humanos. Evaluado en comparación con los datos observados experimentalmente en 7 compartimentos, el modelo de rata se comportó de manera equitativa: para la mayoría de los tejidos, los valores medios previstos por el modelo estaban a menos de un factor de 10 de los valores experimentales promedio. La extrapolación del modelo para predecir la cinética de la flutamida en humanos para dos escenarios diferentes de dosificación (individual y múltiple) también fue similar a los datos observados.

El Capítulo III se enfoca en el desarrollo de un modelo de PBPK durante el embarazo (P-PBPK) para BPA que incluye al feto como un compartimento secundario en la estructura del modelo. En primer lugar, el modelo de PBPK para adultos se desarrolla y valida con los datos toxicocinéticos de BPA humano. Este modelo validado de PBPK se amplía para convertirse en un modelo P-PBPK que incluye los cambios fisiológicos durante el

Resumen

embarazo y el sub-modelo del feto. El modelo P-PBPK desarrollado está en concordancia con los datos de biomonitoreo y muestra que el BPA se transfiere fácilmente al suero fetal y al líquido amniótico después de la exposición materna. El desacoplamiento del BPA conjugado (BPAG) en la placenta y el feto causa una mayor exposición al BPA en la vida fetal temprana. Es importante destacar que el BPA libre en el compartimento fetal se encuentra más estable y persiste incluso cuando el nivel materno de BPA disminuye. Se descubrió que el período de la mitad de la gestación era crítico, ya que durante este tiempo la concentración de BPA en el feto era relativamente alta. Además, este período también se considera crítico para el desarrollo del cuerpo del feto.

El Capítulo IV construye una simulación de réplica in-silico del comportamiento del sistema biológico. Reconstruye la información bioquímica sobre la comunicación de los componentes en ecuaciones matemáticas, incluyendo el desarrollo y la validación de un modelo de sistemas biológicos para ROS (Especies Reactivas de Oxígeno). Primero, se construyeron los modelos *ab initio,* a partir de la fisiología de la respuesta al estrés oxidativo. Posteriormente, se aumentó la complejidad de la red paso a paso. Cada nuevo nivel de complejidad fue agregado siguiendo un efecto dominó que permitió identificar los principios de diseño para la gestión de ROS. Los resultados demuestran que tanto la recuperación mitocondrial como la mitofagia pueden evitar la muerte celular inducida por ROS. El modelo se validó con varios conjuntos de datos in-vitro independientes.

El capítulo V se enfoca en la toxicología de sistemas integradores. Esto implica dos casos: 1) PD acoplado a PBPK con un modelo mecanístico (similar a AOP). El ácido perfluoro octanosulfónico (PFOS) se seleccionó como caso de estudio para ilustrar las formas de incorporar modelos de sistemas biológicos en el campo de la toxicología a través de un modelo de dosimetría de tejidos acoplado a farmacodinámica (PBPK / PD). Un PBPK y un modelo de vía de sistema mecanicista se simularon individualmente para generar los modelos de componentes. Posteriormente, se utilizó el modelo mecánico acoplado PBPK / PD (toxicología de sistemas) para llevar a cabo diferentes simulaciones. Para evaluar el rendimiento del modelo utilizando datos in-vitro se utilizó QIVIVE acoplado al PBPK. 2) PD acoplado a PBPK con el modelo ROS, tomando como caso de estudio la flutamida. Los modelos PBPK de sistemas biológicos para flutamida desarrollados previamente (capítulo 2) y ROS se utilizaron para desarrollar la toxicología integrada de sistemas. Este modelo integral se utilizó para predecir la hepatotoxicidad de la flutamida, alcanzando la aplicación más amplia de la toxicología de sistemas integradores en el campo de las evaluaciones de riesgos para la salud humana.

Samenvatting

In de meeste industrielanden worden grote hoeveelheden chemicaliën geproduceerd en los gelaten in de omgeving. Men verdenkt de ophoping van deze chemicaliën in het ecosysteem en de daardoor veroorzaakte blootstelling van mensen aan die chemicaliën, ervan negatieve effecten te hebben op de menselijk gezondheid. Wat de zogenaamde EDCs (endocrien systeem verstorende verbindingen) betreft, betreffen deze effecten de verstoring van hormoonregulatie. REACH (Registratie, Evaluatie, Autorisering en beperking van CHemicaliën) en 3V (Vervanging, Vermindering, en Verfijning) beginselen zijn respectievelijk voorgesteld door de ECHA (Europese Chemicaliën Agentschap) en de EFSA (Europese Voedsel Veiligheid Autoriteit) om productie en gebruik van zulke chemicaliën aan banden te leggen. Beide beginselen gaan over de bescherming van de menselijke gezondheid en de omgeving door een betere en vroegere vaststelling van wat de intrinsieke eigenschappen zijn van chemische stoffen. Tegelijkertijd richten zij zich op het bieden van een alternatief voor dierproeven door in vitro en in silico methodes te ontwikkelen, door geïntegreerde beoordeling en testbenaderingen (zogenaamde IATAs) mee te nemen, enzovoort. Het tijdig opmerken van schadelijke effecten van chemicaliën gaat gepaard aan verscheidene uitdagingen. Zo geven de complexiteiten die inherent zijn aan de getroffen biologische systemen, de complexe mechanismen rond structuur, stabiliteit, en oplosbaarheid van de chemicaliën zelf, alsook de complexe reacties van organismen in verschillende levensstadia en op verschillende tijdschalen, problemen. De hoge-doorvoer analyses die opduiken, de -ooms, alsmede verschillende in silico methodes zoals PBPK (in fysiologie gefundeerde farmacokinetiek), PD (farmacodynamiek), systeembiologie, en AOPs (paden met schadelijke werking) bieden de gelegenheid meer te begrijpen van de biologische complexiteit en de meerlagige verbondenheid. Het is noodzakelijk om, tezamen met het ontwikkelen van nieuwe methodes en technieken voor toxicologisch onderzoek, bestaande gegevens te her-evalueren, te verbeteren qua opbouw en consistentie, te integreren, en dan op basis van kennis de integrale resultaten hiervan te implementeren in potentiële oplossingen van de vele problemen op dit gebied. Er heerst echter een schaarste aan onderzoek dat in vitro, in vivo en in silico modellen tot platformen integreert an dat de resultaten van de nieuwe gegevens-gedreven benaderingen in direct verband brengt met modellen die schadelijke werkingen voorspellen.

Dit proefschrift beoogt een integratieve systeemtoxicologie methodiek te ontwikkelen die ons in staat stelt om de schadelijke effecten van chemicaliën op een biologische systeem getalsmatig te begrijpen. Deze methodiek dient zich meer te richten op het begrijpen van de mechanismen volgens welke een chemische stof ingrijpt op levende systemen, dan op de conventionele proefondervindelijke eindpunten en dierproeven. De bedoelde benadering dient alle huidige echelons, zoals chemische blootstelling, fysiologie, farmacokinetiek, farmacodynamiek en biologische reactie, mee te nemen.

Samenvatting

In hoofdstuk I wordt de wetenschappelijke literatuur doorgenomen op reeds voorgestelde werkingsmechanismen van EDCs die de interacties van chemicaliën met moleculaire sensoren, enzymen, eiwitten, regulatie van genexpressie, en epigenetica bevatten die op het biologische systeem aangrijpen, tijdens en na de blootstellingsperiode. Dit hoofdstuk onderzoekt ook de normale, endogene paden die de relevante hormonen betreffen, omdat kennisname hiervan het begrip van de fysiologische werking van de overeenkomstige EDCs zou kunnen bevorderen. Dan groepeert het hoofdstuk de EDCs op basis van de organen waarop ze aangrijpen, de hormonen waarvan ze de werking verstoren, de aangrijpingspunten van die hormonen, en de daaruit volgende schadelijke effecten (reacties). Tenslotte wordt een ordeningstrategie voorgesteld die gebaseerd is op overeenkomstige schadelijke effecten. Dit hoofdstuk bespreekt vele complicaties die de quantitatieve risicoanalyse vergezellen, zoals meervoudige mechanismen, vertraagde reacties (tijdsverschil tussen blootstelling en ongewenste effecten), dynamische interacties die lopen via kruisverbanden en gemeenschappelijke mechanismen (complexe mechanismen), en effecten die over generaties heen reiken. Tenslotte wordt een integratieve risicoanalyse voorgesteld die het exposoom, de inwendige blootstelling, en de biologische effecten verbindt aan de schadelijke effecten. Deze benadering maakt gebruik van een PBPK model, van een PD (farmacodynamisch) model en van het aaneenschakelen van deze twee modellen.

Hoofdstuk II bevat de ontwikkeling en validering van een PBPK model in een volwassene, voor di-2-ethylhexyl fthalaat (DEHP) and flutamide, beiden thuishorend in de categorie EDC. Het DEHP model bevat vier afbraakproducten van DHEP, te weten mono-(2-ethylhexyl) fthalaat (MEHP), 5-OH MEHP, 2-ethyl-5-carboxypentyl fthalaat (5-cx MEPP) and 5-oxo MEHP. Een in-vitro naar in-vivo extrapolatie (IVIVE) methode wordt er met succes bij gebruikt om in vivo kinetiek af te leiden uit in vitro studies onder gebruikmaking van de van toepassing zijnde biologische schalen. Een plaatselijke parametergevoeligheidsanalyse wordt uitgevoerd door middel van Monte Carlo simulaties van de onzekerheden in het model. Vervolgens werd het model geëvalueerd ten opzichte van gepubliceerde onafhankelijke gegevens betreffende plasma en urine concentraties van afbraakproducten van DEHP, en dit voor verscheidene doseringsscenarios.

De ontwikkeling van het flutamide PBPK model omvat extrapolatiebenaderingen van onder af, van boven af, alsook vanuit het midden. Eerst wordt het model ontwikkeld voor de rat om vervolgens geëxtrapoleerd te worden naar de mens. Waar het beoordeeld wordt aan de hand van experimenteel waargenomen gegevens aangaande 7 compartimenten, voldoet het rattemodel redelijk: voor de meeste weefsels wijken de door het model voorspelde middenwaardes minder dan een factor 10 af van het experimentele gemiddelde. Resultaten van de extrapolatie van het model naar het voorspellen van flutamide kinetiek in mens voor twee doseerscenarios (enkel- en meervoudig) bleken ook goed in overeenstemming met de experimentele waarnemingen.

Samenvatting

Hoofdstuk III legt de nadruk op de ontwikkeling van een zangerschaps PBPK (P-PBPK) model voor bis-fenol A (BPA) dat de foetus als een subcompartiment beschouwt in de modelstructuur. Eerst wordt het volwassen PBPK model ontwikkeld en gevalideerd aan de hand van menselijke toxicokinetische gegevens over BPA. Dit gevalideerde menselijke PBPK model wordt dan uitgebreid tot een P-PBPK model dat de fysiologische veranderingen accomodeert die optreden tijdens de zwangerschap alsmede het submodel van de foetus. Het hierbij ontwikkelde P-PBPK model blijkt in overeenstemming te zijn met biologische waarnemingen en laat zien dat na blootstelling van de moeder aan BPA deze stof gemakkelijk overgaat naar foetaal bloed en amnionvloeistof. De-conjugatie van het BPAconjugaat in placenta en foetus leidt tot verhoogde blootstelling aan BPA gedurende het foetale leven. Het is van belang dat vrij BPA in het foetale compartiment meer in steady state is en blijft, ook als het maternale BPA niveau daalt. De periode halverwege de zwangerschap wordt kritiek bevonden, omdat in deze tijd de concentratie van BPA in de foetus relatief hoog is. Bovendien wordt deze periode beschouwd als kritiek voor de ontwikkeling van het foetale lichaam.

Hoofdstuk IV bouwt een simulatie van het gedrag van een in silico kopie van het biologische systeem. Het reconstrueert in wiskundige vergelijkingen de biochemische informatie aangaande de communicatie tussen componenten. Het neemt de ontwikkeling en validering van een systeembiologisch model van ROS (reactieve zuurstofsubstanties) in beschouwing. Eerst bouwen we de modellen ab initio, beginnend bij de fysiologie van het reageren op oxidatieve verstoring. Vervolgens verhogen we stap voor stap de complexiteit van het netwerk. Door in een dominobenadering elk nieuw complexiteitsniveau toe te voegen kunnen we beginselen bepalen van hoe het systeem omgaat met ROS. Dit laat zien dat zowel mitochondrieel herstel als mitofagie ROS-geïnduceerde celdood kunnen afwenden. Het model wordt gevalideerd aan de hand van verscheidene groepen van in vitro gegevens.

Hoofdstuk V bevat de integratieve systeemtoxicologie aanpak. Het neemt twee gevallen in beschouwing:

1) Aan PBPK gekoppelde PD met een mechanistisch padenmodel (vergelijkbaar met AOP). Perfluoro octaan sulfonzuur (PFOS) wordt als voorbeeld genomen om de manieren waarop systeembiologisch modelleren ingebouwd wordt in het toxicologieveld via een aan farmacodynamiek gekoppeld weefseldosimetriemodel (PBPK/PD) uit te werken. Een PBPK model en een mechanistisch systeempad model worden elk op zich gesimuleerd om de deelmodellen te maken. Vervolgens wordt het aan het geïntegreerde PBPK/PD gekoppelde mechanistische model gebruikt voor simulaties. QIVIVE (Quantitatieve in-vitro naar in-vivo extrapolatie) tezamen met PBPK wordt gebruikt om de prestaties van het model te qualificeren aan de hand van in vitro gegevens.
2) Aan PBPK gekoppelde PD met het gedetailleerde ROS systeembiologie model in een voorbeeldstudie van flutamide. Het eerder (in Hoofdstuk II) ontwikkelde

Samenvatting

flutamide PBPK model en ROS systeembiologiemodellen worden hier gehanteerd bij de ontwikkeling van integratieve systeemtoxicologie. Het resulterende integrale model wordt gebruikt om de levertoxiciteit van flutamide te voorspellen, daarmee de bredere toepasbaarheid van integratieve systeemtoxicologie bij de beoordeling van risicos voor de menselijk gezondheid illustrerend.

Introduction

1. Endocrine disruptors/Environmental chemicals and human health

Many organic chemicals are produced and released into the environment. The accumulations of these products in the ecosystem are suspected to cause adverse effects on human's health. Human health and wealth benefits greatly from activities that require new (bio) chemical compounds or more of existing ones. These compounds leach into environments, from where they may be taken up into humans, animals or plants. Even without this, animals and plants naturally contain compounds such as hormones. All these compounds may enter humans through nutrition or other contact with their environments and interact with the complex chemical reaction and signalling networks through which human bodies and minds function. This may throw these networks off balance, a bit for some, but more for other human individuals, depending on gender, genome sequence, or life style. USEPA defined EDCs as an exogenous agent that interferes with synthesis, secretion, transport, metabolism, binding action, or elimination of natural blood-borne hormones that are present in the body and are responsible for homeostasis, reproduction, and developmental process (Kavlock et al., 1996).

Quantitative prediction of endocrine disruptor adverse effect on human health poses a large number of challenges particularly due to involvement of hundreds of chemicals and their metabolites, as well as their associated pattern of exposure, retention time in body, generation of toxic metabolites and their wide range action via multiple mechanisms (Ohtake et al. 2003; Welshons et al., 2003; Vandenberg et al., 2013). The advancement in current analytical methods of in-vitro, high throughput screening, genomics, proteomics and metabolomics have led to generate a huge amount of data on toxicological profile. In parallel to this, recently development of systems biology and multiscale modeling has increased the understanding of physiological endogenous pathway and impacts of toxicant on the temporal behaviour of cell, tissue and whole organ system.

In the new EU Framework Programme for Research and Innovation (Horizon 2020), the European Food Safety Agency (EFSA) has identified this area of risk assessment as a priority for development oriented innovations. This thesis will also promote wider Spanish Strategy for Science and Technological Innovation (2013-2020) by promoting the competitiveness.

2. From classical dose response to Integrative Systems Toxicology

The study of toxicology has been focused on quantifying/predicting chemical-induced adverse effects to the biological system. The major challenge in predicting adverse effects of chemicals on the human health are; the inheritance complexity within the biological system and chemical's complex mechanism and, the complex responses of organism over different life stage or time scales. Systems Toxicology is an area, which integrates classic

INTRODUCTION

toxicology (empirical fitting of dose-response curve) with the quantitative analysis of molecular and functional changes that occurs across multiple levels of biological organization (Sturla et al. 2014). The fact that adverse effects cannot be predicted individually by animal testing or in-vitro testing or existing modeling methodologies was the first step on the road of the concept of integrative systems toxicology. An integrative system approach to predict the adverse effects on human health can be described as "viewing the problem in it's entirely as an interconnected system of component operations and functions" and therefore recognizing the full complexity of predicting adverse effects on human health. A Systems Toxicology is aimed at mechanistic understanding of chemical's interaction with living systems versus conventional empirical end points and animal based testing. Several Systems toxicology-modeling approaches have been developed to predict the adverse effects of drugs/chemicals on human health (Bloomingdale et al., 2017). Information regarding the body physiology, pharmacokinetics, pharmacodynamics, chemical exposures, inter-individual variability and covariates relating to toxicity are the integral part of systems toxicology**.**

The classical toxicology involves empirical fitting of external dose (not internal dose) and response (end points) as the basis for the dose-response assessment. This approach lacks the mechanistic understanding of the influence of body physiology onto the chemical's fate and the biological changes at the molecular and functional levels due to chemical interaction with biological target. Later these process are described as Pharmacokinetics (PK) i.e. "what body does to the drug/chemical" and Pharmacodynamics (PD) "what drug/chemical does to the body" respectively. Pharmacokinetics encompasses the four elements absorption, distribution; metabolism and elimination (ADME) that describes the fate of the chemical inside the body. Pharmacodynamics describes the interactions of drugs with biological targets and consequently observed effects.

There are successive development of several pharmacokinetics model describing absorption, distribution, metabolism and elimination of drugs/chemical. Major types of pharmacokinetic models are Non-compartment Analysis (NCA) and compartment physiological analysis (Jusko, 2013). NCA empirically fits experimental data on the time course of plasma drug concentrations. This allows to measure elimination and volume of distribution of chemical inside the body (Gabrielsson and Weiner, 2012). Compartment models can be semi-mechanistic adding improved insights into distribution properties of drugs and physiological properties of organisms. Physiologically-based (PB) Pharmacokinetics (PK), (PBPK) models are systems models where the body is divided into several compartments corresponding to each organ. Organs are connected with each other via the blood circulatory system. The parameters in the model are assigned using physiological measurements (blood flow, organ sizes) and resolved by direct analysis of plasma concentrations and tissue transport, binding, and metabolic properties (Jusko, 2013). Integration of a dynamic change in physiological states related with Age, disease and pregnancy into the PBPK lead to development of person/population specific PBPK model.

INTRODUCTION

Pharmacodynamic (PD) models are empirically fitting of tissue dose and response. PD models are majorly categorized into two types; one is direct effect model that assumes chemical effects are directly proportional to receptor occupancy (i.e. linear transduction), and other is the indirect effect model in which response is due to chemicals indirect effect to the synthesis or degradation of a response variable (Jusko and Ko, 1994).

Both pharmacokinetics and pharmacodynamics can be developed individually and linked together which often referred as PBPK/PD models (Timchalk et al., 2002; Foxenberg et al., 2011). PBPK describes the internal concentrations rather than external exposure. And the key metabolites and their linkage to PD provides a more accurate dose-response relationship. Such integrated PBPK/PD can be able to simultaneously describe chemical ADME at the whole-body level and the resulting drug effect at the cellular or tissue scale (Kuepfer et al., 2016). PBPK/PD has long been used for route-to-route and species-to-species extrapolations and in vitro-to-in vivo extrapolation (IVIVE) (El-Masri, 2013). QIVIVE (quantitative in-vitro in-vivo extrapolation) along with PBPK/PD is used to predict the in-vivo adverse effects based on in-vitro dose response data (Bell et al., 2018; Bessems et al., 2015). However, this model has limitation of not taking into account the process of molecular initiating events (MIEs) to adverse effects and very often, the endpoints are specifically remained single explanatory biomarker. To address this challenges the concept of adverse outcomes pathways (AOPs) and systems toxicology have been developed. Recently, the concept of AOP has been drawn upon a systems biology approach. AOP is defined as "A linear sequence of events commencing with initial interaction(s) of a stressor with a biomolecule within an organism that causes a perturbation in its biology (i.e., molecular initiating event, MIE), which can progress through a dependent series of intermediate key events (KEs) and culminate in an adverse outcome (AO) considered relevant to risk assessment or regulatory decision-making" (Ankley et al., 2010). AOPs do not, however, address the question of what dose of chemical will cause sufficient perturbation to drive the pathways to the adverse outcomes (Ankley et al., 2010). In contrast, Systems toxicology quantifies the effect of chemical's interaction to biological systems across the cellular and multi-tissue level and the observed toxicological effects relevant to the exposure amount of chemical (Sturla et al., 2014). These biological model systems could be comprised of linear signalling pathways such as AOPs to a detailed complex biological pathways (Systems biology). Systems biology comprises genomics, metabolomics, and proteomics rationalizing the functional interaction of biological components in a time-dependent fashion (Aderem, 2005; Kitano, 2002). Coupling a PBPK/PD model and Systems biology together can form a mechanistic framework that enhances the understanding both of biology and of adverse effects due to chemically induced perturbation to the biological systems (Bhattacharya et al., 2012; Gim et al., 2010).

3. Components of Integrative Systems Toxicology and their modelling approach

An essential part of this section is to discuss more about the basic molecular, biochemical and cellular processes responsible for diseases caused by exposure to chemical or physical substances.

Several systems toxicology-modelling approaches have been developed to predict the adverse effects of chemicals on human health. Here we briefly review PBPK, PD, AOPs/Systems biology modelling approaches, since these three are the integral part in the development of integrative systems toxicology models.

3.1. PBPK (Physiologically Based PharmacoKinetics) Models

Physiologically based pharmacokinetic (PBPK) models consist of a series of mathematical representations of biological tissues and physiological processes in the body of target species aimed at describing the absorption, distribution, metabolism, and excretion of chemicals (Fàbrega et al., 2016). When a chemical substances enter the organism, it is usually distributed to various tissues and organs by blood flow (Nestorov, 2007). Following its distribution in tissues, the substance can bind to various proteins and receptors, undergo metabolism, or can be eliminated unchanged. The concentration vs. time profiles of the xenobiotic in different tissues, or the amount of metabolites formed, is often used as surrogate markers of its internal dose or biological activity (Andersen et al., 2005). In a sense, PBPK modelling is an integrated systems approach to both understanding the pharmacokinetic behaviour of compounds and predicting concentration vs time profiles in plasma and tissues (Bois et al. 2010).

The biological response results from the interaction between the toxicant and the target tissue. For this reason, models that can predict the target tissue concentration of the toxicologically-active chemical species (parent compound or metabolite) are especially useful and have been applied in the “exposure–dose–response” paradigm. The internal dose metrics (sometime also referred as biological effective dose) replaces the external exposure dose in the derivation of the quantitative dose-response relationship, with the intent of reducing the uncertainty inherent in human health risk assessments based on external exposure dose estimation.

INTRODUCTION

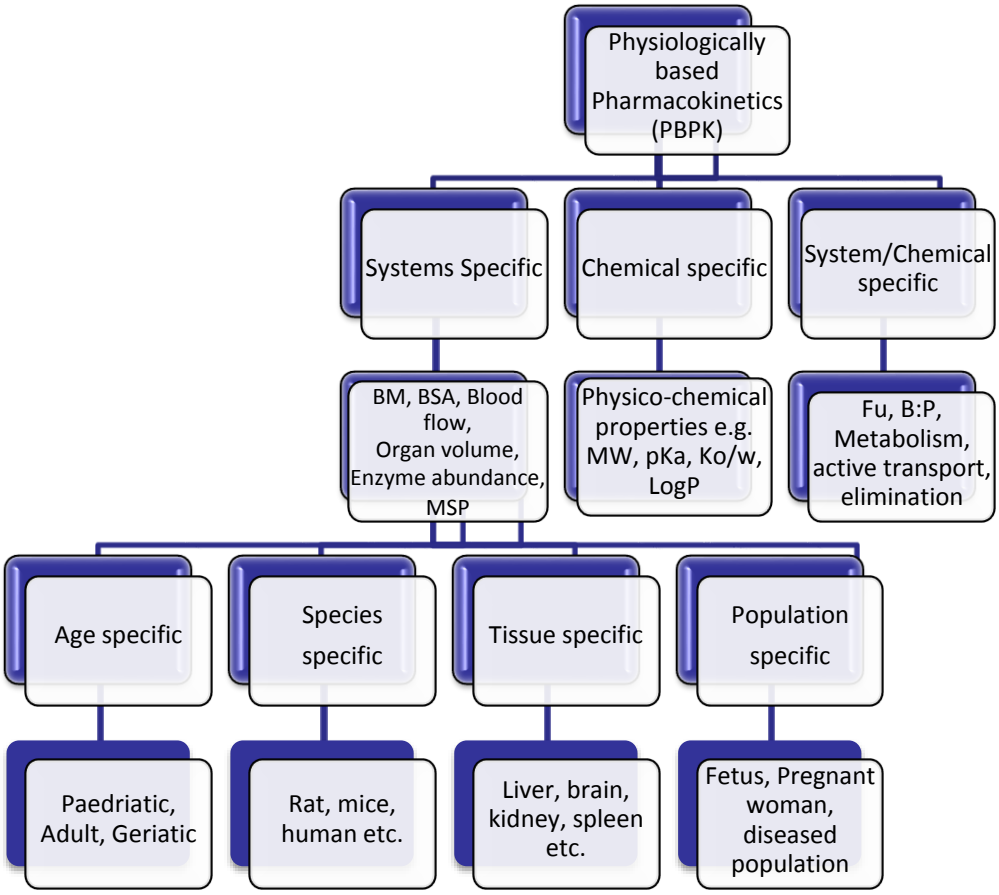

Fig 1. PBPK model structure and approach, representing the model developmental approach and the required parameters input. BM: Body mass; BSA: Body surface area; MW: Molecular weight; $K_{o/w}$: octanol:water partition coefficient; Fu: Fractional unbound concentrations; B:P: blood to plasma ratio; MSP: microsomal protein.

3.1.1. Approaches to building PBPK models

Building a PBPK model requires gathering a considerable amount of data which can be categorised in three groups, namely: the model structure, which refers to the arrangement of tissues and organs included in the model; the system's data (physiological, anatomical, biochemical data) and chemical-specific data (physicochemical) (see Figure 2.1). The transport of xenobiotics (chemicals) in several tissues is determined by two different approaches: (i) permeability limited (also called as flow limited), and (ii) perfusion limited (also called as diffusion limited), (Bois and Paxman, 1992; Gerlowski and Jain, 1983).

Permeability-rate –limited Model: This model is also called diffusion limited and could be applied when the distribution of the substance to a tissue is rate-limited by the drug's permeability across the tissue membrane. That condition is more common with polar compounds and large molecular structures. Consequently, the related PBPK models may exhibit different degrees of complexity.

Perfusion-rate-limited Model: This model is also called flow limited kinetics and could be applied when the tissue membrane presents no barrier to distribution. Here, each tissue is considered to be a well-stirred compartment in which the substance distribution is simply limited by blood flow. Thus, the chemical will be delivered to the tissue via the blood, and is assumed to mix throughout the volume of that compartment immediately and completely and normally partition coefficient is used for the distribution of chemical. Concentrations in the flow limited compartments generally estimated by applying the following equation:

$$\frac{dC_i}{dt} = \frac{Q_i * \left(C_a - \frac{C_i}{K_{i:p}}\right)}{V_i} \quad (1)$$

Where C_i is the concentration in the tissue i (nM), Q_i is the blood flow in the tissue i (L/h), Ca is the arterial concentration (nM), $K_{i:p}$ is the partition coefficient of tissue i, and V_i is the volume of the tissue i (L).

3.1.2 Model Parameterization:

There are two approaches of PBPK model building or parameterization: **bottom-up** and **top-down**. In bottom-up approach, model parameterization is done based on in-silico prediction or in-vitro understanding of chemical-related ADME mechanisms. It mainly depends on tools for translation of in-vitro data to in-vivo such as IVIVE (in vitro-in vivo extrapolation) and several in-silico tools such as QSAR, in a sense its purely predictive model. In contrast top-down approaches rely on estimation of model parameter by fitting to the observed experimental data. Model parameterization requires two specific parameters namely; System's and Chemical's specific input parameters.

System –specific parameters: This comprises of both physiological parameters and biochemical parameters.

Physiological parameters: These parameters are species specific constant. These incudes tissues/organs volume (or weight) and tissues blood flow rate which are specific to the species of interest. These parameters are used to develop species specific PBPK models, the most common being rat, mouse, dog and human. Physiological parameters for developing such models are routinely available in the literatures (Abduljalil et al., 2012; Brown et al., 1997; Sisson et al., 1959; Valentin, 2002).

Biochemical parameters

INTRODUCTION

Biochemical parameters are the hybrid parameters which depend on both chemical and physiology. Among biochemical parameters, chemicals metabolism is considered to be very important parameters, which are generally derived from in-vitro data using IVIVE methodology. The schema of IVIVE has been provided in the figure 2.

IVIVE generally involves the scaling of in-vitro Vmax parameter was done based on microsomal protein content per gram tissue and weight of tissue per kg body weight. Vmax was scaled to in-vivo per kg BW from in-vitro cell line studies by using the following equation:

$$Vmax_{invivo} = (Vmax_{invitro} * MPPGT * V_{tissue})/BW^{.75} \quad (2)$$

Where, $Vmax$ = Maximum metabolic capacity in per gram of microsomal protein, $MPPGT$ = the microsomal protein per gram of tissue, V_{tissue} = the total tissue weight in gram, and BW =is the whole body weight in kg.

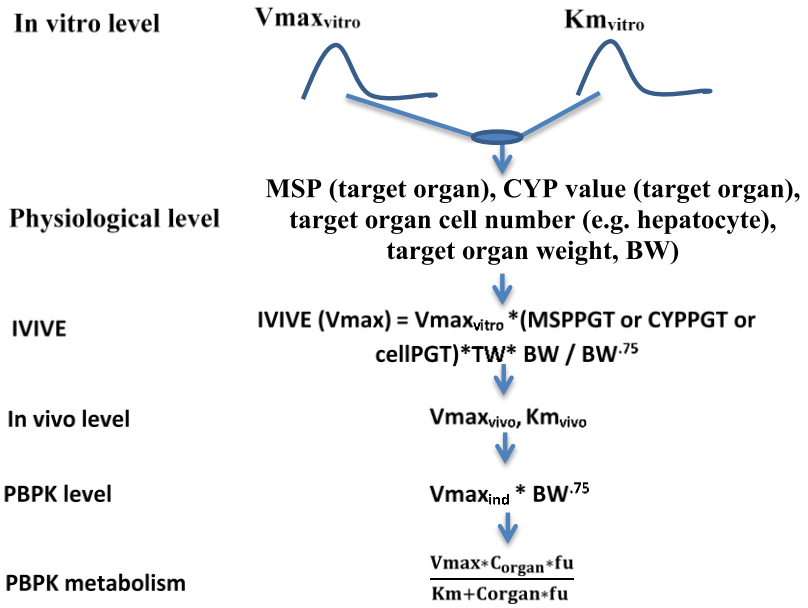

Fig. 2: Illustration of Hierarchical structure model approach for metabolic IVIVE scaling.

Chemical-specific parameters

It can be derived by in vivo or in vitro experiment. However, in certain cases when we lack these data, various in-silico approaches can be useful. Among Physicochemical

INTRODUCTION

parameters partition coefficient is considered one of the most important parameters. It describes the distribution of the chemical between plasma and different organ. There are various tissue composition based algorithm methods to generate partition coefficient data (Poulin and Krishnan, 1996, 1995; Schmitt, 2008; Peyret et al., 2010; Yun et al., 2014).

Tissue composition based algorithm methods for calculating partition coefficients few of them are explained here;

METHOD I (Poulin and Krishnan, 1996, 1995)

$$P_{t:P} = \frac{\left(\left(P_{o:w} * \left(V_{nlt} + 0.3 * V_{pht}\right)\right) + 1\left(V_{wt} + 0.7 * V_{pht}\right)\right)}{\left(P_{o:w} * \left(V_{nlp} + 0.3 * V_{php}\right)\right) + 1\left(V_{wp} + 0.7 * V_{php}\right)} * \frac{fu_p}{fu_t}$$

$$P_{t:P}adipose = \frac{\left(\left(D_{o:w} * \left(V_{nlt} + 0.3 * V_{pht}\right)\right) + 1\left(V_{wt} + 0.7 * V_{pht}\right)\right)}{\left(D_{o:w} * \left(V_{nlp} + 0.3 * V_{php}\right)\right) + 1\left(V_{wp} + 0.7 * V_{php}\right)} * \frac{fu_p}{1}$$

Where,

$P_{t:P}$ = tissue plasma partition coefficient
$P_{o:w}$ = octanol water partition coefficient
V_{nlt} = fractional volume of neutral lipid in tissue
V_{pht} = fractional volume of phospholipid in tissue
V_{nlp} = fractional volume of neutral lipid in plasma
V_{php} = fractional volume of phospholipid in plasma
fu_p = fractional unbound concentration in plasma
fu_t = fractional unbound concentration in tissue
$D_{o:w}$ = olive water partition coefficient
Note: have to take antilog as octanol water partition coefficient always given in log value.
fu_t value, we can calculate by applying formula of = **1/(1+((1-fup)/fup)*RA))**
RA is the ratio of albumin concentration found in tissue over plasma
RA equals 0.15, whereas for nonadipose tissue, RA equal 0.5 (Ellmerer et al., 2000; Poulin and Theil, 2002).

METHOD II: Schmitt Walter (Schmitt, 2008)

$$f_u = \frac{c_u}{c_{total}}$$

$$K_{t:p} = \left(\frac{F_{int}}{f_u^{int}} + \frac{F_{cell}}{f_u^{cell}}\right) * f_u^p$$

Where,

F_{int} = fractional content of interstitial fluid in tissue or volume fraction of interstitial

INTRODUCTION

F_{cell} = fractional content of cell in tissue or volume fraction of cellular
f_u^{int} = unbound fraction in interstitial fluid
f_u^{cell} = unbound fraction in cell
f_u^{p} = unbound fraction in plasma

Calculation of unbound fraction in interstitial space f_u^{int}

Assumption = interstitial fluid is very similar with plasma

Therefore, unbound fraction of interstitium estimated from unbound fraction in plasma

$$\frac{1}{f_u^{int}} = F_w^{int} + \frac{F_p^{int}}{F_p^{pl}} * \left(\frac{1}{f_u^{pl}} - F_w^{pl}\right)$$

Where,

F_w^{int} = fractional water content in interstitial
F_p^{int} = fractional protein content in interstitial
F_w^{pl} = fractional water content in plasma
F_p^{pl} = fractional protein content in plasma
$\frac{F_p^{int}}{F_p^{pl}}$ = 0.37

Calculation of unbound fraction in cellular space f_u^{cell}

$$\frac{1}{f_u^{cell}} = F_w + K_{nl} * F_{nl} + K_{npl} * F_{npl} + K_{apl} * F_{apl} + K_p * F_P$$

Where,

F_w = fractional content of water in cell
K_{nl} = water: neutral lipid partition coefficient
F_{nl} = fractional neutral lipid in cellular space
K_{npl} = water: neutral phospholipid partition coefficient
F_{npl} = fractional neutral phospholipid in cellular space
K_{apl} = water: acidic phospholipid partition coefficient
F_{apl} = fractional content of acidic phospholipid in cell
K_p = water: protein partition coefficient
F_P = fractional content of protein in cell

Calculation of K_{nl}

$$D_{o:w}(pH) = P_{o:w} * \left(\frac{1-\alpha}{1+10^{pH-pKa}} + \alpha\right), \text{ for acid}$$

$D_{o:w}(pH) = P_{o:w} * \left(\frac{1-\alpha}{1+10^{pKa-pH}} + \alpha\right)$, for bases

Calculation of K_{npl}

$D_{pl:w} = 1.294 + .304 * logP$ (Yun et al., 2014)

If $D_{pl:w}$ is not there, we can use Po:w value which is close to that

Here $D_{pl:w}$ is equivalent to K_{npl}

Calculation of K_{apl}

$K_{apl} = K_{npl} * \left(\frac{1}{1+10^{pH-Pka}} + 20 * \left(1 - \frac{1}{1+10^{pH-Pka}}\right)\right)$, for acids

$K_{apl} = K_{npl} * \left(\frac{1}{1+10^{Pka-pH}} + 0.05 * \left(1 - \frac{1}{1+10^{Pka-pH}}\right)\right)$, for base

Calculation of K_p

$K_p = 0.163 + 0.021 * k_{npl}$, protein: water partition coefficient

3.2. Pharmacodynamics Model/Dynamic System Analysis

The interaction of a drug molecule with a receptor causes the initiation of a sequence of molecular events resulting in a pharmacodynamic or pharmacologic response. The term pharmacodynamics refers to the relationship between drug concentrations at the site of action (receptor) and pharmacologic response, including the biochemical and physiological effects that influence the interaction of drug with the receptor.

$$[Chemical] + [Target\ ] \Leftrightarrow [Drug - Target\ complex] \longrightarrow Response$$

The well-known modified Hill equations are used to describe the drug receptor interactions empirically as follows:

Simple E_{max} model

This model was originally derived from the classical theory of drug-receptor interaction.

$$E = E_0 + \frac{E_{max} * C(t)}{EC_{50} + C(t)}$$

Where, E_{max} is the maximum response, EC_{50} is the concentration at which 50% of E_{max} occurs and E_0 is the baseline response. C (t) is the effective chemical concentration i.e. concentration at the target site.

INTRODUCTION

Sigmoid E_{max} model:

This model is a generalization of E_{max} model.

$$E = \frac{E_{max} * C(t)^{\gamma}}{EC_{50} + C(t)^{\gamma}}$$

E_{max}, EC_{50} and E_0 and γ represents the sigmodicity factor or Hill factor, γ=1 for simple E_{max} model and if γ>1 for steeper curve and γ<1 for smoother curve.

Indirect response model

The indirect response models basically assume that the biological response is due to either inhibition or stimulation of the production or degradation as a function of target chemical concentration.

$$\frac{dR}{dt} = K_{in}^{0} * f(t) - K_{out} * f(t) * R$$

Where, K_{in}^{0} is zero order constant for production of response, K_{out} is first order constant for loss of response, R_0 is the basal physiological concentration of response variable.

$f(t)$ is the function that describe the inhibition or stimulation of response variable synthesis or degradation.

$f(t) = S(t) = 1 + \frac{S_{max} * C_t}{SC_{50} + C_t}$; Stimulatory function

$f(t) = I(t) = 1 - \frac{I_{max} * C_i}{IC_{50} + C_i}$; Inhibitory function

S_{max}/ I_{max} is the maximum Stimulatory/inhibitory response, C_i is the concentration at the target site, SC_{50}/IC_{50} is the stimulatory/inhibitory concentration require to produce half maximum response.

There are basically four type of response models:

INTRODUCTION

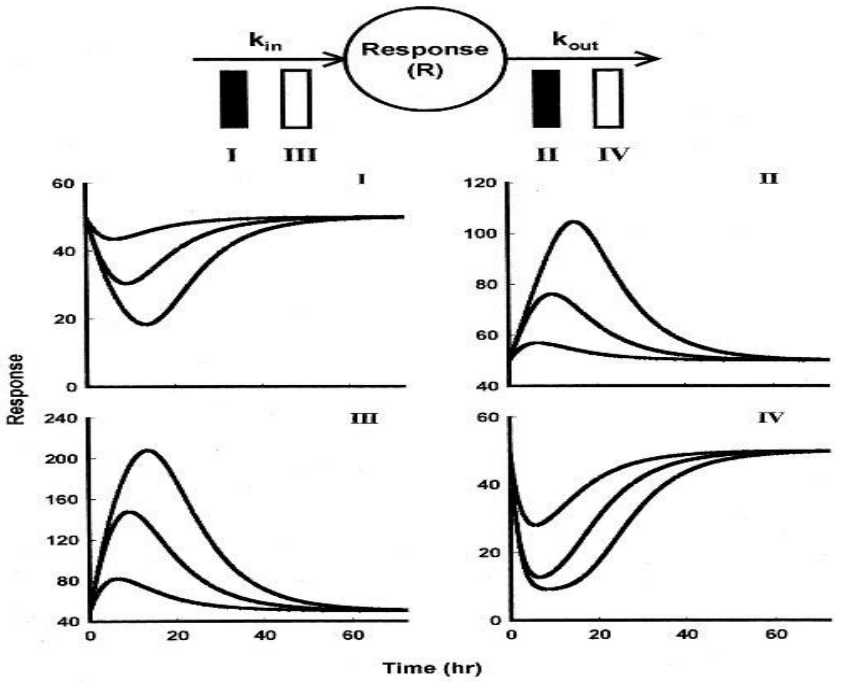

Fig 3. Four type of indirect pharmacodynamic response models. Model I and IV shows inhibition of a response as a result of inhibition of production and stimulation of degradation respectively. Whereas model II and III shows stimulation of a response as a result of inhibition of rate of degradation, and stimulation of rate of synthesis of a response variables respectively (Mager et al., 2003)

Model I

It describes the inhibition of the production rate of response variable (K_{in}).

$$\frac{dR}{dt} = K_{in}^{0} * I(t) - K_{out} * R$$

Model II

It describes inhibition of the degradation rate of response variable (K_{out}).

$$\frac{dR}{dt} = K_{in}^{0} - K_{out} * I(t) * R$$

Both Model I and II leads to higher concentration of the response variable.

Model III

It describes the stimulation of the production rate of response variable (K_{in}).

$$\frac{dR}{dt} = K_{in}^{0} * S(t) - K_{out} * R$$

Model IV

It describes the stimulation of the degradation rate of response variable (K_{in}).

$$\frac{dR}{dt} = K_{in}^{0} - K_{out} * S(t)$$

3.3. QIVIVE

QIVIVE (Quantitative in-vitro to in-vivo extrapolation) is a technique used for the translation of an in-vitro dose-response (DR) to in-vivo dose- response (DR). The reconstruction of in-vivo DR from the in-vitro studies involves the linear interpolation of transduction kinetics of signaling pathway. It assumes that the in-vitro data reflecting DR after target cell exposure, and the in-vitro derived dose-response model must have target cell exposure in input to be consistent. Such *in vivo* target cell (or by extension target organ) exposure, if not measured. So that is obtained by PBPK modeling. This can be done for animals or for humans, or both to help inter-species extrapolation:

A PBPK model along with the QIVIVE has been used to determine the oral equivalent doses corresponding to in-vitro doses. If the determined oral equivalent doses are relevant to the environmental exposure levels, then the response was classified as adverse effect (Rouquié et al., 2015).

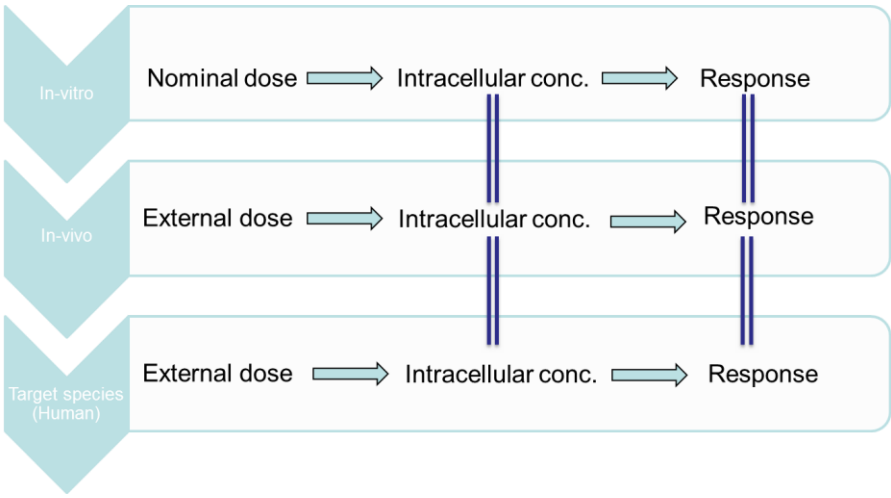

Fig 4. Describes the schema for QIVIVE approach where double lines represent equality assumptions and arrow represents flow of information.

3.4. AOPs

An AOP describes a sequence of events commencing with initial interaction(s) of a stressor with a biomolecule within an organism that causes a perturbation in its biology (i.e., molecular initiating event, MIE), which can progress through a dependent series of intermediate key events (KEs) and culminate in an adverse outcome (AO) considered relevant to risk assessment or regulatory decision-making (Ankley et al., 2010; OECD, 2018, 2016).

A molecular initiating event is "A specialised type of key event that represents the initial point of chemical/stressor interaction at the molecular level within the organism that results in a perturbation that starts the AOP" (OECD, 2018, 2016).

A key event is "A change in biological or physiological state that is both measurable and essential to the progression of a defined biological perturbation leading to a specific adverse outcome" (OECD, 2018, 2016).

A key event relationship is "A scientifically-based relationship that connects one key event to another, defines a causal and predictive relationship between the upstream and downstream event, and thereby facilitates inference or extrapolation of the state of the downstream key event from the known, measured, or predicted state of the upstream key event" (OECD, 2018, 2016).

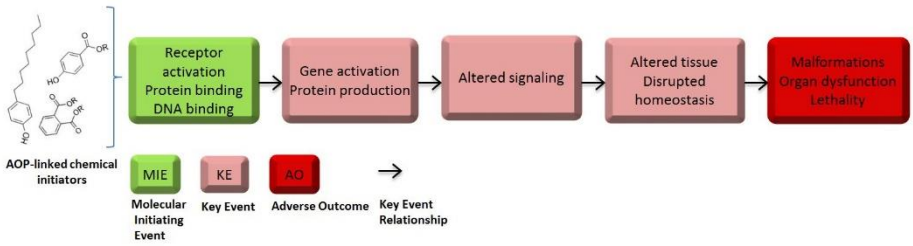

Fig 5. Schematic of AOP network describing the dose response linking the signal transduction pathway, as a series of key events due to chemically induced activation or inhibition of biological target (MIEs), to the adverse effects (https://aopwiki.org/).

3.5. Systems Biology (SBs)

Systems biology provides a platform for integrating multiple components and interactions underlying cell, organ, and organism processes in health and disease (Arrell and Terzic, 2010). It describes the functional interaction of biological components in a time-dependent fashion that uses genomics, metabolomics, and proteomics data (Aderem, 2005; Kitano, 2002). Understanding the biomolecular mechanisms are of great interest to identify the toxicological effects at the advanced stage. Systems biology has long been of great interest in studying the adverse effects on human health which basically involves linking perturbation (result of a chemical interactions with biological target) on the normal biological network to adverse outcome response (Arrell and Terzic, 2010; Auffray et al., 2009; Hood et al., 2004; Kell, 2006).

4. Integrative Systems Toxicology

Currently, there is a paucity of research that integrates all of these above described methods and directly ties the results to a predictive adverse outcomes model. Compared to the traditional dose-response model integrative systems toxicology model implements a more complex structure, as shown in figure 6. In figure 6, Module 1 focuses on the pharmacokinetics describing relationship between the chemical exposures to the plasma concentrations. And this also includes the distribution of chemical to the target tissues (Plasma tissue kinetics; PTK) also called biological effective dose; Module 2 captures the interactions of this biological effective dose with a target receptors (proteins, genes or metabolites) and their intrinsic activity. Module 3 links this perturbation (intrinsic activity) to the signal transduction pathway linking whole biological network (in case of Systems biology models) or simple linear pathway model (in case of AOPs).

INTRODUCTION

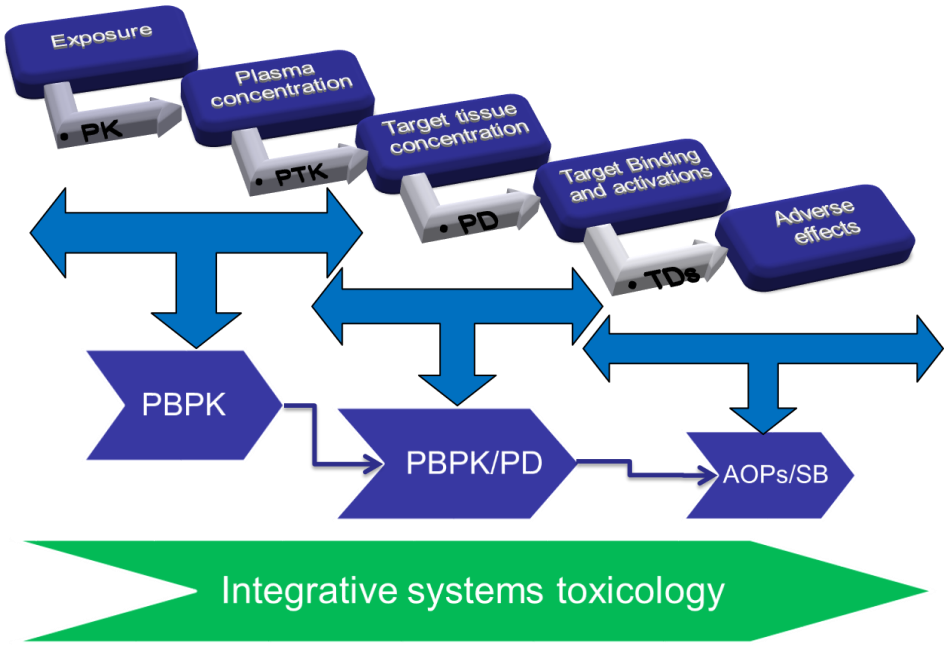

Fig 6. Schematic of integration of several approaches leading to the integrative systems toxicology model. PBPK comprising of both the PK (pharmacokinetics) and PTK (plasma-tissue kinetics) describing the time course of chemical concentration at plasma and tissue. PD is the pharmacodynamics describing the interaction of target tissue dose and biological ligand. Systems toxicology (ST) links the downstream pathway of biological network as a result of perturbed endogenous molecule.

Hypothesis and Objectives

Hypotheses

Along with the development of new tools and techniques in toxicological research, it is necessary to continuous re-evaluation, curation, and integration of existing data, and knowledge-based translation that might be able to solve many current challenges in this field.

Integration of knowledge from a complete pipeline of systems biology into a holistic yet mechanistic framework will enhance the understanding of both biology and adverse effects due to chemically-induced toxicity to human health. The pipeline includes in vivo, in vitro, and in silico data resulting both from genomics and from more targeted studies.

Prediction of Adverse effects of various chemicals on human health may be improved if the time course concentrations of those chemicals in the human body are well known. In silico tools are cheap, quick and reliable techniques to estimate the body burdens of chemicals, being a serious alternative to in vivo or in vitro investigations. PBPK/PD models may simulate and predict the distribution and accumulation of environmental toxicants in the human body. Therefore, they may be a good alternative to biological monitoring of environmental chemicals.

Integration of wide range of in silico tools (QSAR, PBPK/PD, AOP, systems biology models etc.) and databases (OMICS, epidemiological and exposure data), under the umbrella of Integrative Systems toxicology would improve the prediction of chemical-induced adverse effects on human health. This integrative approach would lead to mechanistic understanding of adverse effects vs conventional empirical end points and animal based testing.

Mechanistic understanding of the system as a compendium of interconnected processes would lead to a better integrative in-silico predictive model. It comprises of the chemical exposures to their biological target interactions and subsequently the molecular and functional changes that occurs at the multiple level of biological system.

In a mechanism-based modelling approach it is easy to integrate dynamic physiological changes that occur at life stages. This would allow to develop population and organ specific predictive models. To generate similar predictions without modelling, e.g. based on in experiments only, would be extremely difficult. Overall by improving the toxicity prediction this integrative approach of systems toxicology might also minimize the need of animal testing, reducing the cost and time of toxicity tests.

General Objective

Development of an Integrative Systems Toxicology framework should enable one to understand quantitatively the adverse effects of chemicals on a biological system from the information on the exposure of the system to the sequence of molecular and physiological alteration, through the integration of exposome-internal exposure-molecular/cellular response with adverse effect.

Specific Objectives

1. To review the detailed toxic pathway for the Endocrine disruptors and their classifications based on target organs and their mode of action. Thereby designing principals/framework for the development of the next generation of PBPK/PD – Systems Biology models.
2. Development and Validation of an adult internal dosimetry model (PBPK).
3. Integration of dynamic physiology in the development of PBPK for special populations (Pregnant mother and fetus)
4. Parametrization of PBPK and Systems Biology models using QSAR and in-vitro data.
5. Development and validation of AOPs and Systems Biology Models.
6. To accommodate toxicity prediction of chemicals, by improving mechanistic understanding of chemical effects in dynamic-model-AOPs, through the use of molecular biology and systems toxicology approaches.
7. Coupling PBPK and PD models (AOPs & SB) to develop integrative systems toxicology.
8. Sensitivity and uncertainty analysis of the developed models.

Chapter 1

Sharma, R. P., Schuhmacher., M. and Kumar V

Review on Crosstalk and common mechanisms of endocrine disruptors: scaffolding to improve PBPK / PD model of EDC mixture 'Environmental International, 99:1-14. (2017)

Chapter 1

Review on Crosstalk and common mechanisms of endocrine disruptors: scaffolding to improve PBPK / PD models of EDC mixtures

Abstract

Endocrine disruptor compounds (EDCs) are environment chemicals that cause harmful effects through multiple mechanisms, interfering with hormone systems resulting in alteration of homeostasis, reproduction and developmental effects. Many of these EDCs have concurrent exposure with crosstalk and common mechanisms which may lead to dynamic interactions. To carry out risk assessment of EDCs' mixtures, it is important to know the detailed toxic pathway as well as possible crosstalk with receptors and other factors, like critical window of exposure. In this review, we summarize the major mechanisms of actions of EDCs with the different/same target organs as they interfere with the corresponding hormone pathway by altering synthesis, metabolism, binding and cellular action. To show the impact of EDCs on life stage development, a case study on female fertility is reported on. Based on this summarized discussion, Major groups of EDCs are classified based on their target organ, mode of action and potential risk. Finally, a conceptual model of pharmacodynamic interaction is proposed that integrates the crosstalk and common mechanisms that modulate estrogen level into the predictive mixture dosimetry model. This review will provide new insight for EDCs' risk assessment and can be used to develop next generation PBPK/PD models for EDC mixture analysis.

Highlights

•EDC mechanism involves multiple targets interfering with hormone synthesis, metabolism and their biological action.

•Toxicodynamic interactions like crosstalk and common mechanisms are very important for elucidating the effect of EDC mixture.

•Window of exposure plays an important role in assessing the risk for developmental and reproductive disorders.

•In silico risk prediction can be improved by integrating toxicodynamic interactions of EDCs.

Key words: Endocrine disrupting compounds (EDCs), Toxicity mechanism, Mixture interaction, Common mechanism, Crosstalk, PBPK/PD models

Chapter 1

Abbreviations: 3MC: 3-methylcholanthrene

5α-R: 5 alpha reductase

ACTH: adrenocorticotropic hormone

Ahr: aryl hydrocarbon receptor

Ahrr: aryl hydrocarbon receptor repressor

AKT: serine/threonine kinase

AMH: anti-mullerian hormone

AMPO: ammonium Perflurooctane

ARC: arucate cell

Arnt: aryl nuclear translocator

AVPV: anteroventral periventricular nucleus

BAX: BCL2 associated protein

BCL2: apoptosis regulator

BMP: bone morphogenetic protein

BPA: bisphenol A

CAR: constitutive androstane receptor

CREB: cAMP response-element–binding protein

Cx43: connexin X 43

CYP1A1: cytochrome enzyme A

CYP1B1: cytochrome enzyme B

CYP19A: aromatase enzyme

CYP450scc: cytochrome p450 side chain cleavage

DBT: dibutylin

DEHP: diethylhexyl phthalate

DTCs: dithioarbamate chemicals

ERE: estrogen response element

E2: estrogen

FAK: focal adhesion kinase

Fas- membrane protein

FasL: fas ligand

Figla: factor in the germline alpha

FOXO3: forkhead box proteins

FSH: follicle stimulating hormone

GATA4: transcription factor

GDF: growth differentiation factor

GH: growth hormone

GJA1: gap junction alpha protein

GnRH: gonadotropin releasing hormone

GVBD: germinal vesicle migration and breakdown

HAT: histone acetyl-transferase

HPA- hypothalamus pituitary adrenal axis

HDAC: histone deacetylases

HMT: histone methyl transferase

HPOA: hypothalamus preoptic nucleus

HSDs: hydroxysteroid dehydrogenases

HSP90: heat shock protein 90

IGF-1: insulin growth factor

IGFR: insulin growth factor recptor

Igf2r: insulin like growth factor 2

INH: inhibin

IP3-DAG: inositol triphosphate- diacyglycerol

LH: luteinizing hormone

LHR: luteinizing hormone receptor

LHX8: LIM homeobox 8

LXR: liver X receptor

LXR: liver X receptor

MAPK: mitogen activated protein kinase

MEHP: mono (2-ethylhexyl) phthalate

MMP2: metalloproteinase 2

NCoA: nuclear coactivator

NCoR: nuclear corepressor

Chapter 1

NF-kB: nuclear factor k B

NOBOX: newborn ovary homeobox

NR: notch receptor

p160/SRC: steroid receptor coactivator

P23: protein 23

P4: progesterone

PR: progesterone receptor

PBPK/PD : Physiological based Pharmacokinetics/Pharmaco dynamics modeling

PBR: peripheral type Benzodiazepine receptor

PCBs: polychlorinated biphenyl

PCDDs: polychlorinated dibenzodioxins

Peg3: paternal express gene 3

PEPCK: phosphoenolpyruvate carboxykinase

PFASs: poly-fluorinated alkyl substances

PI3: phosphatidylinositol 3-kinase

PMG: primordial germ cell

PPARs: peroxisome proliferator activated receptors

PTEN: phosphatase and tensin homolog

PXR: pregnane X receptor

RIP140: receptor interacting protein

ROS: reactive oxygen species

RXR: retinoid X receptor

SDM: sexual dimorphism

SF:1-steroidogenesis factor 1

SHBG: steroid hormone binding globulin

SMRT: silencing mediator for retinoid or thyroid-hormone receptors

Sohlh2: spermatogenesis and oogenesis helix-loop-helix 2

SREBP 2: sterol Response Element Binding Protein 2

SREBP1c : sterol Response Element Binding Protein 1c

StAR: steroid acute regulatory protein

SUG 1: suppressor for gal 1

SULTs: sulphotransferase enzyme

TAT: tyrosine aminotransferase

TBG: thyroid binding globulin

TBT: tributyltin

TCDD: 2,3,7,8-tetrachlorodibenzo-p-dioxin

TCPOBOP: 1, 4-bis- [2-(3, 5,-dichloropyridyloxy)] benzene

1. Introduction

The U.S. EPA defines endocrine disruptor compounds (EDCs) as exogenous agents that interfere with synthesis, secretion, transport, metabolism, binding action, or elimination of natural blood-borne hormones that are present in the body and are responsible for homeostasis, reproduction, and developmental process (Kavlock et al., 1996). The WHO extended this definition linking EDCs to adverse health outcomes in an intact organism, or its progeny or subpopulation (WHO, 2002). The Endocrine Society describes EDCs as chemicals that interfere with any aspect of hormone action (Gore et al., 2014). EDCs can be found in daily use products such as detergents, food cans, plastic bottles, children toys, flame retardants, cosmetics, and processed food (Clarkson, 1995; Rudel and Perovich, 2010). EDCs interfere with hormone kinetics and its dynamics causing alteration in hormone level or expression of hormone responsive element (Crisp et al., 1998).

Chapter 1

The aim of hormones is to execute its specific task on specific time with specific amount. There are many studies which link hormone alteration to different disease outcomes. For example, low testosterone and SHBG levels are the early biomarker for the risk of metabolic syndrome (Kupelian et al., 2006); alteration of E2, ERα, PR and the aromatase enzyme is strongly linked with endometriosis and infertility (Kitawaki et al., 2002); alteration in FSH, LH, inhibin B, and testosterone level is associated with decreased sperm quality (Meeker et al., 2006). Earlier assumption that EDCs and hormones would yield the same responses in different cell lines or tissues was found wrong. Now it is well known that EDCs have cell and tissue-specific responses (Lackey et al., 2001). Even at very low concentrations, EDCs can produce significant endocrine disruptive action (Vom Saal and Hughs, 2005; Vandenberg et al., 2012) which challenges classical dose response curve at significantly high doses. Further, EDCs show disparate response at different life-stage dependent physiological concentrations of hormone, challenging current risk assessment methodologies which are not in consonance with life-stage changes (Welshons et al., 2003; Vandenberg et al., 2013). For instance, a study from Ohtake et al. (2003) showed that EDCs can produce a contrary response based on physiological stage of prepuberty and puberty. The interference of EDCs with developmental stages (prenatal-postnatal-early childhood-adulthood) and reproductive stages showed time of exposure as an important factor to determine its potency as well as developmental effect (Haimes, 2009; Gore et al., 2014). For example, there is a strong relationship of EDC exposure affecting HPG axis system and alteration in the age of female puberty showing developmental effect (Wang et al., 2005; Euling et al., 2008). The biological marker like enzyme expression and hormone level can help in assessing developmental risk by knowing the detailed mode of action of EDCs (Rockett et al., 2003).

Humans are subject to continuous and simultaneous exposure to EDCs via its surrounding environment and bioaccumulation becomes inevitable in many cases, which might cause permanent damage following physiological adaptation failure (Vandenberg et al., 2013). Several studies showed that chemicals at the individual level have no observed effect level (NOEL), when exposed simultaneously as a mixture show adverse effect disproving the concept of NOEL and taking more attention towards mixture studies (Rajapakse et al., 2002; Silva et al., 2002). The successive use of the PBPK model in the field of toxicology is commendable since it has great advantage of predicting internal tissue dose by integrating experimental data (both in vivo and in vitro) and extrapolation across species (Caldwell et al., 2012). However, the level of biomarker of exposure (internal tissue dose) is, in many case, not sufficient to predict the toxicity of chemicals and additionally the effect of chemical mixture for certain response deemed to have toxicodynamic interaction. Moreover, many biological responses are the convergence of multiple signaling pathways, which eventually become vulnerable to multiple targets of EDCs. Incorporation of the relationship between the exposure at the sites of action and the response generated can extend the PBPK model to PBPK/PD (Nestorov, 2007). The objective of this review (summarized in Fig. 1) is to understand the mechanism of actions of EDCs which includes interaction of chemicals with molecular receptor, enzymes,

proteins, gene regulatory mechanism or epigenetic process thus affecting biological system, including window of exposure. Besides, this review also investigates the normal endogenous pathway of hormone sidewise to better understand the physiology dependent EDCs' action. The last part of the review includes an example showing common as well as crosstalk mechanism of EDC mixture affecting estrogen kinetics. Improved understanding of common as well as crosstalk mode of action and categorization of chemicals based on similar adverse outcomes may provide better scaffolding for integration of pharmacokinetics and pharmacodynamics into predictive mixture toxicological model of EDCs.

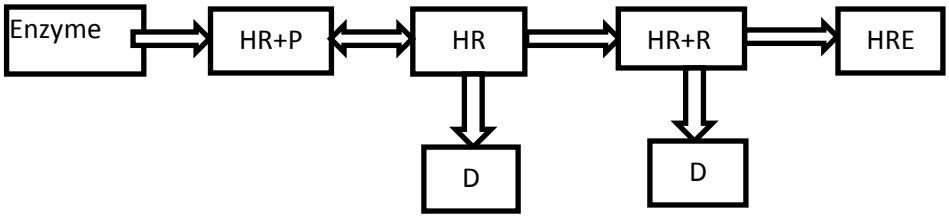

Fig.1. Effects of EDCs on hormone action at different level.
Enzyme responsible for hormone synthesis, HR- hormone, P- hormone binding protein, R- receptor, D- degradation of hormone and its receptor, HRE- hormone response element.

2. Molecular mechanism of EDCs actions on the endocrine system

In general, individual EDCs can affect the endocrine system accounting their synthesis to metabolism; receptor mediated action, various signalling pathways and crosstalk signalling between receptors. In this section, a summarized review of EDCs' effects on major hormones namely thyroid and steroids (corticosteroid and gonadal) is provided.

2.1. EDCs affecting thyroid hormone action

Thyroid hormones (THs) are one of the integral parts of the hormone system required for normal brain and somatic development. It has been seen that EDCs can disrupt the function of the thyroid system possibly through multiple mechanisms such as synthesis, transport, and receptors like TR, Ahr, CAR, PPAR and RXR, mediated function for subsequent action and metabolism of hormone. Various chemicals affect homeostasis of hormones including perchlorates, PCBs, PCDDs and PCDFs (Zoeller, 2010). Perchlorates inhibit uptake of iodide into thyroid follicle (Clewell et al., 2004). PCBs, PCDDs and PCDFs that competitively bind with transthyretin impair transportation (Lans et al., 1994) and their affinity towards the Ahr receptor leads to increase metabolism of hormones (Poland and Knutson, 1982).
The toxicology pathway of EDCs via Ahr is shown in Fig. 2; where Ahr receptor is present in the cytosol in conjugation with subunits like chaperon protein HSP90, regulatory

protein P23 and immunophilin like protein XAP2 (Perdew, 1988; Kazlauskas et al., 1999; Petrulis et al., 2000). Subsequently binding of EDCs with Ahr forms a complex followed by dissociation of Hsp90, P23 and XAP2 and translocation into the nucleus. In the nucleus, Ahr forms a heterodimer complex with Arnt which then binds with XRE causing increase in expression of CYP1A1 and UDPGT1A; and finally leads to increase in

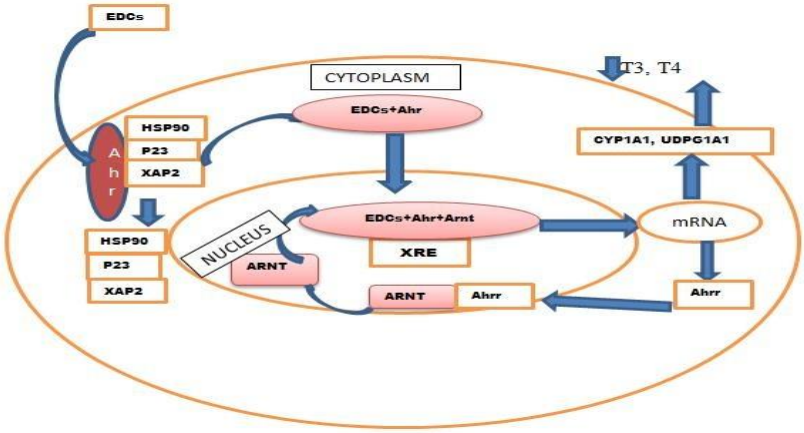

metabolism of thyroid hormone (Hankinson, 1994; Van Birgelen et al., 1995). Simultaneously, there is feedback inhibition of Ahr transactivation by Ahrr (Mimura et al., 1999). Qatanani et al. (2005) reported that EDCs' affinity towards CAR, can be another possible mechanism of metabolism of thyroid, that alters the UGTs and SULT mediated glucuronidation and sulfation of TH, respectively.

Fig.2. Summary of molecular mechanism of EDCs binding with Ahr-. The binding of EDCs like dioxins with Ahr leads to translocation of receptor to nucleus from cytoplasm with dissociation of chaperons, forming Ahr-Arnt complex leading to induction of CYP enzyme, enhancing metabolism of endogenous hormone.

BPA has been reported as an anti-thyroid agent that is mediated via multiple molecular mechanisms, mainly involved in altering receptor gene expression and dynamic stability. It decreases the TRα and TRβ mRNA levels and subsequently suppresses RXR gene expression which is a heterodimer partner of TR. Additionally, it can also inhibit the binding of T3 to TR by recruiting N-CoR (Moriyama et al., 2002; Iwamuro et al., 2006). The isoform of TR remains in dynamically equilibrium state between inactive and active forms to maintain the physiological action. The binding of EDCs with TR favors its inactive isoform (see Fig. 3) via recruitment of (N-CoR). Subsequently, increase in HDAC, HMT, and HDM levels induces the repression of target gene making TR inactive. In contrast, binding of thyroid to TR induces conformation changes and recruits coactivators of p160/SRC (steroid receptor coactivator). These coactivators have inherent histone acetylase activity that recruits complex like histone arginine methyltransferase

(HMT), HAT and chromatin remodeling complex and form active homodimer or heterodimer complex with RXR (Ahuja et al., 2003; Yoon et al., 2005; Flamant et al., 2007). Juge-Aubry et al. (1995) mentioned that RXR was the common partner for both TRs and PPARs to form active heterodimers. Hence, the EDCs having affinity for PPARs or RXR could affect thyroid activity through crosstalk mechanism.

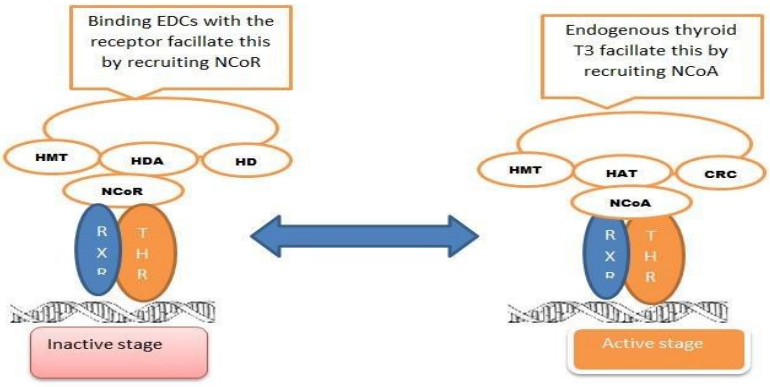

Fig.3. EDCs affecting dynamic state of receptor. Unliganded thyroid receptor resides in nucleus in inactive state by recruiting NCoR and the ligand binding leads to active stage by recruiting NCoA. Binding of EDCs with thyroid receptor induced conformational changes by recruiting nuclear co-repressor facilitates inactive stage leads to inhibition of thyroid action.

2.2. EDCs affecting steroid hormone

2.2.1. EDCs affecting corticosteroid hormone action

Among corticosteroid hormones, glucocorticoids such as cortisol are produced in response to stress and are an integral part of HPA axis involved in cellular homeostasis and different metabolic processes. The enzymes that are responsible for the biosynthesis of these hormones mainly involved CYPs, HSDs and steroid reductases (Miller, 1988). The molecular mechanisms involved in biosynthesis are transfer of cholesterol to inner mitochondrial membrane by regulatory protein StAR (Manna and Stocco, 2005) and conversion of cholesterol to pregnenolone by CYP11A or CYP450scc (Parker and Schimmer, 1995; Manna and Stocco, 2005). Subsequent action of CYP17A and HSD enzyme accomplishes the glucocorticoid synthesis.

The interconversion of cortisol (active) to cortisone (inactive) involves two isoforms of 11β-HSD namely 11β-HSD1 and 11β-HSD2 (Krozowski et al., 1999). This interconversion plays an important role in regulating central adiposity (Stewart et al., 1999) and protecting developing fetus from glucocorticoid excess (Krozowski et al., 1995). EDCs like PFASs, TBT, TPT and dithiocarbamates inhibit 11β-HSD2 isoform (Atanasov et al., 2003; Ohshima et al., 2005; Zhao et al., 2011), and their exposure during pregnancy stage has been found to alter normal fetus development. Wang et al. (2012) reported the role of BPA on increased expression of 11β-HSD1, which results in increased level of cortisol, lipoprotein lipase and PPAR-γ causing higher adipocyte differentiation. The expression of PEPCK and TAT, well characterized metabolic response of

glucocorticoid, was shown to be inhibited by DBT which decreases affinity of glucocorticoid towards its receptor (Gumy et al., 2008). Furthermore, one of the metabolic pathways of steroid involves PXR, a xenobiotic receptor which regulates CYP3A expression. Chemicals like phthalic acid and nonylphenol inhibit PXR degradation, thus enhancing CYP3A expression which leads to alteration in metabolism of steroid hormones (Masuyama et al., 2000, 2002).

2.2.2. EDCs affecting gonadal hormone

The effect of EDCs on the human reproductive system has been linked with infertility, mediated through a diverse mechanism that includes: altering gonadal steroidogenesis, affecting HPA axis and feed-back mechanism, altering receptor biology, crosstalk of receptor signaling, and direct organ toxicity. For the steroidogenesis, cholesterol is the main precursor which can be affected by the EDCs that alter receptor like PPARα and PXR which regulates transporter protein, such as translocator protein (TSPO) or peripheral type Benzodiazepine receptor (PBR) that transports cholesterol from the cytosol to the mitochondria (Hauet et al., 2005; Fan and Papadopoulos, 2012) and the metabolism of cholesterol by regulating transcription of rat CYP7A1 (cholesterol 7α-hydroxylase) gene (Marrapodi and Chiang, 2000; Staudinger et al., 2001; Li et al., 2011). Moreover, the involvement of many supplementary pathways initiated via different receptors like GHR, IGF-1 and (RXR/TR) which regulate the function of steroidogenic enzyme and the affinity of EDCs towards these receptors, makes toxicity mechanism more complex (Chandrashekar and Bartke, 1993; Xu et al., 1995; Hull and Harvey, 2000; Manna et al., 2001; N'Diaye et al., 2002). In addition to that, the central system HPG axis which regulates gonadal cell plays an important role in normal reproductive development process. At the hypothalamic level, kisspeptin neurons express both, ligand KiSS-1 and its receptor GPR54 that regulates the release of GnRH in pituitary which in turn controls the expression of FSHR and LHR in gonadal cell. The kisspeptin neurons also express ER-α which is involved in feedback inhibition of GnRH in response to estrogen stimulation. This feed forward mechanism holds an important role during normal fertility cycle of pre-ovulatory to ovulatory phase (Roseweir and Millar, 2009; Silveira et al., 2010; Hameed et al., 2011). It has been shown in rodent models that exposure of BPA affects HPG axis with different mechanisms depending on life stage of exposure; at prepubertal stage damages kisspeptin neuron and at puberty stage alters ERαmRNA expression (Ceccarelli et al., 2007; Patisaul et al., 2009). Xi et al. (2011) showed that the involvement of BPA on transcript levels of GnRH and FSH in the male and female pup via altering Kiss-1 mRNA expressions further supports the notion of multilevel mechanism of EDCs.

Boberg et al. (2008) reported that exposure to phthalates causes the reduction of anogenital distance, sign of male infertility, via the reduction of leptin level which supports the concept of leptin regulation of LH and FSH via leptin-kisspeptin-GnRH pathway (Neurons et al., 1999; Luque et al., 2007). The leptin synthesis was also found to be inhibited by cadmium exposure (Stasenko et al., 2010). In addition to that the local gonadal enzyme CYP19A (aromatase) catalyses the androgen to estrogen conversion to

Chapter 1

balance androgen-estrogen level which is the prerequisite for the normal fertility in both male and female (Simpson et al., 1994). Several studies have reported that TBT inhibition of aromatase enzyme in granulosa cell results in imposex affecting fertility (Saitoh et al., 2001; Heidrich et al., 2001). Many studies have shown the EDCs' dual action in regard to estrogen level (Ohtake et al., 2003, 2007). For instance dioxin exposure at prepubertal stage, shows estrogenic activity via enhancing binding of ERα to ERE. However at pubertal stage, dioxin-receptor complex represses E2 bound ER function leading to antiestrogenic effects (Ohtake et al., 2003). In another study, Ohtake et al. (2007) reported the antiestrogenic activity of EDCs like TCDD and 3MC via activation of E3 ubiquitin ligase pathway that results in degradation of ERα and Ahr. In contrast to antiestrogenic activity, certain EDCs increase the bioavailability of estrogens via inhibiting principle of estrogen sulphotransferase (SULT1E1) enzyme which causes inactivation of E2 (Kester et al., 2002).

The male sex hormone testosterone biosynthesis has been shown to be affected by TCDD and PFOA via different mechanisms of action that involve altering signaling pathway, regulating expression of enzyme or direct inhibition of enzyme involved in steroidogenesis (Fukuzawa et al., 2004; Lai et al., 2005a; Shi et al., 2009; Zhao et al., 2010; Wan et al., 2011). Saunders et al. (1997) reported that exposure of pregnant mother to octylphenol, decreases the level of testosterone in the fetal rat testis via altering the expression of CYP17α-hydroxylase/C17–20 lyase and steroidogenesis factor 1 (SF-1) leading to reproductive developmental disorder. The local hormone like AMH responsible for sexual differentiation in fetus during embryogenesis also nurtures the testosterone by increasing prenatal proliferation of Leydig cells and maintains the prepubertal stage in male. In parallel, developmental exposure of BPA and PCBs is linked to decreased levels of AMH, LHR, and 17β HSD3 and reduced aromatase activity in the hypothalamus, affecting sexual maturation (Lee and Donahoe, 1993; Hany et al., 1999; Rey et al., 2003; Nanjappa et al., 2012). In addition to that, TBT or TPT is found to inhibit both 5α-R1 and 5α-R2 isoenzymes, responsible for production of active androgen (Svechnikov et al., 2010), affecting male sexual characterization (Doering et al., 2002). Castro et al. (2013) found similar results for BPA, reporting inhibition of both 5α reductases at their synthesis level. Simultaneous exposure of both chemicals (TBT and BPA) could lead to more impact on male fertility. Moreover, exposure to EDCs has shown to induce reproductive toxicity by damaging the integrity of blood testes barrier (BTB) in Sertoli cell that causes impairment in spermatogenesis (Cheng et al., 2011).

EDCs like BPA, PFOS, DEHP and cadmium induced reproductive toxicity are found to be mediated via altering MAPK, PI3K/c-Src/FAK, p38 MAPK and ROS signaling pathway leading to alteration in synthesis and metabolism of different proteins like occludin, ZO-1, Cx43 and catenin affecting BTB integrity (Chitra et al., 2003; Sobarzo et al., 2006; Li et al., 2009; Siu et al., 2009; Cheng et al., 2011; Wong and Cheng, 2011; Qiu et al., 2013; Ansoumane et al., 2014). It has also been found that Sertoli cells have functional Ahr, responsible for TCDD dose-dependent toxicity that alters mRNA level of testin, aromatase, sertolin and MIS which are important for germ cell development (Lai

et al., 2005a, 2005b). Phthalates are well characterized as reproductive toxic agents that cause apoptosis of germ cell by activating caspase pathway which includes: activation of fas by increased expression of fasl (Richburg and Boekelheide, 1996; Lee et al., 1999; Richburg et al., 1999; Koji et al., 2001), accumulation of lipid in somatic cells via increased LXRα mRNA expression (Muczynski et al., 2012) and downregulation of both GJA1 and vocal adhesion molecule vinculin (VCL) by increasing MMP2 (Yao et al., 2012). Subsequently, activation of NFkB via increased expression of TRAIL-R1(DRP4) and TRAIL-R2 (DRP5) leads to increased apoptosis of germ cell without modification of their proliferation (Giammona, 2002; Lambrot et al. 2009). Fig. 4 shows the mechanism of phthalates causing germ cell apoptosis in fetus.

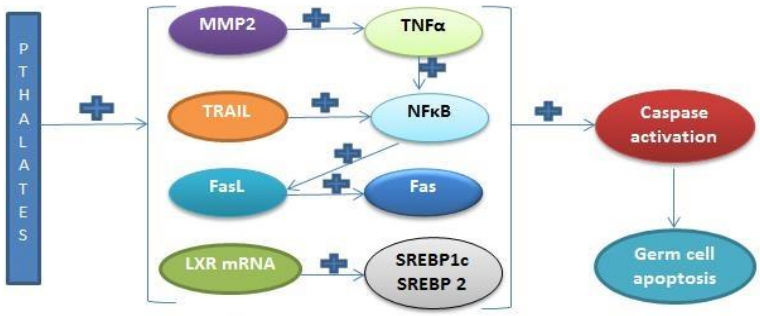

Fig. 4. Mechanism of phthalates causing germ cell apoptosis in fetus. Phthalate exposure at tissue level causes activation of caspase pathway which lead to apoptosis of germ cell through interaction and activation of receptor and gene at the cellular level.

3. Effects of EDCs in different windows of exposure: case study on female fertility effects

It has been shown that EDCs have disparate response at different life-stages, depending on the physiological concentrations of hormones (Ohtake et al., 2003). However, primary concerns for female fertility are exposure to EDCs at prenatal and postnatal stages, which are at higher risk of reproductive failure as well as metabolic disorder and hormonal disorders in their later life. EDCs can alter normal cellular and tissue development and function through their interference in developmental programming of the body (Schug et al., 2011). To study the life stage risk assessment on fertility, it is very important to know the detailed mechanism behind development of germ cell into mature oocyte. This involves complex and sequential biological network of signaling pathway.

3.1. Physiology of development of germ cell into mature oocyte

During epigenetic reprogramming of germ cell, at the very first step, involves DNA demethylation to regain differentiation totipotency which subsequently undergoes mitotic division without completing cytokinesis to the formation of germ cell cyst (Pepling and Spradling, 1998). Before birth, germ cells go through meiosis and arrest in diplotene phase of meiotic prophase until puberty comes. Meanwhile germ cell cyst undergoes apoptosis followed by surrounding of pregranulosa cell forming primordial follicles

Chapter 1

(Borum, 1961; Pepling and Spradling, 2001). After forming primordial follicles, estrogens play a role in maintaining these follicles' pool by inhibiting oocyte nest breakdown through inhibition of BCL-2 gene transcription via both genomic and nongenomic pathways (Perillo et al., 2000; Chen et al., 2007, 2009).

Moreover, additional pathways are also involved in the regulation of primordial follicles which involves Notch signaling, and KIT-KL pathway. Notch signaling activation involves expression of Jagged1 and Jagged2 (ligand), in germ cells and Notch2 (ligand), in granulosa cells to form a receptor ligand complex. The proteolytic cleavage of this complex by γ-secretase produces intracellular domain of Notch (NICD) which translocates into the nucleus and interacts with the CSL family to form the complex. This complex recruits histone acetylase and regulates the expression of LHX8, NOBOX, Figla and Sohlh2 involved in formation of primordial follicles (Baron, 2003; Shih and Wang, 2007; Chen et al., 2014; Vanorny et al., 2014). KIT receptor expressed in oocyte and the KIT ligand that is present in both oocyte and primordial follicle, help in initiation and progression of follicular development (Parrott and Skinner, 1999) via the activation of the MAPK pathway (Jones and Pepling, 2013). GDF9 increases KIT ligand mRNA expression and thus promotes the progression of primary follicle development (Nilsson and Skinner, 2002). BMP4 and BMP7 play a major role in survival and growth of primordial follicle to primary follicle by decreasing KL and TGF-α expression respectively (Nilsson and Skinner, 2003; Lee et al., 2004). Cx43 expressed in both cumulus cell and granulosa cell plays an important role in paracrine signaling and gap junctional intercellular communication between cumulus cell and follicular cell providing follicular development and oocyte quality (Ackert et al., 2001; Gittens et al., 2005; Wang et al., 2009). BMP4, BMP7 and BMP15 downregulate Cx43 in human granulosa cell via smad pathway and thus decrease the gap junctional intercellular communication leading to prevention of premature luteinization (Chang et al., 2013; Chang et al., 2014a, 2014b). The interplay between paracrine hormones is very important for the transition of primordial follicle to primary follicle to become a mature oocyte. AMH inhibits primordial follicles to enter the pool of growing follicles (Durlinger et al., 1999) by decreasing expression of inhibin (Themmen and Themmen, 2009). Billiar et al. (2003) also reported the inhibition of expression of inhibin by the estrogen in pregranulosa and oocyte. Thus, estrogens play an important role in regulating inhibin and follicular development. The TGF-β signaling involves GATA-4 and Smad-3 coordination for activating the inhibin (Anttonen et al., 2006). Androgens play an important role in follicle development via increasing expression of, FOXO-3, GDF9 through PI3/AKT pathway, and, KIT/KL through genomic pathway during primordial follicle to primary follicle stage. Specifically, during the development of primary follicle to antral stage, it inhibits proapoptotic proteins and stimulates FSH mRNA expression, cAMP and p450scc through both genomic and nongenomic i.e. MAPK/ERK pathways which in turn stimulates aromatase enzyme (Prizant et al., 2014). FSH stimulates LHR expression, (Richards et al., 1976) inhibin B production (Lee et al., 1982), and induces aromatase activity in the granulosa cells, which results in more estradiol level (Short, 1962; Richards et al., 1976;

Hillier et al., 1981). Moreover, most FSH sensitive called dominant follicle produces the highest levels of inhibin B and estradiol which in turn causes feedback inhibition of FSH production, required for growth of remnant follicles (Hirshfield and Midgley, 1978). After selection of dominant follicle, subsequently progesterone causes germinal vesicle migration and breakdown (GVBD) for resumption of meiosis at puberty by activating p53 and E2F transcription factor 1 (Garcia-reyero et al., 2015) leading to ovulation. The fertilization of ovum results in formation of zygote and matured follicle after releasing ovum called lutein cell which secretes VEGF. It prolongs the lutein cell function that maintains the progesterone level important for pregnancy development. VEGF function is regulated via PPARγ (Fraser et al., 2000; Kaczmarek et al., 2005).

3.2. EDCs' interaction with target molecules and their pathway

Exposure to Lindane, PCBs and PAHs to embryo has been linked with premature reproductive ageing by causing the apoptosis of germ cell through different pathways such as activation of caspase-3 and poly-ADP ribose polymerase cleavage (PPAR) by Lindane and activation of BAX via Ahr by PAHs (Ronnback and de Rooij, 1994; Matikainen et al., 2002; La Sala et al., 2009; Kee et al., 2010). Phthalate exposure induces primordial follicle recruitment via activation of PI3K/AKT pathway, resulting in premature ovarian follicle and infertility (Hannon et al., 2014). Previously, Castrillon et al. (2003) found development of premature oocyte follicle in FOXO3A knock out mouse which is regulated by the PTEN/PI3K/AKT pathway. Both, phthalates and BPA reduce the expression of LHX8, Nobox, Figla, and Sohlh2, involved in oocyte survival and follicular recruitment to form primordial follicle. In addition to this both compounds alter epigenetic reprogramming of Lhx8 by preventing DNA demethylation (Zhang et al., 2012, 2014). However, BPA shows multiple mechanisms of action, altering steroidogenesis and proliferation of granulosa cell such as: induction of PPARγ causing downregulation of FSH-stimulated IGF-1, SF-1, GATA4, aromatase, and E2 (Kwintkiewicz et al., 2010), decreases both StAR and P450scc mRNA impairing hormone production in the antral follicles (Peretz et al., 2011), and activates nongenomic pathway of estrogen via PKA and PKG pathways associated with phosphorylation of transcription factor CREB and the cell cycle regulator Rb (Bouskine et al., 2009). Additionally, BPA delayed maturation of oocyte by inhibiting resumption of meiosis via altering ER expression, following hypomethylation of imprinted gene Igf2r, Peg3, and GVBD, (Chao et al., 2012). On the other hand, other EDCs like methoxychlor inhibit follicular development by stimulating AMH (Uzumcu et al., 2006). This is further supported by the study of impairmaint of follicular development in neonates on exposure of estradiol benzoate found to be via increased expression of AMH (Ikeda et al., 2002). Moreover, Nagel et al. (1999) shown that BPA even at very low doses can affect sexual dimorphism of infants via its estrogenic action in brain, whereas in normal, prenatal estrogen forms complex with Alpha fetoprotein, protecting the female brain from defeminization and masculinization (Bakker et al., 2006).

EDC contamination in the human follicular micro-environment is associated with a lower chance of an oocyte to develop into a top-quality embryo, leading to lowering in

fertilization rate (Petro et al., 2012). For instance, PCB exposure affects oocyte quality and competence via multiple mechanisms (altered microtubule organization, mRNA polyadenylation levels, redistribution of cortical granules, mitochondrial disorganization) which leads to polyspermy and transcript instability. It can also directly cause cumulus cell apoptosis which is communicator cell between oocyte and follicle mediated via Ahr signaling (Gandolfi et al., 2002; Brevini et al., 2005; Pocar et al., 2006). MEHP an endocrine disruptor inhibits embryonic genome activation (EGA) initiation and maternal-effect genes resulting in the suppression of maternal-to-embryonic transition by generating ROS (Chu et al., 2013).

Fig. 5 summarizes the life stage development of germ cell to oocyte and the possible targets of EDCs. In this turn, Fig. 6 explains the complex signaling pathway for life stage development of germ cell maturation to oocyte.

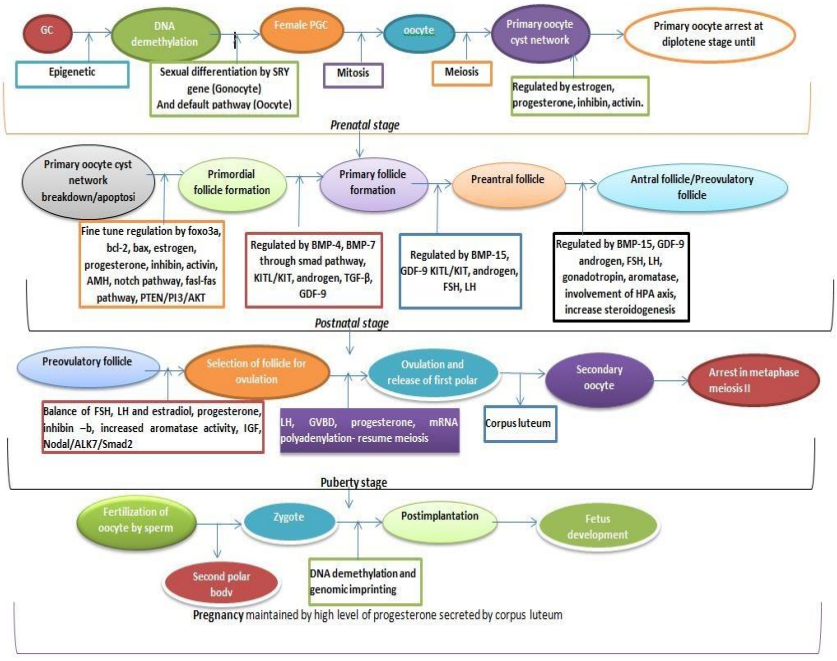

Fig. 5. Life stage development of germ cell and the possible targets of EDCs. The germ cell, basis of future sexual life or transgenerational development, development of oocyte from germ cell starts at embryo stage. Exposure of EDCs to pregnant mother (F0) may cross placental barrier and affect embryonic germ cell in fetus (F1). This could lead to alteration in oocyte quality required for fertilization and transgenerational fetus development (F2). Every stage of development of germ cell to high quality oocyte, demands fine tune balance of endogenous level and interaction pathway. Categorizing development of germ in stages provides information on susceptible targets of EDCs during the journey of germ cell of fetus (F1) residing in mother embryo (F0) to high quality of oocyte, for development of transgenerational fetus (F2).

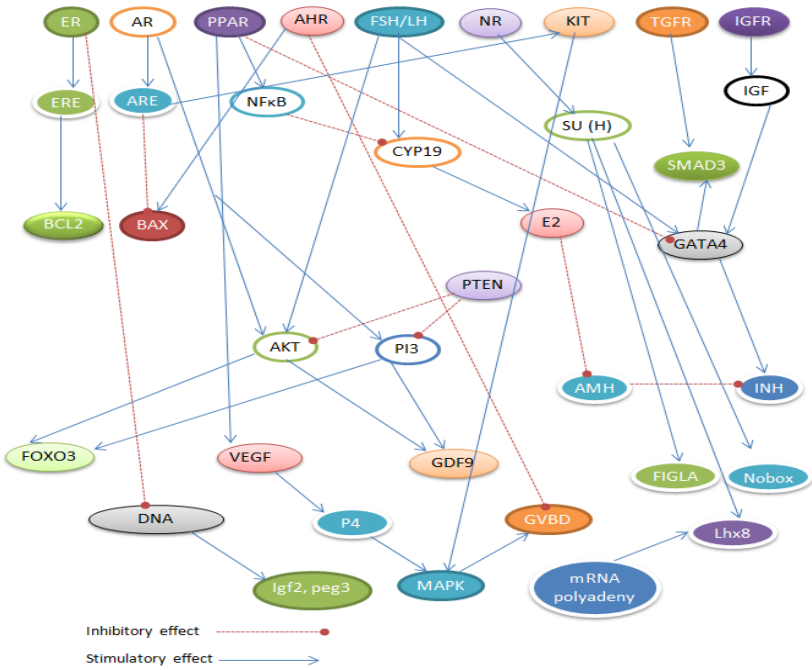

Fig. 6. Signaling pathway for life stage development of germ cell to zygote. The figure depicts the different signaling pathways' initiation via binding of endogenous molecule with receptors, which leads to inhibitory and stimulatory effects on signaling molecule following physiological demand for the development of germ cell into mature oocyte.

4. Grouping strategy and conceptual model of PBPK/PD in assessing risk for chemical mixture

4.1. Grouping strategy

There are numerous classifications of EDCs reported in the literature based on different criteria like pathway of exposure, level of exposure, target hormones, adverse effects, and disease outcomes (Caserta et al., 2008; Wuttke et al., 2010; Craig et al., 2011; Schug et al., 2011; Casals-Casas and Desvergne, 2011; Vandenberg et al., 2012; Hampl et al., 2014). Ongoing discussion of the risk assessment for chemical mixture (EFSA, 2013) needs new grouping strategy which clusters EDCs based on their similar adverse outcomes via independent, crosstalk and common interaction mechanism involving multiple organs and hormones. Similar prerequisite for cumulative risk assessment of chemical mixtures has been cited by EFSA (Kortenkamp, 2007; EFSA, 2013). This type of grouping strategy (based on similar adverse outcomes) could also help in making a decision on whether to go for dose addition or response addition method for mixture interaction study (Culleres et al., 2008). A detailed discussion on classification is beyond the scope of this review. However, a detailed classification for selected chemicals is provided in Table 1 of Annex 1. Classification of EDCs proposed in this review is based on target organs, hormones, biomolecule (MOA) and adverse outcomes, which can

Chapter 1

provide basis for grouping strategy for mixture modeling. Proposed grouping strategy has been illustrated in Fig. 7 by giving a small example of four chemicals (BPA, TCDD, phthalates and PFOS). Some of these chemicals are categorized in one group for mixture study based on their similar adverse outcome including target organs like thyroid gland and Sertoli cell, and in another group with dissimilar mode of action (crosstalk) producing common adverse effect of altering thyroid action and decreasing sperm count, respectively. Similar grouping strategy has been followed in Fig. 9 for the chemicals affecting female fertility.

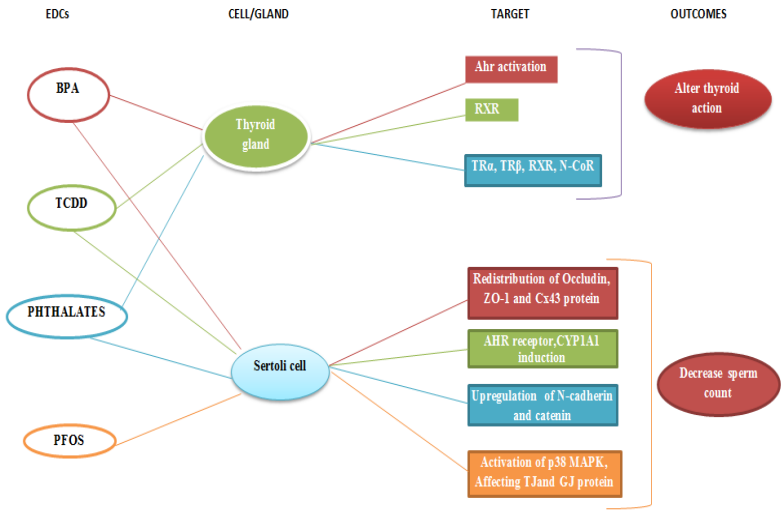

Fig. 7. Endocrine disruptor's classification on the basis of mode of action for selected chemicals (BPA, TCDD, phthalates and PFOS), with different targets on thyroid and Sertoli cell with common adverse effect in respective cell.

4.2. Conceptual model of PBPK/PD

A chemical can alter hormone actions by targeting at the level of epigenetic-gene-enzyme/receptor followed by endogenous intracellular signaling pathway (Grün and Blumberg, 2006; Cruz et al., 2014). Therefore, the mixture of chemicals producing similar adverse outcomes via entirely different modes of action can be categorized in one group in order to analyse the combination effect. Furthermore, timing and level of exposure are also important parameters which can make adverse effects temporary or permanent and have to be included for the risk assessments (Fenton, 2006; Buck Louis et al., 2008; Palanza et al., 2016). Based on methodologies (Fig. 7), we propose a conceptual model which brings the fate and the consequence of chemical mixture in the integrated risk assessment framework of exposome-internal exposure-biological effect to the adverse outcome (Fig. 8).

Chapter 1

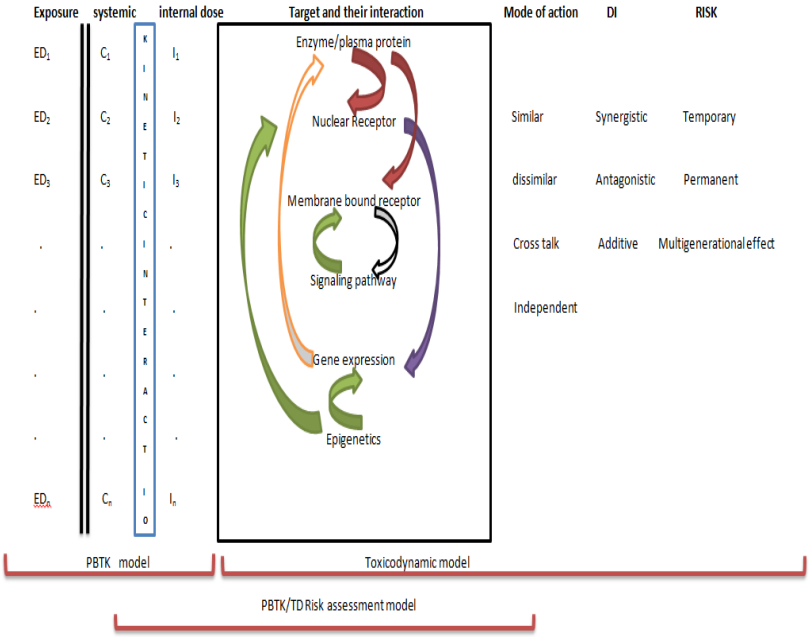

Fig. 8. Conceptual model of PBPK/PD in assessing risk for chemical mixture (ED-endocrine disruptor exposure, C-concentration of ED in systemic circulation, I-concentration of ED in target organ or tissue, DI-dynamic interaction).

PBPK usually well describes the time course of tissue level exposure of chemicals relating environmental exposure by including their absorption, distribution, metabolism and excretion. At the cellular level, the interaction of chemicals with endogenous biomolecules and their pathways which are interrelated with each other results in initiation of an event that could lead to adverse outcomes which can be describe by PBPD model. The integrated PBPK/PD can describe the kinetic as well as dynamic interaction of EDCs giving time course effect of chemicals.

At the dynamic level, integration of individual mechanisms to the dynamic interactions of mixture for assessing risk is still debatable (Lambert and Lipscomb, 2007; EFSA, 2013; Karri et al., 2016). Fig. 9 shows a small example of hypothetical schematic model that integrates individual modes of action based on their target molecule in a system based approach. It includes common, crosstalk as well as dissimilar modes of action based on their targets of common outcome. For instance, the dioxin-like chemicals, DBP, BPA, TOP and PAH-OH alter the estrogen action at different levels of peripheral as well as central mechanism. Their major targets include kisspeptin neuron, CYP19A (aromatase), SHBG, ER, Ahr, ERE CYPA1 and CYPB1 affecting estrogen and progesterone feed forward mechanism, consequently leading to risk of infertility. In fact, EDCs like DBP, BPA and TOP show similar mode of action via targeting CYP19A and SHBG. Dioxin-like substances exhibit dual role such as “antiestrogenic” via Ahr dependent CYPB1 mechanism and “estrogenic” via estrogen receptor showing crosstalk between ER and Ahr. PAH-OH and BPA can interact with other dioxin-like substances in respect to their

targets via crosstalk between Ahr and SULTE1 altering metabolism of estrogen. BPA, PAH-OH and other dioxin-like substance are able to simultaneously interfere with the endocrine system through multiple mechanisms. The mixture effects of these chemicals in system based model can be possible by considering estrogen, progesterone and ERE, as end point biomarker of infertility, and integrating available individual toxicological profile data into a dynamic mixture model of EDCs (PBPK/PD).

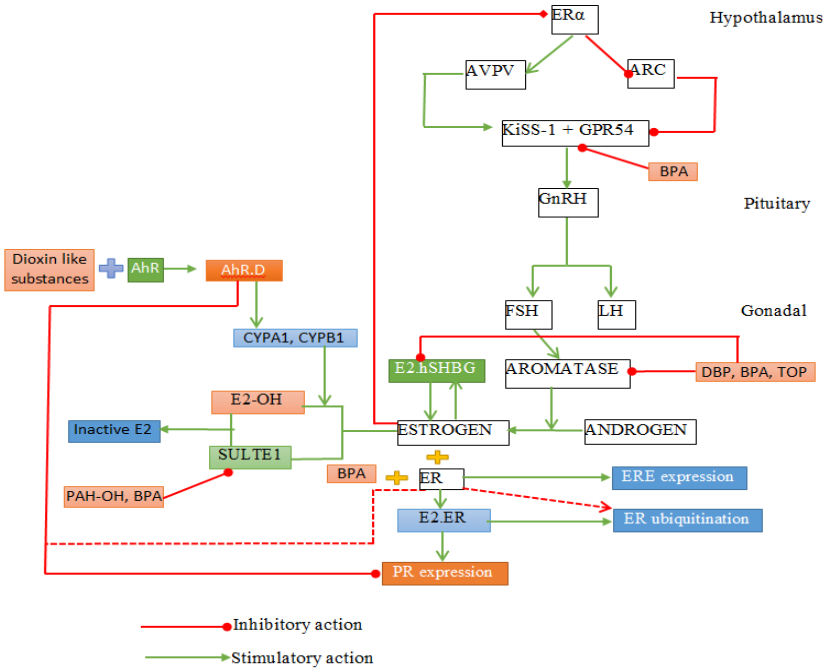

Fig. 9. Schematic model for studying mixture effect in dynamic level.
This figure contains the hypothetical mixture model of characterizing risk through detailed understanding of mode of chemicals' interaction with different biological components of the HPG pathways describing multiple mechanisms.

5. Summary & future perspectives

We have summarized the effects of endocrine disruptors on thyroid, adrenal, and sex hormones accounting their effects on synthesis, metabolisms and actions. Mixture of chemicals can simultaneously interfere with multiple endocrine pathways via multiple mechanisms making mixture effect more pronounced than individual. The EDCs acting on certain hormones via multiple mechanisms (central or peripheral) can be grouped for risk assessment of mixture of chemicals, according to their similar adverse outcomes.
Most of the EDCs have nonmonotonic dose-response curve which is the major drawback when establishing a relationship between the exposure kinetics and elicited response (Vandenberg et al., 2012; Beausoleil et al., 2013; Yang et al., 2016). Additional

Chapter 1

challenges like multiple mechanisms, delayed response (time lag between exposure to adverse outcomes), dynamic interaction involving crosstalk and common mechanisms, and transgenerational effect added more complexity in the quantitative risk assessment (Maffini et al., 2006; Matthiessen and Johnson, 2007; Rubin, 2011; Fowler et al., 2012).

However, understanding the molecular mechanism of interaction of chemicals with endogenous molecules or pathways can explain the variability among chemicals for the same adverse effect (Filby et al., 2007). For instance, BPA shows complex dose-response curve in concentration dependent model which could be explained by the fact that it alters the gene expression through genomic as well as nongenomic pathways (Takayanagi et al., 2006; Vandenberg et al., 2009; Vandenberg, 2014). Similarly, dioxin-like substances show dual response that can be explained by availability of endogenous hormone and their action. The potential dynamic interaction may lead to change in the response curve in case of mixture of chemical, which can be explained by understanding different types of mechanistic interactions like crosstalk or similar or dissimilar MOAs as it has been explained in this review. Similarly, understanding latency of exposure (i.e. lag time between exposure and response) is important as in the case of infertility disorder, which can only be detected after a certain age though exposure occurs at early stage of life.

Lots of experiments have been done on individual EDCs but it is very hard to find mixture level studies. Selecting chemicals and then optimizing the dose for a selected mixture for carrying animal experiment is another difficult task. To know the potency of individual chemical in mixture due to their complex interaction behaviour at different levels, requires large combinatorial experimental design. Normally this kind of experiment requires a large number of animals which will be against the current ethical guideline of risk assessment (EU, 2010). However, tremendous development in in-vitro and in-silico techniques and emerging areas like omics, generating lots of toxicological data leads to new era of quantitative risk assessment (Knudsen et al., 2015).

Incorporation of individual mechanism of chemicals into mixture model provides a platform for assessment of combined risk produced by mixture of chemicals. Understanding individual mechanism and implementing those mechanisms in system based approach will help us in the development of mixture model. This will provide better understanding of the risk produced by chemical mixture exposure and it will further assist in designing animal experiment and optimization of dose which will reduce the use of animals. The European Union (2011) suggested concentration addition method for cumulative risk assessment of chemicals with similar or dissimilar mechanisms of action by considering their common adverse outcomes. But response addition method for a common adverse effect is still not recommended.

Categorization of chemicals in the same group according to similar adverse outcomes, accounting both similar as well as dissimilar mechanisms (crosstalk) of action may provide a sound basis for studying mixture toxicology. Based on this grouping strategy, addressing both kinetic and dynamic interactions of mixture and establishing a relationship between pharmacokinetic-pharmacodynamic-altered molecular events will give a better model to correlate the environment exposure with adverse outcomes. Finally,

integrating individual mode of action of each chemical with the help of mathematical equations into advanced tools such as PBPK/PD would enable the simultaneous assessment of EDC mixtures correlating concentration in various biological matrixes (blood, tissue, urine) with various end points (endocrine diseases). It will also help in finding the toxic equivalent dose of chemicals eliciting similar adverse effects. Similarly, timing and duration of exposure are important factors which need to be considered while assessing the risk. Integrating physiology of the human body at different life stages and respective modes of action of EDCs will help in building life stage dynamic models. For example, dividing life stage into prenatal-postnatal-puberty-menopause and incorporating susceptible gene or receptor or protein at different life stages targeted by EDCs and physiological data provide a model able to predict the risk of infertility in females by exposure to these chemicals in different stages of life.

References

Abduljalil, K., Furness, P., Johnson, T.N., Rostami-Hodjegan, A., Soltani, H., 2012. Anatomical, Physiological and Metabolic Changes with Gestational Age during Normal Pregnancy. Clin. Pharmacokinet. 51, 365–396. https://doi.org/10.2165/11597440-000000000-00000

Abdullah, R., Alhusainy, W., Woutersen, J., Rietjens, I.M.C.M., Punt, A., 2016. Predicting points of departure for risk assessment based on in vitro cytotoxicity data and physiologically based kinetic (PBK) modeling: The case of kidney toxicity induced by aristolochic acid I. Food Chem. Toxicol. 92, 104–116. https://doi.org/10.1016/j.fct.2016.03.017

Adachi, K., Suemizu, H., Murayama, N., Shimizu, M., Yamazaki, H., 2015. Human biofluid concentrations of mono(2-ethylhexyl)phthalate extrapolated from pharmacokinetics in chimeric mice with humanized liver administered with di(2-ethylhexyl)phthalate and physiologically based pharmacokinetic modeling. Environ. Toxicol. Pharmacol. https://doi.org/10.1016/j.etap.2015.02.011

Aderem, A., 2005. Systems biology: Its practice and challenges. Cell 121, 511–513. https://doi.org/10.1016/j.cell.2005.04.020

Akingbemi, B.T., Sottas, C.M., Koulova, A.I., Klinefelter, G.R., Hardy, M.P., 2004. Inhibition of Testicular Steroidogenesis by the Xenoestrogen Bisphenol a Is Associated with Reduced Pituitary Luteinizing Hormone Secretion and Decreased Steroidogenic Enzyme Gene Expression in Rat Leydig Cells. Endocrinology 145, 592–603. https://doi.org/10.1210/en.2003-1174

Andersen, M.E., Krewski, D., 2009. Toxicity testing in the 21st century: Bringing the vision to life. Toxicol. Sci. 107, 324–330. https://doi.org/10.1093/toxsci/kfn255

Andersen, M.E., Thomas, R.S., Gaido, K.W., Conolly, R.B., 2005. Dose-response modeling in reproductive toxicology in the systems biology era. Reprod. Toxicol. 19, 327–337. https://doi.org/10.1016/j.reprotox.2004.12.004

Chapter 1

Andrade, R., Agundez, J., Lucena, M., Martinez, C., Cueto, R., Garcia-Martin, E., 2009. Pharmacogenomics in Drug Induced Liver Injury. Curr. Drug Metab. 10, 956–970. https://doi.org/10.2174/138920009790711805

Ankley, G.T., Bennett, R.S., Erickson, R.J., Hoff, D.J., Hornung, M.W., Johnson, R.D., Mount, D.R., Nichols, J.W., Russom, C.L., Schmieder, P.K., Serrrano, J.A., Tietge, J.E., Villeneuve, D.L., 2010. Adverse outcome pathways: A conceptual framework to support ecotoxicology research and risk assessment. Environ. Toxicol. Chem. 29, 730–741. https://doi.org/10.1002/etc.34

Ansoumane, K., Duan, P., Quan, C., Yaima, M.L.T., Liu, C., Wang, C., Fu, W., Qi, S., Yu, T., Yang, K., 2014. Bisphenol A induced reactive oxygen species (ROS) in the liver and affect epididymal semen quality in adults Sprague-Dawley rats. J. Toxicol. Environ. Heal. Sci. 6, 103–112. https://doi.org/10.5897/JTEHS2014.0309

Aris, A., 2014. Estimation of bisphenol A (BPA) concentrations in pregnant women, fetuses and nonpregnant women in Eastern Townships of Canada. Reprod. Toxicol. 45, 8–13. https://doi.org/10.1016/j.reprotox.2013.12.006

Arrell, D.K., Terzic, a, 2010. Network systems biology for drug discovery. Clin. Pharmacol. Ther. 88, 120–125. https://doi.org/10.1038/clpt.2010.91

Asakawa, N., Koyama, M., Hashimoto, Y., Yamashita, K., 1995. Studies on the Metabolic Fate of Flutamide. (1): Plasma Concentration after Single Administration and Protein Binding in Rats. Drug Metab. Pharmacokinet. 10, 447–453. https://doi.org/10.2133/dmpk.10.447

Atanasov, A.G., Tam, S., Röcken, J.M., Baker, M.E., Odermatt, A., 2003. Inhibition of 11β-hydroxysteroid dehydrogenase type 2 by dithiocarbamates. Biochem. Biophys. Res. Commun. 308, 257–262. https://doi.org/10.1016/S0006-291X(03)01359-7

Auffray, C., Chen, Z., Hood, L., 2009. Systems medicine: the future of medical genomics and healthcare. Genome Med. 1, 2. https://doi.org/10.1186/gm2

Ball, A.L., Kamalian, L., Alfirevic, A., Lyon, J.J., Chadwick, A.E., 2016. Identification of the additional mitochondrial liabilities of 2-hydroxyflutamide when compared with its parent compound, flutamide in HepG2 cells. Toxicol. Sci. 153, 341–351. https://doi.org/10.1093/toxsci/kfw126

Bartel, D.P., 2004. MicroRNAs: Genomics, Biogenesis, Mechanism, and Function. Cell 116, 281–297. https://doi.org/10.1016/S0092-8674(04)00045-5

Bartlett, D.W., Davis, M.E., 2006. Insights into the kinetics of siRNA-mediated gene silencing from live-cell and live-animal bioluminescent imaging. Nucleic Acids Res. 34, 322–333. https://doi.org/10.1093/nar/gkj439

Bell, S.M., Chang, X., Wambaugh, J.F., Allen, D.G., Bartels, M., Brouwer, K.L.R., Casey, W.M., Choksi, N., Ferguson, S.S., Fraczkiewicz, G., Jarabek, A.M., Ke, A., Lumen, A., Lynn, S.G., Paini, A., Price, P.S., Ring, C., Simon, T.W., Sipes,

Chapter 1

N.S., Sprankle, C.S., Strickland, J., Troutman, J., Wetmore, B.A., Kleinstreuer, N.C., 2018. In vitro to in vivo extrapolation for high throughput prioritization and decision making. Toxicol. Vitr. 47, 213–227. https://doi.org/10.1016/j.tiv.2017.11.016

Berson, A., Wolf, C., Chachaty, C., Fisch, C., Fau, D., Eugene, D., Loeper, J., Gauthier, J.-C., Beaune, P., Pompon, D., Maurel, P., Pessayre, D., 1993. Metabolic activation of the nitroaromatic antiandrogen flutamide by rat and human cytochromes P-450, including forms belonging to the 3A and 1A subfamilies. J. Pharmacol. Exp. Ther. 265, 366–372.

Bessems, J., Coecke, S., Gouliarmou, V., Whelan, M., Worth, A., 2015. EURL ECVAM strategy for achieving 3Rs impact in the assessment of toxicokinetics and systemic toxicity 22. https://doi.org/10.2788/197633

Bhattacharya, S., Shoda, L.K.M., Zhang, Q., Woods, C.G., Howell, B.A., Siler, S.Q., Woodhead, J.L., Yang, Y., McMullen, P., Watkins, P.B., Melvin, E.A., 2012. Modeling drug- and chemical-induced hepatotoxicity with systems biology approaches. Front. Physiol. 3 DEC, 1–18. https://doi.org/10.3389/fphys.2012.00462

Birgelen, a Van, Birgelen, a Van, Smit, E., Smit, E., Kampen, I., Kampen, I., 1995. Subchronic effects of 2, 3, 7, 8-TCDD or PCBs on thyroid hormone metabolism: use in risk assessment. Eur. J. Pharmacol. Environ. Toxicol. {…} 293, 77–85.

Bloomingdale, P., Housand, C., Apgar, J.F., Millard, B.L., Mager, D.E., Burke, J.M., Shah, D.K., 2017. Quantitative systems toxicology. Curr. Opin. Toxicol. 4, 79–87. https://doi.org/10.1016/j.cotox.2017.07.003

Boberg, J., Metzdorff, S., Wortziger, R., Axelstad, M., Brokken, L., Vinggaard, A.M., Dalgaard, M., Nellemann, C., 2008. Impact of diisobutyl phthalate and other PPAR agonists on steroidogenesis and plasma insulin and leptin levels in fetal rats. Toxicology 250, 75–81. https://doi.org/10.1016/j.tox.2008.05.020

Boelsterli, U.A., Lim, P.L.K., 2007. Mitochondrial abnormalities—A link to idiosyncratic drug hepatotoxicity? Toxicol. Appl. Pharmacol. 220, 92–107. https://doi.org/10.1016/j.taap.2006.12.013

Bonate, P.L., 2011. Pharmacokinetic-Pharmacodynamic Modeling and Simulation. Springer US, Boston, MA. https://doi.org/10.1007/978-1-4419-9485-1

Boulle, F., van den Hove, D.L. a, Jakob, S.B., Rutten, B.P., Hamon, M., van Os, J., Lesch, K.-P., Lanfumey, L., Steinbusch, H.W., Kenis, G., Hove, D.L.A. Van Den, Jakob, S.B., Rutten, B.P., Hamon, M., Os, J. Van, Lesch, K.-P., van den Hove, D.L. a, Jakob, S.B., Rutten, B.P., Hamon, M., van Os, J., Lesch, K.-P., Lanfumey, L., Steinbusch, H.W., Kenis, G., 2012. Epigenetic regulation of the BDNF gene: implications for psychiatric disorders. Mol. Psychiatry 17, 584–596. https://doi.org/10.1038/mp.2011.107

Bouskine, A., Nebout, M., Brücker-Davis, F., Banahmed, M., Fenichel, P., 2009. Low

doses of bisphenol A promote human seminoma cell proliferation by activating PKA and PKG via a membrane G-protein-coupled estrogen receptor. Environ. Health Perspect. 117, 1053–1058. https://doi.org/10.1289/ehp.0800367

Brahm, J., Brahm, M., Segovia, R., Latorre, R., Zapata, R., Poniachik, J., Buckel, E., Contreras, L., 2011. Acute and fulminant hepatitis induced by flutamide: case series report and review of the literature. Ann. Hepatol. 10, 93–8.

Brown, R.P., Delp, M.D., Lindstedt, S.L., Rhomberg, L.R., Beliles, R.P., 1997. Physiological parameter values for physiologically based pharmacokinetic models. Toxicol. Ind. Health 13, 407–484.

Bursac, N., Kirkton, R.D., Mcspadden, L.C., Liau, B., 2010. Circulating levels of brain-derived neurotrophic factor: correlation with mood, cognition and motor function. Biomark. Med. 4, 871–87.

Calabrese, E.J., Baldwin, L.A., 2003. Toxicology rethinks its central belief. Nature 421, 691–692. https://doi.org/10.1038/421691a

Cao, X.L., Zhang, J., Goodyer, C.G., Hayward, S., Cooke, G.M., Curran, I.H.A., 2012. Bisphenol A in human placental and fetal liver tissues collected from Greater Montreal area (Quebec) during 1998-2008. Chemosphere 89, 505–511. https://doi.org/10.1016/j.chemosphere.2012.05.003

Caputo, V., Sinibaldi, L., Fiorentino, A., Parisi, C., Catalanotto, C., Pasini, A., Cogoni, C., Pizzuti, A., 2011. Brain derived neurotrophic factor (BDNF) expression is regulated by microRNAs miR-26a and miR-26b allele-specific binding. PLoS One 6. https://doi.org/10.1371/journal.pone.0028656

Carlotti, F., Dower, S.K., Qwarnstrom, E.E., 2000. Dynamic shuttling of nuclear factor ??B between the nucleus and cytoplasm as a consequence of inhibitor dissociation. J. Biol. Chem. 275, 41028–41034. https://doi.org/10.1074/jbc.M006179200

Castillo, B., del Cerro, M., Breakefield, X.O., Frim, D.M., Barnstable, C.J., Dean, D.O., Bohn, M.C., 1994. Retinal ganglion cell survival is promoted by genetically modified astrocytes designed to secrete brain-derived neurotrophic factor (BDNF). Brain Res. 647, 30–36. https://doi.org/10.1016/0006-8993(94)91395-1

Castro, B., Sánchez, P., Torres, J.M., Preda, O., del Moral, R.G., Ortega, E., 2013. Bisphenol A Exposure during Adulthood Alters Expression of Aromatase and 5α-Reductase Isozymes in Rat Prostate. PLoS One 8, 1–7. https://doi.org/10.1371/journal.pone.0055905

Chang, Z., Lu, M., Kim, S.S., Park, J.S., 2014. Potential role of HSP90 in mediating the interactions between estrogen receptor (ER) and aryl hydrocarbon receptor (AhR) signaling pathways. Toxicol. Lett. 226, 6–13. https://doi.org/10.1016/j.toxlet.2014.01.032

Chen, N., Li, J., Li, D., Yang, Y., He, D., 2014. Chronic exposure to perfluorooctane

sulfonate induces behavior defects and neurotoxicity through oxidative damages, in Vivo and in Vitro. PLoS One 9, 1–10. https://doi.org/10.1371/journal.pone.0113453

Chitra, K.C., Latchoumycandane, C., Mathur, P.P., 2003. Induction of oxidative stress by bisphenol A in the epididymal sperm of rats. Toxicology 185, 119–127. https://doi.org/10.1016/S0300-483X(02)00597-8

Choi, K., Joo, H., Campbell, J.L., Andersen, M.E., Clewell, H.J., 2013. In vitro intestinal and hepatic metabolism of Di(2-ethylhexyl) phthalate (DEHP) in human and rat. Toxicol. Vitr. 27, 1451–1457. https://doi.org/10.1016/j.tiv.2013.03.012

Clarke, G., Collins, R.A., Leavitt, B.R., Andrews, D.F., Hayden, M.R., Lumsden, C.J., McInnes, R.R., 2000. A one-hit model of cell death in inherited neuronal degenerations. Nature 406, 195–199. https://doi.org/10.1038/35018098

Clewell, H.J., Gearhart, J.M., Gentry, P.R., Covington, T.R., VanLandingham, C.B., Crump, K.S., Shipp, A.M., 1999. Evaluation of the uncertainty in an oral reference dose for methylmercury due to interindividual variability in pharmacokinetics. Risk Anal. 19, 547–558. https://doi.org/10.1023/A:1007017116171

Clewell, R. a, Merrill, E. a, Narayanan, L., Gearhart, J.M., Robinson, P.J., 2004. Evidence for competitive inhibition of iodide uptake by perchlorate and translocation of perchlorate into the thyroid. Int. J. Toxicol. 23, 17–23. https://doi.org/10.1080/10915810490275044

Clewell, R.A., Clewell, H.J., 2008. Development and specification of physiologically based pharmacokinetic models for use in risk assessment. Regul. Toxicol. Pharmacol. 50, 129–43. https://doi.org/10.1016/j.yrtph.2007.10.012

Coe, K.J., Jia, Y., Han, K.H., Rademacher, P., Bammler, T.K., Beyer, R.P., Farin, F.M., Woodke, L., Plymate, S.R., Fausto, N., Nelson, S.D., 2007. Comparison of the cytotoxicity of the nitroaromatic drug flutamide to its cyano analogue in the hepatocyte cell line TAMH: Evidence for complex I inhibition and mitochondrial dysfunction using toxicogenomic screening. Chem. Res. Toxicol. 20, 1277–1290. https://doi.org/10.1021/tx7001349

Coe, K.J., Nelson, S.D., Ulrich, R.G., He, Y., Dai, X., Cheng, O., Caguyong, M., Roberts, C.J., Slatter, J.G., 2006. Profiling the hepatic effects of flutamide in rats: A microarray comparison with classical aryl hydrocarbon receptor ligands and atypical CYP1A inducers. Drug Metab. Dispos. 34, 1266–1275. https://doi.org/10.1124/dmd.105.009159

Cooper, R.L., Stoker, T.E., Tyrey, L., Goldman, J.M., McElroy, W.K., 2000. Atrazine disrupts the hypothalamic control of pituitary-ovarian function. Toxicol. Sci. 53, 297–307. https://doi.org/10.1093/toxsci/53.2.297

Coughlin, J.L., Thomas, P.E., Buckley, B., 2012. Inhibition of genistein glucuronidation by bisphenol A in human and rat liver microsomes. Drug Metab. Dispos. 40, 481–

Chapter 1

485. https://doi.org/10.1124/dmd.111.042366

Csanády, G., Oberste-Frielinghaus, H., Semder, B., Baur, C., Schneider, K., Filser, J., 2002. Distribution and unspecific protein binding of the xenoestrogens bisphenol A and daidzein. Arch. Toxicol. 76, 299–305. https://doi.org/10.1007/s00204-002-0339-5

Cubitt, H.E., Houston, J.B., Galetin, A., 2011. Prediction of human drug clearance by multiple metabolic pathways: Integration of hepatic and intestinal microsomal and cytosolic data. Drug Metab. Dispos. 39, 864–873. https://doi.org/10.1124/dmd.110.036566

Cubitt, H.E., Houston, J.B., Galetin, A., 2009. Relative Importance of Intestinal and Hepatic Glucuronidation—Impact on the Prediction of Drug Clearance. Pharm. Res. 26, 1073–1083. https://doi.org/10.1007/s11095-008-9823-9

Davies, B., Morris, T., 1993. No Title. Pharm. Res. 10, 1093–1095. https://doi.org/10.1023/A:1018943613122

Dieckhaus, C.M., Thompson, C.D., Roller, S.G., Macdonald, T.L., 2002. Mechanisms of idiosyncratic drug reactions: the case of felbamate. Chem. Biol. Interact. 142, 99–117. https://doi.org/10.1016/S0009-2797(02)00057-1

Dinkova-Kostova, A.T., Holtzclaw, W.D., Cole, R.N., Itoh, K., Wakabayashi, N., Katoh, Y., Yamamoto, M., Talalay, P., 2002. Direct evidence that sulfhydryl groups of Keap1 are the sensors regulating induction of phase 2 enzymes that protect against carcinogens and oxidants. Proc. Natl. Acad. Sci. U. S. A. 99, 11908–13. https://doi.org/10.1073/pnas.172398899

Djuranovic, S., Nahvi, A., Green, R., 2011. A Parsimonious Model for Gene Regulation by miRNAs. Science (80-.). 331, 550–553. https://doi.org/10.1126/science.1191138

Doerge, D.R., Twaddle, N.C., Vanlandingham, M., Brown, R.P., Fisher, J.W., 2011. Distribution of bisphenol A into tissues of adult, neonatal, and fetal Sprague–Dawley rats. Toxicol. Appl. Pharmacol. 255, 261–270. https://doi.org/10.1016/j.taap.2011.07.009

Doering, D.D., Steckelbroeck, S., Doering, T., Klingmüller, D., 2002. Effects of butyltins on human 5alpha-reductase type 1 and type 2 activity. Steroids 67, 859–867.

El-Masri, H., 2013. Modeling for Regulatory Purposes (Risk and Safety Assessment), in: Reisfeld, B., Mayeno, A.N. (Eds.), . Humana Press, Totowa, NJ, pp. 297–303. https://doi.org/10.1007/978-1-62703-059-5_13

Espinosa-Diez, C., Miguel, V., Mennerich, D., Kietzmann, T., Sánchez-Pérez, P., Cadenas, S., Lamas, S., 2015. Antioxidant responses and cellular adjustments to oxidative stress. Redox Biol. 6, 183–197. https://doi.org/10.1016/j.redox.2015.07.008

Chapter 1

Fabrega, F., Kumar, V., Schuhmacher, M., Domingo, J.L., Nadal, M., 2014. PBPK modeling for PFOS and PFOA: Validation with human experimental data. Toxicol. Lett. 230, 244–251. https://doi.org/10.1016/j.toxlet.2014.01.007

Fàbrega, F., Nadal, M., Schuhmacher, M., Domingo, J.L., Kumar, V., 2016. Influence of the uncertainty in the validation of PBPK models: A case-study for PFOS and PFOA. Regul. Toxicol. Pharmacol. 77, 230–239. https://doi.org/10.1016/j.yrtph.2016.03.009

Fang, H., Tong, W., Branham, W.S., Moland, C.L., Dial, S.L., Hong, H., Xie, Q., Perkins, R., Owens, W., Sheehan, D.M., 2003. Study of 202 Natural, Synthetic, and Environmental Chemicals for Binding to the Androgen Receptor. Chem. Res. Toxicol. 16, 1338–1358. https://doi.org/10.1021/tx030011g

Fisher, J.W., Twaddle, N.C., Vanlandingham, M., Doerge, D.R., 2011. Pharmacokinetic modeling: Prediction and evaluation of route dependent dosimetry of bisphenol A in monkeys with extrapolation to humans. Toxicol. Appl. Pharmacol. 257, 122–136. https://doi.org/10.1016/j.taap.2011.08.026

Fletcher, J.M., Morton, C.J., Zwar, R.A., Murray, S.S., O'Leary, P.D., Hughes, R.A., 2008. Design of a conformationally defined and proteolytically stable circular mimetic of brain-derived neurotrophic factor. J. Biol. Chem. 283, 33375–33383. https://doi.org/10.1074/jbc.M802789200

Forsby, A., Blaauboer, B., 2007. Integration of in vitro neurotoxicity data with biokinetic modelling for the estimation of in vivo neurotoxicity. Hum. Exp. Toxicol. 26, 333–338. https://doi.org/10.1177/0960327106072994

Foxenberg, R.J., Ellison, C.A., Knaak, J.B., Ma, C., Olson, J.R., 2011. Cytochrome P450-specific human PBPK/PD models for the organophosphorus pesticides: Chlorpyrifos and parathion. Toxicology 285, 57–66. https://doi.org/10.1016/j.tox.2011.04.002

Friedmann, A.S., 2002. Atrazine inhibition of testosterone production in rat males following peripubertal exposure. Reprod. Toxicol. 16, 275–279. https://doi.org/10.1016/S0890-6238(02)00019-9

Fukumitsu, H., Ohtsuka, M., Murai, R., Nakamura, H., Itoh, K., Furukawa, S., 2006. Brain-Derived Neurotrophic Factor Participates in Determination of Neuronal Laminar Fate in the Developing Mouse Cerebral Cortex. J. Neurosci. 26, 13218–13230. https://doi.org/10.1523/JNEUROSCI.4251-06.2006

Fukuzawa, N.H., Ohsako, S., Wu, Q., Sakaue, M., Fujii-Kuriyama, Y., Baba, T., Tohyama, C., 2004. Testicular cytochrome P450scc and LHR as possible targets of 2,3,7,8-tetrachlorodibenzo-p-dioxin (TCDD) in the mouse. Mol. Cell. Endocrinol. 221, 87–96. https://doi.org/10.1016/j.mce.2004.02.005

Gabrielsson, J., Weiner, D., 2012. Non-compartmental Analysis, in: Reisfeld, B., Mayeno, A.N. (Eds.), Methods in Molecular Biology. Humana Press, Totowa, NJ, pp. 377–389. https://doi.org/10.1007/978-1-62703-050-2_16

Chapter 1

García Cortés, M., Andrade, R.J., Lucena, M.I., Sánchez Martínez, H., Fernández, M.C., Ferrer, T., Martín-Vivaldi, R., Peláez, G., Suárez, F., Romero-Gómez, M., Montero, J.L., Fraga, E., Camargo, R., Alcántara, R., Pizarro, M.A., García-Ruiz, E., Rosemary-Gómez, M., 2001. Flutamide-induced hepatotoxicity: report of a case series. Rev. Esp. Enferm. Dig. 93, 423–32.

Generali, J.A., Cada, D.J., 2014. Flutamide: Hirsutism in Women. Hosp. Pharm. 49, 517–520. https://doi.org/10.1310/hpj4906-517

Gentry, P.R., Covington, T.R., Andersen, M.E., Clewell, H.J., 2002. Application of a physiologically based pharmacokinetic model for isopropanol in the derivation of a reference dose and reference concentration. Regul. Toxicol. Pharmacol. 36, 51–68. https://doi.org/S0273230002915400 [pii]

Gerona, R.R., Woodruff, T.J., Dickenson, C.A., Pan, J., Jackie, M., Sen, S., Friesen, M.M., Fujimoto, V.Y., Hunt, P.A., 2014. California population 47. https://doi.org/10.1021/es402764d.Bisphenol-A

Gibbs, J.P., Yang, J.S., Slattery, J.T., 1998. Comparison of human liver and small intestinal glutathione S-transferase-catalyzed busulfan conjugation in vitro. Drug Metab. Dispos. 26, 52–55.

Gillespie, L.N., Clark, G.M., Bartlett, P.F., Marzella, P.L., 2003. BDNF-induced survival of auditory neurons in vivo: Cessation of treatment leads to accelerated loss of survival effects. J. Neurosci. Res. 71, 785–790. https://doi.org/10.1002/jnr.10542

Gim, J., Kim, H.S., Kim, J., Choi, M., Kim, J.R., Chung, Y.J., Cho, K.H., 2010. A system-level investigation into the cellular toxic response mechanism mediated by AhR signal transduction pathway. Bioinformatics 26, 2169–2175. https://doi.org/10.1093/bioinformatics/btq400

Godin, S.J., Scollon, E.J., Hughes, M.F., Potter, P.M., DeVito, M.J., Ross, M.K., 2006. Species differences in the in vitro metabolism of deltamethrin and esfenvalerate: Differential oxidative and hydrolytic metabolism by humans and rats. Drug Metab. Dispos. 34, 1764–1771. https://doi.org/10.1124/dmd.106.010058

Gomez, J.-L., Dupont, A., Cusan, L., Tremblay, M., Suburu, R., Lemay, M., Labrie, F., 1992. Incidence of liver toxicity associated with the use of flutamide in prostate cancer patients. Am. J. Med. 92, 465–470. https://doi.org/10.1016/0002-9343(92)90741-S

Goudarzi, H., Nakajima, S., Ikeno, T., Sasaki, S., Kobayashi, S., Miyashita, C., Ito, S., Araki, A., Nakazawa, H., Kishi, R., 2016. Prenatal exposure to perfluorinated chemicals and neurodevelopment in early infancy: The Hokkaido Study. Sci. Total Environ. 541, 1002–1010. https://doi.org/10.1016/j.scitotenv.2015.10.017

Gumy, C., Chandsawangbhuwana, C., Dzyakanchuk, A. a., Kratschmar, D. V., Baker, M.E., Odermatt, A., 2008. Dibutyltin disrupts glucocorticoid receptor function and impairs glucocorticoid-induced suppression of cytokine production. PLoS

Chapter 1

One 3. https://doi.org/10.1371/journal.pone.0003545

Haley, B., Zamore, P.D., 2004. Kinetic analysis of the RNAi enzyme complex. Nat. Struct. Mol. Biol. 11, 599–606. https://doi.org/10.1038/nsmb780

Hany, J., Lilienthal, H., Sarasin, a, Roth-Härer, a, Fastabend, a, Dunemann, L., Lichtensteiger, W., Winneke, G., 1999. Developmental exposure of rats to a reconstituted PCB mixture or aroclor 1254: effects on organ weights, aromatase activity, sex hormone levels, and sweet preference behavior. Toxicol. Appl. Pharmacol. 158, 231–243. https://doi.org/10.1006/taap.1999.8710

Hayes, T.B., Anderson, L.L., Beasley, V.R., de Solla, S.R., Iguchi, T., Ingraham, H., Kestemont, P., Kniewald, J., Kniewald, Z., Langlois, V.S., Luque, E.H., McCoy, K.A., Muñoz-de-Toro, M., Oka, T., Oliveira, C.A., Orton, F., Ruby, S., Suzawa, M., Tavera-Mendoza, L.E., Trudeau, V.L., Victor-Costa, A.B., Willingham, E., 2011. Demasculinization and feminization of male gonads by atrazine: Consistent effects across vertebrate classes. J. Steroid Biochem. Mol. Biol. 127, 64–73. https://doi.org/10.1016/j.jsbmb.2011.03.015

Heidrich, D.D., Steckelbroeck, S., Klingmuller, D., 2001. Inhibition of human cytochrome P450 aromatase activity by butyltins. Steroids 66, 763–769.

Hood, L., Heath, J.R., Phelps, M.E., Lin, B., 2004. Systems biology and new technologies enable predictive and preventative medicine. Science 306, 640–643. https://doi.org/10.1126/science.1104635

Ikezuki, Y., Tsutsumi, O., Takai, Y., Kamei, Y., Taketani, Y., 2002. Determination of bisphenol A concentrations in human biological fluids reveals significant early prenatal exposure. Hum. Reprod. 17, 2839–2841. https://doi.org/10.1093/humrep/17.11.2839

Jaeschke, H., McGill, M.R., Ramachandran, A., 2012. Oxidant stress, mitochondria, and cell death mechanisms in drug-induced liver injury: lessons learned from acetaminophen hepatotoxicity. Drug Metab. Rev. 44, 88–106. https://doi.org/10.3109/03602532.2011.602688

Johansson, M., Larsson, C., Bergman, a, Lund, B.O., 1998. Structure-activity relationship for inhibition of CYP11B1-dependent glucocorticoid synthesis in Y1 cells by aryl methyl sulfones. Pharmacol. Toxicol. 83, 225–230.

Johansson, N., Fredriksson, A., Eriksson, P., 2008. Neonatal exposure to perfluorooctane sulfonate (PFOS) and perfluorooctanoic acid (PFOA) causes neurobehavioural defects in adult mice. Neurotoxicology 29, 160–169. https://doi.org/10.1016/j.neuro.2007.10.008

Juge-Aubry, C.E., Gorla-Bajszczak, A., Pernin, A., Lemberger, T., Wahli, W., Burger, A.G., Meier, C. a., 1995. Peroxisome proliferator-activated receptor mediates cross-talk with thyroid hormone receptor by competition for retinoid X receptor: Possible role of a leucine zipper-like heptad repeat. J. Biol. Chem. https://doi.org/10.1074/jbc.270.30.18117

Chapter 1

Jusko, W.J., 2013. Moving from basic toward systems pharmacodynamic models. J. Pharm. Sci. 102, 2930–2940. https://doi.org/10.1002/jps.23590

Jusko, W.J., Ko, H.C., 1994. Physiologic indirect response models characterize diverse types of pharmacodynamic effects. Clin. Pharmacol. Ther. 56, 406–419. https://doi.org/10.1038/clpt.1994.155

Kanda, Y., Hinata, T., Kang, S.W., Watanabe, Y., 2011. Reactive oxygen species mediate adipocyte differentiation in mesenchymal stem cells. Life Sci. 89, 250–258. https://doi.org/10.1016/j.lfs.2011.06.007

Kaplowitz, N., 2005. Idiosyncratic drug hepatotoxicity. Nat. Rev. Drug Discov. 4, 489.

Kashimshetty, R., Desai, V.G., Kale, V.M., Lee, T., Moland, C.L., Branham, W.S., New, L.S., Chan, E.C.Y., Younis, H., Boelsterli, U.A., 2009. Underlying mitochondrial dysfunction triggers flutamide-induced oxidative liver injury in a mouse model of idiosyncratic drug toxicity. Toxicol. Appl. Pharmacol. 238, 150–159. https://doi.org/10.1016/j.taap.2009.05.007

Katchen, B., Buxbaum, S., 1975. Disposition of a new, nonsteroid, antiandrogen, alpha,alpha,alpha-trifluoro-2-methyl-4'-nitro-m-propionotoluidide (Flutamide), in men following a single oral 200 mg dose. J. Clin. Endocrinol. Metab. 41, 373–9. https://doi.org/10.1210/jcem-41-2-373

Kawamoto, Y., Matsuyama, W., Wada, M., Hishikawa, J., Chan, M.P.L., Nakayama, A., Morisawa, S., 2007. Development of a physiologically based pharmacokinetic model for bisphenol A in pregnant mice. Toxicol. Appl. Pharmacol. 224, 182–191. https://doi.org/10.1016/j.taap.2007.06.023

Kell, D.B., 2006. Systems biology, metabolic modelling and metabolomics in drug discovery and development. Drug Discov. Today 11, 1085–1092. https://doi.org/10.1016/j.drudis.2006.10.004

Kester, M.H.A., Bulduk, S., Van Toor, H., Tibboel, D., Meinl, W., Glatt, H., Falany, C.N., Coughtrie, M.W.H., Gerlienke Schuur, A., Brouwer, A., Visser, T.J., 2002. Potent inhibition of estrogen sulfotransferase by hydroxylated metabolites of polyhalogenated aromatic hydrocarbons reveals alternative mechanism for estrogenic activity of endocrine disrupters. J. Clin. Endocrinol. Metab. 87, 1142–1150. https://doi.org/10.1210/jc.87.3.1142

Keys, D.A., Wallace, D.G., Kepler, T.B., Conolly, R.B., 2000. Quantitative evaluation of alternative mechanisms of blood disposition of di(n-butyl) phthalate and mono(n-butyl) phthalate in rats. Toxicol. Sci. 53, 173–184. https://doi.org/10.1093/toxsci/53.2.173

Keys, D.A., Wallace, D.G., Kepler, T.B., Conolly, R.B., 1999. Quantitative evaluation of alternative mechanisms of blood and testes disposition of di(2-ethylhexyl) phthalate and mono(2-ethylhexyl) phthalate in rats. Toxicol. Sci. 49, 172–85. https://doi.org/10.1093/toxsci/49.2.172

Chapter 1

Kitano, H., 2002. Systems biology: A brief overview. Sci. (New York, NY) 295, 1662–1664. https://doi.org/10.1126/science.1069492

Kobayashi, Y., Fukami, T.., Shimizu, M., Nakajima, M., Tsuyoshi., Y., 2012. Short Communication Contributions of Arylacetamide Deacetylase and Carboxylesterase 2 to Flutamide Hydrolysis in Human Liver. Drug Metab. Dispos. 40, 1080–1084.

Kohler, J.J., Schepartz, A., 2001. Kinetic Studies of Fos , Jun , DNA Complex Formation : DNA Binding Prior to Dimerization. Biochemistry 40, 130–142. https://doi.org/10.1021/bi001881p

Kortejärvi, H., Urtti, A., Yliperttula, M., 2007. Pharmacokinetic simulation of biowaiver criteria: The effects of gastric emptying, dissolution, absorption and elimination rates. Eur. J. Pharm. Sci. 30, 155–166. https://doi.org/10.1016/j.ejps.2006.10.011

Kuepfer, L., Niederalt, C., Wendl, T., Schlender, J.F., Willmann, S., Lippert, J., Block, M., Eissing, T., Teutonico, D., 2016. Applied Concepts in PBPK Modeling: How to Build a PBPK/PD Model. CPT Pharmacometrics Syst. Pharmacol. 5, 516–531. https://doi.org/10.1002/psp4.12134

Kurebayashi, H., Okudaira, K., Ohno, Y., 2010. Species difference of metabolic clearance of bisphenol A using cryopreserved hepatocytes from rats, monkeys and humans. Toxicol. Lett. 198, 210–215. https://doi.org/10.1016/j.toxlet.2010.06.017

Kuroda, N., Kinoshita, Y., Sun, Y., Wada, M., Kishikawa, N., Nakashima, K., Makino, T., Nakazawa, H., 2003. Measurement of bisphenol A levels in human blood serum and ascitic fluid by HPLC using a fluorescent labeling reagent. J. Pharm. Biomed. Anal. 30, 1743–1749. https://doi.org/10.1016/S0731-7085(02)00516-2

Lai, K.P., Wong, M.H., Wong, C.K.C., 2005a. Inhibition of CYP450scc expression in dioxin-exposed rat Leydig cells. J. Endocrinol. 185, 519–527. https://doi.org/10.1677/joe.1.06054

Lai, K.P., Wong, M.H., Wong, C.K.C., 2005b. Effects of TCDD in modulating the expression of Sertoli cell secretory products and markers for cell-cell interaction. Toxicology 206, 111–123. https://doi.org/10.1016/j.tox.2004.07.002

Lans, M.C., Spiertz, C., Brouwer, a, Koeman, J.H., 1994. Different competition of thyroxine binding to transthyretin and thyroxine-binding globulin by hydroxy-PCBs, PCDDs and PCDFs. Eur. J. Pharmacol. 270, 129–136. https://doi.org/10.1016/0926-6917(94)90054-X

Leclerc, E., Hamon, J., Legendre, A., Bois, F.Y., 2014. Integration of pharmacokinetic and NRF2 system biology models to describe reactive oxygen species production and subsequent glutathione depletion in liver microfluidic biochips after flutamide exposure. Toxicol. Vitr. 28, 1230–1241. https://doi.org/10.1016/j.tiv.2014.05.003

Lee, Y.J., Ryu, H.Y., Kim, H.K., Min, C.S., Lee, J.H., Kim, E., Nam, B.H., Park, J.H., Jung, J.Y., Jang, D.D., Park, E.Y., Lee, K.H., Ma, J.Y., Won, H.S., Im, M.W.,

Chapter 1

Leem, J.H., Hong, Y.C., Yoon, H.S., 2008. Maternal and fetal exposure to bisphenol A in Korea. Reprod. Toxicol. 25, 413–419. https://doi.org/10.1016/j.reprotox.2008.05.058

Lemaire, G., Terouanne, B., Mauvais, P., Michel, S., Rahmani, R., 2004. Effect of organochlorine pesticides on human androgen receptor activation in vitro. Toxicol. Appl. Pharmacol. 196, 235–246. https://doi.org/10.1016/j.taap.2003.12.011

Li, L. a., Wang, P.W., Chang, L.W., 2004. Polychlorinated biphenyl 126 stimulates basal and inducible aldosterone biosynthesis of human adrenocortical H295R cells. Toxicol. Appl. Pharmacol. 195, 92–102. https://doi.org/10.1016/j.taap.2003.11.007

Li, M.W.M., Mruk, D.D., Lee, W.M., Cheng, C.Y., 2009. Disruption of the blood-testis barrier integrity by bisphenol A in vitro: Is this a suitable model for studying blood-testis barrier dynamics? Int. J. Biochem. Cell Biol. 41, 2302–2314. https://doi.org/10.1016/j.biocel.2009.05.016

Li, W., He, Q.Z., Wu, C.Q., Pan, X.Y., Wang, J., Tan, Y., Shan, X.Y., Zeng, H.C., 2015. PFOS Disturbs BDNF-ERK-CREB Signalling in Association with Increased MicroRNA-22 in SH-SY5Y Cells. Biomed Res. Int. 2015. https://doi.org/10.1155/2015/302653

Li, X., Fang, P., Mai, J., Choi, E.T., Wang, H., Yang, X., 2013. Targeting mitochondrial reactive oxygen species as novel therapy for inflammatory diseases and cancers. J. Hematol. Oncol. 6, 19. https://doi.org/10.1186/1756-8722-6-19

Li, Y., Ramdhan, D.H., Naito, H., Yamagishi, N., Ito, Y., Hayashi, Y., Yanagiba, Y., Okamura, A., Tamada, H., Gonzalez, F.J., Nakajima, T., 2011. Ammonium perfluorooctanoate may cause testosterone reduction by adversely affecting testis in relation to PPARα. Toxicol. Lett. 205, 265–272. https://doi.org/10.1016/j.toxlet.2011.06.015

Lipsky, R.H., Marini, A.M., 2007. Brain-derived neurotrophic factor in neuronal survival and behavior-related plasticity. Ann. N. Y. Acad. Sci. 1122, 130–143. https://doi.org/10.1196/annals.1403.009

Long, Y., Wang, Y., Ji, G., Yan, L., Hu, F., Gu, A., 2013. Neurotoxicity of Perfluorooctane Sulfonate to Hippocampal Cells in Adult Mice. PLoS One 8, 1–9. https://doi.org/10.1371/journal.pone.0054176

Lorber, M., Angerer, J., Koch, H.M., 2010. A simple pharmacokinetic model to characterize exposure of Americans to Di-2-ethylhexyl phthalate. J. Expo. Sci. Environ. Epidemiol. 20, 38–53. https://doi.org/10.1038/jes.2008.74

Louisse, J., Beekmann, K., Rietjens, I.M.C.M., 2016. Use of physiologically based kinetic modeling-based reverse dosimetry to predict in vivo toxicity from in vitro data. Chem. Res. Toxicol. acs.chemrestox.6b00302. https://doi.org/10.1021/acs.chemrestox.6b00302

Chapter 1

Lu, B., 2003. Pro-Region of Neurotrophins. Neuron 39, 735–738. https://doi.org/10.1016/S0896-6273(03)00538-5

Lubin, F.D., Roth, T.L., Sweatt, J.D., 2008. Epigenetic regulation of BDNF gene transcription in the consolidation of fear memory. J. Neurosci. 28, 10576–86. https://doi.org/10.1523/JNEUROSCI.1786-08.2008

Ma, E., MacRae, I.J., Kirsch, J.F., Doudna, J.A., 2008. Autoinhibition of Human Dicer by Its Internal Helicase Domain. J. Mol. Biol. 380, 237–243. https://doi.org/10.1016/j.jmb.2008.05.005

Mager, D.E., Woo, S., Jusko, W.J., 2009. Scaling Pharmacodynamics from In Vitro and Preclinical Animal Studies to Humans. Drug Metab. Pharmacokinet. 24, 16–24. https://doi.org/10.2133/dmpk.24.16

Mager, D.E., Wyska, E., Jusko, W.J., 2003. Diversity of mechanism-based pharmacodynamic models. Drug Metab. Dispos. 31, 510–8. https://doi.org/10.1124/DMD.31.5.510

Martínez, M.A., Rovira, J., Prasad Sharma, R., Nadal, M., Schuhmacher, M., Kumar, V., 2018. Comparing dietary and non-dietary source contribution of BPA and DEHP to prenatal exposure: A Catalonia (Spain) case study. Environ. Res. 166, 25–34. https://doi.org/10.1016/j.envres.2018.05.008

Martínez, M.A., Rovira, J., Sharma, R.P., Nadal, M., Schuhmacher, M., Kumar, V., 2017. Prenatal exposure estimation of BPA and DEHP using integrated external and internal dosimetry: A case study. Environ. Res. 158, 566–575. https://doi.org/10.1016/j.envres.2017.07.016

Masuyama, H., Hiramatsu, Y., Kunitomi, M., Kudo, T., MacDonald, P.N., 2000. Endocrine disrupting chemicals, phthalic acid and nonylphenol, activate Pregnane X receptor-mediated transcription. Mol. Endocrinol. 14, 421–428. https://doi.org/10.1210/mend.14.3.0424

Masuyama, H., Inoshita, H., Hiramatsu, Y., Kudo, T., 2002. Ligands have various potential effects on the degradation of pregnane X receptor by proteasome. Endocrinology 143, 55–61. https://doi.org/10.1210/en.143.1.55

Matsuzaki, Y., Nagai, D., Ichimura, E., Goda, R., Tomura, A., Doi, M., Nishikawa, K., 2006. Metabolism and hepatic toxicity of flutamide in cytochrome P450 1A2 knockout SV129 mice. J. Gastroenterol. 41, 231–239. https://doi.org/10.1007/s00535-005-1749-y

Menei, P., Montero-Menei, C., Whittemore, S.R., Bunge, R.P., Bunge, M.B., 1998. Schwann cells genetically modified to secrete human BDNF promote enhanced axonal regrowth across transected adult rat spinal cord. Eur. J. Neurosci. 10, 607–621. https://doi.org/10.1046/j.1460-9568.1998.00071.x

Michael, G.J., Averill, S., Nitkunan, A., Rattray, M., Bennett, D.L., Yan, Q., Priestley, J. V, 1997. Nerve growth factor treatment increases brain-derived neurotrophic

factor selectively in TrkA-expressing dorsal root ganglion cells and in their central terminations within the spinal cord. J. Neurosci. 17, 8476–90.

Mielke, H., Partosch, F., Gundert-Remy, U., 2011. The contribution of dermal exposure to the internal exposure of bisphenol A in man. Toxicol. Lett. 204, 190–198. https://doi.org/10.1016/j.toxlet.2011.04.032

Mikamo, E., Harada, S., Nishikawa, J., Nishihara, T., 2003. Endocrine disruptors induce cytochrome P450 by affecting transcriptional regulation via pregnane X receptor. Toxicol. Appl. Pharmacol. 193, 66–72. https://doi.org/10.1016/j.taap.2003.08.001

Moriyama, K., Tagami, T., Akamizu, T., Usui, T., Saijo, M., Kanamoto, N., Hataya, Y., Shimatsu, A., Kuzuya, H., Nakao, K., 2002. Thyroid hormone action is disrupted by bisphenol A as an antagonist. J. Clin. Endocrinol. Metab. 87, 5185–5190. https://doi.org/10.1210/jc.2002-020209

Mowla, S.J., Pareek, S., Farhadi, H.F., Petrecca, K., Fawcett, J.P., Seidah, N.G., Morris, S.J., Sossin, W.S., Murphy, R. a, 1999. Differential sorting of nerve growth factor and brain-derived neurotrophic factor in hippocampal neurons. J. Neurosci. 19, 2069–2080.

Muiños-Gimeno, M., Espinosa-Parrilla, Y., Guidi, M., Kagerbauer, B., Sipilä, T., Maron, E., Pettai, K., Kananen, L., Navinés, R., Martín-Santos, R., Gratacòs, M., Metspalu, A., Hovatta, I., Estivill, X., 2011. Human microRNAs miR-22, miR-138-2, miR-148a, and miR-488 are associated with panic disorder and regulate several anxiety candidate genes and related pathways. Biol. Psychiatry 69, 526–533. https://doi.org/10.1016/j.biopsych.2010.10.010

Murer, M.., Yan, Q., Raisman-Vozari, R., 2001. Brain-derived neurotrophic factor in the control human brain, and in Alzheimer's disease and Parkinson's disease. Prog. Neurobiol. 63, 71–124. https://doi.org/10.1016/S0301-0082(00)00014-9

Murphy, M.P., 2009. How mitochondria produce reactive oxygen species. Biochem. J. 417, 1–13. https://doi.org/10.1042/BJ20081386

Nestorov, I., 2007. Whole-body physiologically based pharmacokinetic models. Expert Opin. Drug Metab. Toxicol. 3, 235–249. https://doi.org/10.1517/17425255.3.2.235

Nikula, H., Talonpoika, T., Kaleva, M., Toppari, J., 1999. Inhibition of hCG-stimulated steroidogenesis in cultured mouse Leydig tumor cells by bisphenol A and octylphenols. Toxicol. Appl. Pharmacol. 157, 166–173. https://doi.org/10.1006/taap.1999.8674

Niwa, T., Fujimoto, M., Kishimoto, K., Yabusaki, Y., Ishibashi, F., Katagiri, M., 2001. Metabolism and interaction of bisphenol A in human hepatic cytochrome P450 and steroidogenic CYP17. Biol. Pharm. Bull. 24, 1064–1067. https://doi.org/10.1248/bpb.24.1064

O'Leary, P.D., Hughes, R.A., 1998. Structure-activity relationships of conformationally

Chapter 1

constrained peptide analogues of loop 2 of brain-derived neurotrophic factor. J. Neurochem. 70, 1712–21. https://doi.org/10.1046/j.1471-4159.1998.70041712.x

OECD, 2018. "Users'' Handbook supplement to the Guidance Document for developing and assessing Adverse Outcome Pathways", OECD Series on Adverse Outcome Pathways, No. 1, OECD Publishing, Paris."
https://doi.org/10.1787/5jlv1m9d1g32-en

OECD, 2016. "Users'' Handbook supplement to the Guidance Document for developing and assessing Adverse Outcome Pathways", OECD Series on Adverse Outcome Pathways, No. 1, OECD Publishing, Paris" 18.
https://doi.org/10.1787/5jlv1m9d1g32-en

Ohshima, M., Ohno, S., Nakajin, S., 2005. Inhibitory effects of some possible endocrine-disrupting chemicals on the isozymes of human 11beta-hydroxysteroid dehydrogenase and expression of their mRNA in gonads and adrenal glands. Environ. Sci. 12, 219–230.

Ohtake, F., Takeyama, K., Matsumoto, T., Kitagawa, H., Yamamoto, Y., Nohara, K., Tohyama, C., Krust, A., Mimura, J., Chambon, P., Yanagisawa, J., Fujii-Kuriyama, Y., Kato, S., 2003. Modulation of oestrogen receptor signalling by association with the activated dioxin receptor. Nature 423, 545–550.
https://doi.org/10.1038/nature01606

Patisaul, H.B., Todd, K.L., Mickens, J.A., Adewale, H.B., 2009. Impact of neonatal exposure to the ERα agonist PPT, bisphenol-A or phytoestrogens on hypothalamic kisspeptin fiber density in male and female rats. Neurotoxicology 30, 350–357.
https://doi.org/10.1016/j.neuro.2009.02.010

Pérez-Ortín, J.E., Alepuz, P.M., Moreno, J., 2007. Genomics and gene transcription kinetics in yeast. Trends Genet. 23, 250–257.
https://doi.org/10.1016/j.tig.2007.03.006

Perruisseau-Carrier, C., Jurga, M., Forraz, N., McGuckin, C.P., 2011. MiRNAs stem cell reprogramming for neuronal induction and differentiation. Mol. Neurobiol. 43, 215–227. https://doi.org/10.1007/s12035-011-8179-z

Podratz, P.L., Filho, V.S.D., Lopes, P.F.I., Sena, G.C., Matsumoto, S.T., Samoto, V.Y., Takiya, C.M., Miguel, E.D.C., Silva, I.V., Graceli, J.B., 2012. Tributyltin Impairs the Reproductive Cycle in Female Rats. J. Toxicol. Environ. Heal. Part A 75, 1035–1046. https://doi.org/10.1080/15287394.2012.697826

Poland, a, Knutson, J.C., 1982. 2,3,7,8-Tetrachlorodibenzo-P-Dioxin and Related Halogenated Aromatic Hydrocarbons: Examination of the Mechanism of Toxicity. Annu. Rev. Pharmacol. Toxicol. 22, 517–554.
https://doi.org/10.1146/annurev.pa.22.040182.002505

Poulin, P., Krishnan, K., 1996. Molecular Structure-Based Prediction of the Partition Coefficients of Organic Chemicals for Physiological Pharmacokinetic Models. Toxicol. Mech. Methods 6, 117–137. https://doi.org/10.3109/15376519609068458

Chapter 1

Poulin, P., Krishnan, K., 1995. A biologically-based algorithm for predicting human tissue: blood partition coefficients of organic chemicals. Hum Exp Toxicol 14, 273–280.

Poulin, P., Theil, F.P., 2000. A priori prediction of tissue: Plasma partition coefficients of drugs to facilitate the use of physiologically-based pharmacokinetic models in drug discovery. J. Pharm. Sci. 89, 16–35. https://doi.org/10.1002/(SICI)1520-6017(200001)89:1<16::AID-JPS3>3.0.CO;2-E

Qatanani, M., Zhang, J., Moore, D.D., 2005. Role of the constitutive androstane receptor in xenobiotic-induced thyroid hormone metabolism. Endocrinology 146, 995–1002. https://doi.org/10.1210/en.2004-1350

Qiu, L., Zhang, X., Zhang, X., Zhang, Y., Gu, J., Chen, M., Zhang, Z., Wang, X., Wang, S.L., 2013. Sertoli cell is a potential target for perfluorooctane sulfonate-induced reproductive dysfunction in male mice. Toxicol. Sci. 135, 229–240. https://doi.org/10.1093/toxsci/kft129

Radwanski, E., Perentesis, G., Symchowicz, S., Zampaglione, N., 1989. Single and Multiple Dose Pharmacokinetic Evaluation of Flutamide in Normal Geriatric Volunteers. J. Clin. Pharmacol. 29, 554–558. https://doi.org/10.1002/j.1552-4604.1989.tb03381.x

Raun Andersen, H., Vinggaard, A.M., Høj Rasmussen, T., Gjermandsen, I.M., Cecilie Bonefeld-Jørgensen, E., 2002. Effects of Currently Used Pesticides in Assays for Estrogenicity, Androgenicity, and Aromatase Activity in Vitro. Toxicol. Appl. Pharmacol. 179, 1–12. https://doi.org/10.1006/taap.2001.9347

Rey, R., Lukas-Croisier, C., Lasala, C., Bedecarrás, P., 2003. AMH/MIS: What we know already about the gene, the protein and its regulation. Mol. Cell. Endocrinol. 211, 21–31. https://doi.org/10.1016/j.mce.2003.09.007

Rodríguez-Tébar, A., Dechant, G., Götz, R., Barde, Y.A., 1992. Binding of neurotrophin-3 to its neuronal receptors and interactions with nerve growth factor and brain-derived neurotrophic factor. EMBO J. 11, 917–922.

Rouquié, D., Heneweer, M., Botham, J., Ketelslegers, H., Markell, L., Pfister, T., Steiling, W., Strauss, V., Hennes, C., 2015. Contribution of new technologies to characterization and prediction of adverse effects. Crit. Rev. Toxicol. 45, 172–183. https://doi.org/10.3109/10408444.2014.986054

Saitoh, M., Yanase, T., Morinaga, H., Tanabe, M., Mu, Y.M., Nishi, Y., Nomura, M., Okabe, T., Goto, K., Takayanagi, R., Nawata, H., 2001. Tributyltin or triphenyltin inhibits aromatase activity in the human granulosa-like tumor cell line KGN. Biochem. Biophys. Res. Commun. 289, 198–204. https://doi.org/10.1006/bbrc.2001.5952

Sandhya, V.K., Raju, R., Verma, R., Advani, J., Sharma, R., Radhakrishnan, A., Nanjappa, V., Narayana, J., Somani, B.L., Mukherjee, K.K., Pandey, A., Christopher, R., Keshava Prasad, T.S., 2013. A network map of BDNF/TRKB and

Chapter 1

BDNF/p75NTR signaling system. J. Cell Commun. Signal. 7, 301–307. https://doi.org/10.1007/s12079-013-0200-z

Sato, I., Kawamoto, K., Nishikawa, Y., Tsuda, S., Yoshida, M., Yaegashi, K., Saito, N., Liu, W., Jin, Y., 2009. Neurotoxicity of perfluorooctane sulfonate (PFOS) in rats and mice after single oral exposure. J. Toxicol. Sci. 34, 569–574. https://doi.org/10.2131/jts.34.569

Saunders, P.T., Majdic, G., Parte, P., Millar, M.R., Fisher, J.S., Turner, K.J., Sharpe, R.M., 1997. Fetal and perinatal influence of xenoestrogens on testis gene expression. Adv. Exp. Med. Biol. 424, 99–110.

Schmitt, W., 2008. General approach for the calculation of tissue to plasma partition coefficients. Toxicol. Vitr. 22, 457–467. https://doi.org/10.1016/j.tiv.2007.09.010

Schönfelder, G., Wittfoht, W., Hopp, H., Talsness, C.E., Paul, M., Chahoud, I., 2002. Parent bisphenol a accumulation in the human maternal-fetal-placental unit. Environ. Health Perspect. 110, 703–707. https://doi.org/10.1289/ehp.021100703

Seo, J.S., Lee, Y.M., Jung, S.O., Kim, I.C., Yoon, Y.D., Lee, J.S., 2006. Nonylphenol modulates expression of androgen receptor and estrogen receptor genes differently in gender types of the hermaphroditic fish Rivulus marmoratus. Biochem. Biophys. Res. Commun. 346, 213–223. https://doi.org/10.1016/j.bbrc.2006.05.123

Shi, Z., Ding, L., Zhang, H., Feng, Y., Xu, M., Dai, J., 2009. Chronic exposure to perfluorododecanoic acid disrupts testicular steroidogenesis and the expression of related genes in male rats. Toxicol. Lett. 188, 192–200. https://doi.org/10.1016/j.toxlet.2009.04.014

Sisson, T.R., Lund, C.J., Whalen, L.E., Telek, A., 1959. The blood volume of infants. I. The full-term infant in the first year of life. J. Pediatr. 55, 163–79. https://doi.org/10.1016/S0022-3476(59)80084-6

Siu, E.R., Mruk, D.D., Porto, C.S., Cheng, C.Y., 2009. Cadmium-induced testicular injury. Toxicol. Appl. Pharmacol. 238, 240–249. https://doi.org/10.1016/j.taap.2009.01.028

Sjo, E., Lennerna, H., Andersson, T.B., Gråsjo, J., Bredberg, U., 2009. Estimates of Intrinsic Clearance (CL int), Maximum Velocity of the Metabolic Reaction (V max), and Michaelis Constant (K m): Accuracy and Robustness Evaluated through Experimental Data and Monte Carlo Simulations ABSTRACT : Pharmacology 37, 47–58. https://doi.org/10.1124/dmd.108.021477.kinetics

Sjögren, E., Tammela, T.L., Lennernäs, B., Taari, K., Isotalo, T., Malmsten, L.-Å., Axén, N., Lennernäs, H., 2014. Pharmacokinetics of an Injectable Modified-Release 2-Hydroxyflutamide Formulation in the Human Prostate Gland Using a Semiphysiologically Based Biopharmaceutical Model. Mol. Pharm. 11, 3097–3111. https://doi.org/10.1021/mp5002813

Sobarzo, C.M., Lustig, L., Ponzio, R., Denduchis, B., 2006. Effect of di-(2-ethylhexyl)

Chapter 1

phthalate on N-cadherin and catenin protein expression in rat testis. Reprod. Toxicol. 22, 77–86. https://doi.org/10.1016/j.reprotox.2006.02.004

Soetaert, K., Petzoldt, T., 2010. Inverse Modelling, Sensitivity and Monte Carlo Analysis in R Using Package FME. J. Stat. Softw. 33, 2–4. https://doi.org/10.18637/jss.v033.i03

Stasenko, S., Bradford, E.M., Piasek, M., Henson, M.C., Varnai, V.M., Jurasović, J., Kušec, V., 2010. Metals in human placenta: Focus on the effects of cadmium on steroid hormones and leptin. J. Appl. Toxicol. 30, 242–253. https://doi.org/10.1002/jat.1490

Stouder, C., Paoloni-Giacobino, A., 2011. Specific transgenerational imprinting effects of the endocrine disruptor methoxychlor on male gametes. Reproduction 141, 207–216. https://doi.org/10.1530/REP-10-0400

Sturla, S.J., Boobis, A.R., FitzGerald, R.E., Hoeng, J., Kavlock, R.J., Schirmer, K., Whelan, M., Wilks, M.F., Peitsch, M.C., 2014. Systems Toxicology: From Basic Research to Risk Assessment. Chem. Res. Toxicol. 27, 314–329. https://doi.org/10.1021/tx400410s

Teppner, M., Boess, F., Ernst, B., Pähler, A., 2016. Biomarkers of flutamide-bioactivation and oxidative stress in vitro and in vivo. Drug Metab. Dispos. 44, 560–569. https://doi.org/10.1124/dmd.115.066522

Thiel, C., Cordes, H., Conde, I., Castell, J.V., Blank, L.M., Kuepfer, L., 2017. Model-based contextualization of in vitro toxicity data quantitatively predicts in vivo drug response in patients. Arch. Toxicol. 91, 865–883. https://doi.org/10.1007/s00204-016-1723-x

Timchalk, C., Nolan, R.J., Mendrala, A.L., Dittenber, D.A., Brzak, K.A., Mattsson, J.L., 2002. A physiologically based pharmacokinetic and pharmacodynamic (PBPK/PD) model for the organophosphate insecticide chlorpyrifos in rats and humans. Toxicol. Sci. 66, 34–53. https://doi.org/10.1093/toxsci/66.1.34

Toyoda, K., Shibutani, M., Tamura, T., Koujitani, T., Uneyama, C., Hirose, M., 2000. Repeated dose (28 days) oral toxicity study of flutamide in rats, based on the draft protocol for the `Enhanced OECD Test Guideline 407' for screening for endocrine-disrupting chemicals. Arch. Toxicol. 74, 127–132. https://doi.org/10.1007/s002040050664

Trdan Lusin, T., Roskar, R., Mrhar, A., 2012. Evaluation of bisphenol A glucuronidation according to UGT1A1*28 polymorphism by a new LC-MS/MS assay. Toxicology 292, 33–41. https://doi.org/10.1016/j.tox.2011.11.015

Uzumcu, M., Kuhn, P.E., Marano, J.E., Armenti A.E., A.E., Passantino, L., 2006. Early postnatal methoxychlor exposure inhibits folliculogenesis and stimulates anti-Mullerian hormone production in the rat ovary. J. Endocrinol. 191, 549–558. https://doi.org/10.1677/joe.1.06592

Chapter 1

Valentin, J., 2002. Basic anatomical and physiological data for use in radiological protection: reference values. Ann. ICRP 32, 1–277. https://doi.org/10.1016/S0146-6453(03)00002-2

Vuong, A.M., Yolton, K., Webster, G.M., Sjödin, A., Calafat, A.M., Braun, J.M., Dietrich, K.N., Lanphear, B.P., Chen, A., 2016. Prenatal polybrominated diphenyl ether and perfluoroalkyl substance exposures and executive function in school-age children. Environ. Res. 147, 556–564. https://doi.org/10.1016/j.envres.2016.01.008

Wambaugh, J.F., Setzer, R.W., Pitruzzello, A.M., Liu, J., Reif, D.M., Kleinstreuer, N.C., Wang, N.C.Y., Sipes, N., Martin, M., Das, K., DeWitt, J.C., Strynar, M., Judson, R., Houck, K.A., Lau, C., 2013. Dosimetric anchoring of In vivo and In vitro studies for perfluorooctanoate and perfluorooctanesulfonate. Toxicol. Sci. 136, 308–327. https://doi.org/10.1093/toxsci/kft204

Wan, H.T., Zhao, Y.G., Wong, M.H., Lee, K.F., Yeung, W.S.B., Giesy, J.P., Wong, C.K.C., 2011. Testicular signaling is the potential target of perfluorooctanesulfonate-mediated subfertility in male mice. Biol. Reprod. 84, 1016–1023. https://doi.org/10.1095/biolreprod.110.089219

Wang, J., Sun, B., Hou, M., Pan, X., Li, X., 2012. The environmental obesogen bisphenol A promotes adipogenesis by increasing the amount of 11β-hydroxysteroid dehydrogenase type 1 in the adipose tissue of children. Int. J. Obes. 999–1005. https://doi.org/10.1038/ijo.2012.173

Wang, X., Li, Y., Xu, X., Wang, Y. hua, 2010. Toward a system-level understanding of microRNA pathway via mathematical modeling. BioSystems 100, 31–38. https://doi.org/10.1016/j.biosystems.2009.12.005

Waters, M.D., Boorman, G., Bushel, P., Cunningham, M., Irwin, R., Merrick, A., Olden, K., Paules, R., Selkirk, J., Stasiewicz, S., Weis, B., Van Houten, B., Walker, N., Tennant, R., 2003. Systems toxicology and the Chemical Effects in Biological Systems (CEBS) knowledge base. Environ. Health Perspect. 111, 811–824. https://doi.org/10.1289/txg.5971

Wen, B., Coe, K.J., Rademacher, P., Fitch, W.L., Monshouwer, M., Nelson, S.D., 2008. Comparison of in vitro bioactivation of flutamide and its cyano analogue: Evidence for reductive activation by human NADPH:cytochrome P450 reductase. Chem. Res. Toxicol. 21, 2393–2406. https://doi.org/10.1021/tx800281h

Wysowski, D.K., Fourcroy, J.L., 1996. Flutamide Hepatotoxicity. J. Urol. 155, 209–212. https://doi.org/10.1016/S0022-5347(01)66596-0

Xi, W., Lee, C.K.F., Yeung, W.S.B., Giesy, J.P., Wong, M.H., Zhang, X., Hecker, M., Wong, C.K.C., 2011. Effect of perinatal and postnatal bisphenol A exposure to the regulatory circuits at the hypothalamus-pituitary-gonadal axis of CD-1 mice. Reprod. Toxicol. 31, 409–417. https://doi.org/10.1016/j.reprotox.2010.12.002

Yang, J., Wang, C., Nie, X., Shi, S., Xiao, J., Ma, X., Dong, X., Zhang, Y., Han, J., Li,

Chapter 1

T., Mao, J., Liu, X., Zhao, J., Wu, Q., 2015. Perfluorooctane sulfonate mediates microglial activation and secretion of TNF-α through Ca2+-dependent PKC-NF-κB signaling. Int. Immunopharmacol. 28, 52–60. https://doi.org/10.1016/j.intimp.2015.05.019

York, N., 2015. Regulation of Cell Survival by Secreted Proneurotrophins.pdf. Science (80-.). 294, 1945–1949. https://doi.org/10.1126/science.1065057

You, H.J., Park, J.H., Pareja-Galeano, H., Lucia, A., Shin, J. Il, 2016. Targeting MicroRNAs Involved in the BDNF Signaling Impairment in Neurodegenerative Diseases. NeuroMolecular Med. https://doi.org/10.1007/s12017-016-8407-9

Yu, N., Wei, S., Li, M., Yang, J., Li, K., Jin, L., Xie, Y., Giesy, J.P., Zhang, X., Yu, H., 2016. Effects of Perfluorooctanoic Acid on Metabolic Profiles in Brain and Liver of Mouse Revealed by a High-throughput Targeted Metabolomics Approach. Sci. Rep. 6, 23963. https://doi.org/10.1038/srep23963

Yun, Y.E., Cotton, C.A., Edginton, A.N., 2014. Development of a decision tree to classify the most accurate tissue-specific tissue to plasma partition coefficient algorithm for a given compound. J. Pharmacokinet. Pharmacodyn. 41, 1–14. https://doi.org/10.1007/s10928-013-9342-0

Zamkova, M., Khromova, N., Kopnin, B.P., Kopnin, P., 2013. Ras-induced ROS upregulation affecting cell proliferation is connected with cell type-specific alterations of HSF1/SESN3/p21Cip1/WAF1pathways. Cell Cycle 12, 826–836. https://doi.org/10.4161/cc.23723

Zeng, H. cai, Zhang, L., Li, Y. yuan, Wang, Y. jian, Xia, W., Lin, Y., Wei, J., Xu, S. qing, 2011. Inflammation-like glial response in rat brain induced by prenatal PFOS exposure. Neurotoxicology 32, 130–139. https://doi.org/10.1016/j.neuro.2010.10.001

Zhang, J., Cooke, G.M., Curran, I.H.A., Goodyer, C.G., Cao, X.L., 2011. GC-MS analysis of bisphenol A in human placental and fetal liver samples. J. Chromatogr. B Anal. Technol. Biomed. Life Sci. 879, 209–214. https://doi.org/10.1016/j.jchromb.2010.11.031

Zhang, L., Guo, J., Zhang, Q., Zhou, W., Li, J., Yin, J., Cui, L., 2018. Flutamide induces hepatic cell death and mitochondrial dysfunction via inhibition of Nrf2-mediated heme oxygenase-1. Oxid. Med. Cell. Longev.

Zhang, L., Li, Y.-Y., Zeng, H.-C., Wei, J., Wan, Y.-J., Chen, J., Xu, S.-Q., 2011. MicroRNA expression changes during zebrafish development induced by perfluorooctane sulfonate. J. Appl. Toxicol. 31, 210–222. https://doi.org/10.1002/jat.1583

Zhang, T., Sun, H., Kannan, K., 2013. Blood and urinary bisphenol a concentrations in children, adults, and pregnant women from China: Partitioning between blood and urine and maternal and fetal cord blood. Environ. Sci. Technol. 47, 4686–4694. https://doi.org/10.1021/es303808b

Chapter 1

Zhao, B., Hu, G.X., Chu, Y., Jin, X., Gong, S., Akingbemi, B.T., Zhang, Z., Zirkin, B.R., Ge, R.S., 2010. Inhibition of human and rat 3β-hydroxysteroid dehydrogenase and 17β-hydroxysteroid dehydrogenase 3 activities by perfluoroalkylated substances. Chem. Biol. Interact. 188, 38–43. https://doi.org/10.1016/j.cbi.2010.07.001

Chapter 2

Development and validation of Adult PBPK models

2A. Sharma RP, Schuhmacher M, Kumar V. Development of a human physiologically based pharmacokinetic (PBPK) model for phthalate (DEHP) and its metabolites: a bottom up modeling approach. Toxicology Letters, In press. doi: 10.1016/j.toxlet.2018.06.1217

2B. Raju Prasad Sharma, Vikas Kumar, Marta Schuhmacher, Alexey Kolodkin, Frédéric Y. Bois, Hans V. Westerhoff. Development and evaluation of a harmonized whole body physiologically based pharmacokinetic (PBPK) model for flutamide in rats and its extrapolation to human

Chapter 2

2A. Development of a human physiologically based pharmacokinetic (PBPK) model for phthalates and its metabolites: A bottom up modeling approach

Abstract: DEHP exposure to human comes from different sources such as food, diet, cosmetics, toys, medical products, and food wraps. Recently, DEHP and its metabolites were categorized as non-persistent endocrine disrupting compounds (EDCs) by the world health organization (WHO). Rat experimental studies have shown that phthalate and its metabolite(s) can cause hepatic, developmental and reproductive toxicity. In human, DEHP rapidly metabolizes into a toxic metabolite MEHP. This MEHP further metabolizes into the different chemical forms of 5OH-MEHP, 5oxo-MEHP, 5cx-MEPP and phthalic acid. A simple DEHP pharmacokinetics model has been developed, but with a limited number of metabolites. A chemical like DEHP which is extensively metabolized deserves a detail metabolic kinetics study. A physiologically based pharmacokinetics (PBPK) model of DEHP considering all the major metabolites in human, has not been developed yet. The objective of this study is to develop a detailed human PBPK model for DEHP and its major metabolites by using a bottom-up modelling approach with the integration of in vitro metabolic data. We will use an in-vitro-in-vivo extrapolation (IVIVE) and a quantitative structure-activity relationship (QSAR) method for the parameterization of the model. Monte Carlo simulations were performed to estimate the impact of parametric uncertainty on the model predictions. First, the model was calibrated using a control human kinetic study that represents the time course of DEHP metabolites concentrations in both the blood and the urine. Then, the model was evaluated against the published independent data on different dosing scenarios. The results of model predictions for the DEHP metabolites in both the blood and the urine were well within the range of experimentally observed data. The model also captured the time course profile of the observed data, attesting to the model's predictive power. The current developed PBPK model can further be used for the prediction of the time course of chemical concentrations for the different exposure scenarios not only in the blood and the urine but also in the other compartments. Moreover, this model can also be used to explore different biomonitoring studies with respect to human health risk assessment and might be useful for integrative toxicological studies aimed at improving exposure-target tissue dose–response relationship.

Keywords: DEHP; MEHP; Pharmacokinetics; PBPK; Human health Risk assessment; IVIVE; Endocrine disruptors; human biomonitoring

Chapter 2

1. Introduction

Phthalates are ubiquitous environmental contaminants made up of dialkyl esters or alkyl and aryl esters of ortho-phthalic acid (1,2-dicarboxylic acid). Among Phthalates, Di-2-ethylhexyl phthalate (DEHP) is the most important because of its large and widespread uses in industries as a plasticizer. It is found in food, cosmetics, toys, medical products and food packaging, mostly used as a plasticizer. The total dietary intake (TDI) of 50 µg/kg BW/day limit has been set by the EFSA and the European chemical agency (ECHA) to assess the risk related to DEHP exposure (EFSA, 2015; ECHA, 2010). The total mean dietary intake of the DEHP in several cohorts studies estimated in the range of 0.42–11.67 µg/kg bw/ day, which is far below the threshold set by the EFSA and the ECHA (Fromme et al., 2007; Dickson-Spillmann et al., 2009; Sioen et al., 2012; Heinemeyer et al., 2013; Martine et al., 2013; Martínez et al., 2017, 2018).

DEHP has a short half-life and it does not accumulate inside the body (Krotz et al., 2012). DEHP completely metabolizes into a toxic metabolite mono-(2-ethylhexyl) phthalate (MEHP). This MEHP further metabolizes into different chemical forms like 5-hydroxy MEHP, 2- ethyl-5-carboxypentyl phthalate (5-Cx MEPP) and phthalic acid. 5-oxo MEHP is another metabolite result of the 5-OH MEHP metabolism. Temporal variability in phthalate exposure from the different sources and their ability to generate several forms of metabolites can lead to a stable microenvironment exposure of phthalates to internal organs. The microenvironment exposure of the DEHP over a long period of time lead to a pseudo-steady state concentration (Meeker et al., 2009).

Currently, DEHP is of concern in its categorization as a non-persistent endocrine disruptor by the World Health Organization (WHO, 2010). Cobellis (2003) in his epidemiological study has shown the linkage between the exposure of DEHP and the prevalence of endometriosis in women. Other studies have also shown that environment relevant dose of phthalates alters estrous cycle, impaired oocyte maturation, decrease ovulation (Anas et al., 2003; Krisher, 2013; Hannon et al., 2014). DEHP and its toxic metabolite MEHP mainly alter the estrogen productions and its activity in granulosa cell, which are essential for the growth and secretion of the follicles, which might lead to infertility due to hypo-estrogenic, polycystic ovary and anovulatory cycles (Davis et al., 1994; Lovekamp-Swan and Davis, 2003). Many hypotheses of phthalates effect on male reproductive toxicities were proposed based on the animal studies, please refer to the given reference for more information (Richburg and Boekelheide, 1996; Richburg et al., 1999; Lee et al., 1999; Koji et al., 2001; Shelby, 2006; Sharma et al., 2017a). Several cohort studies have shown a correlation between the high levels of DEHP in urine with significant reduction in plasma testosterone concentrations (Duty et al., 2005; Pan et al., 2006).

Understanding the factors that govern the DEHP distribution and metabolisms within the quantitative framework of a physiologically based pharmacokinetic model is essential for better estimation of the physiological concentration of DEHP metabolites in the target tissues such as gonads. The Reliable Physiologically based Pharmacokinetic (PBPK)

Chapter 2

model will be useful for establishing a suitable dose metric for targeted tissues (Fabrega et al., 2014), and exposure-dose-response relationship for the systems toxicology model (Sharma et al., 2017b, 2018). Since 1974, many pharmacokinetic analyses on DEHP and its metabolites have been conducted both in in-vitro and in-vivo (animal and humans) (Daniel and Bratt, 1974; Peck and Albro, 1982; Albro, 1986; Ito et al., 2005; Wittassek and Angerer, 2008; Choi et al., 2013). Several pharmacokinetic (PK) models have been developed accounting its major metabolites using simple compartmental approach (Koch et al., 2003, 2004, 2005, 2006; Lorber et al., 2010). Koch et al. (2003, 2004, 2005) experimentally examined several DEHP secondary metabolites concentration both in the blood and the urine describing their time course kinetics. A PK model developed by Lorber et al. (2010) has predicted the DEHP metabolites concentration both in the blood and urine which includes empirical fitting of the two key parameter against the experimental data namely; first is the fraction of chemicals available to pass through the metabolism; and the other is the rate of dissipation of these metabolites. However, It lacks the mechanistic metabolic kinetics (Michaelis-Menten reaction), considered the most important biotransformation process. Keys et al. (1999) and Cahill et al. (2003) developed a PBPK model of DEHP in both the rats and human, however, these models have not included all the metabolites and their kinetics, which might be due to insufficient data on the DEHP metabolic kinetics at that time. Recently, Choi et al. (2012) has reported on in vitro metabolic kinetics information on the DEHP and its metabolites both in the rat and human using hepatic cell line. To best of our knowledge, there is no published detailed target tissue dosimetry model (PBPK), which becomes essential for the chemical like DEHP that produces many metabolites (Daniel and Bratt, 1974; Ghosh et al., 2010). The purpose of this study is to develop a detailed PBPK model for the DEHP and its major metabolites for the adult human and its evaluation against the experimental data. A bottom-up modeling approach was used to develop the model. It includes the integration of in vitro metabolic and in silico data which uses IVIVE (in-vitro in-vivo extrapolation) and QSAR (Quantitative structure-activity relationship) tools. These tools led to creation of a PBPK model with minimal or no animal experiments, supporting the 3Rs strategies of minimizing the use of animal. An IVIVE tool has been successfully used in connection with a PBPK to derive the in-vivo kinetics from the in vitro studies using biologically appropriate scaling (Yoon et al., 2014; Martin et al., 2015). This work is part of two major EU projects, HEALS and EuroMix, where different aspects of in silico models and its applications in human biomonitoring are investigated (Martínez et al., 2017, 2018).

This article describes the physiologically based pharmacokinetic (PBPK) model that predicts the time variant concentrations of DEHP metabolites such as MEHP 5-OH MEHP, 5-cx MEPP, and 5-oxo MEHP in plasma upon oral dosing of DEHP. The model was used to simulate the cumulative amount of the DEHP metabolites in urine. The in vitro human gut and hepatocyte DEHP metabolic kinetics data were scaled and integrated into the model (Choi et al., 2013). Experimentally observed human DEHP metabolites concentration both in the plasma and the urine are used to calibrate the PBPK model. Further model was evaluated against the independent data on DEHP kinetics for different

dosing scenarios (Anderson et al., 2011). Prior mean parameter values were obtained from the published literature or derived from the in-vitro and in-silico experiments, whilst accounting for uncertainties in the range of± 1 to ± 1.5 standard deviation. After sensitivity analysis the most uncertain parameter yet influential parameters were distributed statistically for Monte Carlo simulations.

2. Models and Methods

2.1 Overview of the modeling approach

The model was coded as a set of ordinary differential equations, written in the GNU MCSim modeling language and solved by numerical integration using the R "deSolve" package (Bois and Maszle, 1997). Model parameters values were derived from in vitro and in-vivo experiments reported in the literature or using the in-silico approach. Sensitivity analysis of the model was done using the mean value of the parameters. After sensitivity analysis, the most uncertain yet influential parameters were distributed statistically for Monte Carlo simulations to estimate the impact on model predictions of uncertainty in all of the selected parameters (Bois et al., 2010; Fàbrega et al., 2016). Model equations are provided in Annex 2.

The exchange of the chemicals between blood and tissue in each organ is described by flow limited processes i.e. we implement a perfusion rate-limited PBPK model (not permeability limited). The model comprises several compartments i.e. gut, liver, blood, fat, gonad and a compartment representing the rest of the body (Fig. 1). The gonad compartment was included in the model for its later use in DEHP reproductive toxicity assessment. The only metabolite MEHP was distributed to the given compartments, while other metabolites were confined to the blood compartment presuming their volume of distribution is equivalent to the plasma volume. All physiological parameters such as blood flows and tissue volumes used in the model were obtained from the published literature and are provided in Table A.1 of Annex 2. The partition coefficients and fractional unbound were obtained from the in-silico approach or literature are provided in Table 1. The calibration of the model was carried out against the human pharmacokinetic experimental data on both the plasma and the urine level of DEHP metabolites reported in Koch et al. (2004, 2005). This involves the plasma concentration data during the first 8 h and the cumulative amount of metabolites in urine over 44 h following an oral dosing of 48.5 mg. Further evaluation of the developed PBPK model was done against the other independent pharmacokinetics study done by Anderson et al. (2011) for two different dosing scenarios. In this study, all major metabolites are considered namely; MEHP, 5-OH MEHP, 5-CX MEPP, 5-Oxo MEHP and phthalic acid. All the metabolic parameters were derived from in vitro cell line study are provided in Table 1.

Chapter 2

2.2. Pharmacokinetics of DEHP and its Metabolites

The rate of metabolite formation is assumed to be equal to the rate of parent compound metabolism. DEHP metabolic pathway is provided in Fig. 2. DEHP metabolizes to MEHP, which metabolizes into different chemical forms such as 5-OH MEHP, 5cx-MEPP, and 2cx-MEPP. Among them, 5-OH MEHP further metabolizes into 5-Oxo MEHP. All the metabolites excrete via urine. Absorption of DEHP from the gut to the liver was described by partition coefficient. Both DEHP and MEHP distributed to compartments such as liver, fat, plasma and gonads. However, due to inadequate data on the partition coefficients for metabolites other than MEHP, their distribution limited to the plasma compartment. And the volume of distribution of these metabolites has set equal to the plasma volume.

Absorption

Koch et al. (2005) in his study reported that DEHP is completely absorbed from the gut and rapidly metabolized into the MEHP in the liver. The distribution of DEHP from the gut to the plasma is described by its partition coefficient between them. The partition coefficient (gut: plasma) was estimated using QSAR approach of Poulin and Krishnan tissue composition method (Poulin and Krishnan, 1996, 1995; Poulin and Theil, 2000). The MEHP uptake from the gut the liver was described by the first order rate constant (Adachi et al., 2015).

Chapter 2

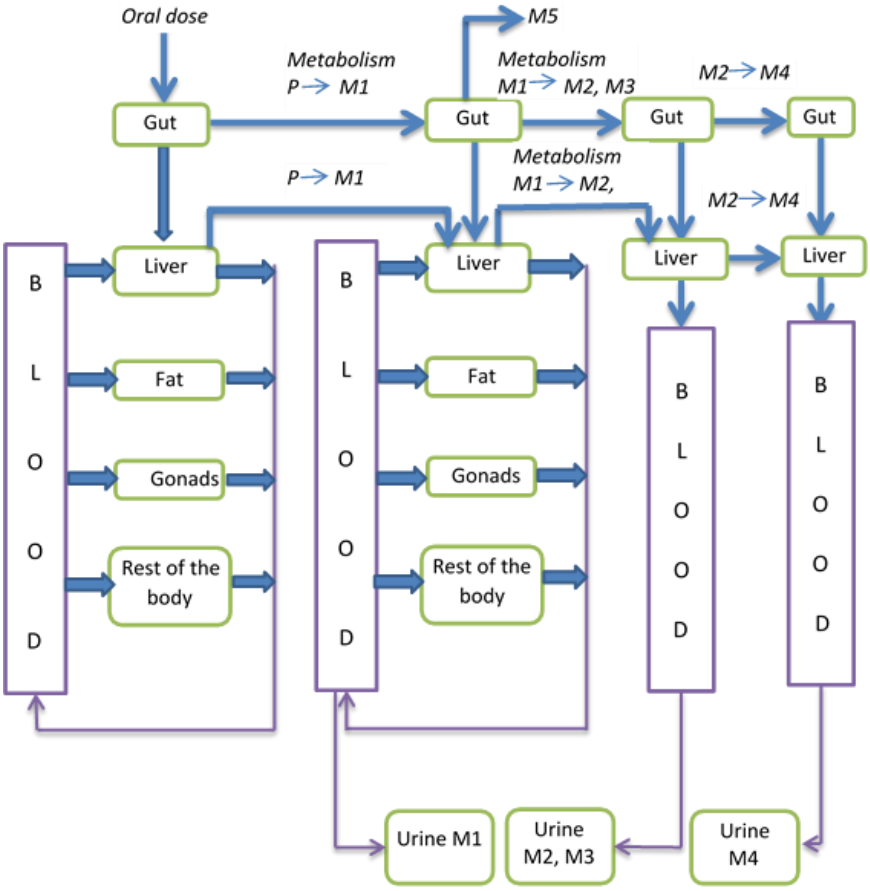

Fig. 1. The figure represents a PBPK model for the DEHP and its metabolites. It includes mainly five compartments and clearance of chemical depends on both metabolism (mainly five metabolites) and urinary elimination. Following oral administration of DEHP (P), it readily metabolizes into MEHP (M1) and MEHP further metabolizes into 5-OH MEHP (M2), 5-cx MEPP (M3) and phthalic acid (M5). 5-OH MEHP (M2) is further metabolizing into 5-oxo MEHP (M4), for detail metabolic scheme refers to Fig. 2. The DEHP and MEHP are distributed to the given compartments. However other metabolites produced in guts and liver are transferred to blood compartments assuming their distribution in a single compartment. The metabolite phthalic acid (M5) was not utilized in this model for its further distribution to blood or its elimination (except for MEHP clearance, metabolic conversion to M5), as no data are available to calibrate its concentration in urine or blood.

Distribution

DEHP and MEHP was distributed to the several compartments using their partition coefficients estimated by in-silico or derived from the published literature and are provided in Table 2. DEHP partition coefficients were estimated using the QSAR approach based on tissue composition method (Poulin and Krishnan, 1996, 1995; Poulin

and Theil, 2000). A log ko/w of 7.6 was used to estimate the tissue: plasma partition coefficients. The MEHP partition coefficient values which was experimentally determined through vial –equilibration method by Keys et al. (2000) was used for the tissue distribution. Other metabolites distributions restricted to the blood compartment only, assuming their volume of distribution equivalent to the plasma volume. The metabolites formed in the liver transfer to the blood using first order uptake rate constants and these parameters were calibrated against the Koch et al. (2005) experimental data.

Elimination

Elimination of DEHP and its metabolites in urine was assumed to be directly proportional to its rate of clearance from the plasma. The model presumed that DEHP clearance solely depends on its metabolism into MEHP (Koch et al., 2004, 2005, 2006; Lorber et al., 2010).

The excretion rates for the MEHP and other metabolites were described by first-order rate equation. These excretion rates were obtained by using the relationship between the elimination rate constant and the chemical's plasma half-life i.e. ratio of ln2 (0.693)/t1/2 (half-life). The mean half-lives for MEHP, 5-OH MEHP and 5-CX MEPP and 5-oxo MEHP was estimated by Lorber et al. (2010) was used for the model parameterization. These parameters values were used for the model simulation and calibration against the reported time course concentration of chemicals in the plasma and cumulative excretion profile in the urine reported (Koch et al., 2005). The elimination rate constant for MEHP was measured using half-life reported by Mittermeier et al. (2016).

2.3. **In vitro intestinal and Hepatocyte metabolic studies**

Metabolism of the DEHP both in the liver and gut to MEHP, 5-OH MEHP, 5oxo-MEHP, 5cx MEPP and phthalic acid was described by the Michaelis Menten equation provided in Eq. (2). This equation includes two important parameters namely Vmax (maximum velocity of metabolic reaction) and Km (affinity i.e. concentration at which reactions occurs at the half maximal rate). The in vitro intestinal and hepatic metabolic rates for several DEHP metabolites were reported in Choi et al. (2012) where the author has described mainly five metabolites (MEHP, 5-OH MEHP, 5oxo-MEHP, 5cx MEPP and phthalic acid) kinetic both in the microsomal and cytosol fraction of the intestine and the liver. A high intrinsic clearance rate i.e. ratio between Vmax and Km for the metabolic conversion of DEHP to MEHP in the cytosolic fraction of intestine and liver was observed (Choi et al., 2012). However, intrinsic clearance for other metabolites in cytosolic fraction was reported to be insignificant. The in-vitro in-vivo extrapolation (IVIVE) method, which involves scaling of in vitro Vmax value to in vivo utilizes physiological specific parameters such as tissue-specific microsomal protein content or cytosol protein, specific tissue volume and, body weight (Yoon et al., 2014) was used to derive the metabolic parameters. The Eq. (1) describes the scaling approach which is used to derive the Vmax value as an input for the PBPK model. The Michaelis constant i.e. Km for the five metabolites in the gut and liver were set equal to the reported in-vitro cell line study provided in Table 1. The reported Vmax in-vitro values the maximum rate of reaction, were scaled to the whole body PBPK using Eq. (1). The reported quantity of MSP in the liver, and the gut is 52.5 mg/g liver and 20.6 mg/g intestine respectively (Cubitt et al., 2011). Mean value of 80.7 mg and 18 mg of cytosolic protein per gram of the liver and

the gut respectively are used for the IVIVE approach. In-vivo scaled Vmax values for each metabolite are provided in Table 2. The schema of metabolism is provided in Fig. 2.

$$Vmax(intestine/liver) = (Vmax_{invitro\ intestine/liver} * MPPGG/MPPGL/ CytosolPGG/CytosolPGL * Vgut/Vliver)/BW^{.75}$$

Eq. (1)

Where,
Vmax is the maximum rate reactions value in the unit of µg/hr/kgBW$^{.75}$; MPPGG is the microsomal protein per gram of gut; MPPGL is the microsomal protein per gram of liver; CytosolPGG is the cytosolic protein per gram of gut; CytosolPGL is the cytosolic protein per gram of liver
Vgut and Vliver is the volume of gut and liver respectively

$$\frac{dA_{mets}}{dt} = \frac{Vmax * C_t * f_u}{km + C_t * f_u}$$

Eq. (2)

Where,
Ct is the corresponding concentration in tissue and fu is the fraction unbound constant.
Vmax (µg/hr/whole body weight) is the maximum rate for the corresponding reactions; Km is the affinity constant concentration at which half of the Vmax occurs.
$\frac{dA_{mets}}{dt}$ is the rate of production of metabolites

Metabolic pathway

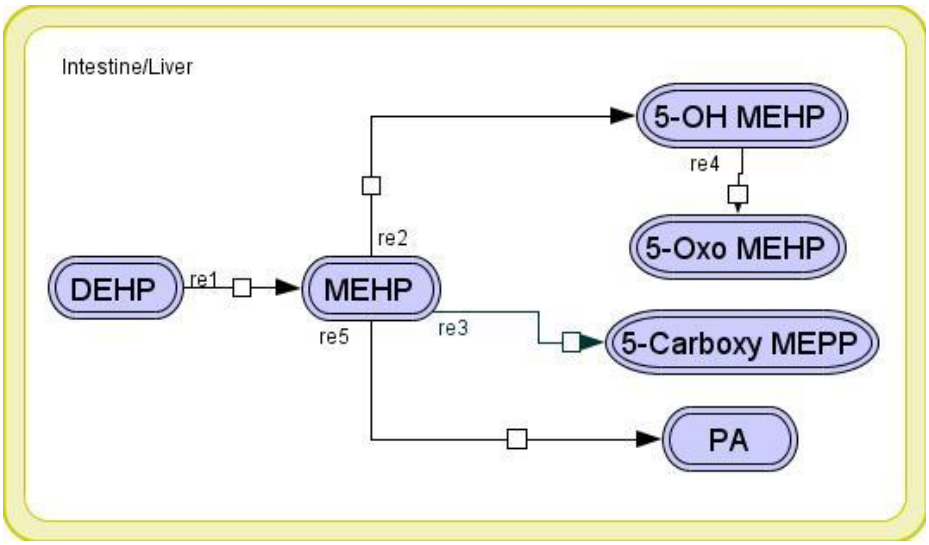

Fig. 2. Represent the schematic metabolic pathway of DEHP in the human gut and liver. The productions of metabolites follow same structure in PBPK and were described using

Chapter 2

Michaelis Menten equation. The corresponding re1, re2, re3, re4, and re5 represent the Michaelis-Menten metabolic reaction used in the model represented in the Eq. (2).

2.4. In vivo Human Pharmacokinetics study

In-vivo pharmacokinetics of DEHP and its metabolites are well characterized in several studies (Koch et al., 2006, 2005, 2004; Anderson et al., 2011; Lorber et al., 2010). Koch et al. (2004, 2005) studies involved the self-dosing of 48.5 mg of D4-DEHP by volunteer (n = 1). The volunteer aged 61, 175 cm tall and weighing 75 kg. Plasma concentrations for MEHP, 5−OH MEHP, 5-oxo MEHP and 5-Cx MEPP were measured at 2,4, 6 and 8.3 h upon DEHP self-dosing. In the same study, urine samples were collected until 44 h and the cumulative amount of DEHP metabolites were reported. This study was accounted for the model calibration. Koch et al. (2005) monitored two metabolites namely 5-cx MEPP and 2cx MMHP in both plasma and urine. Koch et al. (2005) found 5−OH MEHP and 5-cx MEPP as major metabolites in the urine and observed no dose-dependency. The 5-cx MEPP metabolite was not included in the current model since there is no data on its metabolic kinetics (rate of production).

Anderson et al. (2011) analyzed DEHP pharmacokinetics in urine. For this analysis, two scenarios were considered: one at the high dose of 2.8 mg D4-DEHP and second at a low dose of 0.31 mg D4-DEHP. This pharmacokinetics study included 20 volunteers (10 males and 10 females) of following characteristics aged greater than 18 years, BMI between 19 and 32 kg/m2 and body weight greater than 60 kg. The cumulative amount of DEHP metabolites concentration in urine was reported as a percentage of mole dosing. The cumulative DEHP metabolites urine data were used for evaluation of the developed model keeping all the model's parameters same except subject body characteristics such as BW and BMI.

2.5. Sensitivity analysis

A Local sensitivity analysis was carried out for the PBPK model. The R package FME was used, which measures the alteration in model output for variable of interest by changing each parameter by 1 percentage up and down whilst keeping other ones constant. Detailed information about the functions of FME can be found in Soetaert and Petzoldt, (2010).

$$Si,j = \frac{\partial yj}{\partial pi} * \frac{V_{pi}}{V_{yj}}$$

Where,

Si,j is the sensitivity of parameter i for model variable j and is normalized and dimensionless. yj is a model output variable (DEHP Metabolites time-plasma concentration profile) , pi is parameters involved in PBPK model, V_{pi} is the scaling of parameters pi and V_{yj} is the scaling of variable yj.

These sensitivity functions collapsed into a summary of sensitivity values, which includes L1 norm, L2 norm, Mean, Min and Max. The magnitude of the time-averaged sensitivity values were used to rank the parameters.

Where $L1 = \sum \frac{|Sij|}{n}$ and $L2 = \sqrt{\sum \frac{(S_{ij}^2)}{n}}$

2.6. Model parameters

Human physiological data, in vitro data and QSAR estimates, were used for the parameterization of the model. Only Pharmacokinetic specific parameters such as partition coefficients, metabolisms and elimination rate constant are selected for uncertainty analysis. Prior mean parameter values were obtained from in-silico, in-vitro and in-vivo experiments reported in the literature. The model parameters value is provided in Table 1. The model parameters are distributed lognormal in the range of ± 1 to ± 1.5 standard deviations accounting uncertainty on model predictions. Monte Carlo simulations were performed to estimate the uncertainty produced by sampling one random value (out of its assigned distribution) for each selected parameter. The model was then run and its outputs (predictions) recorded. These two steps were iterated 20,000 times, and the collected output values formed a random sample, for with we computed the mean, the SD, and any percentile of interest.

Table 1. DEHP parameter values and statistical distributions

Parameters	**Symbols**	**Units**	**Values or distributions**	**References**
Molecular weight (DEHP)	*MW*	g/mole	391	-
Molecular weight (D4-MEHP)	*MW*	g/mole	281	Anderson et al., (2011)
Molecular weight (MEHP-OH)	*MW*	g/mole	297	Anderson et al., (2011)
Molecular weight (D4-5-oxo MEHP)	*MW*	g/mole	295	Anderson et al., (2011)
Molecular weight (D4-5-cx MEPP)	*MW*	g/mole	311	Anderson et al., (2011)
Octanol:water partition coefficient	*LogKo:w*	-	7.60 [a]	-
Partition coefficients				

Chapter 2

Gut/Plasma	K_gut_plasma		*LN* (12.86, 1.1) [b]	-
Liver /Plasma	K_liver_plasma	-	*LN* (10.16, 1.1) [b]	-
Gonads/Plasma	K_gonads_plasma	-	*LN* (6.5, 1.1) [b]	-
Fat/Plasma	K_fat_plasma	-	*LN* (188, 1.1) [b]	-
Rest of the body/Plasma	K_restbody_plasma	-	*LN* (6.24, 1.1) [b*]	-
Liver/ Plasma	K_liver_plasmaM1	-	*LN* (1.7, 1.1)	(Keys et al., 2000)
Gonads/Plasma	K_gonads_plasmaM1	-	*LN* (0.6, 1.1)	(Keys et al., 2000)
Fat/Plasma	K_fat_plasmaM1	-	*LN* (0.12, 1.1)	(Keys et al., 2000)
Rest of the body/Plasma	K_restbody_plasmaM1	-	*LN* (0.38, 1.1)	Set to slow perfused organ (muscle) (Keys et al., 1999)
Uptake rate of 5-OHMEHP to blood	K_{tM2}	1/h	*LN* (.07, 1.5)	Optimzed against data of koch et al.,(2003, 2005)
Uptake rate of 5-oxo MEHP to the blood	K_{tM4}	1/h	*LN* (0.08, 1.5)	Optimized against data koch et al.,(2003, 2005)
Absorption and elimination parameters				
Unbound fraction in plasma for MEHP	fup	-	0.007	(Adachi et al., 2015)
Oral absorption rate	Kgut	1/h	*LN* (7, 1.5)	(Adachi et al., 2015)

Chapter 2

Elimination rate constant (M1)	KurineM1	1/h	*LN* (0.35, 1.1) [c]	Calculated
Elimination rate constant (M2)	KurineM2	1/h	*LN* (0.69, 1.1) [c]	Calculated
Elimination rate constant (M3)	KurineM3	1/h	*LN* (0.69, 1.1) [c]	Calculated
Elimination rate constant (M4)	KurineM4	1/h	*LN* (3.47, 1.1) [c]	Calculated
Metabolic parameters for DEHP and its metabolites in gut				
DEHP to MEHP in intestinal MSP maximum reaction value	Vmaxgut M1	µg/min/ mg MSP	LN (0.11,1.1)[d]	(Choi et al., 2013)
Conc. at half maximum value	KmgutM1	µg/L	6956	(Choi et al., 2013)
DEHP to MEHP in gut cytosol maximum reaction value	Vmaxgut M1cyt_in vitro	µg/min/ mg cytosol	LN (0.312, 1.1) [d]	(Choi et al., 2013)
Conc. at half maximum value	Kmgut_cytM1	µg/L	7038	(Choi et al., 2013)
MEHP to 5-OH MEHP maximum reaction value	Vmaxgut M2_invitro	µg/min/ mg MSP	LN (0.0012, 1.1) [d]	(Choi et al., 2013)
Conc. at half maximum value	KmgutM2	µg/L	22508	(Choi et al., 2013)
MEHP to 5-carboxy MEPP maximum reaction value	Vmaxgut M3_invitro	µg/min/ mg MSP	0	(Choi et al., 2013)
Conc. at half maximum value	KmgutM3	µg/L	0	(Choi et al., 2013)
MEHP-OH to 5-oxo MEHP maximum reaction value	Vmaxgut M4_invitro	µg/min/ mg MSP	LN (0.0012, 1.5) [d]	(Choi et al., 2013)

Chapter 2

Conc. at half maximum value	KmgutM4	µg/L	219076	(Choi et al., 2013)
MEHP to phthalic acid maximum reaction value	Vmaxgut M5_invitr o	µg/min/ mg MSP	LN (0.285, 1.1) [d]	(Choi et al., 2013)
Conc. at half maximum value	KmgutM5	µg/L	187652	(Choi et al., 2013)
Metabolic parameters for DEHP and its metabolites in liver				
DEHP to MEHP in liver MSP maximum reaction value	Vmaxliv M1	µg/min/ mg MSP	LN (0.112, 1.1) [d]	(Choi et al., 2013)
Conc. at half maximum value	KmlivM1	µg/L	11847.3	(Choi et al., 2013)
DEHP to MEHP in liver cytosol maximum reaction value	Vmaxliv M1cyt_in vitro	µg/min/ mg cytosol	LN (0.036, 1.1) [d]	(Choi et al., 2013)
Conc. at half maximum value	Kmliv_cyt M1	µg/L	2228.7	(Choi et al., 2013)
MEHP to 5-OH MEHP maximum reaction value	Vmaxliv M2_invitr o	µg/min/ mg MSP	LN (0.172, 1.1) [d]	(Choi et al., 2013)
Conc. at half maximum value	KmlivM2	µg/L	7980.4	(Choi et al., 2013)
MEHP to 5-carboxy MEPP maximum reaction value	Vmaxliv M3_invitr o	µg/min/ mg MSP	LN (0.0023, 1.5) [d]	(Choi et al., 2013)
Conc. at half maximum value	KmlivM3	µg/L	1124	(Choi et al., 2013)
MEHP-OH to 5-oxo MEHP maximum reaction value	Vmaxliv M4_invitr o	µg/min/ mg MSP	LN (0.003, 1.1) [d]	(Choi et al., 2013)

Conc. at half maximum value	KmlivM4	µg/L	23,117.7	(Choi et al., 2013)
MEHP to phthalic acid maximum reaction value	Vmaxliv M5_invitr o	µg/min/ mg MSP	LN (0.088, 1.1) [d]	(Choi et al., 2013)
Conc. at half maximum value	KmlivM5	µg/L	141315	(Choi et al., 2013)

a = value taken form PubChem
b = partition coefficient calculated based on tissue composition method using (Poulin and Krishnan, 1996, 1995; Poulin and Theil, 2000)
c = value is first estimated applying the following relationship i.e. elimination rate constant = 0.693/$t_{1/2}$
d = parameters value needs to scale to whole body weight prior to use in model

3. Results and Discussions

In this study, parameters such as partition coefficient, biochemical (metabolism), absorption, elimination as an input and target variables such as DEHP metabolites concentration as a model output, were considered to conduct sensitivity analysis and uncertainty analysis. The bottom- up approach was used to develop the PBPK model and all necessary parameters were derived from in-silico (QSAR), in vitro (metabolism) and published literature. The results are described and discussed in the following subsection.

3.1. Sensitivity analysis results

The local sensitivity analysis was carried out for all the kinetic parameters that were used in the development of the PBPK model. Human physiological parameters were included neither in the Monte Carlo model nor in the sensitivity analysis in view of their inherent variability. The sensitivity coefficient of parameters was estimated using the R FME package (Soetaert and Petzoldt, 2010) (described in Section 2.5), which uses the initial parameter value with allowable relative changes in that parameter, taking the parameters one by one. The results are provided in Table 2. It includes L1 and L2, norm, mean, minimum, maximum, and ranking. The table summarizes the statistics of the normalized and dimensionless parameter sensitivity results. The parameters were ranked based on the L1 value. A higher value of L1 signifies a higher sensitivity of the model output to changes in the parameter. The biochemical parameters such as V_{max} and K_m value have very close sensitivity coefficient. The mean sensitivity coefficient of V_{max} has the negative

Chapter 2

effect and the K_m has the positive effect on the model output. Hence in uncertainty analysis, instead of both Vmax and Km, only Vmax was distributed statistically as result of sensitivity shows that they are highly correlated with each other. The VmaxliverM2 (metabolism of MEHP to MEHP−OH) is the most sensitive parameter (Rank 1) following partition coefficient of liver: plasma (Rank 3). The partition coefficient for the rest of the body and the metabolism of DEHP in the cytosol fraction of both gut and liver are under the rank of 10 which shows their high sensitivity compared to other parameters. The plots for sensitive analysis output i.e. mean sensitivity coefficient are provided in Fig. A.1 (Annex 2). The summary statistics tables of parameters' sensitivities for the output of DEHP metabolites concentration in plasma is provided in Tables A.5–A.8 (Annex 2).

Table 2. Summary statistics of parameters' sensitivities

Parameters	L1	L2	Mean	Min	Max	Rank
VmaxliverM2	0.61	0.01	-0.45	-3.40	1.00	1
KmliverM2	0.60	0.01	0.44	-1.00	3.39	2
K_liver_plasma	0.57	0.01	-0.57	-2.08	0.00	3
VmaxliverM4	0.43	0.01	-0.36	-3.63	0.99	4
KmliverM4	0.38	0.01	0.32	-0.99	3.39	5
K_restbody_plasma	0.32	0.01	0.27	-0.92	3.85	6
Vmaxgut_cytM1	0.30	0.00	-0.29	-8.86	0.54	7
K_liver_plasmaM1	0.29	0.00	-0.14	-1.00	0.40	8
Vmaxliver_cytM1	0.21	0.00	-0.21	-3.09	0.12	9
Kmliver_cytM1	0.20	0.00	0.20	-0.12	3.04	10
VmaxliverM3	0.19	0.00	0.08	-0.32	1.00	11
KmliverM3	0.18	0.00	-0.07	-1.00	0.32	12
KurineM3	0.17	0.00	-0.15	-2.79	1.00	13
KtM2	0.17	0.00	0.05	-0.67	1.00	14
KtM4	0.15	0.00	0.15	0.00	1.00	15
Kmgut_cytM1	0.15	0.00	0.15	-0.30	6.45	16
KurineM2	0.15	0.00	-0.13	-2.20	1.00	17

Chapter 2

KurineM1	0.13	0.00	-0.03	-0.47	1.00	18
VmaxgutM1	0.12	0.00	-0.12	-3.57	0.22	19
KurineM4	0.10	0.00	-0.09	-1.13	0.98	20
K_restbody_plasmaM1	0.09	0.00	-0.08	-0.71	0.20	21
VmaxliverM1	0.08	0.00	-0.08	-1.18	0.05	22
KmliverM1	0.08	0.00	0.08	-0.05	1.17	23
kmgutM1	0.06	0.00	0.06	-0.12	2.59	24
k_gut_plasma	0.05	0.00	0.05	0.00	0.37	25
k_gonads_plasma	0.04	0.00	0.04	-0.04	1.59	26
VmaxgutM2	0.03	0.00	0.03	-0.05	1.00	27
KmgutM2	0.03	0.00	-0.03	-1.00	0.00	28
Vplasmad	0.03	0.00	-0.03	-1.00	0.00	29
KmliverM5	0.02	0.00	0.02	-0.06	0.10	30
VmaxliverM5	0.02	0.00	-0.02	-0.10	0.03	31
K_fat_plasmaM1	0.02	0.00	0.00	-0.10	0.74	32
K_fat_plasma	0.01	0.00	-0.01	-0.23	0.08	33
K_gonads_plasmaM1	0.01	0.00	0.01	-0.02	0.66	34
VmaxgutM5	0.00	0.00	0.00	-0.03	0.03	35
KmgutM5	0.00	0.00	0.00	-0.01	0.03	36
VmaxgutM4	0.00	0.00	0.00	0.00	0.01	37
KmgutM4	0.00	0.00	0.00	-0.01	0.00	38

Table 2: Sensitivity results for both the rat and human PBPK model. It includes L1 and L2 norm, mean, minimum, maximum, and ranking. Ranking of parameter sensitivity coefficient was done based on L1 norm.

3.2. PBPK model calibration results and its evaluation with independent data

The time course of DEHP metabolites concentration in plasma and the cumulative amount in urine were predicted at the median, 2.5 and 97.5 percentiles and 20 random predictions.

Chapter 2

PBPK model has accounted the parameter statistical distribution followed by sampling one random value (out of its assigned distribution) and performing Monte Carlo simulation reflecting uncertainty in the model. The model does not include any variability factor related to physiological parameters. For the metabolic uncertainties, only Vmax values were statistically distributed but not Km considering that they are highly correlated with each other. Single oral dose of 48.5 mg DEHP as an input and the observed concentration of metabolites both in the blood and urine as an output were used to calibrate the model. Most of the parameters were derived via either from in-silico (estimation of the partition coefficient) (Poulin and Krishnan, 1996, 1995; Poulin and Theil, 2000) or from in vitro such as, partition coefficient determined (Keys et al., 2000) and in vitro metabolic data (human hepatocyte and intestinal cell line) (Choi et al., 2013). The parameters such as elimination rate constants for the metabolites are derived using a mathematical relationship described in models and methods section. The absorption rates of metabolites (mass transfer) from the gut to the liver were set as one (complete mass transfer) except MEHP whose absorption rate constant was derived from the literature (Adachi et al., 2015). The mass transfer rate of metabolites from the liver to the blood was calibrated against the observed data (Koch et al., 2005). The model was developed using the parameters derived from in-silico, in vitro data, and previously published literature, and certain default parameter values, which needed to be calibrate. Instead of optimizing all the parameters very specifically to get a point to point prediction against the observed data rather we statistically distributed all the parameters in a range of 1–1.5 ± SD (standard deviation) providing range of predictions. Then the model was verified against the blood and urine metabolites concentration data reported by Koch et al. (2005), so that observed data for all metabolites fall within the range (2.5th –97.5th) of model predictions. The predictions of the DEHP metabolites concentration in blood and urine included their metabolic kinetics both in the gut and the liver described by Michaelis Menten equation. And the parameters such as Vmax and Km were estimated in vitro by Choi et al. (2013) were scaled to the whole body (based on organ weight) and integrated into the model. Fig. 3(a–d) represents the PBPK model predictions for plasma concentrations of four DEHP metabolites. It can be observed that the model predictions agree quite closely to the observed data. The cumulative excretion of DEHP metabolites is also adequately predicted by the model represented in Fig. 4(a–d) and Table 2. The recently reported in vitro metabolism data shows that the production rate of MEHP from the DEHP is very high (Choi et al., 2013). A similar trend of the kinetic profile was also reported by Koch et al. (2005) where he observed very low or undetectable DEHP blood concentration. Given the above facts, the clearance of DEHP is presumed to completely depend on its metabolic conversion to MEHP. The Fig. 3(a) shows that predicted Cmax (highest chemical plasma concentration) of the MEHP is slightly lower than the observed data even at 97.5 percentile simulation. However, the time course trend of chemical concentrations in plasma is similar to the observed data points. In addition to that, post-Cmax, the predictability of the model are in close agreement with the observed points. The clearance of MEHP from the body includes both its metabolism and the urinary elimination.

Fig. 3(b) represents the model predictions for MEHP−OH concentrations in blood at 2.5, 50 (median) and 97.5th percentiles including 20 random simulations, and the observed data in green dots. The blood Cmax value for 5−OH MEHP is lower than MEHP and 5-Cx MEPP and more than its metabolite 5-oxo MEHP. The observed data points at the terminal elimination are predicted at the lower boundary of the model, where almost all

chemicals are eliminated. All the observed blood data points are within the range of the model prediction (2.5, 50 and 97.5th percentiles). The observed production rate of 5−OH MEHP in gut and liver i.e. in vitro metabolism data (Vmax) is higher than the other metabolites (Choi et al., 2013). However, reported blood concentration by Koch et al. (2005) is less than 5-Cx MEPP, another metabolite. The reason for its lower blood plasma concentration is might be due to its higher volume of distribution than the other metabolites, the similar observation was noted previously by Lorber et al. (2010) during the calibration of the model. The other reasons might be its higher clearance to the urine and its further metabolism to 5-oxo MEHP. The production of 5−OH MEHP depends on the MEHP concentration in both the liver and the gut, and then its distribution to the blood. The transfer of 5−OH MEHP from the liver to blood was done using first order rate constant and is calibrated against the observed data. 5−OH MEHP clearance was done based on both its metabolism to the 5-oxo MEHP and the urinary elimination. The urinary elimination was described using first order using first order rate constant.

Similarly, PBPK model predictions for 5-cx MEPP plasma concentrations as shown in Fig. 3(c), which is the metabolite of MEHP, appears to be in close agreement with the observed data points. The volume of distribution (Vd) was confined to the plasma compartment volume since the distribution of the compound is unknown. The production of 5-cx MEPP metabolite from the MEHP in the gut was reported to be null in the in vitro experiment (Choi et al., 2013). So, the concentration of 5-oxo MEPP only depends on its production in the liver from the MEHP. Its clearance was described using first order rate constant from the blood to urine.

The model predictions for 5-oxo MEHP plasma concentrations as shown in Fig. 3(d), results from metabolism of 5−OH MEHP in both gut and liver, are in close agreements with the observed concentrations. All the observed data points are in compliance with the predicted range of percentile. Its production in gut and liver from the 5−OH MEHP is described using Michaelis Menten reaction. Its volume of distribution is confined to a single compartment of plasma volume. The urinary elimination was described using first order elimination rate from the systemic circulation.

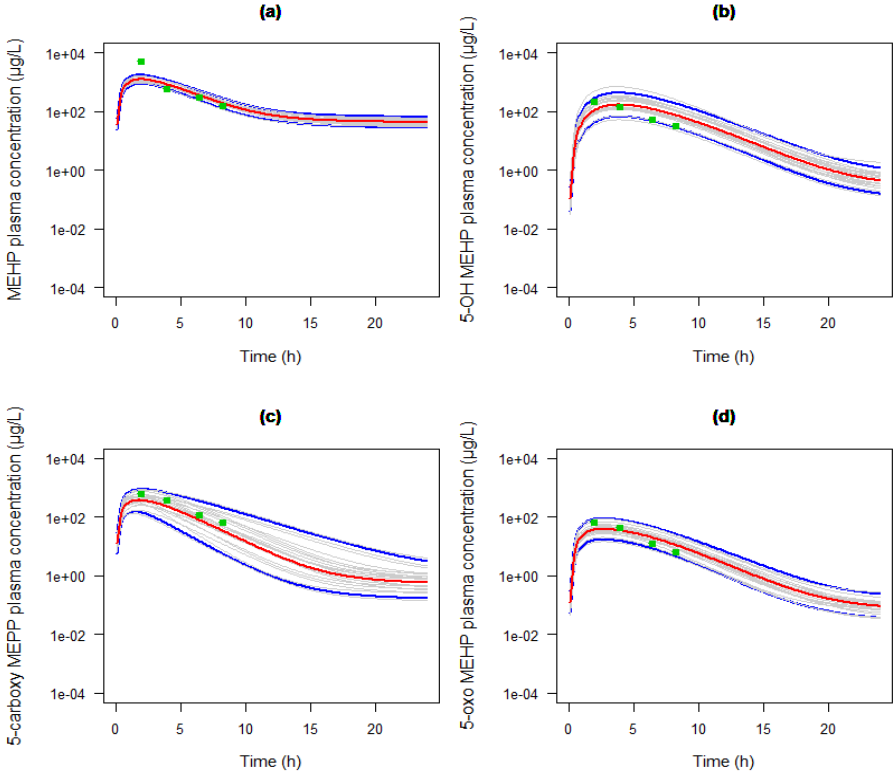

Fig. 3. PBPK model prediction of DEHP metabolites plasma concentrations upon 48.5 mg oral dosing in human. Red lines: median predictions; blue lines: 2.5 and 97.5 percentiles; gray lines: 20 random simulations. (a) Represents MEHP plasma concentration. (b) Represents 5-hyroxy MEHP plasma concentration. (c) Represents 5-carboxy MEPP plasma concentration. (d) Represents 5-oxo MEHP plasma concentration. The green dotes indicate the observed concentrations reported in (Lorber et al., 2010). Dose unit is converted to microgram prior to use as an input for the model.

The four metabolites' blood concentrations are not only in close agreement with the observed data points but also captured the time course profile. The Fig. 4(a–d), presented PBPK prediction of the cumulative amount (µg) urinary excretion of four metabolites for 44h at median, 2.5 and 97.5 percentiles and for 20 random simulations. The simulated urinary amount of DEHP metabolites (cumulative amount) are also in compliance with the experimentally observed cumulative amount (Koch et al., 2005), results are provided in Table 2. It also summarizes the predicted vs observed metabolites elimination as a percent of applied dose in mole for three dosing scenarios based on Koch et al. (2005) study. The observed metabolites as a percentage of mole doses are within the range of predictions of the model not only for high dose (use for calibration) but also for other two independent dosing scenarios such as medium (2.15 mg) and low dose (0.35 mg).

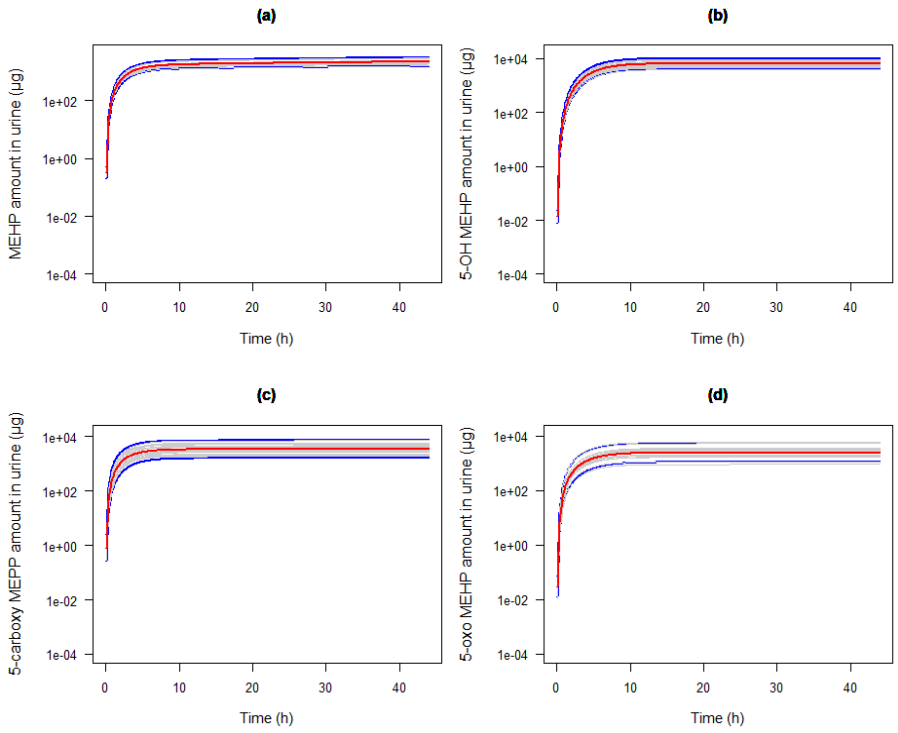

Fig. 4. PBPK model predictions of DEHP metabolites amount in urine following 48.5 mg oral dose. Red lines: median predictions; blue lines: 2.5 and 97.5 percentiles; gray lines: 20 random simulations. (a) Represents MEHP cumulative amount (µg) in urine. (b) Represents 5-hyroxy MEHP cumulative amount (µg) in urine. (c) Represents 5-carboxy MEPP cumulative amount (µg) in urine. (d) Represents 5-oxo MEHP cumulative amount (µg) in urine. Dose unit is converted to microgram prior to use as an input for the PBPK model.

Table 3. Observed and PBPK predicted amount of DEHP (µg) metabolites in urine

	Cumulative amount of Metabolites (µg) of the D4-DEHP in urine					
Study involved	**Dose**	**MEHP**	**5OH-MEHP**	**5cx-MEPP**	**5oxo-MEHP**	**Total dose in µg or percent**
Koch et al., (2005) [a]	48,500	2500	9000	7500	5000	23500

Chapter 2

Present study **2.5th - 97.5th (median)**	48,500	1548.2-3122.7 (2230.5)	3988.6-10148 (6511)	1585.4-7086 (3397)	1087-5497 (2432)	8209.2-25853.7 (14570.5)
Metabolites of the D4-DEHP Dose as percent of applied dose (mol)						
Koch et al., (2005)	48,500	7.3	24.1	20.7	14.6	66.7 %
Present study **2.5th - 97.5th (median)**	48,500	4.4-8.9 (6.4)	10.8-27.5 (17.6)	4.1-18.3 (8.8)	3.0-15.0 (6.6)	22.3-69.7 (39.44) %
Koch et al., (2005)	2,150	4.3	22.7	19.4	13.0	59.4 %
Present study **2.5th - 97.5th (median)**	2,150	4.3-8.7 (6.2)	8.9-23.3 (14.6)	4.3-19.0 (9.2)	3.02-15.3 (6.7)	20.52-66.3 (36.7) %
Koch et al., (2005)	350	6.2	23.1	15.5	17.3	62.1 %
Present study **2.5th - 97.5th (median)**	350	4.3-8.7 (6.2)	8.8-23.2 (14.5)	4.3-19.0 (9.2)	3.1-15.3 (6.8)	20.5-66.2 (36.7) %

a = values are extracted from the graph presented in manuscript by Koch et al., (2005)
Dose unit is converted to microgram prior to use as an input for the PBPK model.

Chapter 2

Given that the model predictions fit the DEHP metabolites namely MEHP and other metabolites 5−OH MEHP, 5-cx MEPP and 5-oxo MEHP concentration in the blood and urine upon 48.5 mg of a single oral dose of DEHP. The structure of the model and the model parameters remained unchanged from their calibrated values, and the predicted percentage mole elimination data for four metabolites in urine were compared with the data reported in Anderson et al. (2011) for the evaluation of model credibility. The study included 20 subjects, 10 male, and 10 female, and their overall mean body weight was 74.8 kg. The only additional change in the model is subject body weight. The present model does not include gender variability among 20 subjects, and the mean body weight was taken as an input for model simulation, as current model only accounted for the parametric uncertainty, not the variability. Two dosing scenarios namely high dose; a single oral dose of 2.8 mg DEHP and low dose; a single oral dose of 0.31 mg was used for the model simulations. The subject characteristic and dosing for respective studies are provided in Table A. (1–3). The predicted urinary data were converted into moles based on their molecular weight in order to standardize the exposure unit data. Then the relation; ((predicted amounts of metabolites in urine (moles)/amounts dose (moles)) *100), is used to calculate the percentage molar eliminations on moles basis (Anderson et al., 2011; Koch et al., 2005). The detailed summarized tables are provided in Tables A.5–A.7. The PBPK predicted a range of metabolites elimination as a percentage of doses in mole reflecting the uncertainty in the model. The model output was compared with the observed experimental data. Table 3 summarizes the predicted vs observed percentage amount elimination of metabolites. The experimentally observed cumulative amount of all metabolites in the urine is well within the range of PBPK simulation (Table 4).

Table 4. Fraction excretion value (mole percentage) for observed and PBPK predicted of DEHP metabolites

	Metabolites of the D4-DEHP Dose (% mol elimination)					
Study involved	**Dose**	**MEHP**	**5OH-MEHP**	**5cx-MEPP**	**5oxo-MEHP**	**Total molar elimination (%)**
Anderson et al., (2011)	310µg	6.94	16.33	15.90	12.53	51.70
Present study **2.5th - 97.5th (median)**	310µg	4.3-8.7 (6.3)	8.8-22.9 (14.6)	4.3-18.5 (9.2)	3.0-15.2 (6.8)	20.4 -65.2 (36.9)
Anderson et al., (2011)	2800µg	5.67	14.86	11.97	10.00	42.51

Present study	2800µg	4.4-8.7 (6.3)	9.0-23.2 (14.8)	4.3-18.9 (9.2)	3.0-15.3 (6.8)	20.7-66.1 (37.1)
2.5^{th} - 97.5^{th} (median)						

4. Conclusions and future work

The results showed that the current developed model can able to predict the plasma and the cumulative urine concentration of the DEHP metabolites for the different exposure scenario. The current model included four metabolites and the generation of metabolites was described mechanistically using integrated physiological parameters and Michaelis-Menten (M-M) parameters such as Vmax and Km derived from a human hepatic/intestine cell line. The sensitive analysis was done for all parameters and the metabolic parameters were found to be more sensitive than other parameters. Monte Carlo simulation was used accounting probabilistic information about pharmacokinetics parameters that estimated DEHP metabolites concentration in both the plasma and the urine at three percentile considering the uncertainty into the model. Some of the major strength of current predictive model over previously developed models for DEHP are: (1) it's a detail PBPK model that predict the compound(s) or metabolite(s) concentration using the in vitro metabolism data with the application of IVIVE instead of using animal experimental data for its calibration or fitting, (2) production of metabolites was described using saturation kinetics (M-M equations) which retains its biological plausibility, (3) model can be individualized (personalized) for different populations by implementing the physiological variability into the model, (4) it can be used to predict the target tissue internal concentrations for further toxicodynamics study and human health risk assessments. The current developed model did not account for the 2-cx MEPP metabolite due to lack of in vitro metabolic data, considered to be another important metabolite for the biomonitoring study. The current PBPK model can be further extended for 2-cx MEPP, once the metabolic data are available. Detailed rat's pharmacokinetic studies that include all metabolites could be very useful for further understanding metabolites tissue distribution. The current developed model can be applied in the biomonitoring and exposome studies for the human health risk assessment (Martínez et al., 2017, 2018). The developed model can be further extended for the development of an integrated PBPK/PD systems toxicology model (integrative systems toxicology) to establish the exposure-internal dose- response relationship (Sharma et al., 2017b)

Acknowledgement

Preparation of this manuscript was supported in part by European Union's projects, HEALS (Health and Environment-wide Associations via Large population Surveys) by the FP7 Programme under grant agreement no. 603946 and EuroMix (European Test and Risk Assessment Strategies for Mixtures) by the Horizon 2020 Framework Programme under grant agreement no. 633172. Raju Prasad Sharma has received a doctoral fellowship from Universitat Rovira i Virgili under Martí-Franquès Research Grants Programme. V. Kumar has received funds from Health Department of Catalonia

Chapter 2

Government trough "Pla Estratègic de Recerca i Innovació en salut" (PERIS 2016-2020). This publication reflects only the authors' views. The Community and other funding organizations are not liable for any use made of the information contained therein.

References

Abduljalil, K., Furness, P., Johnson, T.N., Rostami-Hodjegan, A., Soltani, H., 2012. Anatomical, Physiological and Metabolic Changes with Gestational Age during Normal Pregnancy. Clin. Pharmacokinet. 51, 365–396. https://doi.org/10.2165/11597440-000000000-00000

Abdullah, R., Alhusainy, W., Woutersen, J., Rietjens, I.M.C.M., Punt, A., 2016. Predicting points of departure for risk assessment based on in vitro cytotoxicity data and physiologically based kinetic (PBK) modeling: The case of kidney toxicity induced by aristolochic acid I. Food Chem. Toxicol. 92, 104–116. https://doi.org/10.1016/j.fct.2016.03.017

Adachi, K., Suemizu, H., Murayama, N., Shimizu, M., Yamazaki, H., 2015. Human biofluid concentrations of mono(2-ethylhexyl)phthalate extrapolated from pharmacokinetics in chimeric mice with humanized liver administered with di(2-ethylhexyl)phthalate and physiologically based pharmacokinetic modeling. Environ. Toxicol. Pharmacol. https://doi.org/10.1016/j.etap.2015.02.011

Aderem, A., 2005. Systems biology: Its practice and challenges. Cell 121, 511–513. https://doi.org/10.1016/j.cell.2005.04.020

Akingbemi, B.T., Sottas, C.M., Koulova, A.I., Klinefelter, G.R., Hardy, M.P., 2004. Inhibition of Testicular Steroidogenesis by the Xenoestrogen Bisphenol a Is Associated with Reduced Pituitary Luteinizing Hormone Secretion and Decreased Steroidogenic Enzyme Gene Expression in Rat Leydig Cells. Endocrinology 145, 592–603. https://doi.org/10.1210/en.2003-1174

Andersen, M.E., Krewski, D., 2009. Toxicity testing in the 21st century: Bringing the vision to life. Toxicol. Sci. 107, 324–330. https://doi.org/10.1093/toxsci/kfn255

Andersen, M.E., Thomas, R.S., Gaido, K.W., Conolly, R.B., 2005. Dose-response modeling in reproductive toxicology in the systems biology era. Reprod. Toxicol. 19, 327–337. https://doi.org/10.1016/j.reprotox.2004.12.004

Andrade, R., Agundez, J., Lucena, M., Martinez, C., Cueto, R., Garcia-Martin, E., 2009. Pharmacogenomics in Drug Induced Liver Injury. Curr. Drug Metab. 10, 956–970. https://doi.org/10.2174/138920009790711805

Ankley, G.T., Bennett, R.S., Erickson, R.J., Hoff, D.J., Hornung, M.W., Johnson, R.D., Mount, D.R., Nichols, J.W., Russom, C.L., Schmieder, P.K., Serrrano, J.A., Tietge, J.E., Villeneuve, D.L., 2010. Adverse outcome pathways: A conceptual framework to support ecotoxicology research and risk assessment. Environ. Toxicol. Chem. 29, 730–741. https://doi.org/10.1002/etc.34

Ansoumane, K., Duan, P., Quan, C., Yaima, M.L.T., Liu, C., Wang, C., Fu, W., Qi, S.,

Chapter 2

Yu, T., Yang, K., 2014. Bisphenol A induced reactive oxygen species (ROS) in the liver and affect epididymal semen quality in adults Sprague-Dawley rats. J. Toxicol. Environ. Heal. Sci. 6, 103–112. https://doi.org/10.5897/JTEHS2014.0309

Aris, A., 2014. Estimation of bisphenol A (BPA) concentrations in pregnant women, fetuses and nonpregnant women in Eastern Townships of Canada. Reprod. Toxicol. 45, 8–13. https://doi.org/10.1016/j.reprotox.2013.12.006

Arrell, D.K., Terzic, a, 2010. Network systems biology for drug discovery. Clin. Pharmacol. Ther. 88, 120–125. https://doi.org/10.1038/clpt.2010.91

Asakawa, N., Koyama, M., Hashimoto, Y., Yamashita, K., 1995. Studies on the Metabolic Fate of Flutamide. (1): Plasma Concentration after Single Administration and Protein Binding in Rats. Drug Metab. Pharmacokinet. 10, 447–453. https://doi.org/10.2133/dmpk.10.447

Atanasov, A.G., Tam, S., Röcken, J.M., Baker, M.E., Odermatt, A., 2003. Inhibition of 11β-hydroxysteroid dehydrogenase type 2 by dithiocarbamates. Biochem. Biophys. Res. Commun. 308, 257–262. https://doi.org/10.1016/S0006-291X(03)01359-7

Auffray, C., Chen, Z., Hood, L., 2009. Systems medicine: the future of medical genomics and healthcare. Genome Med. 1, 2. https://doi.org/10.1186/gm2

Ball, A.L., Kamalian, L., Alfirevic, A., Lyon, J.J., Chadwick, A.E., 2016. Identification of the additional mitochondrial liabilities of 2-hydroxyflutamide when compared with its parent compound, flutamide in HepG2 cells. Toxicol. Sci. 153, 341–351. https://doi.org/10.1093/toxsci/kfw126

Bartel, D.P., 2004. MicroRNAs: Genomics, Biogenesis, Mechanism, and Function. Cell 116, 281–297. https://doi.org/10.1016/S0092-8674(04)00045-5

Bartlett, D.W., Davis, M.E., 2006. Insights into the kinetics of siRNA-mediated gene silencing from live-cell and live-animal bioluminescent imaging. Nucleic Acids Res. 34, 322–333. https://doi.org/10.1093/nar/gkj439

Bell, S.M., Chang, X., Wambaugh, J.F., Allen, D.G., Bartels, M., Brouwer, K.L.R., Casey, W.M., Choksi, N., Ferguson, S.S., Fraczkiewicz, G., Jarabek, A.M., Ke, A., Lumen, A., Lynn, S.G., Paini, A., Price, P.S., Ring, C., Simon, T.W., Sipes, N.S., Sprankle, C.S., Strickland, J., Troutman, J., Wetmore, B.A., Kleinstreuer, N.C., 2018. In vitro to in vivo extrapolation for high throughput prioritization and decision making. Toxicol. Vitr. 47, 213–227. https://doi.org/10.1016/j.tiv.2017.11.016

Berson, A., Wolf, C., Chachaty, C., Fisch, C., Fau, D., Eugene, D., Loeper, J., Gauthier, J.-C., Beaune, P., Pompon, D., Maurel, P., Pessayre, D., 1993. Metabolic activation of the nitroaromatic antiandrogen flutamide by rat and human cytochromes P-450, including forms belonging to the 3A and 1A subfamilies. J. Pharmacol. Exp. Ther. 265, 366–372.

Chapter 2

Bessems, J., Coecke, S., Gouliarmou, V., Whelan, M., Worth, A., 2015. EURL ECVAM strategy for achieving 3Rs impact in the assessment of toxicokinetics and systemic toxicity 22. https://doi.org/10.2788/197633

Bhattacharya, S., Shoda, L.K.M., Zhang, Q., Woods, C.G., Howell, B.A., Siler, S.Q., Woodhead, J.L., Yang, Y., McMullen, P., Watkins, P.B., Melvin, E.A., 2012. Modeling drug- and chemical-induced hepatotoxicity with systems biology approaches. Front. Physiol. 3 DEC, 1–18. https://doi.org/10.3389/fphys.2012.00462

Birgelen, a Van, Birgelen, a Van, Smit, E., Smit, E., Kampen, I., Kampen, I., 1995. Subchronic effects of 2, 3, 7, 8-TCDD or PCBs on thyroid hormone metabolism: use in risk assessment. Eur. J. Pharmacol. Environ. Toxicol. {…} 293, 77–85.

Bloomingdale, P., Housand, C., Apgar, J.F., Millard, B.L., Mager, D.E., Burke, J.M., Shah, D.K., 2017. Quantitative systems toxicology. Curr. Opin. Toxicol. 4, 79–87. https://doi.org/10.1016/j.cotox.2017.07.003

Boberg, J., Metzdorff, S., Wortziger, R., Axelstad, M., Brokken, L., Vinggaard, A.M., Dalgaard, M., Nellemann, C., 2008. Impact of diisobutyl phthalate and other PPAR agonists on steroidogenesis and plasma insulin and leptin levels in fetal rats. Toxicology 250, 75–81. https://doi.org/10.1016/j.tox.2008.05.020

Boelsterli, U.A., Lim, P.L.K., 2007. Mitochondrial abnormalities—A link to idiosyncratic drug hepatotoxicity? Toxicol. Appl. Pharmacol. 220, 92–107. https://doi.org/10.1016/j.taap.2006.12.013

Bonate, P.L., 2011. Pharmacokinetic-Pharmacodynamic Modeling and Simulation. Springer US, Boston, MA. https://doi.org/10.1007/978-1-4419-9485-1

Boulle, F., van den Hove, D.L. a, Jakob, S.B., Rutten, B.P., Hamon, M., van Os, J., Lesch, K.-P., Lanfumey, L., Steinbusch, H.W., Kenis, G., Hove, D.L.A. Van Den, Jakob, S.B., Rutten, B.P., Hamon, M., Os, J. Van, Lesch, K.-P., van den Hove, D.L. a, Jakob, S.B., Rutten, B.P., Hamon, M., van Os, J., Lesch, K.-P., Lanfumey, L., Steinbusch, H.W., Kenis, G., 2012. Epigenetic regulation of the BDNF gene: implications for psychiatric disorders. Mol. Psychiatry 17, 584–596. https://doi.org/10.1038/mp.2011.107

Bouskine, A., Nebout, M., Brücker-Davis, F., Banahmed, M., Fenichel, P., 2009. Low doses of bisphenol A promote human seminoma cell proliferation by activating PKA and PKG via a membrane G-protein-coupled estrogen receptor. Environ. Health Perspect. 117, 1053–1058. https://doi.org/10.1289/ehp.0800367

Brahm, J., Brahm, M., Segovia, R., Latorre, R., Zapata, R., Poniachik, J., Buckel, E., Contreras, L., 2011. Acute and fulminant hepatitis induced by flutamide: case series report and review of the literature. Ann. Hepatol. 10, 93–8.

Brown, R.P., Delp, M.D., Lindstedt, S.L., Rhomberg, L.R., Beliles, R.P., 1997. Physiological parameter values for physiologically based pharmacokinetic models. Toxicol. Ind. Health 13, 407–484.

Chapter 2

Bursac, N., Kirkton, R.D., Mcspadden, L.C., Liau, B., 2010. Circulating levels of brain-derived neurotrophic factor: correlation with mood, cognition and motor function. Biomark. Med. 4, 871–87.

Calabrese, E.J., Baldwin, L.A., 2003. Toxicology rethinks its central belief. Nature 421, 691–692. https://doi.org/10.1038/421691a

Cao, X.L., Zhang, J., Goodyer, C.G., Hayward, S., Cooke, G.M., Curran, I.H.A., 2012. Bisphenol A in human placental and fetal liver tissues collected from Greater Montreal area (Quebec) during 1998-2008. Chemosphere 89, 505–511. https://doi.org/10.1016/j.chemosphere.2012.05.003

Caputo, V., Sinibaldi, L., Fiorentino, A., Parisi, C., Catalanotto, C., Pasini, A., Cogoni, C., Pizzuti, A., 2011. Brain derived neurotrophic factor (BDNF) expression is regulated by microRNAs miR-26a and miR-26b allele-specific binding. PLoS One 6. https://doi.org/10.1371/journal.pone.0028656

Carlotti, F., Dower, S.K., Qwarnstrom, E.E., 2000. Dynamic shuttling of nuclear factor ??B between the nucleus and cytoplasm as a consequence of inhibitor dissociation. J. Biol. Chem. 275, 41028–41034. https://doi.org/10.1074/jbc.M006179200

Castillo, B., del Cerro, M., Breakefield, X.O., Frim, D.M., Barnstable, C.J., Dean, D.O., Bohn, M.C., 1994. Retinal ganglion cell survival is promoted by genetically modified astrocytes designed to secrete brain-derived neurotrophic factor (BDNF). Brain Res. 647, 30–36. https://doi.org/10.1016/0006-8993(94)91395-1

Castro, B., Sánchez, P., Torres, J.M., Preda, O., del Moral, R.G., Ortega, E., 2013. Bisphenol A Exposure during Adulthood Alters Expression of Aromatase and 5α-Reductase Isozymes in Rat Prostate. PLoS One 8, 1–7. https://doi.org/10.1371/journal.pone.0055905

Chang, Z., Lu, M., Kim, S.S., Park, J.S., 2014. Potential role of HSP90 in mediating the interactions between estrogen receptor (ER) and aryl hydrocarbon receptor (AhR) signaling pathways. Toxicol. Lett. 226, 6–13. https://doi.org/10.1016/j.toxlet.2014.01.032

Chen, N., Li, J., Li, D., Yang, Y., He, D., 2014. Chronic exposure to perfluorooctane sulfonate induces behavior defects and neurotoxicity through oxidative damages, in Vivo and in Vitro. PLoS One 9, 1–10. https://doi.org/10.1371/journal.pone.0113453

Chitra, K.C., Latchoumycandane, C., Mathur, P.P., 2003. Induction of oxidative stress by bisphenol A in the epididymal sperm of rats. Toxicology 185, 119–127. https://doi.org/10.1016/S0300-483X(02)00597-8

Choi, K., Joo, H., Campbell, J.L., Andersen, M.E., Clewell, H.J., 2013. In vitro intestinal and hepatic metabolism of Di(2-ethylhexyl) phthalate (DEHP) in human and rat. Toxicol. Vitr. 27, 1451–1457. https://doi.org/10.1016/j.tiv.2013.03.012

Chapter 2

Clarke, G., Collins, R.A., Leavitt, B.R., Andrews, D.F., Hayden, M.R., Lumsden, C.J., McInnes, R.R., 2000. A one-hit model of cell death in inherited neuronal degenerations. Nature 406, 195–199. https://doi.org/10.1038/35018098

Clewell, H.J., Gearhart, J.M., Gentry, P.R., Covington, T.R., VanLandingham, C.B., Crump, K.S., Shipp, A.M., 1999. Evaluation of the uncertainty in an oral reference dose for methylmercury due to interindividual variability in pharmacokinetics. Risk Anal. 19, 547–558. https://doi.org/10.1023/A:1007017116171

Clewell, R. a, Merrill, E. a, Narayanan, L., Gearhart, J.M., Robinson, P.J., 2004. Evidence for competitive inhibition of iodide uptake by perchlorate and translocation of perchlorate into the thyroid. Int. J. Toxicol. 23, 17–23. https://doi.org/10.1080/10915810490275044

Clewell, R.A., Clewell, H.J., 2008. Development and specification of physiologically based pharmacokinetic models for use in risk assessment. Regul. Toxicol. Pharmacol. 50, 129–43. https://doi.org/10.1016/j.yrtph.2007.10.012

Coe, K.J., Jia, Y., Han, K.H., Rademacher, P., Bammler, T.K., Beyer, R.P., Farin, F.M., Woodke, L., Plymate, S.R., Fausto, N., Nelson, S.D., 2007. Comparison of the cytotoxicity of the nitroaromatic drug flutamide to its cyano analogue in the hepatocyte cell line TAMH: Evidence for complex I inhibition and mitochondrial dysfunction using toxicogenomic screening. Chem. Res. Toxicol. 20, 1277–1290. https://doi.org/10.1021/tx7001349

Coe, K.J., Nelson, S.D., Ulrich, R.G., He, Y., Dai, X., Cheng, O., Caguyong, M., Roberts, C.J., Slatter, J.G., 2006. Profiling the hepatic effects of flutamide in rats: A microarray comparison with classical aryl hydrocarbon receptor ligands and atypical CYP1A inducers. Drug Metab. Dispos. 34, 1266–1275. https://doi.org/10.1124/dmd.105.009159

Cooper, R.L., Stoker, T.E., Tyrey, L., Goldman, J.M., McElroy, W.K., 2000. Atrazine disrupts the hypothalamic control of pituitary-ovarian function. Toxicol. Sci. 53, 297–307. https://doi.org/10.1093/toxsci/53.2.297

Coughlin, J.L., Thomas, P.E., Buckley, B., 2012. Inhibition of genistein glucuronidation by bisphenol A in human and rat liver microsomes. Drug Metab. Dispos. 40, 481–485. https://doi.org/10.1124/dmd.111.042366

Csanády, G., Oberste-Frielinghaus, H., Semder, B., Baur, C., Schneider, K., Filser, J., 2002. Distribution and unspecific protein binding of the xenoestrogens bisphenol A and daidzein. Arch. Toxicol. 76, 299–305. https://doi.org/10.1007/s00204-002-0339-5

Cubitt, H.E., Houston, J.B., Galetin, A., 2011. Prediction of human drug clearance by multiple metabolic pathways: Integration of hepatic and intestinal microsomal and cytosolic data. Drug Metab. Dispos. 39, 864–873. https://doi.org/10.1124/dmd.110.036566

Chapter 2

Cubitt, H.E., Houston, J.B., Galetin, A., 2009. Relative Importance of Intestinal and Hepatic Glucuronidation—Impact on the Prediction of Drug Clearance. Pharm. Res. 26, 1073–1083. https://doi.org/10.1007/s11095-008-9823-9

Davies, B., Morris, T., 1993. No Title. Pharm. Res. 10, 1093–1095. https://doi.org/10.1023/A:1018943613122

Dieckhaus, C.M., Thompson, C.D., Roller, S.G., Macdonald, T.L., 2002. Mechanisms of idiosyncratic drug reactions: the case of felbamate. Chem. Biol. Interact. 142, 99–117. https://doi.org/10.1016/S0009-2797(02)00057-1

Dinkova-Kostova, A.T., Holtzclaw, W.D., Cole, R.N., Itoh, K., Wakabayashi, N., Katoh, Y., Yamamoto, M., Talalay, P., 2002. Direct evidence that sulfhydryl groups of Keap1 are the sensors regulating induction of phase 2 enzymes that protect against carcinogens and oxidants. Proc. Natl. Acad. Sci. U. S. A. 99, 11908–13. https://doi.org/10.1073/pnas.172398899

Djuranovic, S., Nahvi, A., Green, R., 2011. A Parsimonious Model for Gene Regulation by miRNAs. Science (80-.). 331, 550–553. https://doi.org/10.1126/science.1191138

Doerge, D.R., Twaddle, N.C., Vanlandingham, M., Brown, R.P., Fisher, J.W., 2011. Distribution of bisphenol A into tissues of adult, neonatal, and fetal Sprague–Dawley rats. Toxicol. Appl. Pharmacol. 255, 261–270. https://doi.org/10.1016/j.taap.2011.07.009

Doering, D.D., Steckelbroeck, S., Doering, T., Klingmüller, D., 2002. Effects of butyltins on human 5alpha-reductase type 1 and type 2 activity. Steroids 67, 859–867.

El-Masri, H., 2013. Modeling for Regulatory Purposes (Risk and Safety Assessment), in: Reisfeld, B., Mayeno, A.N. (Eds.), . Humana Press, Totowa, NJ, pp. 297–303. https://doi.org/10.1007/978-1-62703-059-5_13

Espinosa-Diez, C., Miguel, V., Mennerich, D., Kietzmann, T., Sánchez-Pérez, P., Cadenas, S., Lamas, S., 2015. Antioxidant responses and cellular adjustments to oxidative stress. Redox Biol. 6, 183–197. https://doi.org/10.1016/j.redox.2015.07.008

Fabrega, F., Kumar, V., Schuhmacher, M., Domingo, J.L., Nadal, M., 2014. PBPK modeling for PFOS and PFOA: Validation with human experimental data. Toxicol. Lett. 230, 244–251. https://doi.org/10.1016/j.toxlet.2014.01.007

Fàbrega, F., Nadal, M., Schuhmacher, M., Domingo, J.L., Kumar, V., 2016. Influence of the uncertainty in the validation of PBPK models: A case-study for PFOS and PFOA. Regul. Toxicol. Pharmacol. 77, 230–239. https://doi.org/10.1016/j.yrtph.2016.03.009

Fang, H., Tong, W., Branham, W.S., Moland, C.L., Dial, S.L., Hong, H., Xie, Q., Perkins, R., Owens, W., Sheehan, D.M., 2003. Study of 202 Natural, Synthetic,

Chapter 2

and Environmental Chemicals for Binding to the Androgen Receptor. Chem. Res. Toxicol. 16, 1338–1358. https://doi.org/10.1021/tx030011g

Fisher, J.W., Twaddle, N.C., Vanlandingham, M., Doerge, D.R., 2011. Pharmacokinetic modeling: Prediction and evaluation of route dependent dosimetry of bisphenol A in monkeys with extrapolation to humans. Toxicol. Appl. Pharmacol. 257, 122–136. https://doi.org/10.1016/j.taap.2011.08.026

Fletcher, J.M., Morton, C.J., Zwar, R.A., Murray, S.S., O'Leary, P.D., Hughes, R.A., 2008. Design of a conformationally defined and proteolytically stable circular mimetic of brain-derived neurotrophic factor. J. Biol. Chem. 283, 33375–33383. https://doi.org/10.1074/jbc.M802789200

Forsby, A., Blaauboer, B., 2007. Integration of in vitro neurotoxicity data with biokinetic modelling for the estimation of in vivo neurotoxicity. Hum. Exp. Toxicol. 26, 333–338. https://doi.org/10.1177/0960327106072994

Foxenberg, R.J., Ellison, C.A., Knaak, J.B., Ma, C., Olson, J.R., 2011. Cytochrome P450-specific human PBPK/PD models for the organophosphorus pesticides: Chlorpyrifos and parathion. Toxicology 285, 57–66. https://doi.org/10.1016/j.tox.2011.04.002

Friedmann, A.S., 2002. Atrazine inhibition of testosterone production in rat males following peripubertal exposure. Reprod. Toxicol. 16, 275–279. https://doi.org/10.1016/S0890-6238(02)00019-9

Fukumitsu, H., Ohtsuka, M., Murai, R., Nakamura, H., Itoh, K., Furukawa, S., 2006. Brain-Derived Neurotrophic Factor Participates in Determination of Neuronal Laminar Fate in the Developing Mouse Cerebral Cortex. J. Neurosci. 26, 13218–13230. https://doi.org/10.1523/JNEUROSCI.4251-06.2006

Fukuzawa, N.H., Ohsako, S., Wu, Q., Sakaue, M., Fujii-Kuriyama, Y., Baba, T., Tohyama, C., 2004. Testicular cytochrome P450scc and LHR as possible targets of 2,3,7,8-tetrachlorodibenzo-p-dioxin (TCDD) in the mouse. Mol. Cell. Endocrinol. 221, 87–96. https://doi.org/10.1016/j.mce.2004.02.005

Gabrielsson, J., Weiner, D., 2012. Non-compartmental Analysis, in: Reisfeld, B., Mayeno, A.N. (Eds.), Methods in Molecular Biology. Humana Press, Totowa, NJ, pp. 377–389. https://doi.org/10.1007/978-1-62703-050-2_16

García Cortés, M., Andrade, R.J., Lucena, M.I., Sánchez Martínez, H., Fernández, M.C., Ferrer, T., Martín-Vivaldi, R., Peláez, G., Suárez, F., Romero-Gómez, M., Montero, J.L., Fraga, E., Camargo, R., Alcántara, R., Pizarro, M.A., García-Ruiz, E., Rosemary-Gómez, M., 2001. Flutamide-induced hepatotoxicity: report of a case series. Rev. Esp. Enferm. Dig. 93, 423–32.

Generali, J.A., Cada, D.J., 2014. Flutamide: Hirsutism in Women. Hosp. Pharm. 49, 517–520. https://doi.org/10.1310/hpj4906-517

Gentry, P.R., Covington, T.R., Andersen, M.E., Clewell, H.J., 2002. Application of a

Chapter 2

physiologically based pharmacokinetic model for isopropanol in the derivation of a reference dose and reference concentration. Regul. Toxicol. Pharmacol. 36, 51–68. https://doi.org/S0273230002915400 [pii]

Gerona, R.R., Woodruff, T.J., Dickenson, C.A., Pan, J., Jackie, M., Sen, S., Friesen, M.M., Fujimoto, V.Y., Hunt, P.A., 2014. California population 47. https://doi.org/10.1021/es402764d.Bisphenol-A

Gibbs, J.P., Yang, J.S., Slattery, J.T., 1998. Comparison of human liver and small intestinal glutathione S-transferase-catalyzed busulfan conjugation in vitro. Drug Metab. Dispos. 26, 52–55.

Gillespie, L.N., Clark, G.M., Bartlett, P.F., Marzella, P.L., 2003. BDNF-induced survival of auditory neurons in vivo: Cessation of treatment leads to accelerated loss of survival effects. J. Neurosci. Res. 71, 785–790. https://doi.org/10.1002/jnr.10542

Gim, J., Kim, H.S., Kim, J., Choi, M., Kim, J.R., Chung, Y.J., Cho, K.H., 2010. A system-level investigation into the cellular toxic response mechanism mediated by AhR signal transduction pathway. Bioinformatics 26, 2169–2175. https://doi.org/10.1093/bioinformatics/btq400

Godin, S.J., Scollon, E.J., Hughes, M.F., Potter, P.M., DeVito, M.J., Ross, M.K., 2006. Species differences in the in vitro metabolism of deltamethrin and esfenvalerate: Differential oxidative and hydrolytic metabolism by humans and rats. Drug Metab. Dispos. 34, 1764–1771. https://doi.org/10.1124/dmd.106.010058

Gomez, J.-L., Dupont, A., Cusan, L., Tremblay, M., Suburu, R., Lemay, M., Labrie, F., 1992. Incidence of liver toxicity associated with the use of flutamide in prostate cancer patients. Am. J. Med. 92, 465–470. https://doi.org/10.1016/0002-9343(92)90741-S

Goudarzi, H., Nakajima, S., Ikeno, T., Sasaki, S., Kobayashi, S., Miyashita, C., Ito, S., Araki, A., Nakazawa, H., Kishi, R., 2016. Prenatal exposure to perfluorinated chemicals and neurodevelopment in early infancy: The Hokkaido Study. Sci. Total Environ. 541, 1002–1010. https://doi.org/10.1016/j.scitotenv.2015.10.017

Gumy, C., Chandsawangbhuwana, C., Dzyakanchuk, A. a., Kratschmar, D. V., Baker, M.E., Odermatt, A., 2008. Dibutyltin disrupts glucocorticoid receptor function and impairs glucocorticoid-induced suppression of cytokine production. PLoS One 3. https://doi.org/10.1371/journal.pone.0003545

Haley, B., Zamore, P.D., 2004. Kinetic analysis of the RNAi enzyme complex. Nat. Struct. Mol. Biol. 11, 599–606. https://doi.org/10.1038/nsmb780

Hany, J., Lilienthal, H., Sarasin, a, Roth-Härer, a, Fastabend, a, Dunemann, L., Lichtensteiger, W., Winneke, G., 1999. Developmental exposure of rats to a reconstituted PCB mixture or aroclor 1254: effects on organ weights, aromatase activity, sex hormone levels, and sweet preference behavior. Toxicol. Appl. Pharmacol. 158, 231–243. https://doi.org/10.1006/taap.1999.8710

Chapter 2

Hayes, T.B., Anderson, L.L., Beasley, V.R., de Solla, S.R., Iguchi, T., Ingraham, H., Kestemont, P., Kniewald, J., Kniewald, Z., Langlois, V.S., Luque, E.H., McCoy, K.A., Muñoz-de-Toro, M., Oka, T., Oliveira, C.A., Orton, F., Ruby, S., Suzawa, M., Tavera-Mendoza, L.E., Trudeau, V.L., Victor-Costa, A.B., Willingham, E., 2011. Demasculinization and feminization of male gonads by atrazine: Consistent effects across vertebrate classes. J. Steroid Biochem. Mol. Biol. 127, 64–73. https://doi.org/10.1016/j.jsbmb.2011.03.015

Heidrich, D.D., Steckelbroeck, S., Klingmuller, D., 2001. Inhibition of human cytochrome P450 aromatase activity by butyltins. Steroids 66, 763–769.

Hood, L., Heath, J.R., Phelps, M.E., Lin, B., 2004. Systems biology and new technologies enable predictive and preventative medicine. Science 306, 640–643. https://doi.org/10.1126/science.1104635

Ikezuki, Y., Tsutsumi, O., Takai, Y., Kamei, Y., Taketani, Y., 2002. Determination of bisphenol A concentrations in human biological fluids reveals significant early prenatal exposure. Hum. Reprod. 17, 2839–2841. https://doi.org/10.1093/humrep/17.11.2839

Jaeschke, H., McGill, M.R., Ramachandran, A., 2012. Oxidant stress, mitochondria, and cell death mechanisms in drug-induced liver injury: lessons learned from acetaminophen hepatotoxicity. Drug Metab. Rev. 44, 88–106. https://doi.org/10.3109/03602532.2011.602688

Johansson, M., Larsson, C., Bergman, a, Lund, B.O., 1998. Structure-activity relationship for inhibition of CYP11B1-dependent glucocorticoid synthesis in Y1 cells by aryl methyl sulfones. Pharmacol. Toxicol. 83, 225–230.

Johansson, N., Fredriksson, A., Eriksson, P., 2008. Neonatal exposure to perfluorooctane sulfonate (PFOS) and perfluorooctanoic acid (PFOA) causes neurobehavioural defects in adult mice. Neurotoxicology 29, 160–169. https://doi.org/10.1016/j.neuro.2007.10.008

Juge-Aubry, C.E., Gorla-Bajszczak, A., Pernin, A., Lemberger, T., Wahli, W., Burger, A.G., Meier, C. a., 1995. Peroxisome proliferator-activated receptor mediates cross-talk with thyroid hormone receptor by competition for retinoid X receptor: Possible role of a leucine zipper-like heptad repeat. J. Biol. Chem. https://doi.org/10.1074/jbc.270.30.18117

Jusko, W.J., 2013. Moving from basic toward systems pharmacodynamic models. J. Pharm. Sci. 102, 2930–2940. https://doi.org/10.1002/jps.23590

Jusko, W.J., Ko, H.C., 1994. Physiologic indirect response models characterize diverse types of pharmacodynamic effects. Clin. Pharmacol. Ther. 56, 406–419. https://doi.org/10.1038/clpt.1994.155

Kanda, Y., Hinata, T., Kang, S.W., Watanabe, Y., 2011. Reactive oxygen species mediate adipocyte differentiation in mesenchymal stem cells. Life Sci. 89, 250–258. https://doi.org/10.1016/j.lfs.2011.06.007

Chapter 2

Kaplowitz, N., 2005. Idiosyncratic drug hepatotoxicity. Nat. Rev. Drug Discov. 4, 489.

Kashimshetty, R., Desai, V.G., Kale, V.M., Lee, T., Moland, C.L., Branham, W.S., New, L.S., Chan, E.C.Y., Younis, H., Boelsterli, U.A., 2009. Underlying mitochondrial dysfunction triggers flutamide-induced oxidative liver injury in a mouse model of idiosyncratic drug toxicity. Toxicol. Appl. Pharmacol. 238, 150–159. https://doi.org/10.1016/j.taap.2009.05.007

Katchen, B., Buxbaum, S., 1975. Disposition of a new, nonsteroid, antiandrogen, alpha,alpha,alpha-trifluoro-2-methyl-4'-nitro-m-propionotoluidide (Flutamide), in men following a single oral 200 mg dose. J. Clin. Endocrinol. Metab. 41, 373–9. https://doi.org/10.1210/jcem-41-2-373

Kawamoto, Y., Matsuyama, W., Wada, M., Hishikawa, J., Chan, M.P.L., Nakayama, A., Morisawa, S., 2007. Development of a physiologically based pharmacokinetic model for bisphenol A in pregnant mice. Toxicol. Appl. Pharmacol. 224, 182–191. https://doi.org/10.1016/j.taap.2007.06.023

Kell, D.B., 2006. Systems biology, metabolic modelling and metabolomics in drug discovery and development. Drug Discov. Today 11, 1085–1092. https://doi.org/10.1016/j.drudis.2006.10.004

Kester, M.H.A., Bulduk, S., Van Toor, H., Tibboel, D., Meinl, W., Glatt, H., Falany, C.N., Coughtrie, M.W.H., Gerlienke Schuur, A., Brouwer, A., Visser, T.J., 2002. Potent inhibition of estrogen sulfotransferase by hydroxylated metabolites of polyhalogenated aromatic hydrocarbons reveals alternative mechanism for estrogenic activity of endocrine disrupters. J. Clin. Endocrinol. Metab. 87, 1142–1150. https://doi.org/10.1210/jc.87.3.1142

Keys, D.A., Wallace, D.G., Kepler, T.B., Conolly, R.B., 2000. Quantitative evaluation of alternative mechanisms of blood disposition of di(n-butyl) phthalate and mono(n-butyl) phthalate in rats. Toxicol. Sci. 53, 173–184. https://doi.org/10.1093/toxsci/53.2.173

Keys, D.A., Wallace, D.G., Kepler, T.B., Conolly, R.B., 1999. Quantitative evaluation of alternative mechanisms of blood and testes disposition of di(2-ethylhexyl) phthalate and mono(2-ethylhexyl) phthalate in rats. Toxicol. Sci. 49, 172–85. https://doi.org/10.1093/toxsci/49.2.172

Kitano, H., 2002. Systems biology: A brief overview. Sci. (New York, NY) 295, 1662–1664. https://doi.org/10.1126/science.1069492

Kobayashi, Y., Fukami, T.., Shimizu, M., Nakajima, M., Tsuyoshi., Y., 2012. Short Communication Contributions of Arylacetamide Deacetylase and Carboxylesterase 2 to Flutamide Hydrolysis in Human Liver. Drug Metab. Dispos. 40, 1080–1084.

Kohler, J.J., Schepartz, A., 2001. Kinetic Studies of Fos , Jun , DNA Complex Formation : DNA Binding Prior to Dimerization. Biochemistry 40, 130–142. https://doi.org/10.1021/bi001881p

Chapter 2

Kortejärvi, H., Urtti, A., Yliperttula, M., 2007. Pharmacokinetic simulation of biowaiver criteria: The effects of gastric emptying, dissolution, absorption and elimination rates. Eur. J. Pharm. Sci. 30, 155–166. https://doi.org/10.1016/j.ejps.2006.10.011

Kuepfer, L., Niederalt, C., Wendl, T., Schlender, J.F., Willmann, S., Lippert, J., Block, M., Eissing, T., Teutonico, D., 2016. Applied Concepts in PBPK Modeling: How to Build a PBPK/PD Model. CPT Pharmacometrics Syst. Pharmacol. 5, 516–531. https://doi.org/10.1002/psp4.12134

Kurebayashi, H., Okudaira, K., Ohno, Y., 2010. Species difference of metabolic clearance of bisphenol A using cryopreserved hepatocytes from rats, monkeys and humans. Toxicol. Lett. 198, 210–215. https://doi.org/10.1016/j.toxlet.2010.06.017

Kuroda, N., Kinoshita, Y., Sun, Y., Wada, M., Kishikawa, N., Nakashima, K., Makino, T., Nakazawa, H., 2003. Measurement of bisphenol A levels in human blood serum and ascitic fluid by HPLC using a fluorescent labeling reagent. J. Pharm. Biomed. Anal. 30, 1743–1749. https://doi.org/10.1016/S0731-7085(02)00516-2

Lai, K.P., Wong, M.H., Wong, C.K.C., 2005a. Inhibition of CYP450scc expression in dioxin-exposed rat Leydig cells. J. Endocrinol. 185, 519–527. https://doi.org/10.1677/joe.1.06054

Lai, K.P., Wong, M.H., Wong, C.K.C., 2005b. Effects of TCDD in modulating the expression of Sertoli cell secretory products and markers for cell-cell interaction. Toxicology 206, 111–123. https://doi.org/10.1016/j.tox.2004.07.002

Lans, M.C., Spiertz, C., Brouwer, a, Koeman, J.H., 1994. Different competition of thyroxine binding to transthyretin and thyroxine-binding globulin by hydroxy-PCBs, PCDDs and PCDFs. Eur. J. Pharmacol. 270, 129–136. https://doi.org/10.1016/0926-6917(94)90054-X

Leclerc, E., Hamon, J., Legendre, A., Bois, F.Y., 2014. Integration of pharmacokinetic and NRF2 system biology models to describe reactive oxygen species production and subsequent glutathione depletion in liver microfluidic biochips after flutamide exposure. Toxicol. Vitr. 28, 1230–1241. https://doi.org/10.1016/j.tiv.2014.05.003

Lee, Y.J., Ryu, H.Y., Kim, H.K., Min, C.S., Lee, J.H., Kim, E., Nam, B.H., Park, J.H., Jung, J.Y., Jang, D.D., Park, E.Y., Lee, K.H., Ma, J.Y., Won, H.S., Im, M.W., Leem, J.H., Hong, Y.C., Yoon, H.S., 2008. Maternal and fetal exposure to bisphenol A in Korea. Reprod. Toxicol. 25, 413–419. https://doi.org/10.1016/j.reprotox.2008.05.058

Lemaire, G., Terouanne, B., Mauvais, P., Michel, S., Rahmani, R., 2004. Effect of organochlorine pesticides on human androgen receptor activation in vitro. Toxicol. Appl. Pharmacol. 196, 235–246. https://doi.org/10.1016/j.taap.2003.12.011

Li, L. a., Wang, P.W., Chang, L.W., 2004. Polychlorinated biphenyl 126 stimulates basal and inducible aldosterone biosynthesis of human adrenocortical H295R cells. Toxicol. Appl. Pharmacol. 195, 92–102.

Chapter 2

https://doi.org/10.1016/j.taap.2003.11.007

Li, M.W.M., Mruk, D.D., Lee, W.M., Cheng, C.Y., 2009. Disruption of the blood-testis barrier integrity by bisphenol A in vitro: Is this a suitable model for studying blood-testis barrier dynamics? Int. J. Biochem. Cell Biol. 41, 2302–2314. https://doi.org/10.1016/j.biocel.2009.05.016

Li, W., He, Q.Z., Wu, C.Q., Pan, X.Y., Wang, J., Tan, Y., Shan, X.Y., Zeng, H.C., 2015. PFOS Disturbs BDNF-ERK-CREB Signalling in Association with Increased MicroRNA-22 in SH-SY5Y Cells. Biomed Res. Int. 2015. https://doi.org/10.1155/2015/302653

Li, X., Fang, P., Mai, J., Choi, E.T., Wang, H., Yang, X., 2013. Targeting mitochondrial reactive oxygen species as novel therapy for inflammatory diseases and cancers. J. Hematol. Oncol. 6, 19. https://doi.org/10.1186/1756-8722-6-19

Li, Y., Ramdhan, D.H., Naito, H., Yamagishi, N., Ito, Y., Hayashi, Y., Yanagiba, Y., Okamura, A., Tamada, H., Gonzalez, F.J., Nakajima, T., 2011. Ammonium perfluorooctanoate may cause testosterone reduction by adversely affecting testis in relation to PPARα. Toxicol. Lett. 205, 265–272. https://doi.org/10.1016/j.toxlet.2011.06.015

Lipsky, R.H., Marini, A.M., 2007. Brain-derived neurotrophic factor in neuronal survival and behavior-related plasticity. Ann. N. Y. Acad. Sci. 1122, 130–143. https://doi.org/10.1196/annals.1403.009

Long, Y., Wang, Y., Ji, G., Yan, L., Hu, F., Gu, A., 2013. Neurotoxicity of Perfluorooctane Sulfonate to Hippocampal Cells in Adult Mice. PLoS One 8, 1–9. https://doi.org/10.1371/journal.pone.0054176

Lorber, M., Angerer, J., Koch, H.M., 2010. A simple pharmacokinetic model to characterize exposure of Americans to Di-2-ethylhexyl phthalate. J. Expo. Sci. Environ. Epidemiol. 20, 38–53. https://doi.org/10.1038/jes.2008.74

Louisse, J., Beekmann, K., Rietjens, I.M.C.M., 2016. Use of physiologically based kinetic modeling-based reverse dosimetry to predict in vivo toxicity from in vitro data. Chem. Res. Toxicol. acs.chemrestox.6b00302. https://doi.org/10.1021/acs.chemrestox.6b00302

Lu, B., 2003. Pro-Region of Neurotrophins. Neuron 39, 735–738. https://doi.org/10.1016/S0896-6273(03)00538-5

Lubin, F.D., Roth, T.L., Sweatt, J.D., 2008. Epigenetic regulation of BDNF gene transcription in the consolidation of fear memory. J. Neurosci. 28, 10576–86. https://doi.org/10.1523/JNEUROSCI.1786-08.2008

Ma, E., MacRae, I.J., Kirsch, J.F., Doudna, J.A., 2008. Autoinhibition of Human Dicer by Its Internal Helicase Domain. J. Mol. Biol. 380, 237–243. https://doi.org/10.1016/j.jmb.2008.05.005

Chapter 2

Mager, D.E., Woo, S., Jusko, W.J., 2009. Scaling Pharmacodynamics from In Vitro and Preclinical Animal Studies to Humans. Drug Metab. Pharmacokinet. 24, 16–24. https://doi.org/10.2133/dmpk.24.16

Mager, D.E., Wyska, E., Jusko, W.J., 2003. Diversity of mechanism-based pharmacodynamic models. Drug Metab. Dispos. 31, 510–8. https://doi.org/10.1124/DMD.31.5.510

Martínez, M.A., Rovira, J., Prasad Sharma, R., Nadal, M., Schuhmacher, M., Kumar, V., 2018. Comparing dietary and non-dietary source contribution of BPA and DEHP to prenatal exposure: A Catalonia (Spain) case study. Environ. Res. 166, 25–34. https://doi.org/10.1016/j.envres.2018.05.008

Martínez, M.A., Rovira, J., Sharma, R.P., Nadal, M., Schuhmacher, M., Kumar, V., 2017. Prenatal exposure estimation of BPA and DEHP using integrated external and internal dosimetry: A case study. Environ. Res. 158, 566–575. https://doi.org/10.1016/j.envres.2017.07.016

Masuyama, H., Hiramatsu, Y., Kunitomi, M., Kudo, T., MacDonald, P.N., 2000. Endocrine disrupting chemicals, phthalic acid and nonylphenol, activate Pregnane X receptor-mediated transcription. Mol. Endocrinol. 14, 421–428. https://doi.org/10.1210/mend.14.3.0424

Masuyama, H., Inoshita, H., Hiramatsu, Y., Kudo, T., 2002. Ligands have various potential effects on the degradation of pregnane X receptor by proteasome. Endocrinology 143, 55–61. https://doi.org/10.1210/en.143.1.55

Matsuzaki, Y., Nagai, D., Ichimura, E., Goda, R., Tomura, A., Doi, M., Nishikawa, K., 2006. Metabolism and hepatic toxicity of flutamide in cytochrome P450 1A2 knockout SV129 mice. J. Gastroenterol. 41, 231–239. https://doi.org/10.1007/s00535-005-1749-y

Menei, P., Montero-Menei, C., Whittemore, S.R., Bunge, R.P., Bunge, M.B., 1998. Schwann cells genetically modified to secrete human BDNF promote enhanced axonal regrowth across transected adult rat spinal cord. Eur. J. Neurosci. 10, 607–621. https://doi.org/10.1046/j.1460-9568.1998.00071.x

Michael, G.J., Averill, S., Nitkunan, A., Rattray, M., Bennett, D.L., Yan, Q., Priestley, J. V, 1997. Nerve growth factor treatment increases brain-derived neurotrophic factor selectively in TrkA-expressing dorsal root ganglion cells and in their central terminations within the spinal cord. J. Neurosci. 17, 8476–90.

Mielke, H., Partosch, F., Gundert-Remy, U., 2011. The contribution of dermal exposure to the internal exposure of bisphenol A in man. Toxicol. Lett. 204, 190–198. https://doi.org/10.1016/j.toxlet.2011.04.032

Mikamo, E., Harada, S., Nishikawa, J., Nishihara, T., 2003. Endocrine disruptors induce cytochrome P450 by affecting transcriptional regulation via pregnane X receptor. Toxicol. Appl. Pharmacol. 193, 66–72. https://doi.org/10.1016/j.taap.2003.08.001

Chapter 2

Moriyama, K., Tagami, T., Akamizu, T., Usui, T., Saijo, M., Kanamoto, N., Hataya, Y., Shimatsu, A., Kuzuya, H., Nakao, K., 2002. Thyroid hormone action is disrupted by bisphenol A as an antagonist. J. Clin. Endocrinol. Metab. 87, 5185–5190. https://doi.org/10.1210/jc.2002-020209

Mowla, S.J., Pareek, S., Farhadi, H.F., Petrecca, K., Fawcett, J.P., Seidah, N.G., Morris, S.J., Sossin, W.S., Murphy, R. a, 1999. Differential sorting of nerve growth factor and brain-derived neurotrophic factor in hippocampal neurons. J. Neurosci. 19, 2069–2080.

Muiños-Gimeno, M., Espinosa-Parrilla, Y., Guidi, M., Kagerbauer, B., Sipilä, T., Maron, E., Pettai, K., Kananen, L., Navinés, R., Martín-Santos, R., Gratacòs, M., Metspalu, A., Hovatta, I., Estivill, X., 2011. Human microRNAs miR-22, miR-138-2, miR-148a, and miR-488 are associated with panic disorder and regulate several anxiety candidate genes and related pathways. Biol. Psychiatry 69, 526–533. https://doi.org/10.1016/j.biopsych.2010.10.010

Murer, M.., Yan, Q., Raisman-Vozari, R., 2001. Brain-derived neurotrophic factor in the control human brain, and in Alzheimer's disease and Parkinson's disease. Prog. Neurobiol. 63, 71–124. https://doi.org/10.1016/S0301-0082(00)00014-9

Murphy, M.P., 2009. How mitochondria produce reactive oxygen species. Biochem. J. 417, 1–13. https://doi.org/10.1042/BJ20081386

Nestorov, I., 2007. Whole-body physiologically based pharmacokinetic models. Expert Opin. Drug Metab. Toxicol. 3, 235–249. https://doi.org/10.1517/17425255.3.2.235

Nikula, H., Talonpoika, T., Kaleva, M., Toppari, J., 1999. Inhibition of hCG-stimulated steroidogenesis in cultured mouse Leydig tumor cells by bisphenol A and octylphenols. Toxicol. Appl. Pharmacol. 157, 166–173. https://doi.org/10.1006/taap.1999.8674

Niwa, T., Fujimoto, M., Kishimoto, K., Yabusaki, Y., Ishibashi, F., Katagiri, M., 2001. Metabolism and interaction of bisphenol A in human hepatic cytochrome P450 and steroidogenic CYP17. Biol. Pharm. Bull. 24, 1064–1067. https://doi.org/10.1248/bpb.24.1064

O'Leary, P.D., Hughes, R.A., 1998. Structure-activity relationships of conformationally constrained peptide analogues of loop 2 of brain-derived neurotrophic factor. J. Neurochem. 70, 1712–21. https://doi.org/10.1046/j.1471-4159.1998.70041712.x

OECD, 2018. "Users'' Handbook supplement to the Guidance Document for developing and assessing Adverse Outcome Pathways", OECD Series on Adverse Outcome Pathways, No. 1, OECD Publishing, Paris." https://doi.org/10.1787/5jlv1m9d1g32-en

OECD, 2016. "Users'' Handbook supplement to the Guidance Document for developing and assessing Adverse Outcome Pathways", OECD Series on Adverse Outcome Pathways, No. 1, OECD Publishing, Paris" 18.

Chapter 2

https://doi.org/10.1787/5jlv1m9d1g32-en

Ohshima, M., Ohno, S., Nakajin, S., 2005. Inhibitory effects of some possible endocrine-disrupting chemicals on the isozymes of human 11beta-hydroxysteroid dehydrogenase and expression of their mRNA in gonads and adrenal glands. Environ. Sci. 12, 219–230.

Ohtake, F., Takeyama, K., Matsumoto, T., Kitagawa, H., Yamamoto, Y., Nohara, K., Tohyama, C., Krust, A., Mimura, J., Chambon, P., Yanagisawa, J., Fujii-Kuriyama, Y., Kato, S., 2003. Modulation of oestrogen receptor signalling by association with the activated dioxin receptor. Nature 423, 545–550. https://doi.org/10.1038/nature01606

Patisaul, H.B., Todd, K.L., Mickens, J.A., Adewale, H.B., 2009. Impact of neonatal exposure to the ERα agonist PPT, bisphenol-A or phytoestrogens on hypothalamic kisspeptin fiber density in male and female rats. Neurotoxicology 30, 350–357. https://doi.org/10.1016/j.neuro.2009.02.010

Pérez-Ortín, J.E., Alepuz, P.M., Moreno, J., 2007. Genomics and gene transcription kinetics in yeast. Trends Genet. 23, 250–257. https://doi.org/10.1016/j.tig.2007.03.006

Perruisseau-Carrier, C., Jurga, M., Forraz, N., McGuckin, C.P., 2011. MiRNAs stem cell reprogramming for neuronal induction and differentiation. Mol. Neurobiol. 43, 215–227. https://doi.org/10.1007/s12035-011-8179-z

Podratz, P.L., Filho, V.S.D., Lopes, P.F.I., Sena, G.C., Matsumoto, S.T., Samoto, V.Y., Takiya, C.M., Miguel, E.D.C., Silva, I.V., Graceli, J.B., 2012. Tributyltin Impairs the Reproductive Cycle in Female Rats. J. Toxicol. Environ. Heal. Part A 75, 1035–1046. https://doi.org/10.1080/15287394.2012.697826

Poland, a, Knutson, J.C., 1982. 2,3,7,8-Tetrachlorodibenzo-P-Dioxin and Related Halogenated Aromatic Hydrocarbons: Examination of the Mechanism of Toxicity. Annu. Rev. Pharmacol. Toxicol. 22, 517–554. https://doi.org/10.1146/annurev.pa.22.040182.002505

Poulin, P., Krishnan, K., 1996. Molecular Structure-Based Prediction of the Partition Coefficients of Organic Chemicals for Physiological Pharmacokinetic Models. Toxicol. Mech. Methods 6, 117–137. https://doi.org/10.3109/15376519609068458

Poulin, P., Krishnan, K., 1995. A biologically-based algorithm for predicting human tissue: blood partition coefficients of organic chemicals. Hum Exp Toxicol 14, 273–280.

Poulin, P., Theil, F.P., 2000. A priori prediction of tissue: Plasma partition coefficients of drugs to facilitate the use of physiologically-based pharmacokinetic models in drug discovery. J. Pharm. Sci. 89, 16–35. https://doi.org/10.1002/(SICI)1520-6017(200001)89:1<16::AID-JPS3>3.0.CO;2-E

Qatanani, M., Zhang, J., Moore, D.D., 2005. Role of the constitutive androstane

Chapter 2

receptor in xenobiotic-induced thyroid hormone metabolism. Endocrinology 146, 995–1002. https://doi.org/10.1210/en.2004-1350

Qiu, L., Zhang, X., Zhang, X., Zhang, Y., Gu, J., Chen, M., Zhang, Z., Wang, X., Wang, S.L., 2013. Sertoli cell is a potential target for perfluorooctane sulfonate-induced reproductive dysfunction in male mice. Toxicol. Sci. 135, 229–240. https://doi.org/10.1093/toxsci/kft129

Radwanski, E., Perentesis, G., Symchowicz, S., Zampaglione, N., 1989. Single and Multiple Dose Pharmacokinetic Evaluation of Flutamide in Normal Geriatric Volunteers. J. Clin. Pharmacol. 29, 554–558. https://doi.org/10.1002/j.1552-4604.1989.tb03381.x

Raun Andersen, H., Vinggaard, A.M., Høj Rasmussen, T., Gjermandsen, I.M., Cecilie Bonefeld-Jørgensen, E., 2002. Effects of Currently Used Pesticides in Assays for Estrogenicity, Androgenicity, and Aromatase Activity in Vitro. Toxicol. Appl. Pharmacol. 179, 1–12. https://doi.org/10.1006/taap.2001.9347

Rey, R., Lukas-Croisier, C., Lasala, C., Bedecarrás, P., 2003. AMH/MIS: What we know already about the gene, the protein and its regulation. Mol. Cell. Endocrinol. 211, 21–31. https://doi.org/10.1016/j.mce.2003.09.007

Rodríguez-Tébar, A., Dechant, G., Götz, R., Barde, Y.A., 1992. Binding of neurotrophin-3 to its neuronal receptors and interactions with nerve growth factor and brain-derived neurotrophic factor. EMBO J. 11, 917–922.

Rouquié, D., Heneweer, M., Botham, J., Ketelslegers, H., Markell, L., Pfister, T., Steiling, W., Strauss, V., Hennes, C., 2015. Contribution of new technologies to characterization and prediction of adverse effects. Crit. Rev. Toxicol. 45, 172–183. https://doi.org/10.3109/10408444.2014.986054

Saitoh, M., Yanase, T., Morinaga, H., Tanabe, M., Mu, Y.M., Nishi, Y., Nomura, M., Okabe, T., Goto, K., Takayanagi, R., Nawata, H., 2001. Tributyltin or triphenyltin inhibits aromatase activity in the human granulosa-like tumor cell line KGN. Biochem. Biophys. Res. Commun. 289, 198–204. https://doi.org/10.1006/bbrc.2001.5952

Sandhya, V.K., Raju, R., Verma, R., Advani, J., Sharma, R., Radhakrishnan, A., Nanjappa, V., Narayana, J., Somani, B.L., Mukherjee, K.K., Pandey, A., Christopher, R., Keshava Prasad, T.S., 2013. A network map of BDNF/TRKB and BDNF/p75NTR signaling system. J. Cell Commun. Signal. 7, 301–307. https://doi.org/10.1007/s12079-013-0200-z

Sato, I., Kawamoto, K., Nishikawa, Y., Tsuda, S., Yoshida, M., Yaegashi, K., Saito, N., Liu, W., Jin, Y., 2009. Neurotoxicity of perfluorooctane sulfonate (PFOS) in rats and mice after single oral exposure. J. Toxicol. Sci. 34, 569–574. https://doi.org/10.2131/jts.34.569

Saunders, P.T., Majdic, G., Parte, P., Millar, M.R., Fisher, J.S., Turner, K.J., Sharpe, R.M., 1997. Fetal and perinatal influence of xenoestrogens on testis gene

Chapter 2

expression. Adv. Exp. Med. Biol. 424, 99–110.

Schmitt, W., 2008. General approach for the calculation of tissue to plasma partition coefficients. Toxicol. Vitr. 22, 457–467. https://doi.org/10.1016/j.tiv.2007.09.010

Schönfelder, G., Wittfoht, W., Hopp, H., Talsness, C.E., Paul, M., Chahoud, I., 2002. Parent bisphenol a accumulation in the human maternal-fetal-placental unit. Environ. Health Perspect. 110, 703–707. https://doi.org/10.1289/ehp.021100703

Seo, J.S., Lee, Y.M., Jung, S.O., Kim, I.C., Yoon, Y.D., Lee, J.S., 2006. Nonylphenol modulates expression of androgen receptor and estrogen receptor genes differently in gender types of the hermaphroditic fish Rivulus marmoratus. Biochem. Biophys. Res. Commun. 346, 213–223. https://doi.org/10.1016/j.bbrc.2006.05.123

Shi, Z., Ding, L., Zhang, H., Feng, Y., Xu, M., Dai, J., 2009. Chronic exposure to perfluorododecanoic acid disrupts testicular steroidogenesis and the expression of related genes in male rats. Toxicol. Lett. 188, 192–200. https://doi.org/10.1016/j.toxlet.2009.04.014

Sisson, T.R., Lund, C.J., Whalen, L.E., Telek, A., 1959. The blood volume of infants. I. The full-term infant in the first year of life. J. Pediatr. 55, 163–79. https://doi.org/10.1016/S0022-3476(59)80084-6

Siu, E.R., Mruk, D.D., Porto, C.S., Cheng, C.Y., 2009. Cadmium-induced testicular injury. Toxicol. Appl. Pharmacol. 238, 240–249. https://doi.org/10.1016/j.taap.2009.01.028

Sjo, E., Lennerna, H., Andersson, T.B., Gråsjo, J., Bredberg, U., 2009. Estimates of Intrinsic Clearance (CL int), Maximum Velocity of the Metabolic Reaction (V max), and Michaelis Constant (K m): Accuracy and Robustness Evaluated through Experimental Data and Monte Carlo Simulations ABSTRACT : Pharmacology 37, 47–58. https://doi.org/10.1124/dmd.108.021477.kinetics

Sjögren, E., Tammela, T.L., Lennernäs, B., Taari, K., Isotalo, T., Malmsten, L.-Å., Axén, N., Lennernäs, H., 2014. Pharmacokinetics of an Injectable Modified-Release 2-Hydroxyflutamide Formulation in the Human Prostate Gland Using a Semiphysiologically Based Biopharmaceutical Model. Mol. Pharm. 11, 3097–3111. https://doi.org/10.1021/mp5002813

Sobarzo, C.M., Lustig, L., Ponzio, R., Denduchis, B., 2006. Effect of di-(2-ethylhexyl) phthalate on N-cadherin and catenin protein expression in rat testis. Reprod. Toxicol. 22, 77–86. https://doi.org/10.1016/j.reprotox.2006.02.004

Soetaert, K., Petzoldt, T., 2010. Inverse Modelling, Sensitivity and Monte Carlo Analysis in R Using Package FME. J. Stat. Softw. 33, 2–4. https://doi.org/10.18637/jss.v033.i03

Stasenko, S., Bradford, E.M., Piasek, M., Henson, M.C., Varnai, V.M., Jurasović, J., Kušec, V., 2010. Metals in human placenta: Focus on the effects of cadmium on steroid hormones and leptin. J. Appl. Toxicol. 30, 242–253.

Chapter 2

https://doi.org/10.1002/jat.1490

Stouder, C., Paoloni-Giacobino, A., 2011. Specific transgenerational imprinting effects of the endocrine disruptor methoxychlor on male gametes. Reproduction 141, 207–216. https://doi.org/10.1530/REP-10-0400

Sturla, S.J., Boobis, A.R., FitzGerald, R.E., Hoeng, J., Kavlock, R.J., Schirmer, K., Whelan, M., Wilks, M.F., Peitsch, M.C., 2014. Systems Toxicology: From Basic Research to Risk Assessment. Chem. Res. Toxicol. 27, 314–329. https://doi.org/10.1021/tx400410s

Teppner, M., Boess, F., Ernst, B., Pähler, A., 2016. Biomarkers of flutamide-bioactivation and oxidative stress in vitro and in vivo. Drug Metab. Dispos. 44, 560–569. https://doi.org/10.1124/dmd.115.066522

Thiel, C., Cordes, H., Conde, I., Castell, J.V., Blank, L.M., Kuepfer, L., 2017. Model-based contextualization of in vitro toxicity data quantitatively predicts in vivo drug response in patients. Arch. Toxicol. 91, 865–883. https://doi.org/10.1007/s00204-016-1723-x

Timchalk, C., Nolan, R.J., Mendrala, A.L., Dittenber, D.A., Brzak, K.A., Mattsson, J.L., 2002. A physiologically based pharmacokinetic and pharmacodynamic (PBPK/PD) model for the organophosphate insecticide chlorpyrifos in rats and humans. Toxicol. Sci. 66, 34–53. https://doi.org/10.1093/toxsci/66.1.34

Toyoda, K., Shibutani, M., Tamura, T., Koujitani, T., Uneyama, C., Hirose, M., 2000. Repeated dose (28 days) oral toxicity study of flutamide in rats, based on the draft protocol for the `Enhanced OECD Test Guideline 407' for screening for endocrine-disrupting chemicals. Arch. Toxicol. 74, 127–132. https://doi.org/10.1007/s002040050664

Trdan Lusin, T., Roskar, R., Mrhar, A., 2012. Evaluation of bisphenol A glucuronidation according to UGT1A1*28 polymorphism by a new LC-MS/MS assay. Toxicology 292, 33–41. https://doi.org/10.1016/j.tox.2011.11.015

Uzumcu, M., Kuhn, P.E., Marano, J.E., Armenti A.E., A.E., Passantino, L., 2006. Early postnatal methoxychlor exposure inhibits folliculogenesis and stimulates anti-Mullerian hormone production in the rat ovary. J. Endocrinol. 191, 549–558. https://doi.org/10.1677/joe.1.06592

Valentin, J., 2002. Basic anatomical and physiological data for use in radiological protection: reference values. Ann. ICRP 32, 1–277. https://doi.org/10.1016/S0146-6453(03)00002-2

Vuong, A.M., Yolton, K., Webster, G.M., Sjödin, A., Calafat, A.M., Braun, J.M., Dietrich, K.N., Lanphear, B.P., Chen, A., 2016. Prenatal polybrominated diphenyl ether and perfluoroalkyl substance exposures and executive function in school-age children. Environ. Res. 147, 556–564. https://doi.org/10.1016/j.envres.2016.01.008

Chapter 2

Wambaugh, J.F., Setzer, R.W., Pitruzzello, A.M., Liu, J., Reif, D.M., Kleinstreuer, N.C., Wang, N.C.Y., Sipes, N., Martin, M., Das, K., DeWitt, J.C., Strynar, M., Judson, R., Houck, K.A., Lau, C., 2013. Dosimetric anchoring of In vivo and In vitro studies for perfluorooctanoate and perfluorooctanesulfonate. Toxicol. Sci. 136, 308–327. https://doi.org/10.1093/toxsci/kft204

Wan, H.T., Zhao, Y.G., Wong, M.H., Lee, K.F., Yeung, W.S.B., Giesy, J.P., Wong, C.K.C., 2011. Testicular signaling is the potential target of perfluorooctanesulfonate-mediated subfertility in male mice. Biol. Reprod. 84, 1016–1023. https://doi.org/10.1095/biolreprod.110.089219

Wang, J., Sun, B., Hou, M., Pan, X., Li, X., 2012. The environmental obesogen bisphenol A promotes adipogenesis by increasing the amount of 11β-hydroxysteroid dehydrogenase type 1 in the adipose tissue of children. Int. J. Obes. 999–1005. https://doi.org/10.1038/ijo.2012.173

Wang, X., Li, Y., Xu, X., Wang, Y. hua, 2010. Toward a system-level understanding of microRNA pathway via mathematical modeling. BioSystems 100, 31–38. https://doi.org/10.1016/j.biosystems.2009.12.005

Waters, M.D., Boorman, G., Bushel, P., Cunningham, M., Irwin, R., Merrick, A., Olden, K., Paules, R., Selkirk, J., Stasiewicz, S., Weis, B., Van Houten, B., Walker, N., Tennant, R., 2003. Systems toxicology and the Chemical Effects in Biological Systems (CEBS) knowledge base. Environ. Health Perspect. 111, 811–824. https://doi.org/10.1289/txg.5971

Wen, B., Coe, K.J., Rademacher, P., Fitch, W.L., Monshouwer, M., Nelson, S.D., 2008. Comparison of in vitro bioactivation of flutamide and its cyano analogue: Evidence for reductive activation by human NADPH:cytochrome P450 reductase. Chem. Res. Toxicol. 21, 2393–2406. https://doi.org/10.1021/tx800281h

Wysowski, D.K., Fourcroy, J.L., 1996. Flutamide Hepatotoxicity. J. Urol. 155, 209–212. https://doi.org/10.1016/S0022-5347(01)66596-0

Xi, W., Lee, C.K.F., Yeung, W.S.B., Giesy, J.P., Wong, M.H., Zhang, X., Hecker, M., Wong, C.K.C., 2011. Effect of perinatal and postnatal bisphenol A exposure to the regulatory circuits at the hypothalamus-pituitary-gonadal axis of CD-1 mice. Reprod. Toxicol. 31, 409–417. https://doi.org/10.1016/j.reprotox.2010.12.002

Yang, J., Wang, C., Nie, X., Shi, S., Xiao, J., Ma, X., Dong, X., Zhang, Y., Han, J., Li, T., Mao, J., Liu, X., Zhao, J., Wu, Q., 2015. Perfluorooctane sulfonate mediates microglial activation and secretion of TNF-α through Ca2+-dependent PKC-NF-κB signaling. Int. Immunopharmacol. 28, 52–60. https://doi.org/10.1016/j.intimp.2015.05.019

York, N., 2015. Regulation of Cell Survival by Secreted Proneurotrophins.pdf. Science (80-.). 294, 1945–1949. https://doi.org/10.1126/science.1065057

You, H.J., Park, J.H., Pareja-Galeano, H., Lucia, A., Shin, J. Il, 2016. Targeting MicroRNAs Involved in the BDNF Signaling Impairment in Neurodegenerative

Chapter 2

Diseases. NeuroMolecular Med. https://doi.org/10.1007/s12017-016-8407-9

Yu, N., Wei, S., Li, M., Yang, J., Li, K., Jin, L., Xie, Y., Giesy, J.P., Zhang, X., Yu, H., 2016. Effects of Perfluorooctanoic Acid on Metabolic Profiles in Brain and Liver of Mouse Revealed by a High-throughput Targeted Metabolomics Approach. Sci. Rep. 6, 23963. https://doi.org/10.1038/srep23963

Yun, Y.E., Cotton, C.A., Edginton, A.N., 2014. Development of a decision tree to classify the most accurate tissue-specific tissue to plasma partition coefficient algorithm for a given compound. J. Pharmacokinet. Pharmacodyn. 41, 1–14. https://doi.org/10.1007/s10928-013-9342-0

Zamkova, M., Khromova, N., Kopnin, B.P., Kopnin, P., 2013. Ras-induced ROS upregulation affecting cell proliferation is connected with cell type-specific alterations of HSF1/SESN3/p21Cip1/WAF1pathways. Cell Cycle 12, 826–836. https://doi.org/10.4161/cc.23723

Zeng, H. cai, Zhang, L., Li, Y. yuan, Wang, Y. jian, Xia, W., Lin, Y., Wei, J., Xu, S. qing, 2011. Inflammation-like glial response in rat brain induced by prenatal PFOS exposure. Neurotoxicology 32, 130–139. https://doi.org/10.1016/j.neuro.2010.10.001

Zhang, J., Cooke, G.M., Curran, I.H.A., Goodyer, C.G., Cao, X.L., 2011. GC-MS analysis of bisphenol A in human placental and fetal liver samples. J. Chromatogr. B Anal. Technol. Biomed. Life Sci. 879, 209–214. https://doi.org/10.1016/j.jchromb.2010.11.031

Zhang, L., Guo, J., Zhang, Q., Zhou, W., Li, J., Yin, J., Cui, L., 2018. Flutamide induces hepatic cell death and mitochondrial dysfunction via inhibition of Nrf2-mediated heme oxygenase-1. Oxid. Med. Cell. Longev.

Zhang, L., Li, Y.-Y., Zeng, H.-C., Wei, J., Wan, Y.-J., Chen, J., Xu, S.-Q., 2011. MicroRNA expression changes during zebrafish development induced by perfluorooctane sulfonate. J. Appl. Toxicol. 31, 210–222. https://doi.org/10.1002/jat.1583

Zhang, T., Sun, H., Kannan, K., 2013. Blood and urinary bisphenol a concentrations in children, adults, and pregnant women from China: Partitioning between blood and urine and maternal and fetal cord blood. Environ. Sci. Technol. 47, 4686–4694. https://doi.org/10.1021/es303808b

Zhao, B., Hu, G.X., Chu, Y., Jin, X., Gong, S., Akingbemi, B.T., Zhang, Z., Zirkin, B.R., Ge, R.S., 2010. Inhibition of human and rat 3β-hydroxysteroid dehydrogenase and 17β-hydroxysteroid dehydrogenase 3 activities by perfluoroalkylated substances. Chem. Biol. Interact. 188, 38–43. https://doi.org/10.1016/j.cbi.2010.07.001

Chapter 2

Chapter 2

2B. Development and evaluation of a harmonized whole body physiologically based pharmacokinetic (PBPK) model for flutamide in rats and its extrapolation to humans

Abstract:

By their definition, inadvertent exposure to endocrine disruptors Compounds (EDCs) intervenes with the endocrine signalling system, even at low dose. On the one hand, some EDCs are used as important pharmaceutical drugs that one would not want to dismiss. On the other hand, they thereby enter the human environment with subsequent implications for environmental toxicology. Flutamide, one of the top pharmaceutical products marketed all over the world for the treatment of prostate cancer, is also a pollutant. Its therapeutic action mainly depends on targeting the androgen receptors and inhibiting the androgen action that is essential for growth and survival of prostate tissue. Currently flutamide is of concern with respect to its categorization as an endocrine disruptor.

In this chapters we show a developed physiologically based pharmacokinetic (PBPK) model of flutamide that could serve as a standard tool for its human risk assessment. First we built the model for rat (where many parameters have been measured). The rat PBPK model was extrapolated to human where the re-parameterization involved human specific physiology and metabolism parameters. Then the model was used to simulate different exposure scenarios and the results were compared against the observed data. Both uncertainty and sensitivity analysis were assessed.

Since this new whole-body PBPK model can predict flutamide concentrations not only in plasma but also in various organs, the model may have clinical applications in efficacy and safety assessment of flutamide. The model can also be used for reverse dosimetry in the context of interpreting the available biomonitoring data to estimate the degree to which the population is currently being exposed, a way for the pharmaceutical companies to validate the estimated Permitted Daily Exposure (PDE) for flutamide.

Highlights:

- In-vitro metabolic kinetics was integrated into PBPK to characterize in-vivo kinetics.
- PBPK model of flutamide was calibrated in rats.
- PBPK model of flutamide was extrapolated to humans and validated.
- The dose-dependent kinetics of flutamide was captured after single and multiple dose scenarios in humans.

Chapter 2

1. Introduction

Flutamide is one of the top pharmaceutical products marketed universally all over the world for the treatment of prostate cancer. Its therapeutic action mainly depends on its metabolite flutamide hydroxide, which is a competitive inhibitor of endogenous androgens for binding to their receptors in prostate (Brogden and Clissold 1989). Several rat studies revealed flutamide off target effects, such as decreased weight of the accessory gland, alteration in sex hormone levels in the male rat, and prolongation of the oestrous cycle in female rats (Shin et al. 2002; Toyoda et al. 2000a). Miyata et al. (2002) have linked flutamide exposure to its endocrine related effects in rats. Patients treated with flutamide at its therapeutic dose are always at a higher risk of liver toxicity (Brahm et al. 2011; Tavakkoli et al. 2011), which is presumed to be its idiosyncratic adverse effect. Consequent to an OECD-guideline, repeated-dose, screening for endocrine disruptors compounds (EDCs), flutamide was listed as one of the EDCs (Toyoda et al. 2000b). Endocrine disruptor's chemicals can elucidate toxicity even at low dose (Blumberg et al. 2011). The estimated no observed effect level (NOEL) for flutamide is 0.25 mg/kg/day (Toyoda et al. 2000b). Mimicking endogenous hormones is considered to be one of the important mechanisms of EDCs.

The current guideline set by European Medicines Agency (EMEA) requires that pharmaceutical companies relate the Permitted Daily Exposure (PDE) (EMEA 2014) of API (active pharmaceutical ingredients) to their specific toxicological end points. Residuals of active chemicals generated during the manufacturing cycle and exposure to humans via cross contaminated medicinal products should be considered for estimating the PDE (Hayes et al. 2016). Recently flutamide's PDE of 0.025 mg/day was established as safe dose in the context of reproductive and development disorders end points (Zacharia 2017). Knowing the target tissue concentration and its further integration to the toxicodynamic model should help predict toxicological endpoints (Sharma et al. 2017a, 2017b).

Upon rapid absorption after oral administration, flutamide undergoes extensive hepatic first-pass metabolism in humans generating several metabolites (Katchen and Buxbaum 1975). Flutamide metabolites differs between species due to different tissue distribution and different enzyme activities (Kobayashi et al., 2012). Liver CYP1A2 metabolizes flutamide to flutamide hydroxide (Flu-OH) (Radwanski et al. 1989; Shet et al. 1997; Sjo et al. 2009; Sjögren et al. 2014a). Other metabolites include 4-nitro-3-(trifluoromethyl)-aniline (FLU-1) and 2-methyl-N-(4′-amino-3′ [trifluoromethyl] phenyl) propanamide (FLU-6) (Kobayashi et al., 2012; Wen et al., 2008). Wen et al. (2008) showed that NADPH: cytochrome P450 reductase (CPR) was involved in producing FLU-6 in liver by nitro reduction of flutamide, which enhances hepatocytes cytotoxicity. Complete elimination of flutamide and its metabolites takes 5 days according to an in-vivo human study (Katchen and Buxbaum 1975).

PBPKs models have been applied successfully in toxicology and welcomed by pharmaceutical companies (Jones et al. 2015; Zhuang and Lu 2016). Not only do they estimate target tissue concentrations, but they also allow interspecies extrapolation, intraspecies dose interpolation, and exposure dose reconstruction. PBPK models are mathematical representations of compartments corresponding to the various physiological organs of the body, linked by the circulating blood system. Each compartment is described

by a tissue volume and blood flow rate that is specific to the species of interest. PBPK describes the bio-distribution (absorption, distribution, metabolism and elimination, referred as ADME) and generates time course profiles of chemicals inside the body. A semi-physiologically based biopharmaceutical model has been developed in human for the injectable flutamide hydroxide to estimate the local distribution of the chemical to prostate tissue (Sjögren et al., 2014a). However, to our knowledge there is no full scale PBPK model for flutamide, neither for rats nor for humans.

This article presents physiologically based pharmacokinetic (PBPK) models predicting the time variant concentrations of flutamide in plasma and other organs upon oral dosing in rats and humans. The models were used to simulate single and multiple dose scenarios. The simulated data were compared against the data observed in plasma. In the case of the human PBPK, data referring to the flutamide and its metabolite Flu-OH were taken into consideration. Both the bottom up and the top down approach were applied to the development of the model. Prior mean parameter values were obtained either from the published literature or via in-silico or in-vitro and in-vivo experiments, whilst accounting for uncertainties in the range of ±1 to ±1.5 standard deviations. After a sensitivity analysis, the most uncertain yet influential parameters were distributed statistically for Monte Carlo simulations. We conclude that the models should be suitable for the assessment of flutamide as endocrine disruptor.

2. Material and Methods

2.1. PBPK model development

For both rat and human our PBPK model comprises nine compartments, i.e. gut, liver, plasma, lungs, kidney, fat, gonads, prostate and a compartment representing the rest of the body (Fig. 1). The model is flutamide-specific which includes prostate and gonads; flutamide is used in prostate cancer therapy. The exchange of the flutamide between blood and tissue in each organ is described by flow limited processes i.e. we implemented a perfusion rate-limited PBPK model (not permeability limited). This model works under the assumption that total chemical concentration in the tissue and in the plasma at steady state are in equilibrium with each other. First the model was developed in rats and then extrapolated to humans. Because for the animal models there are more data sets available remaining unmeasurable parameters can be fitted more readily to one group of data sets, whilst using remaining data sets for validation. Accordingly, our strategy was to make an optimal model for rat and then extrapolate this to the human. Oral dosing is considered to be main route. After an oral exposure, flutamide is rapidly absorbed by the system, in a process described using a first order rate constant. Plasma protein binding of flutamide and of its main metabolite (flutamide hydroxide; considered only for human model) was made to conform to the experimentally measured fixed ratio values. The fraction of chemical not bound to plasma proteins is the only fraction of a chemical that is available for transport into organs for metabolism and for clearance.

Distribution parameters such as partition coefficients describe steady state ratios of the concentrations in the plasma and the different organs. Partition coefficients for different organs were derived from the detailed rat in-vivo studies (Asakawa et al., (1995a) using AUC (area under the curve) data. The same partition coefficients were then used for both rat and human PBPK model development. Elimination pathways included both chemical

Chapter 2

metabolism and its urinary excretion. The metabolism of the flutamide was described using the Michaelis-Menten and Hill equations. Data from literature in-vitro cell line studies for both rat and human were scaled to respective in-vivo using IVIVE approach (in-vitro in-vivo extrapolation) (Howgate et al. 2006). Validation of the rat model included several in-vivo kinetic data sets for rat resolving 7 compartments, i.e. plasma, liver, lung, kidney, fat, gonads and prostate. For the validation of the human model, kinetic data sets for flutamide and its metabolite flutamide hydroxide in plasma (Radwanski et al. 1989) were used, as well as multiple dose scenario kinetic data sets (Radwanski et al. 1989). Concentrations of the chemical in any compartment were estimated by applying Eq. (1) without metabolism; however metabolic equation, Eq. (3), is included in the respective compartment responsible for metabolism of chemical. A more detailed model description including the equations used for each compartment is available in the Supplementary file (A).

$$\frac{dCi}{dt} = \frac{Qi \times \left(Ca - \frac{Ci}{Ki:p} \right)}{Vi} \qquad \textbf{Eq. (1)}$$

Here, C_i is the concentration in the tissue i (µg/L), Q_i is the blood flow in the tissue i (L/h), C_a is the arterial concentration (ng/L), $K_{i:p}$ is the partition coefficient of tissue i, and V_i is the volume of the tissue i (L). The blood is considered to flow into a well-mixed extracellular compartment in the tissue where the drug is at partition equilibrium with the intracellular drug. Should there be active drug efflux or influx pumping, this is rather a partition steady state where the partition coefficient becomes dependent on the cells' energy state.

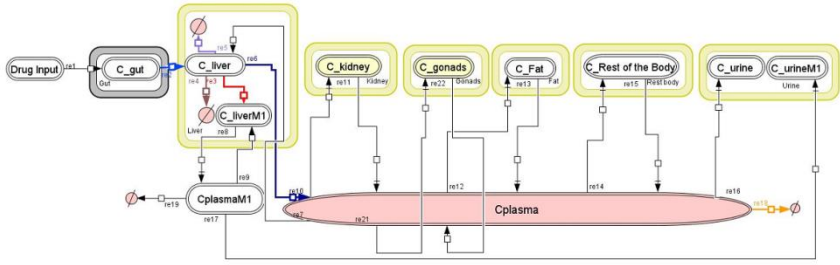

Fig. 1: Minimal PBPK model structure for flutamide and its metabolite flutamide hydroxide. Six tissues, each with a concentration (C) of flutamide (and similarly for flutamide hydroxide) are connected through the blood (plasma). Each compartment has a passive uptake from (as indicated near the beginning of each arrow, reactions re7, re9, re10,re12, re14, re21) and an active release (re6, re8, re11, re22, re13, re15) into the blood, but only the liver can metabolize (reaction re3, re4, re5) and destroy it in its cytosol. re18,

re19 corresponds to flutamide and its metabolite flu-OH protein binding. re16, re17 corresponds to urinary excretion of flutamide and its metabolite flu-OH.

2.2. PBPK Model parameterization

PBPK model parameterization requires physiological parameters, physiochemical properties (fraction unbound and partition coefficient, estimated either by in silico or animal experimentation), and biochemical parameters such as for metabolism (Vmax and Km and other relevant kinetic constants). Our baseline model was for rat and we extrapolated this to the human by adapting the tissue volumes, blood flows through the tissues and the Vmax per unit microsomal protein, and the fraction of microsomal protein per organ on the basis of experimental data. The partition coefficients were considered the same for rat and human.

All the physiological parameters such as blood flow to tissue as a fraction of cardiac blood flow and tissue volume as a fraction of body weight for both rats and human are provided in Table A.1 and A.2 Supplementary Information (SI). Chemical rate constants and metabolic parameters are provided in Table 1. We have estimated prostate volume and blood flow from the reported literature data, for humans (Inaba 1992; Sjögren et al. 2014b) and for rats (Shimizu et al. 2015). As per requirement of PBPK, these data were converted into fraction of body weight and fraction of cardiac blood flow, respectively and are provided in Table A.1 and A.2 (SI)). The oral absorption process for the flutamide was described through a first order absorption rate constant 0.62 h-1 (Xu and Li 1998). The same absorption rate was taken for single and multiple oral doses simulations of the human PBPK model.

We interpreted detailed rat in-vivo data reported in Asakawa et al. (1995) through a method introduced by Gallo et al. (1987) and effectively adapted by others (Lin et al. 2016), This method uses the trapezoidal rule to derive tissue partition coefficients (Kpt) from the AUC (area under the curve) observed in in-vivo animal kinetic profile data of plasma and tissues (The corresponding excel file is provided as supplementary material)

$$K_{i:p} = \frac{AUC_{tissue(0-48)}}{AUC_{plasma(0-48)}} \qquad \textbf{Eq. (2)}$$

Where, AUC_tissue(0-48) represents the area under the curve for the tissue concentration-time curves from 0 to 48 h. AUC_plasma(0-48) represents the area under the curve for the plasma concentrations-time profile from 0 to 48 h. The values of partition coefficients for different organs used in our rat PBPK model are provided in Table 1.

The average binding percentage of flutamide with plasma protein was reported for rats and human as 60.6 and 91.9 %, respectively (Asakawa et al. 1995a). The reported mean value of 95% for Flu-OH (flutamide hydroxide) for human was used to derive the fraction unbound for Flu-OH, which has also been previously used by Sjögren et al. (2014a) for the development of a semi physiologically based pharmacokinetic model. We assumed that intracellularly the same fraction of flutamide is bound to intracellular proteins. The fractional unbound (fu) for both flutamide and its metabolite flutamide hydroxide are provided in Table 1.

Chapter 2

Flutamide metabolism is described as a saturable process utilizing the Michaelis-Menten equation (Eq.3) with parameters Vmax (maximum velocity of metabolic reaction) and Km (1/affinity, i.e. concentration at which reaction occurs at half maximal rate). The reported in-vitro Vmax values for the tissue microsomal fraction were scaled to in-vivo values using the IVIVE approach (Howgate et al. 2006), whereas Km values were kept the same as the in-vitro value. The in-vitro in-vivo extrapolation (IVIVE) approach utilizes physiological specific parameters such as tissue specific microsomal protein content, specific tissue volume and body weight described in Eq. (4) (Yoon et al., 2014).

$$v_{A_{mets}} = \frac{Vmax * C_t * f_u}{Km + C_t * f_u} \quad \textbf{Eq. (3)}$$

Where, Ct is the corresponding concentration in tissue and fu is the fraction unbound.

$v_{A_{mets}}$ is the rate of production of metabolites.

$$Vmax_{invivo} = (Vmax_{invitro} * MSPPGT * V_{tissue})/BW^{.75} \quad \textbf{Eq. (4)}$$

Where, MSPPGT is the microsomal protein per gram tissue; Vtissue is the volume of tissue; BW is the body weight and its power to .75 is to normalize the scaled Vmax for different body weight persons.

The in-vitro data such as Vmax and Km for flutamide metabolism in rats were taken from Yuki Kobayashi et al. (2012). This study reported on flutamide metabolism in different tissue cell lines. The in vitro measured specific activity (Vmax) for liver, lung and kidney provided in Table 1 were scaled to whole body in order to obtain the in-vivo specific intrinsic clearance. For the development of the human PBPK model, the biochemical parameters such as Vmax and Km describing metabolism of flutamide into 3 different metabolites (Fig. 2) were taken from in-vitro hepatic cell line studies (Kobayashi et al., 2012; Sjo et al., 2009; Wen et al., 2008); the corresponding values are provided in Table 1. Eq. (3), basically involves the extrapolation of the specific activity from in-vitro measured to in-vivo whole body, used for the both rat and human using species specific physiological data such as microsomal protein content of tissue, tissue volume and body weight provided in Table A. (1& 2) (SI). Our human PBPK model involves three metabolic reactions producing three different metabolites. However, only flutamide hydroxide, which is the major metabolite, was distributed to plasma from the liver site using the same partition coefficient to that of the parent compound. Due to lack of specific data on the generation of different metabolites, no metabolites were included in the current rat PBPK model. However clearance of flutamide is considered in that model, including its metabolism in rat lung, rat liver and rat kidney as reported by Yuki Kobayashi et al., (2012) in in-vitro cell line studies. Elimination rate constants for both flutamide and flutamide hydroxide were visually optimized to fit the plasma data of human studies carried out by (Radwanski et al., 1989). The flutamide elimination rate constant was needed to optimize in order to match the observed data knowing the fact that there are some unknown flutamide catabolism pathways.

Chapter 2

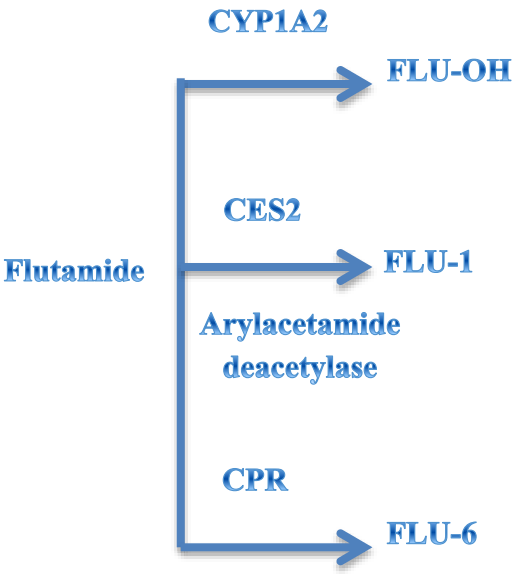

FLU-OH = 2 hydroxy flutamide

FLU-1 = 4-nitro-3-(**trifluoromethyl**)-aniline

FLU-6 = 2-methyl-N-(4′-amino-3′-[trifluoromethyl]phenyl)propanamide

CYP1= cytochrome P450 1A2

CES2 = carboxy esterase CPR = NADPH: cytochrome P450 reductase

Figure2: Schema for human flutamide metabolism; Liver CYP1A2 metabolizes flutamide into flutamide hydroxide, main metabolite. Deacetylation of flutamide by carboxylesterase generates Flu-1. Reduction of aromatic nitro group into amino group by cytochrome reductase results in conversion of Flutamide to FLU-6.

2.3. Sensitivity analysis

A sensitivity analysis (i.e. not global) was carried out both for the rat and for the human PBPK model. The R package FME was used, which measures the alteration in model output for variable of interest by changing each parameter by 1% change up and down whilst keeping the other ones constant. Detailed information about the functions of FME can be found in Soetaert and Petzoldt (2010).

$$Sflutamide,j(t) = \frac{\partial[flutamide(t)]}{\partial p_j} * \frac{p_j}{[flutamide(t)]} = \frac{\partial \ln[flutamide(t)]}{\partial \ln p_j}$$

Where,

$S[flutamide(t)],j$ is the sensitivity of the flutamide concentration to any time-independent parameter p_j, normalized by both the model variable and the parameter value and thereby dimensionless. pj is any parameter of the PBPK model and $[flutamide(t)]$ is the scaling of variable i.e. flutamide plasma concentration.

These sensitivity functions collapsed into a summary of sensitivity values. The magnitude of the time-averaged sensitivity values were used to rank the parameters. This includes the absolute values of the sensitivity coefficients |S| i.e. $\text{flutamide(t)} - \text{flutamide(t)(pj)}$ termed as least absolute deviation, the average of their squares S2 termed as least square

Chapter 2

error, and their average S_{mean} (t), their lowest S_{min} and their highest value (S_{max}), where $|S|_{norm}(t) = \sum_{j=1}^{n_p} \frac{|Sj(t)|}{n_p}$ and $S^2 = \sqrt{\sum \frac{(S_{ij}^2)}{n}}$.

There are two different time average S coefficients: one takes the time average of the coefficients. The other takes the sensitivity of the time average.

The former is:

$$\frac{1}{T} \cdot \sum_{t=0}^{t=T} \frac{\partial \ln[flutamide(t)]}{\partial \ln p_j}$$

The latter is:

$$\frac{\partial \ln\left(\frac{1}{T} \cdot \sum_{t=0}^{t=T}[flutamide(t)]\right)}{\partial \ln p_j} = \frac{\frac{1}{T} \cdot \partial \ln(AUC)}{\partial \ln p_j}$$

2.4. Model Simulation

The PBPK model was developed using ordinary differential equations describing the kinetics of flutamide. The equations were written in the GNU MCSim modeling language (Bois and Maszle 1997) and solved by numerical integration with the GNU MCSim, using the R platform. And a priori information was taken from in vitro and in-vivo experiments reported in the literature. Sensitivity analysis considered mean values of parameters. Monte Carlo simulations were performed to estimate the impact on model predictions of uncertainty in all of the rate constants, the partition coefficients, and the Vmax of the metabolizing enzyme. MC simulation consisted of 15,000 iterations and each corresponded to simulation of the model equations with parameter set defined by a random sample from the probability distributions provided in Table 1. The model was considered to be fit, if all the observed data fell within the range of output simulation between the 2.5th and 97.5th percentile.

2.5. Calibration and Evaluation of PBPK model

First the calibration and then validation of the model was done using data on several compartments. Most of the data were taken from the in-vitro and in-vivo experiments. The unknown parameters prior values were first calibrated against the observed in-vivo data and the logarithms of their values were then assigned a normal distribution. To validate the rat PBPK model, rat experimental data for different organs were used from the Asakawa et al., (1995a) study involving a single oral administration of flutamide at a dose 5 mg/kg. The mean weight of the rats was 250 gram. The time course profile of flutamide concentration in plasma and different organs were recorded at 0.5, 2, 8, 24 and 48 h. The output concentrations data were expressed as the mean (µg/ml) ± SD. The units were converted into µg/L in order to make simulation output and observed data uniform. The kinetic profile for seven compartments, namely plasma, liver, lung, kidney, fat, gonads and prostate were used to evaluate the performance of the model.

Chapter 2

An experimental human study by Radwanski et al., (1989) in which volunteers were orally administered 0.25 g of flutamide was used to evaluate the human PBPK model. The subject characteristics include mean weight, height and age of 89 kg, 180 cm and 66 year, respectively. The study involved two case scenarios: One was administration of a single oral dose of 0.25 g and then measuring the time course profile of flutamide and its metabolite flutamide hydroxide in plasma at 0, 0.5, 1, 1.5, 2, 3, 4, 6 h and at 0, 0.5, 1, 1.5, 2, 3, 4, 6, 8, 12, 16, 24 h, respectively. The second scenario included multiple dosing, i.e. on the first day a single oral dose of 0.25 g, then a dose of 0.25 g three times a day from the 2nd to the 8th day. The observed concentration in plasma on the 6th and the 9th day were recorded for both flutamide and flutamide hydroxide. The data were expressed in mean (ng/ml) and CV.

Table 1: Flutamide chemical and biochemical specific parameter values and its statistical distributions. LN: LOG NORMAL LN(a,b) means a = ln(mean) and b=sd in ln space

Parameters	Symbols	Units	Values or distributions	References
Partition coefficients				-
Liver /Plasma	Kpt:liver/plasma		LN (5.57, 1.5)	a
Lung /Plasma	Kpt:lung/plasma		LN (1.65, 1.1)	a
Kidney/Plasma	Kpt:kidney_plasma	-	LN (2.63, 1.5)	a
Fat/Plasma	Kpt:fat_plasma	-	LN (2.78, 1.1)	a
gonads/Plasma	Kpt:gonads_plasma	-	LN (1.7, 1.5)	a
prostate/Plasma	Kpt:prostate_plasma	-	LN (2.17, 1.1)	a
Rest of the body/Plasma	Kpt:restbody_plasma	-	LN (5.57, 1.1)	a
Liver/ Plasma (FLU-OH)	Kpt:liver_plasmaM1	-	LN (5.57, 1.5)	a
Absorption and elimination parameters				
Unbound fraction in plasma (Flutamide)	fu	-	0.09	(Asakawa et al., 1995)
Unbound fraction in plasma (Flu-OH)	fu1	-	0.05	Sjogren et al. (2014)

Chapter 2

Oral absorption rate	Kgut	1/h	LN (0.64, 1.1)	a
Elimination rate	Kurine	1/h	LN (1.25, 1.5)	optimized
Elimination rate (FLU-OH)	KurineM1	1/h	LN (1.85, 1.5)	optimized
Metabolic parameters for human				
Flu to Flu-OH maximum reaction value	VmaxlivM1_invitro	µg/min/mg MSP	LN (0.079,1.1)[b]	(Sjo et al., 2009)
Conc. at half maximum value	KmliverM1	mg/L	1.113	(Sjo et al., 2009)
Flu to Flu-6 maximum reaction value	VmaxlivM2_invitro	µg/min/mg MSP	LN (0.052, 1.1) [b]	(Wen et al., 2008)
Conc. at half maximum value	KmliverM2	mg/L	23.754	(Wen et al., 2008)
Flu to Flu-1 maximum reaction value	VmaxlivM3_invitro	µg/min/mg MSP	LN (0.31, 1.1) [b]	(Kobayashi et al., 2012)
Conc. at half maximum value	KmliverM3	mg/L	82.863	(Kobayashi et al., 2012)
Metabolic parameters for rat				
Unbound fraction in plasma	fu	-	LN (0.4,1.5)	(Asakawa et al., 1995)
Flu metabolism in liver	VmaxlivM1_inviro	µg/min/mg MSP	LN (0.8,1.2) [b]	(Kobayashi et al., 2012)
Conc. at half maximum value	KmliverM1	g/L	0.276	(Kobayashi et al., 2012)
Flu metabolism in kidney	VmaxkidM1_invitro	µg/min/mg MSP	LN (0.75, 1.1) [b]	(Kobayashi et al., 2012)
Conc. at half maximum value	KmkidneyM1	g/L	1.6	(Kobayashi et al., 2012)
Flutamide metabolism in lung	VmaxlungM1_invitro	µg/min/mg MSP	LN (0.028, 1.1) [b]	(Kobayashi et al., 2012)
Conc. at half maximum value	KmlungM1	g/L	0.193	(Kobayashi et al., 2012)
Oral absorption rate	Kgut	1/h	LN (0.64, 1.1)	a
Renal clearance	Cl_R	L/h	LN (0.07, 1.5) [c]	optimized

a derived from sources explained in parameterization section 2.2 and using same value in case of both rat and human PBPK model
b parameters are scaled to whole body species prior to use in model
c Rat glomeration filtration rate was considered

3. Results

3.1. Rat PBPK Model

The rat PBPK model was used to simulate the experimental data obtained by Asakawa et al. (1995a) for seven different compartments after oral administration of 5 mg/kg to the rat. The model prediction results are presented in Fig.3 (a-g) for 20 random predictions; their median (red), and their two extremes corresponds to 2.5 and 97.5 percentiles (blue). The green points represent the experimentally observed mean concentrations, the black bars represents ±standard deviation. Overall, the experimental in-vivo time course concentrations for several organs Fig.3 (a-g) were adequately predicted by the model. In most of the compartments, model slightly under-predicted the rate of appearance i.e. initial observed experimental points are at or near the 97.5th of the modelling percentile. This indicates that model prediction uncertainty is still much higher than experimental uncertainty: the model uncertainty exceeds the experimental noise and it should therefore be possible to improve the model further by a more precise determination of its parameters. The under-prediction of initial time points by the model could be due to the under-estimation of the gut absorption rate constant parameter. This fact is further supported by the sensitivity results (Table 2), where the gut absorption rate constant parameter has high positive sensitivity coefficient among all other parameters. However, terminal experimental points are close to the predicted median line.

The results also show that the flutamide concentrations in plasma (Fig.3a) were lower than in the other compartments. Fig.4 (a) shows the flutamide concentrations in various organs relative to the concentration in the prostate, again as a function of time. An optimal drug against prostate cancer should have a much lower concentration in gonads and liver, i.e. in organs where this drug is suspected to have side effects than in prostate, where it is supposed to be active against the tumor. And it should have a much lower concentration in liver, where it is removed by metabolism and where metabolic products may cause idiosyncratic liver damage. None of this is true, neither for the model nor for the experimental results. Endocrine related adverse effects shown by flutamide are thought to be mediated by its action in gonads. Here PBPK model shows that flutamide concentrations in the gonad is higher than in the plasma, indicating importance of knowing target concentration and thus risk assessment based on tissue dosimetry model.

Fig. 4 (b) shows the results of AUC as a function of time for plasma, liver, gonads and prostate. After an hour, these organs have had their 90% integral dose. This suggests that multiple low dose would be advantageous than high dosing once a day. With multiple dosing scenarios, one may able to maintain the therapeutic concentrations at target site with minimal exposure to off target organ such as gonads. In contrast single high dosing of flutamide could increase its non-target organs exposure where drug flushes out slowly (mean residence time is higher).

Chapter 2

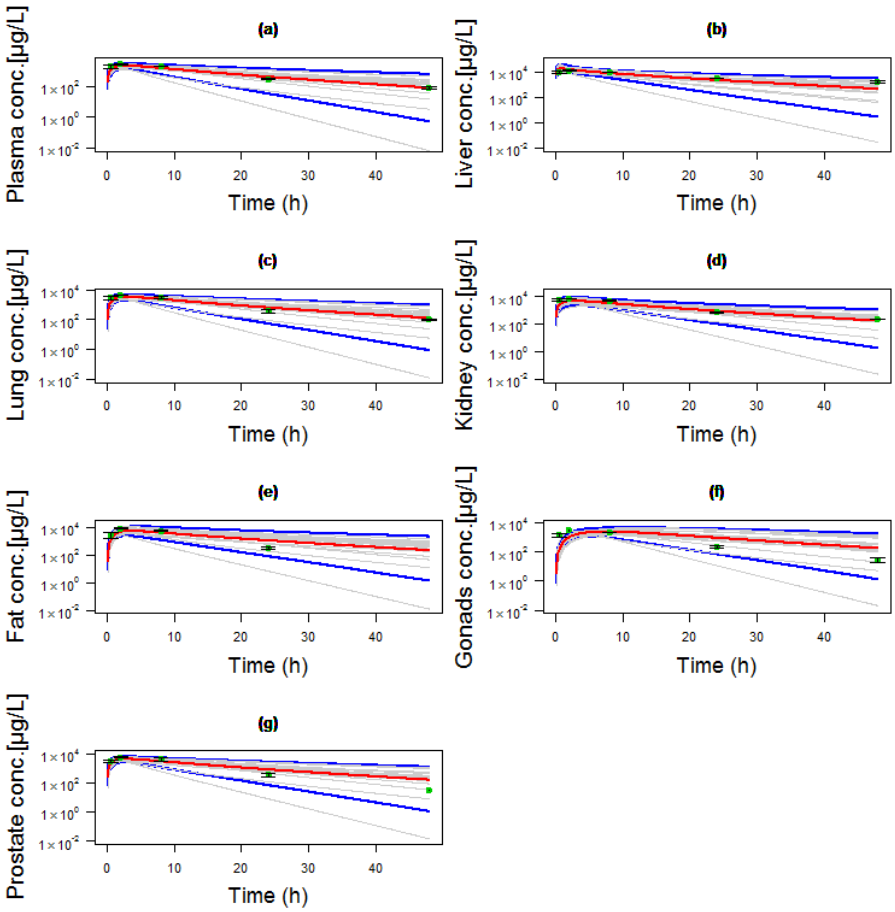

Figure 3: PBPK model predictions of flutamide concentration in various rat compartments following 5 mg/kg oral dose of flutamide. Blue lines: 2.5 and 97.5 percentiles; Gray lines: 20 simulations chosen at random from the ensemble of 15000 models where the parameters were chosen at random within the confines of their log normal distribution parameterized as provided in Table 1. Red lines: median prediction taken from the ensemble of 15000 models; The green dots indicate the mean concentrations and black lines indicate the mean +/- sd reported in (Asakawa et al., (1995a). For the fat compartment (e), the data for 48 h was not available.

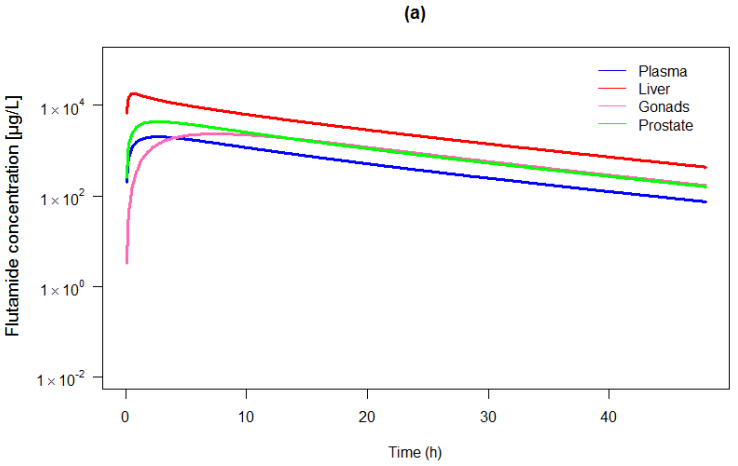

Fig. 4 (a) shows the flutamide concentration as a function of time for plasma, liver, gonads and prostate in log scale, after an oral dosing of 5mg/kg body weight to the rats.

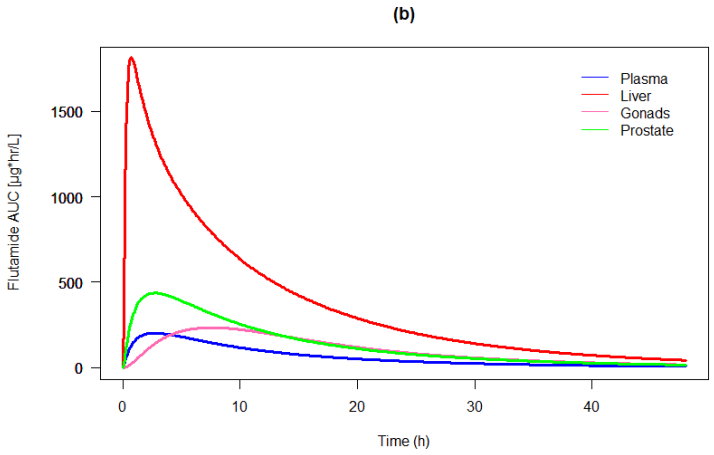

Fig. 4 (b) shows the AUC as a function of time for plasma, liver, gonads and prostate, after an oral dosing of 5mg/kg body weight to the rats.

3.2. Human PBPK model

When simulating tissue concentrations for the human model, the partition coefficients parameters were kept the same than for rat model, whereas the rate constant for absorption was estimated by using the reported (Xu and Li 1998) absorption half-life of 1-2 hour. Fig.5 (A-B) represents the simulated time course of flutamide and its metabolite flutamide

hydroxide in plasma following a single oral dose of 0.25 g. Remarkably, for this extrapolation from rat to human, the 2.5-97.5 percentile of the distribution of the modelling results still includes the experimental results. For flutamide itself, the variation in model prediction is now virtually equal to the experimental variability, suggesting that no further model improvement is called for. Here the experimental reproducibility should be enhanced if it is due to experimental error, or, if it is due to biological variability between individual humans, we therefore should move to individualized models. For flutamide hydroxide the model variability is still a wee bit higher than the experimental variability; here some parameters need to be improved.

Fig.5 (A) shows a small over-prediction by the model of the flutamide concentrations at early times after administration, as compared to the experimental results. At early times, flutamide hydroxide is under-predicted. This suggests that the model underestimates flutamide catabolism to flutamide hydroxide.

The flutamide concentrations decreased within 24 h to significantly lower levels. Therefore, we also simulated repeated dosing of the drug. All the parameters were kept same for the multiple dose scenario simulations, which involved 1st day single dose of 0.25 g and then three times in day from 2nd to 8th day oral dose of 0.25 g and the results are presented in Fig.6 (A-B). Again, all the observed mean points are within the simulated range shows data agreement between simulated and observed. The increase in concentration of flutamide and flutamide for multiple oral doses was captured by the model which has been also observed in human experimental study.

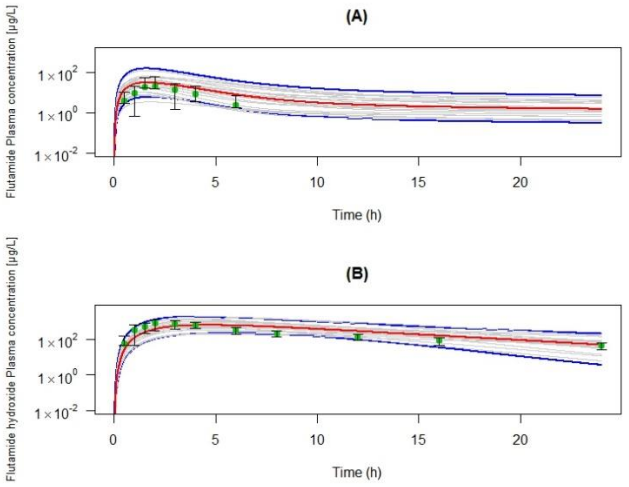

Fig 5: PBPK model predictions of flutamide (A) and flutamide hydroxide (B) concentrations in human plasma following a 0.25 g oral dose of flutamide. Red lines: median predictions; blue lines: 2.5 and 97.5 percentiles; gray lines: 20 random simulations. The green dots and black lines indicate the mean +/- sd concentrations reported in Radwanski et al. (1989).

Chapter 2

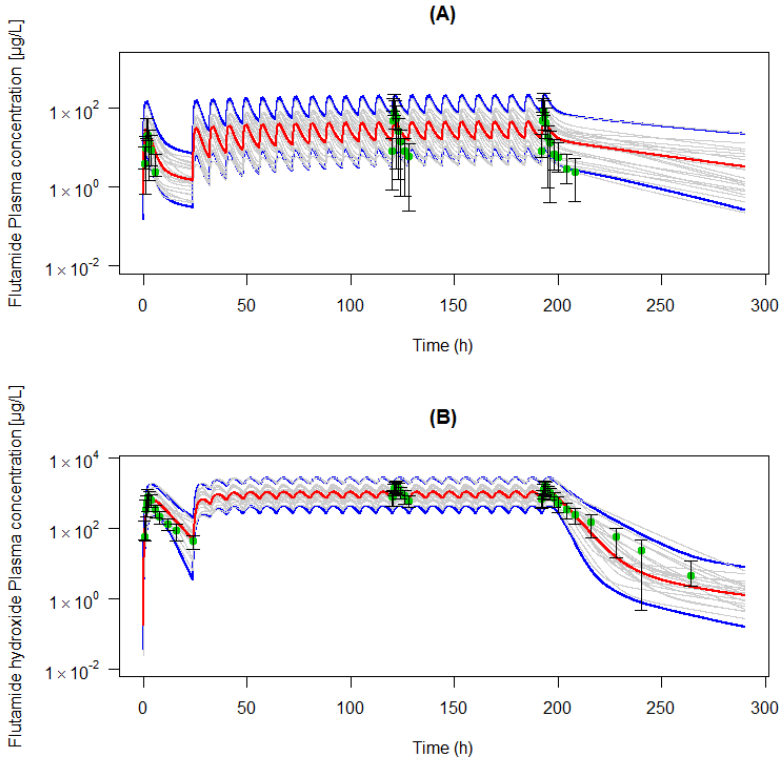

Fig 6: PBPK model predictions of flutamide (A) and flutamide hydroxide (B) plasma concentration in human following a 0.25 g oral dose of flutamide at first day and then 0.25 g three times a day on the 2nd to 8th day. Red line: median prediction; blue lines: 2.5 and 97.5 percentiles; gray lines: 20 random simulations. The green dots and black lines indicate the mean +/- sd concentrations reported in Radwanski et al., (1989).

A further simulation for 48 h after a single oral dose of 0.25 g for several compartments keeping all parameters equal is presented in Fig.7 (A-F). As expected, initially the liver gets a very high concentration of flutamide and then decreases very rapidly as liver actively metabolizes it. Flutamide concentrations into fat and gonads are much lower than in other compartments. Fig 7(D & E) kinetics profile shows that flutamide concentration in these two organs might have longer residence time. This observation should be further investigated, which might be very important as the endocrine effects of flutamide are mainly targeted to the gonads.

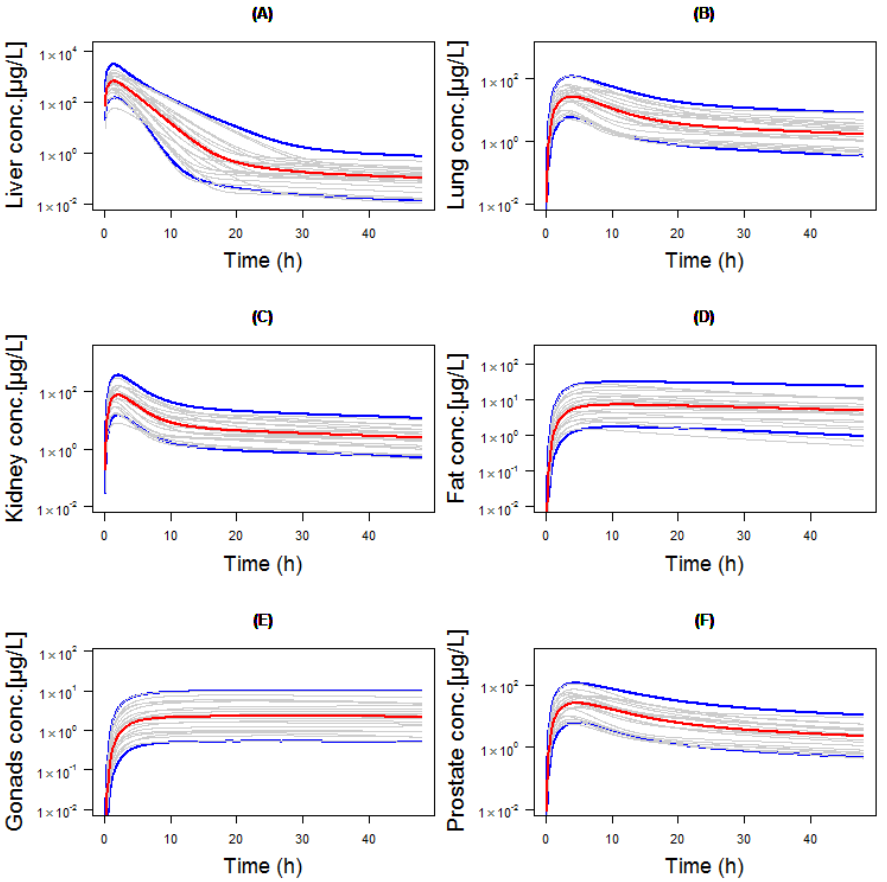

Fig 7: PBPK model predictions of flutamide concentration for 48hr in several human organs following a 0.25 g of single oral dose. Red lines: median predictions; blue lines: 2.5 and 97.5 percentiles; gray lines: 20 random simulations.

3.3. Parameter Sensitivity

A sensitivity analysis was carried out for all the parameters that were used for the development of the PBPK model. The summarized table results for the rat and human PBPK models are provided in Table 2. It includes |S| and |S2| norm, mean, minimum, maximum, and ranking. The table summarizes the statistics of the normalized and dimensionless parameter sensitivity results. Ranking of parameter sensitivity coefficient was done based on |S| that measures least absolute deviation of output (here flutamide plasma concentration)

Sensitivity coefficients results for different parameters are provided in Table 2 (A-B). In turn Fig.8 (A-B) represents the mean sensitivity coefficients. As expected, the sensitivity coefficients of the flutamide concentrations to urine is negative: urine secretes the compound. In humans, the flutamide level in plasma is modelled to be strongly

Chapter 2

influenced by diuresis: its sensitivity coefficient is -1, meaning that a 10 % activation of urination should decrease the flutamide level by 10%. Surprisingly, the sensitivity towards the gut activity is much smaller than expected in the rat model and even negative in the human. The latter finding suggests that the activation of flutamide uptake from the gut cause a decrease in the level of flutamide in the plasma. The explanation is that increased liver uptake of the flutamide activates flutamide degradation earlier; initially the plasma flutamide concentration is may be higher, but the drug is removed more quickly from the body by liver detoxification (first pass metabolic effect). Indeed, in the human the plasma flutamide concentration depends strongly on the drug detoxification reaction in liver, at a sensitivity coefficient of around -1. This shows that flutamide metabolism is an important process for determining the flutamide concentration in plasma. The mean sensitivity coefficient of Vmax is negative and Km is positive. This result suggests that adding these two parameters have opposite effect on flutamide concentration. Statistical distribution of both parameters simultaneously would result in compensation into the output variable i.e. flutamide plasma concentrations. Thus, we restricted probability distributions to Vmax only for the uncertainty analysis, so that it would not influence the output result.

The expectation that the binding fraction to proteins (fu) has a negative control over the free plasma flutamide concentrations was expected because the binding will lower its free concentration. Likewise one should expect that the partition coefficients exert negative control on the plasma flutamide concentrations. The sensitive coefficient at min and max of partition coefficients for liver, kidney exert negative effect or no effect (zero) on flutamide concentration (Table 2.(A)). Indeed, both the liver and the kidney causes clearance of flutamide; in other word, flutamide is not retained in these organs. But for the other tissues such as fat, gonads, lung and prostate, sensitivity coefficient ranges from negative to positive. This indicates that their partition coefficient exert a positive control on the flutamide concentration at the later times. It could be explained by the fact that drug might be retained for longer in these organs, as these are non-metabolizing organs. Accordingly to the results showed in Table 2 (B), the maximum sensitivity coefficient values are in this order: Rest of the body > Fat > gonads > lung > prostate.

Table 2. (A) Summary statistics of parameters' sensitivities

Response variable: Flutamide Plasma concentrations in rat

Parameters	**|S|**	**|S2|**	**S_{mean}**	**S_{min}**	**S_{max}**	**Rank**
kgut	1.826	0.134	0.3	-1.04	63.48	1
fu	1.581	0.048	-1.579	-3.028	0.564	2
kurine	1.076	0.033	-1.076	-2.199	0	3
K_kidney_plasma	1.069	0.033	-1.069	-2.178	0	4
K_restbody_plasma	0.742	0.023	0.607	-0.533	1.643	5
KmliverM1	0.736	0.02	0.736	0	0.974	6

Chapter 2

K_liver_plasma	0.616	0.017	-0.616	-0.96	0	7
VmaxliverM1	0.409	0.011	-0.409	-0.542	0	8
K_fat_plasma	0.142	0.004	0.116	-0.095	0.318	9
K_gonads_plasma	0.008	0	0.006	-0.004	0.023	10
K_lung_plasma	0.007	0	0.006	-0.009	0.015	11
K_prostate_plasma	0.003	0	0.002	-0.006	0.005	12
KmkidneyM1	0.002	0	0.002	-0.001	0.003	13
VmaxkidneyM1	0.001	0	-0.001	-0.008	0.004	14
KmlungM1	0	0	0	-0.002	0.001	15
VmaxlungM1	0	0	0	0	0	16
K_liver_plasmaM1	0	0	0	0	0	17

Table 2. (B) Summary statistics of parameters' sensitivities

Response variable: Flutamide Plasma concentrations in human

Parameters	**|S|**	**|S2|**	**S_{mean}**	**S_{min}**	**S_{max}**	**Rank**
k_liver_plasma	0.987	0.037	-0.987	-0.997	0	1
vmaxliverM1	0.95	0.035	-0.95	-0.992	0	2
kmliverM1	0.904	0.034	0.904	0	0.928	3
k_restbody_plasma	0.513	0.021	-0.513	-0.721	0	4
kurine	0.408	0.016	-0.408	-0.51	0	5
kgut	0.348	0.02	-0.239	-1.126	1.006	6
fu	0.294	0.014	-0.065	-0.837	0.798	7
vmaxliverM3	0.053	0.002	-0.053	-0.057	0	8
kmliverM3	0.053	0.002	0.053	0	0.057	9
k_fat_plasma	0.051	0.002	-0.051	-0.071	0	10

Chapter 2

vmaxliverM2	0.031	0.001	-0.031	-0.034	0	11
kmliverM2	0.031	0.001	0.031	0	0.034	12
k_lung_plasma	0.023	0.001	0.017	-0.024	0.051	13
k_kidney_plasma	0.01	0.001	0.006	-0.048	0.032	14
k_prostate_plasma	0.001	0	0.001	-0.004	0.005	15
k_gonads_plasma	0	0	0	-0.00012	-0.0002	16
k_liver_plasmaM1	0	0	0	0	0	17
kurineM1	0	0	0	0	0	17
fu1	0	0	0	0	0	17

Table 2: Sensitivity results for both the rat and human PBPK model. It includes |S| and $|S^2|$ norm, mean, minimum, maximum, and ranking. Ranking of parameter sensitivity coefficient was done based on |S| that measures least absolute deviation of output (here flutamide plasma concentration)

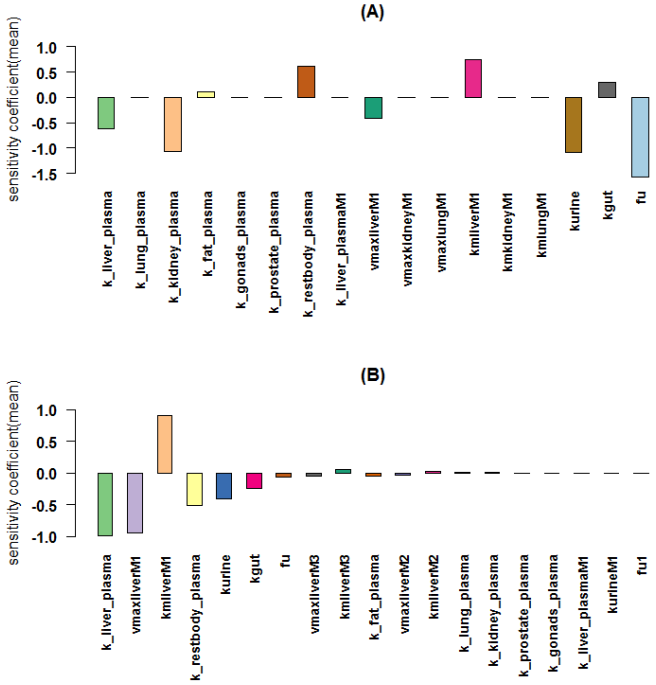

Fig.8. Normalized sensitivity coefficients for the dependence of plasma flutamide concentration 24h after dosing on partition coefficient, Vmax's and KM's, as obtained from simulated time course data of flutamide for 24hr. (A), represents sensitivity coefficients for rat PBPK and (B), represents sensitivity coefficients for human PBPK.

4. Discussion

The present study is the first attempt to develop a two species (Rat and Humans) PBPK model simulating the concentrations of flutamide in various tissues following a single or repetitive oral dose. The model was parameterized on the basis of species-specific physiological data, physicochemical data and independent biochemical data on metabolism such as in-vitro data for both rats and humans. The human model was made specific by inserting human specific data for enzyme activities, organ volumes and blood flow through each organ. Partition coefficients were kept the same as for the rat model. Parameter uncertainties were handled by running multiple models with various values for each uncertain parameter in parallel. This led to uncertainties in the predicted dynamic behavior of flutamide concentrations in the various tissues.

When comparing to dynamic distribution of flutamide over seven rat tissues, the model performed fairly: the median values predicted by the model were less than a factor of 10 away from the average experimental value, for most tissues. In other words, the robustness of the developed PBPK model for predicting flutamide levels in different compartments was substantial. Although the model pointed out high uncertainties in the predictions for some compartments (Fig.3), the observed concentrations were well captured by the predicted intervals (within uncertainty range).

The uncertainty in the rat model predictions was about five times larger than the experimental uncertainty, when evaluated at the 2.5; 97.5 percentile. Surprisingly, predictions for the human plasma levels, although requiring more uncertain steps in model formulation was actually better: the median model values were mostly less than a factor of 4 away from the average experimental value, being the model uncertainty at par with the experimental uncertainty. This suggests that further average model refinement makes no sense, because of limitations in the experimental values.

The limitations in the apparent accuracy of the experimental values could be for either of two reasons: The experimental variability may be due to experimental error, or due to biological variation between individuals. Inspecting the original experimental publications, we conclude that the latter explanation is the more likely one. This implies that rather than looking into improvement of the model or for improvement of the experimental methodology, one should begin to make the models in an individualized way.

The extrapolation of the model to predicting flutamide kinetics in humans with two scenarios of dosing (single and multiple) (Fig. 5 and 6) were also in good agreement with the observed data. Moreover, the prediction of flutamide hydroxide and its agreement with observed data (Fig. 5B and 6B), confirmed that the metabolic kinetic for the production of metabolite in liver (flutamide hydroxide) and its distribution to the plasma was well captured. In the model, flutamide hydroxide was confined to liver and plasma,

Chapter 2

not distributed over all the given compartments owing to the fact of not having data on its bio-distributions. In the worst case scenarios, it would be possible to distribute the flutamide hydroxide presuming its partition coefficient similar with its parent compound or using in-silico approach.

The predictions of flutamide and its metabolite flutamide hydroxide kinetics in human plasma for different dose scenarios suggested that the dose dependency of flutamide kinetics was modelled correctly. This might enhance the model's applicability optimization of doses regimens based on not only the parent compound (usual approach) but also its main metabolite flutamide hydroxide, presumably responsible for pharmacological effects. The current model could be useful for extrapolating low dose scenarios that are relevant for environmental exposure of flutamide as a result of pharmaceutical residuals as well as for verifying low dose animal testing endocrine effects.

However additional research is required to better characterize the flutamide kinetics: the dose dependency that we implemented in the model is uncertain as flutamide is degraded by two different enzymes namely carboxylesterase and arylacetamide deacetylase depending on its concentration (Kobayashi et al., 2012; Watanabe et al., 2009). It should also be useful to measure the kinetics of flutamide simultaneously in plasma and urine in case of the humans, as this should give an additional mode of model validation. Although in this study we have considered the metabolism of flutamide into three different metabolites (assuming hepatic clearance of flutamide), reported studies shows that flutamide can produce even more metabolites in humans, which could lead to a decrease in its own concentration. This would allow for the confirmation of the total observed clearance of flutamide (hepatic and renal) being faster experimentally than in the present model. It also could allow the prediction of other important metabolites as a function of flutamide exposure in the PBPK model and reduce the uncertainties in parameters particularly associated with metabolism and elimination to which the predicted flutamide concentration is sensitive (Fig 8 and Table 2). Additionally, capturing metabolic variation of flutamide due to variation in enzyme level at target metabolizing tissue (liver), correlating with genetic predisposition, and accounting for changes in CYP activity, could enhance our understanding at the level of a personalized PBPK model for flutamide.

The results of this study are promising for application of PBPK modeling in risk assessments of flutamide in human populations in the context of target tissue concentration. To date, no tool has been developed to predict in humans the chemical kinetics in plasma and more importantly tissues concentration along with time. Several future uses of the PBPK model of flutamide could be considered. Here the model could serve to relate the levels to which humans are exposed to the levels attained in various target organs, suspected to be involved in toxicity. By in vitro tissue-specific cell line experiments one could then determine whether those levels should be expected to be toxic or tumorigenic for those tissues. In other words, the current model could be used in a reverse dosimetry context to interpret the available in vitro biomonitoring data so as to estimate the degree to which the population is currently being exposed, an alternative solution to validate the estimated PDE for flutamide for the pharmaceutical companies.

An important issue for EDCs is their idiosyncrasies, i.e. the phenomenon that even if non-toxic for most of the human population, a fraction of the population may

suffer from exposure. One of the origins of this idiosyncrasy may reside in inter-individual differences based on genomic, nutritional or behavioral differences. Such idiosyncrasies are often thought to occur in the PD, i.e. in the effect the EDC has on the body. We suspect that idiosyncrasies may also arise in the PBPK, by some individuals having strongly altered parameters in PD, such as modelled by our model. In future work we shall account for mechanism in or model (or in extended versions thereof) that are affected by known SNPs in the human population. These could reside in drug metabolism, or in drug pumping alterations.

Physiologically specific in nature, the current PBPK model for flutamide could also be adapted to the context of a large human population by considering their metabolic and genetic diversity. This could add explanations of otherwise unexpected sensitivities of small fractions of the population to flutamide and corresponding idiosyncrasies.

Acknowledgement

Preparation of this manuscript was supported in part by the European Union projects HEALS (Health and Environment-wide Associations via Large population Surveys; FP7 Programme under grant agreement no. 603946, EuroMix (European Test and Risk Assessment Strategies for Mixtures); Horizon 2020 Framework Programme under grant agreement no. 633172) Raju Prasad Sharma has received a doctoral fellowship from Universitat Rovira i Virgili under the Martí-Franquès Research Grants Programme. This work was further supported various systems biology grants to HVW, including Synpol: EU-FP7 (KBBE.2012.3.4-02 #311815), Corbel: EU-H2020 (NFRADEV-4-2014-2015 #654248), Epipredict: EU-H2020 MSCA-ITN-2014-ETN: Marie Skłodowska-Curie Innovative Training Networks (ITN-ETN) #642691, BBSRC China: BB/J020060/1.

References

Abduljalil, K., Furness, P., Johnson, T.N., Rostami-Hodjegan, A., Soltani, H., 2012. Anatomical, Physiological and Metabolic Changes with Gestational Age during Normal Pregnancy. Clin. Pharmacokinet. 51, 365–396. https://doi.org/10.2165/11597440-000000000-00000

Abdullah, R., Alhusainy, W., Woutersen, J., Rietjens, I.M.C.M., Punt, A., 2016. Predicting points of departure for risk assessment based on in vitro cytotoxicity data and physiologically based kinetic (PBK) modeling: The case of kidney toxicity induced by aristolochic acid I. Food Chem. Toxicol. 92, 104–116. https://doi.org/10.1016/j.fct.2016.03.017

Adachi, K., Suemizu, H., Murayama, N., Shimizu, M., Yamazaki, H., 2015. Human biofluid concentrations of mono(2-ethylhexyl)phthalate extrapolated from pharmacokinetics in chimeric mice with humanized liver administered with di(2-ethylhexyl)phthalate and physiologically based pharmacokinetic modeling. Environ. Toxicol. Pharmacol. https://doi.org/10.1016/j.etap.2015.02.011

Aderem, A., 2005. Systems biology: Its practice and challenges. Cell 121, 511–513.

Chapter 2

https://doi.org/10.1016/j.cell.2005.04.020

Akingbemi, B.T., Sottas, C.M., Koulova, A.I., Klinefelter, G.R., Hardy, M.P., 2004. Inhibition of Testicular Steroidogenesis by the Xenoestrogen Bisphenol a Is Associated with Reduced Pituitary Luteinizing Hormone Secretion and Decreased Steroidogenic Enzyme Gene Expression in Rat Leydig Cells. Endocrinology 145, 592–603. https://doi.org/10.1210/en.2003-1174

Andersen, M.E., Krewski, D., 2009. Toxicity testing in the 21st century: Bringing the vision to life. Toxicol. Sci. 107, 324–330. https://doi.org/10.1093/toxsci/kfn255

Andersen, M.E., Thomas, R.S., Gaido, K.W., Conolly, R.B., 2005. Dose-response modeling in reproductive toxicology in the systems biology era. Reprod. Toxicol. 19, 327–337. https://doi.org/10.1016/j.reprotox.2004.12.004

Andrade, R., Agundez, J., Lucena, M., Martinez, C., Cueto, R., Garcia-Martin, E., 2009. Pharmacogenomics in Drug Induced Liver Injury. Curr. Drug Metab. 10, 956–970. https://doi.org/10.2174/138920009790711805

Ankley, G.T., Bennett, R.S., Erickson, R.J., Hoff, D.J., Hornung, M.W., Johnson, R.D., Mount, D.R., Nichols, J.W., Russom, C.L., Schmieder, P.K., Serrrano, J.A., Tietge, J.E., Villeneuve, D.L., 2010. Adverse outcome pathways: A conceptual framework to support ecotoxicology research and risk assessment. Environ. Toxicol. Chem. 29, 730–741. https://doi.org/10.1002/etc.34

Ansoumane, K., Duan, P., Quan, C., Yaima, M.L.T., Liu, C., Wang, C., Fu, W., Qi, S., Yu, T., Yang, K., 2014. Bisphenol A induced reactive oxygen species (ROS) in the liver and affect epididymal semen quality in adults Sprague-Dawley rats. J. Toxicol. Environ. Heal. Sci. 6, 103–112. https://doi.org/10.5897/JTEHS2014.0309

Aris, A., 2014. Estimation of bisphenol A (BPA) concentrations in pregnant women, fetuses and nonpregnant women in Eastern Townships of Canada. Reprod. Toxicol. 45, 8–13. https://doi.org/10.1016/j.reprotox.2013.12.006

Arrell, D.K., Terzic, a, 2010. Network systems biology for drug discovery. Clin. Pharmacol. Ther. 88, 120–125. https://doi.org/10.1038/clpt.2010.91

Asakawa, N., Koyama, M., Hashimoto, Y., Yamashita, K., 1995. Studies on the Metabolic Fate of Flutamide. (1): Plasma Concentration after Single Administration and Protein Binding in Rats. Drug Metab. Pharmacokinet. 10, 447–453. https://doi.org/10.2133/dmpk.10.447

Atanasov, A.G., Tam, S., Röcken, J.M., Baker, M.E., Odermatt, A., 2003. Inhibition of 11β-hydroxysteroid dehydrogenase type 2 by dithiocarbamates. Biochem. Biophys. Res. Commun. 308, 257–262. https://doi.org/10.1016/S0006-291X(03)01359-7

Auffray, C., Chen, Z., Hood, L., 2009. Systems medicine: the future of medical genomics and healthcare. Genome Med. 1, 2. https://doi.org/10.1186/gm2

Chapter 2

Ball, A.L., Kamalian, L., Alfirevic, A., Lyon, J.J., Chadwick, A.E., 2016. Identification of the additional mitochondrial liabilities of 2-hydroxyflutamide when compared with its parent compound, flutamide in HepG2 cells. Toxicol. Sci. 153, 341–351. https://doi.org/10.1093/toxsci/kfw126

Bartel, D.P., 2004. MicroRNAs: Genomics, Biogenesis, Mechanism, and Function. Cell 116, 281–297. https://doi.org/10.1016/S0092-8674(04)00045-5

Bartlett, D.W., Davis, M.E., 2006. Insights into the kinetics of siRNA-mediated gene silencing from live-cell and live-animal bioluminescent imaging. Nucleic Acids Res. 34, 322–333. https://doi.org/10.1093/nar/gkj439

Bell, S.M., Chang, X., Wambaugh, J.F., Allen, D.G., Bartels, M., Brouwer, K.L.R., Casey, W.M., Choksi, N., Ferguson, S.S., Fraczkiewicz, G., Jarabek, A.M., Ke, A., Lumen, A., Lynn, S.G., Paini, A., Price, P.S., Ring, C., Simon, T.W., Sipes, N.S., Sprankle, C.S., Strickland, J., Troutman, J., Wetmore, B.A., Kleinstreuer, N.C., 2018. In vitro to in vivo extrapolation for high throughput prioritization and decision making. Toxicol. Vitr. 47, 213–227. https://doi.org/10.1016/j.tiv.2017.11.016

Berson, A., Wolf, C., Chachaty, C., Fisch, C., Fau, D., Eugene, D., Loeper, J., Gauthier, J.-C., Beaune, P., Pompon, D., Maurel, P., Pessayre, D., 1993. Metabolic activation of the nitroaromatic antiandrogen flutamide by rat and human cytochromes P-450, including forms belonging to the 3A and 1A subfamilies. J. Pharmacol. Exp. Ther. 265, 366–372.

Bessems, J., Coecke, S., Gouliarmou, V., Whelan, M., Worth, A., 2015. EURL ECVAM strategy for achieving 3Rs impact in the assessment of toxicokinetics and systemic toxicity 22. https://doi.org/10.2788/197633

Bhattacharya, S., Shoda, L.K.M., Zhang, Q., Woods, C.G., Howell, B.A., Siler, S.Q., Woodhead, J.L., Yang, Y., McMullen, P., Watkins, P.B., Melvin, E.A., 2012. Modeling drug- and chemical-induced hepatotoxicity with systems biology approaches. Front. Physiol. 3 DEC, 1–18. https://doi.org/10.3389/fphys.2012.00462

Birgelen, a Van, Birgelen, a Van, Smit, E., Smit, E., Kampen, I., Kampen, I., 1995. Subchronic effects of 2, 3, 7, 8-TCDD or PCBs on thyroid hormone metabolism: use in risk assessment. Eur. J. Pharmacol. Environ. Toxicol. {…} 293, 77–85.

Bloomingdale, P., Housand, C., Apgar, J.F., Millard, B.L., Mager, D.E., Burke, J.M., Shah, D.K., 2017. Quantitative systems toxicology. Curr. Opin. Toxicol. 4, 79–87. https://doi.org/10.1016/j.cotox.2017.07.003

Boberg, J., Metzdorff, S., Wortziger, R., Axelstad, M., Brokken, L., Vinggaard, A.M., Dalgaard, M., Nellemann, C., 2008. Impact of diisobutyl phthalate and other PPAR agonists on steroidogenesis and plasma insulin and leptin levels in fetal rats. Toxicology 250, 75–81. https://doi.org/10.1016/j.tox.2008.05.020

Boelsterli, U.A., Lim, P.L.K., 2007. Mitochondrial abnormalities—A link to

Chapter 2

idiosyncratic drug hepatotoxicity? Toxicol. Appl. Pharmacol. 220, 92–107. https://doi.org/10.1016/j.taap.2006.12.013

Bonate, P.L., 2011. Pharmacokinetic-Pharmacodynamic Modeling and Simulation. Springer US, Boston, MA. https://doi.org/10.1007/978-1-4419-9485-1

Boulle, F., van den Hove, D.L. a, Jakob, S.B., Rutten, B.P., Hamon, M., van Os, J., Lesch, K.-P., Lanfumey, L., Steinbusch, H.W., Kenis, G., Hove, D.L.A. Van Den, Jakob, S.B., Rutten, B.P., Hamon, M., Os, J. Van, Lesch, K.-P., van den Hove, D.L. a, Jakob, S.B., Rutten, B.P., Hamon, M., van Os, J., Lesch, K.-P., Lanfumey, L., Steinbusch, H.W., Kenis, G., 2012. Epigenetic regulation of the BDNF gene: implications for psychiatric disorders. Mol. Psychiatry 17, 584–596. https://doi.org/10.1038/mp.2011.107

Bouskine, A., Nebout, M., Brücker-Davis, F., Banahmed, M., Fenichel, P., 2009. Low doses of bisphenol A promote human seminoma cell proliferation by activating PKA and PKG via a membrane G-protein-coupled estrogen receptor. Environ. Health Perspect. 117, 1053–1058. https://doi.org/10.1289/ehp.0800367

Brahm, J., Brahm, M., Segovia, R., Latorre, R., Zapata, R., Poniachik, J., Buckel, E., Contreras, L., 2011. Acute and fulminant hepatitis induced by flutamide: case series report and review of the literature. Ann. Hepatol. 10, 93–8.

Brown, R.P., Delp, M.D., Lindstedt, S.L., Rhomberg, L.R., Beliles, R.P., 1997. Physiological parameter values for physiologically based pharmacokinetic models. Toxicol. Ind. Health 13, 407–484.

Bursac, N., Kirkton, R.D., Mcspadden, L.C., Liau, B., 2010. Circulating levels of brain-derived neurotrophic factor: correlation with mood, cognition and motor function. Biomark. Med. 4, 871–87.

Calabrese, E.J., Baldwin, L.A., 2003. Toxicology rethinks its central belief. Nature 421, 691–692. https://doi.org/10.1038/421691a

Cao, X.L., Zhang, J., Goodyer, C.G., Hayward, S., Cooke, G.M., Curran, I.H.A., 2012. Bisphenol A in human placental and fetal liver tissues collected from Greater Montreal area (Quebec) during 1998-2008. Chemosphere 89, 505–511. https://doi.org/10.1016/j.chemosphere.2012.05.003

Caputo, V., Sinibaldi, L., Fiorentino, A., Parisi, C., Catalanotto, C., Pasini, A., Cogoni, C., Pizzuti, A., 2011. Brain derived neurotrophic factor (BDNF) expression is regulated by microRNAs miR-26a and miR-26b allele-specific binding. PLoS One 6. https://doi.org/10.1371/journal.pone.0028656

Carlotti, F., Dower, S.K., Qwarnstrom, E.E., 2000. Dynamic shuttling of nuclear factor ??B between the nucleus and cytoplasm as a consequence of inhibitor dissociation. J. Biol. Chem. 275, 41028–41034. https://doi.org/10.1074/jbc.M006179200

Castillo, B., del Cerro, M., Breakefield, X.O., Frim, D.M., Barnstable, C.J., Dean, D.O.,

Chapter 2

Bohn, M.C., 1994. Retinal ganglion cell survival is promoted by genetically modified astrocytes designed to secrete brain-derived neurotrophic factor (BDNF). Brain Res. 647, 30–36. https://doi.org/10.1016/0006-8993(94)91395-1

Castro, B., Sánchez, P., Torres, J.M., Preda, O., del Moral, R.G., Ortega, E., 2013. Bisphenol A Exposure during Adulthood Alters Expression of Aromatase and 5α-Reductase Isozymes in Rat Prostate. PLoS One 8, 1–7. https://doi.org/10.1371/journal.pone.0055905

Chang, Z., Lu, M., Kim, S.S., Park, J.S., 2014. Potential role of HSP90 in mediating the interactions between estrogen receptor (ER) and aryl hydrocarbon receptor (AhR) signaling pathways. Toxicol. Lett. 226, 6–13. https://doi.org/10.1016/j.toxlet.2014.01.032

Chen, N., Li, J., Li, D., Yang, Y., He, D., 2014. Chronic exposure to perfluorooctane sulfonate induces behavior defects and neurotoxicity through oxidative damages, in Vivo and in Vitro. PLoS One 9, 1–10. https://doi.org/10.1371/journal.pone.0113453

Chitra, K.C., Latchoumycandane, C., Mathur, P.P., 2003. Induction of oxidative stress by bisphenol A in the epididymal sperm of rats. Toxicology 185, 119–127. https://doi.org/10.1016/S0300-483X(02)00597-8

Choi, K., Joo, H., Campbell, J.L., Andersen, M.E., Clewell, H.J., 2013. In vitro intestinal and hepatic metabolism of Di(2-ethylhexyl) phthalate (DEHP) in human and rat. Toxicol. Vitr. 27, 1451–1457. https://doi.org/10.1016/j.tiv.2013.03.012

Clarke, G., Collins, R.A., Leavitt, B.R., Andrews, D.F., Hayden, M.R., Lumsden, C.J., McInnes, R.R., 2000. A one-hit model of cell death in inherited neuronal degenerations. Nature 406, 195–199. https://doi.org/10.1038/35018098

Clewell, H.J., Gearhart, J.M., Gentry, P.R., Covington, T.R., VanLandingham, C.B., Crump, K.S., Shipp, A.M., 1999. Evaluation of the uncertainty in an oral reference dose for methylmercury due to interindividual variability in pharmacokinetics. Risk Anal. 19, 547–558. https://doi.org/10.1023/A:1007017116171

Clewell, R. a, Merrill, E. a, Narayanan, L., Gearhart, J.M., Robinson, P.J., 2004. Evidence for competitive inhibition of iodide uptake by perchlorate and translocation of perchlorate into the thyroid. Int. J. Toxicol. 23, 17–23. https://doi.org/10.1080/10915810490275044

Clewell, R.A., Clewell, H.J., 2008. Development and specification of physiologically based pharmacokinetic models for use in risk assessment. Regul. Toxicol. Pharmacol. 50, 129–43. https://doi.org/10.1016/j.yrtph.2007.10.012

Coe, K.J., Jia, Y., Han, K.H., Rademacher, P., Bammler, T.K., Beyer, R.P., Farin, F.M., Woodke, L., Plymate, S.R., Fausto, N., Nelson, S.D., 2007. Comparison of the cytotoxicity of the nitroaromatic drug flutamide to its cyano analogue in the hepatocyte cell line TAMH: Evidence for complex I inhibition and mitochondrial

Chapter 2

dysfunction using toxicogenomic screening. Chem. Res. Toxicol. 20, 1277–1290. https://doi.org/10.1021/tx7001349

Coe, K.J., Nelson, S.D., Ulrich, R.G., He, Y., Dai, X., Cheng, O., Caguyong, M., Roberts, C.J., Slatter, J.G., 2006. Profiling the hepatic effects of flutamide in rats: A microarray comparison with classical aryl hydrocarbon receptor ligands and atypical CYP1A inducers. Drug Metab. Dispos. 34, 1266–1275. https://doi.org/10.1124/dmd.105.009159

Cooper, R.L., Stoker, T.E., Tyrey, L., Goldman, J.M., McElroy, W.K., 2000. Atrazine disrupts the hypothalamic control of pituitary-ovarian function. Toxicol. Sci. 53, 297–307. https://doi.org/10.1093/toxsci/53.2.297

Coughlin, J.L., Thomas, P.E., Buckley, B., 2012. Inhibition of genistein glucuronidation by bisphenol A in human and rat liver microsomes. Drug Metab. Dispos. 40, 481–485. https://doi.org/10.1124/dmd.111.042366

Csanády, G., Oberste-Frielinghaus, H., Semder, B., Baur, C., Schneider, K., Filser, J., 2002. Distribution and unspecific protein binding of the xenoestrogens bisphenol A and daidzein. Arch. Toxicol. 76, 299–305. https://doi.org/10.1007/s00204-002-0339-5

Cubitt, H.E., Houston, J.B., Galetin, A., 2011. Prediction of human drug clearance by multiple metabolic pathways: Integration of hepatic and intestinal microsomal and cytosolic data. Drug Metab. Dispos. 39, 864–873. https://doi.org/10.1124/dmd.110.036566

Cubitt, H.E., Houston, J.B., Galetin, A., 2009. Relative Importance of Intestinal and Hepatic Glucuronidation—Impact on the Prediction of Drug Clearance. Pharm. Res. 26, 1073–1083. https://doi.org/10.1007/s11095-008-9823-9

Davies, B., Morris, T., 1993. No Title. Pharm. Res. 10, 1093–1095. https://doi.org/10.1023/A:1018943613122

Dieckhaus, C.M., Thompson, C.D., Roller, S.G., Macdonald, T.L., 2002. Mechanisms of idiosyncratic drug reactions: the case of felbamate. Chem. Biol. Interact. 142, 99–117. https://doi.org/10.1016/S0009-2797(02)00057-1

Dinkova-Kostova, A.T., Holtzclaw, W.D., Cole, R.N., Itoh, K., Wakabayashi, N., Katoh, Y., Yamamoto, M., Talalay, P., 2002. Direct evidence that sulfhydryl groups of Keap1 are the sensors regulating induction of phase 2 enzymes that protect against carcinogens and oxidants. Proc. Natl. Acad. Sci. U. S. A. 99, 11908–13. https://doi.org/10.1073/pnas.172398899

Djuranovic, S., Nahvi, A., Green, R., 2011. A Parsimonious Model for Gene Regulation by miRNAs. Science (80-.). 331, 550–553. https://doi.org/10.1126/science.1191138

Doerge, D.R., Twaddle, N.C., Vanlandingham, M., Brown, R.P., Fisher, J.W., 2011. Distribution of bisphenol A into tissues of adult, neonatal, and fetal Sprague–

Chapter 2

Dawley rats. Toxicol. Appl. Pharmacol. 255, 261–270. https://doi.org/10.1016/j.taap.2011.07.009

Doering, D.D., Steckelbroeck, S., Doering, T., Klingmüller, D., 2002. Effects of butyltins on human 5alpha-reductase type 1 and type 2 activity. Steroids 67, 859–867.

El-Masri, H., 2013. Modeling for Regulatory Purposes (Risk and Safety Assessment), in: Reisfeld, B., Mayeno, A.N. (Eds.), . Humana Press, Totowa, NJ, pp. 297–303. https://doi.org/10.1007/978-1-62703-059-5_13

Espinosa-Diez, C., Miguel, V., Mennerich, D., Kietzmann, T., Sánchez-Pérez, P., Cadenas, S., Lamas, S., 2015. Antioxidant responses and cellular adjustments to oxidative stress. Redox Biol. 6, 183–197. https://doi.org/10.1016/j.redox.2015.07.008

Fabrega, F., Kumar, V., Schuhmacher, M., Domingo, J.L., Nadal, M., 2014. PBPK modeling for PFOS and PFOA: Validation with human experimental data. Toxicol. Lett. 230, 244–251. https://doi.org/10.1016/j.toxlet.2014.01.007

Fàbrega, F., Nadal, M., Schuhmacher, M., Domingo, J.L., Kumar, V., 2016. Influence of the uncertainty in the validation of PBPK models: A case-study for PFOS and PFOA. Regul. Toxicol. Pharmacol. 77, 230–239. https://doi.org/10.1016/j.yrtph.2016.03.009

Fang, H., Tong, W., Branham, W.S., Moland, C.L., Dial, S.L., Hong, H., Xie, Q., Perkins, R., Owens, W., Sheehan, D.M., 2003. Study of 202 Natural, Synthetic, and Environmental Chemicals for Binding to the Androgen Receptor. Chem. Res. Toxicol. 16, 1338–1358. https://doi.org/10.1021/tx030011g

Fisher, J.W., Twaddle, N.C., Vanlandingham, M., Doerge, D.R., 2011. Pharmacokinetic modeling: Prediction and evaluation of route dependent dosimetry of bisphenol A in monkeys with extrapolation to humans. Toxicol. Appl. Pharmacol. 257, 122–136. https://doi.org/10.1016/j.taap.2011.08.026

Fletcher, J.M., Morton, C.J., Zwar, R.A., Murray, S.S., O'Leary, P.D., Hughes, R.A., 2008. Design of a conformationally defined and proteolytically stable circular mimetic of brain-derived neurotrophic factor. J. Biol. Chem. 283, 33375–33383. https://doi.org/10.1074/jbc.M802789200

Forsby, A., Blaauboer, B., 2007. Integration of in vitro neurotoxicity data with biokinetic modelling for the estimation of in vivo neurotoxicity. Hum. Exp. Toxicol. 26, 333–338. https://doi.org/10.1177/0960327106072994

Foxenberg, R.J., Ellison, C.A., Knaak, J.B., Ma, C., Olson, J.R., 2011. Cytochrome P450-specific human PBPK/PD models for the organophosphorus pesticides: Chlorpyrifos and parathion. Toxicology 285, 57–66. https://doi.org/10.1016/j.tox.2011.04.002

Friedmann, A.S., 2002. Atrazine inhibition of testosterone production in rat males

Chapter 2

following peripubertal exposure. Reprod. Toxicol. 16, 275–279. https://doi.org/10.1016/S0890-6238(02)00019-9

Fukumitsu, H., Ohtsuka, M., Murai, R., Nakamura, H., Itoh, K., Furukawa, S., 2006. Brain-Derived Neurotrophic Factor Participates in Determination of Neuronal Laminar Fate in the Developing Mouse Cerebral Cortex. J. Neurosci. 26, 13218–13230. https://doi.org/10.1523/JNEUROSCI.4251-06.2006

Fukuzawa, N.H., Ohsako, S., Wu, Q., Sakaue, M., Fujii-Kuriyama, Y., Baba, T., Tohyama, C., 2004. Testicular cytochrome P450scc and LHR as possible targets of 2,3,7,8-tetrachlorodibenzo-p-dioxin (TCDD) in the mouse. Mol. Cell. Endocrinol. 221, 87–96. https://doi.org/10.1016/j.mce.2004.02.005

Gabrielsson, J., Weiner, D., 2012. Non-compartmental Analysis, in: Reisfeld, B., Mayeno, A.N. (Eds.), Methods in Molecular Biology. Humana Press, Totowa, NJ, pp. 377–389. https://doi.org/10.1007/978-1-62703-050-2_16

García Cortés, M., Andrade, R.J., Lucena, M.I., Sánchez Martínez, H., Fernández, M.C., Ferrer, T., Martín-Vivaldi, R., Peláez, G., Suárez, F., Romero-Gómez, M., Montero, J.L., Fraga, E., Camargo, R., Alcántara, R., Pizarro, M.A., García-Ruiz, E., Rosemary-Gómez, M., 2001. Flutamide-induced hepatotoxicity: report of a case series. Rev. Esp. Enferm. Dig. 93, 423–32.

Generali, J.A., Cada, D.J., 2014. Flutamide: Hirsutism in Women. Hosp. Pharm. 49, 517–520. https://doi.org/10.1310/hpj4906-517

Gentry, P.R., Covington, T.R., Andersen, M.E., Clewell, H.J., 2002. Application of a physiologically based pharmacokinetic model for isopropanol in the derivation of a reference dose and reference concentration. Regul. Toxicol. Pharmacol. 36, 51–68. https://doi.org/S0273230002915400 [pii]

Gerona, R.R., Woodruff, T.J., Dickenson, C.A., Pan, J., Jackie, M., Sen, S., Friesen, M.M., Fujimoto, V.Y., Hunt, P.A., 2014. California population 47. https://doi.org/10.1021/es402764d.Bisphenol-A

Gibbs, J.P., Yang, J.S., Slattery, J.T., 1998. Comparison of human liver and small intestinal glutathione S-transferase-catalyzed busulfan conjugation in vitro. Drug Metab. Dispos. 26, 52–55.

Gillespie, L.N., Clark, G.M., Bartlett, P.F., Marzella, P.L., 2003. BDNF-induced survival of auditory neurons in vivo: Cessation of treatment leads to accelerated loss of survival effects. J. Neurosci. Res. 71, 785–790. https://doi.org/10.1002/jnr.10542

Gim, J., Kim, H.S., Kim, J., Choi, M., Kim, J.R., Chung, Y.J., Cho, K.H., 2010. A system-level investigation into the cellular toxic response mechanism mediated by AhR signal transduction pathway. Bioinformatics 26, 2169–2175. https://doi.org/10.1093/bioinformatics/btq400

Godin, S.J., Scollon, E.J., Hughes, M.F., Potter, P.M., DeVito, M.J., Ross, M.K., 2006.

Chapter 2

Species differences in the in vitro metabolism of deltamethrin and esfenvalerate: Differential oxidative and hydrolytic metabolism by humans and rats. Drug Metab. Dispos. 34, 1764–1771. https://doi.org/10.1124/dmd.106.010058

Gomez, J.-L., Dupont, A., Cusan, L., Tremblay, M., Suburu, R., Lemay, M., Labrie, F., 1992. Incidence of liver toxicity associated with the use of flutamide in prostate cancer patients. Am. J. Med. 92, 465–470. https://doi.org/10.1016/0002-9343(92)90741-S

Goudarzi, H., Nakajima, S., Ikeno, T., Sasaki, S., Kobayashi, S., Miyashita, C., Ito, S., Araki, A., Nakazawa, H., Kishi, R., 2016. Prenatal exposure to perfluorinated chemicals and neurodevelopment in early infancy: The Hokkaido Study. Sci. Total Environ. 541, 1002–1010. https://doi.org/10.1016/j.scitotenv.2015.10.017

Gumy, C., Chandsawangbhuwana, C., Dzyakanchuk, A. a., Kratschmar, D. V., Baker, M.E., Odermatt, A., 2008. Dibutyltin disrupts glucocorticoid receptor function and impairs glucocorticoid-induced suppression of cytokine production. PLoS One 3. https://doi.org/10.1371/journal.pone.0003545

Haley, B., Zamore, P.D., 2004. Kinetic analysis of the RNAi enzyme complex. Nat. Struct. Mol. Biol. 11, 599–606. https://doi.org/10.1038/nsmb780

Hany, J., Lilienthal, H., Sarasin, a, Roth-Härer, a, Fastabend, a, Dunemann, L., Lichtensteiger, W., Winneke, G., 1999. Developmental exposure of rats to a reconstituted PCB mixture or aroclor 1254: effects on organ weights, aromatase activity, sex hormone levels, and sweet preference behavior. Toxicol. Appl. Pharmacol. 158, 231–243. https://doi.org/10.1006/taap.1999.8710

Hayes, T.B., Anderson, L.L., Beasley, V.R., de Solla, S.R., Iguchi, T., Ingraham, H., Kestemont, P., Kniewald, J., Kniewald, Z., Langlois, V.S., Luque, E.H., McCoy, K.A., Muñoz-de-Toro, M., Oka, T., Oliveira, C.A., Orton, F., Ruby, S., Suzawa, M., Tavera-Mendoza, L.E., Trudeau, V.L., Victor-Costa, A.B., Willingham, E., 2011. Demasculinization and feminization of male gonads by atrazine: Consistent effects across vertebrate classes. J. Steroid Biochem. Mol. Biol. 127, 64–73. https://doi.org/10.1016/j.jsbmb.2011.03.015

Heidrich, D.D., Steckelbroeck, S., Klingmuller, D., 2001. Inhibition of human cytochrome P450 aromatase activity by butyltins. Steroids 66, 763–769.

Hood, L., Heath, J.R., Phelps, M.E., Lin, B., 2004. Systems biology and new technologies enable predictive and preventative medicine. Science 306, 640–643. https://doi.org/10.1126/science.1104635

Ikezuki, Y., Tsutsumi, O., Takai, Y., Kamei, Y., Taketani, Y., 2002. Determination of bisphenol A concentrations in human biological fluids reveals significant early prenatal exposure. Hum. Reprod. 17, 2839–2841. https://doi.org/10.1093/humrep/17.11.2839

Jaeschke, H., McGill, M.R., Ramachandran, A., 2012. Oxidant stress, mitochondria, and cell death mechanisms in drug-induced liver injury: lessons learned from

Chapter 2

acetaminophen hepatotoxicity. Drug Metab. Rev. 44, 88–106. https://doi.org/10.3109/03602532.2011.602688

Johansson, M., Larsson, C., Bergman, a, Lund, B.O., 1998. Structure-activity relationship for inhibition of CYP11B1-dependent glucocorticoid synthesis in Y1 cells by aryl methyl sulfones. Pharmacol. Toxicol. 83, 225–230.

Johansson, N., Fredriksson, A., Eriksson, P., 2008. Neonatal exposure to perfluorooctane sulfonate (PFOS) and perfluorooctanoic acid (PFOA) causes neurobehavioural defects in adult mice. Neurotoxicology 29, 160–169. https://doi.org/10.1016/j.neuro.2007.10.008

Juge-Aubry, C.E., Gorla-Bajszczak, A., Pernin, A., Lemberger, T., Wahli, W., Burger, A.G., Meier, C. a., 1995. Peroxisome proliferator-activated receptor mediates cross-talk with thyroid hormone receptor by competition for retinoid X receptor: Possible role of a leucine zipper-like heptad repeat. J. Biol. Chem. https://doi.org/10.1074/jbc.270.30.18117

Jusko, W.J., 2013. Moving from basic toward systems pharmacodynamic models. J. Pharm. Sci. 102, 2930–2940. https://doi.org/10.1002/jps.23590

Jusko, W.J., Ko, H.C., 1994. Physiologic indirect response models characterize diverse types of pharmacodynamic effects. Clin. Pharmacol. Ther. 56, 406–419. https://doi.org/10.1038/clpt.1994.155

Kanda, Y., Hinata, T., Kang, S.W., Watanabe, Y., 2011. Reactive oxygen species mediate adipocyte differentiation in mesenchymal stem cells. Life Sci. 89, 250–258. https://doi.org/10.1016/j.lfs.2011.06.007

Kaplowitz, N., 2005. Idiosyncratic drug hepatotoxicity. Nat. Rev. Drug Discov. 4, 489.

Kashimshetty, R., Desai, V.G., Kale, V.M., Lee, T., Moland, C.L., Branham, W.S., New, L.S., Chan, E.C.Y., Younis, H., Boelsterli, U.A., 2009. Underlying mitochondrial dysfunction triggers flutamide-induced oxidative liver injury in a mouse model of idiosyncratic drug toxicity. Toxicol. Appl. Pharmacol. 238, 150–159. https://doi.org/10.1016/j.taap.2009.05.007

Katchen, B., Buxbaum, S., 1975. Disposition of a new, nonsteroid, antiandrogen, alpha,alpha,alpha-trifluoro-2-methyl-4'-nitro-m-propionotoluidide (Flutamide), in men following a single oral 200 mg dose. J. Clin. Endocrinol. Metab. 41, 373–9. https://doi.org/10.1210/jcem-41-2-373

Kawamoto, Y., Matsuyama, W., Wada, M., Hishikawa, J., Chan, M.P.L., Nakayama, A., Morisawa, S., 2007. Development of a physiologically based pharmacokinetic model for bisphenol A in pregnant mice. Toxicol. Appl. Pharmacol. 224, 182–191. https://doi.org/10.1016/j.taap.2007.06.023

Kell, D.B., 2006. Systems biology, metabolic modelling and metabolomics in drug discovery and development. Drug Discov. Today 11, 1085–1092. https://doi.org/10.1016/j.drudis.2006.10.004

Chapter 2

Kester, M.H.A., Bulduk, S., Van Toor, H., Tibboel, D., Meinl, W., Glatt, H., Falany, C.N., Coughtrie, M.W.H., Gerlienke Schuur, A., Brouwer, A., Visser, T.J., 2002. Potent inhibition of estrogen sulfotransferase by hydroxylated metabolites of polyhalogenated aromatic hydrocarbons reveals alternative mechanism for estrogenic activity of endocrine disrupters. J. Clin. Endocrinol. Metab. 87, 1142–1150. https://doi.org/10.1210/jc.87.3.1142

Keys, D.A., Wallace, D.G., Kepler, T.B., Conolly, R.B., 2000. Quantitative evaluation of alternative mechanisms of blood disposition of di(n-butyl) phthalate and mono(n-butyl) phthalate in rats. Toxicol. Sci. 53, 173–184. https://doi.org/10.1093/toxsci/53.2.173

Keys, D.A., Wallace, D.G., Kepler, T.B., Conolly, R.B., 1999. Quantitative evaluation of alternative mechanisms of blood and testes disposition of di(2-ethylhexyl) phthalate and mono(2-ethylhexyl) phthalate in rats. Toxicol. Sci. 49, 172–85. https://doi.org/10.1093/toxsci/49.2.172

Kitano, H., 2002. Systems biology: A brief overview. Sci. (New York, NY) 295, 1662–1664. https://doi.org/10.1126/science.1069492

Kobayashi, Y., Fukami, T.., Shimizu, M., Nakajima, M., Tsuyoshi., Y., 2012. Short Communication Contributions of Arylacetamide Deacetylase and Carboxylesterase 2 to Flutamide Hydrolysis in Human Liver. Drug Metab. Dispos. 40, 1080–1084.

Kohler, J.J., Schepartz, A., 2001. Kinetic Studies of Fos , Jun , DNA Complex Formation : DNA Binding Prior to Dimerization. Biochemistry 40, 130–142. https://doi.org/10.1021/bi001881p

Kortejärvi, H., Urtti, A., Yliperttula, M., 2007. Pharmacokinetic simulation of biowaiver criteria: The effects of gastric emptying, dissolution, absorption and elimination rates. Eur. J. Pharm. Sci. 30, 155–166. https://doi.org/10.1016/j.ejps.2006.10.011

Kuepfer, L., Niederalt, C., Wendl, T., Schlender, J.F., Willmann, S., Lippert, J., Block, M., Eissing, T., Teutonico, D., 2016. Applied Concepts in PBPK Modeling: How to Build a PBPK/PD Model. CPT Pharmacometrics Syst. Pharmacol. 5, 516–531. https://doi.org/10.1002/psp4.12134

Kurebayashi, H., Okudaira, K., Ohno, Y., 2010. Species difference of metabolic clearance of bisphenol A using cryopreserved hepatocytes from rats, monkeys and humans. Toxicol. Lett. 198, 210–215. https://doi.org/10.1016/j.toxlet.2010.06.017

Kuroda, N., Kinoshita, Y., Sun, Y., Wada, M., Kishikawa, N., Nakashima, K., Makino, T., Nakazawa, H., 2003. Measurement of bisphenol A levels in human blood serum and ascitic fluid by HPLC using a fluorescent labeling reagent. J. Pharm. Biomed. Anal. 30, 1743–1749. https://doi.org/10.1016/S0731-7085(02)00516-2

Lai, K.P., Wong, M.H., Wong, C.K.C., 2005a. Inhibition of CYP450scc expression in dioxin-exposed rat Leydig cells. J. Endocrinol. 185, 519–527. https://doi.org/10.1677/joe.1.06054

Chapter 2

Lai, K.P., Wong, M.H., Wong, C.K.C., 2005b. Effects of TCDD in modulating the expression of Sertoli cell secretory products and markers for cell-cell interaction. Toxicology 206, 111–123. https://doi.org/10.1016/j.tox.2004.07.002

Lans, M.C., Spiertz, C., Brouwer, a, Koeman, J.H., 1994. Different competition of thyroxine binding to transthyretin and thyroxine-binding globulin by hydroxy-PCBs, PCDDs and PCDFs. Eur. J. Pharmacol. 270, 129–136. https://doi.org/10.1016/0926-6917(94)90054-X

Leclerc, E., Hamon, J., Legendre, A., Bois, F.Y., 2014. Integration of pharmacokinetic and NRF2 system biology models to describe reactive oxygen species production and subsequent glutathione depletion in liver microfluidic biochips after flutamide exposure. Toxicol. Vitr. 28, 1230–1241. https://doi.org/10.1016/j.tiv.2014.05.003

Lee, Y.J., Ryu, H.Y., Kim, H.K., Min, C.S., Lee, J.H., Kim, E., Nam, B.H., Park, J.H., Jung, J.Y., Jang, D.D., Park, E.Y., Lee, K.H., Ma, J.Y., Won, H.S., Im, M.W., Leem, J.H., Hong, Y.C., Yoon, H.S., 2008. Maternal and fetal exposure to bisphenol A in Korea. Reprod. Toxicol. 25, 413–419. https://doi.org/10.1016/j.reprotox.2008.05.058

Lemaire, G., Terouanne, B., Mauvais, P., Michel, S., Rahmani, R., 2004. Effect of organochlorine pesticides on human androgen receptor activation in vitro. Toxicol. Appl. Pharmacol. 196, 235–246. https://doi.org/10.1016/j.taap.2003.12.011

Li, L. a., Wang, P.W., Chang, L.W., 2004. Polychlorinated biphenyl 126 stimulates basal and inducible aldosterone biosynthesis of human adrenocortical H295R cells. Toxicol. Appl. Pharmacol. 195, 92–102. https://doi.org/10.1016/j.taap.2003.11.007

Li, M.W.M., Mruk, D.D., Lee, W.M., Cheng, C.Y., 2009. Disruption of the blood-testis barrier integrity by bisphenol A in vitro: Is this a suitable model for studying blood-testis barrier dynamics? Int. J. Biochem. Cell Biol. 41, 2302–2314. https://doi.org/10.1016/j.biocel.2009.05.016

Li, W., He, Q.Z., Wu, C.Q., Pan, X.Y., Wang, J., Tan, Y., Shan, X.Y., Zeng, H.C., 2015. PFOS Disturbs BDNF-ERK-CREB Signalling in Association with Increased MicroRNA-22 in SH-SY5Y Cells. Biomed Res. Int. 2015. https://doi.org/10.1155/2015/302653

Li, X., Fang, P., Mai, J., Choi, E.T., Wang, H., Yang, X., 2013. Targeting mitochondrial reactive oxygen species as novel therapy for inflammatory diseases and cancers. J. Hematol. Oncol. 6, 19. https://doi.org/10.1186/1756-8722-6-19

Li, Y., Ramdhan, D.H., Naito, H., Yamagishi, N., Ito, Y., Hayashi, Y., Yanagiba, Y., Okamura, A., Tamada, H., Gonzalez, F.J., Nakajima, T., 2011. Ammonium perfluorooctanoate may cause testosterone reduction by adversely affecting testis in relation to PPARα. Toxicol. Lett. 205, 265–272. https://doi.org/10.1016/j.toxlet.2011.06.015

Chapter 2

Lipsky, R.H., Marini, A.M., 2007. Brain-derived neurotrophic factor in neuronal survival and behavior-related plasticity. Ann. N. Y. Acad. Sci. 1122, 130–143. https://doi.org/10.1196/annals.1403.009

Long, Y., Wang, Y., Ji, G., Yan, L., Hu, F., Gu, A., 2013. Neurotoxicity of Perfluorooctane Sulfonate to Hippocampal Cells in Adult Mice. PLoS One 8, 1–9. https://doi.org/10.1371/journal.pone.0054176

Lorber, M., Angerer, J., Koch, H.M., 2010. A simple pharmacokinetic model to characterize exposure of Americans to Di-2-ethylhexyl phthalate. J. Expo. Sci. Environ. Epidemiol. 20, 38–53. https://doi.org/10.1038/jes.2008.74

Louisse, J., Beekmann, K., Rietjens, I.M.C.M., 2016. Use of physiologically based kinetic modeling-based reverse dosimetry to predict in vivo toxicity from in vitro data. Chem. Res. Toxicol. acs.chemrestox.6b00302. https://doi.org/10.1021/acs.chemrestox.6b00302

Lu, B., 2003. Pro-Region of Neurotrophins. Neuron 39, 735–738. https://doi.org/10.1016/S0896-6273(03)00538-5

Lubin, F.D., Roth, T.L., Sweatt, J.D., 2008. Epigenetic regulation of BDNF gene transcription in the consolidation of fear memory. J. Neurosci. 28, 10576–86. https://doi.org/10.1523/JNEUROSCI.1786-08.2008

Ma, E., MacRae, I.J., Kirsch, J.F., Doudna, J.A., 2008. Autoinhibition of Human Dicer by Its Internal Helicase Domain. J. Mol. Biol. 380, 237–243. https://doi.org/10.1016/j.jmb.2008.05.005

Mager, D.E., Woo, S., Jusko, W.J., 2009. Scaling Pharmacodynamics from In Vitro and Preclinical Animal Studies to Humans. Drug Metab. Pharmacokinet. 24, 16–24. https://doi.org/10.2133/dmpk.24.16

Mager, D.E., Wyska, E., Jusko, W.J., 2003. Diversity of mechanism-based pharmacodynamic models. Drug Metab. Dispos. 31, 510–8. https://doi.org/10.1124/DMD.31.5.510

Martínez, M.A., Rovira, J., Prasad Sharma, R., Nadal, M., Schuhmacher, M., Kumar, V., 2018. Comparing dietary and non-dietary source contribution of BPA and DEHP to prenatal exposure: A Catalonia (Spain) case study. Environ. Res. 166, 25–34. https://doi.org/10.1016/j.envres.2018.05.008

Martínez, M.A., Rovira, J., Sharma, R.P., Nadal, M., Schuhmacher, M., Kumar, V., 2017. Prenatal exposure estimation of BPA and DEHP using integrated external and internal dosimetry: A case study. Environ. Res. 158, 566–575. https://doi.org/10.1016/j.envres.2017.07.016

Masuyama, H., Hiramatsu, Y., Kunitomi, M., Kudo, T., MacDonald, P.N., 2000. Endocrine disrupting chemicals, phthalic acid and nonylphenol, activate Pregnane X receptor-mediated transcription. Mol. Endocrinol. 14, 421–428. https://doi.org/10.1210/mend.14.3.0424

Chapter 2

Masuyama, H., Inoshita, H., Hiramatsu, Y., Kudo, T., 2002. Ligands have various potential effects on the degradation of pregnane X receptor by proteasome. Endocrinology 143, 55–61. https://doi.org/10.1210/en.143.1.55

Matsuzaki, Y., Nagai, D., Ichimura, E., Goda, R., Tomura, A., Doi, M., Nishikawa, K., 2006. Metabolism and hepatic toxicity of flutamide in cytochrome P450 1A2 knockout SV129 mice. J. Gastroenterol. 41, 231–239. https://doi.org/10.1007/s00535-005-1749-y

Menei, P., Montero-Menei, C., Whittemore, S.R., Bunge, R.P., Bunge, M.B., 1998. Schwann cells genetically modified to secrete human BDNF promote enhanced axonal regrowth across transected adult rat spinal cord. Eur. J. Neurosci. 10, 607–621. https://doi.org/10.1046/j.1460-9568.1998.00071.x

Michael, G.J., Averill, S., Nitkunan, A., Rattray, M., Bennett, D.L., Yan, Q., Priestley, J. V, 1997. Nerve growth factor treatment increases brain-derived neurotrophic factor selectively in TrkA-expressing dorsal root ganglion cells and in their central terminations within the spinal cord. J. Neurosci. 17, 8476–90.

Mielke, H., Partosch, F., Gundert-Remy, U., 2011. The contribution of dermal exposure to the internal exposure of bisphenol A in man. Toxicol. Lett. 204, 190–198. https://doi.org/10.1016/j.toxlet.2011.04.032

Mikamo, E., Harada, S., Nishikawa, J., Nishihara, T., 2003. Endocrine disruptors induce cytochrome P450 by affecting transcriptional regulation via pregnane X receptor. Toxicol. Appl. Pharmacol. 193, 66–72. https://doi.org/10.1016/j.taap.2003.08.001

Moriyama, K., Tagami, T., Akamizu, T., Usui, T., Saijo, M., Kanamoto, N., Hataya, Y., Shimatsu, A., Kuzuya, H., Nakao, K., 2002. Thyroid hormone action is disrupted by bisphenol A as an antagonist. J. Clin. Endocrinol. Metab. 87, 5185–5190. https://doi.org/10.1210/jc.2002-020209

Mowla, S.J., Pareek, S., Farhadi, H.F., Petrecca, K., Fawcett, J.P., Seidah, N.G., Morris, S.J., Sossin, W.S., Murphy, R. a, 1999. Differential sorting of nerve growth factor and brain-derived neurotrophic factor in hippocampal neurons. J. Neurosci. 19, 2069–2080.

Muiños-Gimeno, M., Espinosa-Parrilla, Y., Guidi, M., Kagerbauer, B., Sipilä, T., Maron, E., Pettai, K., Kananen, L., Navinés, R., Martín-Santos, R., Gratacòs, M., Metspalu, A., Hovatta, I., Estivill, X., 2011. Human microRNAs miR-22, miR-138-2, miR-148a, and miR-488 are associated with panic disorder and regulate several anxiety candidate genes and related pathways. Biol. Psychiatry 69, 526–533. https://doi.org/10.1016/j.biopsych.2010.10.010

Murer, M.., Yan, Q., Raisman-Vozari, R., 2001. Brain-derived neurotrophic factor in the control human brain, and in Alzheimer's disease and Parkinson's disease. Prog. Neurobiol. 63, 71–124. https://doi.org/10.1016/S0301-0082(00)00014-9

Murphy, M.P., 2009. How mitochondria produce reactive oxygen species. Biochem. J. 417, 1–13. https://doi.org/10.1042/BJ20081386

Chapter 2

Nestorov, I., 2007. Whole-body physiologically based pharmacokinetic models. Expert Opin. Drug Metab. Toxicol. 3, 235–249. https://doi.org/10.1517/17425255.3.2.235

Nikula, H., Talonpoika, T., Kaleva, M., Toppari, J., 1999. Inhibition of hCG-stimulated steroidogenesis in cultured mouse Leydig tumor cells by bisphenol A and octylphenols. Toxicol. Appl. Pharmacol. 157, 166–173. https://doi.org/10.1006/taap.1999.8674

Niwa, T., Fujimoto, M., Kishimoto, K., Yabusaki, Y., Ishibashi, F., Katagiri, M., 2001. Metabolism and interaction of bisphenol A in human hepatic cytochrome P450 and steroidogenic CYP17. Biol. Pharm. Bull. 24, 1064–1067. https://doi.org/10.1248/bpb.24.1064

O'Leary, P.D., Hughes, R.A., 1998. Structure-activity relationships of conformationally constrained peptide analogues of loop 2 of brain-derived neurotrophic factor. J. Neurochem. 70, 1712–21. https://doi.org/10.1046/j.1471-4159.1998.70041712.x

OECD, 2018. "Users'' Handbook supplement to the Guidance Document for developing and assessing Adverse Outcome Pathways", OECD Series on Adverse Outcome Pathways, No. 1, OECD Publishing, Paris." https://doi.org/10.1787/5jlv1m9d1g32-en

OECD, 2016. "Users'' Handbook supplement to the Guidance Document for developing and assessing Adverse Outcome Pathways", OECD Series on Adverse Outcome Pathways, No. 1, OECD Publishing, Paris" 18. https://doi.org/10.1787/5jlv1m9d1g32-en

Ohshima, M., Ohno, S., Nakajin, S., 2005. Inhibitory effects of some possible endocrine-disrupting chemicals on the isozymes of human 11beta-hydroxysteroid dehydrogenase and expression of their mRNA in gonads and adrenal glands. Environ. Sci. 12, 219–230.

Ohtake, F., Takeyama, K., Matsumoto, T., Kitagawa, H., Yamamoto, Y., Nohara, K., Tohyama, C., Krust, A., Mimura, J., Chambon, P., Yanagisawa, J., Fujii-Kuriyama, Y., Kato, S., 2003. Modulation of oestrogen receptor signalling by association with the activated dioxin receptor. Nature 423, 545–550. https://doi.org/10.1038/nature01606

Patisaul, H.B., Todd, K.L., Mickens, J.A., Adewale, H.B., 2009. Impact of neonatal exposure to the ERα agonist PPT, bisphenol-A or phytoestrogens on hypothalamic kisspeptin fiber density in male and female rats. Neurotoxicology 30, 350–357. https://doi.org/10.1016/j.neuro.2009.02.010

Pérez-Ortín, J.E., Alepuz, P.M., Moreno, J., 2007. Genomics and gene transcription kinetics in yeast. Trends Genet. 23, 250–257. https://doi.org/10.1016/j.tig.2007.03.006

Perruisseau-Carrier, C., Jurga, M., Forraz, N., McGuckin, C.P., 2011. MiRNAs stem cell reprogramming for neuronal induction and differentiation. Mol. Neurobiol.

Chapter 2

43, 215–227. https://doi.org/10.1007/s12035-011-8179-z

Podratz, P.L., Filho, V.S.D., Lopes, P.F.I., Sena, G.C., Matsumoto, S.T., Samoto, V.Y., Takiya, C.M., Miguel, E.D.C., Silva, I.V., Graceli, J.B., 2012. Tributyltin Impairs the Reproductive Cycle in Female Rats. J. Toxicol. Environ. Heal. Part A 75, 1035–1046. https://doi.org/10.1080/15287394.2012.697826

Poland, a, Knutson, J.C., 1982. 2,3,7,8-Tetrachlorodibenzo-P-Dioxin and Related Halogenated Aromatic Hydrocarbons: Examination of the Mechanism of Toxicity. Annu. Rev. Pharmacol. Toxicol. 22, 517–554. https://doi.org/10.1146/annurev.pa.22.040182.002505

Poulin, P., Krishnan, K., 1996. Molecular Structure-Based Prediction of the Partition Coefficients of Organic Chemicals for Physiological Pharmacokinetic Models. Toxicol. Mech. Methods 6, 117–137. https://doi.org/10.3109/15376519609068458

Poulin, P., Krishnan, K., 1995. A biologically-based algorithm for predicting human tissue: blood partition coefficients of organic chemicals. Hum Exp Toxicol 14, 273–280.

Poulin, P., Theil, F.P., 2000. A priori prediction of tissue: Plasma partition coefficients of drugs to facilitate the use of physiologically-based pharmacokinetic models in drug discovery. J. Pharm. Sci. 89, 16–35. https://doi.org/10.1002/(SICI)1520-6017(200001)89:1<16::AID-JPS3>3.0.CO;2-E

Qatanani, M., Zhang, J., Moore, D.D., 2005. Role of the constitutive androstane receptor in xenobiotic-induced thyroid hormone metabolism. Endocrinology 146, 995–1002. https://doi.org/10.1210/en.2004-1350

Qiu, L., Zhang, X., Zhang, X., Zhang, Y., Gu, J., Chen, M., Zhang, Z., Wang, X., Wang, S.L., 2013. Sertoli cell is a potential target for perfluorooctane sulfonate-induced reproductive dysfunction in male mice. Toxicol. Sci. 135, 229–240. https://doi.org/10.1093/toxsci/kft129

Radwanski, E., Perentesis, G., Symchowicz, S., Zampaglione, N., 1989. Single and Multiple Dose Pharmacokinetic Evaluation of Flutamide in Normal Geriatric Volunteers. J. Clin. Pharmacol. 29, 554–558. https://doi.org/10.1002/j.1552-4604.1989.tb03381.x

Raun Andersen, H., Vinggaard, A.M., Høj Rasmussen, T., Gjermandsen, I.M., Cecilie Bonefeld-Jørgensen, E., 2002. Effects of Currently Used Pesticides in Assays for Estrogenicity, Androgenicity, and Aromatase Activity in Vitro. Toxicol. Appl. Pharmacol. 179, 1–12. https://doi.org/10.1006/taap.2001.9347

Rey, R., Lukas-Croisier, C., Lasala, C., Bedecarrás, P., 2003. AMH/MIS: What we know already about the gene, the protein and its regulation. Mol. Cell. Endocrinol. 211, 21–31. https://doi.org/10.1016/j.mce.2003.09.007

Rodríguez-Tébar, A., Dechant, G., Götz, R., Barde, Y.A., 1992. Binding of neurotrophin-3 to its neuronal receptors and interactions with nerve growth factor

Chapter 2

and brain-derived neurotrophic factor. EMBO J. 11, 917–922.

Rouquié, D., Heneweer, M., Botham, J., Ketelslegers, H., Markell, L., Pfister, T., Steiling, W., Strauss, V., Hennes, C., 2015. Contribution of new technologies to characterization and prediction of adverse effects. Crit. Rev. Toxicol. 45, 172–183. https://doi.org/10.3109/10408444.2014.986054

Saitoh, M., Yanase, T., Morinaga, H., Tanabe, M., Mu, Y.M., Nishi, Y., Nomura, M., Okabe, T., Goto, K., Takayanagi, R., Nawata, H., 2001. Tributyltin or triphenyltin inhibits aromatase activity in the human granulosa-like tumor cell line KGN. Biochem. Biophys. Res. Commun. 289, 198–204. https://doi.org/10.1006/bbrc.2001.5952

Sandhya, V.K., Raju, R., Verma, R., Advani, J., Sharma, R., Radhakrishnan, A., Nanjappa, V., Narayana, J., Somani, B.L., Mukherjee, K.K., Pandey, A., Christopher, R., Keshava Prasad, T.S., 2013. A network map of BDNF/TRKB and BDNF/p75NTR signaling system. J. Cell Commun. Signal. 7, 301–307. https://doi.org/10.1007/s12079-013-0200-z

Sato, I., Kawamoto, K., Nishikawa, Y., Tsuda, S., Yoshida, M., Yaegashi, K., Saito, N., Liu, W., Jin, Y., 2009. Neurotoxicity of perfluorooctane sulfonate (PFOS) in rats and mice after single oral exposure. J. Toxicol. Sci. 34, 569–574. https://doi.org/10.2131/jts.34.569

Saunders, P.T., Majdic, G., Parte, P., Millar, M.R., Fisher, J.S., Turner, K.J., Sharpe, R.M., 1997. Fetal and perinatal influence of xenoestrogens on testis gene expression. Adv. Exp. Med. Biol. 424, 99–110.

Schmitt, W., 2008. General approach for the calculation of tissue to plasma partition coefficients. Toxicol. Vitr. 22, 457–467. https://doi.org/10.1016/j.tiv.2007.09.010

Schönfelder, G., Wittfoht, W., Hopp, H., Talsness, C.E., Paul, M., Chahoud, I., 2002. Parent bisphenol a accumulation in the human maternal-fetal-placental unit. Environ. Health Perspect. 110, 703–707. https://doi.org/10.1289/ehp.021100703

Seo, J.S., Lee, Y.M., Jung, S.O., Kim, I.C., Yoon, Y.D., Lee, J.S., 2006. Nonylphenol modulates expression of androgen receptor and estrogen receptor genes differently in gender types of the hermaphroditic fish Rivulus marmoratus. Biochem. Biophys. Res. Commun. 346, 213–223. https://doi.org/10.1016/j.bbrc.2006.05.123

Shi, Z., Ding, L., Zhang, H., Feng, Y., Xu, M., Dai, J., 2009. Chronic exposure to perfluorododecanoic acid disrupts testicular steroidogenesis and the expression of related genes in male rats. Toxicol. Lett. 188, 192–200. https://doi.org/10.1016/j.toxlet.2009.04.014

Sisson, T.R., Lund, C.J., Whalen, L.E., Telek, A., 1959. The blood volume of infants. I. The full-term infant in the first year of life. J. Pediatr. 55, 163–79. https://doi.org/10.1016/S0022-3476(59)80084-6

Siu, E.R., Mruk, D.D., Porto, C.S., Cheng, C.Y., 2009. Cadmium-induced testicular

Chapter 2

injury. Toxicol. Appl. Pharmacol. 238, 240–249. https://doi.org/10.1016/j.taap.2009.01.028

Sjo, E., Lennerna, H., Andersson, T.B., Gråsjo, J., Bredberg, U., 2009. Estimates of Intrinsic Clearance (CL int), Maximum Velocity of the Metabolic Reaction (V max), and Michaelis Constant (K m): Accuracy and Robustness Evaluated through Experimental Data and Monte Carlo Simulations ABSTRACT : Pharmacology 37, 47–58. https://doi.org/10.1124/dmd.108.021477.kinetics

Sjögren, E., Tammela, T.L., Lennernäs, B., Taari, K., Isotalo, T., Malmsten, L.-Å., Axén, N., Lennernäs, H., 2014. Pharmacokinetics of an Injectable Modified-Release 2-Hydroxyflutamide Formulation in the Human Prostate Gland Using a Semiphysiologically Based Biopharmaceutical Model. Mol. Pharm. 11, 3097–3111. https://doi.org/10.1021/mp5002813

Sobarzo, C.M., Lustig, L., Ponzio, R., Denduchis, B., 2006. Effect of di-(2-ethylhexyl) phthalate on N-cadherin and catenin protein expression in rat testis. Reprod. Toxicol. 22, 77–86. https://doi.org/10.1016/j.reprotox.2006.02.004

Soetaert, K., Petzoldt, T., 2010. Inverse Modelling, Sensitivity and Monte Carlo Analysis in R Using Package FME. J. Stat. Softw. 33, 2–4. https://doi.org/10.18637/jss.v033.i03

Stasenko, S., Bradford, E.M., Piasek, M., Henson, M.C., Varnai, V.M., Jurasović, J., Kušec, V., 2010. Metals in human placenta: Focus on the effects of cadmium on steroid hormones and leptin. J. Appl. Toxicol. 30, 242–253. https://doi.org/10.1002/jat.1490

Stouder, C., Paoloni-Giacobino, A., 2011. Specific transgenerational imprinting effects of the endocrine disruptor methoxychlor on male gametes. Reproduction 141, 207–216. https://doi.org/10.1530/REP-10-0400

Sturla, S.J., Boobis, A.R., FitzGerald, R.E., Hoeng, J., Kavlock, R.J., Schirmer, K., Whelan, M., Wilks, M.F., Peitsch, M.C., 2014. Systems Toxicology: From Basic Research to Risk Assessment. Chem. Res. Toxicol. 27, 314–329. https://doi.org/10.1021/tx400410s

Teppner, M., Boess, F., Ernst, B., Pähler, A., 2016. Biomarkers of flutamide-bioactivation and oxidative stress in vitro and in vivo. Drug Metab. Dispos. 44, 560–569. https://doi.org/10.1124/dmd.115.066522

Thiel, C., Cordes, H., Conde, I., Castell, J.V., Blank, L.M., Kuepfer, L., 2017. Model-based contextualization of in vitro toxicity data quantitatively predicts in vivo drug response in patients. Arch. Toxicol. 91, 865–883. https://doi.org/10.1007/s00204-016-1723-x

Timchalk, C., Nolan, R.J., Mendrala, A.L., Dittenber, D.A., Brzak, K.A., Mattsson, J.L., 2002. A physiologically based pharmacokinetic and pharmacodynamic (PBPK/PD) model for the organophosphate insecticide chlorpyrifos in rats and humans. Toxicol. Sci. 66, 34–53. https://doi.org/10.1093/toxsci/66.1.34

Chapter 2

Toyoda, K., Shibutani, M., Tamura, T., Koujitani, T., Uneyama, C., Hirose, M., 2000. Repeated dose (28 days) oral toxicity study of flutamide in rats, based on the draft protocol for the `Enhanced OECD Test Guideline 407' for screening for endocrine-disrupting chemicals. Arch. Toxicol. 74, 127–132. https://doi.org/10.1007/s002040050664

Trdan Lusin, T., Roskar, R., Mrhar, A., 2012. Evaluation of bisphenol A glucuronidation according to UGT1A1*28 polymorphism by a new LC-MS/MS assay. Toxicology 292, 33–41. https://doi.org/10.1016/j.tox.2011.11.015

Uzumcu, M., Kuhn, P.E., Marano, J.E., Armenti A.E., A.E., Passantino, L., 2006. Early postnatal methoxychlor exposure inhibits folliculogenesis and stimulates anti-Mullerian hormone production in the rat ovary. J. Endocrinol. 191, 549–558. https://doi.org/10.1677/joe.1.06592

Valentin, J., 2002. Basic anatomical and physiological data for use in radiological protection: reference values. Ann. ICRP 32, 1–277. https://doi.org/10.1016/S0146-6453(03)00002-2

Vuong, A.M., Yolton, K., Webster, G.M., Sjödin, A., Calafat, A.M., Braun, J.M., Dietrich, K.N., Lanphear, B.P., Chen, A., 2016. Prenatal polybrominated diphenyl ether and perfluoroalkyl substance exposures and executive function in school-age children. Environ. Res. 147, 556–564. https://doi.org/10.1016/j.envres.2016.01.008

Wambaugh, J.F., Setzer, R.W., Pitruzzello, A.M., Liu, J., Reif, D.M., Kleinstreuer, N.C., Wang, N.C.Y., Sipes, N., Martin, M., Das, K., DeWitt, J.C., Strynar, M., Judson, R., Houck, K.A., Lau, C., 2013. Dosimetric anchoring of In vivo and In vitro studies for perfluorooctanoate and perfluorooctanesulfonate. Toxicol. Sci. 136, 308–327. https://doi.org/10.1093/toxsci/kft204

Wan, H.T., Zhao, Y.G., Wong, M.H., Lee, K.F., Yeung, W.S.B., Giesy, J.P., Wong, C.K.C., 2011. Testicular signaling is the potential target of perfluorooctanesulfonate-mediated subfertility in male mice. Biol. Reprod. 84, 1016–1023. https://doi.org/10.1095/biolreprod.110.089219

Wang, J., Sun, B., Hou, M., Pan, X., Li, X., 2012. The environmental obesogen bisphenol A promotes adipogenesis by increasing the amount of 11β-hydroxysteroid dehydrogenase type 1 in the adipose tissue of children. Int. J. Obes. 999–1005. https://doi.org/10.1038/ijo.2012.173

Wang, X., Li, Y., Xu, X., Wang, Y. hua, 2010. Toward a system-level understanding of microRNA pathway via mathematical modeling. BioSystems 100, 31–38. https://doi.org/10.1016/j.biosystems.2009.12.005

Waters, M.D., Boorman, G., Bushel, P., Cunningham, M., Irwin, R., Merrick, A., Olden, K., Paules, R., Selkirk, J., Stasiewicz, S., Weis, B., Van Houten, B., Walker, N., Tennant, R., 2003. Systems toxicology and the Chemical Effects in Biological Systems (CEBS) knowledge base. Environ. Health Perspect. 111, 811–824. https://doi.org/10.1289/txg.5971

Chapter 2

Wen, B., Coe, K.J., Rademacher, P., Fitch, W.L., Monshouwer, M., Nelson, S.D., 2008. Comparison of in vitro bioactivation of flutamide and its cyano analogue: Evidence for reductive activation by human NADPH:cytochrome P450 reductase. Chem. Res. Toxicol. 21, 2393–2406. https://doi.org/10.1021/tx800281h

Wysowski, D.K., Fourcroy, J.L., 1996. Flutamide Hepatotoxicity. J. Urol. 155, 209–212. https://doi.org/10.1016/S0022-5347(01)66596-0

Xi, W., Lee, C.K.F., Yeung, W.S.B., Giesy, J.P., Wong, M.H., Zhang, X., Hecker, M., Wong, C.K.C., 2011. Effect of perinatal and postnatal bisphenol A exposure to the regulatory circuits at the hypothalamus-pituitary-gonadal axis of CD-1 mice. Reprod. Toxicol. 31, 409–417. https://doi.org/10.1016/j.reprotox.2010.12.002

Yang, J., Wang, C., Nie, X., Shi, S., Xiao, J., Ma, X., Dong, X., Zhang, Y., Han, J., Li, T., Mao, J., Liu, X., Zhao, J., Wu, Q., 2015. Perfluorooctane sulfonate mediates microglial activation and secretion of TNF-α through Ca2+-dependent PKC-NF-κB signaling. Int. Immunopharmacol. 28, 52–60. https://doi.org/10.1016/j.intimp.2015.05.019

York, N., 2015. Regulation of Cell Survival by Secreted Proneurotrophins.pdf. Science (80-.). 294, 1945–1949. https://doi.org/10.1126/science.1065057

You, H.J., Park, J.H., Pareja-Galeano, H., Lucia, A., Shin, J. Il, 2016. Targeting MicroRNAs Involved in the BDNF Signaling Impairment in Neurodegenerative Diseases. NeuroMolecular Med. https://doi.org/10.1007/s12017-016-8407-9

Yu, N., Wei, S., Li, M., Yang, J., Li, K., Jin, L., Xie, Y., Giesy, J.P., Zhang, X., Yu, H., 2016. Effects of Perfluorooctanoic Acid on Metabolic Profiles in Brain and Liver of Mouse Revealed by a High-throughput Targeted Metabolomics Approach. Sci. Rep. 6, 23963. https://doi.org/10.1038/srep23963

Yun, Y.E., Cotton, C.A., Edginton, A.N., 2014. Development of a decision tree to classify the most accurate tissue-specific tissue to plasma partition coefficient algorithm for a given compound. J. Pharmacokinet. Pharmacodyn. 41, 1–14. https://doi.org/10.1007/s10928-013-9342-0

Zamkova, M., Khromova, N., Kopnin, B.P., Kopnin, P., 2013. Ras-induced ROS upregulation affecting cell proliferation is connected with cell type-specific alterations of HSF1/SESN3/p21Cip1/WAF1pathways. Cell Cycle 12, 826–836. https://doi.org/10.4161/cc.23723

Zeng, H. cai, Zhang, L., Li, Y. yuan, Wang, Y. jian, Xia, W., Lin, Y., Wei, J., Xu, S. qing, 2011. Inflammation-like glial response in rat brain induced by prenatal PFOS exposure. Neurotoxicology 32, 130–139. https://doi.org/10.1016/j.neuro.2010.10.001

Zhang, J., Cooke, G.M., Curran, I.H.A., Goodyer, C.G., Cao, X.L., 2011. GC-MS analysis of bisphenol A in human placental and fetal liver samples. J. Chromatogr. B Anal. Technol. Biomed. Life Sci. 879, 209–214. https://doi.org/10.1016/j.jchromb.2010.11.031

Chapter 2

Zhang, L., Guo, J., Zhang, Q., Zhou, W., Li, J., Yin, J., Cui, L., 2018. Flutamide induces hepatic cell death and mitochondrial dysfunction via inhibition of Nrf2-mediated heme oxygenase-1. Oxid. Med. Cell. Longev.

Zhang, L., Li, Y.-Y., Zeng, H.-C., Wei, J., Wan, Y.-J., Chen, J., Xu, S.-Q., 2011. MicroRNA expression changes during zebrafish development induced by perfluorooctane sulfonate. J. Appl. Toxicol. 31, 210–222. https://doi.org/10.1002/jat.1583

Zhang, T., Sun, H., Kannan, K., 2013. Blood and urinary bisphenol a concentrations in children, adults, and pregnant women from China: Partitioning between blood and urine and maternal and fetal cord blood. Environ. Sci. Technol. 47, 4686–4694. https://doi.org/10.1021/es303808b

Zhao, B., Hu, G.X., Chu, Y., Jin, X., Gong, S., Akingbemi, B.T., Zhang, Z., Zirkin, B.R., Ge, R.S., 2010. Inhibition of human and rat 3β-hydroxysteroid dehydrogenase and 17β-hydroxysteroid dehydrogenase 3 activities by perfluoroalkylated substances. Chem. Biol. Interact. 188, 38–43. https://doi.org/10.1016/j.cbi.2010.07.001

Chapter 3

Sharma, R.P., Schuhmacher, M., Kumar, V., 2018. The development of a pregnancy PBPK Model for Bisphenol A and its evaluation with the available biomonitoring data. Sci. Total Environ. 624, 55–68. doi:10.1016/j.scitotenv.2017.12.023

Chapter 3

The development of a pregnancy PBPK Model for Bisphenol A and its evaluation with the available biomonitoring data

Abstract

Recent studies suggest universal fetal exposure to Bisphenol A (BPA) and its association with adverse birth outcomes. Estimation of the fetal plasma BPA concentration from the maternal plasma BPA would be highly useful to predict its associated risk to this specific population. The objective of current work is to develop a pregnancy–physiologically based pharmacokinetic (P-PBPK) model to predict the toxicokinetic profile of BPA in the fetus during gestational growth, and to evaluate the developed model using biomonitoring data obtained from different pregnancy cohort studies. To achieve this objective, first, the adult PBPK model was developed and validated with the human BPA toxicokinetic data. This validated human PBPK model was extended to develop a P-PBPK model, which included the physiological changes during pregnancy both in mother and in the fetus sub-model. The developed model would be able to predict the BPA pharmacokinetics (PKs) in both mother and fetus. Transplacental BPA kinetics parameters for this study were taken from a previous pregnant mice study. Both oral and dermal exposure routes were included into the model to simulate total BPA internal exposure. The impact of conjugation and deconjugation of the BPA and its metabolites on fetal PKs was investigated. The developed P-PBPK model was evaluated against the observed BPA concentrations in cord blood, fetus liver and amniotic fluid considering maternal blood concentration as an exposure source. A range of maternal exposure dose for the oral and dermal routes was estimated, so that simulation concentration matched the observed highest and lowest mother plasma concentration in different cohorts' studies. The developed model could be used to address the concerns regarding possible adverse health effects in the fetus being exposed to BPA and might be useful in identifying critical windows of exposure during pregnancy.

Highlights

•Developed P-PBPK model for BPA can describe and predict the fetus toxicokinetic profiles based on mother’s exposure scenario.
•Conjugation-deconjugation of BPA in placenta and fetus is a key issue for the fetal exposure to parent BPA.
•Amniotic fluid BPA concentration can be a good biomarker for identifying the critical window of exposure in fetus.
•Fetal exposure was characterized by a low but sustained basal BPA concentration due to their low metabolic activity.

Keywords: Bisphenol A, Pregnancy-PBPK, Fetal exposure, Biomonitoring, Window of exposure

Chapter 3

1. Introduction

BPA is produced at over 2 billion pounds/year and is found in wide variety of dietary and non-dietary products. The dietary sources include both canned and non-canned foods categories ranging from “meat and meat products”, “vegetables and vegetable products”, and other packaged foods, and food handling consumer products like baby bottles, beverage containers etc. (WHO, 2010; EFSA, 2015). The non-dietary sources include medical devices, dental sealants, dust, thermal papers, toys and cosmetics (Mendum et al., 2011; EFSA, 2015). Although ingestion of the BPA from food or water is the predominant route of exposure (Lorber et al., 2015), there are other non-dietary routes, which also equally contributes to the total BPA exposure, such as inhalation of free BPA (concentrations in indoor and outdoor air), indirect ingestion (dust, soil, and toys), and dermal route (contact with thermal papers and application of dental treatment) (Myridakis et al., 2016). Recently reported studies have found relatively more contribution of the dermal route to overall internal BPA concentration than the oral route's exposure (Biedermann et al., 2010; Mielke et al., 2011). In addition, recent studies (De Coensel et al., 2009; Sungur et al., 2014) show that temperature has a major impact on the BPA migration level into water; an increase from 40 °C to 60 °C can lead to a 6–10 fold increase in the migration level.

BPA and its metabolites have been detected in maternal blood, amniotic fluid, follicular fluid, placental tissue, umbilical cord blood, urine and breast milk (Schönfelder et al., 2002; Ikezuki et al., 2002; Kuroda et al., 2003; Kuruto-Niwa et al., 2007; Lee et al., 2008; Zhang et al., 2011, 2013; Cao et al., 2012; Muna et al., 2013; Gerona et al., 2014; Teeguarden et al., 2016). In different rodents' studies, it has been seen that low dose of bisphenol exposure during the gestational period has effects on the fertility, brain development, and the behavioural changes in their later life stages, signify BPA pleiotropic effects (Palanza et al., 2002; Cabaton et al., 2013; Snijder et al., 2013; Harley et al., 2013). Rubin and Soto (2009) reviewed the prenatal BPA exposure and its effects on adipocytes differentiation, a major cause of obesity. U.S. Environmental Protection Agency (EPA) has declared the BPA as an endocrine-modifying chemical, which has been found to be reproductive, developmental, systemic toxicant, obesogenic and, weakly estrogenic (Moriyama et al., 2002; Rey et al., 2003; Patisaul et al., 2009; Xi et al., 2011; Wang et al., 2012; Vafeiadi et al., 2016; Sharma et al., 2017).

Adult human studies have reported that BPA has a very short half-life. It rapidly detoxifies to nontoxic conjugate substance such as BPA-glucuronide (BPAG) and BPA-sulfate (BPAS), collectively called as BPA conjugates (BPA-C), by glucuronidation and sulfation metabolic process (Völkel et al., 2002; Teeguarden et al., 2015; Thayer et al., 2015). However, in the case of the specific populations such as developing fetus, growing infants, and young children, whose chemical metabolizing systems are underdeveloped, even moderate exposure can lead to higher internal concentration of BPA (Divakaran et al., 2014). Moreover, the reactivation of these conjugates (deconjugation), BPAG and BPAS, by the fetal tissue and the placenta has been reported (Ginsberg and Rice, 2009; Muna et al., 2013), causing an increase in BPA internal exposure to the fetus. The recent human pharmacokinetics studies showed low amount of BPA plasma concentration even with the high oral dose, in contrast, exposure amount of BPA for the different cohorts are estimated to be very low against higher BPA plasma concentration obtained in biomonitoring studies (Völkel et al., 2005, 2002; Teeguarden et al., 2015; Thayer et al.,

Chapter 3

2015). Mielke and Gundert-Remy (2009) compared the observed biomonitoring data of Schönfelder et al. (2002) study against the model predicted plasma concentrations of BPA using the simple kinetic approach and physiological based pharmacokinetic (PBPK) model, and found 3000 fold lower difference between the model prediction and the observed biomonitoring data. This wide discrepancy between the pharmacokinetic models' prediction and the biomonitoring data could be due to physiological variation, genetic polymorphisms among populations, exposure variation and exclusion of non-oral routes of exposure. However, the possible contamination during sample collection and analysis could be one reason for this discrepancy (Longnecker et al., 2013; Ye et al., 2013) but it is beyond the scope of this paper. Functional polymorphism in glucuronidation enzyme responsible for the BPA metabolisms has been reported by Trdan Lusin et al. (2012). It has been found that BPA after dermal exposure has a longer half-life of 8 h as it bypass the first pass metabolism, and attains the steady state in blood by the 4th day, whereas single oral dose intake completely eliminates in 6–8 h and never reach steady state even with daily dosing (Biedermann et al., 2010; Mielke et al., 2011; Mielke and Gundert-Remy, 2012; Gundert-Remy et al., 2013).

In recent years, use of physiologically based pharmacokinetic (PBPK) modeling has been quite popular in the human health risk assessment (Clewell and Clewell, 2008, Schuhmacher et al, 2014, Fabrega et al, 2015, Fabrega et al, 2016, Sharma et al, 2017). Previously, adult human, rat and monkey PBPK models have been developed for the BPA and its conjugates (Shin et al., 2004; Edginton and Ritter, 2009; Fisher et al., 2011; Yang et al., 2015, 2013; Yang and Fisher, 2015). The pregnancy physiologically-based pharmacokinetic (P-PBPK) models have long been used to estimate the exposure of the chemical to the fetus (Corley et al., 2003). The P-PBPK model for mice was previously developed (Kawamoto et al., 2007), which showed the potential exposure of BPA to the fetus. However, a P-PBPK model for the human has not yet been developed. The pharmacokinetic data for chemicals are often limited in specific populations of pregnant mother and fetus, due to the ethical and technical reason, which often lead to difficulties in building a kinetic model. However, the use of a physiological based pharmacokinetic model can simplify this complexity, based on its capability to predict the kinetics of chemical via a mechanistic understanding of its absorption, distribution, metabolisms, and elimination inside the body. The overall aim of this study was to improve the understanding of the chemical toxicokinetic relationship between the mother and the fetus by developing a P-PBPK model for the BPA and its conjugates. This would enable to predict the fetus plasma and organs BPA concentration by estimating the mother plasma BPA concentration and, thus helps in identifying the critical window(s) of exposure to the fetus during its gestational period of development. The conceptual model diagram is provided in Fig. 1 showing the study design undertaken for this work. The P-PBPK model development has followed following phases: a) development and validation of the adult PBPK model, b) extension of the developed adult PBPK model to a P-PBPK with the inclusions of dynamic physiological changes during the pregnancy and the prediction of chemical toxicokinetic profile in both mother and fetus compartment and c) evaluation of developed P-PBPK model against the biomonitoring data of available pregnant cohort population. An additional case study of this model has been recently published in Martínez et al. (2017), where simulation of prenatal BPA exposure via dietary intake of pregnant women recruited from Tarragona County was performed.

Chapter 3

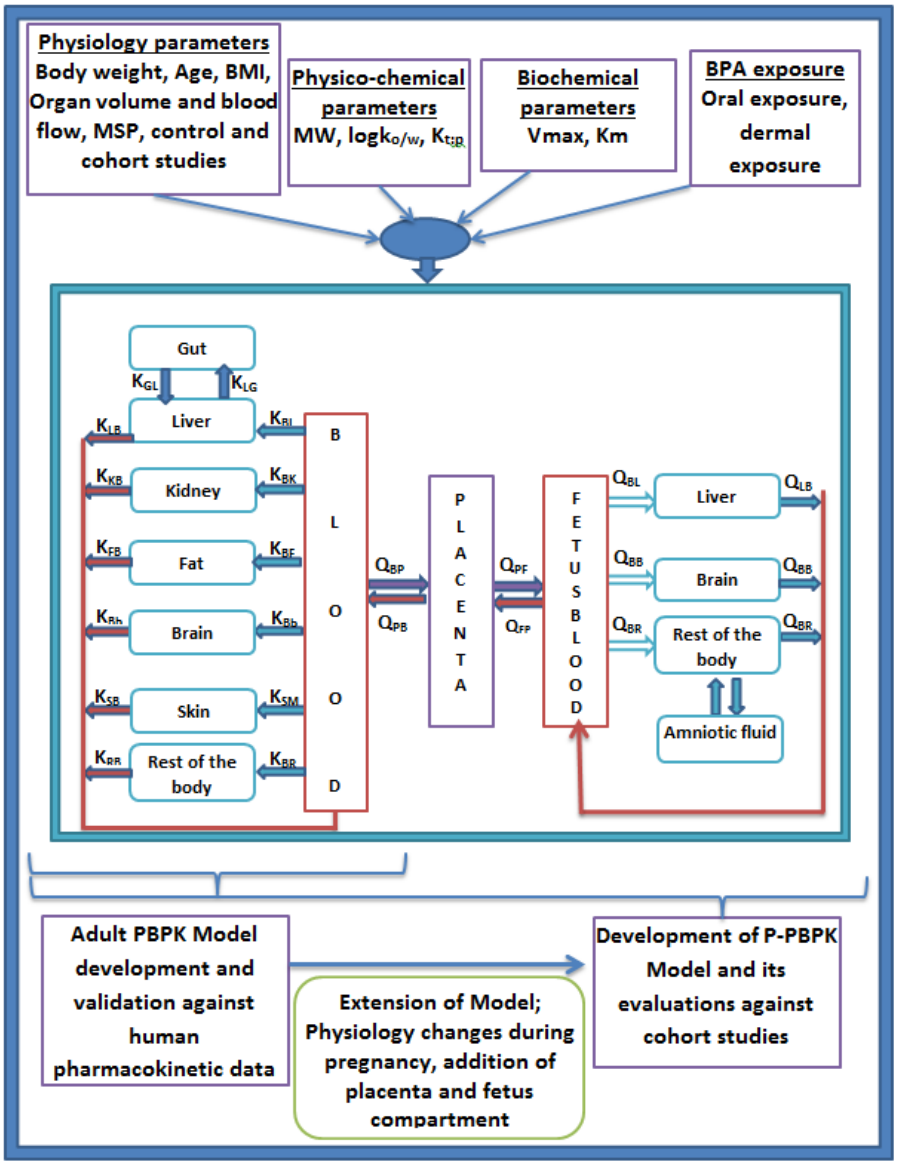

Fig. 1. A conceptual model for the development of P-PBPK model. It involves the development of the adult PBPK model and extension of this model to the P-PBPK model with the addition of placenta and fetus sub-compartment. MW = molecular weight, BMI = basal metabolic index, MSP = microsomal protein, K = partition coefficient and subscripts L = Liver, B = blood, b = brain, K = kidney, S = skin, R = rest organ, G = gut, Q = cardiac blood flow, P = placenta, F = fetus.

Chapter 3

2. Methodology and parameterization

Development of the P-PBPK model retains entire feature that used to describes the adult BPA and BPA-C (BPAG and BPAS) kinetics like partition coefficient for the organs, fraction unbound, metabolism (Vmax and Km) and elimination (urinary elimination). The physiological changes that occur during pregnancy like changes in plasma volume, fat volume, and amniotic fluid, placental and fetal growth are described as dynamic parameters that depend on the gestational period (Gentry et al., 2003; Abduljalil et al., 2012). Besides the oral mode of exposure, dermal mode of exposure was included in the development of the pregnancy-PBPK model. The oral exposure was divided into three equal doses and dermal as a single dose. Considering the gestational growth physiology in the case of the pregnant mother and fetus, the development of a P-PBPK model has been described in the following section. The model was coded in the R (version 3.2.3), and model equations are provided in the supplementary material (Annex 3).

2.1. General pregnancy-PBPK Model structure

The basic structure of the P-PBPK model has been adapted from an adult model, which included plasma, liver, kidneys, fat, brain, skin and a rest of the body compartment for the remaining tissues. The placenta and the fetus compartments were added into the model. The fetus compartment is further extended to fetus sub-model considering liver, kidney, brain, and plasma as fetus sub-compartments. The fetus sub-model considered the fetus-specific metabolic processes and included important target organs for the prediction of internal target dosimetry. The physiological and metabolic parameters were applied for the fetus model as dynamic parameters of gestational period and chemical-specific parameters such as partition coefficient were kept similar to the adult human model in the case of both Mother and fetus organs.

The source of exposure to the fetus was via unbound concentration of the chemical in the mother placenta, assuming only the mother directly exposed to the chemical. The placental-fetal unit assumes a bidirectional transfer process describing BPA and BPA-G transfer between mother placenta to fetus plasma and vice versa. The transfer rate was assumed as a simple diffusion process. Transport of chemical from fetal plasma into the fetal compartments like liver, kidney, brain, and rest of the body was assumed to be simple diffusion described by partition coefficient (same as of mother tissue). The amniotic fluid compartment was included in the current P-PBPK model. Transfer rates between the amniotic fluid compartment and the fetal body were described as a simple diffusion process.

The elimination of BPA in the mother was assumed to be similar to adult human, which occurs via its rapid metabolism in the liver and intestine, subsequently excreted via urine. However, the clearance of BPA and its conjugates in the fetus was described with first order transfer rate from fetus plasma to mother plasma via the placenta.

2.2. Gestational growth physiology model

The dynamic physiological parameters for the pregnant mother that changes during the gestational period such as plasma volume, hematocrit percentage, the fetus and the

Chapter 3

placental growth were accounted for the development of P-PBPK model. The increase in maternal body weight was accounted by considering the dynamic growth of mother's organ and fetus growth into the model. The volumes of liver, kidney, skin, brain, and gut of mother were calculated by taking constant fractions of the non-pregnant maternal body weight (Davies and Morris, 1993; Brown et al., 1997) provided in Table A.1. For the rest of the body compartment for pregnant mother and fetus was calculated by subtracting the sum of all organs volume from the total maternal and fetus body weight respectively. Additionally, the increased blood flow to the organs such as kidney, fat and placenta were considered to calculate the increase in maternal cardiac output (O'Flaherty et al., 1992; Gentry et al., 2003, 2002). All physiological parameters were considered as a function of gestational day and the model equations were adapted from different literature sources (Sisson et al., 1959; O'Flaherty et al., 1992; Gentry et al., 2003, 2002; (Clewell and Clewell, 2008); Abduljalil et al., 2012) and are provided in appendix-I.

The fetus model was sub compartmentalized into liver, plasma, brain, amniotic fluid and rest of the body. Fetal body and mother placental volume was modelled by using Eqs. (1) and (2), respectively, described by Gentry et al. (2003). The quantity of amniotic fluid for the gestational day was calculated by applying polynomial Eq. (3), as described by Abduljalil et al. (2012). Fetal blood flow was defined as a function of fetal blood volume and is adapted from the Clewell et al. (1999). Fetus plasma blood flow to the individual organs was calculated using Eq. (5) that implies multiplication of the fetal cardiac output with a constant fraction of the fetal blood flows to those organs, which assumed to be same as mother, as described by Gentry et al. (2003). Blood plasma flow to the rest of body was derived by subtracting the sum of total blood plasma flow to the organ from the total fetal cardiac output. The dynamic growth of the fetus volume was calculated during its gestational growth using Eq. (1). The fetus growth data provided by Brown et al. (1997) and ICRP (2002) were used to calculate the fetus organ weight as a constant fraction of its body weight which is dynamic parameter described in Eq. (1). Thus the fetus organ volume was estimated by multiplying fetal body volume with constant fraction value of the organs described in Eq. (4).

The fetus, placenta, and amniotic fluid growth kinetics were calculated by applying the following equations:

$$V\_fetus = (3.779 * \exp(-16.081 * (\exp(-5.67e-4 * (GD * 24)))) + 3.883 * \exp(-140.178 * (\exp(-7.01e-4 * (24 * GD)))) \quad (1)$$

$$V\_placenta = 0.85 * (\exp(-9.434 * \exp(-5.23e-4 * (GD24)))) \quad (2)$$

$$V_{aminiotic}fluid = 1.9648 * \left(\frac{GD}{7}\right) - 1.2056 * \left(\frac{GD}{7}\right)^2 + 0.2064 * \left(\frac{GD}{7}\right)^3 - 0.0061 * (GD/7)\text{^}4 + 0.00005 * (GD/7)\text{^}5 \quad (3)$$

Where, V_fetus = volume of fetus as a function of gestational day in L, GD = gestational day, V_placenta = volume of placenta in L, and V_aminitoic fluid = volume of aminiotic fluid in mL.

The blood flow to the fetus organ was calculatd by using the following general equation:

Chapter 3

$$Q\text{organ}_{\text{fetus}} = \text{FQorgan}_{\text{mother}} * \text{QCplasma}_{\text{fetus}} \quad (4)$$

Where, $Qorgan_{fetus}$ = the blood flow to organ in L, $FQogran_{mother}$ = constant fraction of cardiac blood flow to organ in mother, and $QCplasma_{fetus}$ = the fetus cardiac output.

The organ volume of the fetus was scaled by using the following general equation:

$$Vorgan_{fetus} = Forgan_{fetus} * V\_fetus \quad (5)$$

Where, $Vorgan_{fetus}$ = the organ volume in L, $Forgan_{fetus}$ = constant fraction of organ of fetus as a funciton of gestational day, and V_fetus = the total volume of fetus as a function of gestational day.

All the physiological parameters are provided in the annex 3 (Table A.1). The dynamic growth pregnancy physiology equations are taken from previous studies (Gentry et al., 2003; Abduljalil et al., 2012) summarized in Table 1.

Table 1. Parameterization of pregnant mother and fetus physiology

Mother Tissue volume	
Liver volume [b]	$\text{V\_Liver} = \text{F}_{\text{Liver}} * \text{BWinit}$
Kidney Volume [b]	$\text{V\_Kidney} = \text{F}_{\text{kidney}} * \text{BWinit}$
Gut volume[b]	$\text{V\_Gut} = \text{F}_{\text{Gut}} * \text{BWinit}$
Brain Volume[b]	$\text{V\_Brain} = \text{F}_{\text{Brain}} * \text{BWinit}$
Plasma volume [c]	$\text{V}_{\text{Plasma}} = (2.50 - 0.0223\text{GA} + 0.0042 * \text{GA}^2 - 0.00007 * \text{GA}^3) * \text{BW}$
Initial fat volume[a]	$\text{V\_Fat}_{\text{init}} = \text{BWInit} * \text{F}_{\text{fat}}$
Fat volume [a]	$\text{V\_Fat} = \text{BWInit} * (\text{F}_{\text{fat}} + 0.09 * \text{e}^{-12.90995862} * \text{e}^{-0.000797} * \text{GD} * 24)$
HCT[c]	$\text{HCT} = 39.1 - 0.0544 * (\text{GA} * 7) - 0.0021 * (\text{GA} * 7)^2$
Placenta Volume[a]	$\text{V\_placenta} = .85 * \left(\text{e}^{-9.434 * \text{e}^{-5.23\text{E}-4 * \text{GD} * 24}}\right)$

Chapter 3

Increase in Body weight of pregnant women as due to change in fat, placenta, feus and amniotic fluid weight	$BW = BWinit + \left(V_{Fat} - V_{Fat_{init}}\right) + V\_placenta + V\_fetus + V\_Aminiotic\ fluid$
Fetus tissue volume	
Fetus volume [a]	$V\_fetus = 3.779 * \left(e^{-16.08*e^{-5.67*e^{-4}*GD*24}}\right) + \left(e^{-140.78*e^{-7.01*e^{-4}*24*GD}}\right)$
Fetal plasma volume [b]	$V_{Plasma_{fetus}} = F_{Plasma_{fet}} * V_{fetus}$
Fetus liver volume [b]	$V\_liver\_fetus = F_{liverfet} * V\_fetus$
Fetus kidney volume [b]	$V\_kidney\_fetus = F_{kidneyfet} * V\_fetus$
Fetus brain volume [b]	$V\_brain\_fetus = F_{brainfet} * V\_fetus$
Amniotic fluid volume[c]	$V\_Aminiotic\ fluid = 0 + 1.9648 * GA - 1.2056 * GA^2 + 0.2064 * GA^3 - 0.0061 * GA^4 + 0.00005 * GA^5$
Fetus rest of body volume	$V\_restbody\_fetus = (0.92 * V\_fetus) - (V\_Plasma\_fetus + V\_liver\_fetus + V\_kidney\_fetus + V\_brain\_fetus)$
Blood flow to mother tissue (L/h)	
Initial cardiac output for blood [b]	$QC\_Blood\_init = QCC * BWinit^{(.75)}$
Adjust initial cardiac output for plasma flow [b]	$QC\_Plasma\_init = QC_{init} * (1 - HCT)$
Plasma flow to liver [b]	$Q\_Liver = F\_QLiver * QC\_Plasma\_init$
Plasma flow to gut [b]	$Q\_Gut = F\_QGut * QC\_Plasma\_init$

Chapter 3

Initial flow to fat [b]	$Q\_Fat_{init} = F\_QFat * QC\_Plasma\_init$
Changing flow to the fat [a]	$Q\_Fat = Q\_Fat_{init} * \left(\frac{V_{Fat}}{V_{Fat_{init}}}\right)$
Blood flow to placenta[a]	$Q\_Placenta\_blood = 58.5 * V\_placenta$
Plasma flow to placenta	$Q\_Placenta = Q\_Placenta\_blood * (1 - HTC)$
Renal plasma flow[c]	$QKidney = 53 + 2.6616 * GA - 0.0389 * GA^2$
Cardiac output[b]	$QC = QC\_init + (Q\_Fat - Q\_(Fat\_init)) + (QKidney - QKidney\_int) + QPlacenta$
Blood flow to fetus (L/h)	
Cardiac output for fetus[b]	$QCblood\_fetus = FQfetus * V\_Plasma\_fetus$
Fetal cardiac output adjusted to plasma[b]	$Qplasma\_fetus = QC\_Blood\_fetus * (1 - HCT_{fetus})$
Fetal liver blood flow [b]	$QLiver\_fetus = FQLiver * QC\_Plasmafetus$
Fetal kidney blood flow [b]	$QKideny\_fetus = FQKidney * QC\_Plasmafetus$
Fetal brain blood flow [b]	$QBrain\_fetus = FQBrain * QC\_Plasmafetus$

a = (Gentry et al., 2002), b = standard scaling method for PBPK, c = (Abduljalil et al., 2012)
GD= Gestational day, GA = Gestational age in week

2.3. BPA pharmacokinetics

The conceptual schema has been provided in the Fig. 2 showing distribution of BPA and its metabolites in the body.

Chapter 3

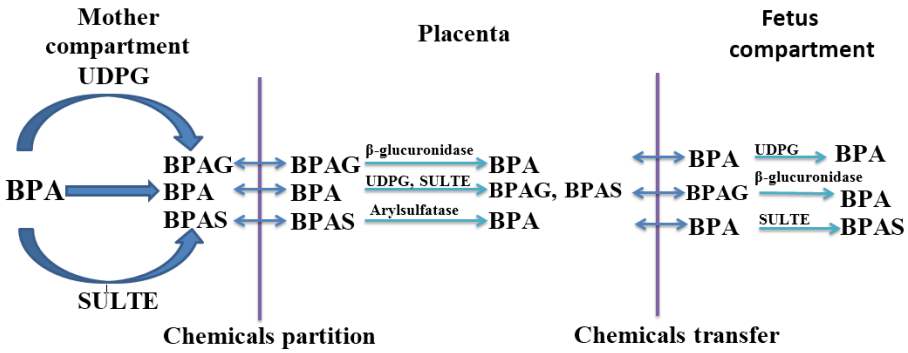

Fig. 2. The pharmacokinetics of BPA and its conjugates in both mother and fetus. The placental-fetal unit assumes a bidirectional transfer process of BPA and BPA-C describing the distribution of BPA and its metabolites in mother and fetus body.

In the present P-PBPK model of BPA, physiological changes during pregnancy were included. Metabolism in pregnancy was introduced via scaling of the in-vitro Vmax for glucuronidation and sulfation, considering the pre-pregnancy body weight. The BPA metabolism data for the fetus was scaled using human in-vitro data and fetus microsomal protein content, and, growing fetus liver and body weight. Two metabolic kinetic parameters namely Vmax (maximum rate of reaction) and Km (affinity of the substrate for the enzyme), for mother and fetus, is taken from in-vitro studies and has been scaled to in-vivo. The pharmacokinetic data are provided in the annex 3 (Table A.2).

2.3.1. Oral uptake and gut metabolism

Generally, the oral ingestion of BPA through diet is considered as the major route of exposure (WHO, 2010). It is rapidly absorbed through the gut and maximum concentration in the blood achieves at 0.42–1 h. Studies have shown that oral bioavailability of BPA is very low, as it passes through first pass metabolism, in the intestine and liver, being completely absorbed from the gut (Völkel et al., 2005, 2002; Mielke and Gundert-Remy, 2012).

Both BPA and BPAG uptake from the gut to the system was described by first order reaction, considering gastric emptying delay for BPA arrival to the gut (Kortejärvi et al., 2007). The oral absorption rate of the BPA was optimized against the Yang et al. (2015) data. The data on uptake of BPAG from the intestine to the liver was taken from the previous study of Yang and Fisher (2015).

Most of the oral administered BPA metabolizes into BPAG by intestinal UDPGT (Mazur et al., 2010; Trdan Lusin et al., 2012). The in-vitro in-vivo extrapolation (IVIVE) approach and saturation metabolism kinetic (Eq. (6)) were applied for describing BPA glucuronidation in the mother intestine (Cubitt et al., 2009; Yoon et al., 2014). The scaling of in-vitro Vmax parameter to in-vivo (IVIVE) was done applying Eq. (7) that used microsomal protein content per gram tissue and weight of tissue per kg body weight. For the scaling of Vmax, the amount of microsomal protein in the gut of 3 mg/g (MPPGG)

and the weight of human gut 30 g/kg body weight was taken into account (Yang and Fisher, 2015).

The metabolism is described by using the following equation:

$$\frac{dAmet}{\mathrm{dt}} = \frac{\mathrm{Vmax}*\mathrm{C_{organ}}*\mathrm{fu}}{\mathrm{Km}+\mathrm{Corgan}*\mathrm{fu}} \quad (6)$$

Where, $\frac{\mathrm{dAmet}}{\mathrm{dt}}$ = the amount of metabolism produced with time, Vmax = the maximum metabolism rate, Km = the concentration of substrate required to attain 50 percent of its Vmax, Corgan = the concentration of substrate at target metabolism organ, and fu = fractional unbound.

Vmax was scaled to in-vivo per kg BW from in-vitro cell line studies by using the following method:

$$Vmax(intestine) = (Vmax_{invitro} * MPPGG * Vgut)/BW^{.75} \quad (7)$$

Where, $Vmax_{invitro}$ = in-vitro value of metabolic capacity in per gram of microsomal protein (intestinal cell line) , $MPPGG$ = microsomal protein per gram of gut , Vgut = total gut weight in gram, and BW = whole body weight in kg.

2.3.2. Dermal absorption and metabolism

Recently published papers raised the issue of underestimation of BPA exposure via the dermal route given that BPA presence in materials that frequently comes in contact with the human skin (Biedermann et al., 2010; Lassen et al., 2011; Mendum et al., 2011). In-vitro viable skin culture model experiments showed that the skin has potential to absorb and metabolize BPA into BPAG and BPAS (Kaddar et al., 2008; Zalko et al., 2011a). Recently, Mielke et al. (2011) published internal dosimetry model of BPA compared oral route with 90% absorption rate, with dermal route considering different reported absorption rates such as 10 (EU, 2003), 13 (Morck et al., 2010), 46 (Zalko et al., 2011b), and 60 (Biedermann et al., 2010) and showed importance of the dermal absorption for the estimation of BPA internal exposure level.

In the present study, the dermal route of exposure was considered for the development of P-PBPK model. Considering the fact of wide variation of the absorption rate of BPA via skin, highest reported permeability coefficient (kas = 0.25 1/h), data for the adult model provided by Mielke et al. (2011) was used to develop the P-PBPK model. The following Eq. (8) was applied for calculating skin absorption:

$$\frac{d}{dt}skin = Qskin * (Cplasma * fu - Cskin * \frac{fu}{K\_skin\_plasma}) + (Capp\_skin - cskin/K\_skin\_vehicle) * t\_df * kas * A/1000 \quad (8)$$

Where, Qskin = the cardiac blood flow to skin, Cplasma = the plasma chemical concentration, fu = the fractional unbound, K_skin_ plasma = the plasma skin partition

coefficient, Capp_skin = the applied concentration of chemical to the skin surface, Cskin = the concentration of chemical in the skin compartment, K_skin_ vehicle = the vehicle skin partition coefficient, t_df = the time delay factor for absorption to reach to plasma, A = skin surface area and kas = the permeability rate constant.

2.3.3. Metabolism in the adult liver

Phase-II glucuronidation reaction is a major pathway in human for chemicals or drugs detoxification. The resulting conjugates of glucuronic acid to the chemicals increase its hydrophilicity and are generally considered to be pharmacologically inactive (Sperker et al., 1997b). BPA undergoes rapid metabolism to form glucuronidation and sulfation conjugates in the liver by uridine-diphospho-Glucoronide transferase (UDPGTs) and sulfotransferase (SULT) enzyme respectively (Kim et al., 2003; Hanioka et al., 2008; Hanioka et al., 2011). The reported values of Vmax and Km for glucuronidation from different in vitro studies show variability in glucuronidation (Elsby et al., 2001; Kuester and Sipes, 2007; Kurebayashi et al., 2010; Mazur et al., 2010; Trdan Lusin et al., 2012).

In the present study, the rate of reaction for both glucuronidation and sulfation for the PBPK model was derived by IVIVE scaling approach. The current hepatic in-vitro cell line data were used for deriving maximum reaction velocity (Coughlin et al., 2012) using Eq. (9) that accounts microsomal protein value (32 mg/g of liver) and liver weight (2.6 percentage of BW). The metabolism was described based on Michaelis-Menten equations using Eq. (6) and implemented into the current PBPK model. The fraction unbound in the microsomes was not accounted for in the calculation of the in vivo values.

$$Vmax(liver) = (Vmax_{invitro} * MPPGL * Vliver)/BW^{.75} \quad (9)$$

Where, $Vmax_{invitro}$ = in-vitro value of metabolic capacity in per gram of microsomal protein (hepatic cell line), $MPPGL$ = the microsomal protein per gram of Liver, Vliver = the total liver weight in gram, and BW =the whole body weight in kg

2.3.4. BPA metabolism in the human fetal liver

Formation of the glucuronide conjugates involves following steps such as rate of supply of substrate (chemicals to be conjugate), the rate of formation and supply of the co-substrate i.e., glucuronic acid, and the expression and the specific activity of the enzyme responsible for glucuronidation i.e., uridine-diphospho-Glucoronide transferase (UDP-GTs). The concentrations (µmol/Kg wet weight) of UDPGLcUA were 59.4 ± 11.3 (fetal liver), 301 ± 119 (adult liver), 17.8 ± 1.8 (mid-term placenta) and 17.0 ± 1.7 (near term placenta) (Beach et al., 1978; Cappiello et al., 2000; Coughtrie et al., 1988; Kawade and Onishi, 1981). The above data shows that the UDPGLcUA is present in the human fetal liver at a 5-fold lower concentration than in the adult liver. Another study has shown that the activity of UDPGT was null at an early stage of the fetus, showing glucuronidation as a potential limiting factor in the human fetus (Strassburg et al., 2002). The expression of these two isoforms UGT2B15 and 2B7 are detectable in human fetal livers during the second trimester of pregnancy and has been stated to account for 18% of the values calculated in adults (Divakaran et al., 2014).

Chapter 3

In the present study, the glucuronidation of BPA in the model was considered for the fetus. The scaling of Vmax in the case of the fetus liver has been done before by Gentry et al. (2003). However, Gentry method considers the fixed value of Vmax and uses fetus enzyme activity as a fraction of the adult value for the scaling method. For this study, similar to adult's scaling, the metabolism in the fetus liver was directly scaled from the in vitro hepatocyte data, considering the developmental changes in the fetus. The reported microsomal protein content per gram of fetus liver at the age of 9–22 gestational week was 10–16 mg (Pelkonen, 1973) and 26 mg (Pelkonen et al., 1973) in two different studies and for the scaling purpose 26 mg/g liver was taken presumably a realistic value at near term of pregnancy, when fetal metabolic capacity is matured. The liver weight for the fetus was provided as a dynamic parameter, which was scaled by taking constant fraction value of liver from ICRP (2002) data, (provided in the annex Table A.1) and its multiplication with growing fetus body (dynamic equation as a function of the gestational day). The concentration of microsomal fraction content per gram liver was assumed to be constant throughout the gestational day. This approach represents an increase in liver enzyme activity with the increase in the fetus liver and body weight. Thus the Vmax value increases with gestational age. The Vmax, maximum velocity reaction for BPA in the fetal liver was derived by using following equation:

$$Vmax_{fetus} = (Vmax_{invitro} * MPPGL_{fetus} * Vliver_{fetus})/BW\_fetus^{.75} \quad (10)$$

Where, $Vmax_{fetus}$ = maximum metabolism rate of fetus liver, $Vmax_{invitro}$ = reported in-vitro metabolism rate, $MPPGL_{fetus}$ = microsomal protein per gram of fetus liver, and $Vliver_{fetus}$ = liver volume of fetus.

2.3.5. Deglucuronidation in fetus compartment

β-Glucuronidase is an enzyme, which deconjugates the glucuronide conjugate xenobiotics (Sperker et al., 1997a). There is evidence for a significant role of the β-Glucuronidase in the fetus, although the role has not been well understood so far in the fetus kinetic modeling. In the animal fetus development studies, it has been found that deglucoronidation activity is more than glucuronidation at the developmental stage (Mccance et al., 1949; Lucier and Sonawane, 1977). In contrast at near term, a fetus glucuronidation activity is higher than deconjugation (Corbel et al., 2015). Domoradzki et al. (2003) studies in the fetus rats at different gestational age showed deconjugation activity of 443 nmol/h/mgMSP at the age of 22 weeks showing the importance of deglucuronidation in the fetus. Moreover, glucuronide conjugate versus free BPA ratio in the placenta and fetus showed that β glucuronidase is present at high concentration in placenta and other various tissues in the fetus (Ginsberg and Rice, 2009).

2.4. Fetoplacental BPA kinetics

Placenta acts as a barrier against xenobiotics such as chemicals and drugs to protect the fetus from being exposed to them. Morck et al. (2010), in an ex vivo placental perfusion study showed that BPA can easily cross the human placenta. Further, Borrirukwisitsak et al. (2012) reported that due to its lipophilic nature, BPA can easily cross the placental barrier. The finding of free BPA in fetus plasma in human biomonitoring (Schönfelder et

al., 2002; Ikezuki et al., 2002; Kuroda et al., 2003; Lee et al., 2008; Zhang et al., 2013), showed evidence of transfer of BPA through the placenta. In contrast, very low level of BPAG in the fetus was found (Muna et al., 2013; Gerona et al., 2014) assuming due to the deglucuronidation in both placenta and fetus liver (Muna et al., 2013; Gerona et al., 2014). In fact, Nishikawa et al. (2010) uterine perfusion experiments showed that small amount of BPAG is transferred to the fetus across the placenta showing very low bidirectional transfer of BPAG.

The mother plasma and placenta partition coefficient value for BPA and BPAG were taken from a previous study of Csanády et al. (2002) and Kawamoto et al. (2007) respectively. In this model distribution of sulfation conjugate of BPA (BPAS) to the fetus compartment was not considered due to lack of data in placental transfer. The transfer rate constants for BPAG in this model were taken from the pregnant mice PBPK model and scaled to fetal body weight (Kawamoto et al., 2007), as there is no available human data. Additionally, the glucuronidation of BPA in placenta was described, considering Vmax and Km value from an in-vitro hepatic cell line (Coughlin et al., 2012). The in-vivo Vmax for the placenta was calculated using placenta microsomal content i.e., 11.3 mg/g (McLaughlin et al., 2000), placenta volume and the body weight. The scaling of Vmax for placenta glucuronidation was done using following equations:

$$Vmax_{placenta} = (Vmax_{invitro} * (MPPGP) * V\_placenta)/BW^{.75} \quad (11)$$

Where, $V\_placenta$ is the volume of placenta and it is a dynamic parameter, which depends on the Gestational day can be seen in equation 2. $MPPGP$ is microsomal protein per gram of placenta.

2.5. Amniotic fluid BPA kinetics

The human biomonitoring data had reported the presence of BPA and BPAG concentration in amniotic fluid. The increase in free BPA concentration with the increase in the gestational period was observed, as from second trimester to the third trimester (Edlow et al., 2012). Ikezuki et al. (2002) reported the five-fold higher concentration of free BPA at an early stage of pregnancy in comparison to the late week of gestational. This phenomenon might be due to the low metabolic capacity of fetus organ as well as the low volume of amniotic fluid at an early stage of pregnancy. Further, the activity of beta-glucuronidase measured in amniotic fluid at early stage found to be higher than the later week of gestation. Whereas, glucuronidase activity is found to be higher in the later week of gestation (Matysek, 1980; Fetus et al., 1993). The above finding of increased activity in glucuronidase at an early stage of pregnancy could be some of the possible reasons for the increased level of free BPA at the early gestational age.

2.6. Partition coefficient for pregnant mother and fetus organs

The partition coefficient (PC) for liver, fat, brain, and skin were taken from the study done by Doerge et al., (2011) and Fisher et al. (2011). The placental and kidney partition coefficient for BPA were taken from Csanády et al. (2002) and the BPAS was not distributed to fetus tissues. However, to measure BPAG concentration in the fetus plasma, BPAG was distributed to maternal placenta using placenta partition coefficient taken from

the previous mice study (Kawamoto et al., 2007). For other fetus compartments, partition coefficients were kept similar to as mother's organs partition coefficients. The partition coefficients used in the P-PBPK model are provided in the annex 3 (Table A.2).

2.7. Pregnancy cohort studies

For this study, we have used 5 different pregnancy cohort studies that measure the BPA concentration in different matrices. Subject characterics are provided in the Table A.3, which was used as an input variable for the case specific scenario. Summary of the biomonitoring data is provided in the annex 3 (Table A.4). Schönfelder et al. (2002) studies included 37 samples of both mother and fetus plasma (umbilical cord) between the gestational age of 32 to 41 week. Pregnant women of age ranging from 22 to 44 years old were recruited from Berlin and samples were collected at Benjamin Franklin Medical Center. In another study by Aris (2014), which included 61 pregnant women recruited from the eastern township of Canada at delivery time and both mother plasma and fetal cord blood BPA was analyzed.

Zhang et al. (2011) study included each 21 samples of human placental and fetal liver at the gestational age of 12.3–20 weeks and 11.3–22, respectively. Samples were obtained after elective pregnancy termination during 1998–2006 in the Greater Montreal area of Quebec. In addition, Cao et al. (2012) study included a large number of placenta and liver samples from the same population i.e. 128 and 28, respectively. In addition, Schönfelder et al. (2002) also studied placenta BPA concentration at the delivery time. Ikezuki et al. (2002) studied includes Japan population of each 37 women with an early and late pregnancy, where 37 maternal (late pregnancy) and 32 umbilical cord blood samples were collected at full-term delivery. In addition, 32 and 38 amniotic fluids samples were collected at 15–18 weeks gestation (early pregnancy) and at full-term (late pregnancy), respectively.

3. Results

3.1. Simulation and validation of adult human PBPK model

Validation of the developed adult PBPK model was performed by comparing the model predictions with plasma data obtained from the human study by Thayer et al. (2015) in which volunteers were orally administered 100 µg/kg BW dose of deuterated BPA. These predictions were performed by taking into account only female volunteers, and their individual BMI and body weight. The exposure dose was normalized according to body weight and the fat content of individual volunteers was calculated based on body weight and BMI of the respective subject. Out of 14 subjects (male and female), only 7 female subjects were considered from Thayer's study and simulated time-plasma BPA data profile were validated against their observed data. The total duration of simulation was 24 h. Fig. 3A, B and C depict the concentration–time profiles after single oral dosing of adult females (n = 7) for BPA (d6-BPA), and observations made by Thayer et al. (2015).

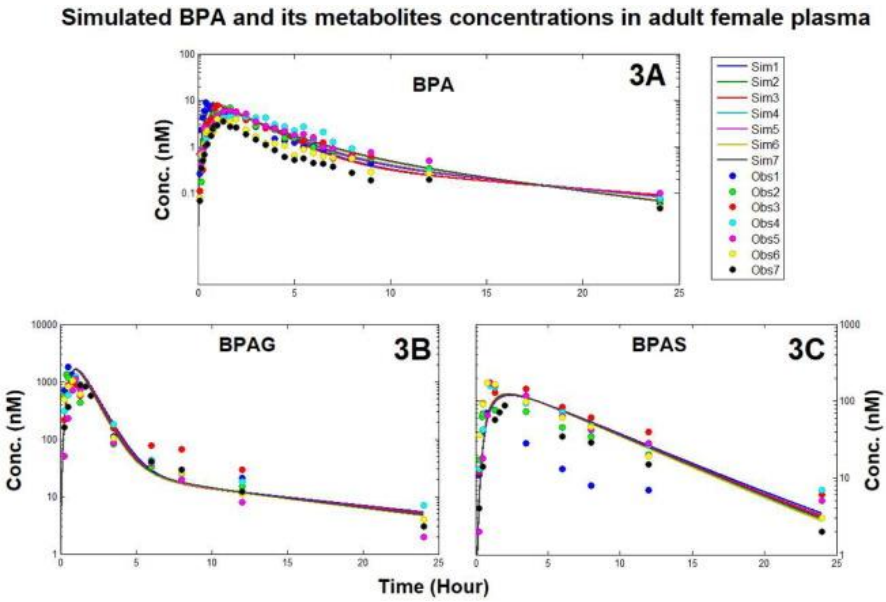

Fig. 3. Concentrations–time profiles after oral dosing of adult females (n = 7) with 100 µg/kg of deuterated BPA (d6-BPA) (Thayer et al., 2015). A) Simulated individual (solid color lines) and observed individual plasma (dot points) d6-BPA concentrations; B) Simulated individual (solid color lines) and observed individual plasma (dot points) d6-BPAG concentrations; C) Simulated individual (solid color lines) and observed individual plasma (dot points) d6-BPAS concentrations. Simulations of individual patients were performed using individual body weights and their fat content while keeping other model parameters constant.

3.2. Simulation and evaluation of P-PBPK Model

Most of the reported human biomonitoring data for the fetus is for BPA and generally, BPAG and BPAS studies are under-reported (Ikezuki et al., 2002; Schönfelder et al., 2002; Kuroda et al., 2003; Lee et al., 2008; Zhang et al., 2013). Development of the present model includes BPAG and BPAS conjugates in the mother, whereas in the case of the fetus only BPAG has been accounted, which is the major metabolite produced in the mother. For this study, the distribution of BPA and BPAG from mother plasma to the placenta is described via partition coefficient. Following that transfer of both BPA and BPAG across the placenta was described as simple diffusion process between the placenta and fetus plasma. Human Biomonitoring data showed the presence of higher concentration of free BPA in the amniotic fluid in early pregnancy than compared to late pregnancy (Ikezuki et al., 2002; Edlow et al., 2012). The reason behind this difference could be the higher beta-glucuronidase activity in early and mid-gestational periods (Matysek, 1980). However, in the later week of gestation, as the fetus liver develops and matures that might increase the liver glucuronidation activity.

Though there is a lack of glucuronidase data specific to the fetus deconjugation, presuming deconjugation process as an important toxicokinetic process, in the present P-

Chapter 3

PBPK model it was taken into account for the fetus compartment. The assumption has made that deconjugation of the BPAG to BPA was based on first-order rate transfer constant. The half-life of the chemicals is used to establish the rate of deconjugation estimated to be 0.35 h−1 (k = 0.693/t1/2).The same value is used in the case of both placental and fetus deconjugation for simplification. A similar approach has been used in the previous study (Lorber et al., 2010) for transfer of one metabolite to another, but it should be considered as worst case scenario and it shows clearly there is a need for proper studies to parameterise this process. These steps would result in increased level of free BPA in the fetus plasma. To maintain the cyclic deconjugation and conjugation reaction into the model, the available free BPA undergoes simultaneously for glucuronidation into the liver following distribution to the liver compartment to mimic the real biological phenomena.

The lack of validation of a model for the estimated exposure (for respective cohort) against biomonitoring data for cohorts via PBPK model has been observed in the previous study by Mielke and Gundert-Remy (2009). Additionally, finding of differences in the biomonitoring data for free BPA concentration within the cohort and in between cohorts is observed in different biomonitoring studies (Ikezuki et al., 2002; Schönfelder et al., 2002; Kuroda et al., 2003; Lee et al., 2008; Zhang et al., 2013). Several possible reasons can be put forward to explain this inconsistency among which underestimation of exposure levels and not considering other routes of exposure than oral has been questioned by researchers (Mielke et al., 2011). The timing of sampling is one of the major concern that has not been accounted in biomonitoring data, which can be another source of variability in biomonitoring data due to fast absorption and elimination of BPA that never reach steady state concentration even with multiple doses. In targeted human kinetic studies (Völkel et al., 2002; Thayer et al., 2015), the observation of Cmax (maximum concentration) and elimination half-life within 1–3 h of BPA exposure shows how crucial is the time of sampling. However variability due to the analytical method, contamination, source and route of exposure (EFSA, 2015; Longnecker et al., 2013; Ye et al., 2013), and importantly metabolic variation among population cannot be ruled out (Partosch et al., 2013; Nachman et al., 2014), which is beyond the scope of this manuscript.

Another complexity with the prediction of concentration for such chemicals might be due to their narrow time interval between the Cmax (the highest concentration) and Cmin (minimum concentration after exposure of chemical during 24 h or before subsequent exposure of chemical) rising a question on observed biomonitoring data is because of high/low exposure or because of the schedule of sampling. Therefore evaluation of the developed model has two possibilities first; either by changing exposure dose for each biomonitoring study, second; by using two extreme exposure scenarios (low-high). In this study, it was assumed that sampled biomonitoring data can be from any point of the time-concentration profile and the exposure dose was estimated for the observed high and low mother plasma concentration. This assumption seems conservative, but for the current scenario, this might be the best solution, instead of estimating exposure for each biomonitoring study. Exposure dose for the biomonitoring data was estimated by taking the reference of a previous study (Mielke et al., 2011). In the present study, the oral exposure was divided into three equal doses keeping dermal exposure as a single dose. Exposure dose for both the oral and dermal was estimated that matches the observed highest and lowest mother plasma concentration in different biomonitoring studies. This

Chapter 3

was done by simply applying trial and error method, a similar method was used before for other environment chemicals (Loccisano et al., 2013). Then the estimated dose was used for the simulation of a model that predicts the fetus plasma and organs concentrations at the different gestational period.

We have selected 5 different pregnancy cohort studies that measure the BPA concentration in different matrices. Two scenarios were selected for the simulation of PBPK model: one with the observed high mother plasma concentration population (Schönfelder et al., 2002), in turn dose of 44 μg/kg/BW thrice in a day (TID) oral dose and 20 μg/kg/BW single dermal exposure and other with the observed low mother plasma concentration (Ikezuki et al., 2002), in turn dose estimated to be 20 μg/kg/BW (TID) oral dose and 9 μg/kg/BW single dermal exposure.

Since the BPA has a very short half-life, even with well-distributed dosing schedule, the BPA plasma concentration shows sharp elimination curve profile and did not arrive at the steady state; a similar observation has been made by Mielke et al. (2011). In order to cover all the simulated data points considering essential for comparisons against the observed biomonitoring data points which could be either result of random samples at any point of time not knowing the exact exposure time or exposure variability in sample subjects (VandeVoort et al., 2016). The model output data were summarized into boxplot for each gestational week, which included the range of value from higher to lower concentration.

The simulation was done for different matrices and results were presented in different figures, a number from 4 to 7. Figs. 4 & 5 show the simulated results for mother and fetus BPA plasma concentration for the selected high and low dose exposure scenario respectively. Fig. 6 shows the simulation results for the BPA concentration in liver and placenta during the mid-gestational week and the results were compared with the biomonitoring data obtained from Zhang et al. (2011) study. Fig. 7 shows the BPA concentration in amniotic fluid. The amniotic fluid concentration of BPA by Ikezuki et al. (2002) was monitored at two stages, early and full term pregnancy. The low dose scenario was simulated for the Ikezuki et al. (2002) data on the concentration of BPA in mother and fetus plasma (Fig. 5) and amniotic fluid concentration (Fig. 7). The Fig. 7 shows the predicted BPA concentration in amniotic fluid is well matched with the observed concentration. Moreover, the observed mother and fetus plasma concentration (mean ± SD) by Ikezuki et al. (2002) is within the range of simulated low dose exposure scenario (Fig. 8).

Chapter 3

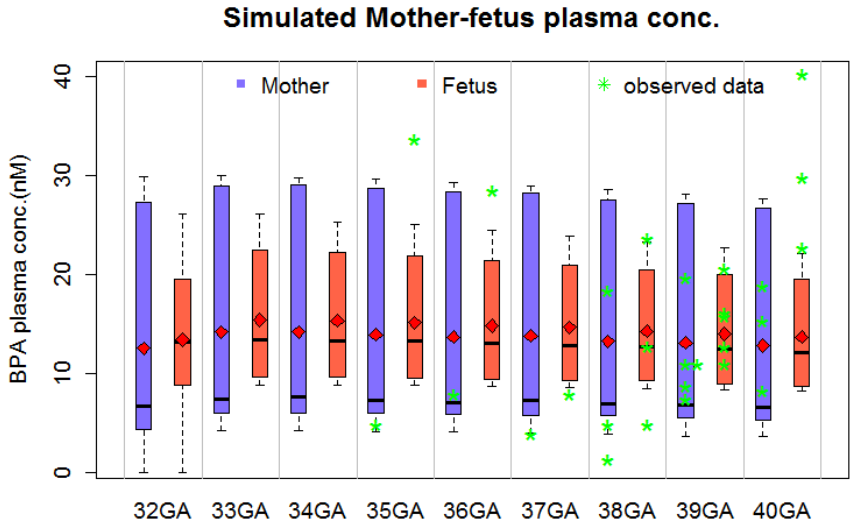

Fig. 4. Observed vs predicted mother plasma and fetus plasma of volunteer participated in Schönfelder et al. (2002) study for 32 to 41 week of GA; box plot containing mean (red diamond), median (horizontal line of boxplot), highest (upper bar of boxplot), lowest (lower bar of boxplot) value and observed value marked as green star.

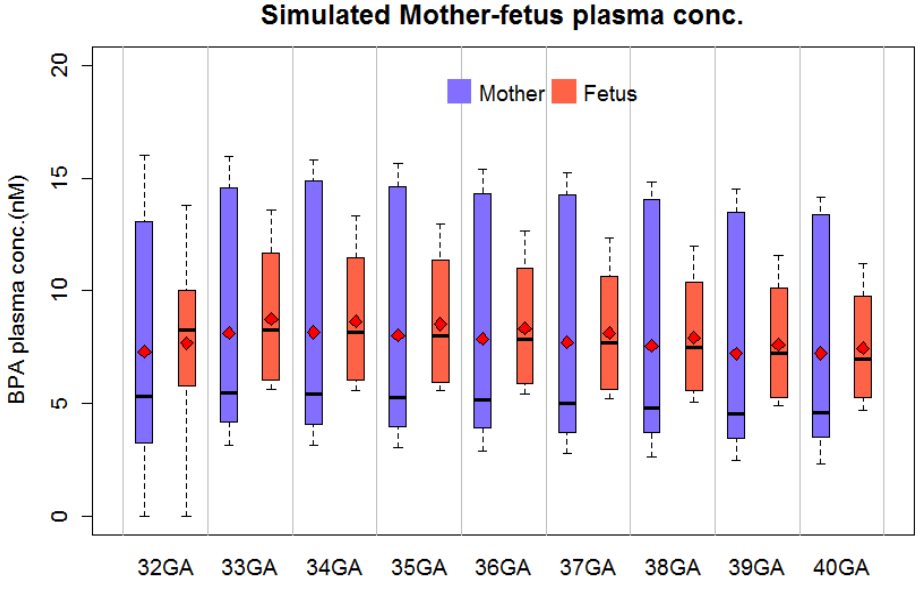

Fig. 5. Predicted mother plasma and fetus plasma for low dose scenario, estimated from the Ikezuki et al. (2002) mother plasma concentration, for 32 to 41 week of GA; box plot

containing mean (red diamond), median (horizontal line of boxplot), highest (upper bar of boxplot), and lowest (lower bar of boxplot) value.

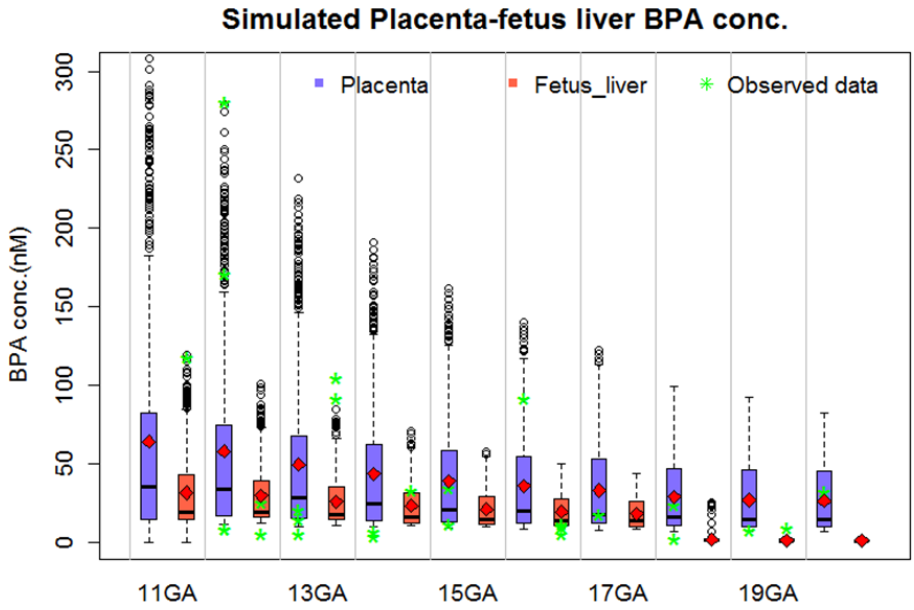

Fig. 6. Observed vs predicted placenta and fetal liver for higher exposure scenario for 11 to 22 week of GA; box plot containing mean (red diamond), median (horizontal line of boxplot), highest (upper bar of boxplot), lowest (lower bar of boxplot) and observed value (Zhang et al., 2011) marked as green star.

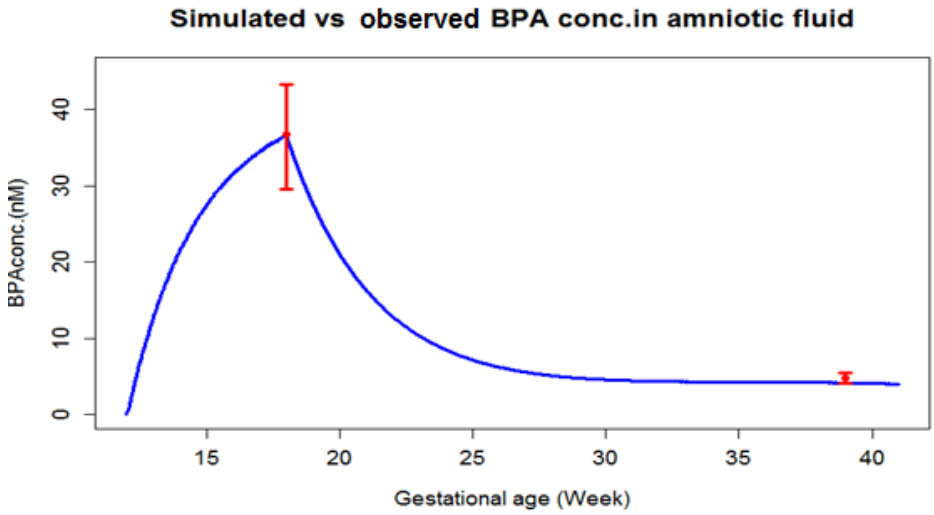

Fig. 7. Simulated low dose exposure scenario for amniotic BPA concentration starting from early mid-gestational to late gestational period (blue line curve) vs. observed (mean ± SD) concentration in Ikezuki et al. (2002) studied during 15–18 and 32–40 weeks of pregnancy (red error bar).

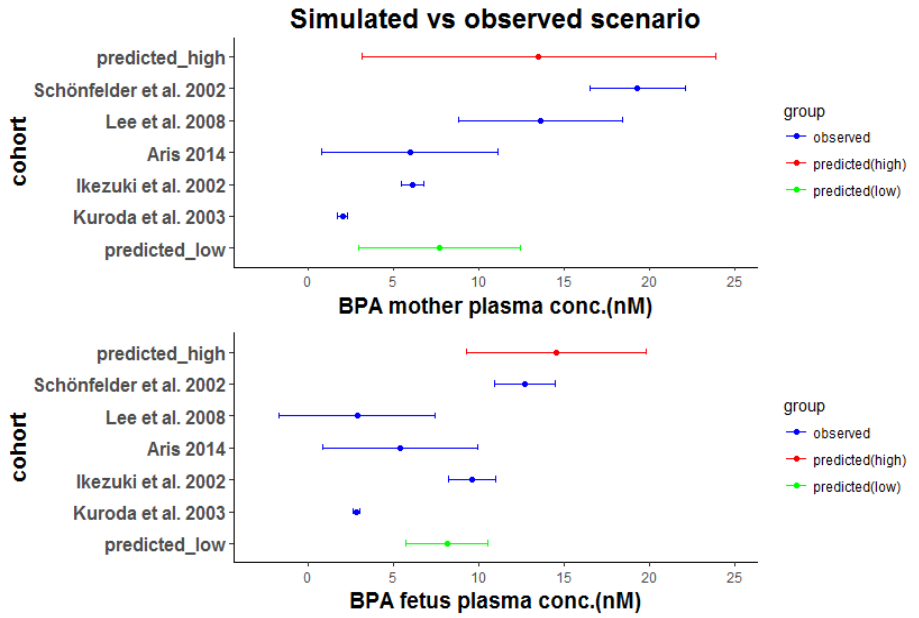

Fig. 8. Simulated mean ± SD of BPA for two exposure scenario (high and low dose) for the period of 32–40 GA and the observed mean ± SD of BPA in different studies for both mother and fetus BPA plasma concentration.

Fig. 8 shows the predicted mean ± SD for the high and low dose scenario vs. observed mean ± SD of different cohort studies for the period during 32–40 week of gestation. Most of the observed mean concentration was covered by a simulated scenario in case of mother plasma given the large range between Cmax and Cmin. However, in the case of the fetus some observed mean values were not in the range, which could be due to the various factors such as; variability in the gender of fetus previously reported as significant, metabolic variability due to polymorphism (not considered in this study) and process of deglucuronidation, which need proper in-vitro investigation for parameterization.

4. Discussions

The present study involved development and validation of the adult PBPK model and then an extension of this model to the pregnant mother to predict the toxicokinetic profile of BPA for both mother and fetus organs. Following the same parameterization of the previously developed model (Yang et al., 2015), in the present study, it was observed that results under predicts the free BPA and BPAS in plasma serum. The reason behind this could be the low absorption rate constant for free BPA, which leads to higher concentration available in the gut for the metabolism. The present adult model was slightly modified optimizing absorption rate constant and then the model was validated

against the Thayer et al. (2015) human experimental data. For the validation of the adult model, only female subjects were taken into consideration and the simulation for the individual subjects was done considering their physiological parameters such as body weight and body mass index. The adult pharmacokinetic results have shown that BPA has very fast absorption and elimination process (Schönfelder et al., 2002) as it undergoes first pass metabolism and rapidly converted into more polar compounds (glucuronide conjugates). Due to high metabolic activity for BPA, even higher or multiple doses has very less effect on time-concentration curve characteristic. However, variability in the BPA plasma concentration with respect to the time-concentration curve is much higher than inter-individual variation among subjects, showed plasma concentration is not only sensitive to dose but to time as well. The sudden drop in BPA concentration at peak is due to its higher metabolism rate, making a very sharp curve, which can be considered as benchmark characteristics of BPA. Even within a small fraction of the time, a large difference in BPA concentration was observed in this study. There were no significant changes in BPA plasma concentration observed among subjects, even individual fat content, calculated from body weight and BMI, has very little or no impact on plasma concentration. Although, some study has shown the genetic and gender variability in metabolism among the population (Hanioka et al., 2011). It has been reported that the concentration of BPA varies among different population cohorts such as male and female, pregnant and non-pregnant, adult, neonates, and children (Kim et al., 2003; Calafat et al., 2005; Vandenberg et al., 2010; Zhang et al., 2013; Aris, 2014). Polymorphism has been found to be one of the important factors in metabolic variability (Trdan Lusin et al., 2012). However, there are very few data available on functional polymorphism among the population causing metabolic differences in BPA metabolism (Hanioka et al., 2011). In the present study, polymorphism variability has not been accounted, however, it cannot be ruled out. Further, the variation in biomonitoring data shows the need for considering different physiological states into the PBPK models. Some specific physiological parameter such as body weight, height, and dynamic physiological changes in the specific population such as pregnancy and fetus were accounted to capture variability. A number of P-PBPK models have been developed for various environmental chemicals in the past for the risk assessment application (O'Flaherty et al., 1992; Gentry et al., 2003, 2002; Loccisano et al., 2013). Similar approach has been taken for the current P-PBPK model. However, in the current model approach, the model has included detailed chemical metabolism concept in both mother and fetus considering their dynamic growth parameters in order to mimic the real physiological process during gestational period.

The observed concentration in different cohorts during pregnancy was used for model evaluation. For instance, maternal blood concentration during pregnancy or at the delivery time was used for exposure estimation accounting both dermal and oral exposure. In the development of P-PBPK model, pregnancy growth dynamic equations were implemented into the model that mimics the physiology of pregnant mother, and the inclusion of the fetus compartment and its communication with the mother was done via placenta blood flow. The metabolism of the BPA in placenta and fetus liver is found to be key parameters for the understanding of fetal exposure to parent BPA. The human hepatocyte in-vitro data was scaled to calculate the fetus liver metabolic activity. For the scaling of Vmax, the reported fetus microsomal protein content was used in place of adult microsomal content. The deglucuronidation process for the fetus liver and amniotic fluid was applied into plasma compartment for the simplification of the model. The P-PBPK model predictions were compared with different sets of the BPA biomonitoring data available in

Chapter 3

the literature. Simulation-matched study designs were used based on information in the original studies.

In order to predict the BPA concentration in fetus plasma for various population studies, observed maternal BPA plasma concentration during pregnancy was used for exposure estimation accounting both dermal and oral exposure. The predicted exposure concentrations for two scenarios (high and low mother plasma concentration considering Schönfelder et al., 2002 and Ikezuki et al., 2002 studies respectively), were chosen and seems to be significantly higher than the generally estimated exposure. A similar observation about predicted and observed concentrations of these two references (Schönfelder et al. (2002) and Ikezuki et al. (2002)) were made in previous studies (Mielke and Gundert-Remy, 2009; Mielke and Gundert-Remy, 2012). The exposure scenarios used in this study are: high dose scenario with 44 μg/kg/BW thrice in a day (TID) oral dose and 20 μg/kg/BW single dermal exposure and, low dose scenario with 20 μg/kg/BW (TID) thrice in a day (TID) oral dose and 9 μg/kg/BW single dermal exposure. A similar exposure dose was previously estimated by Mielke et al. (2011). However, in this study, the estimated dose is lower, given the fact that single oral dose was equally divided into three doses and lag time for dermal dose was included. The simulated results for mother and fetus plasma concentration for two exposure scenario showing median, mean, high and low value for each gestational week were presented in Figs. 4 and 5. Most of the biomonitoring observed data are within the simulated results represented in Fig. 8. Limited data availability for each gestational week is one of the limitations of the model validation. However, in some cases, fetus plasma of BPA was much higher (Fig. 4), which might be explained by gender difference observed previously (Schönfelder et al., 2002), which was not included in the present model. Considering the mean value for each simulated week shown in Figs. 4 and 5, fetus BPA mean concentration value is higher than the BPA in mother plasma, which could be explained by the fact that the elimination process in the fetus is not so effective and solely depends on diffusion of chemical back to mother plasma via placenta or to amniotic fluid. Additionally, the model predicted the Cmax and Cmin relatively higher value for the mother plasma than the fetus plasma concentration.

Detailed biomonitoring sample of liver and placenta during 11 to 20 weeks of gestational has been reported (Zhang et al., 2011). It was observed that after the 17th week of gestational, free BPA concentration starts to decrease and appearance of BPAG in the liver, showing the development of the metabolic capacity of the fetus at this stage. To mimic this condition, metabolic activity in fetus liver and placenta was introduced at 17th gestational week. The simulated results for both fetus liver and placenta during mid-gestational were compared with the biomonitoring study of Zhang et al. (2011) (Fig. 6). However, some observed data points were below the range of predicted value. An increase in metabolic capacity was observed with the increase in liver weight during the gestational development, which could explain the result of decreasing free BPA concentration.

The recent biomonitoring data by Aris (2014) showed that BPA exposure to the fetus during the mid- gestational is very high ranging from LOD to 229 nM. This biomonitoring data shows that mid-gestational is a very critical window of exposure to the fetus. The developed P-PBPK model has also shown the higher BPA value during mid-gestational weeks compared to near term or at delivery. The reason of relatively higher exposure

could be the fetus volume, which is very less at mid-gestational, and also the metabolic capacity, which is presumably active after the 18th week of gestational.

The pharmacokinetic differences for the fetus seem to be very dramatic as fetus metabolic capacity and organ physiology system are relatively immature at an early stage of fetal development. The faster chemical metabolism and elimination of the BPA by the maternal system ameliorate BPA kinetics in the fetus to a great degree. However, evidence of finding higher free BPA (Ikezuki et al., 2002; Schönfelder et al., 2002; Aris, 2014) in cord blood as compared to maternal blood in various populations indicates higher fetal exposure and sensitivity to BPA due to pharmacokinetic factors.

The simulation of the model for BPA concentration in amniotic fluid during mid-gestation (Fig. 7) to near term showed the increasing concentration of the BPA with an increase in the gestational period. The BPA concentration increased until mid-gestational and then slowly started to decrease reaching to almost one and a half fold less than the observed mother plasma concentration. The predicted results are in agreement with observed data of Ikezuki et al. (2002), and have a linear relation with gestational time (less fluctuation in BPA concentration) suggesting amniotic fluid BPA concentration as a good biomarker for identifying the critical window of exposure to the fetus. The prediction of the concentration of free BPA in amniotic fluid was slightly less than reported biomonitoring data observed in late gestational. This could be due to the prediction of slightly high amniotic fluid volume than normally observed in the late gestational period. Factors such as local deconjugation in placenta, the lipophilicity of chemical, relatively higher deconjugation than conjugation in the fetal compartment can affect the propensity for chemicals to reach a higher concentration in the fetal compartment (Nachman et al., 2014).

The developed P-PBPK model is in concordance with biomonitoring data and showed that BPA readily transferred to fetal serum and amniotic fluid after mother's exposure. Even, fast metabolism and rapid excretion of BPA and BPA-C are unable to prevent the BPA fetal exposure. The transfer rates of BPA from the placenta to the fetal compartment varied considerably. Deconjugation in placenta and fetus body is of major concern at early fetal life, where metabolism capacity is low, causing an increased level of unconjugated BPA in the fetus. Importantly, free BPA in the fetal compartment are more in steady state and persists even as the maternal level of BPA declines. The consideration of mechanistic approach such as dynamic growth parameters and their governing equations, and model structure could be useful for the development of P-PBPK model for different chemicals.

5. Conclusion

The present study proposed and prospectively developed a P-PBPK model for BPA that describes and predicts the fetus blood and tissues concentrations time profiles based on the mother's exposure scenario. Detail metabolic toxicokinetics in mother and fetus was reviewed and included in the proposed model. Glucuronidation and deglucuronidation in both mother and fetus liver and placenta are found to be an important mechanism that alters BPA toxicokinetic profile. For the development of the model, a two-stage approach was employed: first the development and validation of the adult PBPK model against the kinetic data from control human experimental study and second extension of the adult model to the P-PBPK model and further evaluation with the available BPA biomonitoring

cohort studies. The prediction of higher concentration of BPA during the mid-gestational period in the amniotic fluid, placenta, and the fetus liver are in accordance with biomonitoring data, indicating mid-gestational period might be the critical window of exposure for the fetus. Due to the fast absorption and short half-life of BPA, it is showing extreme concentration variability with respect to time, which makes the task of prediction of biomonitoring data very difficult. This study considered two extreme dose scenarios (min-max) for the simulation and in turn plotting of simulated data under the box plot to capture all the data set that allows comparing with biomonitoring data. It has an assumption that biomonitoring sample can be from any time point. However, in order to address the issue of temporal variation of short life chemical, there is a need to have very control case studies dealing with the timing of exposure (food intake) and schedule of sampling. In this study, there are several data gaps identified, which need to be addressed to improve the model. For example, kinetics of BPA glucuronidation/sulfation and deglucoronidation/desulfation at the fetus level, and placental BPA conjugation and deconjugation, and metabolic variation due to functional polymorphism among the different population, are some of the major concern.

Acknowledgement

Preparation of this manuscript was supported in part for European Union's projects, HEALS (Health and Environment-wide Associations via Large population Surveys) by the FP7 Programme under grant agreement no. 603946 and EuroMix (European Test and Risk Assessment Strategies for Mixtures) by the Horizon 2020 Framework Programme under grant agreement no. 633172. Raju Prasad Sharma has received a doctoral fellowship from Universitat Rovira i Virgili under Martí-Franquès Research Grants Programme. This publication reflects only the authors' views. The Community and other funding organizations are not liable for any use made of the information contained therein.

References

Abduljalil, K., Furness, P., Johnson, T.N., Rostami-Hodjegan, A., Soltani, H., 2012. Anatomical, Physiological and Metabolic Changes with Gestational Age during Normal Pregnancy. Clin. Pharmacokinet. 51, 365–396. doi:10.2165/11597440-000000000-00000

Aris, A., 2014. Estimation of bisphenol A (BPA) concentrations in pregnant women, fetuses and nonpregnant women in Eastern Townships of Canada. Reprod. Toxicol. 45, 8–13. doi:10.1016/j.reprotox.2013.12.006

Beach, L., Adminisrration, V., Hospital, L.K., Angeles, L., 1978. Reduced Hepatic Bilirubin Uridine Diphosphate Glucuronyl Transferase and Uridine Diphosphate Glucose Dehydrogenase Activity in the Human Fetus. Pediat. Res. 12, 838–840.

Biedermann, S., Tschudin, P., Grob, K., 2010. Transfer of bisphenol A from thermal printer paper to the skin. Anal. Bioanal. Chem. 398, 571–576. doi:10.1007/s00216-010-3936-9

Borrirukwisitsak, S., Keenan, H.E., Gauchotte-lindsay, C., 2012. Effects of Salinity , pH and Temperature on the Octanol-Water Partition Coefficient of Bisphenol A. Int. J. Environ. Sci. Dev. 3, 460–464.

Chapter 3

Brown, R.P., Delp, M.D., Lindstedt, S.L., Rhomberg, L.R., Beliles, R.P., 1997. Physiological parameter values for physiologically based pharmacokinetic models. Toxicol. Ind. Health 13, 407–484.

Cabaton, N.J., Canlet, C., Wadia, P.R., Tremblay-Franco, M., Gautier, R., Molina, J., Sonnenschein, C., Cravedi, J.P., Rubin, B.S., Soto, A.M., Zalko, D., 2013. Effects of low doses of bisphenol a on the metabolome of perinatally exposed CD-1 mice. Environ. Health Perspect. 121, 586–593. doi:10.1289/ehp.1205588

Calafat, A.M., Kuklenyik, Z., Reidy, J.A., Caudill, S.P., Ekong, J., Needham, L.L., 2005. Urinary concentrations of bisphenol A and 4-Nonylphenol in a human reference population. Environ. Health Perspect. 113, 391–395. doi:10.1289/ehp.7534

Cao, X.L., Zhang, J., Goodyer, C.G., Hayward, S., Cooke, G.M., Curran, I.H.A., 2012. Bisphenol A in human placental and fetal liver tissues collected from Greater Montreal area (Quebec) during 1998-2008. Chemosphere 89, 505–511. doi:10.1016/j.chemosphere.2012.05.003

Cappiello, M., Giuliani, L., Ranee, A., Pacificr, G.M., 2000. Uridine 5 '-Diphosphoglucuronic acid (UDPGLcUA) in the human fetal liver , kidney and placenta. Eur. J. Drug Metab. Pharmacokinet. 25, 161–163.

Clewell, H.J., Gearhart, J.M., Gentry, P.R., Covington, T.R., VanLandingham, C.B., Crump, K.S., Shipp, A.M., 1999. Evaluation of the uncertainty in an oral reference dose for methylmercury due to interindividual variability in pharmacokinetics. Risk Anal. 19, 547–558. doi:10.1023/A:1007017116171

Clewell, R.A., Clewell, H.J., 2008. Development and specification of physiologically based pharmacokinetic models for use in risk assessment. Regul. Toxicol. Pharmacol. 50, 129–43. doi:10.1016/j.yrtph.2007.10.012

Corbel, T., Perdu, E., Gayrard, V., Puel, S., Lacroix, M.Z., Viguié, C., Toutain, P.L., Zalko, D., Picard-Hagen, N., 2015. Conjugation and deconjugation reactions within the fetoplacental compartment in a sheep model: A key factor determining bisphenol a fetal exposure. Drug Metab. Dispos. 43, 467–476. doi:10.1124/dmd.114.061291

Corley, R. a, Mast, T.J., Carney, E.W., Rogers, J.M., Daston, G.P., 2003. Evaluation of physiologically based models of pregnancy and lactation for their application in children's health risk assessments. Crit. Rev. Toxicol. 33, 137–211. doi:10.1080/713611035

Coughlin, J.L., Thomas, P.E., Buckley, B., 2012. Inhibition of genistein glucuronidation by bisphenol A in human and rat liver microsomes. Drug Metab. Dispos. 40, 481–485. doi:10.1124/dmd.111.042366

Coughtrie, M.W., Burchell, B., Leakey, J.E., Hume, R., 1988. The inadequacy of perinatal glucuronidation: immunoblot analysis of the developmental expression of individual UDP-glucuronosyltransferase isoenzymes in rat and human liver microsomes. Mol. Pharmacol. 34, 729–735.

Chapter 3

Csanády, G., Oberste-Frielinghaus, H., Semder, B., Baur, C., Schneider, K., Filser, J., 2002. Distribution and unspecific protein binding of the xenoestrogens bisphenol A and daidzein. Arch. Toxicol. 76, 299–305. doi:10.1007/s00204-002-0339-5

Cubitt, H.E., Houston, J.B., Galetin, A., 2009. Relative Importance of Intestinal and Hepatic Glucuronidation-Impact on the Prediction of Drug Clearance. Pharm. Res. 26, 1073–1083. doi:10.1007/s11095-008-9823-9

Davies, B., Morris, T., 1993. Physiological parameters in laboratory animals and humans. Pharm. Res. doi:10.1023/A:1018943613122

Divakaran, K., Hines, R.N., McCarver, D.G., 2014. Human hepatic UGT2B15 developmental expression. Toxicol. Sci. 141, 292–299. doi:10.1093/toxsci/kfu126

Doerge, D.R., Twaddle, N.C., Vanlandingham, M., Brown, R.P., Fisher, J.W., 2011. Distribution of bisphenol A into tissues of adult, neonatal, and fetal Sprague–Dawley rats. Toxicol. Appl. Pharmacol. 255, 261–270. doi:10.1016/j.taap.2011.07.009

Domoradzki, J.Y., Pottenger, L.H., Thornton, C.M., Hansen, S.C., Card, T.L., Markham, D.A., Dryzga, M.D., Shiotsuka, R.N., Waechter, J.M., 2003. Metabolism and pharmacokinetics of bisphenol A (BPA) and the embryo-fetal distribution of BPA and BPA-monoglucuronide in CD Sprague-Dawley rats at three gestational stages. Toxicol. Sci. 76, 21–34. doi:10.1093/toxsci/kfg206

Edginton, A.N., Ritter, L., 2009. Predicting plasma concentrations of bisphenol A in children younger than 2 years of age after typical feeding schedules, using a physiologically based toxicokinetic model. Environ. Health Perspect. 117, 645–652. doi:10.1289/ehp.0800073

Edlow, A.G., Chen, M., Smith, N.A., Lu, C., McElrath, T.F., 2012. Fetal bisphenol A exposure: Concentration of conjugated and unconjugated bisphenol A in amniotic fluid in the second and third trimesters. Reprod. Toxicol. 34, 1–7. doi:10.1016/j.reprotox.2012.03.009

EFSA, 2015. Scientific Opinion on the risks to public health related to the presence of bisphenol A (BPA) in foodstuffs: Executive summary. EFSA J. 13, 4002. doi:10.2903/j.efsa.2015.4002

Elsby, R., Maggs, J.L., Ashby, J., Park, B.K., 2001. Comparison of the modulatory effects of human and rat liver microsomal metabolism on the estrogenicity of bisphenol A: implications for extrapolation to humans. J. Pharmacol. Exp. Ther. 297, 103–113.

EU, 2003. European Union, Risk Assessment Report on 4,4'-isopropylidenediphenol (bisphenol- A). Eur. Chem. Bur. 302.

Fetus, A.N.A., Sampling, W.S., Villus, C., Fluid, A., 1993. β-glucuronidase deficiency : identification of an affected fetus with simultaneous sampling of chorionic villus and amniotic fluid. Prenat. Diagn. 13, 429–433.

Chapter 3

Fisher, J.W., Twaddle, N.C., Vanlandingham, M., Doerge, D.R., 2011. Pharmacokinetic modeling: Prediction and evaluation of route dependent dosimetry of bisphenol A in monkeys with extrapolation to humans. Toxicol. Appl. Pharmacol. 257, 122–136. doi:10.1016/j.taap.2011.08.026

Gentry, P.R., Covington, T.R., Andersen, M.E., Clewell, H.J., 2002. Application of a physiologically based pharmacokinetic model for isopropanol in the derivation of a reference dose and reference concentration. Regul. Toxicol. Pharmacol. 36, 51–68. doi:S0273230002915400 [pii]

Gentry, P.R., Covington, T.R., Clewell, H.J., 2003. Evaluation of the potential impact of pharmacokinetic differences on tissue dosimetry in offspring during pregnancy and lactation. Regul. Toxicol. Pharmacol. 38, 1–16. doi:10.1016/S0273-2300(03)00047-3

Gerona, R.R., Woodruff, T.J., Dickenson, C.A., Pan, J., Jackie, M., Sen, S., Friesen, M.M., Fujimoto, V.Y., Hunt, P.A., 2014. California population 47. doi:10.1021/es402764d.Bisphenol-A

Ginsberg, G., Rice, D.C., 2009. Does rapid metabolism ensure negligible risk from bisphenol A? Environ. Health Perspect. 117, 1639–1643. doi:10.1289/ehp.0901010

Gundert-Remy, U., Mielke, H., Bernauer, U., 2013. Commentary: Dermal penetration of bisphenol A-Consequences for risk assessment. Toxicol. Lett. 217, 159–161. doi:10.1016/j.toxlet.2012.12.009

Hanioka, N., Naito, T., Narimatsu, S., 2008. Human UDP-glucuronosyltransferase isoforms involved in bisphenol A glucuronidation. Chemosphere 74, 33–36. doi:10.1016/j.chemosphere.2008.09.053

Hanioka, N., Oka, H., Nagaoka, K., Ikushiro, S., Narimatsu, S., 2011. Effect of UDP-glucuronosyltransferase 2B15 polymorphism on bisphenol A glucuronidation. Arch. Toxicol. 85, 1373–1381. doi:10.1007/s00204-011-0690-5

ICRP, 2002. Basic anatomical and physiological data for use in radiological protection: reference values. Ann. ICRP 32, 1–277. doi:10.1016/S0146-6453(03)00002-2

Ikezuki, Y., Tsutsumi, O., Takai, Y., Kamei, Y., Taketani, Y., 2002. Determination of bisphenol A concentrations in human biological fluids reveals significant early prenatal exposure. Hum. Reprod. 17, 2839–2841. doi:10.1093/humrep/17.11.2839

Kaddar, N., Harthé, C., Déchaud, H., Mappus, E., Pugeat, M., 2008. Cutaneous penetration of bisphenol A in pig skin. J. Toxicol. Environ. Health. A 71, 471–3. doi:10.1080/15287390801906824

Kawade, N., Onishi, S., 1981. The prenatal and postnatal development of UDP-glucuronyltransferase activity towards bilirubin and the effect of premature birth on this activity in the human liver. Biochem. J. 196, 257–60.

Kawamoto, Y., Matsuyama, W., Wada, M., Hishikawa, J., Chan, M.P.L., Nakayama, A., Morisawa, S., 2007. Development of a physiologically based pharmacokinetic model for

Chapter 3

bisphenol A in pregnant mice. Toxicol. Appl. Pharmacol. 224, 182–191. doi:10.1016/j.taap.2007.06.023

Kim, Y.H., Kim, C.S., Park, S., Han, S.Y., Pyo, M.Y., Yang, M., 2003. Gender differences in the levels of bisphenol A metabolites in urine. Biochem. Biophys. Res. Commun. 312, 441–448. doi:10.1016/j.bbrc.2003.10.135

Kortejärvi, H., Urtti, A., Yliperttula, M., 2007. Pharmacokinetic simulation of biowaiver criteria: The effects of gastric emptying, dissolution, absorption and elimination rates. Eur. J. Pharm. Sci. 30, 155–166. doi:10.1016/j.ejps.2006.10.011

Kuester, R.K., Sipes, I.G., 2007. Prediction of Metabolic Clearance of Bisphenol A (4 ,4' -Dihydroxy- 2 , 2-diphenylpropane) using Cryopreserved Human Hepatocytes. Drug Metab. Dispos. 35, 1910–1915. doi:10.1124/dmd.107.014787.

Kurebayashi, H., Okudaira, K., Ohno, Y., 2010. Species difference of metabolic clearance of bisphenol A using cryopreserved hepatocytes from rats, monkeys and humans. Toxicol. Lett. 198, 210–215. doi:10.1016/j.toxlet.2010.06.017

Kuroda, N., Kinoshita, Y., Sun, Y., Wada, M., Kishikawa, N., Nakashima, K., Makino, T., Nakazawa, H., 2003. Measurement of bisphenol A levels in human blood serum and ascitic fluid by HPLC using a fluorescent labeling reagent. J. Pharm. Biomed. Anal. 30, 1743–1749. doi:10.1016/S0731-7085(02)00516-2

Kuruto-Niwa, R., Tateoka, Y., Usuki, Y., Nozawa, R., 2007. Measurement of bisphenol A concentrations in human colostrum. Chemosphere 66, 1160–1164. doi:10.1016/j.chemosphere.2006.06.073

Lassen, C., Mikkelsen, S.H., Brandt, U.K., Cowi, A.S., 2011. Migration of bisphenol A from cash register receipts and baby dummies. Surv. Chem. Consum. Prod. Danish Minist. Environ.

Lee, Y.J., Ryu, H.Y., Kim, H.K., Min, C.S., Lee, J.H., Kim, E., Nam, B.H., Park, J.H., Jung, J.Y., Jang, D.D., Park, E.Y., Lee, K.H., Ma, J.Y., Won, H.S., Im, M.W., Leem, J.H., Hong, Y.C., Yoon, H.S., 2008. Maternal and fetal exposure to bisphenol A in Korea. Reprod. Toxicol. 25, 413–419. doi:10.1016/j.reprotox.2008.05.058

Loccisano, A.E., Longnecker, M.P., Campbell, J.L., Andersen, M.E., Clewell, H.J., 2013. Development of Pbpk Models for PFOA and PFOS for Human Pregnancy and Lactation Life Stages. J. Toxicol. Environ. Heal. Part A 76, 25–57. doi:10.1080/15287394.2012.722523

Longnecker, M.P., Harbak, K., Kissling, G.E., Hoppin, J.A., Eggesbo, M., Jusko, T.A., Eide, J., Koch, H.M., 2013. The concentration of bisphenol A in urine is affected by specimen collection, a preservative, and handling. Environ. Res. 126, 211–214. doi:10.1016/j.envres.2013.07.002

Lorber, M., Angerer, J., Koch, H.M., 2010. A simple pharmacokinetic model to characterize exposure of Americans to Di-2-ethylhexyl phthalate. J. Expo. Sci. Environ. Epidemiol. 20, 38–53. doi:10.1038/jes.2008.74

Chapter 3

Lucier, W., Sonawane, B.R., 1977. Glucuronidation and deglucuronidation reactions in hepatic and extrahepatic tissues during perinatal development. Drug Metab. Dispos. 5, 279–287.

Martínez, M.A., Rovira, J., Sharma, R.P., Nadal, M., Schuhmacher, M., Kumar, V., 2017. Prenatal exposure estimation of BPA and DEHP using integrated external and internal dosimetry: A case study. Environ. Res. 158, 566–575. doi:10.1016/j.envres.2017.07.016

Matysek, P., 1980. β-Glucuronidase Activity in Amniotic Fluid. J. Clin. Chem. Clin. Biochem. 18, 611–614.

Mazur, C.S., Kenneke, J.F., Hess-Wilson, J.K., Lipscomb, J.C., 2010. Differences between human and rat intestinal and hepatic bisphenol a glucuronidation and the influence of alamethicin on in vitro kinetic measurements. Drug Metab. Dispos. 38, 2232–2238. doi:10.1124/dmd.110.034819

Mccance, R.A., Dean, R.F.A., Jones, P.E.H., 1949. The Glucuronide-synthesizing System in the Mouse and its Relationship to β-Glucuronidase. Biochem. J. 45, 496–499.

McLaughlin, B.E., Hutchinson, J.M., Graham, C.H., Smith, G.N., Marks, G.S., Nakatsu, K., Brien, J.F., 2000. Heme oxygenase activity in term human placenta. Placenta 21, 870–873. doi:10.1053/plac.2000.0574

Mendum, T., Stoler, E., VanBenschoten, H., Warner, J.C., 2011. Concentration of bisphenol A in thermal paper. Green Chem. Lett. Rev. 4, 81–86. doi:10.1080/17518253.2010.502908

Mielke, H., Gundert-Remy, U., 2012. Physiologically based toxicokinetic modelling as a tool to support risk assessment: Three case studies. J. Toxicol. 2012. doi:10.1155/2012/359471

Mielke, H., Gundert-Remy, U., 2009. Bisphenol A levels in blood depend on age and exposure. Toxicol. Lett. 190, 32–40. doi:10.1016/j.toxlet.2009.06.861

Mielke, H., Partosch, F., Gundert-Remy, U., 2011. The contribution of dermal exposure to the internal exposure of bisphenol A in man. Toxicol. Lett. 204, 190–198. doi:10.1016/j.toxlet.2011.04.032

Morck, T.J., Sorda, G., Bechi, N., Rasmussen, B.S., Nielsen, J.B., Ietta, F., Rytting, E., Mathiesen, L., Paulesu, L., Knudsen, L.E., 2010. Placental transport and in vitro effects of Bisphenol A. Reprod. Toxicol. 30, 131–137. doi:10.1016/j.reprotox.2010.02.007

Moriyama, K., Tagami, T., Akamizu, T., Usui, T., Saijo, M., Kanamoto, N., Hataya, Y., Shimatsu, A., Kuzuya, H., Nakao, K., 2002. Thyroid hormone action is disrupted by bisphenol A as an antagonist. J. Clin. Endocrinol. Metab. 87, 5185–5190. doi:10.1210/jc.2002-020209

Muna S. Nahar, Chunyang Liao, Kurunthachalam Kannan, and D.C.D., 2013. Fetal Liver Bisphenol A Concentrations and Biotransformation Gene Expression Reveal Variable

Chapter 3

Exposure and Altered Capacity for Metabolism in Humans. J. Biochem. Mol. Toxicol. 27, 116–123. doi:10.1002/jbt

Nachman, R.M., Hartle, J.C., Lees, P.S.J., Groopman, J.D., 2014. Early Life Metabolism of Bisphenol A: A Systematic Review of the Literature. Curr. Environ. Heal. reports 1, 90–100. doi:10.1007/s40572-013-0003-7

Nishikawa, M., Iwano, H., Yanagisawa, R., Koike, N., Inoue, H., Yokota, H., 2010. Placental transfer of conjugated bisphenol A and subsequent reactivation in the rat fetus. Environ. Health Perspect. 118, 1196–1203. doi:10.1289/ehp.0901575

O'Flaherty, E.J., Scott, W., Schreiner, C., Beliles, R.P., 1992. A physiologically based kinetic model of rat and mouse gestation: disposition of a weak acid. Toxicol. Appl. Pharmacol. 112, 245–56.

Palanza, P., Howdeshell, K.L., Parmigiani, S., vom Saal, F.S., 2002. Exposure to a low dose of bisphenol A during fetal life or in adulthood alters maternal behavior in mice. Environ. Health Perspect. 110, 415–422. doi:10.1289/ehp.02110s3415

Partosch, F., Mielke, H., Gundert-Remy, U., 2013. Functional UDP-glucuronyltransferase 2B15 polymorphism and bisphenol A concentrations in blood: Results from physiologically based kinetic modelling. Arch. Toxicol. 87, 1257–1264. doi:10.1007/s00204-013-1022-8

Patisaul, H.B., Todd, K.L., Mickens, J.A., Adewale, H.B., 2009. Impact of neonatal exposure to the ERα agonist PPT, bisphenol-A or phytoestrogens on hypothalamic kisspeptin fiber density in male and female rats. Neurotoxicology 30, 350–357. doi:10.1016/j.neuro.2009.02.010

Pelkonen, O., 1973. Drug metabolism in the human fetal liver. Relationship to fetal age. Arch. Int. Pharmacodyn. Ther. 202, 281—287.

Pelkonen, O., Kaltiala, E.H., Larmi, T.K.I., Karki, N.T., 1973. Comparison of activities of drug-metabolizing enzymes in human fetal and adult livers. Clin. Pharmacol. Ther. 14, 840–846.

Rey, R., Lukas-Croisier, C., Lasala, C., Bedecarrás, P., 2003. AMH/MIS: What we know already about the gene, the protein and its regulation. Mol. Cell. Endocrinol. 211, 21–31. doi:10.1016/j.mce.2003.09.007

Rubin, B.S., Soto, A.M., 2009. Bisphenol A: Perinatal exposure and body weight. Mol. Cell. Endocrinol. 304, 55–62. doi:10.1016/j.mce.2009.02.023

Schönfelder, G., Wittfoht, W., Hopp, H., Talsness, C.E., Paul, M., Chahoud, I., 2002. Parent bisphenol a accumulation in the human maternal-fetal-placental unit. Environ. Health Perspect. 110, 703–707. doi:10.1289/ehp.021100703

Sharma, R.P., Schuhmacher, M., Kumar, V., 2017. Review on crosstalk and common mechanisms of endocrine disruptors: Scaffolding to improve PBPK/PD model of EDC mixture. Environ. Int. 99, 1–14. doi:10.1016/j.envint.2016.09.016

Chapter 3

Shin, B.S., Kim, C.H., Jun, Y.S., Kim, D.H., Lee, B.M., Yoon, C.H., Park, E.H., Lee, K.C., Han, S.-Y., Park, K.L., Kim, H.S., Yoo, S.D., 2004. Physiologically Based Pharmacokinetics of Bisphenol a. J. Toxicol. Environ. Heal. Part A 67, 1971–1985. doi:10.1080/15287390490514615

Sisson, T.R., Lund, C.J., Whalen, L.E., Telek, A., 1959. The blood volume of infants. I. The full-term infant in the first year of life. J. Pediatr. 55, 163–79. doi:10.1016/S0022-3476(59)80084-6

Snijder, C.A., Heederik, D., Pierik, F.H., Hofman, A., Jaddoe, V.W., Koch, H.M., Longnecker, M.P., Burdorf, A., 2013. Fetal growth and prenatal exposure to bisphenol A: The generation R study. Environ. Health Perspect. 121, 393–396. doi:10.1289/ehp.1205296

Sperker, B., Backman, J.T., Kroemer, H.K., 1997a. The role of beta-glucuronidase in drug disposition and drug targeting in humans. Clin.Pharmacokinet. 33, 18–31.

Sperker, B., Mürdter, T.E., Schick, M., Eckhardt, K., Bosslet, K., Kroemer, H.K., 1997b. Interindividual variability in expression and activity of human beta-glucuronidase in liver and kidney: consequences for drug metabolism. J. Pharmacol. Exp. Ther. 281, 914–20.

Strassburg, C.P., Strassburg, a, Kneip, S., Barut, a, Tukey, R.H., Rodeck, B., Manns, M.P., 2002. Developmental aspects of human hepatic drug glucuronidation in young children and adults. Gut 50, 259–65. doi:10.1136/gut.50.2.259

Teeguarden, J.G., Twaddle, N.C., Churchwell, M.I., Doerge, D.R., 2016. Urine and serum biomonitoring of exposure to environmental estrogens I: Bisphenol A in pregnant women. Food Chem. Toxicol. 92, 129–142. doi:10.1016/j.fct.2016.03.023

Teeguarden, J.G., Twaddle, N.C., Churchwell, M.I., Yang, X., Fisher, J.W., Seryak, L.M., Doerge, D.R., 2015. 24-hour human urine and serum profiles of bisphenol A: Evidence against sublingual absorption following ingestion in soup. Toxicol. Appl. Pharmacol. 288, 131–142. doi:10.1016/j.taap.2015.01.009

Thayer, K.A., Doerge, D.R., Hunt, D., Schurman, S.H., Twaddle, N.C., Churchwell, M.I., Garantziotis, S., Kissling, G.E., Easterling, M.R., Bucher, J.R., Birnbaum, L.S., 2015. Pharmacokinetics of bisphenol A in humans following a single oral administration. Environ. Int. 83, 107–115. doi:10.1016/j.envint.2015.06.008

Trdan Lusin, T., Roskar, R., Mrhar, A., 2012. Evaluation of bisphenol A glucuronidation according to UGT1A1*28 polymorphism by a new LC-MS/MS assay. Toxicology 292, 33–41. doi:10.1016/j.tox.2011.11.015

Vafeiadi, M., Roumeliotaki, T., Myridakis, A., Chalkiadaki, G., Fthenou, E., Dermitzaki, E., Karachaliou, M., Sarri, K., Vassilaki, M., Stephanou, E.G., Kogevinas, M., Chatzi, L., 2016. Association of early life exposure to bisphenol A with obesity and cardiometabolic traits in childhood. Environ. Res. 146, 379–387. doi:10.1016/j.envres.2016.01.017

Vandenberg, L.N., Chahoud, I., Heindel, J.J., Padmanabhan, V., Paumgartten, F.J.R., Schoenfelder, G., 2010. Urinary, circulating, and tissue biomonitoring studies indicate

Chapter 3

widespread exposure to bisphenol A. Environ. Health Perspect. 118, 1055–1070. doi:10.1289/ehp.0901716

VandeVoort, C.A., Gerona, R.R., vom Saal, F.S., Tarantal, A.F., Hunt, P.A., Hillenweck, A., Zalko, D., 2016. Maternal and Fetal Pharmacokinetics of Oral Radiolabeled and Authentic Bisphenol A in the Rhesus Monkey. PLoS One 11, e0165410. doi:10.1371/journal.pone.0165410

Völkel, W., Bittner, N., Dekant, W., 2005. Quantitation of Bisphenol a and Bisphenol a Glucuronide in Biological Samples By High Performance Liquid Chromatography-Tandem Mass Abstract : Drug Metab Dispos 33, 1748–1757. doi:10.1124/dmd.105.005454.unintentionally

Völkel, W., Colnot, T., Csanády, G.A., Filser, J.G., Dekant, W., 2002. Metabolism and kinetics of bisphenol a in humans at low doses following oral administration. Chem. Res. Toxicol. 15, 1281–1287. doi:10.1021/tx025548t

Wang, J., Sun, B., Hou, M., Pan, X., Li, X., 2012. The environmental obesogen bisphenol A promotes adipogenesis by increasing the amount of 11β-hydroxysteroid dehydrogenase type 1 in the adipose tissue of children. Int. J. Obes. 999–1005. doi:10.1038/ijo.2012.173

WHO, F. and A.O. of the U.N., 2010. Toxicological and Health Aspects of Bisphenol A. World Heal. Organ. 60.

Xi, W., Lee, C.K.F., Yeung, W.S.B., Giesy, J.P., Wong, M.H., Zhang, X., Hecker, M., Wong, C.K.C., 2011. Effect of perinatal and postnatal bisphenol A exposure to the regulatory circuits at the hypothalamus-pituitary-gonadal axis of CD-1 mice. Reprod. Toxicol. 31, 409–417. doi:10.1016/j.reprotox.2010.12.002

Yang, X., Doerge, D.R., Fisher, J.W., 2013. Prediction and evaluation of route dependent dosimetry of BPA in rats at different life stages using a physiologically based pharmacokinetic model. Toxicol. Appl. Pharmacol. 270, 45–59. doi:10.1016/j.taap.2013.03.022

Yang, X., Doerge, D.R., Teeguarden, J.G., Fisher, J.W., 2015. Development of a physiologically based pharmacokinetic model for assessment of human exposure to bisphenol A. Toxicol. Appl. Pharmacol. 289, 442–456. doi:10.1016/j.taap.2015.10.016

Yang, X., Fisher, J.W., 2015. Unraveling bisphenol A pharmacokinetics using physiologically based pharmacokinetic modeling. Front. Pharmacol. 6, 1–7. doi:10.3389/fphar.2015.00292

Ye, X., Zhou, X., Hennings, R., Kramer, J., Calafat, A.M., 2013. Potential External Contamination with Bisphenol A and Other Ubiquitous Organic Environmental Chemicals during Biomonitoring Analysis: An Elusive Laboratory Challenge. Environ. Health Perspect. 121, 283–286. doi:10.1289/ehp.1206093

Yoon, M., Efremenko, A., Blaauboer, B.J., Clewell, H.J., 2014. Evaluation of simple in vitro to in vivo extrapolation approaches for environmental compounds. Toxicol. Vitr. 28, 164–170. doi:10.1016/j.tiv.2013.10.023

Chapter 3

Zalko, D., Jacques, C., Duplan, H., Bruel, S., Perdu, E., 2011a. Viable skin efficiently absorbs and metabolizes bisphenol A. Chemosphere 82, 424–430. doi:10.1016/j.chemosphere.2010.09.058

Zalko, D., Jacques, C., Duplan, H., Bruel, S., Perdu, E., 2011b. Viable skin efficiently absorbs and metabolizes bisphenol A. Chemosphere 82, 424–430. doi:10.1016/j.chemosphere.2010.09.058

Zhang, J., Cooke, G.M., Curran, I.H.A., Goodyer, C.G., Cao, X.L., 2011. GC-MS analysis of bisphenol A in human placental and fetal liver samples. J. Chromatogr. B Anal. Technol. Biomed. Life Sci. 879, 209–214. doi:10.1016/j.jchromb.2010.11.031

Zhang, T., Sun, H., Kannan, K., 2013. Blood and urinary bisphenol a concentrations in children, adults, and pregnant women from China: Partitioning between blood and urine and maternal and fetal cord blood. Environ. Sci. Technol. 47, 4686–4694. doi:10.1021/es303808b

Chapter 4

Dynamic networks of oxidative stress: From disease maps to design principles suggesting personalised therapies for Parkinson's disease

Alexey Kolodkin, Raju Prasad Sharma,Vikas Kumar, Andrew Ignatenko, Nathan Brady, Evangelos Simeonidis, Danyel Jennen, Jacco J. Briede, Matteo Barberis, Thierry D.G.A. Mondeel, Nilgun Sahin, Stephan Gebel, Lilia Alberghina, Anna Maria Colangelo, Bernhard Peters, Alex Skupin,Rudi Balling, Hans V. Westerhoff

Chapter 4

Dynamic networks of oxidative stress: From disease maps to design principles suggesting personalised therapies for Parkinson's disease

Abstract

The regulatory network protecting the cell against oxidative stress is eminently complex. It surfaces in several disease maps, including that of Parkinson's disease (PD). How this molecular networking achieves its various functionalities was hitherto ununderstood. How a network of processes operating at the seconds-minutes time scale may cause a disease at the century time scale was likewise enigmatic.

By computational analysis, we disentangle the reactive oxygen species (ROS) regulatory network into a hierarchy of subnetworks and show that each corresponds to a different functionality. In parallel with achieving an understanding of the design principles of the network we thereby obtained a detailed dynamic model of ROS management. This model could fit two independent data sets from in vitro experiments performed in two different laboratories, at University Milano-Bicocca (Italy) and Maastricht University (the Netherlands).

The resulting detailed model shows effective ROS-management for a prolonged time, followed by a sudden system's collapse due to the loss of p62 protein required for mitophagy. Parkinson's disease (PD) related conditions, e.g. lack of DJ-1 protein (encoded by Park7) or increased concentration of alfa-synuclein accelerated the system's collapse under oxidative stress. Analysing in silico various hypothetical interventions (e.g. addition of antioxidants or activation of Nrf2 signalling system by caffeine uptake) that may slow down the collapse of the system under oxidative stress, we show how recognition of the network's design principles may help design personalised PD therapies.

Keywords:

Systems biology/dynamic modelling/oxidative stress/reactive oxygen species/Parkinson's disease

Chapter 4

1. Introduction

Reactive Oxygen Species (ROS) are chemically reactive small molecules containing oxygen, such as superoxide anion, peroxides, hydroxyl radicals and singlet oxygen, generated in various intracellular processes: they may be (i) produced in the cytoplasm from redox reactions such as the Fenton reaction (1), (ii) released from the Endoplasmic Reticulum (2), (iii) formed from reactive nitrogen species (3) and, more commonly, (iv) generated when electrons escape from the Electron Transport Chain (ETC). Around 0.1-2% of ETC electrons escape and form active radicals by single electron reduction (4).

ROS play three main roles: (i) "killing" in the immune response (5), (ii) signalling in cell differentiation (6-12) and proliferation (13), and also (iii) damaging components leading to cell death (1). Indeed, oxygen radicals damage DNA and this leads to mutations. They also oxidise various organic molecules including mitochondrial lipids, which leads to mitochondrial dysfunction and initiates a positive feedback loop leading to the propagation if not amplification of the active radicals.

Excessive ROS may be removed enzymatically, e.g. by superoxide dismutase (14), or scavenged by various antioxidants (15). Should these processes fail, the removal of damaged mitochondria may be initiated (16-18). The latter is called mitoptosis as it averts cell death (19-23). Alternatively, damaged mitochondria may be recycled into undamaged mitochondria via mitochondria-derived vesicles (MDVs). All these processes appear to be coordinated by an ROS-induced signalling network, with rather complicated cross-talk mechanisms (24-26).

More than the topology of a network such as that around ROS, it is its dynamic response to perturbations that determines the fitness of organisms and their cellular constituents. This response is determined by a sequel of nonlinear interactions producing the functionality that is absent from the components. Disease then corresponds to failure of the network to produce that functionality and this failure can be produced by various combinations of component failures (see also Westerhoff and Alberghina book, Barabasi, 2012).

Mistuning of ROS management has been implicated in many diseases, including diabetes (27, 28), cancer (29) and neurodegenerative diseases (25, 26, 30). This is reflected in the recurrence of ROS management in several disease maps. Any such disease map is based on extensive literature data mining and thorough curation by many experts. It summarizes the substantial efforts of the scientific community at large with respect to the disease. The map of Parkinson's disease (PD) may serve as an example (Fujita et al, 2014).

A network module through which many diseases overlap has been called a disease module (Barabasi, 2012). The ROS management network may constitute an example of such a disease module. Since a disease module is a dynamic network itself (44), it may be difficult to identify a single trigger and a unique scenario of its malfunction. Understanding the emergence of diseased behaviour in a disease module may be beyond the capacity of the naked human brain (45, 46): nonlinear interactions require more information for their specification than linear interactions do, the networks tend to consist of many components, and it is hard to foresee what comes from nonlinear interactions. Systems biology suggests a solution to this problem – to reconstruct the biological

Chapter 4

behaviour in an in silico replica of the system. Biological emergence (47, 48) may be reconstructed by translating the information about how components communicate into mathematical equations (45, 49, 50). By integrating the resulting system of mathematical equations in a computer, one should be able to simulate the biological system's behaviour. Whilst we hereby delegate our understanding of the system to the computer model, we may subsequently analyse the mathematical model and identify 'design principles' of the system. The robustness of the operation of these design principles to perturbations associated with disease may then also be calculated and this may be used for computational medicine. The present paper implements this approach with the aim of understanding the complexity of ROS management in the context of Parkinson's disease (PD).

Parkinson's disease is the second (after Alzheimer's disease) most prevalent neurodegenerative disorder, affecting 1-3% of the population over 65 years old. PD is characterized by symptomatic motor disorders related to lack of dopamine secretion by dopaminergic neurons (31). PD is associated with diverse genetic and environmental factors. On a growing list of recessive PD-related mutations (32), mutations in alfa-synuclein (33), ubiquitin E3 ligase Parkin (34) and in Park 7 (DJ-1) (35) are prominent. With respect to environment and nutrition, there is a positive correlation between PD risk and exposure to pesticides (36), and a negative correlation between PD and increased coffee consumption (37-40). On the anatomical level, the disease may be attributed to processes inside the dopaminergic neurons in the substantia nigra, to disruptions of inter-cellular communication between neuronal and glial cells, to inflammation, or even to the pathogenic spread of unfolded alfa-synuclein or tau proteins between cells (41, 42).

On the molecular level, the plethora of above mentioned factors associated with PD may converge to three main mechanisms underlying the lack of dopamine secretion: (i) a lack of substrates required to produce dopamine, e.g. lack of tyrosine in the case of parkinsonism in phenylketonuria (43), (ii) lack of ATP required to secrete dopamine and to maintain neuron functionality, which leads to shrinking and ultimately to neuron degeneration,(iii) an excess of ROS leading to mitochondrial damage, cytochrome c (CytC) release and apoptotic death of dopaminergic neurons. These three mechanisms may interlink in the ROS management disease module in a highly non-linear manner and network perturbations that correspond to disease may be triggered by various events. For example, such a perturbation may start with mitochondrial malfunctioning, when, due to genetic predisposition and/or a certain constellation of environmental factors, mitochondria start producing more ROS. In the absence of a negative genetic predisposition, mitochondria would be healthy initially, but excessive ROS may be a by-product of pesticides detoxification. In either case, the increase of ROS generation would damage mitochondria further, thereby initiating a positive feed-back loop resulting in a further increase in this ROS production. Although the resulting oxidative stress would happen throughout the entire organism, dopaminergic neurons should suffer most, because, compared with other cells, they need more energy to secrete dopamine and maintain a higher level of oxidative phosphorylation, hence a higher activity of the ETC. In such cases it should be very hard to distinguish between cause and effect since the increased level of ROS could be both the triggering event and the consequence of many other events.

Chapter 4

Yet one of the usual aims of Medicine is to establish 'the cause' of disease and to then remove that cause. Approaches such as GWAS have met with limited success. If single reproducible causes of the same network disease do not exist, how then should one go about identifying the 'network causes' that should be more robustly related to the disease? And how should one then approach the therapy of network diseases, i.e. how should one with, mostly molecular drugs, expect to redress the faltering network back to fulfilling its physiological functions properly? And, would it then become possible to integrate pharmaceutical, nutritional and life-style therapies in a more rational way than has hitherto been possible?

We will here approach these three challenges. We will first construct a core model of ROS management. We will then increase the complexity of this model by adding new details step-by-step. After each new step, we will use computational analysis to identify the ROS-management design principles arising with the complexification of the system in that step. We will hereby find a hierarchy of design principles, corresponding to a hierarchy of modes of operation of the ROS network. This hierarchy enables the network to carry out its functions and is violated in disease. We will discuss the results in the context of PD personalised medicine and the three above challenges.

2. Methods

Model diagrams (e.g. Figures 2(a-h)) were generated using CellDesigner (v4.0.1; Systems Biology Institute, http://celldesigner.org/index.html), a graphical front-end for creating process diagrams of biochemical networks in systems Biology Markup Language (28).

CellDesigner-generated models were transferred to COPASI (v4.6, build 32) (www.copasi.org), which is another Systems Biology Markup Language-compliant programme, but with a wider variety of analysis options. For each reaction, a kinetic term can be included, detailing the mathematics underlying the interaction between the species (e.g. the description of ROS detailed model equations in Annex 4). A number of the parameter values used within the model were fitted to the known biological behaviour of the system, while maintaining these parameters within previously determined biologically realistic bounds.

3. Results

ROS-induced mitochondrial aging. Mitophagy helps protect mitochondria by providing stability (design principle 1, Model 1)

Our proposed core (design principle 1A, model 1A) of the ROS network consists of healthy mitochondria, damaged mitochondria, and ROS. In this model, the concentration of healthy mitochondria is fixed, and damaged mitochondria are produced in a ROS dependent reaction (denoted by 're1'). Damaged mitochondria catalyse ROS generation (re2) and this additional ROS damages healthy mitochondria further, forming a positive feedback loop. The higher is the concentration of ROS, the higher is the mitochondrial damage and the higher will be ROS generation (Figure 1A). Our model allows two interpretations of what "healthy" and what "damaged" mitochondria mean: (i) the fraction of healthy and damaged mitochondria respectively in the total mitochondria pool, or (ii) the degree of damage in every mitochondrion assuming the population is homogeneous.

Chapter 4

If indeed all mitochondria are interconnected and undergo continuous fusion and fission and constitute one big mitochondrion, both interpretations converge.

On the basis of this network structure, we built a dynamic model 1A (model_1A). This model produced an explosion of both ROS and damaged mitochondria (Comparisons of models 1A-1C, Figure 1A).

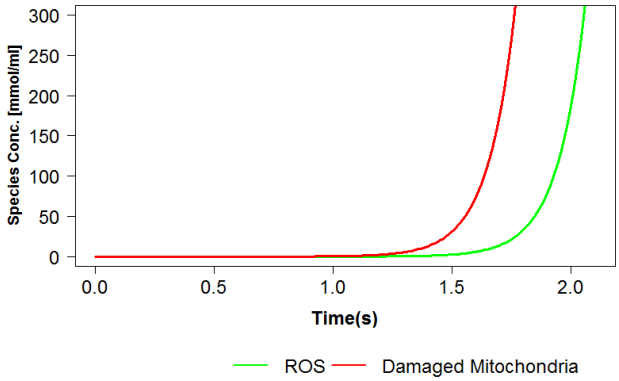

Fig 1A. Concentration of ROS and damaged mitochondria in model 1A.

For simulation model 1A was used. Simulations strarts with initial conditions where the concentration of ROS was equal to 1 x 10^{-5} and the concentration of damaged mitochondria was eqal to 1 x 10^{-5}. Time courses for ROS and Damaged Mitochondria were simulated. No steady state was observed. The concentration of both ROS and Damaged Mitochondria exponentially explodes.

Paradoxically, the incorporation of both a so-called antioxidant response that removed ROS (re3), and of mitophagy, which removed damaged mitochondria with the help of p62 (re4) (see design 1B, model_1B) did not eliminate the compromised stability associated with this explosion (Compare models 1A-1C): A steady state was found only for a very precise balance between the rate at which the damaged mitochondria were removed (Figure 1B).

Chapter 4

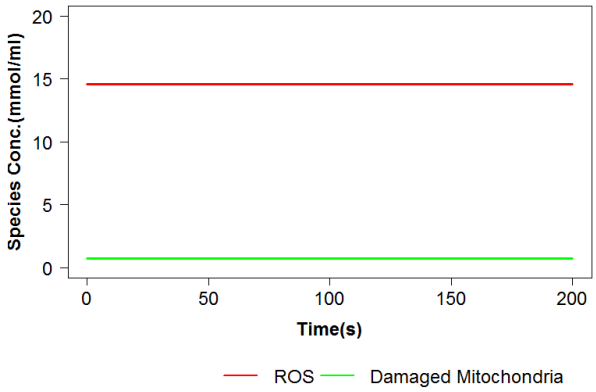

Fig 1B: Concentration of ROS and damaged mitochondria in model 1B
For a very precise balance rate of mitophagy a steady state was achived for both ROS and damaged mitochondria.

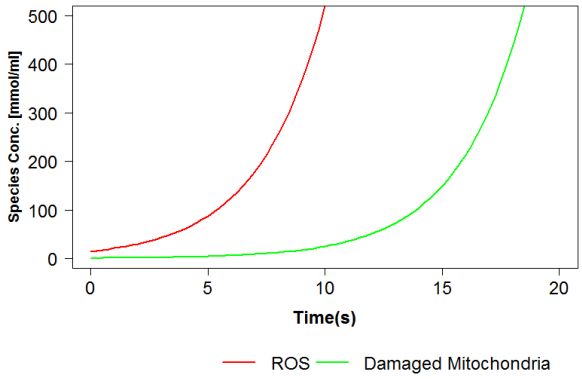

Fig 1B.1: Concentration of ROS and damaged mitochondria in model 1B

For simulation model 1B was used. The concentration of both ROS and damaged mitochondria exponentially explodes, upon 10 percent increase in ROS generation rate

On the other hand, with a rate of ROS generation only slightly below the balancing rate, the concentration of damaged mitochondria would drop to 0 (Figure 1B.2, Model 1B-ROS synt decreased 10%.cps):

Chapter 4

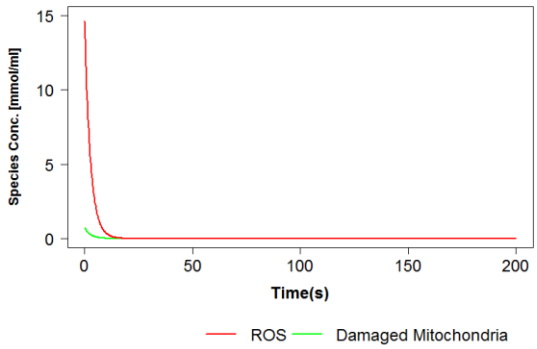

Fig 1B.2: Concentration of ROS and damaged mitochondria in model 1B
The concentration of both ROS and damaged mitochondria goes to zero, upon 10 percent decrease in ROS generation rate.

Moreover, when exposed to a sudden injection of ROS, the system maintained the new ROS concentration rather than returning homeostatically to the pre-existing steady state. Here it did adjust the concentration of damaged mitochondria (Figure 1B.3 ROS initial concentration was increased 10 fold. Model1Bs-ROS initial Increased 10 fold.cps):

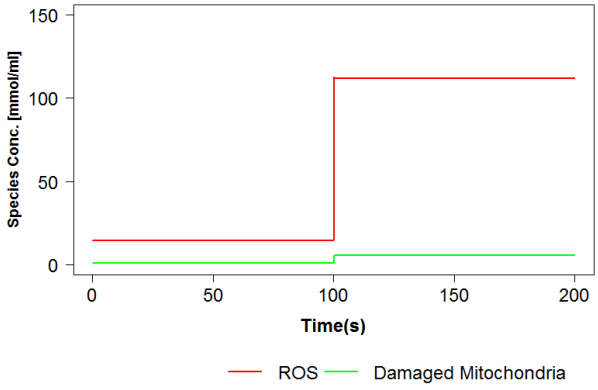

Figure 1B.3: Concentration of ROS and damaged mitochondria in model 1B
Transient perturbation of ROS upon increasing ROS initial concentration, both the ROS and damaged mitochondria attained new steady state.

These results demonstrated that this model is both structurally and dynamically unstable. Taking into account random biological fluctuations, the system with both damaged and healthy mitochondria coexisting would not persist. Ultimately, ROS synthesis would fluctuate below the threshold and system will become "perfect" with only healthy mitochondria, without any damaged mitochondria and without ROS. The rate of ROS generation and mitochondrial damage would then ultimately drop to zero as in Figure 1B.2.

Chapter 4

However, neither a complete absence of ROS nor perfectly healthy mitochondria may be realistic, nor the assumption that ROS be only produced by damaged mitochondria. Most probably, also mitochondria not yet damaged by ROS produce superoxide anion, which is converted by superoxide dismutase to hydrogen peroxide. Because of the presence of ferrous iron in the mitochondrial respiratory chain, the hydrogen peroxide is converted by the inorganic Fenton reaction to the highly reactive ROS hydroxyl.

Thus, we added a reaction of ROS generation by healthy mitochondria (Model 1B). Then, when ROS generation by damaged mitochondria was low because few of these mitochondria were left, ROS concentration was also low but not equal to 0 as it was still produced, be it at a lower rate, by the healthy mitochondria.

ROSgeneration(t) =ROSsynCoeficient*([DamagedMitochondria(t)]+kbasalROS)

First, we decreased total ROS generation proportionally by healthy and damaged mitochondria. In the reaction of ROS generation, where

ROSgeneration(t) =ROSsynCoeficient*([DamagedMitochondria(t)]+kbasalROS),
ROSsynCoefficient was decreased twice. Then the concentration of ROS and of damaged mitochondria deceased, and the concentration of healthy mitochondria increased, but reached new steady state. Thus, when ROS influx rate was decreased in a sustained manner, the ROS concentration and levels of healthy and damaged mitochondria changes but reach new steady again.

Then we returned ROS generation back to the initial level and system came back to the initial steady state. This all shows that with the additional ROS influx the system had become stable (Figure 1B.4).

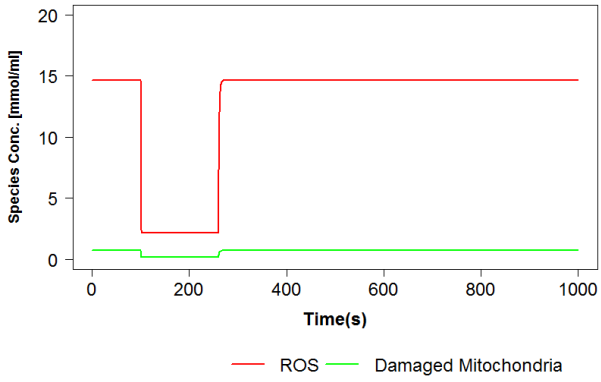

Fig 1.B.4: ROS concentration and Impaired Mitochondria in the model of basal ROS generation ROS and the damaged mitochondira respond to transient decrease in ROS synthesis to 2 fold. Removing the transient decrease of ROS generation, systems able to recovered back to initial states.

Chapter 4

However the stability was limited. When total ROS generation flux was increased 2 fold higher, the system would explode in terms of ROS concentration and levels of damaged mitochondria (Figure 1.B.5):

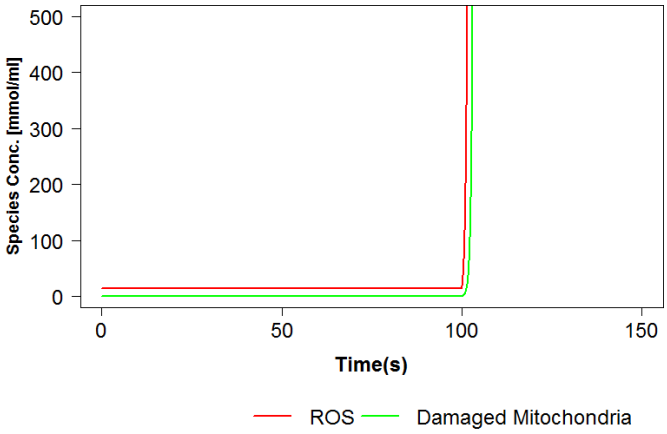

Figure 1.B.5: ROS concentration and Impaired Mitochondria in the model 1b with basal ROS generation
The concentration of both ROS and damaged mitochondria exponentially explodes, upon increased ROS generation flux 2 fold.
In reality the cell has a limited capacity to synthesise new mitochondria and thereby to maintain the level of healthy mitochondria constant, hence independent of ROS damage. The sustained damage to mitochondria consequent to increased ROS should in reality work to decrease the pool of healthy mitochondria. Accommodating this by making the pool of healthy mitochondria a variable rather than a constant we also added a reaction of mitochondrial synthesis (see design 1C) at a constant flux. We did this in order to maintain the possibility of the system reaching steady state.

Then, when ROS generation by the healthy mitochondria was increased 2 fold, the system no longer exploded in terms of ROS levels and damaged mitochondria (Model 1C).

This process of synthesis of new healthy mitochondria rather than a fixed level of heathy mitochondria sufficed to provide: When we removed basal synthesis of ROS and basal mitochondrial aging, mitochondria and ROS did explode either when ROS generation was increased twice or decreased half (model 1C, Figure 1C.1 & 1C.2):

Chapter 4

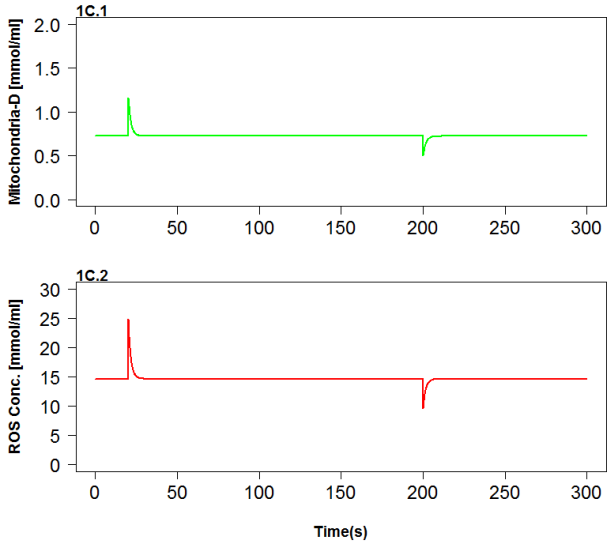

Figure 1C: Damaged mitochondria (1C.1) ROS concentration (1C.2) in the model of Basal Mitochondrial aging. ROS initial concentration was increased and decreased twice. The damaged mitochondria and the ROS are able to recovered back to its initial states. The model nither explodes nor goes to zero when ROS generation was increased or decrease twice.

To summarize, comparative analysis of models 1A, 1B and 1C revealed that a reduction of the abundance of mitochondria with increased ROS should insure that stable steady states are achieved. Thus, paradoxically, the, limited, removal of mitochondria may be essential to protect the cell (comparing models 1A-1C). We then subjected model 1C to a repetitive step-up of ROS generation. This led to an almost proportional variation of the ROS concentration attained at the end of each step-up period (Fig. 3B) with the ROS influx rate, with little sustained effect on the level of damaged mitochondria, but leading to very high ROS levels at high challenges (Fig. 3f).

We then used a dynamic challenge to study the properties of model 1C (Fig.2): a temporal step-up of ROS generation (Fig. 3A). This showed an almost linear variation of the ROS concentration attained at the end of each step-up period (Fig. 3B), with little sustained effect on the level of damaged mitochondria, but leading to very high ROS levels at high challenges (Fig. 3f). Stable steady states were reached however and this is what we identify as design principle 1: The limited synthesis of healthy mitochondria and the mitophagy together produce robust steady states. Thus, mitophagy might protect against PD by removing the potential time-bomb of explosive ROS generation inherent in the mitochondria. And, failure of mitophagy or unlimited synthesis of healthy mitochondria should cause ROS related disease.

The Keap1-Nrf2 module provides homeostasis through negative feed-back (design principle 2, Model 2)

Chapter 4

We then added synthesis and degradation of p62 as well as the antioxidant response (design 1D on Figure 1D; Model 1D). For fixed rates constants of the p62 processes one can then balance synthesis and degradation in such a way that the steady state concentrations of p62 and antioxidant response would be identical to their concentrations in Model 1C and this is what we did. Then Model 1D and Model 1C would exhibit a very similar (not distinguishable) response to oxidative stress and we can therefore use Model 1C as a representative model (so-called model 1) for design 1.

Subsequently we increased the complexity by incorporating the Keap1-Nrf2 system, which is capable of modulating mitophagy (by changing the p62 concentration), as well as an antioxidant response (by changing the concentration of antioxidant response species). Keap1 is a ROS sensor that regulates Nrf2 degradation and intracellular localisation (25). When active, Keap1 binds to Nrf2 and both immobilises Nrf2 in the cytoplasm, and marks (through ubiquitination) Nrf2 for degradation. When ROS oxidize cysteine residues in the Keap1 molecule, Keap1 changes its conformation and becomes inactive. Nrf2 is a transcription factor that actively shuttles between nucleus and cytoplasm (24) and regulates the expression of p62 and genes responsible for an antioxidant response. The higher is the concentration of ROS, the less active is Keap1, and consequently, the more active nuclear Nrf2 should be. An elevated expression of p62 (activation of mitophagy) and a higher antioxidant response should ensue. This dynamic networking will be called ‘design 2’ and simulated by model 2 (see Model 2 in Figure 2e, Model 2 in Figure 3.

The addition of the Keap1-Nrf2 module changed the behaviour of the system qualitatively: upon an increase of ROS generation, the ROS concentration first increased but then decreased again, presumably due to the negative feed-back loop which activated the antioxidant response and mitophagy and enabled homeostatic dynamic adaptation (Figure 3C-E). By contrast, the dynamic response of model 1 to the temporal step-up of ROS generation (Fig. 3A) showed an almost linear variation of the ROS concentration attained at the end of each step-up period (see above and Figure 2B). In model 2, the curve showing the variation of ROS generation rate with ROS ‘steady state’ concentration was progressively less than linear, and less steep. The transient oscillations obtained I Model 2 after each step-up of ROS production, decreased in amplitude with increasing ROS production.

This can be summarised in design principle 2: Addition of Nrf2-Keap1 feedback provides for the emergence of homeostatic adaptation. Thus, xenobiotics (like coffee) interfering with the Keap1-Nrf2 system may affect the response to oxidative stress by affecting homeostasis.

NFkB by itself activates recovery of damaged mitochondria and reduces the liability to necrosis (design 3, Model 3)

Mitophagy of damaged mitochondria averts excessive ROS generation thus preventing the cell from ROS-induced damage (corresponding to CytC release leading to apoptosis), but may lead to the loss of mitochondria. Such a loss could lead to necrosis due to the consequent drop in ATP concentration. There is a physiological mechanism where, instead of being degraded in mitophagy, damaged mitochondria are repaired. We incorporated this mechanism into the next model (see Model 3, Figure 2F; Model 3 in

Chapter 4

Figure 3) where NFkB-signalling activates mitochondrial recovery. Here we kept the NFkB loop by itself insensitive to intracellular signals such as related to ROS levels; it just served to activate repair of impaired mitochondria. Likewise we use a fixed first order rate constant for reaction 18 (making that rate strictly proportional to the level of impaired mitochondria. Upon the first increase in ROS generation, the activation of reaction 18 by the transiently increased level of damaged mitochondria was beneficial in keep the concentration of impaired mitochondria lower and more steady; the transient oscillations of Model 2 disappeared in this Model 3 (Figure 3D). The ratio of impaired mitochondria to healthy mitochondria (Figure 3E) was higher however, due to a stronger reduction in the level of healthy mitochondria (Figure 3C). However, the protective role of reaction 18 disappeared with further increases in ROS production rate constant (Figure 3).

We investigated this paradox in more detail by applying a different time series of ROS production (Fig. 4A). When we applied the first increase in ROS generation rate constant (at time zero in Figure 4A, setting up zone 1), reaction 18 helped to obtain strong homeostasis – the concentration of healthy mitochondria did not change significantly (zone 1 Figure 4 B); high ROS generation was compensated by the high rate of mitochondrial recovery. When ROS generation was brought back to the standard production rate (zone 2, Figure 4A), healthy mitochondria accumulated (Figure 4B). We might expect this to be advantageous. However, paradoxically, this brings a potential danger – when, healthy mitochondria are accumulated and ROS generation is suddenly increased (zone 3, Figure 4), because accumulated healthy mitochondria serve as a substrate for the production of damaged mitochondria. Because the concentration of substrate is high, there will be also a high rate of mitochondrial damage and ROS generation. This triggers a positive feed-back loop: ROS damage mitochondria and damaged mitochondria produce more ROS. When the concentration of damaged mitochondria accumulates faster than it can be utilised in mitophagy, a sharp peaks of damaged mitochondria and of ROS are observed (zone 3, Figure 4C&D). A vicious cycle fed by the high initial concentration of healthy mitochondria then leads to a collapse of the whole system. To avoid this mitochondrial catastrophe, the rate of reaction 18 should adapt to ROS concentrations. By other words, reaction 18 should be "democratic" and "listen" to other parts of the system: there should be little mitochondrial repair for low ROS concentration and higher mitochondrial repair for higher ROS concentrations.

Design principle 3: NFkB signalling by itself prevents necrosis at high ROS levels by enabling the synthesis of healthy mitochondria from impaired mitochondria. However, the increased level of healthy mitochondria makes the cell liable to sudden increases of ROS and consequent catastrophes

DJ-1 is a ROS sensor that coordinates Nrf2 and NFkB signalling so as to achieve almost perfect homeostasis (model 4). (Figure 3)

DJ-1 protein is one of the sensors of ROS. When oxidised by ROS, the conformation of DJ-1 is changed. DJ-1 becomes active and modulates the activity of various pathways, including those around NFkB and Nrf2. To examine what functionality DJ-1 might contribute, we added the DJ-1 module to our model (Model 4A, Figure 5). Activated DJ-1 activates the rate of mitochondrial recovery (reaction 18) via NFkB but now in a ROS dependent manner. In addition, it activates both mitophagy and antioxidant response via

amplifying ROS-induces Nrf2-Keap1 signalling. This helps to adapt to the changes in ROS concentration and reach dynamic homeostasis. Although the concentration of healthy mitochondria was a bit lower in Model 4 as compared with Model 2 (Figure 3C), the concentration of impaired mitochondria (Figure 3D) and the ratio of impaired to healthy mitochondria in the total mitochondrial pool (Figure 3F) were substantially lower. Furthermore, the peak of ROS concentration (Figure 3E) and the steady state of ROS is much lower than in other models. Overall we can conclude that Model 4 is the most robust to the increases in ROS generation. This optimal functioning of Model 4 was observed for realistic parameters obtained from the literature.

Design principle 4: DJ-1 coordinates mitochondrial recovery and amplification of Nrf2 signalling and helps to bring dynamic homeostasis close to perfect adaptation. Thus, mutations in DJ-1 could lead to PD in cases where the network is challenged by large perturbations.

In vitro experiments for validation of the ROS-management model

The model was fitted to two independent data sets from In vitro experiments performed in two different laboratories on different cell types.

In vitro experiments of cell response to oxidative stress were performed on the human hepatoma cell line HepG2 exposed to menadione, a compound inducing ROS generation (51, 52). Time course transcriptomics data of cell response to oxidative stress were obtained.

We added the module consisting of menadione to model 5. The model was then converted into a Simulink representation and computation environment. Then parameters related to menadione module were adjusted in the way that the experimentally observed time-dependent curve of ROS concentration was reproduced in the model simulations (Figure 5A). Then we compared the behaviour of the antioxidant response in terms of p62, Bclxl, and NFkB simulated by the model with those obtained in our experiments. The model showed very good predictions for an antioxidant response, p62 increase and Bclxl (Figure 5B).

Then we added the module consisting of peroxide to detailed model parameters related to peroxide module were adjusted in the way that the experimentally observed time-dependent peroxide data were reproduced in the model at three different dose levels (Figure 5C and 5D). We used one pulse and periodic peroxide additions both in model and in experiments.

Detailed model of ROS management: Simulation of stress and distress (Figure 6)

On the basis of literature information, we then further increased the resolution of the ROS management model (Model 5). Several additional species and interactions were added: Pink1, which affects mitochondrial functioning (54, 55) and activates Parkin E3 (56, 57), an ATP module, Keap1 ubiquitination of both Nrf2 and p62 marking the latter two for degradation, an mRNA layer for several proteins, as well as more details of NFkB signalling (58, 59).

Chapter 4

Oxidative stress in model 5 was now simulated by consecutive pulses of increased rate of ROS generation, together forming a sine wave (Fig. 6a). In the short term, model 5 behaved similar to the much simpler model 4 (Figure 6 A-D) demonstrates homeostatic adaptation to stress. However, in contrast to model 4, model 5 exhibits a new emergent property. This a collapse of the system in the long term. In Model 5, ultimately all mitochondria are lost (Figure 6D). As a result, all ATP is lost as well. The explanation is routed in the continuous loss of p62 that is the net non-linear effect of several reactions involved in p62 degradation when those reactions are affected by the mechanism involved in compensation to the increased ROS generation. This is a bi-stable system. If the rate of p62 synthesis remains above the 'trash line', then the system never collapses, but with insufficient p62 synthesis, the system will collapse, even after a long time.

Model 5 allows to simulate how perturbations in various components of the ROS-managing network affect the system's dynamics and more in particular also the time when the system collapses. For example, activation of Nrf2 synthesis prolongs the time of system's functioning (Figure 7A). This demonstrates that the activation of Nrf2 does not change the main trend of stress accumulation but can substantially delay the stress effect. Indeed, Nrf2 synthesis might be activated by different drugs or biologically active compounds, such as caffeine, and perhaps other components of coffee that fits well with the observation that drinking coffee correlates negatively with the PD progression (37).

Design principle 5: Strong adaptation runs out with ageing. The system is robust to different perturbations (ROS generation, mitochondrial synthesis), because some parts of the network are more fragile (p62 synthesis).

ROS-management model and the Parkinson's disease map: Towards personalised PD medicine (Figure 7)

At this moment, we have overlaid the detailed model 5 built ab initio, starting from the physiology of ROS management, over the Parkinson's disease map rooted in literature and experimental data and integrating molecular mechanisms involved in PD development (71). All components of model 5 and their interconnections were found in the PD map. Thus, a subnetwork corresponding exactly to a detailed model 5 could be extracted from PD map. PD map is online and we have a sub-map there with the model.

We have previously identified that the system's fragility was concentrated in the reaction of p62 synthesis, and that a p62 perturbation may be associated with many cases of Parkinson's disease. As reflected in the PD map, on the one hand, p62 may be sequestered by misfolded alfa-synuclein (33). On the other hand, synthesis of p62 is regulated by DJ-1 via Nrf2-Keap1 signalling, and DJ-1 may be downregulated in some PD cases (35). Apart from p62, other components of the ROS-managing network are also perturbed in PD. The PD map allows to display various experimental subsets as a layer over the network diagram. The projection of the transcriptomics analysis of PD post-mortal substantia nigra onto the PD network. In supplemental material shows that PD samples exhibit upregulation of keap1, and downregulation of Pink1, VDAC1 and the above mentioned DJ-1 (shown in PD map; PD substantia nigra data sets at http://minerva.uni.lu/MapViewer/). p62 expression was upregulated in this data set. The latter may indicate the activation of mitophagy. The upregulation of p62 transcription is

found in experiment. Also in our model. We upregulate p62 synthesis as compensatory mechanism, but still it is not enough to compensate the loss of p62 protein in mitophagy.

Using the PD map, we may identify several scenarios of PD development. In the present study we have chosen two of them, corresponding to two hypothetical patients: patient 1 with a substantial increase of alfa-synuclein which is oxidised by ROS, forms aggregates and sequesters p62, and patient 2 with a decreased DJ-1 concentration.

B. ATP concentrations time courses

In steady state, without excessive ROS generation, both hypothetical patients behaved very similarly to the healthy situation (Figure 7). However, upon increase of ROS generation under oxidative stress, both PD-patients lost healthy mitochondria and ATP much earlier that what was predicted for the healthy case (Figure 7).

From the previous chapter, we might expect that activation of Nrf2-Keap1 signalling (e.g. by caffeine and other coffee components) might be helpful to protect from oxidative stress. Our simulations confirm that PD-related collapse during oxidative stress might be delayed under coffee-based treatment (Figure 7). The activation of nrf2 signalling accompanying simultaneously the increase of ROS generation helps to protect from oxidative stress and helps even more if the Nrf2 system is activated prior to the increase of ROS generation (Figure 7).

Design principle 6: preconditioning (pre-treatment by Nrf2 activation) may play PD protective role.

Out simulations demonstrated as well, that patient 1 was affected by Nrf2 activation much stronger than patient 2 (Figure 7). This suggests that only a fraction of PD patients may benefit from a certain treatment (in this case coffee-induced nrf2 signalling). Taking into account the possibility to identify those patients for targeted personalised treatment, coffee – based PD medicine could be even more promising than what is inspired by population or randomised case studies where negative correlations between PD and coffee consumption were observed (37-40).

Design principle 7: Inter-individual variations cause disease variability between individuals that provides a foundation for the development of personalised medicine.

4. Discussion

Our models demonstrated that both mitochondrial recovery and mitophagy may avert ROS-induced cell death. The fine-tuning and coordination of those processes are crucial. This is related to two paradoxes which we have identified and explained using dynamic models: (i) mitophagy saves mitochondria by making steady states stable (design principle 1) and (ii) a high rate of mitochondrial recovery is not always beneficial but harms the cell if ROS generation suddenly increases (design principle 3).

Mitochondrial recovery and mitophagy should also be coordinated with an antioxidant response. We have identified roles of Nrf2-Keap1 (design principle 2) and DJ-1 (design principle 4) in this coordination. The Nrf2-Keap1 system works as ROS sensor and forms the first contour of the defence by activating antioxidant response and mitophagy (60).

Chapter 4

DJ-1 is an additional ROS-sensor that amplifies the activity of Nrf2-Keap1 signalling and coordinates it with mitochondrial recovery (61). Our models predicted that DJ-1 upregulation increases the cell's robustness and downregulation makes the system more sensitive to oxidative stress. Indeed, some cancers are associated with upregulation of DJ-1 (62), while some cases of neurodegeneration are related to DJ-1 downregulation (35). These are interesting examples where the same components are oppositely mistuned in opposing diseases: in cancer, the cell survives elevated ROS and in neurodegeneration, the cell dies from ROS. Taking into account that DJ-1 is localised mostly in the mitochondria, but Keap1 is localised in the cytoplasm, one could have foreseen the importance of adding a spatial aspect to the complexity of ROS-management.

When we increased the resolution of model 4 to obtain model 5, we observed the emergence of dynamic homeostasis: several consecutive pulses of increased ROS generation (mild oxidative stress), "trained" ROS management system to deal with subsequent larger stresses (63). This may explain several paradoxes reported in the literature, for example, those related to the observations that antioxidants may exhibit a hormetic response (64) and, in some cases, that antioxidant therapies come with disappointing clinical experience (65).

We have observed that consecutive pulses of increased ROS generation applied for a long time, can exhaust the adaptation and system ultimately collapses (design principle 5). A similar phenomenon of the accumulation of oxidative stress has been reported in the literature (66). In the terminology of Hans Seley, eustress (stress when the system can adapt) may convert into distress (the stress causing the collapse of the system) when the eustress persists for too long. Our modeling results are also compatible with publications (67, 68), demonstrating how the sequence of oxidative stress events may lead to the development of PD via the mechanism of a vicious cycle. For example, when rats were exposed to 3 pulses of paraquat (PQ) imitating the oxidative stress, the first addition of PQ had an observed effect, the second addition allowed the system almost perfectly to compensate for a stress (adaptation), and the third pulse of PQ addition caused again a larger effect (and ultimately perhaps system collapse) (3). Authors explained the phenomena by already existing mathematical models exhibiting bistability (67, 68). Our models may provide an additional interpretation: the first pulse of PQ leads to adaptation (eustress) via activation of antioxidants response and mitophagy that makes the system more tolerant to the consecutive mild stress, but the third pulse exceeds the protective potential and causes the collapse of the system (distress).

Taken into account the stochastic difference between neurons (neurons are not identical and differ in concentrations of various proteins) we should not expect synchronized death of all neurons at once. Likewise, limited neuronal loss can be compensated for, at least to some extent. However, when damage accumulates and exceeds a certain threshold, the neurodegenerative pathology develops. This correlates well with clinical observations that there is a gradual age-related loss of dopaminergic neurons, but the first PD motor disorders appear only when already 50-70 % of dopaminergic neurons are lost (69).

In several simulations, we observed that Nrf2 oscillated transiently (e.g. model 3). This correlates with literature data (70) showing that Nrf2 undergoes autonomous frequency-modulated oscillations between cytoplasm and nucleus. Oscillations occurred (70) when cells were stimulated at physiological levels of activators, they decreased in period and

Chapter 4

amplitude and then evoked a cytoprotective transcriptional response. According to the data shown in (24), Nrf2 is activated in cells without a change in total cellular Nrf2 protein concentration. In our models, there is also the conserved moiety of total Nrf2, an increase of nuclear localization of Nrf2 corresponds to an increase of Nrf2 activity.

Our Model 5 is an interesting example where a slow aging process emerges from quick processes in the network. Apparently, minor differences in persons' genomes (or expressomes) that do not affect unchallenged function may become crucial when challenged with oxidative stress.

First, we have built our models ab initio, starting from the physiology of the response to oxidative stress and increasing the complexity of the network step by step. Adding every new level of complexity in a domino approach enabled us to identify design principles of ROS management. At the same time, our most complex model, which still comprised these design principles, became a blueprint model where the information accumulated in these maps may be projected. This produced the ability to tuning this blueprint map into a patient-specific model. Overall, our calculations may serve as case studies connecting data-driven biomedical disease maps with systems biological dynamic models built *ab initio*, and as prove of concept showing how personalised medicine may benefit from this connection and how fundamental design principles study may face practical biomedical questions.

Chapter 4

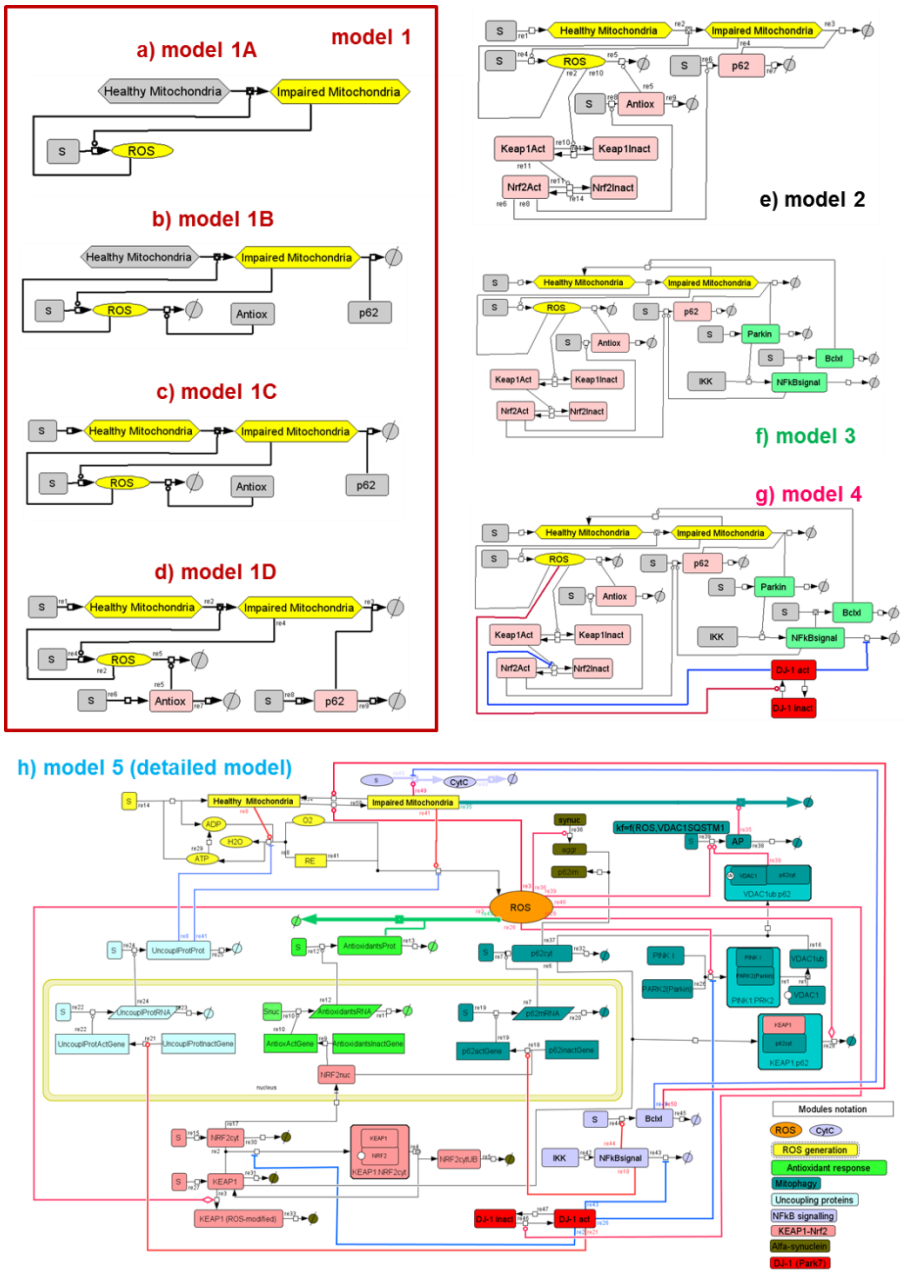

Figure 2. Network diagrams describing 5 principles (with 4 subprinciples for level 1) of ROS management. Level 1, i.e any of the models 1, is comprised in level 2 (model 2) and level 2 in level 3, etc., thereby forming a hierarchy of networks and corresponding models). By co-determining level 5 functionality each of these corresponds to a subnetwork of ROS-associated disease.

Chapter 4

(A) Model 1A. The simplest model. Healthy Mitochondria damaged by ROS are converted into Impaired Mitochondria. Impaired Mitochondria produce ROS. (B) Model 1 B. Adding ROS and Impaired Mitochondria removal. The node called Aniox comprises the total pool of all antioxidant response, both metabolites (e.g. various antioxidants) and enzymes (e.g. superoxide dismutase) catalyzing ROS removal. P62 is required for mitophagy (removal of Impaired Mitochondria) and is removed together with the impaired mitochodnria in the process. (C) Model 1 C. Adding synthesis of Healthy Mitochondria. The reaction where Healthy Mitochondria are constantly synthesized has been added. (D) Model 1 D. Adding synthesis and degradation of Antiox and p62 species. Aniox and p62 specie are constantly synthesized and degraded. Their synthesis and degradation rates are balance in the way to obtain steady state concentrations equal to ones in model 1C. (E) Model 2. Adding keap1-Nrf2 signaling system. Pink species (pink tile) represent Keap1 – Nrf2 module. Reactions 10 and 21 are two directions of the reversible transition of keap1 between active and non-active (oxidized) form. Reaction 11 and 22 are two directions of the reversible transition of Nrf2 between active and non-active (ubiquitinated, marked for degradation and localized in the cytoplasm) form. ROS catalyze reaction 10 and shift the equilibrium towards a higher rate of keap1 oxidation (deactivation); thus ROS inactivates keap1. Keap1 catalyzes reaction 11 and shift the equilibrium towards the higher fraction of inactive Nrf2. When active, Nrf2 activates the expression of p62 (reaction 6) and the antioxidant response (reaction 8). (F) Model 3. Adding the NF-kB signaling system. The violet species (violet tile) represent NFkB signaling. Parkin activates NFkB signaling via IKK (reaction 14). NfkB activates the expression of Bclxl (reaction 16) and p62 (reaction 6). Bclxl activates the protection of mitochondria via biosynthesis (reaction 18). Parkin is removed together with p62 in mitophagy (G) Model 4. Adding DJ-1 sensor system. Red species (red tile) represent DJ1 regulatory module. DJ1 is a protein that may be present in two active (oxidized) and non-active conformations. DJ1 activation is the net effect of two reactions of protein conformation change: activation catalyzed by ROS (reaction 19) and deactivation (reaction 20). When active, DJ1 inhibits deactivation of Nrf2 (reaction 11) and also inhibits removal of NfkB signaling (reaction 15). (H) Model 5. Our most complete and detailed model of ROS management. The resolution of the model was increased, e.g. the nucleus and cytoplasm compartmentalization were added: Pink1, that affects mitochondrial functioning and activates parkin E3, ATP module Keap1 ubiquitination of both Nrf2 and p62 marking them for degradation; mRNA layer for several proteins; more details of NFkB signalling. In these diagrams SBGN notation is used, i.e. –o for stimulation, -| for inhibition and – for co-reaction

Chapter 4

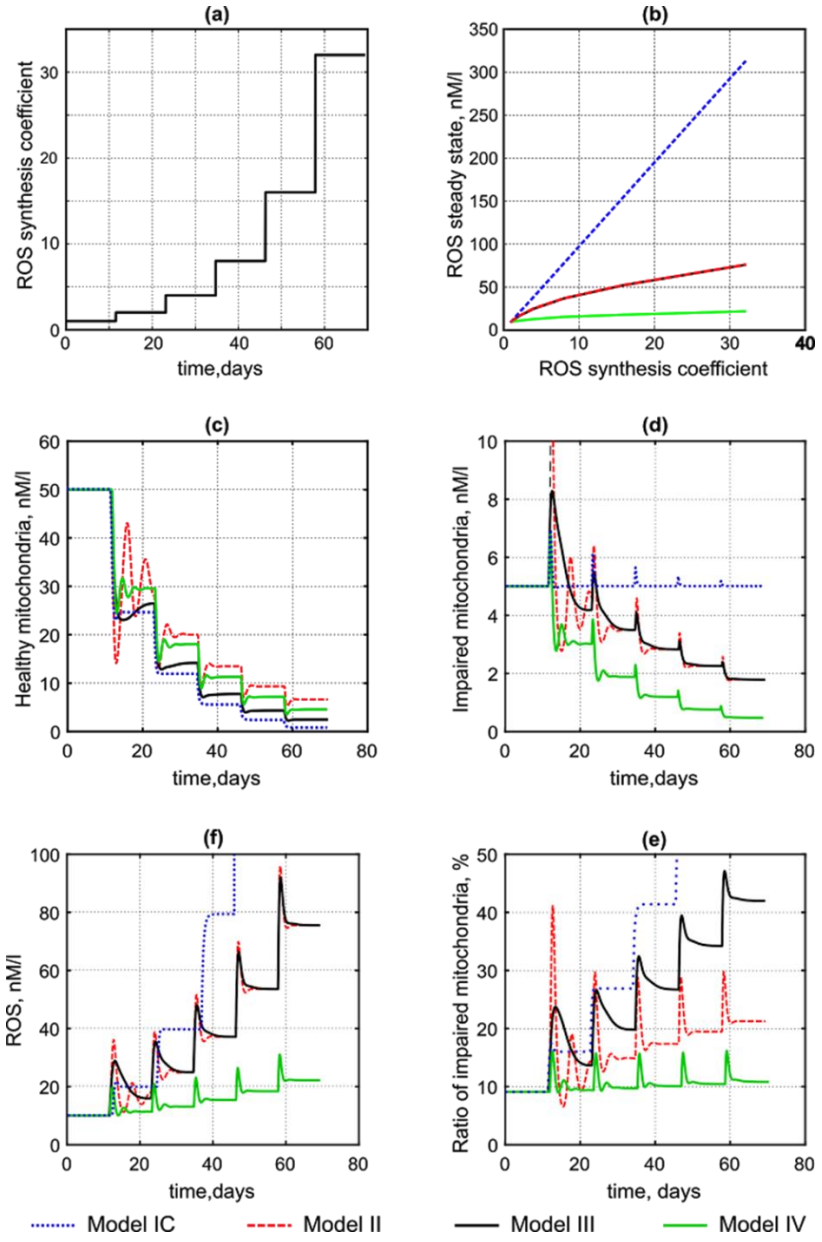

Figure 3

The response of models 1-4 to a challenge of stepwise increased ROS generation.

A. The stepwise increase in ROS generation (effected by increasing the ROS synthesis coefficient) that was used to examine the dynamic response of the ROS networks of higher complexity. The

Chapter 4

step increase of the ROS generation consists of a doubling of the **rate of ROS synthesis per impaired mitochondria (rate constant in reaction 4) every 11 days.**

B. The dependence of steady state concentration of ROS on the ROS synthesis coefficient (rate constant of the reaction 4). The results of Model 2 and Model 3 overlap.

C. The Response of the concentration of Healthy Mitochondria in models 1-4 upon the step increase of ROS generation.

The concentration of Healthy Mitochondria decreases with the step increase of ROS generation. The concentration of Healthy Mitochondria goes to the new steady state upon the increase in ROS synthesis coefficient. In model 1 (blue line) Healthy Mitochondria steady state concentration drops the most severely. In Model 2 (red line), model 3 (black line) and model 4 (green line) we observe homeostasis. Healthy Mitochondria steady state concentration first decreases upon the increase of ROS synthesis but then recovers back to some extent. Model 4 performs stronger homeostasis than model 3 and model 2 has the strongest homeostasis of Healthy Mitochondria.

D. The Response of the concentration of Impaired Mitochondria in models 1-4 upon the step increase of ROS generation.

The concentration of Impaired Mitochondria first increases upon the step increase of ROS generation. Then the concentration of Impaired Mitochondria goes to the new steady state. Paradoxically the increase of ROS generation helps to clear out damaged mitochondria (due to increased mitophagy). The strength of the capacity to clear out Impaired Mitochondria increases respectively from model 1 (blue line) to model 2 (red line), to model 3 (black line), and to model 4 (pink line).

E. The Response of the ratio of Impaired/Healthy Mitochondria in models 1-4 upon the step increase of ROS generation.

The ratio of Impaired/Healthy Mitochondria increases upon the step increase of ROS generation. In model 1 (blue line), the doubling of ROS generation results in the increase of Impaired/Healthy Mitochondria ratio twice as well. In model 2 (red line), model 3 (black line) and model 4 (green line) Impaired/Healthy Mitochondria ratio first increases twice and then drops back (homeostasis). In model 4, Impaired/Healthy Mitochondria ratio drops to the almost initial steady state level.

F. The Response of the ROS concentration in models 1-4 upon the step increase of ROS generation.

ROS concentration increases upon the step increase of ROS generation. In model 1 (blue line), the doubling of ROS generation results in the increase of ROS concentration twice as well. In model 2 (red line), model 3 (black line) and model 4 (green line) homeostasis; system counteracts perturbation and exhibit the tendency to decrease both ROS peak and ROS steady state concentration. Model 4 exhibit the strongest homeostasis.

Chapter 4

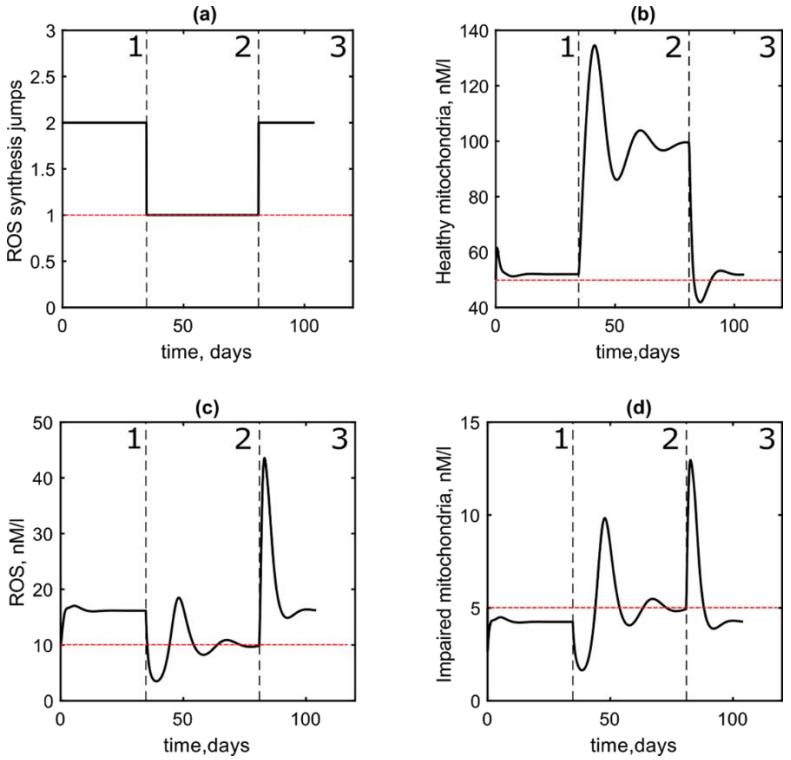

Figure 4

Fig NF-kB signaling: response of Model 3 to 2 consecutive pulses of increased ROS generation. Red dotted lines correspond to the steady state levels maintained in the absence of the pulses

(A) The causal variation of ROS production rate constant applied, which was 1 before time zero. 2 long pulses of ROS generation were applied to model 3: zone 1 and zone 2. (B) The response in the concentration of Healthy Mitochondria to the 2 pulses of increased ROS generation. (**C)** The response in the concentration of ROS to the 2 pulses of increased ROS generation. (**D)** The response in the concentration of Impaired Mitochondria to the 2 pulses of increased ROS generation.

Chapter 4

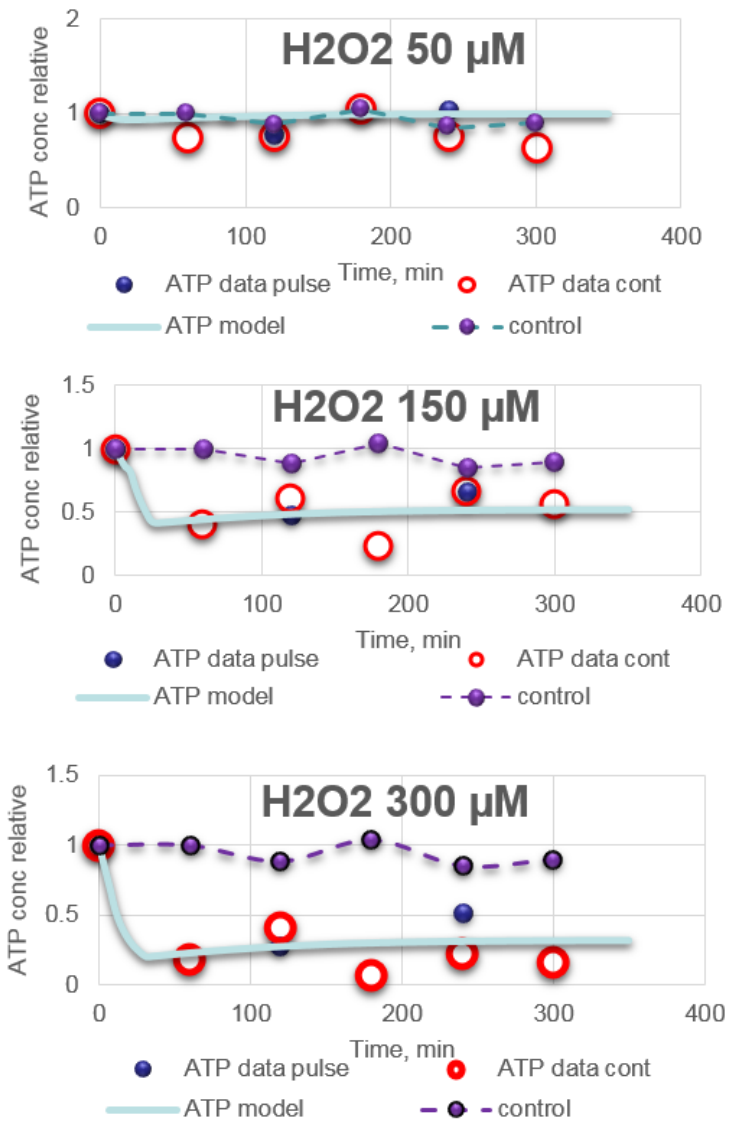

Fig.5A: Model validation. (I) model 5's dynamics of the relative ATP concentration upon the addition of peroxide at three different dose level with pulse treatment (Milano data). The light purple dots are the experimentally observed control data points. The red dots are experimentally observed data upon addition of peroxide to a cell culture and relative ATP concentration was determined. The ligh blue line is the predicted relative ATP concentration by the model.

Chapter 4

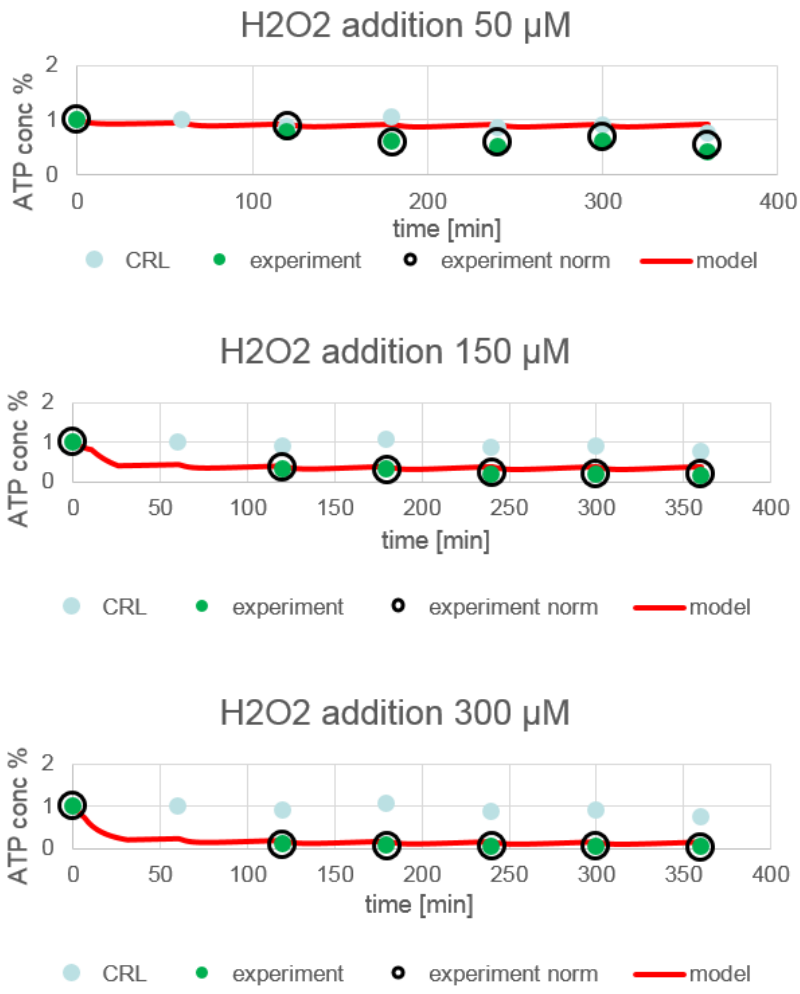

Fig.5B: Model validation. (I) model 5's dynamics of the relative ATP concentration upon the addition of peroxide at three different dose level with repeated treatment (Milano data). The light blue dots are the experimentally observed control data points. The green dots are experimentally observed data upon addition of peroxide to a cell culture and relative ATP concentration was determined. The red line is the predicted relative ATP concentration by the model.

Chapter 4

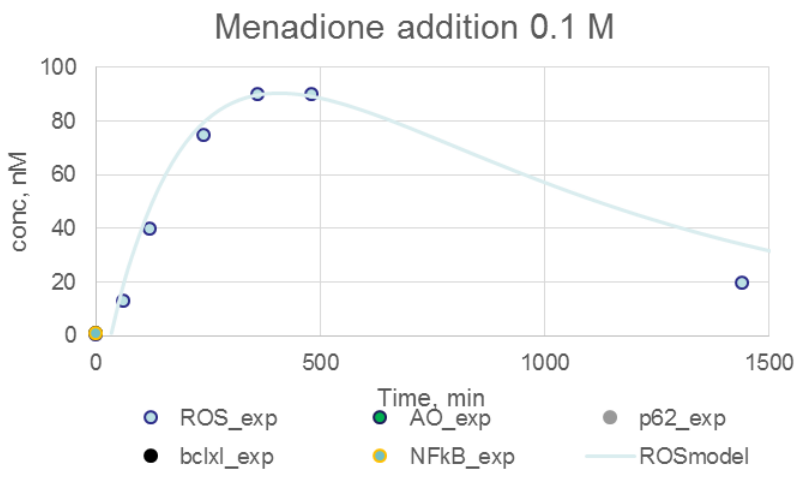

Fig.5C: Model validation. Model 5's dynamics of the change of ROS concentration upon the addition of menadione was fitted to experimental data. The light blue dots are the experimentally observed data points. 0.1M of menadione was added to a culture of HepG2 cells and total ROS concentration was determined. The blue line is the predicted ROS concentration by the model.

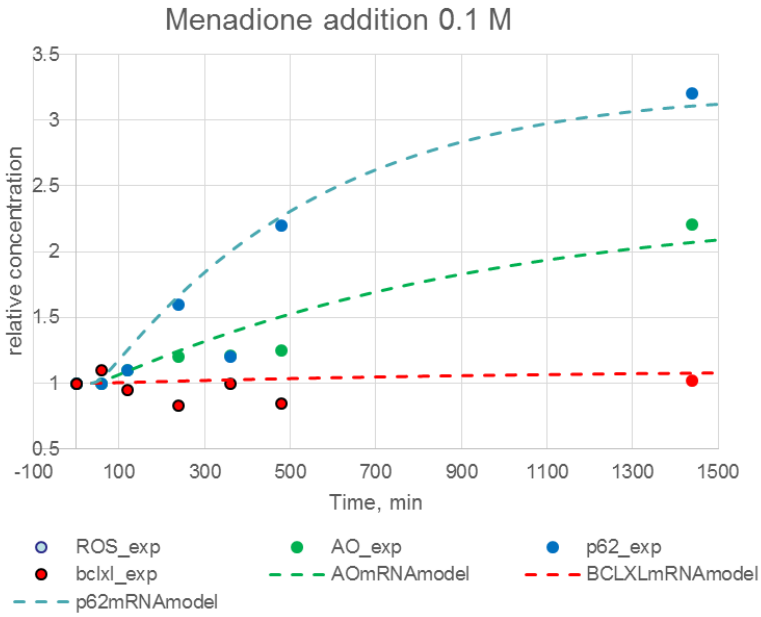

Fig.5D: Model validation. Model 5's dynamics of the relative change of species such as Antioxidant mRNA expression, P62mRNA expression and BCLxL mRNA expression upon the addition of menadione was fitted to experimental data upon addition of 0.1M mendione into the cell culture. The green dots (experimentally observed) and line (model predicted) are corresponds to relative Antioxidant mRNA; blue dots (experimentally observed) and line (model predicted) are

corresponds to relative P62mRNA expression; red dots (experimentally observed) and line (model predicted) are corresponds to relative BCLxL mRNA expression.

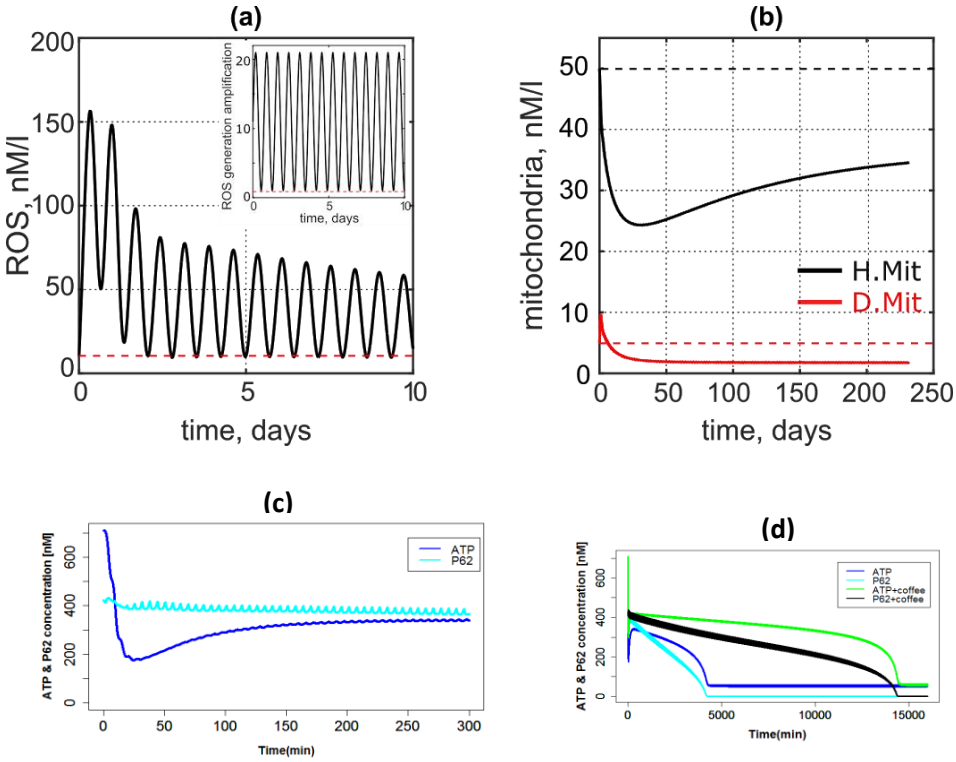

Figure 6. Simulations of the response to oxidative stress in simplified (A-B) and detailed (C-D) models.

Oxidative stress was simulated as oscillations of increased ROS generation (over the initial base line) (subgraph in A)

A. The response of ROS concentration on the oscillatory increase of ROS generation.

First pulses of increased ROS generation affected ROS concentration to a higher extent than consecutive pulses.

B. The response of Healthy and Impaired Mitochondria concentration on the oscillatory increase of ROS generation.

First pulses of increased ROS generation caused the decrease of Healthy and the increase of Impaired Mitochondria. However, the system counteracted this changes and the concentration of Healthy Mitochondria increases again while the concentration of Impaired Mitochondria decreases back.

C. The response of ATP on the oscillatory increase of ROS generation in the detailed model in the short term.

First pulses of increased ROS generation caused the decrease of ATP concentrations. However, the system counteracted this changes and the concentration of ATP recovers back.

D. The response of ATP and p62 on the oscillatory increase of ROS generation in the detailed model in the long term.

Although the concentration of ATP is recovered in the short term, the system collapses and all ATP is lost in the long term because the damage (lost of p62) is accumulated.

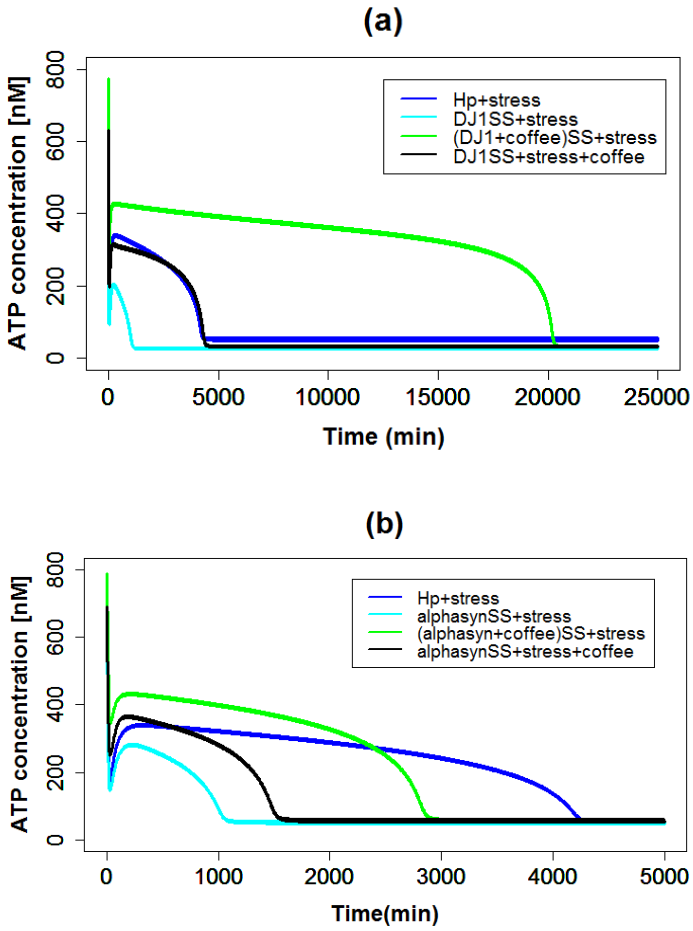

Figure 7. Parkinson's disease (PD) and personalized medicine. (A). ATP concentrations time courses in a virtual patient 1 with increased alfa-synuclein and (B) in virtual patient 2 with a decreased DJ-1 concentration. Both are compared to a healthy person.

Chapter 4

References

1. Kell DB. Towards a unifying, systems biology understanding of large-scale cellular death and destruction caused by poorly liganded iron: Parkinson's, Huntington's, Alzheimer's, prions, bactericides, chemical toxicology and others as examples. Archives of toxicology. 2010;84(11):825-89. Epub 2010/10/23.
2. Kim HR, Lee GH, Cho EY, Chae SW, Ahn T, Chae HJ. Bax inhibitor 1 regulates ER-stress-induced ROS accumulation through the regulation of cytochrome P450 2E1. Journal of cell science. 2009;122(Pt 8):1126-33. Epub 2009/04/03.
3. Finnerty NJ, O'Riordan SL, Lowry JP, Cloutier M, Wellstead P. Continuous real-time in vivo measurement of cerebral nitric oxide supports theoretical predictions of an irreversible switching in cerebral ROS after sufficient exposure to external toxins. Journal of Parkinson's disease. 2013;3(3):351-62. Epub 2013/08/29.
4. Li X, Fang P, Mai J, Choi ET, Wang H, Yang XF. Targeting mitochondrial reactive oxygen species as novel therapy for inflammatory diseases and cancers. Journal of hematology & oncology. 2013;6:19. Epub 2013/02/28.
5. Hall CJ, Boyle RH, Astin JW, Flores MV, Oehlers SH, Sanderson LE, et al. Immunoresponsive gene 1 augments bactericidal activity of macrophage-lineage cells by regulating beta-oxidation-dependent mitochondrial ROS production. Cell Metab. 2013;18(2):265-78. Epub 2013/08/13.
6. Juntilla MM, Patil VD, Calamito M, Joshi RP, Birnbaum MJ, Koretzky GA. AKT1 and AKT2 maintain hematopoietic stem cell function by regulating reactive oxygen species. Blood. 2010;115(20):4030-8. Epub 2010/04/01.
7. Kinder M, Wei C, Shelat SG, Kundu M, Zhao L, Blair IA, et al. Hematopoietic stem cell function requires 12/15-lipoxygenase-dependent fatty acid metabolism. Blood. 2010;115(24):5012-22. Epub 2010/04/02.
8. Lewandowski D, Barroca V, Duconge F, Bayer J, Van Nhieu JT, Pestourie C, et al. In vivo cellular imaging pinpoints the role of reactive oxygen species in the early steps of adult hematopoietic reconstitution. Blood. 2010;115(3):443-52. Epub 2009/10/03.
9. Chaudhari P, Ye Z, Jang YY. Roles of reactive oxygen species in the fate of stem cells. Antioxidants & redox signaling. 2014;20(12):1881-90. Epub 2012/10/17.
10. Kanda Y, Hinata T, Kang SW, Watanabe Y. Reactive oxygen species mediate adipocyte differentiation in mesenchymal stem cells. Life Sci. 2011;89(7-8):250-8. Epub 2011/07/05.
11. Le Belle JE, Orozco NM, Paucar AA, Saxe JP, Mottahedeh J, Pyle AD, et al. Proliferative neural stem cells have high endogenous ROS levels that regulate self-renewal and neurogenesis in a PI3K/Akt-dependant manner. Cell stem cell. 2011;8(1):59-71. Epub 2011/01/08.
12. Limoli CL, Rola R, Giedzinski E, Mantha S, Huang TT, Fike JR. Cell-density-dependent regulation of neural precursor cell function. Proceedings of the National Academy of Sciences of the United States of America. 2004;101(45):16052-7. Epub 2004/11/04.

Chapter 4

13. Zamkova M, Khromova N, Kopnin BP, Kopnin P. Ras-induced ROS upregulation affecting cell proliferation is connected with cell type-specific alterations of HSF1/SESN3/p21Cip1/WAF1 pathways. Cell cycle. 2013;12(5):826-36. Epub 2013/02/08.
14. Afonso V, Champy R, Mitrovic D, Collin P, Lomri A. Reactive oxygen species and superoxide dismutases: role in joint diseases. Joint, bone, spine : revue du rhumatisme. 2007;74(4):324-9. Epub 2007/06/26.
15. Oyewole AO, Birch-Machin MA. Mitochondrial-targeted antioxidants. FASEB J. 2015. Epub 2015/08/09.
16. Brady NR, Elmore SP, van Beek JJ, Krab K, Courtoy PJ, Hue L, et al. Coordinated behavior of mitochondria in both space and time: a reactive oxygen species-activated wave of mitochondrial depolarization. Biophysical journal. 2004;87(3):2022-34. Epub 2004/09/04.
17. Kane LA, Lazarou M, Fogel AI, Li Y, Yamano K, Sarraf SA, et al. PINK1 phosphorylates ubiquitin to activate Parkin E3 ubiquitin ligase activity. The Journal of cell biology. 2014;205(2):143-53. Epub 2014/04/23.
18. Koyano F, Okatsu K, Kosako H, Tamura Y, Go E, Kimura M, et al. Ubiquitin is phosphorylated by PINK1 to activate parkin. Nature. 2014. Epub 2014/05/03.
19. Cui T, Fan C, Gu L, Gao H, Liu Q, Zhang T, et al. Silencing of PINK1 induces mitophagy via mitochondrial permeability transition in dopaminergic MN9D cells. Brain research. 2011;1394:1-13. Epub 2011/01/26.
20. Wang X, Winter D, Ashrafi G, Schlehe J, Wong YL, Selkoe D, et al. PINK1 and Parkin Target Miro for Phosphorylation and Degradation to Arrest Mitochondrial Motility. Cell. 2011;147(4):893-906. Epub 2011/11/15.
21. Fedorowicz MA, de Vries-Schneider RL, Rub C, Becker D, Huang Y, Zhou C, et al. Cytosolic cleaved PINK1 represses Parkin translocation to mitochondria and mitophagy. EMBO Rep. 2014;15(1):86-93. Epub 2013/12/21.
22. Ivatt RM, Whitworth AJ. The many faces of mitophagy. EMBO Rep. 2014;15(1):5-6. Epub 2014/01/09.
23. Allen GF, Toth R, James J, Ganley IG. Loss of iron triggers PINK1/Parkin-independent mitophagy. EMBO Rep. 2013;14(12):1127-35. Epub 2013/11/02.
24. Xue M, Momiji H, Rabbani N, Barker G, Bretschneider T, Shmygol A, et al. Frequency Modulated Translocational Oscillations of Nrf2 Mediate the Antioxidant Response Element Cytoprotective Transcriptional Response. Antioxidants & redox signaling. 2014. Epub 2014/09/03.
25. Williamson TP, Johnson DA, Johnson JA. Activation of the Nrf2-ARE pathway by siRNA knockdown of Keap1 reduces oxidative stress and provides partial protection from MPTP-mediated neurotoxicity. Neurotoxicology. 2012;33(3):272-9. Epub 2012/02/22.
26. Joselin AP, Hewitt SJ, Callaghan SM, Kim RH, Chung YH, Mak TW, et al. ROS-dependent regulation of Parkin and DJ-1 localization during oxidative stress in neurons. Human molecular genetics. 2012;21(22):4888-903. Epub 2012/08/09.

Chapter 4

27. Santiago JA, Potashkin JA. Shared dysregulated pathways lead to Parkinson's disease and diabetes. Trends in molecular medicine. 2013;19(3):176-86. Epub 2013/02/05.
28. Soleimanpour SA, Gupta A, Bakay M, Ferrari AM, Groff DN, Fadista J, et al. The diabetes susceptibility gene clec16a regulates mitophagy. Cell. 2014;157(7):1577-90. Epub 2014/06/21.
29. Matsuda S, Nakanishi A, Minami A, Wada Y, Kitagishi Y. Functions and characteristics of PINK1 and Parkin in cancer. Front Biosci (Landmark Ed). 2015;20:491-501. Epub 2015/01/02.
30. Varcin M, Bentea E, Michotte Y, Sarre S. Oxidative stress in genetic mouse models of Parkinson's disease. Oxidative medicine and cellular longevity. 2012;2012:624925. Epub 2012/07/26.
31. Kruger R, Hilker R, Winkler C, Lorrain M, Hahne M, Redecker C, et al. Advanced stages of PD: interventional therapies and related patient-centered care. Journal of neural transmission. 2015. Epub 2015/07/04.
32. Nalls MA, Pankratz N, Lill CM, Do CB, Hernandez DG, Saad M, et al. Large-scale meta-analysis of genome-wide association data identifies six new risk loci for Parkinson's disease. Nat Genet. 2014. Epub 2014/07/30.
33. Tran HT, Chung CH, Iba M, Zhang B, Trojanowski JQ, Luk KC, et al. alpha-Synuclein Immunotherapy Blocks Uptake and Templated Propagation of Misfolded alpha-Synuclein and Neurodegeneration. Cell reports. 2014. Epub 2014/06/17.
34. Charan RA, Johnson BN, Zaganelli S, Nardozzi JD, LaVoie MJ. Inhibition of apoptotic Bax translocation to the mitochondria is a central function of parkin. Cell death & disease. 2014;5:e1313. Epub 2014/07/06.
35. Wang Y, Liu W, He X, Zhou F. Parkinson's disease-associated DJ-1 mutations increase abnormal phosphorylation of tau protein through Akt/GSK-3beta pathways. Journal of molecular neuroscience : MN. 2013;51(3):911-8. Epub 2013/08/28.
36. Pfeiffer R, Wszolek ZK, Ebadi MS. Parkinson's disease. Boca Raton, FL: CRC Press; 2012. Available from: http://www.crcnetbase.com/isbn/978-1-4398-0714-9.
37. Bjorklund A, Cenci MA. Recent advances in Parkinson's disease: basic research. Amsterdam etc.: Elsevier; 2010. Available from: http://www.sciencedirect.com/science/bookseries/00796123/183.
38. Palacios N, Gao X, McCullough ML, Schwarzschild MA, Shah R, Gapstur S, et al. Caffeine and risk of Parkinson's disease in a large cohort of men and women. Movement disorders : official journal of the Movement Disorder Society. 2012;27(10):1276-82. Epub 2012/08/29.
39. Postuma RB, Lang AE, Munhoz RP, Charland K, Pelletier A, Moscovich M, et al. Caffeine for treatment of Parkinson disease: a randomized controlled trial. Neurology. 2012;79(7):651-8. Epub 2012/08/03.
40. van der Mark M, Nijssen PC, Vlaanderen J, Huss A, Mulleners WM, Sas AM, et al. A case-control study of the protective effect of alcohol, coffee, and cigarette consumption on Parkinson disease risk: time-since-cessation modifies the effect of tobacco smoking. PloS one. 2014;9(4):e95297. Epub 2014/05/03.

Chapter 4

41. Lee SJ, Lim HS, Masliah E, Lee HJ. Protein aggregate spreading in neurodegenerative diseases: Problems and perspectives. Neuroscience research. 2011;70(4):339-48. Epub 2011/06/01.
42. Walsh DM, Selkoe DJ. A critical appraisal of the pathogenic protein spread hypothesis of neurodegeneration. Nat Rev Neurosci. 2016;17(4):251-60. Epub 2016/03/19.
43. Velema M, Boot E, Engelen M, Hollak C. Parkinsonism in phenylketonuria: a consequence of dopamine depletion? JIMD reports. 2015;20:35-8. Epub 2015/01/24.
44. del Sol A, Balling R, Hood L, Galas D. Diseases as network perturbations. Curr Opin Biotechnol. 2010;21(4):566-71. Epub 2010/08/17.
45. Boogerd FC, Bruggeman, F., Hofmeyr, J.H.S., Westerhoff, H.V. Systems Biology Philosophical Foundations. 2007:342 p.
46. Kolodkin A, Simeonidis E, Westerhoff HV. Computing life: Add logos to biology and bios to physics. Prog Biophys Mol Biol. 2012. Epub 2012/10/30.
47. Westerhoff HV, Kolodkin A, Conradie R, Wilkinson SJ, Bruggeman FJ, Krab K, et al. Systems biology towards life in silico: mathematics of the control of living cells. J Math Biol. 2009;58(1-2):7-34. Epub 2008/02/19.
48. Alberghina L, Westerhoff, H.V. . Systems Biology: Definitions and Perspectives. 2005:408.
49. Boogerd FC, Bruggeman FJ, Richardson RC, Stephan A, Westerhoff HV. Emergence and its place in nature: A case study of biochemical networks (vol 145, pg 131, 2005). Synthese. 2005;145(3):501-.
50. Kolodkin AN, Boogerd FC, Bruggeman FJ, Westerhoff HV. Modeling Approaches in Systems Biology, Including Silicon Cell Models. In: Pas tMFW, Woelders H, Bannink A, editors. Systems Biology and Livestock Science. Oxford, UK: Wiley-Blackwell; 2011.
51. Criddle DN, Gillies S, Baumgartner-Wilson HK, Jaffar M, Chinje EC, Passmore S, et al. Menadione-induced reactive oxygen species generation via redox cycling promotes apoptosis of murine pancreatic acinar cells. The Journal of biological chemistry. 2006;281(52):40485-92. Epub 2006/11/08.
52. Loor G, Kondapalli J, Schriewer JM, Chandel NS, Vanden Hoek TL, Schumacker PT. Menadione triggers cell death through ROS-dependent mechanisms involving PARP activation without requiring apoptosis. Free radical biology & medicine. 2010;49(12):1925-36. Epub 2010/10/13.
53. Nelson DE, Ihekwaba AE, Elliott M, Johnson JR, Gibney CA, Foreman BE, et al. Oscillations in NF-kappaB signaling control the dynamics of gene expression. Science. 2004;306(5696):704-8. Epub 2004/10/23.
54. Morais VA, Haddad D, Craessaerts K, De Bock PJ, Swerts J, Vilain S, et al. PINK1 loss-of-function mutations affect mitochondrial complex I activity via NdufA10 ubiquinone uncoupling. Science. 2014;344(6180):203-7. Epub 2014/03/22.
55. Rakovic A, Shurkewitsch K, Seibler P, Grunewald A, Zanon A, Hagenah J, et al. Phosphatase and tensin homolog (PTEN)-induced putative kinase 1 (PINK1)-dependent ubiquitination of endogenous Parkin attenuates mitophagy: study in human primary

Chapter 4

fibroblasts and induced pluripotent stem cell-derived neurons. The Journal of biological chemistry. 2013;288(4):2223-37. Epub 2012/12/06.
56. Sha D, Chin LS, Li L. Phosphorylation of parkin by Parkinson disease-linked kinase PINK1 activates parkin E3 ligase function and NF-kappaB signaling. Human molecular genetics. 2010;19(2):352-63. Epub 2009/11/03.
57. Muller-Rischart AK, Pilsl A, Beaudette P, Patra M, Hadian K, Funke M, et al. The E3 Ligase Parkin Maintains Mitochondrial Integrity by Increasing Linear Ubiquitination of NEMO. Mol Cell. 2013;49(5):908-21. Epub 2013/03/05.
58. Arena G, Gelmetti V, Torosantucci L, Vignone D, Lamorte G, De Rosa P, et al. PINK1 protects against cell death induced by mitochondrial depolarization, by phosphorylating Bcl-xL and impairing its pro-apoptotic cleavage. Cell death and differentiation. 2013;20(7):920-30. Epub 2013/03/23.
59. Kodama T, Takehara T, Hikita H, Shimizu S, Shigekawa M, Li W, et al. BH3-only activator proteins Bid and Bim are dispensable for Bak/Bax-dependent thrombocyte apoptosis induced by Bcl-xL deficiency: molecular requisites for the mitochondrial pathway to apoptosis in platelets. The Journal of biological chemistry. 2011;286(16):13905-13. Epub 2011/03/04.
60. Lewis KN, Wason E, Edrey YH, Kristan DM, Nevo E, Buffenstein R. Regulation of Nrf2 signaling and longevity in naturally long-lived rodents. Proceedings of the National Academy of Sciences of the United States of America. 2015;112(12):3722-7. Epub 2015/03/17.
61. Ariga H, Takahashi-Niki K, Kato I, Maita H, Niki T, Iguchi-Ariga SM. Neuroprotective function of DJ-1 in Parkinson's disease. Oxidative medicine and cellular longevity. 2013;2013:683920. Epub 2013/06/15.
62. Li Y, Cui J, Zhang CH, Yang DJ, Chen JH, Zan WH, et al. High-expression of DJ-1 and loss of PTEN associated with tumor metastasis and correlated with poor prognosis of gastric carcinoma. International journal of medical sciences. 2013;10(12):1689-97. Epub 2013/10/25.
63. Yun J, Finkel T. Mitohormesis. Cell Metab. 2014;19(5):757-66. Epub 2014/02/25.
64. Shore DE, Carr CE, Ruvkun G. Induction of cytoprotective pathways is central to the extension of lifespan conferred by multiple longevity pathways. PLoS genetics. 2012;8(7):e1002792. Epub 2012/07/26.
65. Bjelakovic G, Gluud C. Surviving antioxidant supplements. Journal of the National Cancer Institute. 2007;99(10):742-3. Epub 2007/05/17.
66. Bodea LG, Wang Y, Linnartz-Gerlach B, Kopatz J, Sinkkonen L, Musgrove R, et al. Neurodegeneration by activation of the microglial complement-phagosome pathway. The Journal of neuroscience : the official journal of the Society for Neuroscience. 2014;34(25):8546-56. Epub 2014/06/21.
67. Cloutier M, Middleton R, Wellstead P. Feedback motif for the pathogenesis of Parkinson's disease. IET systems biology. 2012;6(3):86-93. Epub 2012/07/05.

Chapter 4

68. Cloutier M, Wellstead P. Dynamic modelling of protein and oxidative metabolisms simulates the pathogenesis of Parkinson's disease. IET systems biology. 2012;6(3):65-72. Epub 2012/07/05.
69. Cheng HC, Ulane CM, Burke RE. Clinical progression in Parkinson disease and the neurobiology of axons. Annals of neurology. 2010;67(6):715-25. Epub 2010/06/03.
70. DeNicola GM, Karreth FA, Humpton TJ, Gopinathan A, Wei C, Frese K, et al. Oncogene-induced Nrf2 transcription promotes ROS detoxification and tumorigenesis. Nature. 2011;475(7354):106-9. Epub 2011/07/08.
71. Fujita KA, Ostaszewski M, Matsuoka Y, Ghosh S, Glaab E, Trefois C, et al. Integrating pathways of Parkinson's disease in a molecular interaction map. Molecular neurobiology. 2014;49(1):88-102. Epub 2013/07/09.
72. Ray PD, Huang BW, Tsuji Y. Reactive oxygen species (ROS) homeostasis and redox regulation in cellular signaling. Cell Signal. 2012;24(5):981-90. Epub 2012/01/31.
73. Squadrito GL, Pryor WA. Oxidative chemistry of nitric oxide: the roles of superoxide, peroxynitrite, and carbon dioxide. Free radical biology & medicine. 1998;25(4-5):392-403. Epub 1998/09/19.
74. Dijkstra G, Blokzijl H, Bok L, Homan M, van Goor H, Faber KN, et al. Opposite effect of oxidative stress on inducible nitric oxide synthase and haem oxygenase-1 expression in intestinal inflammation: anti-inflammatory effect of carbon monoxide. The Journal of pathology. 2004;204(3):296-303. Epub 2004/10/12.
75. Guzik TJ, West NE, Pillai R, Taggart DP, Channon KM. Nitric oxide modulates superoxide release and peroxynitrite formation in human blood vessels. Hypertension. 2002;39(6):1088-94. Epub 2002/06/08.
76. Zulueta JJ, Sawhney R, Kayyali U, Fogel M, Donaldson C, Huang H, et al. Modulation of inducible nitric oxide synthase by hypoxia in pulmonary artery endothelial cells. Am J Respir Cell Mol Biol. 2002;26(1):22-30. Epub 2001/12/26.
77. Tanner FC, Meier P, Greutert H, Champion C, Nabel EG, Luscher TF. Nitric oxide modulates expression of cell cycle regulatory proteins: a cytostatic strategy for inhibition of human vascular smooth muscle cell proliferation. Circulation. 2000;101(16):1982-9. Epub 2000/04/26.
78. Scicinski J, Oronsky B, Ning S, Knox S, Peehl D, Kim MM, et al. NO to cancer: The complex and multifaceted role of nitric oxide and the epigenetic nitric oxide donor, RRx-001. Redox biology. 2015;6:1-8. Epub 2015/07/15.
79. Chang CF, Diers AR, Hogg N. Cancer cell metabolism and the modulating effects of nitric oxide. Free radical biology & medicine. 2015;79:324-36. Epub 2014/12/03.
80. Jahani-Asl A, Bonni A. iNOS: a potential therapeutic target for malignant glioma. Current molecular medicine. 2013;13(8):1241-9. Epub 2013/04/18.
81. Somasundaram V, Nadhan R, S KH, Kumar Sengodan S, Srinivas P. Nitric oxide and reactive oxygen species: Clues to target oxidative damage repair defective breast cancers. Critical reviews in oncology/hematology. 2016. Epub 2016/03/28.

Chapter 5

Integrative Systems Toxicology models

5A. Sharma, R. P., Schuhmacher. M., Kumar V., 2017. Developing Integrated PBPK/PD Coupled mechanistic pathway model (miRNA-BDNF): an approach towards Systems toxicology, Toxicology Letters 280:79-91.

5B. Sharma, R.P., Alexey Kolodkin., Schuhmacher, M., Kumar, V., Hans V. Westerhoff., 2018. All- in-One-Model to understand hepatotoxicity: From organ-specific pharmacokinetics of Flutamide to predicting its personalised pharmacodynamics effects (under revision).

Chapter 5

5A. Developing an Integrated PBPK/PD Coupled mechanistic pathway model (miRNA-BDNF): an approach towards Systems Toxicology

Abstract

Integration of a dynamic signal transduction pathway into the tissue dosimetry model is a major advancement in the area of computational toxicology. This paper illustrates the ways to incorporate existing systems biological models in the field of toxicology via its coupling to the Physiologically based Pharmacokinetics and Pharmacodynamics (PBPK/PD) model. This expansion framework of integrated PBPK/PD coupled mechanistic system pathway model can be identified as systems toxicology that describes the kinetics of both the chemicals and the biomolecules, help us to understand the dynamic and steady-state behaviors of molecular pathways under perturbed condition. The objective of this article is to illustrate a systems toxicology based approach by developing a PBPK/PD integrated with miRNA-BDNF pathway model and to demonstrate its application by taking a case study of PFOS mediated neurotoxicity. System dynamics involves miRNA-mediated BDNF regulation, which plays an important role in the control of neuronal cell proliferation, differentiation, and survivability.

Key words: PBPK/PD, miRNA, BDNF, Neuroendocrine, System biology, PFOS

Highlights

- mi-RNA-based post-transcription regulations of BDNF was modeled and proposed.
- The model simplifies the mechanistic features of BDNF induces cell survivability.
- BDNF can be a good biomarker linking environmental exposure to neuronal disorders.
- Integrated PBPK/PD for the PFOS induced neurotoxicity was proposed.

Chapter 5

1. Introduction

In the field of quantitative risk assessment, a journey of classical dose-response models is categorized into different classes for the better quantification and estimation of early possible risk (Andersen et al. 2005). These include –a) Physiological based pharmacokinetic and pharmacodynamic modeling (PBPK) for the quantification of internal biophase concentrations in different tissues, b) pharmacodynamics (PD) model quantifies the interactions of chemicals with target biomolecules c) Systems Biology describes the dynamic relationship of biological components for a robust physiological response. Perturbation of these biological components can be quantified through the integration of PBPK/PD model into the system biological models providing a predictive tool for measuring toxicological impact at the cellular and biomolecular level (Andersen et al. 2005; Gohlke et al. 2005; Zhao and Ricci 2010).

The PBPK model in the area of dosimetry risk assessment has been widely accepted and applied and it is among the top priority tool recommended in the vision of toxicity testing in the 21st century (Andersen and Krewski, 2009). PBPK model has been extended to develop the PBPK/PD for certain pesticides (Timchalk et al., 2002; Foxenberg et al., 2011). The integration of PD was generally done with the quantification of the response variable (biomarker) effect of an interaction of a chemical (biophase concentration estimated by PBPK) with a target biomolecule (mainly receptors). But it has a certain limitation such as lack of robust biology (biomarker relation to endpoint), and very often the endpoints are specifically remained single explanatory biomarker. Coupling of PBPK/PD model and system biology together can enlighten the effect of changes in key biomolecules considering the whole biological system. System biology comprising of genomics, metabolomics, and proteomics which rationalizes the functional interaction of biological components in a time-dependent fashion (Aderem, 2005; Kitano, 2002). Thus, it could be useful in systems toxicology for understanding the altered biological pathway due to chemical induced perturbation of certain key biomolecule in a system, illustrating differences from normal pathway (Arrell and Terzic, 2010; Auffray et al., 2009; Hood et al., 2004; Kell, 2006). Understanding the biomolecular mechanisms are of great interest to identify the toxicological effects at the very early stages of the disease (toxicological response). However, often we lack sufficient information to link chemically perturbed biological components (molecular biomarker) to an altered biological system. This lead to the use of the simplified dose-response model (simple PD) to predict the adverse outcome (disease) for a target chemical(Calabrese and Baldwin, 2003). In the field of toxicology, there is limited use of these system biology models (Waters et al., 2003). The wide use of systems toxicology in human environmental risk assessment has a time lag in comparison with pharmaceuticals science as it lacks experimental data, has complex interaction pathways of environmental chemicals than the target specific drugs, and low commercial priority of applied toxicological science.

Recently use of the integrated PBPK/PD models in a field of environmental toxicology, enables development of a quantitative biologically based risk model which increases our understanding towards the relationship between tissue bio-phase concentration of chemicals and endogenous biomolecule (Timchalk et al., 2002; Foxenberg et al., 2011). Furthermore, signaling pathways could be used as an extension of PBPK/PD, given dynamic interactions of chemicals with biological components are known, the first step towards systems toxicology (Bhattacharya et al., 2012; Gim et al., 2010). It has benefits

Chapter 5

such as: easy to implement if the signaling pathway already developed, often data from the dose-response experiments for known biomolecules can be used, a good step to use Adverse Outcome Pathways (AOPs) knowledge to develop the generic PBPK/PD model for multi-species and multi-chemicals.

Neuroendocrine or neurotrophins such as nerve growth factors, BDNF and neurotrophin-3 are proteins, basically processed and secreted in constitutive and regulatory fashion in non-neuron, neurons and neuroendocrine cells (Lu, 2003; Mowla et al., 1999). Among them, BDNF is immensely expressed and extensively scattered than other neurotrophins, and play an important role in neuronal survival and differentiation (Boulle et al., 2012; Michael et al., 1997; Murer et al., 2001). BDNF binds with a Tropomyosin receptor kinase B (TrkB) presents on the neuronal cell surface causing sequential activation of following pathways such as Mitogen-activated protein kinases (MAPKs), Extracellular-signal-regulated kinase (ERK), and Protein kinase B (AKT) that are mainly involved in differentiation and survivability of neurons (Michael et al., 1997; Murer et al., 2001 Bursac et al., 2010; Boulle et al., 2012). It has been seen that reduced BDNF protein and mRNA expression is linked with several neurological disorders such as Alzheimer's and Parkinson's (Bursac et al., 2010). Moreover, dopaminergic, GABAergic, cholinergic, and serotonergic neurons are known to require BDNF for their proper development and survival (Lipsky and Marini, 2007; Murer et al., 2001), signifies BDNF as an important biomarker for neurodevelopmental function.

It has been reported that miRNA regulates the synthesis of BDNF via posttranscriptional modification of BDNFmRNA (Caputo et al., 2011; You et al., 2016). Muiños-Gimeno et al., (2011) reported the involvement of miRNA-22 associated panic disorders in the Spanish and North European population. Later, the transcriptomic analysis studied by Li et al., (2015) in SH-SY5Y cell line also found the involvement of miRNA-22 dependent decrease in the BDNF level and neuronal cell survivability. The miRNAs are turning out to be significant regulators of mRNAs and the related proteins. In this proposed study, miRNA (micro-RNA) regulated BDNF (Brain- derived neurotropic factor) and its effect on neuronal survivability mechanisms was selected for the development of the mechanistic base model. Perfluorooctanesulfonic acid (PFOS) was selected as a case study to illustrate the ways to incorporate the use of system biological model in the field of toxicology via Pharmacodynamic coupled tissue dosimetry model (PBPK/PD).

1.1. Case studies on PFOS

PFOS is well recognized among industrial chemicals that can easily cross the BBB (blood brain barrier) (Sato et al., 2009) and its exposure was related to several developmental neurotoxicity effects (Johansson et al., 2008; Yang et al., 2015; Goudarzi et al., 2016; Vuong et al., 2016) . For instance, it was found that PFOS exposure to zebrafish causing an alteration in the expression of more than 40 different type of miRNAs allied with the developmental toxicities (L. Zhang et al., 2011). The several mechanisms were hypothesized for the PFOS causing development neurotoxicity disorders such as oxidative stress, altering neurotransmitters level and upregulation and downregulation of apoptotic and pro-survival factors from various animals and cell line studies (Long et al., 2013; Chen et al., 2014; Yu et al., 2016). In a recent study, it was found that PFOS can decrease the neuronal cell survivability by altering the level of miRNA in human neuroblastoma cell line(Li et al., 2015). This could be an important mechanism of PFOS

as it has been seen that miRNAs regulate the proteins level by regulating their mRNAs expression level. The purpose of our model is to test the hypothesis that PFOS perturbed the miRNA affecting neuronal survivability via regulating BDNF at mRNA level. The human dosimetry study has shown the longer residence time of PFOS inside the body and relatively higher concentration in the brain tissue than comparing to other perfluoroalkyl substances (PFASs) (Fabrega et al., 2014). Furthermore, its continuous exposure and potential to cross the BBB could put the humans at high risk of neurodevelopmental disorders which is in consonance with recently published paper related to neurotoxicity of PFOS (Yang et al., 2015; Vuong et al., 2016). The PFOS PBPK model has been well developed previously by Fabrega et al., (2014) that predicts internal tissue dose. However, for a better understanding of toxicological mechanisms in the context of risk assessment, we would need one more step towards the systems toxicology. This gap could fill by coupling integrated PBPK/PD model into a mechanistic system model.

The objective of this study was the development of a mechanistic pathway system (miRNA-BDNF mRNA- BDNF- cell survivability) model and coupling of above model with a PBPK/PD taking a case study of the PFOS induced neurotoxicity.

2. Materials and Methods

2.1. **miRNA-mRNA-BDNF-cell survival mechanistic pathway (figure 1)**

Generally, miRNA post-transcriptionally regulates the protein molecule via binding at 3´UTR of mRNA (Perruisseau-Carrier et al., 2011). It has been found that miRNA decreases the level of BDNF either via degradation of mRNA or facilitating ribosome induced silencing complex formation with mRNA (RISCm) (Bartel 2004; Djuranovic et al. 2011). The other mechanism involves miRNA inhibits the BDNF regulation by down regulating the expression ofcyclic response element-binding protein (CREB) (Caputo et al. 2011;You et al. 2016).

Nonetheless, the numbers of the regulatory pathways have been proposed (Zeng et al., 2 011; Sandhya et al., 2013; York, 2015). Moreover, a study on population affected with neuronal disorders showed an inverse relationship between miRNA and BDNF level (M uiños-Gimeno et al., 2011) strengthens the evidence of regulation of BDNF via miRNA. BDNF dependent cell survival pathways can be extremely important from a regulatory perspective. The relationship between BDNF concentration and cell survival are quite well known via the dose-response curve obtained from the in-vitro cell line study (O'Leary and Hughes, 1998). Nevertheless, intermediate molecular signaling pathways are prevailed in-between the binding of BDNF with TrkB receptors to the effects on the neuronal cell. This involves activation of MAPK/ERK and AKT-PI3K pathways that increase the neuronal survival and differentiation process via increasing expression of CREB (Michael et al., 1997; Murer et al., 2001 Bursac et al., 2010; Boulle et al., 2012). The conceptual diagram is provided in figure 1.

Chapter 5

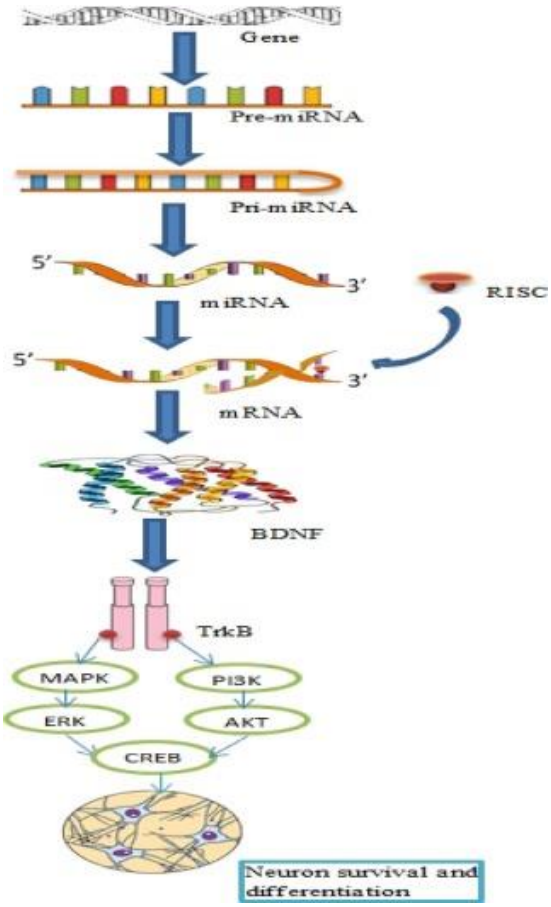

2.1.1. miRNA regulatory BDNF pathway model

The regulatory pathway of BDNF involves different intermediate biomolecules. However, in this study, the generic miRNA-BDNF pathway was adapted from the previously published work of Wang et al., (2010) to developed exclusively miRNA regulatory BDNF model. The whole pathways are modeled by applying mass balance equation based on reaction kinetics applying ordinary differential equations. This allows the estimation of a biomolecule given the model parameter corresponds to the reaction rates. BDNF is the output of the miRNA-BDNF model, which was then used as an input for the estimation of neuronal survival. The generic form of the system dynamic model is as follow:

Chapter 5

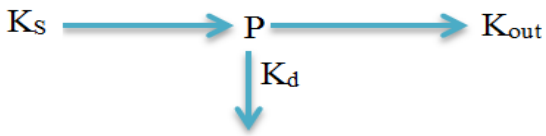

Where ks is synthesis rate constant for the endogenous molecules, P is the concentration of an endogenous molecule, kd is the degradation rate constant, kout is the dissipation rate constant of P available for the synthesis of the subsequent endogenous molecule. Following this schematic, concentration of endogenous biomolecules is estimated by the following differential equation;

$$\frac{\mathrm{d}}{\mathrm{dt}}(\mathrm{P}) = \mathrm{ks} - \mathrm{Kd} * \mathrm{P} - \mathrm{kout} * \mathrm{P} \quad \textbf{(1)}$$

2.1.2. BDNF - cell survival Emax model-

To simplify the model, we have applied hills sigmoid equations to get the output of the neuronal survival by applying Emax and EC50 value of BDNF for neuronal cell survival from experimental data (O'Leary and Hughes, 1998). The percentage of cell survivability with respect to BDNF concentration was estimated by the use of sigmoid Emax model applying the following equations;

$$\text{Cell survivablity} = \mathrm{E0} + ((\mathrm{Emax} * \mathrm{C}^{\mathrm{n}})/\ (\mathrm{EC50} + \ \mathrm{C}^{\mathrm{n}})) \quad \textbf{(2)}$$

Where, Cell survivability = percentage of cell survivability as function of BDNF conc., Eo = baseline response, Emax = maximum response, C= BDNF concentration, EC50= concentration at which BDNF shows 50% response of Emax, n= hill coefficient

This developed Emax model was integrated into indirect response model eq. (3) that provides the neuronal cell survivability as a function of time. More details on indirect response models can be found in Bonate, (2011).

$$\frac{d}{dt} Cell\ survivablity\ = kout\_BDNF * cell\ survivablity - kd * cell\ survivability(t) \quad \textbf{(3)}$$

Where, $\frac{\mathrm{d}}{\mathrm{dt}}$Cell survivability $=$ percentage of cell survivability in the time domain, kout_BDNF is BDNF conc. assumed to be responsible for neuronal cell survivability, kd is the degradation rate of the neuronal cell.

2.2. PFOS PBPK (a case study)

The PBPK model of PFOS was adapted from the previously published model (Fabrega et al., 2014). The concentration of PFOS in a brain considered as the effective target dose (target tissue dosimetry), considering the brain as a target organ in relation to potential neurodevelopment deficit disorders. PBPK model generates time course of PFOS concentration in the brain, which is used as input for the mechanistic pathway model. At the end, integration of the PBPK model of PFOS into the mechanistic BDNF –cell

survivability model analyzes the perturbation of PFOS on the whole pathway results in decreased in neuronal cell survival rate. The conceptual model for this integration is provided in figure 2.

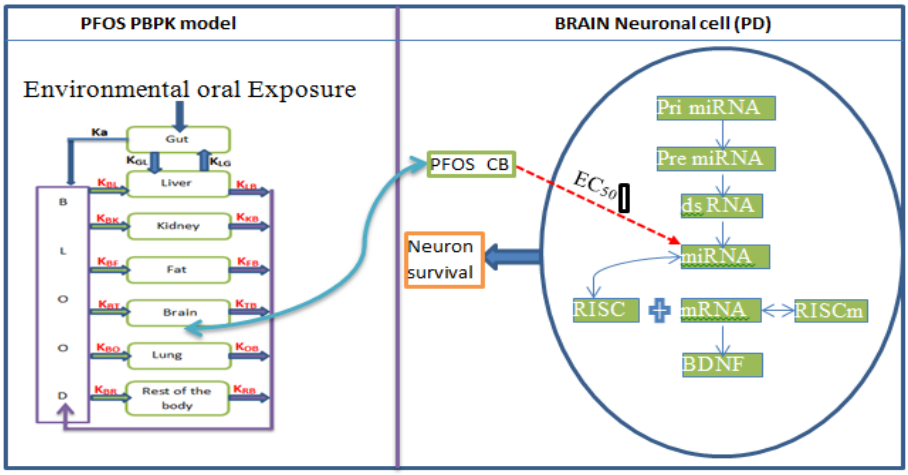

Concentrations in the respective compartment (muscle, richly perfused, fat, kidney, Brain and liver) are estimated by applying the following equation:

$$\frac{dCi}{dt} = \frac{Qi \times \left(Ca - \frac{Ci}{Ki:p} \right)}{Vi} \qquad \textbf{(4)}$$

Where, Ci is the concentration in the tissue i (ng/L), Qi is the blood flow in the tissue i (L/h), Ca is the arterial concentration (ng/L), Ki: p is the partition coefficient of tissue i, and Vi is the volume of the tissue i (L). Detail description of PBPK model can be found in our other publications (Fabrega et al., 2014; Fàbrega et al., 2016).

All the physiological, physicochemical parameters and model equations for the PBPK are provided in the Annex-5

2.3. IVIVE for dose Equivalency

In-vitro in-vivo extrapolation (IVIVE) method was used in order to estimate the oral equivalent dose from the given in-vitro dose. It has an assumption that the in-vitro area under the curve (AUC), calculated by multiplying dose with the total duration of exposure, would be similar with the AUC of target in-vivo organ (in this case Brain).

Li et al., (2015) in-vitro studies on SH-SY5Y cell line was selected, where a decrease in neuronal cell survivability found to depend on miRNA and BDNF. In Li et al., an

Chapter 5

experiment they used 12 in-vitro doses (6 doses each for 24hr and 48 hr) for that corresponding in vivo doses was determined. The assumption was made that in-vitro doses are equivalent to internal target concentration (brain). For the reconstructing equivalent oral dose, the AUC value was calculated for each in-vitro conc., based on their duration of treatment (In this case 24hr and 48 hr). The conceptual schematic for dose reconstruction is provided in figure 3. The calculated AUC was assumed to be equivalent with in-vivo AUC brain. Dose reconstruction approach has been used, so that the given equivalent oral dose will provide the AUC in the brain that matches the AUC for the 12 different in-vitro doses (6 for 24hr and 6 for 48hr), a similar approach has been used in the previous study (Thiel et al., 2017). The oral equivalent doses were estimated to be way higher, as the PFOS concentration reaching to the brain was found to be relatively very low(Fabrega et al., 2014; Fàbrega et al., 2016). The estimated oral equivalent doses for the corresponding in-vitro doses are provided in Table 1.

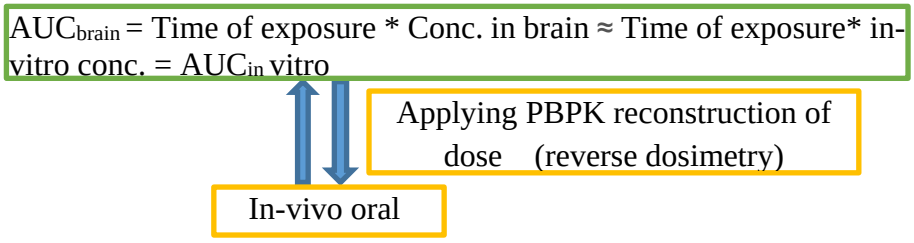

Figure 3. Describes the schema for the estimation of in-vivo oral dose

Table 1: oral equivalent dose calculated based on AUC extrapolation method

in-vitro dose (µM)	AUC_24 (nM*hr)	AUC_48 (nM*hr)	in-vivo **dose (nM)**(24**hr**)	in-vivo **dose (**nM**)** (48**hr**)
1	24000	48000	86925	130570
10	240000	480000	896550	1362850
50	1200000	2400000	4494910	6839718
100	2400000	4800000	8992868	13685810
150	3600000	7200000	13490820	20531899
200	4800000	9600000	17988780	27378025

Chapter 5

2.4. Integrated PBPK/PD coupled miRNA-BDNF-cell survival pathway

Coupling of PBPK to mechanistic miRNA-BDNF pathway model has been done with the integration of brain PFOS concentration as a target input that perturbs key component miRNA of the pathway. The interaction of the PFOS with the miRNA has done based on empirical evidence but the mechanism behind the interaction is still not clear. The coupling was done by applying stimulatory Emax model that assumes PFOS increase the concentration of miRNA via increasing their synthesis rate. Finally the output we measured as a percentage of neuronal survival rate considering two scenarios; with and without PFOS exposure. The conceptual diagram is provided in figure 4.

The integration of PFOS into the BDNF pathway is done by indirect pharmacodynamic interaction model with the following equation;

$$\frac{d}{dt}(miRNA) = K_{in_{miRNA}} * \left(1 + \frac{Emax*C}{EC_{50}+C}\right) - K_{out_{miRNA}} * miRNA_0 \quad \textbf{(5)}$$

Where, $K_{in_{miRNA}}$ = synthesis rate constant of miRNA, $K_{out_{miRNA}}$ = dissipation rate of miRNA, $miRNA_0$ = initial value of miRNA, Emax = maximum response for miRNA, C = brain concentration of PFOS, EC50 = concentration at which PFOS shows 50% response of Emax.

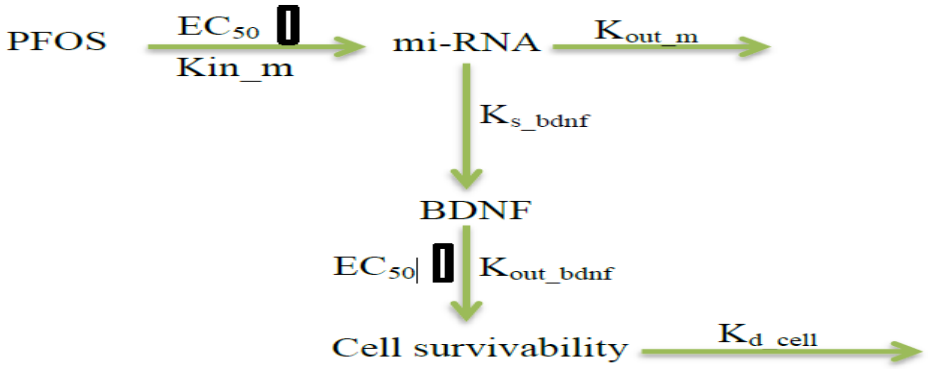

Fig. 4. Represents the pharmacodynamics interaction of PFOS-miRNA and the consequent effect on neuronal survivability rate.

2.5 Model parameterization

The mi-RNA-mRNA-Protein pathway parameters were taken from the previously published model (Wang et al., 2010). Specifically, BDNF protein synthesis rate was used instead of generic protein synthesis. There was no BDNFmRNA synthesis rate data available in the literature and for that generic BDNFmRNA rate constant was used. BDNF synthesis rate was taken from the Castillo et al., (1994) and Menei et al., (1998). Furthermore, the synthesis rate was scaled accounting number of neuronal cells to the whole body per kg weight nmol/hr/kg$^{(0.75)}$. The degradation rate of BDNF was

Chapter 5

parameterized from half- life by using the following relationship: degradation rate = $Ln2/t_{1/2}$.

For the quantification of neuronal survival against BDNF exposure, the required Emax and EC50 parameters for establishing sigmoid Emax model were taken from O'Leary and Hughes,(1998). The Emax and EC50 values for the reaction are implemented as such as these parameters tend to have a similar trend across species (Mager et al., 2009). PBPK parameters for the PFOS were used from the previously published article (Fabrega et al., 2014). The dynamic interaction data for the PFOS to miRNA, such as EC50 estimated from Li et al., (2015). All the parameters that were used for developing mechanistic model are provided in Table 2. All the model equations for the mechanistic and integrated PBPK/PD-mechanistic models are provided in the Annex-5

Table 2. Scaled parameters for Coupled PBPK/PD mechanistic pathway model.

Description	**Parameter symbol**	**Value**	**References**
BDNF synthesis rate	Kin_BDNF	0.023 nM/hr/kg 0.75	(Menei et al., 1998)
BDNF dissipation rate	Kout_BDNF	$0.231hr^{-1}$	(Fukumitsu et al., 2006)
Maximum BDNF effect on cell survival	Emax	100	Assumed
Half maximum concentration of BDNF for neuron survivability	EC50_BDNF	$5\ X10^{-3}$ nM	(O'Leary and Hughes, 1998)
Cell degradation constant	Kd_cell	$2.45\ X\ 10^{-5}$ hr^{-1}	(Clarke et al., 2000)
Maximum PFOS effect on miRNA	Emax_miRNA	2.4	Fixed as similar with maximum fold change(Li et al., 2015)
Half maximum stimulatory concentration of PFOS for miRNA	EC50_PFOS	1000 nM	(Li et al., 2015)

Chapter 5

Volume of cytoplasm	V_cyt	4 $X10^{-12}$ L	(Bartlett and Davis, 2006)
Volume of nucleus	V_nucleus	4 X 10^{-13} L	(Carlotti et al., 2000)
Pri miRNA synthesis rate	k_primiRNA	3.6 nM/hr	(Pérez-Ortín et al., 2007)
mRNA synthesis rate	k_mRNA	0.36 nM/hr	(Bartlett and Davis, 2006)
Adjusted Coefficient of R promoting pri-miRNA maturation	R_miRNA	0.001 nM	(Wang et al., 2010)
pri-miRNA to pre-miRNA(n) catalyzed by R	k_primiRNA-premiRNA	360 hr^{-1}	(Wang et al., 2010)
premiRNA transport rate	T_premiRNA	180 hr^{-1}	(Wang et al., 2010)
Rate of premiRNA(c) conversion to dsmRNA	k_premiRNA-dsmRNA	36 hr^{-1}	(Ma et al., 2008)
miRNA formation rate	k_miRNA	36 hr^{-1}	(Kohler and Schepartz, 2001)
miRNA-induced RISC formation rate	k_RISC	108 hr^{-1}	(Bartlett and Davis, 2006)
mRNA-RISC complex formation rate	k_[mRNA-RISC]	3.6 nM/hr	(Haley and Zamore, 2004)
mRNA cleavage rate	kc_mRNA	25.27 hr^{-1}	(Haley and Zamore, 2004)
Dissociation rate of RISC complex	kd_[mRNA-RISC]	3.6 hr^{-1}	(Wang et al., 2010)

Rate of pri-miRNA degradation	d_primiRNA	0.9 hr^{-1}	(Wang et al., 2010)
Rate of pre-miRNA(c) degradation	d_premiRNA	0.9 hr^{-1}	(Wang et al., 2010)
Rate of dsRNA degradation	d_dsRNA	3.96 hr^{-1}	(Wang et al., 2010)
Rate of miRNA degradation	d_miRNA	0.9 hr^{-1}	(Wang et al., 2010)
Rate of RISC degradation	d_RISC	0.36 hr^{-1}	(Wang et al., 2010)
Rate of mRNA-bound RISC complex degradation	d_[mRNA-RISC]	0.077 hr^{-1}	(Wang et al., 2010)
Rate of mRNA degradation	d_mRNA	0.36 hr^{-1}	(Wang et al., 2010)

3. Results

The simulation of the model is divided into two parts; first simulations of a PBPK and a mechanistic system pathway model individually to get the base model. Later simulation of integrated PBPK/PD coupled mechanistic model (systems toxicology) was done. The integration of Pharmacodynamic interaction between PFOS and target biomolecule was done by using indirect response model. The equivalent exposure doses for the PFOS were extrapolated from the in-vitro study of Li et al., (2015). Neuronal survivability was chosen as an end point biomarker for the model and mapping of in-vitro data (neuronal survivability) to in-vivo was done based on linear interpolation method. The PFOS PBPK model codes are provided by Fabrega et al., (2014) which was used in this paper to simulate PBPK model.

The mechanistic system model simulations were performed for the miRNA-BDNF signaling pathway and the resulting time course of BDNF was recorded as model output. The output of the BDNF time course data was used for performing the simulation to get the percentage of cell survivability by applying indirect sigmoid response model. This part of simulation results recorded as the normal baseline value for the model. The figure 6 (base model of the mechanistic pathway) showed the baseline value of important endogenous biomolecules like miRNA, BDNF, RISC(RNA- induced silencing complex), RISCm (complex form between BDNFmRNA and RISC) and percentage of neuronal cell survivability. The mechanistic system model has optimized to achieve the maximum neuronal cell survivability steady state which is in compliance with experiment data given

Chapter 5

by Gillespie et al., (2003). The model has been simulated for 20 days in order to achieve the steady state. The miRNA regulation of BDNF via forming a complex between RISC and BDNFmRNA called RISCm has been documented can be seen in the base model figure number 6 which is in compliance with Wang et al., (2010) model. This complex formation between RISC and BDNFmRNA was enhanced by the miRNA resulting in a decrease of BDNF protein synthesis. The RISC complex binds with the mRNA at the 3' UTR and inhibits its further translation to protein. The base model also able to capture the phenomena of regulating BDNF protein by miRNA considered to be one of the important biological processes. The behavior of model curve for BDNF and cell survival are in a similar trend, which was also observed in in-vivo experiments (Rodríguez-Tébar et al., 1992; O'Leary and Hughes, 1998; Fletcher et al., 2008). The model shows BDNF maintains cell survivability at the steady state level of around 95 percent. In Figure (6), a sudden drop in the cell survivability to 40 percent level could be explained considering the lag time in the attainment of BDNF steady state level. The simulation of the base model (Figure 6) shows that model able to retain the steady state for cell survivability at 95% once BDNF attained a steady state. A similar observation was reported by Gillespie et al., (2003) experimental study that survivability of neuron in presence and absence of BDNF were 90 percent and 40 percent respectively.

The PBPK model simulation was carried out for the PFOS for the estimated oral equivalent dose (12 doses) given as a single dose. Figure 5 shows the simulation of the internal target tissue (brain) concentration of PFOS with 12 different dose levels providing different Cmax in dose dependent manner over the time period. The dose was given at the 240hr as shown in figure 6 when the mechanistic base model reaches steady state.

The figure shows a simulation of the time course of PFOS concentration in the brain for each 12 different doses corresponding to in-vitro dose. The single oral dose was given at 240hr.

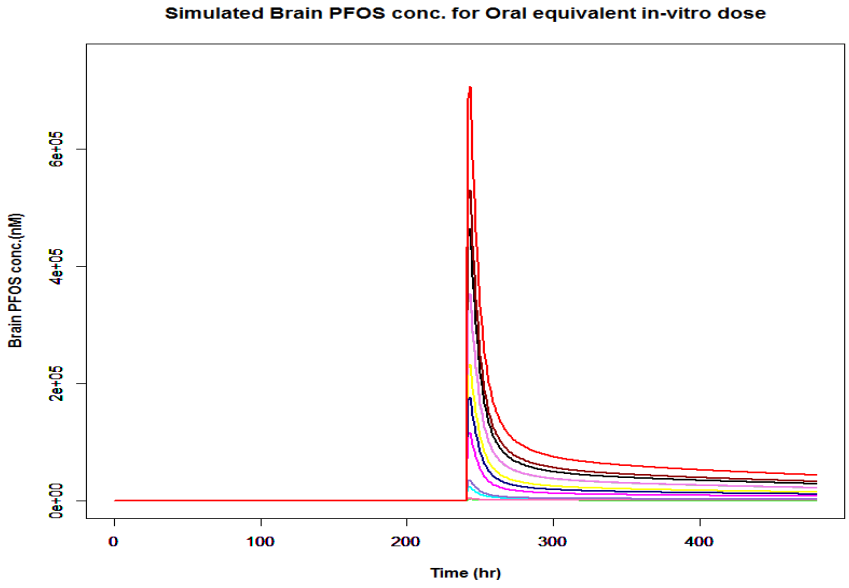

Chapter 5

Fig. 5. **Simulated brain concentrations of PFOS over the time period:** This figure shows a simulation of the time course of PFOS concentration in the brain for each 12 different doses corresponding to in-vitro dose. The single oral dose was given at 240hr.

The coupling of PBPK into the mechanistic model was done by fitting in-vitro data, estimated from Li et al., (2015) study, via applying Emax sigmoid model. The developed coupled PBPK/PD-mechanistic model quantifies the dynamic of the endogenous biomolecular concentration of different species at the different level of PFOS exposure that perturb key components of the system (in the miRNA model). The interaction of the PFOS to the given pathway was modeled by implementing indirect sigmoid response model **Eq. (5)** for PFOS-miRNA interaction. Consequently, dynamic changes in miRNA level as a function of PFOS concentration over time was observed (figure 7). The PFOS alter the steady state of all biological components involved in the pathway via stimulating input of miRNA disturbing whole mechanistic pathway. The integrated model was simulated for 12 different in-vitro equivalent in-vivo doses describing the whole system as one unit rendering time course of endogenous concentration after exposure to environment chemicals distinct from normal condition (Base model).

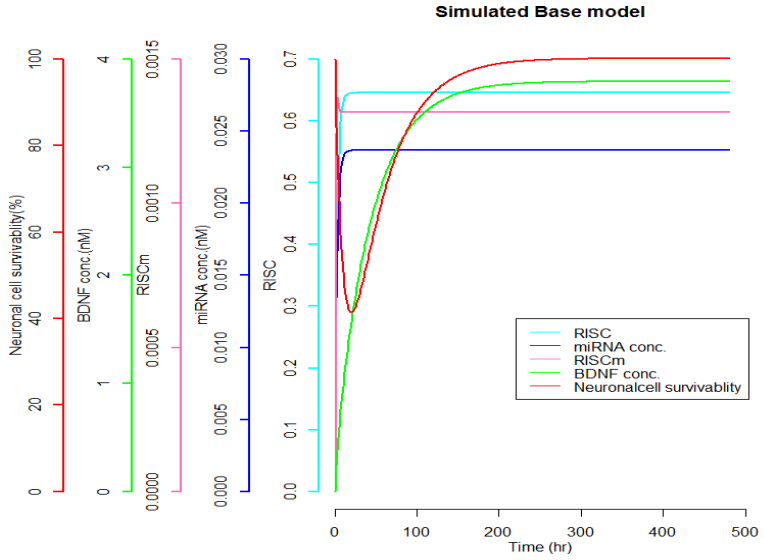

Fig. 6. **Mechanistic base models**

The figure shows simulated key biomolecules such as RISC, miRNA, RISCm, BDNF and percentage neuronal cell survivability.

Chapter 5

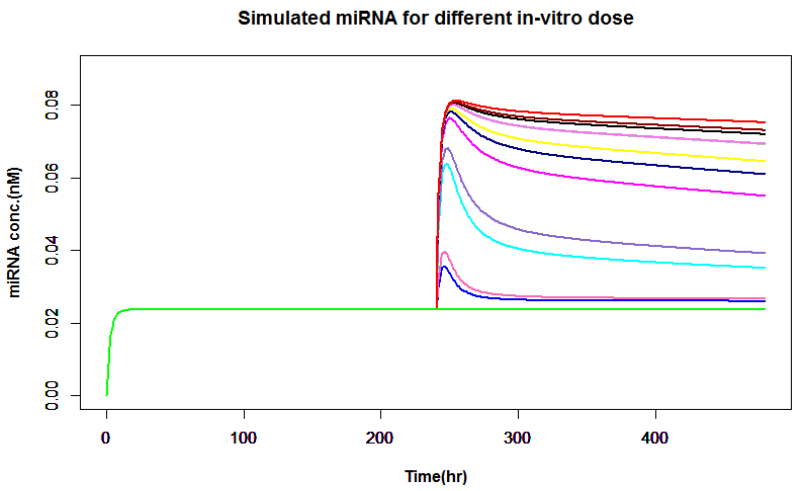

Fig.7. **Simulated time vs miRNA level:** Figure depicts simulated miRNA concentration after single oral dose of PFOS for 12 different dose levels.

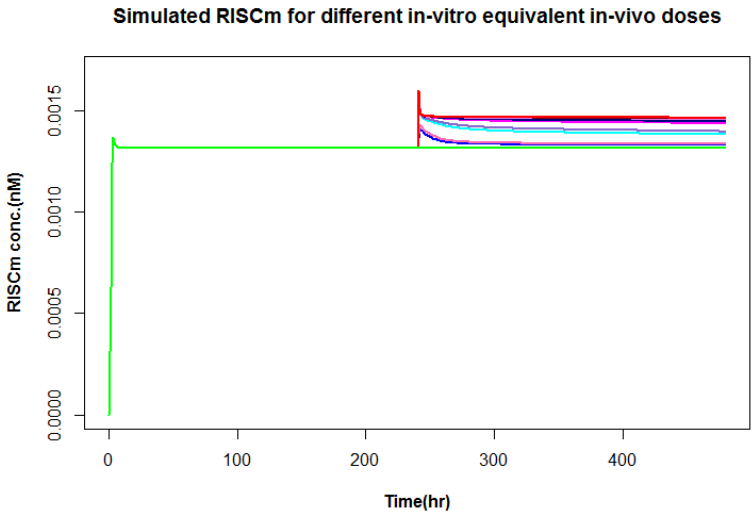

Fig. 8. Simulated time vs RISCm level. The figure shows the increase in RISCm level after single oral dose of PFOS for 12 different dose levels.

Chapter 5

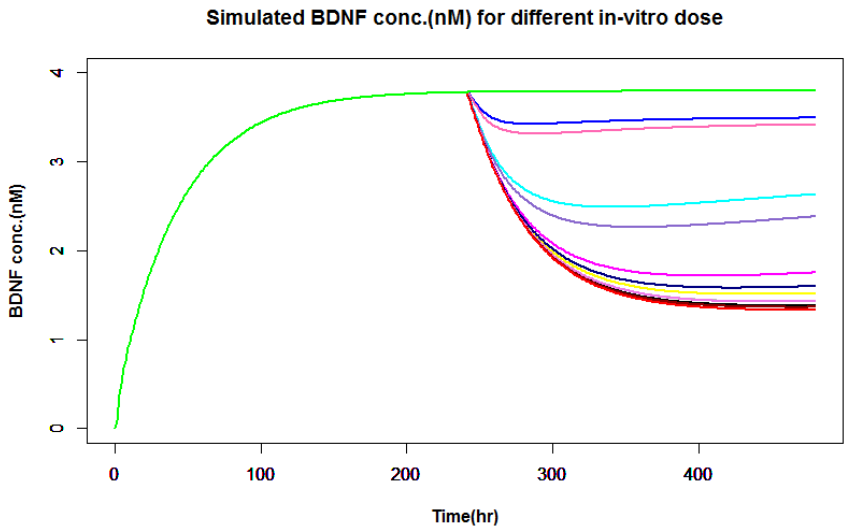

Fig. 9. Simulated time vs BDNF level. The figure depicts simulated BDNF concentration after single oral dose of PFOS for 12 different dose levels.

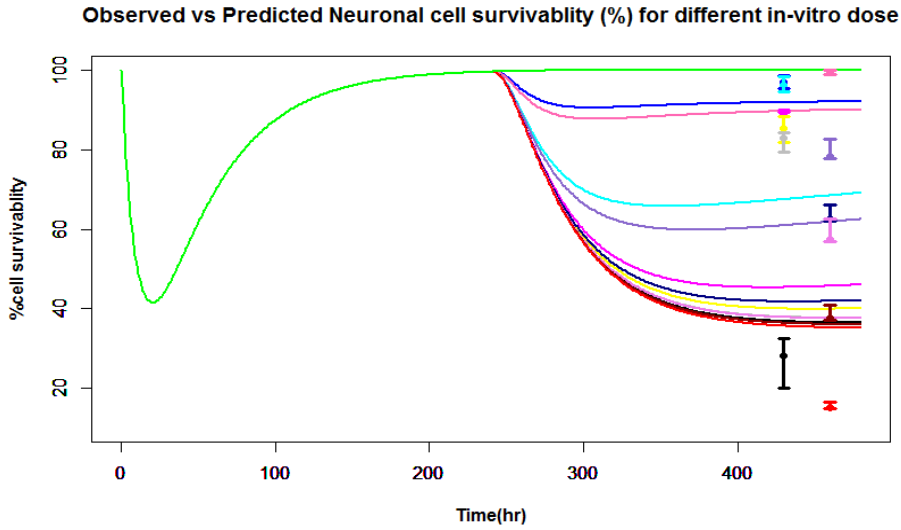

Fig. 10. Simulated vs predicted neuronal cell survivability (percentage). The figure depicts simulated vs observed neuronal cell survivability (percentage) after single oral dose of PFOS for 12 different dose levels.

The figure 7, 8, 9 and 10 shows the effect of a chemical on the endogenous biomolecule concentration (miRNA, RISCm, BDNF) and cell survivability (in percentage) respectively over the time period. Figure 7 illustrates the dose depended effects of PFOS

on miRNA level following single exposure to PFOS (dose given at 240hr). Figure 8 illustrates the increase in the formation of the RISCm complex after the PFOS exposure. The increase of RISCm complex concentration is due to increase of miRNA level which can be considered as an indirect action of PFOS. The highest level of miRNA is observed at tmax (time point of Cmax) of PFOS and, with the elimination of PFOS from the system, shifting of miRNA level to steady state concentration at the level higher than baseline concentration was observed. Consequently, a decrease in the level of BDNF (figure 9) was noted as increase miRNA level facilitates the formation of the RISCm (figure 8), posttranscriptional regulatory mechanism of miRNA (explained in 2.1). With the increase in dose level, the difference between base steady state concentration and shifted steady state concentration was higher that can be seen in figure 7, 8, 9 and 10. Figure 10, illustrates the time vs neuronal survivability that describes the effect of PFOS over time as an end point biomarker.

4. Discussion and Conclusions

In this study, an attempt was made for the development of an integrated PBPK/PD coupled mechanistic model that allows assessing or characterizing the potential impact of environmental chemicals on a biological system. An Integrated PBPK/PD PFOS model and a mechanistic (miRNA-BDNF-neuronal survival) system model were evaluated individually. The generic mi-RNA model was adapted with a modification in BDNF as a target output protein. The regulation of BDNF involves several pathways among which miRNA-dependent pathway is an important one. The endogenous level of BDNF has an important effect on the survivability of neurons. For example principal hierarchy of BDNF signaling and consequently activation of MAPK/ERK/AKT pathway is well understood (Michael et al., 1997; Murer et al., 2001 Bursac et al., 2010; Boulle et al., 2012), but how these events control cellular survival are not well understood. The reported relation between chemical exposure and significant changes in BDNF level, consequently neuronal adverse outcomes, made a plausible argument of considering BDNF as a good biomarker. To keep biological plausibility intact in our mathematical expression, we restrict our model to the miRNA-BDNF pathway, and later linking it to the cell survivability as a function of the time course of BDNF concentration by applying Emax model. The developed mechanistic model shows miRNA-dependent regulation of BDNF which is a natural phenomenon of this model retaining the regulatory mechanism of miRNA on BDNF. The mechanistic base model (figure 6) well predicted the percentage of cell survivability as a function of BDNF concentration. The PBPK model was used to estimate the internal target dose of chemicals. The output of PBPK in target organ is used as input for the mechanistic system model providing integrated coupled PBPK/PD-mechanistic system model. This will describe the whole system as one unit rendering time course of endogenous biomolecules concentration and their steady state level with and without chemical exposure marking the difference between the normal and altered biology of the pathway.

The integrated PBPK/PD- coupled mechanistic system model well describes the observed changes in endogenous molecules level during and after discontinuation of exposure to the chemical. It can predict the adverse effect of environment chemicals considering both; the nature of changes in the system (altered biology) with respect to normal biology, and, the capability of an endogenous molecule to retain homeostasis, mimicking the real in vivo physiological scenario. Therefore, this kind of model (integrated PBPK/PD- coupled

Chapter 5

mechanistic system model) can predict risk in more quantitatively as well as mechanistically considering pharmacokinetic, pharmacodynamic and relative altered biology from normal biology pathway as a consequence of chemical exposure. The advantage of Coupled integrated PBPK/PD- mechanistic system model is; it provides more understanding towards risk not only based on the target tissue concentration but also their effect on the target molecule participating in the biological network. Integrated PBPK/PD coupled mechanistic model are able to predict endogenous molecule concentration involved in pathway over their time course as a function of chemical exposure, which was shown by current developed model as a case study for PFOS

In summary, a molecular/cellular model that presented in this article mechanistically links BDNF involved in directed neuronal growth and neuronal survival, two distinct neurodevelopmental processes that use an overlapping molecular (that is genetic) machinery. The model does not provide further insights into which of these neurodevelopmental processes would be most relevant to the etiology of neurotoxicity, or where in the brain these processes are localized to selectively impact on neural circuitry. Although epigenetically regulation of BDNF (Lubin et al., 2008) in the brain by miRNA is very important were observed from literature in the theoretical network, it is unlikely that there would just be a single explanatory model that connects to BDNF on a molecular level and corresponding neuronal adverse outcomes. Rather, several etiological cascades contributing to neuronal adverse outcome are likely to exist. However, the currently developed model considered the following pathway for a series of signaling cascade biomolecules such as chemicals-miRNA-mRNA-RISCm-BDNF-neuronal survivability, previously described in the conceptual model (figure 2). For the currently selected pathway model predicts BDNF as a very sensitive endogenous species biomolecule, which maintains the cell survivability at steady state. Although, PFOS does not directly target BDNF in our model it still remains the sensitive target which could be due to its regulation is highly dependent on miRNA level. Comparison of figure 9 and 10 allow us to see the decrease in neuronal survivability (figure 10) is highly sensitive towards BDNF level (figure 9). The model shows that BDNF regulation (miRNA based regulation) is very much important for neuronal cell survivability. This shows BDNF could be an interesting species (biomarker) which can link between both environmental exposure and neuronal adverse outcomes.

There was an assumption of the existence of an empirical relation between the in-vitro toxicity to in-vivo toxicity (Wambaugh et al., 2013). Moreover, tools have been developed to translate in-vitro toxicity dose-response to predict the in-vivo toxicity by applying reverse dosimetry concept that provides equivalent in-vivo dose required to produce in-vitro toxicity, eventually validation of model was done by comparing POD (point of departure) from predicted in vivo dose response with reported POD of chemicals (Abdullah et al., 2016; Forsby and Blaauboer, 2007; Louisse et al., 2016; Wambaugh et al., 2013). In this case study of PFOS model (PBPK/PD coupled mechanistic model) due to lack of in-vivo data particularly for the following proposed mechanistic pathway, in worst case scenario we constrained to in-vitro data for qualitative or partial validation of the developed model. To check the performance of the developed PBPK/PD coupled mechanistic model, neuronal cell survivability was selected as an end point. Two approaches were used for this purpose; first reconstructing oral in-vivo equivalent dose for an in-vitro dose; second, response data are generated for identified in vivo doses by mapping in vitro toxicity data (in this case neuronal cell survivability). Figure 10

illustrates, the simulated response variable (% neuronal survivability), for dose equivalent to in-vitro conc., vs observed linear interpolated response variable. Although model could not able to predict all the observed data, however, most of them were within the simulated range. The simulated maximum % of neuronal cell survivability on the lower side was around 35%, which is higher than the experimental observation of around 16 to 20%. This could be possibly explained by several facts such as current model uses adaptability mechanism which lacks in the in-vitro system, only one pathway has been accounted, neglecting the possibility of several mechanisms, empirical estimation of PFOS-miRNA interaction and the inherent uncertainty in in-vitro data and model.

The purpose of this work was to develop a simple model which combines pharmacokinetic model like PBPK predicting the internal tissue dosimetry and mechanistic system model via quantifying the Pharmacodynamic interaction of chemicals with key biomolecule components involved in the mechanistic system of biology. The measurement of mi-RNA, mRNA, BDNF in the brain at different time points gives evidence in parallel changes and difference in between them; significantly improves the understanding of relation with neuronal adverse outcomes. Here in this model, the mechanistic pathway can be considered as an equivalent AOP pathway for neurotoxicity. However, this can be further extended by integrating identified new pathways responsible for neurotoxicity. There are many ways that model can be extended to increase its utility, but certainly, the mi-RNA-based post-transcription regulation of BDNF not limited to PFOS. The same concept can further be applied to other environmental chemicals altering the similar system.

In this paper, we have partially validated our model, considering our objective of this paper is to focus on the illustration of tools that use simple integrated PBPK/PD-coupled mechanistic pathway model involving three main steps 1.Development of PBPK model, 2. Development of mechanistic system model, 3. Couple PBPK with the mechanistic model by integrating PD model that quantify perturbed biomolecule (a component of the mechanistic model) as a result of chemical exposure. This step developed a new framework that could utilize the existing normal mechanistic pathways model and integrated PBPK/PD model, a step towards systems toxicology based models.

Acknowledgement

Preparation of this manuscript was supported in part for European Union's projects, HEALS (Health and Environment-wide Associations via Large population Surveys) by the FP7 Programme under grant agreement no. 603946 and EuroMix (European Test and Risk Assessment Strategies for Mixtures) by the Horizon 2020 Framework Programme under grant agreement no. 633172. Raju Prasad Sharma has received a doctoral fellowship from Universitat Rovira i Virgili under Martí-Franquès Research Grants Programme. This publication reflects only the authors' views. The European Commission and other funding organizations are not liable for any use made of the information contained therein.

References

Abduljalil, K., Furness, P., Johnson, T.N., Rostami-Hodjegan, A., Soltani, H., 2012. Anatomical, Physiological and Metabolic Changes with Gestational Age during

Chapter 5

Normal Pregnancy. Clin. Pharmacokinet. 51, 365–396. https://doi.org/10.2165/11597440-000000000-00000

Abdullah, R., Alhusainy, W., Woutersen, J., Rietjens, I.M.C.M., Punt, A., 2016. Predicting points of departure for risk assessment based on in vitro cytotoxicity data and physiologically based kinetic (PBK) modeling: The case of kidney toxicity induced by aristolochic acid I. Food Chem. Toxicol. 92, 104–116. https://doi.org/10.1016/j.fct.2016.03.017

Adachi, K., Suemizu, H., Murayama, N., Shimizu, M., Yamazaki, H., 2015. Human biofluid concentrations of mono(2-ethylhexyl)phthalate extrapolated from pharmacokinetics in chimeric mice with humanized liver administered with di(2-ethylhexyl)phthalate and physiologically based pharmacokinetic modeling. Environ. Toxicol. Pharmacol. https://doi.org/10.1016/j.etap.2015.02.011

Aderem, A., 2005. Systems biology: Its practice and challenges. Cell 121, 511–513. https://doi.org/10.1016/j.cell.2005.04.020

Akingbemi, B.T., Sottas, C.M., Koulova, A.I., Klinefelter, G.R., Hardy, M.P., 2004. Inhibition of Testicular Steroidogenesis by the Xenoestrogen Bisphenol a Is Associated with Reduced Pituitary Luteinizing Hormone Secretion and Decreased Steroidogenic Enzyme Gene Expression in Rat Leydig Cells. Endocrinology 145, 592–603. https://doi.org/10.1210/en.2003-1174

Andersen, M.E., Krewski, D., 2009. Toxicity testing in the 21st century: Bringing the vision to life. Toxicol. Sci. 107, 324–330. https://doi.org/10.1093/toxsci/kfn255

Andersen, M.E., Thomas, R.S., Gaido, K.W., Conolly, R.B., 2005. Dose-response modeling in reproductive toxicology in the systems biology era. Reprod. Toxicol. 19, 327–337. https://doi.org/10.1016/j.reprotox.2004.12.004

Andrade, R., Agundez, J., Lucena, M., Martinez, C., Cueto, R., Garcia-Martin, E., 2009. Pharmacogenomics in Drug Induced Liver Injury. Curr. Drug Metab. 10, 956–970. https://doi.org/10.2174/138920009790711805

Ankley, G.T., Bennett, R.S., Erickson, R.J., Hoff, D.J., Hornung, M.W., Johnson, R.D., Mount, D.R., Nichols, J.W., Russom, C.L., Schmieder, P.K., Serrrano, J.A., Tietge, J.E., Villeneuve, D.L., 2010. Adverse outcome pathways: A conceptual framework to support ecotoxicology research and risk assessment. Environ. Toxicol. Chem. 29, 730–741. https://doi.org/10.1002/etc.34

Ansoumane, K., Duan, P., Quan, C., Yaima, M.L.T., Liu, C., Wang, C., Fu, W., Qi, S., Yu, T., Yang, K., 2014. Bisphenol A induced reactive oxygen species (ROS) in the liver and affect epididymal semen quality in adults Sprague-Dawley rats. J. Toxicol. Environ. Heal. Sci. 6, 103–112. https://doi.org/10.5897/JTEHS2014.0309

Aris, A., 2014. Estimation of bisphenol A (BPA) concentrations in pregnant women, fetuses and nonpregnant women in Eastern Townships of Canada. Reprod. Toxicol. 45, 8–13. https://doi.org/10.1016/j.reprotox.2013.12.006

Chapter 5

Arrell, D.K., Terzic, a, 2010. Network systems biology for drug discovery. Clin. Pharmacol. Ther. 88, 120–125. https://doi.org/10.1038/clpt.2010.91

Asakawa, N., Koyama, M., Hashimoto, Y., Yamashita, K., 1995. Studies on the Metabolic Fate of Flutamide. (1): Plasma Concentration after Single Administration and Protein Binding in Rats. Drug Metab. Pharmacokinet. 10, 447–453. https://doi.org/10.2133/dmpk.10.447

Atanasov, A.G., Tam, S., Röcken, J.M., Baker, M.E., Odermatt, A., 2003. Inhibition of 11β-hydroxysteroid dehydrogenase type 2 by dithiocarbamates. Biochem. Biophys. Res. Commun. 308, 257–262. https://doi.org/10.1016/S0006-291X(03)01359-7

Auffray, C., Chen, Z., Hood, L., 2009. Systems medicine: the future of medical genomics and healthcare. Genome Med. 1, 2. https://doi.org/10.1186/gm2

Ball, A.L., Kamalian, L., Alfirevic, A., Lyon, J.J., Chadwick, A.E., 2016. Identification of the additional mitochondrial liabilities of 2-hydroxyflutamide when compared with its parent compound, flutamide in HepG2 cells. Toxicol. Sci. 153, 341–351. https://doi.org/10.1093/toxsci/kfw126

Bartel, D.P., 2004. MicroRNAs: Genomics, Biogenesis, Mechanism, and Function. Cell 116, 281–297. https://doi.org/10.1016/S0092-8674(04)00045-5

Bartlett, D.W., Davis, M.E., 2006. Insights into the kinetics of siRNA-mediated gene silencing from live-cell and live-animal bioluminescent imaging. Nucleic Acids Res. 34, 322–333. https://doi.org/10.1093/nar/gkj439

Bell, S.M., Chang, X., Wambaugh, J.F., Allen, D.G., Bartels, M., Brouwer, K.L.R., Casey, W.M., Choksi, N., Ferguson, S.S., Fraczkiewicz, G., Jarabek, A.M., Ke, A., Lumen, A., Lynn, S.G., Paini, A., Price, P.S., Ring, C., Simon, T.W., Sipes, N.S., Sprankle, C.S., Strickland, J., Troutman, J., Wetmore, B.A., Kleinstreuer, N.C., 2018. In vitro to in vivo extrapolation for high throughput prioritization and decision making. Toxicol. Vitr. 47, 213–227. https://doi.org/10.1016/j.tiv.2017.11.016

Berson, A., Wolf, C., Chachaty, C., Fisch, C., Fau, D., Eugene, D., Loeper, J., Gauthier, J.-C., Beaune, P., Pompon, D., Maurel, P., Pessayre, D., 1993. Metabolic activation of the nitroaromatic antiandrogen flutamide by rat and human cytochromes P-450, including forms belonging to the 3A and 1A subfamilies. J. Pharmacol. Exp. Ther. 265, 366–372.

Bessems, J., Coecke, S., Gouliarmou, V., Whelan, M., Worth, A., 2015. EURL ECVAM strategy for achieving 3Rs impact in the assessment of toxicokinetics and systemic toxicity 22. https://doi.org/10.2788/197633

Bhattacharya, S., Shoda, L.K.M., Zhang, Q., Woods, C.G., Howell, B.A., Siler, S.Q., Woodhead, J.L., Yang, Y., McMullen, P., Watkins, P.B., Melvin, E.A., 2012. Modeling drug- and chemical-induced hepatotoxicity with systems biology approaches. Front. Physiol. 3 DEC, 1–18.

Chapter 5

https://doi.org/10.3389/fphys.2012.00462

Birgelen, a Van, Birgelen, a Van, Smit, E., Smit, E., Kampen, I., Kampen, I., 1995. Subchronic effects of 2, 3, 7, 8-TCDD or PCBs on thyroid hormone metabolism: use in risk assessment. Eur. J. Pharmacol. Environ. Toxicol. {…} 293, 77–85.

Bloomingdale, P., Housand, C., Apgar, J.F., Millard, B.L., Mager, D.E., Burke, J.M., Shah, D.K., 2017. Quantitative systems toxicology. Curr. Opin. Toxicol. 4, 79–87. https://doi.org/10.1016/j.cotox.2017.07.003

Boberg, J., Metzdorff, S., Wortziger, R., Axelstad, M., Brokken, L., Vinggaard, A.M., Dalgaard, M., Nellemann, C., 2008. Impact of diisobutyl phthalate and other PPAR agonists on steroidogenesis and plasma insulin and leptin levels in fetal rats. Toxicology 250, 75–81. https://doi.org/10.1016/j.tox.2008.05.020

Boelsterli, U.A., Lim, P.L.K., 2007. Mitochondrial abnormalities—A link to idiosyncratic drug hepatotoxicity? Toxicol. Appl. Pharmacol. 220, 92–107. https://doi.org/10.1016/j.taap.2006.12.013

Bonate, P.L., 2011. Pharmacokinetic-Pharmacodynamic Modeling and Simulation. Springer US, Boston, MA. https://doi.org/10.1007/978-1-4419-9485-1

Boulle, F., van den Hove, D.L. a, Jakob, S.B., Rutten, B.P., Hamon, M., van Os, J., Lesch, K.-P., Lanfumey, L., Steinbusch, H.W., Kenis, G., Hove, D.L.A. Van Den, Jakob, S.B., Rutten, B.P., Hamon, M., Os, J. Van, Lesch, K.-P., van den Hove, D.L. a, Jakob, S.B., Rutten, B.P., Hamon, M., van Os, J., Lesch, K.-P., Lanfumey, L., Steinbusch, H.W., Kenis, G., 2012. Epigenetic regulation of the BDNF gene: implications for psychiatric disorders. Mol. Psychiatry 17, 584–596. https://doi.org/10.1038/mp.2011.107

Bouskine, A., Nebout, M., Brücker-Davis, F., Banahmed, M., Fenichel, P., 2009. Low doses of bisphenol A promote human seminoma cell proliferation by activating PKA and PKG via a membrane G-protein-coupled estrogen receptor. Environ. Health Perspect. 117, 1053–1058. https://doi.org/10.1289/ehp.0800367

Brahm, J., Brahm, M., Segovia, R., Latorre, R., Zapata, R., Poniachik, J., Buckel, E., Contreras, L., 2011. Acute and fulminant hepatitis induced by flutamide: case series report and review of the literature. Ann. Hepatol. 10, 93–8.

Brown, R.P., Delp, M.D., Lindstedt, S.L., Rhomberg, L.R., Beliles, R.P., 1997. Physiological parameter values for physiologically based pharmacokinetic models. Toxicol. Ind. Health 13, 407–484.

Bursac, N., Kirkton, R.D., Mcspadden, L.C., Liau, B., 2010. Circulating levels of brain-derived neurotrophic factor: correlation with mood, cognition and motor function. Biomark. Med. 4, 871–87.

Calabrese, E.J., Baldwin, L.A., 2003. Toxicology rethinks its central belief. Nature 421, 691–692. https://doi.org/10.1038/421691a

Chapter 5

Cao, X.L., Zhang, J., Goodyer, C.G., Hayward, S., Cooke, G.M., Curran, I.H.A., 2012. Bisphenol A in human placental and fetal liver tissues collected from Greater Montreal area (Quebec) during 1998-2008. Chemosphere 89, 505–511. https://doi.org/10.1016/j.chemosphere.2012.05.003

Caputo, V., Sinibaldi, L., Fiorentino, A., Parisi, C., Catalanotto, C., Pasini, A., Cogoni, C., Pizzuti, A., 2011. Brain derived neurotrophic factor (BDNF) expression is regulated by microRNAs miR-26a and miR-26b allele-specific binding. PLoS One 6. https://doi.org/10.1371/journal.pone.0028656

Carlotti, F., Dower, S.K., Qwarnstrom, E.E., 2000. Dynamic shuttling of nuclear factor ??B between the nucleus and cytoplasm as a consequence of inhibitor dissociation. J. Biol. Chem. 275, 41028–41034. https://doi.org/10.1074/jbc.M006179200

Castillo, B., del Cerro, M., Breakefield, X.O., Frim, D.M., Barnstable, C.J., Dean, D.O., Bohn, M.C., 1994. Retinal ganglion cell survival is promoted by genetically modified astrocytes designed to secrete brain-derived neurotrophic factor (BDNF). Brain Res. 647, 30–36. https://doi.org/10.1016/0006-8993(94)91395-1

Castro, B., Sánchez, P., Torres, J.M., Preda, O., del Moral, R.G., Ortega, E., 2013. Bisphenol A Exposure during Adulthood Alters Expression of Aromatase and 5α-Reductase Isozymes in Rat Prostate. PLoS One 8, 1–7. https://doi.org/10.1371/journal.pone.0055905

Chang, Z., Lu, M., Kim, S.S., Park, J.S., 2014. Potential role of HSP90 in mediating the interactions between estrogen receptor (ER) and aryl hydrocarbon receptor (AhR) signaling pathways. Toxicol. Lett. 226, 6–13. https://doi.org/10.1016/j.toxlet.2014.01.032

Chen, N., Li, J., Li, D., Yang, Y., He, D., 2014. Chronic exposure to perfluorooctane sulfonate induces behavior defects and neurotoxicity through oxidative damages, in Vivo and in Vitro. PLoS One 9, 1–10. https://doi.org/10.1371/journal.pone.0113453

Chitra, K.C., Latchoumycandane, C., Mathur, P.P., 2003. Induction of oxidative stress by bisphenol A in the epididymal sperm of rats. Toxicology 185, 119–127. https://doi.org/10.1016/S0300-483X(02)00597-8

Choi, K., Joo, H., Campbell, J.L., Andersen, M.E., Clewell, H.J., 2013. In vitro intestinal and hepatic metabolism of Di(2-ethylhexyl) phthalate (DEHP) in human and rat. Toxicol. Vitr. 27, 1451–1457. https://doi.org/10.1016/j.tiv.2013.03.012

Clarke, G., Collins, R.A., Leavitt, B.R., Andrews, D.F., Hayden, M.R., Lumsden, C.J., McInnes, R.R., 2000. A one-hit model of cell death in inherited neuronal degenerations. Nature 406, 195–199. https://doi.org/10.1038/35018098

Clewell, H.J., Gearhart, J.M., Gentry, P.R., Covington, T.R., VanLandingham, C.B., Crump, K.S., Shipp, A.M., 1999. Evaluation of the uncertainty in an oral reference dose for methylmercury due to interindividual variability in

Chapter 5

pharmacokinetics. Risk Anal. 19, 547–558. https://doi.org/10.1023/A:1007017116171

Clewell, R. a, Merrill, E. a, Narayanan, L., Gearhart, J.M., Robinson, P.J., 2004. Evidence for competitive inhibition of iodide uptake by perchlorate and translocation of perchlorate into the thyroid. Int. J. Toxicol. 23, 17–23. https://doi.org/10.1080/10915810490275044

Clewell, R.A., Clewell, H.J., 2008. Development and specification of physiologically based pharmacokinetic models for use in risk assessment. Regul. Toxicol. Pharmacol. 50, 129–43. https://doi.org/10.1016/j.yrtph.2007.10.012

Coe, K.J., Jia, Y., Han, K.H., Rademacher, P., Bammler, T.K., Beyer, R.P., Farin, F.M., Woodke, L., Plymate, S.R., Fausto, N., Nelson, S.D., 2007. Comparison of the cytotoxicity of the nitroaromatic drug flutamide to its cyano analogue in the hepatocyte cell line TAMH: Evidence for complex I inhibition and mitochondrial dysfunction using toxicogenomic screening. Chem. Res. Toxicol. 20, 1277–1290. https://doi.org/10.1021/tx7001349

Coe, K.J., Nelson, S.D., Ulrich, R.G., He, Y., Dai, X., Cheng, O., Caguyong, M., Roberts, C.J., Slatter, J.G., 2006. Profiling the hepatic effects of flutamide in rats: A microarray comparison with classical aryl hydrocarbon receptor ligands and atypical CYP1A inducers. Drug Metab. Dispos. 34, 1266–1275. https://doi.org/10.1124/dmd.105.009159

Cooper, R.L., Stoker, T.E., Tyrey, L., Goldman, J.M., McElroy, W.K., 2000. Atrazine disrupts the hypothalamic control of pituitary-ovarian function. Toxicol. Sci. 53, 297–307. https://doi.org/10.1093/toxsci/53.2.297

Coughlin, J.L., Thomas, P.E., Buckley, B., 2012. Inhibition of genistein glucuronidation by bisphenol A in human and rat liver microsomes. Drug Metab. Dispos. 40, 481–485. https://doi.org/10.1124/dmd.111.042366

Csanády, G., Oberste-Frielinghaus, H., Semder, B., Baur, C., Schneider, K., Filser, J., 2002. Distribution and unspecific protein binding of the xenoestrogens bisphenol A and daidzein. Arch. Toxicol. 76, 299–305. https://doi.org/10.1007/s00204-002-0339-5

Cubitt, H.E., Houston, J.B., Galetin, A., 2011. Prediction of human drug clearance by multiple metabolic pathways: Integration of hepatic and intestinal microsomal and cytosolic data. Drug Metab. Dispos. 39, 864–873. https://doi.org/10.1124/dmd.110.036566

Cubitt, H.E., Houston, J.B., Galetin, A., 2009. Relative Importance of Intestinal and Hepatic Glucuronidation—Impact on the Prediction of Drug Clearance. Pharm. Res. 26, 1073–1083. https://doi.org/10.1007/s11095-008-9823-9

Davies, B., Morris, T., 1993. No Title. Pharm. Res. 10, 1093–1095. https://doi.org/10.1023/A:1018943613122

Chapter 5

Dieckhaus, C.M., Thompson, C.D., Roller, S.G., Macdonald, T.L., 2002. Mechanisms of idiosyncratic drug reactions: the case of felbamate. Chem. Biol. Interact. 142, 99–117. https://doi.org/10.1016/S0009-2797(02)00057-1

Dinkova-Kostova, A.T., Holtzclaw, W.D., Cole, R.N., Itoh, K., Wakabayashi, N., Katoh, Y., Yamamoto, M., Talalay, P., 2002. Direct evidence that sulfhydryl groups of Keap1 are the sensors regulating induction of phase 2 enzymes that protect against carcinogens and oxidants. Proc. Natl. Acad. Sci. U. S. A. 99, 11908–13. https://doi.org/10.1073/pnas.172398899

Djuranovic, S., Nahvi, A., Green, R., 2011. A Parsimonious Model for Gene Regulation by miRNAs. Science (80-.). 331, 550–553. https://doi.org/10.1126/science.1191138

Doerge, D.R., Twaddle, N.C., Vanlandingham, M., Brown, R.P., Fisher, J.W., 2011. Distribution of bisphenol A into tissues of adult, neonatal, and fetal Sprague–Dawley rats. Toxicol. Appl. Pharmacol. 255, 261–270. https://doi.org/10.1016/j.taap.2011.07.009

Doering, D.D., Steckelbroeck, S., Doering, T., Klingmüller, D., 2002. Effects of butyltins on human 5alpha-reductase type 1 and type 2 activity. Steroids 67, 859–867.

El-Masri, H., 2013. Modeling for Regulatory Purposes (Risk and Safety Assessment), in: Reisfeld, B., Mayeno, A.N. (Eds.), . Humana Press, Totowa, NJ, pp. 297–303. https://doi.org/10.1007/978-1-62703-059-5_13

Espinosa-Diez, C., Miguel, V., Mennerich, D., Kietzmann, T., Sánchez-Pérez, P., Cadenas, S., Lamas, S., 2015. Antioxidant responses and cellular adjustments to oxidative stress. Redox Biol. 6, 183–197. https://doi.org/10.1016/j.redox.2015.07.008

Fabrega, F., Kumar, V., Schuhmacher, M., Domingo, J.L., Nadal, M., 2014. PBPK modeling for PFOS and PFOA: Validation with human experimental data. Toxicol. Lett. 230, 244–251. https://doi.org/10.1016/j.toxlet.2014.01.007

Fàbrega, F., Nadal, M., Schuhmacher, M., Domingo, J.L., Kumar, V., 2016. Influence of the uncertainty in the validation of PBPK models: A case-study for PFOS and PFOA. Regul. Toxicol. Pharmacol. 77, 230–239. https://doi.org/10.1016/j.yrtph.2016.03.009

Fang, H., Tong, W., Branham, W.S., Moland, C.L., Dial, S.L., Hong, H., Xie, Q., Perkins, R., Owens, W., Sheehan, D.M., 2003. Study of 202 Natural, Synthetic, and Environmental Chemicals for Binding to the Androgen Receptor. Chem. Res. Toxicol. 16, 1338–1358. https://doi.org/10.1021/tx030011g

Fisher, J.W., Twaddle, N.C., Vanlandingham, M., Doerge, D.R., 2011. Pharmacokinetic modeling: Prediction and evaluation of route dependent dosimetry of bisphenol A in monkeys with extrapolation to humans. Toxicol. Appl. Pharmacol. 257, 122–136. https://doi.org/10.1016/j.taap.2011.08.026

Chapter 5

Fletcher, J.M., Morton, C.J., Zwar, R.A., Murray, S.S., O'Leary, P.D., Hughes, R.A., 2008. Design of a conformationally defined and proteolytically stable circular mimetic of brain-derived neurotrophic factor. J. Biol. Chem. 283, 33375–33383. https://doi.org/10.1074/jbc.M802789200

Forsby, A., Blaauboer, B., 2007. Integration of in vitro neurotoxicity data with biokinetic modelling for the estimation of in vivo neurotoxicity. Hum. Exp. Toxicol. 26, 333–338. https://doi.org/10.1177/0960327106072994

Foxenberg, R.J., Ellison, C.A., Knaak, J.B., Ma, C., Olson, J.R., 2011. Cytochrome P450-specific human PBPK/PD models for the organophosphorus pesticides: Chlorpyrifos and parathion. Toxicology 285, 57–66. https://doi.org/10.1016/j.tox.2011.04.002

Friedmann, A.S., 2002. Atrazine inhibition of testosterone production in rat males following peripubertal exposure. Reprod. Toxicol. 16, 275–279. https://doi.org/10.1016/S0890-6238(02)00019-9

Fukumitsu, H., Ohtsuka, M., Murai, R., Nakamura, H., Itoh, K., Furukawa, S., 2006. Brain-Derived Neurotrophic Factor Participates in Determination of Neuronal Laminar Fate in the Developing Mouse Cerebral Cortex. J. Neurosci. 26, 13218–13230. https://doi.org/10.1523/JNEUROSCI.4251-06.2006

Fukuzawa, N.H., Ohsako, S., Wu, Q., Sakaue, M., Fujii-Kuriyama, Y., Baba, T., Tohyama, C., 2004. Testicular cytochrome P450scc and LHR as possible targets of 2,3,7,8-tetrachlorodibenzo-p-dioxin (TCDD) in the mouse. Mol. Cell. Endocrinol. 221, 87–96. https://doi.org/10.1016/j.mce.2004.02.005

Gabrielsson, J., Weiner, D., 2012. Non-compartmental Analysis, in: Reisfeld, B., Mayeno, A.N. (Eds.), Methods in Molecular Biology. Humana Press, Totowa, NJ, pp. 377–389. https://doi.org/10.1007/978-1-62703-050-2_16

García Cortés, M., Andrade, R.J., Lucena, M.I., Sánchez Martínez, H., Fernández, M.C., Ferrer, T., Martín-Vivaldi, R., Peláez, G., Suárez, F., Romero-Gómez, M., Montero, J.L., Fraga, E., Camargo, R., Alcántara, R., Pizarro, M.A., García-Ruiz, E., Rosemary-Gómez, M., 2001. Flutamide-induced hepatotoxicity: report of a case series. Rev. Esp. Enferm. Dig. 93, 423–32.

Generali, J.A., Cada, D.J., 2014. Flutamide: Hirsutism in Women. Hosp. Pharm. 49, 517–520. https://doi.org/10.1310/hpj4906-517

Gentry, P.R., Covington, T.R., Andersen, M.E., Clewell, H.J., 2002. Application of a physiologically based pharmacokinetic model for isopropanol in the derivation of a reference dose and reference concentration. Regul. Toxicol. Pharmacol. 36, 51–68. https://doi.org/S0273230002915400 [pii]

Gerona, R.R., Woodruff, T.J., Dickenson, C.A., Pan, J., Jackie, M., Sen, S., Friesen, M.M., Fujimoto, V.Y., Hunt, P.A., 2014. California population 47. https://doi.org/10.1021/es402764d.Bisphenol-A

Chapter 5

Gibbs, J.P., Yang, J.S., Slattery, J.T., 1998. Comparison of human liver and small intestinal glutathione S-transferase-catalyzed busulfan conjugation in vitro. Drug Metab. Dispos. 26, 52–55.

Gillespie, L.N., Clark, G.M., Bartlett, P.F., Marzella, P.L., 2003. BDNF-induced survival of auditory neurons in vivo: Cessation of treatment leads to accelerated loss of survival effects. J. Neurosci. Res. 71, 785–790. https://doi.org/10.1002/jnr.10542

Gim, J., Kim, H.S., Kim, J., Choi, M., Kim, J.R., Chung, Y.J., Cho, K.H., 2010. A system-level investigation into the cellular toxic response mechanism mediated by AhR signal transduction pathway. Bioinformatics 26, 2169–2175. https://doi.org/10.1093/bioinformatics/btq400

Godin, S.J., Scollon, E.J., Hughes, M.F., Potter, P.M., DeVito, M.J., Ross, M.K., 2006. Species differences in the in vitro metabolism of deltamethrin and esfenvalerate: Differential oxidative and hydrolytic metabolism by humans and rats. Drug Metab. Dispos. 34, 1764–1771. https://doi.org/10.1124/dmd.106.010058

Gomez, J.-L., Dupont, A., Cusan, L., Tremblay, M., Suburu, R., Lemay, M., Labrie, F., 1992. Incidence of liver toxicity associated with the use of flutamide in prostate cancer patients. Am. J. Med. 92, 465–470. https://doi.org/10.1016/0002-9343(92)90741-S

Goudarzi, H., Nakajima, S., Ikeno, T., Sasaki, S., Kobayashi, S., Miyashita, C., Ito, S., Araki, A., Nakazawa, H., Kishi, R., 2016. Prenatal exposure to perfluorinated chemicals and neurodevelopment in early infancy: The Hokkaido Study. Sci. Total Environ. 541, 1002–1010. https://doi.org/10.1016/j.scitotenv.2015.10.017

Gumy, C., Chandsawangbhuwana, C., Dzyakanchuk, A. a., Kratschmar, D. V., Baker, M.E., Odermatt, A., 2008. Dibutyltin disrupts glucocorticoid receptor function and impairs glucocorticoid-induced suppression of cytokine production. PLoS One 3. https://doi.org/10.1371/journal.pone.0003545

Haley, B., Zamore, P.D., 2004. Kinetic analysis of the RNAi enzyme complex. Nat. Struct. Mol. Biol. 11, 599–606. https://doi.org/10.1038/nsmb780

Hany, J., Lilienthal, H., Sarasin, a, Roth-Härer, a, Fastabend, a, Dunemann, L., Lichtensteiger, W., Winneke, G., 1999. Developmental exposure of rats to a reconstituted PCB mixture or aroclor 1254: effects on organ weights, aromatase activity, sex hormone levels, and sweet preference behavior. Toxicol. Appl. Pharmacol. 158, 231–243. https://doi.org/10.1006/taap.1999.8710

Hayes, T.B., Anderson, L.L., Beasley, V.R., de Solla, S.R., Iguchi, T., Ingraham, H., Kestemont, P., Kniewald, J., Kniewald, Z., Langlois, V.S., Luque, E.H., McCoy, K.A., Muñoz-de-Toro, M., Oka, T., Oliveira, C.A., Orton, F., Ruby, S., Suzawa, M., Tavera-Mendoza, L.E., Trudeau, V.L., Victor-Costa, A.B., Willingham, E., 2011. Demasculinization and feminization of male gonads by atrazine: Consistent effects across vertebrate classes. J. Steroid Biochem. Mol. Biol. 127, 64–73. https://doi.org/10.1016/j.jsbmb.2011.03.015

Chapter 5

Heidrich, D.D., Steckelbroeck, S., Klingmuller, D., 2001. Inhibition of human cytochrome P450 aromatase activity by butyltins. Steroids 66, 763–769.

Hood, L., Heath, J.R., Phelps, M.E., Lin, B., 2004. Systems biology and new technologies enable predictive and preventative medicine. Science 306, 640–643. https://doi.org/10.1126/science.1104635

Ikezuki, Y., Tsutsumi, O., Takai, Y., Kamei, Y., Taketani, Y., 2002. Determination of bisphenol A concentrations in human biological fluids reveals significant early prenatal exposure. Hum. Reprod. 17, 2839–2841. https://doi.org/10.1093/humrep/17.11.2839

Jaeschke, H., McGill, M.R., Ramachandran, A., 2012. Oxidant stress, mitochondria, and cell death mechanisms in drug-induced liver injury: lessons learned from acetaminophen hepatotoxicity. Drug Metab. Rev. 44, 88–106. https://doi.org/10.3109/03602532.2011.602688

Johansson, M., Larsson, C., Bergman, a, Lund, B.O., 1998. Structure-activity relationship for inhibition of CYP11B1-dependent glucocorticoid synthesis in Y1 cells by aryl methyl sulfones. Pharmacol. Toxicol. 83, 225–230.

Johansson, N., Fredriksson, A., Eriksson, P., 2008. Neonatal exposure to perfluorooctane sulfonate (PFOS) and perfluorooctanoic acid (PFOA) causes neurobehavioural defects in adult mice. Neurotoxicology 29, 160–169. https://doi.org/10.1016/j.neuro.2007.10.008

Juge-Aubry, C.E., Gorla-Bajszczak, A., Pernin, A., Lemberger, T., Wahli, W., Burger, A.G., Meier, C. a., 1995. Peroxisome proliferator-activated receptor mediates cross-talk with thyroid hormone receptor by competition for retinoid X receptor: Possible role of a leucine zipper-like heptad repeat. J. Biol. Chem. https://doi.org/10.1074/jbc.270.30.18117

Jusko, W.J., 2013. Moving from basic toward systems pharmacodynamic models. J. Pharm. Sci. 102, 2930–2940. https://doi.org/10.1002/jps.23590

Jusko, W.J., Ko, H.C., 1994. Physiologic indirect response models characterize diverse types of pharmacodynamic effects. Clin. Pharmacol. Ther. 56, 406–419. https://doi.org/10.1038/clpt.1994.155

Kanda, Y., Hinata, T., Kang, S.W., Watanabe, Y., 2011. Reactive oxygen species mediate adipocyte differentiation in mesenchymal stem cells. Life Sci. 89, 250–258. https://doi.org/10.1016/j.lfs.2011.06.007

Kaplowitz, N., 2005. Idiosyncratic drug hepatotoxicity. Nat. Rev. Drug Discov. 4, 489.

Kashimshetty, R., Desai, V.G., Kale, V.M., Lee, T., Moland, C.L., Branham, W.S., New, L.S., Chan, E.C.Y., Younis, H., Boelsterli, U.A., 2009. Underlying mitochondrial dysfunction triggers flutamide-induced oxidative liver injury in a mouse model of idiosyncratic drug toxicity. Toxicol. Appl. Pharmacol. 238, 150–159. https://doi.org/10.1016/j.taap.2009.05.007

Chapter 5

Katchen, B., Buxbaum, S., 1975. Disposition of a new, nonsteroid, antiandrogen, alpha,alpha,alpha-trifluoro-2-methyl-4'-nitro-m-propionotoluidide (Flutamide), in men following a single oral 200 mg dose. J. Clin. Endocrinol. Metab. 41, 373–9. https://doi.org/10.1210/jcem-41-2-373

Kawamoto, Y., Matsuyama, W., Wada, M., Hishikawa, J., Chan, M.P.L., Nakayama, A., Morisawa, S., 2007. Development of a physiologically based pharmacokinetic model for bisphenol A in pregnant mice. Toxicol. Appl. Pharmacol. 224, 182–191. https://doi.org/10.1016/j.taap.2007.06.023

Kell, D.B., 2006. Systems biology, metabolic modelling and metabolomics in drug discovery and development. Drug Discov. Today 11, 1085–1092. https://doi.org/10.1016/j.drudis.2006.10.004

Kester, M.H.A., Bulduk, S., Van Toor, H., Tibboel, D., Meinl, W., Glatt, H., Falany, C.N., Coughtrie, M.W.H., Gerlienke Schuur, A., Brouwer, A., Visser, T.J., 2002. Potent inhibition of estrogen sulfotransferase by hydroxylated metabolites of polyhalogenated aromatic hydrocarbons reveals alternative mechanism for estrogenic activity of endocrine disrupters. J. Clin. Endocrinol. Metab. 87, 1142–1150. https://doi.org/10.1210/jc.87.3.1142

Keys, D.A., Wallace, D.G., Kepler, T.B., Conolly, R.B., 2000. Quantitative evaluation of alternative mechanisms of blood disposition of di(n-butyl) phthalate and mono(n-butyl) phthalate in rats. Toxicol. Sci. 53, 173–184. https://doi.org/10.1093/toxsci/53.2.173

Keys, D.A., Wallace, D.G., Kepler, T.B., Conolly, R.B., 1999. Quantitative evaluation of alternative mechanisms of blood and testes disposition of di(2-ethylhexyl) phthalate and mono(2-ethylhexyl) phthalate in rats. Toxicol. Sci. 49, 172–85. https://doi.org/10.1093/toxsci/49.2.172

Kitano, H., 2002. Systems biology: A brief overview. Sci. (New York, NY) 295, 1662–1664. https://doi.org/10.1126/science.1069492

Kobayashi, Y., Fukami, T.., Shimizu, M., Nakajima, M., Tsuyoshi., Y., 2012. Short Communication Contributions of Arylacetamide Deacetylase and Carboxylesterase 2 to Flutamide Hydrolysis in Human Liver. Drug Metab. Dispos. 40, 1080–1084.

Kohler, J.J., Schepartz, A., 2001. Kinetic Studies of Fos , Jun , DNA Complex Formation : DNA Binding Prior to Dimerization. Biochemistry 40, 130–142. https://doi.org/10.1021/bi001881p

Kortejärvi, H., Urtti, A., Yliperttula, M., 2007. Pharmacokinetic simulation of biowaiver criteria: The effects of gastric emptying, dissolution, absorption and elimination rates. Eur. J. Pharm. Sci. 30, 155–166. https://doi.org/10.1016/j.ejps.2006.10.011

Kuepfer, L., Niederalt, C., Wendl, T., Schlender, J.F., Willmann, S., Lippert, J., Block, M., Eissing, T., Teutonico, D., 2016. Applied Concepts in PBPK Modeling: How to Build a PBPK/PD Model. CPT Pharmacometrics Syst. Pharmacol. 5, 516–531.

Chapter 5

https://doi.org/10.1002/psp4.12134

Kurebayashi, H., Okudaira, K., Ohno, Y., 2010. Species difference of metabolic clearance of bisphenol A using cryopreserved hepatocytes from rats, monkeys and humans. Toxicol. Lett. 198, 210–215. https://doi.org/10.1016/j.toxlet.2010.06.017

Kuroda, N., Kinoshita, Y., Sun, Y., Wada, M., Kishikawa, N., Nakashima, K., Makino, T., Nakazawa, H., 2003. Measurement of bisphenol A levels in human blood serum and ascitic fluid by HPLC using a fluorescent labeling reagent. J. Pharm. Biomed. Anal. 30, 1743–1749. https://doi.org/10.1016/S0731-7085(02)00516-2

Lai, K.P., Wong, M.H., Wong, C.K.C., 2005a. Inhibition of CYP450scc expression in dioxin-exposed rat Leydig cells. J. Endocrinol. 185, 519–527. https://doi.org/10.1677/joe.1.06054

Lai, K.P., Wong, M.H., Wong, C.K.C., 2005b. Effects of TCDD in modulating the expression of Sertoli cell secretory products and markers for cell-cell interaction. Toxicology 206, 111–123. https://doi.org/10.1016/j.tox.2004.07.002

Lans, M.C., Spiertz, C., Brouwer, a, Koeman, J.H., 1994. Different competition of thyroxine binding to transthyretin and thyroxine-binding globulin by hydroxy-PCBs, PCDDs and PCDFs. Eur. J. Pharmacol. 270, 129–136. https://doi.org/10.1016/0926-6917(94)90054-X

Leclerc, E., Hamon, J., Legendre, A., Bois, F.Y., 2014. Integration of pharmacokinetic and NRF2 system biology models to describe reactive oxygen species production and subsequent glutathione depletion in liver microfluidic biochips after flutamide exposure. Toxicol. Vitr. 28, 1230–1241. https://doi.org/10.1016/j.tiv.2014.05.003

Lee, Y.J., Ryu, H.Y., Kim, H.K., Min, C.S., Lee, J.H., Kim, E., Nam, B.H., Park, J.H., Jung, J.Y., Jang, D.D., Park, E.Y., Lee, K.H., Ma, J.Y., Won, H.S., Im, M.W., Leem, J.H., Hong, Y.C., Yoon, H.S., 2008. Maternal and fetal exposure to bisphenol A in Korea. Reprod. Toxicol. 25, 413–419. https://doi.org/10.1016/j.reprotox.2008.05.058

Lemaire, G., Terouanne, B., Mauvais, P., Michel, S., Rahmani, R., 2004. Effect of organochlorine pesticides on human androgen receptor activation in vitro. Toxicol. Appl. Pharmacol. 196, 235–246. https://doi.org/10.1016/j.taap.2003.12.011

Li, L. a., Wang, P.W., Chang, L.W., 2004. Polychlorinated biphenyl 126 stimulates basal and inducible aldosterone biosynthesis of human adrenocortical H295R cells. Toxicol. Appl. Pharmacol. 195, 92–102. https://doi.org/10.1016/j.taap.2003.11.007

Li, M.W.M., Mruk, D.D., Lee, W.M., Cheng, C.Y., 2009. Disruption of the blood-testis barrier integrity by bisphenol A in vitro: Is this a suitable model for studying blood-testis barrier dynamics? Int. J. Biochem. Cell Biol. 41, 2302–2314. https://doi.org/10.1016/j.biocel.2009.05.016

Chapter 5

Li, W., He, Q.Z., Wu, C.Q., Pan, X.Y., Wang, J., Tan, Y., Shan, X.Y., Zeng, H.C., 2015. PFOS Disturbs BDNF-ERK-CREB Signalling in Association with Increased MicroRNA-22 in SH-SY5Y Cells. Biomed Res. Int. 2015. https://doi.org/10.1155/2015/302653

Li, X., Fang, P., Mai, J., Choi, E.T., Wang, H., Yang, X., 2013. Targeting mitochondrial reactive oxygen species as novel therapy for inflammatory diseases and cancers. J. Hematol. Oncol. 6, 19. https://doi.org/10.1186/1756-8722-6-19

Li, Y., Ramdhan, D.H., Naito, H., Yamagishi, N., Ito, Y., Hayashi, Y., Yanagiba, Y., Okamura, A., Tamada, H., Gonzalez, F.J., Nakajima, T., 2011. Ammonium perfluorooctanoate may cause testosterone reduction by adversely affecting testis in relation to PPARα. Toxicol. Lett. 205, 265–272. https://doi.org/10.1016/j.toxlet.2011.06.015

Lipsky, R.H., Marini, A.M., 2007. Brain-derived neurotrophic factor in neuronal survival and behavior-related plasticity. Ann. N. Y. Acad. Sci. 1122, 130–143. https://doi.org/10.1196/annals.1403.009

Long, Y., Wang, Y., Ji, G., Yan, L., Hu, F., Gu, A., 2013. Neurotoxicity of Perfluorooctane Sulfonate to Hippocampal Cells in Adult Mice. PLoS One 8, 1–9. https://doi.org/10.1371/journal.pone.0054176

Lorber, M., Angerer, J., Koch, H.M., 2010. A simple pharmacokinetic model to characterize exposure of Americans to Di-2-ethylhexyl phthalate. J. Expo. Sci. Environ. Epidemiol. 20, 38–53. https://doi.org/10.1038/jes.2008.74

Louisse, J., Beekmann, K., Rietjens, I.M.C.M., 2016. Use of physiologically based kinetic modeling-based reverse dosimetry to predict in vivo toxicity from in vitro data. Chem. Res. Toxicol. acs.chemrestox.6b00302. https://doi.org/10.1021/acs.chemrestox.6b00302

Lu, B., 2003. Pro-Region of Neurotrophins. Neuron 39, 735–738. https://doi.org/10.1016/S0896-6273(03)00538-5

Lubin, F.D., Roth, T.L., Sweatt, J.D., 2008. Epigenetic regulation of BDNF gene transcription in the consolidation of fear memory. J. Neurosci. 28, 10576–86. https://doi.org/10.1523/JNEUROSCI.1786-08.2008

Ma, E., MacRae, I.J., Kirsch, J.F., Doudna, J.A., 2008. Autoinhibition of Human Dicer by Its Internal Helicase Domain. J. Mol. Biol. 380, 237–243. https://doi.org/10.1016/j.jmb.2008.05.005

Mager, D.E., Woo, S., Jusko, W.J., 2009. Scaling Pharmacodynamics from In Vitro and Preclinical Animal Studies to Humans. Drug Metab. Pharmacokinet. 24, 16–24. https://doi.org/10.2133/dmpk.24.16

Mager, D.E., Wyska, E., Jusko, W.J., 2003. Diversity of mechanism-based pharmacodynamic models. Drug Metab. Dispos. 31, 510–8. https://doi.org/10.1124/DMD.31.5.510

Chapter 5

Martínez, M.A., Rovira, J., Prasad Sharma, R., Nadal, M., Schuhmacher, M., Kumar, V., 2018. Comparing dietary and non-dietary source contribution of BPA and DEHP to prenatal exposure: A Catalonia (Spain) case study. Environ. Res. 166, 25–34. https://doi.org/10.1016/j.envres.2018.05.008

Martínez, M.A., Rovira, J., Sharma, R.P., Nadal, M., Schuhmacher, M., Kumar, V., 2017. Prenatal exposure estimation of BPA and DEHP using integrated external and internal dosimetry: A case study. Environ. Res. 158, 566–575. https://doi.org/10.1016/j.envres.2017.07.016

Masuyama, H., Hiramatsu, Y., Kunitomi, M., Kudo, T., MacDonald, P.N., 2000. Endocrine disrupting chemicals, phthalic acid and nonylphenol, activate Pregnane X receptor-mediated transcription. Mol. Endocrinol. 14, 421–428. https://doi.org/10.1210/mend.14.3.0424

Masuyama, H., Inoshita, H., Hiramatsu, Y., Kudo, T., 2002. Ligands have various potential effects on the degradation of pregnane X receptor by proteasome. Endocrinology 143, 55–61. https://doi.org/10.1210/en.143.1.55

Matsuzaki, Y., Nagai, D., Ichimura, E., Goda, R., Tomura, A., Doi, M., Nishikawa, K., 2006. Metabolism and hepatic toxicity of flutamide in cytochrome P450 1A2 knockout SV129 mice. J. Gastroenterol. 41, 231–239. https://doi.org/10.1007/s00535-005-1749-y

Menei, P., Montero-Menei, C., Whittemore, S.R., Bunge, R.P., Bunge, M.B., 1998. Schwann cells genetically modified to secrete human BDNF promote enhanced axonal regrowth across transected adult rat spinal cord. Eur. J. Neurosci. 10, 607–621. https://doi.org/10.1046/j.1460-9568.1998.00071.x

Michael, G.J., Averill, S., Nitkunan, A., Rattray, M., Bennett, D.L., Yan, Q., Priestley, J. V, 1997. Nerve growth factor treatment increases brain-derived neurotrophic factor selectively in TrkA-expressing dorsal root ganglion cells and in their central terminations within the spinal cord. J. Neurosci. 17, 8476–90.

Mielke, H., Partosch, F., Gundert-Remy, U., 2011. The contribution of dermal exposure to the internal exposure of bisphenol A in man. Toxicol. Lett. 204, 190–198. https://doi.org/10.1016/j.toxlet.2011.04.032

Mikamo, E., Harada, S., Nishikawa, J., Nishihara, T., 2003. Endocrine disruptors induce cytochrome P450 by affecting transcriptional regulation via pregnane X receptor. Toxicol. Appl. Pharmacol. 193, 66–72. https://doi.org/10.1016/j.taap.2003.08.001

Moriyama, K., Tagami, T., Akamizu, T., Usui, T., Saijo, M., Kanamoto, N., Hataya, Y., Shimatsu, A., Kuzuya, H., Nakao, K., 2002. Thyroid hormone action is disrupted by bisphenol A as an antagonist. J. Clin. Endocrinol. Metab. 87, 5185–5190. https://doi.org/10.1210/jc.2002-020209

Mowla, S.J., Pareek, S., Farhadi, H.F., Petrecca, K., Fawcett, J.P., Seidah, N.G., Morris, S.J., Sossin, W.S., Murphy, R. a, 1999. Differential sorting of nerve growth factor and brain-derived neurotrophic factor in hippocampal neurons. J. Neurosci. 19,

Chapter 5

2069–2080.

Muiños-Gimeno, M., Espinosa-Parrilla, Y., Guidi, M., Kagerbauer, B., Sipilä, T., Maron, E., Pettai, K., Kananen, L., Navinés, R., Martín-Santos, R., Gratacòs, M., Metspalu, A., Hovatta, I., Estivill, X., 2011. Human microRNAs miR-22, miR-138-2, miR-148a, and miR-488 are associated with panic disorder and regulate several anxiety candidate genes and related pathways. Biol. Psychiatry 69, 526–533. https://doi.org/10.1016/j.biopsych.2010.10.010

Murer, M.., Yan, Q., Raisman-Vozari, R., 2001. Brain-derived neurotrophic factor in the control human brain, and in Alzheimer's disease and Parkinson's disease. Prog. Neurobiol. 63, 71–124. https://doi.org/10.1016/S0301-0082(00)00014-9

Murphy, M.P., 2009. How mitochondria produce reactive oxygen species. Biochem. J. 417, 1–13. https://doi.org/10.1042/BJ20081386

Nestorov, I., 2007. Whole-body physiologically based pharmacokinetic models. Expert Opin. Drug Metab. Toxicol. 3, 235–249. https://doi.org/10.1517/17425255.3.2.235

Nikula, H., Talonpoika, T., Kaleva, M., Toppari, J., 1999. Inhibition of hCG-stimulated steroidogenesis in cultured mouse Leydig tumor cells by bisphenol A and octylphenols. Toxicol. Appl. Pharmacol. 157, 166–173. https://doi.org/10.1006/taap.1999.8674

Niwa, T., Fujimoto, M., Kishimoto, K., Yabusaki, Y., Ishibashi, F., Katagiri, M., 2001. Metabolism and interaction of bisphenol A in human hepatic cytochrome P450 and steroidogenic CYP17. Biol. Pharm. Bull. 24, 1064–1067. https://doi.org/10.1248/bpb.24.1064

O'Leary, P.D., Hughes, R.A., 1998. Structure-activity relationships of conformationally constrained peptide analogues of loop 2 of brain-derived neurotrophic factor. J. Neurochem. 70, 1712–21. https://doi.org/10.1046/j.1471-4159.1998.70041712.x

OECD, 2018. "Users'' Handbook supplement to the Guidance Document for developing and assessing Adverse Outcome Pathways", OECD Series on Adverse Outcome Pathways, No. 1, OECD Publishing, Paris." https://doi.org/10.1787/5jlv1m9d1g32-en

OECD, 2016. "Users'' Handbook supplement to the Guidance Document for developing and assessing Adverse Outcome Pathways", OECD Series on Adverse Outcome Pathways, No. 1, OECD Publishing, Paris" 18. https://doi.org/10.1787/5jlv1m9d1g32-en

Ohshima, M., Ohno, S., Nakajin, S., 2005. Inhibitory effects of some possible endocrine-disrupting chemicals on the isozymes of human 11beta-hydroxysteroid dehydrogenase and expression of their mRNA in gonads and adrenal glands. Environ. Sci. 12, 219–230.

Ohtake, F., Takeyama, K., Matsumoto, T., Kitagawa, H., Yamamoto, Y., Nohara, K.,

Chapter 5

Tohyama, C., Krust, A., Mimura, J., Chambon, P., Yanagisawa, J., Fujii-Kuriyama, Y., Kato, S., 2003. Modulation of oestrogen receptor signalling by association with the activated dioxin receptor. Nature 423, 545–550. https://doi.org/10.1038/nature01606

Patisaul, H.B., Todd, K.L., Mickens, J.A., Adewale, H.B., 2009. Impact of neonatal exposure to the ERα agonist PPT, bisphenol-A or phytoestrogens on hypothalamic kisspeptin fiber density in male and female rats. Neurotoxicology 30, 350–357. https://doi.org/10.1016/j.neuro.2009.02.010

Pérez-Ortín, J.E., Alepuz, P.M., Moreno, J., 2007. Genomics and gene transcription kinetics in yeast. Trends Genet. 23, 250–257. https://doi.org/10.1016/j.tig.2007.03.006

Perruisseau-Carrier, C., Jurga, M., Forraz, N., McGuckin, C.P., 2011. MiRNAs stem cell reprogramming for neuronal induction and differentiation. Mol. Neurobiol. 43, 215–227. https://doi.org/10.1007/s12035-011-8179-z

Podratz, P.L., Filho, V.S.D., Lopes, P.F.I., Sena, G.C., Matsumoto, S.T., Samoto, V.Y., Takiya, C.M., Miguel, E.D.C., Silva, I.V., Graceli, J.B., 2012. Tributyltin Impairs the Reproductive Cycle in Female Rats. J. Toxicol. Environ. Heal. Part A 75, 1035–1046. https://doi.org/10.1080/15287394.2012.697826

Poland, a, Knutson, J.C., 1982. 2,3,7,8-Tetrachlorodibenzo-P-Dioxin and Related Halogenated Aromatic Hydrocarbons: Examination of the Mechanism of Toxicity. Annu. Rev. Pharmacol. Toxicol. 22, 517–554. https://doi.org/10.1146/annurev.pa.22.040182.002505

Poulin, P., Krishnan, K., 1996. Molecular Structure-Based Prediction of the Partition Coefficients of Organic Chemicals for Physiological Pharmacokinetic Models. Toxicol. Mech. Methods 6, 117–137. https://doi.org/10.3109/15376519609068458

Poulin, P., Krishnan, K., 1995. A biologically-based algorithm for predicting human tissue: blood partition coefficients of organic chemicals. Hum Exp Toxicol 14, 273–280.

Poulin, P., Theil, F.P., 2000. A priori prediction of tissue: Plasma partition coefficients of drugs to facilitate the use of physiologically-based pharmacokinetic models in drug discovery. J. Pharm. Sci. 89, 16–35. https://doi.org/10.1002/(SICI)1520-6017(200001)89:1<16::AID-JPS3>3.0.CO;2-E

Qatanani, M., Zhang, J., Moore, D.D., 2005. Role of the constitutive androstane receptor in xenobiotic-induced thyroid hormone metabolism. Endocrinology 146, 995–1002. https://doi.org/10.1210/en.2004-1350

Qiu, L., Zhang, X., Zhang, X., Zhang, Y., Gu, J., Chen, M., Zhang, Z., Wang, X., Wang, S.L., 2013. Sertoli cell is a potential target for perfluorooctane sulfonate-induced reproductive dysfunction in male mice. Toxicol. Sci. 135, 229–240. https://doi.org/10.1093/toxsci/kft129

Chapter 5

Radwanski, E., Perentesis, G., Symchowicz, S., Zampaglione, N., 1989. Single and Multiple Dose Pharmacokinetic Evaluation of Flutamide in Normal Geriatric Volunteers. J. Clin. Pharmacol. 29, 554–558. https://doi.org/10.1002/j.1552-4604.1989.tb03381.x

Raun Andersen, H., Vinggaard, A.M., Høj Rasmussen, T., Gjermandsen, I.M., Cecilie Bonefeld-Jørgensen, E., 2002. Effects of Currently Used Pesticides in Assays for Estrogenicity, Androgenicity, and Aromatase Activity in Vitro. Toxicol. Appl. Pharmacol. 179, 1–12. https://doi.org/10.1006/taap.2001.9347

Rey, R., Lukas-Croisier, C., Lasala, C., Bedecarrás, P., 2003. AMH/MIS: What we know already about the gene, the protein and its regulation. Mol. Cell. Endocrinol. 211, 21–31. https://doi.org/10.1016/j.mce.2003.09.007

Rodríguez-Tébar, A., Dechant, G., Götz, R., Barde, Y.A., 1992. Binding of neurotrophin-3 to its neuronal receptors and interactions with nerve growth factor and brain-derived neurotrophic factor. EMBO J. 11, 917–922.

Rouquié, D., Heneweer, M., Botham, J., Ketelslegers, H., Markell, L., Pfister, T., Steiling, W., Strauss, V., Hennes, C., 2015. Contribution of new technologies to characterization and prediction of adverse effects. Crit. Rev. Toxicol. 45, 172–183. https://doi.org/10.3109/10408444.2014.986054

Saitoh, M., Yanase, T., Morinaga, H., Tanabe, M., Mu, Y.M., Nishi, Y., Nomura, M., Okabe, T., Goto, K., Takayanagi, R., Nawata, H., 2001. Tributyltin or triphenyltin inhibits aromatase activity in the human granulosa-like tumor cell line KGN. Biochem. Biophys. Res. Commun. 289, 198–204. https://doi.org/10.1006/bbrc.2001.5952

Sandhya, V.K., Raju, R., Verma, R., Advani, J., Sharma, R., Radhakrishnan, A., Nanjappa, V., Narayana, J., Somani, B.L., Mukherjee, K.K., Pandey, A., Christopher, R., Keshava Prasad, T.S., 2013. A network map of BDNF/TRKB and BDNF/p75NTR signaling system. J. Cell Commun. Signal. 7, 301–307. https://doi.org/10.1007/s12079-013-0200-z

Sato, I., Kawamoto, K., Nishikawa, Y., Tsuda, S., Yoshida, M., Yaegashi, K., Saito, N., Liu, W., Jin, Y., 2009. Neurotoxicity of perfluorooctane sulfonate (PFOS) in rats and mice after single oral exposure. J. Toxicol. Sci. 34, 569–574. https://doi.org/10.2131/jts.34.569

Saunders, P.T., Majdic, G., Parte, P., Millar, M.R., Fisher, J.S., Turner, K.J., Sharpe, R.M., 1997. Fetal and perinatal influence of xenoestrogens on testis gene expression. Adv. Exp. Med. Biol. 424, 99–110.

Schmitt, W., 2008. General approach for the calculation of tissue to plasma partition coefficients. Toxicol. Vitr. 22, 457–467. https://doi.org/10.1016/j.tiv.2007.09.010

Schönfelder, G., Wittfoht, W., Hopp, H., Talsness, C.E., Paul, M., Chahoud, I., 2002. Parent bisphenol a accumulation in the human maternal-fetal-placental unit. Environ. Health Perspect. 110, 703–707. https://doi.org/10.1289/ehp.021100703

Chapter 5

Seo, J.S., Lee, Y.M., Jung, S.O., Kim, I.C., Yoon, Y.D., Lee, J.S., 2006. Nonylphenol modulates expression of androgen receptor and estrogen receptor genes differently in gender types of the hermaphroditic fish Rivulus marmoratus. Biochem. Biophys. Res. Commun. 346, 213–223. https://doi.org/10.1016/j.bbrc.2006.05.123

Shi, Z., Ding, L., Zhang, H., Feng, Y., Xu, M., Dai, J., 2009. Chronic exposure to perfluorododecanoic acid disrupts testicular steroidogenesis and the expression of related genes in male rats. Toxicol. Lett. 188, 192–200. https://doi.org/10.1016/j.toxlet.2009.04.014

Sisson, T.R., Lund, C.J., Whalen, L.E., Telek, A., 1959. The blood volume of infants. I. The full-term infant in the first year of life. J. Pediatr. 55, 163–79. https://doi.org/10.1016/S0022-3476(59)80084-6

Siu, E.R., Mruk, D.D., Porto, C.S., Cheng, C.Y., 2009. Cadmium-induced testicular injury. Toxicol. Appl. Pharmacol. 238, 240–249. https://doi.org/10.1016/j.taap.2009.01.028

Sjo, E., Lennerna, H., Andersson, T.B., Gråsjo, J., Bredberg, U., 2009. Estimates of Intrinsic Clearance (CL int), Maximum Velocity of the Metabolic Reaction (V max), and Michaelis Constant (K m): Accuracy and Robustness Evaluated through Experimental Data and Monte Carlo Simulations ABSTRACT : Pharmacology 37, 47–58. https://doi.org/10.1124/dmd.108.021477.kinetics

Sjögren, E., Tammela, T.L., Lennernäs, B., Taari, K., Isotalo, T., Malmsten, L.-Å., Axén, N., Lennernäs, H., 2014. Pharmacokinetics of an Injectable Modified-Release 2-Hydroxyflutamide Formulation in the Human Prostate Gland Using a Semiphysiologically Based Biopharmaceutical Model. Mol. Pharm. 11, 3097–3111. https://doi.org/10.1021/mp5002813

Sobarzo, C.M., Lustig, L., Ponzio, R., Denduchis, B., 2006. Effect of di-(2-ethylhexyl) phthalate on N-cadherin and catenin protein expression in rat testis. Reprod. Toxicol. 22, 77–86. https://doi.org/10.1016/j.reprotox.2006.02.004

Soetaert, K., Petzoldt, T., 2010. Inverse Modelling, Sensitivity and Monte Carlo Analysis in R Using Package FME. J. Stat. Softw. 33, 2–4. https://doi.org/10.18637/jss.v033.i03

Stasenko, S., Bradford, E.M., Piasek, M., Henson, M.C., Varnai, V.M., Jurasović, J., Kušec, V., 2010. Metals in human placenta: Focus on the effects of cadmium on steroid hormones and leptin. J. Appl. Toxicol. 30, 242–253. https://doi.org/10.1002/jat.1490

Stouder, C., Paoloni-Giacobino, A., 2011. Specific transgenerational imprinting effects of the endocrine disruptor methoxychlor on male gametes. Reproduction 141, 207–216. https://doi.org/10.1530/REP-10-0400

Sturla, S.J., Boobis, A.R., FitzGerald, R.E., Hoeng, J., Kavlock, R.J., Schirmer, K., Whelan, M., Wilks, M.F., Peitsch, M.C., 2014. Systems Toxicology: From Basic Research to Risk Assessment. Chem. Res. Toxicol. 27, 314–329.

Chapter 5

https://doi.org/10.1021/tx400410s

Teppner, M., Boess, F., Ernst, B., Pähler, A., 2016. Biomarkers of flutamide-bioactivation and oxidative stress in vitro and in vivo. Drug Metab. Dispos. 44, 560–569. https://doi.org/10.1124/dmd.115.066522

Thiel, C., Cordes, H., Conde, I., Castell, J.V., Blank, L.M., Kuepfer, L., 2017. Model-based contextualization of in vitro toxicity data quantitatively predicts in vivo drug response in patients. Arch. Toxicol. 91, 865–883. https://doi.org/10.1007/s00204-016-1723-x

Timchalk, C., Nolan, R.J., Mendrala, A.L., Dittenber, D.A., Brzak, K.A., Mattsson, J.L., 2002. A physiologically based pharmacokinetic and pharmacodynamic (PBPK/PD) model for the organophosphate insecticide chlorpyrifos in rats and humans. Toxicol. Sci. 66, 34–53. https://doi.org/10.1093/toxsci/66.1.34

Toyoda, K., Shibutani, M., Tamura, T., Koujitani, T., Uneyama, C., Hirose, M., 2000. Repeated dose (28 days) oral toxicity study of flutamide in rats, based on the draft protocol for the `Enhanced OECD Test Guideline 407' for screening for endocrine-disrupting chemicals. Arch. Toxicol. 74, 127–132. https://doi.org/10.1007/s002040050664

Trdan Lusin, T., Roskar, R., Mrhar, A., 2012. Evaluation of bisphenol A glucuronidation according to UGT1A1*28 polymorphism by a new LC-MS/MS assay. Toxicology 292, 33–41. https://doi.org/10.1016/j.tox.2011.11.015

Uzumcu, M., Kuhn, P.E., Marano, J.E., Armenti A.E., A.E., Passantino, L., 2006. Early postnatal methoxychlor exposure inhibits folliculogenesis and stimulates anti-Mullerian hormone production in the rat ovary. J. Endocrinol. 191, 549–558. https://doi.org/10.1677/joe.1.06592

Valentin, J., 2002. Basic anatomical and physiological data for use in radiological protection: reference values. Ann. ICRP 32, 1–277. https://doi.org/10.1016/S0146-6453(03)00002-2

Vuong, A.M., Yolton, K., Webster, G.M., Sjödin, A., Calafat, A.M., Braun, J.M., Dietrich, K.N., Lanphear, B.P., Chen, A., 2016. Prenatal polybrominated diphenyl ether and perfluoroalkyl substance exposures and executive function in school-age children. Environ. Res. 147, 556–564. https://doi.org/10.1016/j.envres.2016.01.008

Wambaugh, J.F., Setzer, R.W., Pitruzzello, A.M., Liu, J., Reif, D.M., Kleinstreuer, N.C., Wang, N.C.Y., Sipes, N., Martin, M., Das, K., DeWitt, J.C., Strynar, M., Judson, R., Houck, K.A., Lau, C., 2013. Dosimetric anchoring of In vivo and In vitro studies for perfluorooctanoate and perfluorooctanesulfonate. Toxicol. Sci. 136, 308–327. https://doi.org/10.1093/toxsci/kft204

Wan, H.T., Zhao, Y.G., Wong, M.H., Lee, K.F., Yeung, W.S.B., Giesy, J.P., Wong, C.K.C., 2011. Testicular signaling is the potential target of perfluorooctanesulfonate-mediated subfertility in male mice. Biol. Reprod. 84,

Chapter 5

1016–1023. https://doi.org/10.1095/biolreprod.110.089219

Wang, J., Sun, B., Hou, M., Pan, X., Li, X., 2012. The environmental obesogen bisphenol A promotes adipogenesis by increasing the amount of 11β-hydroxysteroid dehydrogenase type 1 in the adipose tissue of children. Int. J. Obes. 999–1005. https://doi.org/10.1038/ijo.2012.173

Wang, X., Li, Y., Xu, X., Wang, Y. hua, 2010. Toward a system-level understanding of microRNA pathway via mathematical modeling. BioSystems 100, 31–38. https://doi.org/10.1016/j.biosystems.2009.12.005

Waters, M.D., Boorman, G., Bushel, P., Cunningham, M., Irwin, R., Merrick, A., Olden, K., Paules, R., Selkirk, J., Stasiewicz, S., Weis, B., Van Houten, B., Walker, N., Tennant, R., 2003. Systems toxicology and the Chemical Effects in Biological Systems (CEBS) knowledge base. Environ. Health Perspect. 111, 811–824. https://doi.org/10.1289/txg.5971

Wen, B., Coe, K.J., Rademacher, P., Fitch, W.L., Monshouwer, M., Nelson, S.D., 2008. Comparison of in vitro bioactivation of flutamide and its cyano analogue: Evidence for reductive activation by human NADPH:cytochrome P450 reductase. Chem. Res. Toxicol. 21, 2393–2406. https://doi.org/10.1021/tx800281h

Wysowski, D.K., Fourcroy, J.L., 1996. Flutamide Hepatotoxicity. J. Urol. 155, 209–212. https://doi.org/10.1016/S0022-5347(01)66596-0

Xi, W., Lee, C.K.F., Yeung, W.S.B., Giesy, J.P., Wong, M.H., Zhang, X., Hecker, M., Wong, C.K.C., 2011. Effect of perinatal and postnatal bisphenol A exposure to the regulatory circuits at the hypothalamus-pituitary-gonadal axis of CD-1 mice. Reprod. Toxicol. 31, 409–417. https://doi.org/10.1016/j.reprotox.2010.12.002

Yang, J., Wang, C., Nie, X., Shi, S., Xiao, J., Ma, X., Dong, X., Zhang, Y., Han, J., Li, T., Mao, J., Liu, X., Zhao, J., Wu, Q., 2015. Perfluorooctane sulfonate mediates microglial activation and secretion of TNF-α through Ca2+-dependent PKC-NF-κB signaling. Int. Immunopharmacol. 28, 52–60. https://doi.org/10.1016/j.intimp.2015.05.019

York, N., 2015. Regulation of Cell Survival by Secreted Proneurotrophins.pdf. Science (80-.). 294, 1945–1949. https://doi.org/10.1126/science.1065057

You, H.J., Park, J.H., Pareja-Galeano, H., Lucia, A., Shin, J. Il, 2016. Targeting MicroRNAs Involved in the BDNF Signaling Impairment in Neurodegenerative Diseases. NeuroMolecular Med. https://doi.org/10.1007/s12017-016-8407-9

Yu, N., Wei, S., Li, M., Yang, J., Li, K., Jin, L., Xie, Y., Giesy, J.P., Zhang, X., Yu, H., 2016. Effects of Perfluorooctanoic Acid on Metabolic Profiles in Brain and Liver of Mouse Revealed by a High-throughput Targeted Metabolomics Approach. Sci. Rep. 6, 23963. https://doi.org/10.1038/srep23963

Yun, Y.E., Cotton, C.A., Edginton, A.N., 2014. Development of a decision tree to classify the most accurate tissue-specific tissue to plasma partition coefficient

Chapter 5

algorithm for a given compound. J. Pharmacokinet. Pharmacodyn. 41, 1–14. https://doi.org/10.1007/s10928-013-9342-0

Zamkova, M., Khromova, N., Kopnin, B.P., Kopnin, P., 2013. Ras-induced ROS upregulation affecting cell proliferation is connected with cell type-specific alterations of HSF1/SESN3/p21Cip1/WAF1pathways. Cell Cycle 12, 826–836. https://doi.org/10.4161/cc.23723

Zeng, H. cai, Zhang, L., Li, Y. yuan, Wang, Y. jian, Xia, W., Lin, Y., Wei, J., Xu, S. qing, 2011. Inflammation-like glial response in rat brain induced by prenatal PFOS exposure. Neurotoxicology 32, 130–139. https://doi.org/10.1016/j.neuro.2010.10.001

Zhang, J., Cooke, G.M., Curran, I.H.A., Goodyer, C.G., Cao, X.L., 2011. GC-MS analysis of bisphenol A in human placental and fetal liver samples. J. Chromatogr. B Anal. Technol. Biomed. Life Sci. 879, 209–214. https://doi.org/10.1016/j.jchromb.2010.11.031

Zhang, L., Guo, J., Zhang, Q., Zhou, W., Li, J., Yin, J., Cui, L., 2018. Flutamide induces hepatic cell death and mitochondrial dysfunction via inhibition of Nrf2-mediated heme oxygenase-1. Oxid. Med. Cell. Longev.

Zhang, L., Li, Y.-Y., Zeng, H.-C., Wei, J., Wan, Y.-J., Chen, J., Xu, S.-Q., 2011. MicroRNA expression changes during zebrafish development induced by perfluorooctane sulfonate. J. Appl. Toxicol. 31, 210–222. https://doi.org/10.1002/jat.1583

Zhang, T., Sun, H., Kannan, K., 2013. Blood and urinary bisphenol a concentrations in children, adults, and pregnant women from China: Partitioning between blood and urine and maternal and fetal cord blood. Environ. Sci. Technol. 47, 4686–4694. https://doi.org/10.1021/es303808b

Zhao, B., Hu, G.X., Chu, Y., Jin, X., Gong, S., Akingbemi, B.T., Zhang, Z., Zirkin, B.R., Ge, R.S., 2010. Inhibition of human and rat 3β-hydroxysteroid dehydrogenase and 17β-hydroxysteroid dehydrogenase 3 activities by perfluoroalkylated substances. Chem. Biol. Interact. 188, 38–43. https://doi.org/10.1016/j.cbi.2010.07.001

Chapter 5

Chapter 5

5B. All- in-One-Model for understanding ROS induced hepatotoxicity: From organ-specific pharmacokinetics of Flutamide to predicting its toxic-dynamics effects

Abstract:

Flutamide is a selective androgen receptor antagonist widely used for prostate cancer and is also an EDC (endocrine disrupting chemical). Flutamide treatment patients are at a risk of developing liver toxicity due to its idiosyncratic adverse effect. The desired effects are achieved when the concentration of the chemical is tuned well. So as, to minimize adverse actions off-target, it is necessary to consider (epi-) genetic heterogeneity of the population at both the levels of kinetics and dynamics models. In vitro assays identified alterations of mitochondrial respiration and generation of reactive oxygen species as potential mechanisms underlying flutamide hepatotoxicity. This study details the application of integrative systems toxicology to determine whether these mechanisms could account for the liver toxicity observed in in-vivo and in-vitro assays. Integrative systems toxicology included physiologically based pharmacokinetics simulation to estimate the internal exposure of the hepatic cell to flutamide and its metabolites. Then coupling of estimated tissue dose of flutamide and consequent perturbation in endogenous ROS was carried out using direct pharmacodynamics response models. This perturbation (changes in the ROS level) was dynamically linked to a systems biology model of ROS. This integrative approach allowed us to predict several variables of ROS model such as antioxidant regulated genes, mitochondrial respiration and ATP level as a function of flutamide dosing.

Keywords: PBPK, PD, Systems biology, ROS, Integrative systems toxicology

Chapter 5

1. Introduction

Flutamide is a selective androgen receptor antagonist. It exerts its action by inhibiting androgen binding to its receptor or by inhibiting its uptake in target tissue (prostrate). It is used for the management of locally confined Stage B2-C and Stage D2 metastatic carcinoma of the prostate either alone or in combination with luteinizing hormone-releasing hormone agonists (LHRH). Flutamide produces liver toxicity at its therapeutic dose and the rate of serious liver injury (patient death) is estimated to be 3 per 10,000 users (Wysowski and Fourcroy, 1996). It shows a high incidence of hepatic side effects especially in women using the drug off-label for the treatment of polycystic ovarian disorder and hirsutism (Generali and Cada, 2014). The development of hepatotoxicity during flutamide treatment is presumed to be its idiosyncratic adverse reaction (García Cortés et al., 2001; Gomez et al., 1992; Wysowski and Fourcroy, 1996).

Idiosyncratic adverse effects are characterized by their delayed onset, occurrence in a unique, small proportion of individuals depending on their genetic background and other factors such as generation of reactive metabolites (Dieckhaus et al., 2002). Particularly in the case of liver idiosyncratic adverse reaction, the role of variability between patients in the activity of metabolic enzymes in the generation of oxidative stress and in the consequent mitochondrial dysfunction needs to be better understood (Andrade et al., 2009; Boelsterli and Lim, 2007). Hence, detailed pharmacokinetics of the responsible chemical as well as of other factors affecting the generation of reactive metabolites and their linking with a systems biology describing molecular and functional changes due to perturbation and adaptation in biological pathways should be an useful approach towards understanding the causes of chemical-induced idiosyncratic liver toxicity (Kaplowitz, 2005).

Flutamide undergoes oxidative metabolism by CYP450 generating reactive metabolite(s) such as: flutamide hydroxide (Flu-OH), 4-nitro-3-(trifluoromethyl)-aniline (FLU-1) and 2-methyl-N-(4′-amino-3′ [trifluoromethyl] phenyl) propanamide (FLU-6) (Katchen and Buxbaum 1975 ; Shet et al. 1997; Kobayashi et al. 2012; Toyoda et al. 2000; Wen et al. 2008). The reaction catalysed via CYP3A and CYP1A generates oxidative metabolites responsible for covalent binding to microsomal protein (Berson et al., 1993). Wen et al. (2008) reported that FLU-6 i.e. the product of nitro reduction of flutamide by NADPH: cytochrome P450 reductase (CPR) enhanced the hepatocyte cytotoxicity. it has been found that FLU induces the expression of CYP1A, CYP2B and CYP3A enzyme (Coe et al., 2006).

Both in-vitro and in-vivo rat studies identified alterations of mitochondrial respiration and generation of Reactive Oxygen Species (ROS) as potential mechanisms underlying flutamide hepatotoxicity (Coe et al., 2007; Teppner et al., 2016). Moreover, an inhibitory effect of flutamide hydroxide on mitochondrial respiration chain was reported (Teppner et al., 2016). This might be a contributing factor to the idiosyncratic adverse effect of flutamide due to metabolic variation among individuals. However, Flutamide dosing of 800 mg/kg/day to CYP1A2 knockout mice showed no sign of hepatic toxicity, except in combination with glutathione depletion these mice developed hepatotoxicity (Matsuzaki et al., 2006), emphasizing the importance of glutathione mediated antioxidant defence mechanism. Flutamide treated $Sod2^{+/-}$ (mitochondrial superoxide dismutase) mice were

Chapter 5

more sensitive to hepatotoxicity than wild type (Kashimshetty et al., 2009). This may be important for genotypic variation in SOD2 and glutathione peroxidase (GPX1) in the human population. All these factors indicate that flutamide toxicity is multifactorial: various factors such as generation of the reactive oxygen species, inhibitions of mitochondrial respiration, and underlying mitochondrial abnormalities i.e. genotypic variation in SOD2 etc. all together can lead to hepatic toxicity. The additional mitochondrial effects of 2-hydroxyflutamide, compared with its parent drug, have been related to idiosyncratic DILI in flutamide-treated patients (Ball et al. 2016).

Reactive oxygen species (ROS) are important intracellular signalling molecules produced via various processes particularly in redox inside the cell, viz. reactions involving leakage, such as from the mitochondrial electron transfer chain and from peroxisomal processes., ROS released from mitochondria and endoplasmic reticulum engages in regulation so as to meet the energy demand through transcriptional changes allowing proliferation and differentiation of cell (Kanda et al., 2011; Li et al., 2013; Murphy, 2009; Zamkova et al., 2013). The generated ROS detoxifies through antioxidant defence mechanisms such as the one involving Superoxide dismutase, catalase etc. (Espinosa-Diez et al., 2015). The catabolism and metabolism of ROS run parallel to each other and imbalance of these process can cause intracellular cell damage (Jaeschke et al., 2012).

Integrative systems toxicology comprising of PBPK, QIVIVE and Systems biology can be used to evaluate how flutamide induces hepatotoxicity integrating in-vitro, in-vivo and in-silico approaches. PBPK being mechanistic, it can be used to describe the time course of drug concentration at the cellular level in different species like rat, mice and human. QIVIVE is very useful in constructing in-vivo dose-response from the in-vitro data along with PBPK. Systems biology model here in this case is the detailed ROS model that includes several processes viz. antioxidant defence mechanisms, mitophagy, autophagy and apoptosis etc. and their functional interactions across multiple levels of biological organization. This integrative framework would allow to investigate how *in vivo* exposure to drugs and their major metabolites induces ROS generation and consequently to predict their effect on endogenous molecule that may then lead to hepatocyte death. Hence, the objective of this study is to develop an integrative tool that describes both the kinetic and dynamic effects of Flutamide via coupling physiologically based pharmacokinetics of the drug (PBPK) to a systems biology model of ROS effects. To achieve this objective, two levels of hierarchy were used: First both a PBPK model describing the drug-concentration time-course inside the body and a systems biology model describing ROS generation in liver, were made. Second, the two models were coupled so as to predict Flutamide toxicity in liver at therapeutic doses.

In this study, putative mechanisms of flutamide toxicity identified in several in-vivo and in vitro assays were evaluated for biological plausibility as the underlying drivers of observed liver injury using our new integrative systems toxicology approach. Further, PBPK and systems biology models were used independently to test the hypothesis that both variations in drug metabolism and variations in capability of antioxidant defence with consequent variations mitochondrial dysfunction and ATP depletion, constitute mechanisms of flutamide toxicity. The developed integrative systems toxicology model was used to explore how inter-patient variability impacted flutamide-induced liver

toxicity. This was done by creating virtual populations with variation in anthropometrics and biochemistry.

2. Material and Methods

2.1. Integrative systems toxicology overview

Integrative systems toxicology is a multi-scale approach that includes study of chemicals' kinetics i.e. ADME (absorption, distribution, Metabolism and Elimination), and, their interactions (target dose) with a biological target. Then it arrives at a quantitative analysis of molecular and functional changes that occurs across multiple levels of biological organization. Here, integrative systems toxicology model has several interacting sub-models: physiologically based pharmacokinetics (PBPK), pharmacodynamics (PD) and systems biology. Coupling of a target tissue dose quantified through PBPK with a biological target of ROS network (Systems biology model) is done by using pharmacodynamics model.

Simulations for the current study were conducted in both rat and human model. First in-vitro rat hepatocyte data were used to simulate the ROS SB model and results were compared with experimental data. The previously developed rat flutamide PBPK model was used to simulate the flutamide concentrations in plasma and liver using experimental dose. Then the integrative model was used to simulate the several components of the ROS network and the results were compared with in-vivo rat data to check the performance of the model. Then the model is used to investigate the susceptibility of flutamide- induced hepatotoxicity in humans by testing our underlying hypothesis. Models are developed in both R and COPASI.

2.2. Model hypotheses and assumptions

Four alternative hypotheses representing four putative mechanisms of actions were formulated in six different models. These hypotheses are as follows: 1) exposure to flutamide increases ROS levels in target organ. 2) Not only flutamide but also its metabolite flutamide hydroxide increases the ROS. 3) Metabolic activation of CYP1A2 by flutamide leads to more ROS generation due to higher affinity for flutamide metabolites than for flutamide itself. 4) Functional variation in superoxide dismutase 2 (SOD2) activities could greatly affect flutamide toxicity. Three models were created based on the first three hypotheses and rest three model were created by combining superoxide dismutase 2 variations factor (4^{th} hypothesis) with each of the rest three hypotheses.

The PK/PD link is made based on the assumption that flutamide levels in situ determine the increase in ROS synthesis.

2.3. In-vivo and in-vitro information input to the model

Chapter 5

Coe et al. (2006) through rat experimental study reported that flutamide induced a 10 fold change in CYP1A2 and a 7 fold change in NAD(P)H dehydrogenase, quinone 1(NQO1). The increase in CYP1A2 level was mediated through the flutamide –induced Ahr activation (Coe et al. 2006). NQO1 is a cytoprotective gene which generally detoxifies ROS and thus protects cells against oxidative stress. The induction of NQO1 following an increase in oxidative stress was mediated through the KEAP1(Kelch Like ECH Associated Protein 1)/ Nrf2 (nuclear factor- erythroid-derived 2) like 2/ARE signalling pathway (Dinkova-Kostova et al., 2002). This observation was further supported by the two experiments; one involves experiment on HepG2 cell line which shows that both the flutamide and its metabolite flutamide hydroxide have capability to increase the superoxide (ROS) to a very high level (Ball et al., 2016); and the other, flutamide increases the Nrf2 regulated antioxidant genes (Coe et al. 2007). In another experiment of the in-vitro rat hepatocyte and the in-vivo rat, induction of Nrf2-regulated mRNA expression such as glutathione s transferase Π 1 (GSH Π 1), heme oxygenase 1 (HMOX1) and NAD(P)H:quinone oxidoreductase 1 (NQO1) was reported upon the exposure of flutamide (Teppner et al., 2016). Teppner et al. (2016) experiment involves estimation of both the flutamide plasma concentration and the Nrf2-regulated mRNA expression level in rats plasma for two different time points (3 hr and 24 hr) upon dosing of 500 mg/kg BW of flutamide. Simutanously he also measured the ATP level and Nrf2-regulated mRNA expression in two different time points following exposure of the flutamide to the rat in-vitro hepatocyte cell line. Ball et al. (2016) carried out the experiment on HepaG2 cell line and observed that 2-Hydroxyfltuamide, metabolite of flutamide, significantly reduced the respiratory complex I in addition to its parent compound flutamide and thus increasing the probability of mitochondrial damage. Recently, Zhang et al. (2018) reported flutamide-induced hepatotoxicity by inhibiting the Nrf2/HO-1 pathway, in that they estimated the ATP content, flutamide-induced ROS generation and Nrf2 expression in human hepatocyte cell line for a dose ranging from 12.5 to 100μM. Majorly, Flutamide induced liver toxicity is manifested by loss of ATP and mitochondrial dysfunction, which is accompanied by several proposed mechanisms among them increase in oxidative stress was found to be critical.

2.4. ROS SB model

The SB ROS model represents the generation of reactive oxygen species in response to normal physiological stress. It is fundamentally based on several design principles namely; ROS-induced mitochondrial aging, protection of mitochondria by providing stability; the Keap1-Nrf2 module, providing homeostasis by regulating antioxidant response elements (ARE); the NFκB component as a survivability factor, helping in recovering damaged mitochondria; and DJ-1, a ROS sensor that coordinates Nrf2 and NFκB. The model that has been developed and validated with experimental data previously (Kolodkin et al., 2018), will be used in this study.

2.5. Flutamide PBPK model

The previously developed and validated PBPK model was taken from Chapter 2.B (Sharma et al., 2018). This PBPK model comprises nine compartments, i.e. gut, liver, plasma, lungs, kidney, fat, gonads, prostate and a compartment representing the rest of the body. The exchange of the flutamide between blood and tissue in each organ is

described by flow limited processes under the assumption that at steady state the total chemical concentration in the tissue and in the plasma are in equilibrium with each other. Our previously developed rat model was used to simulate the (Teppner et al., 2016) rat experimental kinetic data obtained by Teppner et al. (2016). This experiment had involved administering the flutamide orally at 0.5 g/kg to six male F344 rats and estimating flutamide plasma concentration at 3 hr and 24 hr. The PBPK model will here be used to predict the intracellular concentrations (target concentrations) for both flutamide and its metabolite as a function of time after oral administration of the drug. This target/biophase concentration is the dose available to interact(s)/perturb the biological target(s)/systems. The computations were carried out for 15000 individual model instantiations. Instantiations differed in the value of one parameter at a time from the set of kinetic parameters marked in chapter 2B Table 1. Parameter values were drawn at random from log normal distributions about the mean with standard deviations of ±1.5.

3. Results

3.1. Pharmacokinetics of flutamide in rat (PBPK model)

The flutamide PBPK model reported in chapter 2B was used to simulate the time course of plasma and liver flutamide concentrations (Fig. 1& 2) for 24 hr. The model input of the rats' body weight ranged from 250 to 300 g and a flutamide oral dosing of 500 mg/kg body weight was considered, as reported in Teppner et al. (2016).

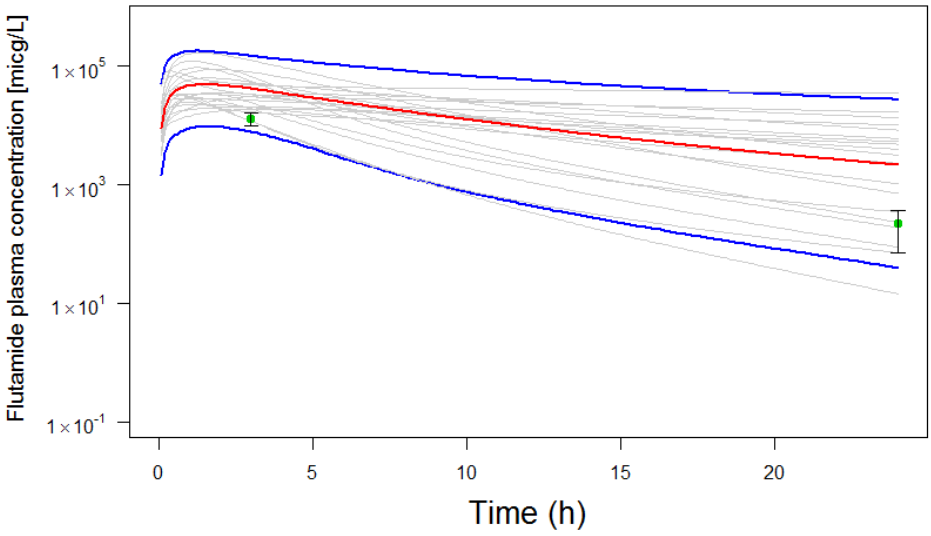

Fig.1: Simulation of flutamide plasma concentrations in the rat after an oral dosing of 0.50 g/kg BW. Blue lines: 2.5 and 97.5 percentiles of flutamide concentration distribution function estimated throught 15,000 iterations taking random values from the distribution

functions of the parameters. Gray lines: 20 simulations chosen at random from the 15,000 iterations. Red line: median prediction. The green dots indicate the experimental observed mean concentrations in the rat after an oral dosing of 0.5 mg/kg BW. Black lines indicate the +/- sd reported in Teppner et al. (2016).

The model of Sharma et al. (2018) over-predicted flutamide plasma concentrations at higher dose (Fig.1), possibly due to dose dependent CYP enzymes' induction by the flutamide via Ahr activation (Coe et al., 2006). Coe et al reported a ^{10}log[CYP1A2] increase in the range of 0.6 to 1.1 (i.e. a 4 to 13 fold change) for dosing in a range of 16 to 500 mg/kg/day. The current study involves simulation of flutamide concentration for 500 mg/kg BW oral dosing to the rats, which is 100 times higher than the dosing of 5 mg/kg on the basis of which the previous model (Sharma et al., 2018) was developed. The extrapolation of the model from a low dose to this much higher dose may lead to changes in dose dependent kinetics particularly in absorption and metabolism rates. For this reason, we here taken a high uncertainty (±2SD) for the parameter value of the fraction absorbed by the gut, assuming high dosing might cause chemicals to be left unabsorbed. We also consider high uncertainty (±2SD) for metabolic parameters assuming there might be a dose dependent metabolic effect. Although there might be additional experimental uncertainties associated with the limited number of animals that could be sued per experimental time point, as well as gender and species variations and plain experimental error, with these minor modifications, the experimentally observed concentrations fell within the model's output range. The model prediction could be improved taking into account the enzyme induction in IVIVE (scaling of metabolism data from in-vitro to in-vivo).

Then this model was used to simulate the flutamide concentrations inside the liver which is the target organ of interest in this study. Fig 2 represents the resulting flutamide liver concentrations in rats as a function of time after oral dosing. The flutamide concentration inside the liver was modelled to be higher than its plasma concentration, which is obvious as the chemical absorbed by the gut has to pass the liver through the portal vein before reaching the plasma. A similar trend was observed in the previous study (Sharma et al., 2018; Chapter 2B).

Chapter 5

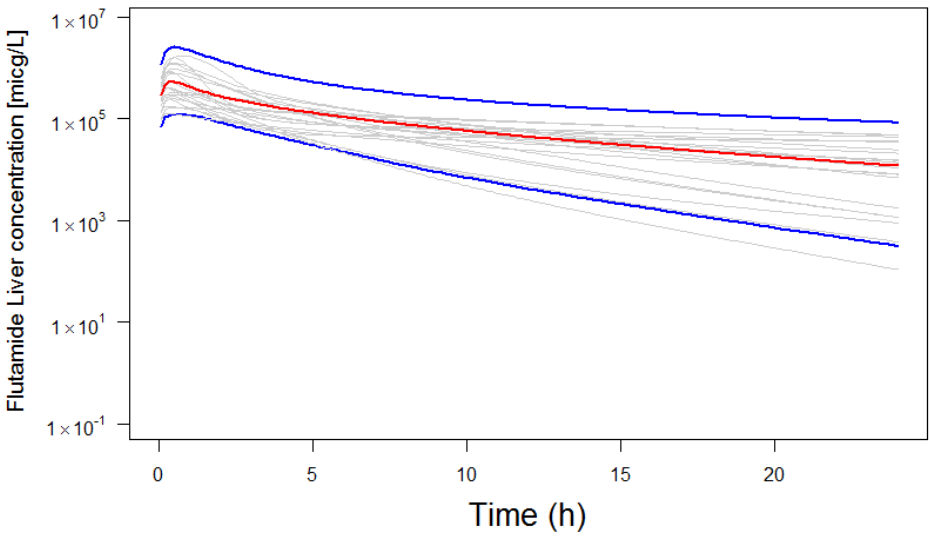

Fig. 2: Simulation of flutamide liver concentrations in the rat after an oral dosing of 0.5 mg/kg BW. Blue lines: 2.5 and 97.5 percentiles; Gray lines: 20 simulations chosen at random from the 15,000 iterations. Red line: median prediction.

3.2. Pharmacokinetics of flutamide in human (PBPK model)

The model built previously by Sharma et al. (2018) (Chapter2B) was used to predict the transport and distribution of flutamide in the human body. This should also allow simulating flutamide dynamics in the particular target cells, e.g. hepatocytes. This model was used to simulate a multiple dose scenario, which involved 1st day single dose of 0.25 g and then a dose of 0.25 g three times a day from the 2nd to the 8th day. The results are presented for plasma both for flutamide and its metabolite flutamide hydroxide and liver in figures 3(A & B) and 4, respectively. The concentration in the liver was again approximately 10 to 15 times higher than the plasma flutamide concentrations. However, flutamide was rapidly cleared from the liver, as compared to the plasma. The output of this PBPK model, i.e. the flutamide concentration in the liver as a function of time, was used as an input to the integrative systems toxicology model.

Chapter 5

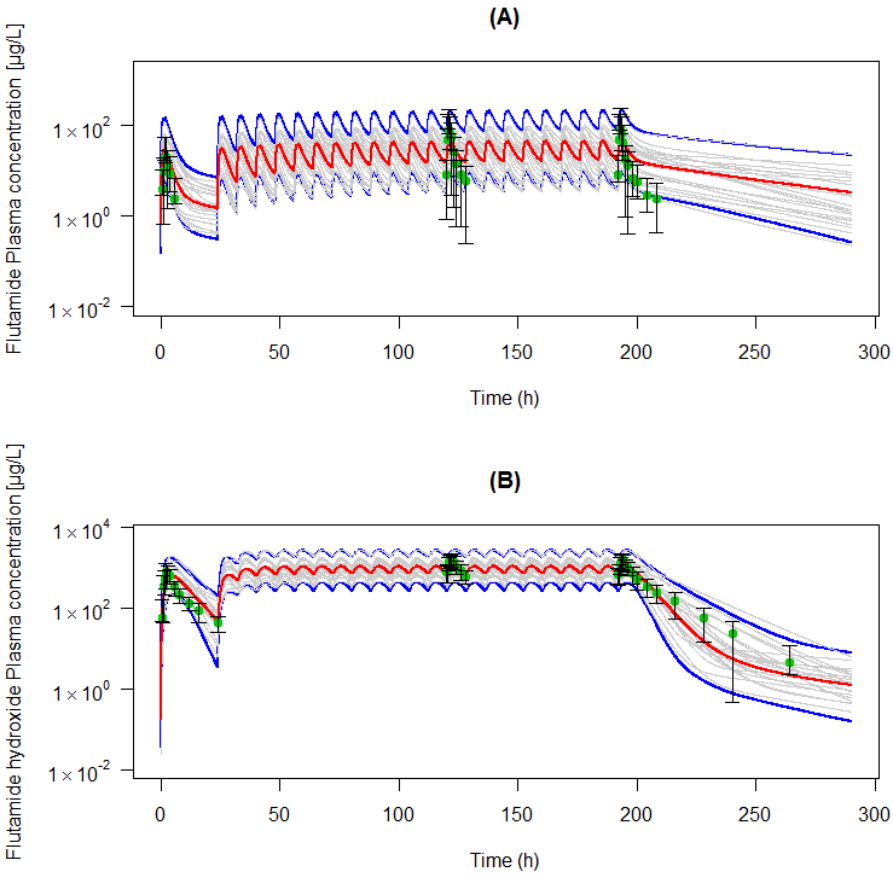

Figure 3: PBPK model predictions of flutamide (A) and flutamide hydroxide (B) plasma concentration in human following a 0.25 g oral dose of flutamide on a first day and then 0.25 g three times a day from the 2nd to 8th day. Red lines: median predictions; blue lines: 2.5 and 97.5 percentiles; gray lines: 20 random simulations. The green dots and black lines indicate the mean +/- sd concentrations reported in Radwanski et al., (1989).

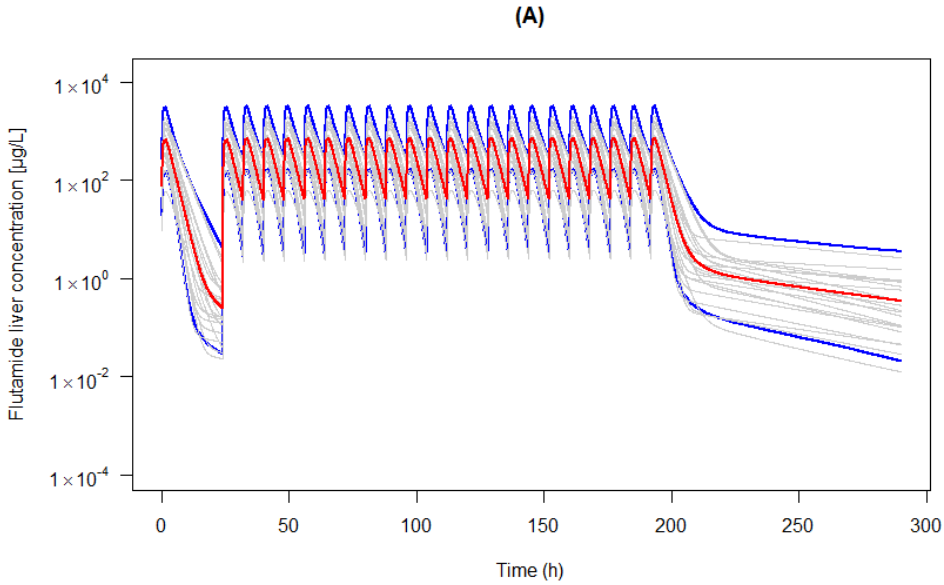

Figure.4: PBPK model predictions of flutamide liver concentration in human following a 0.25 g oral dose of flutamide on a first day and then 0.25 g doses three times a day from the 2nd to the 8th day. Red line: median prediction; blue lines: 2.5 and 97.5 percentiles; gray lines: 20 random simulations.

3.3. In-vitro experiments simulation (ROS SB model)

In this section, our integration of the Flutamide PK model with the dynamic intracellular model of oxidative stress effect is documented. The rate constant for the induction of endogenous ROS was optimized against the observed in-vitro experimental data and was found to be close i.e. 1.2 X 10^{-4} hr^{-1} to the value reported by Leclerc et al. (2014). The PK-ROS (in-vitro) systems biology (SB) model was then used to simulate several components of ROS for various in-vitro concentrations of flutamide at different time points. Results are presented in figures (5-8). Superoxide ($O_2^{\bullet -}$) is considered to be the proximal mitochondrial ROS (Murphy, 2009). The experimentally observed mitochondrial superoxide (mitoSoX) and hydrogen peroxide (H_2O_2) levels were used to simulate the flutamide induced oxidative stress and to check the performance of the model (Fig 5). Flutamide concentrations ranging from 0.05 to 500 µM were used as an input for the model to simulate and the respective responses at 2, 6 and 24 hr were plotted with their means and standard deviations. The mean and standard deviation were calculated for the ensemble of 15000 instantiations of the same model, which were created based on a lognormal statistical distribution of two parameters, i.e. the flutamide-induced ROS synthesis rate constant, and the internal degradation rate constant of flutamide. The model suggested that at 500 µM concentration, ROS levels between 2h and 24 h should vary greatly (Fig. 5A & C; blue bar). This might be due to the fact that increase in ROS level

activates the Nrf2-KEAP1 which in turn regulates the ROS by increasing the synthesis of ARE (Kolodkin et al., 2018; Chapter 4).

The model showed a good prediction of the experimental data. The simulated results of several doses at different time points showed increasing ATP depletion with the increasing concentration for initial time points. The simulated and observed ATP concentrations for the 300 µM dose were much lower that these concentrations for the lower doses ranging from 0.05 to 100 µM. At the dose of 300µM, the model predicted a high amount of ROS, which caused a massive depletion in ATP at initial time points. Comparing ATP level between figure 6.A and 6.C at 24hr one could see, the ATP started to recover. Eventually, after stopping the dosing, the ATP able to recovered back to its initial steady state magnitude after a 3 to 4 days approximately (data has not shown).

Figure 7 shows the simulated vs experiment data on NQO1 and HOMOX1 leves at three different time points (2, 6 and 24hr) at 50 µM and 100 µM in-vitro concentrations. The time dependent increase in the level of the Nrf2-regulated Antioxidant Response Element (ARE) (NQO1) can be observed. In figure 7B, initially there is increase in Nrf2-regulated HOMOX1 which then slowly decreased. Figure 7, the time dependent increase in concentration of of Nrf2 regulated NQO1 (Antioxidant response element) was observed. The synthesis of antioxidant elements involves the activation of the downstream signalling cascade loop (Nrf2-KEAP1-ARE) (Chapter 4). The time lag between the ROS induced Nrf2 activation and antioxidant response elements (ARE) activation peak concentration should be the time required for the system to find a new balance. In other words, this may be the time required to back regulate the ROS to a new steady state where the cells can maintain enough ATP and healthy mitochondria for their survival.

Figure 8 represents the observed vs predicted relative expression of P62mRNA. The model predicts the minor time-dependent and flutamide dose-dependent increases in expression of P62mRNA observed experimentally.

Chapter 5

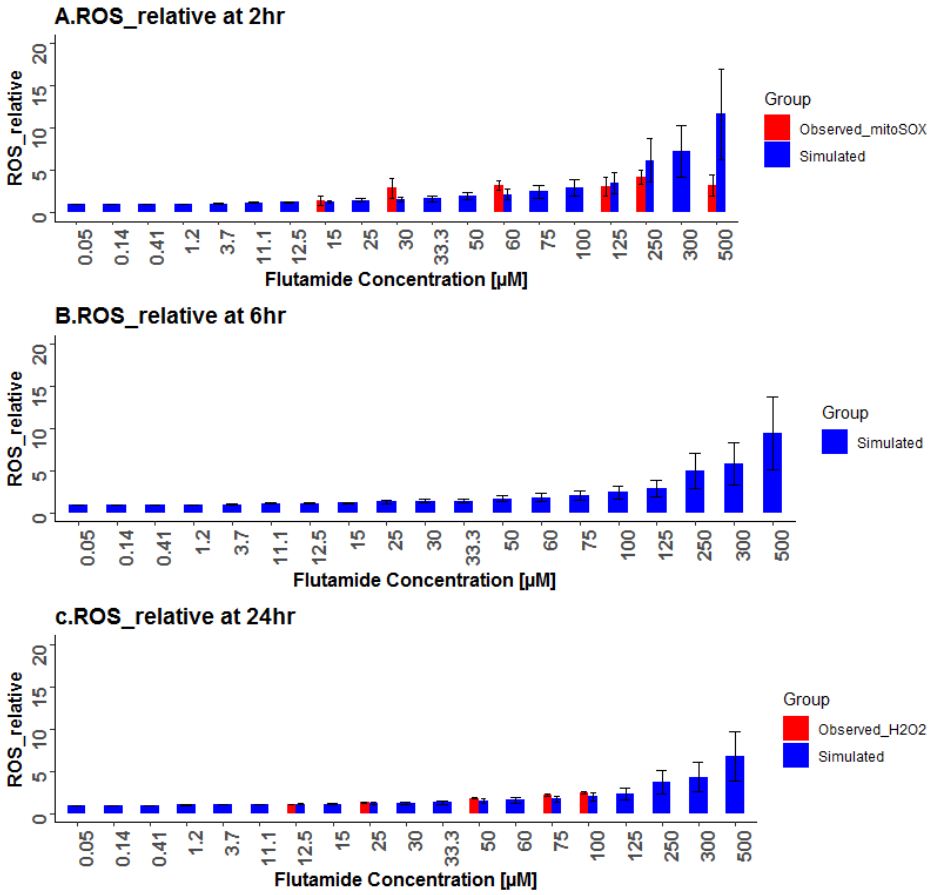

Fig 5. Flutamide in-vitro concentrations-response relationship for relative ROS levels at three different time points computed for the in-vitro setting of incubating cells from time zero onwards in a medium containing flutamide at various concentrations. A) corresponds to 2 hr, B) corresponds to 6 hr and C) corresponds to 24 hr. The PK-SB model simulated for various in-vitro concentrations (provided in the abscissa of the figure). The results were compared against the corresponding experimental data reported in the literature. Blue bars indicate simulated data with the black bar representing ±SD which is calculated from the ensemble of 15000 models. The red bars are experimentally observed data relative mitoSoX (mitochondrial superoxide) at 2hr reported in (Ball et al., 2016)and relative H_2O_2 at 24 hr reported in (Zhang et al., 2018).

Chapter 5

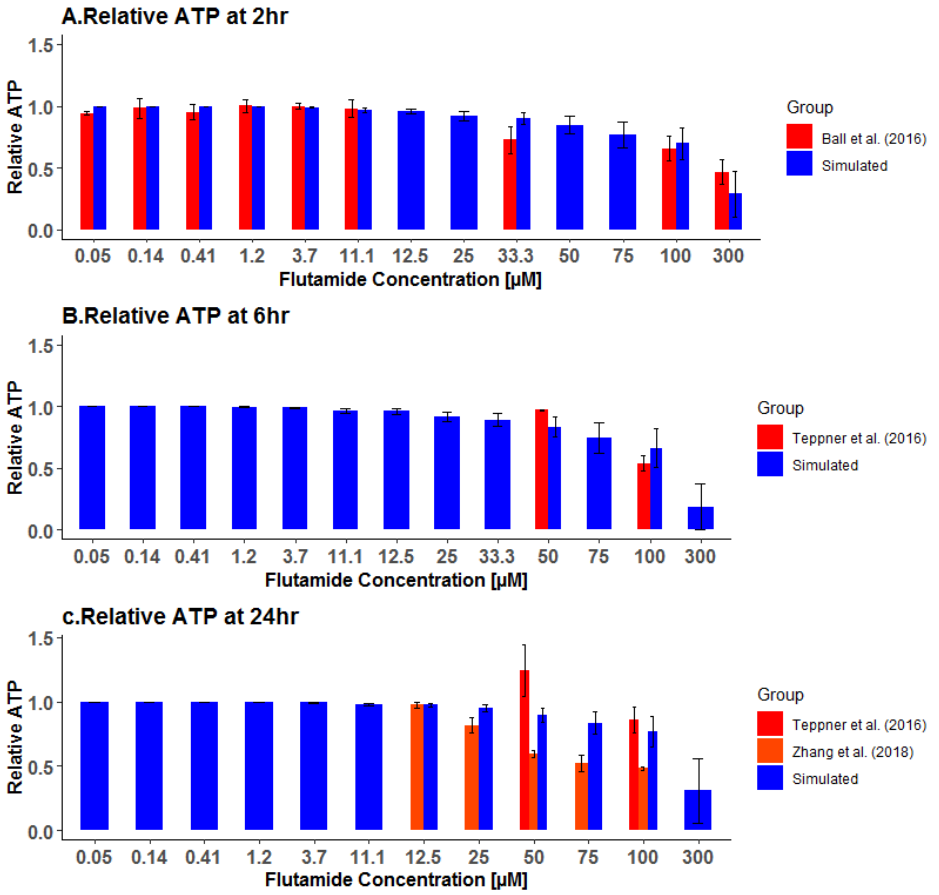

Fig 6. Flutamide in-vitro concentrations-response relationship for intra-hepatocyte ATP concentration at various time points after incubation from time zero in a medium containing flutamide at the concentration indicated A) corresponds to 2 hr, B) corresponds to 6 hr and C) corresponds to 24 hr. The PK-SB model was simulated for the various concentrations provided on the abscissa of the figure. The calculated ATP concentrations relative to the one at zero dose (blue bars) are compared against the experimentally observed data reported in the literature (red and orange bars). The black lines represent ±SD which is calculated from the ensemble of 15000 models. A) The red bars are the experimentally observed data reported in Ball et al. (2016) (relative to the ATP concentration at 2hr), B) red bars reported in Teppner et al. (2016) (relative to ATP at 6hr) and (C) red and orange bars experimentally observed relative to [ATP] at 24hr as reported in Teppner et al. (2016) and Zhang et al. (2018) respectively.

Chapter 5

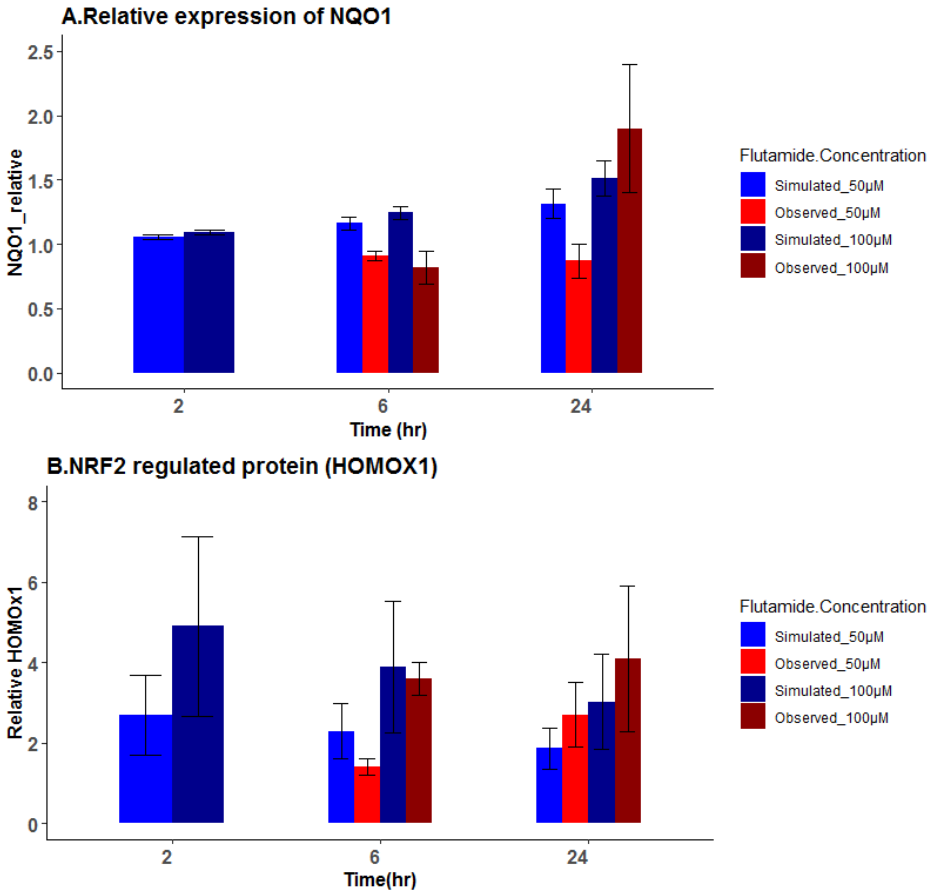

Fig 7. Flutamide in-vitro concentrations-Response Bar-plot; A) relative NQO1 value at different time points (2, 6 and 24 hr) B) Relative Nrf2 value at different time points (2, 6 and 24 hr). The PK-SB model was simulated for different doses (as indicated on the right-hand side of the figure) and the results were compared against the experimentally observed data reported in the literature. Blue bar plots indicate simulated data with black bar representing ±SD, which was calculated from the ensemble of 15000 models. Gradient red color bars are experimentally observed data reported in (Teppner et al., 2016).

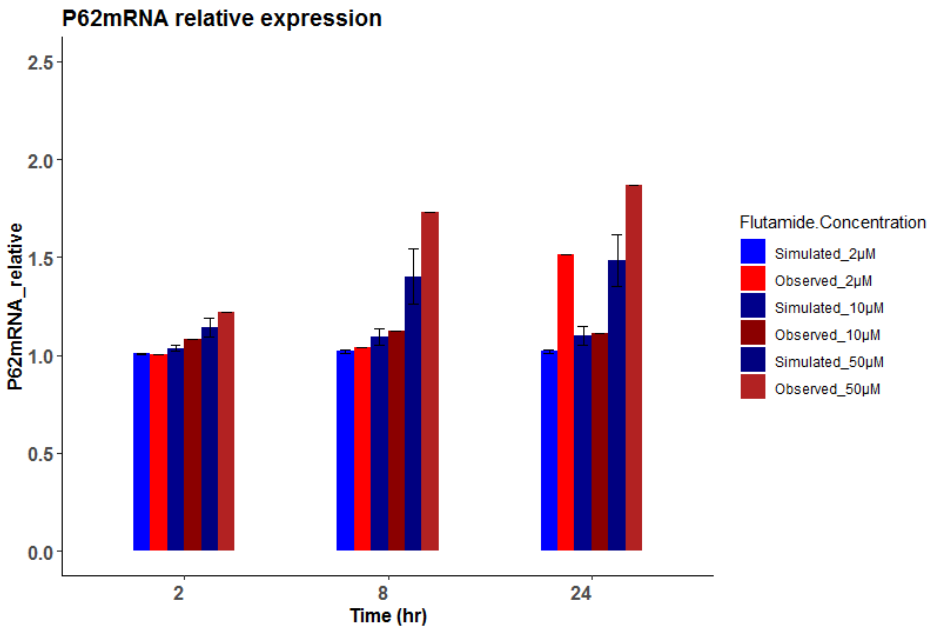

Fig 8. Flutamide in vitro concentration-Response Bar-plot for relative P62mRNA level at different time points after cells' incubation with flutamide. The PK-SB model was simulated for different flutamide concentrations (as indicated below the abscissa) and the results were compared against transcriptomic data (http://toxygates.nibiohn.go.jp/toxygates/). Thin black lines indicate ±SD, which was calculated from the ensemble of 15,000 model instantiations. The gradient red color bars present the experimentally derived expression data.

3.4. Integrative systems toxicology

Then, the validated PBPK model and ROS SB model were coupled with the aim of obtaining an integrative systems toxicology model. In the previous section, the ROS SB model was made flutamide-specific by introducing the rate constant for flutamide-induced ROS synthesis externally and by comparing the output of the model against the experimental data (section 3.3). In the present section the output of the PBPK models of sections 3.1 and 3.2, i.e. the cellular concentration of flutamide (in liver) was used as an input to the ROS model. In this section we examine whether this indeed allows us to predict dynamically the response variables of the ROS model as a function of flutamide dose. We used both rat- and human- specific PBPK model for this coupling to the SB model (the SB model was kept the same for both species), presuming that pharmacokinetic differences alone would already lead to the disparate response. Three main components of ROS SB, i.e. ATP, Nrf2 and Cytc were simulated in response to flutamide liver concentrations. ATP and Cytc levels were taken to represent to

mitochondrial function and cell survivability, respectively, whilst Nrf2 should corresponds to the antioxidant functionality.

3.4.1. Integrative systems toxicology for rat

Three main components of ROS SB, i.e. ATP, Nrf2 and Cytc in rat liver were simulated in response to oral dosing of rat with flutamide. The results are presented in Figure 9. Upon dosing of the flutamide at 0.5 g/kg BW, the Nrf2 protein level increased to its maximum level responding to an increase in ROS as a function of flutamide-induced ROS (Fig 9.A). As the flutamide concentration declined in the liver, the Nrf2 level also decreased until it reached its steady state level. However, in some model instantiations, flutamide-induced ROS caused an initially rather strong drop in the ATP level (lower blue line) which did not recover back to its basal steady state level in 24 hr, whilst the model simulation at median and 97.5th percentile recovered very fast (Fig 9.B). The ATP levels in the former case were low enough to be lethal. Fig 9C represents the cytochrome C level. Initially it went up, but very soon thereafter its level decreased. Cytochrome C generally indicates the cell apoptosis process, apoptosis being promoted by high levels. The level of Cytc predicted by the model showed no sign of apoptosis. The strong decrease in the cytochrome c level in some cells might block the electron transfer chain, cause an increased reduction of its bc1 complex and an increased ROS production by NADH dehydrogenase (Complex I). Similar results were obtained by Teppner et al. (2016) in a rat experimental study These authors also measured the Nrf2 regulated genes where they observed a 94±40 fold change for NQO1. A highly expressed Nrf2 regulated gene suggests that there is a significant increase in the expression of the antioxidant genes that it regulates. Our model results (Fig 9D) showed a 10 to 100 fold increase in Nrf2 expression (2.5-97.5 percentile).

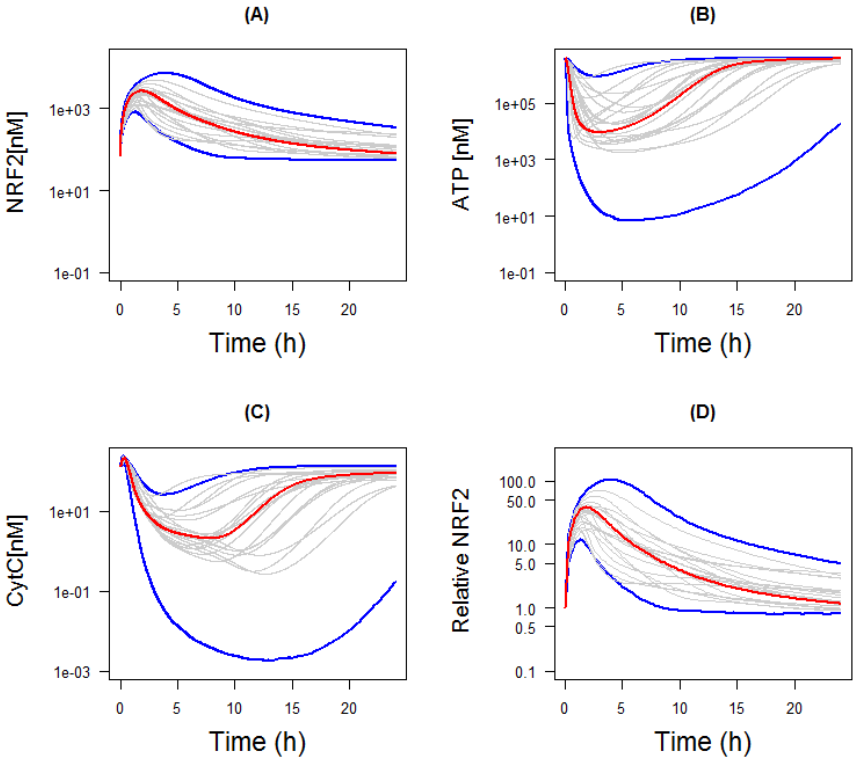

Figure 9: PBPK/ROS SB (Integrative systems toxicology) model predictions of the effect of flutamide on various components of the ROS systems biology network in response to an administration of a 0.50 g/kg BW oral dose of flutamide to the rats; A) Nrf2 protein, B) ATP, C) Cytochrome c, D) Relative Nrf2 expression, Red lines: median predictions; blue lines: 2.5 and 97.5 percentiles; gray lines: 20 random simulations.

3.4.2. Integrative systems toxicology for the human

The validated human PBPK model was used as an input function to the SB model. The same output response variables were simulated as in the case of rat. Here the dosing scenarios are the normal regimen that prostate cancer patients follow. This regimen includes a 250 mg oral dose thrice in day. The flutamide liver concentration was taken into account as a target organ concentrations predicted by PBPK model (see section 3.2, figure 4). The integrative systems toxicology model was simulated for the same dosing scenario as the PBPK had been. The results are presented in figure 10 (A to C). After administration of the flutamide, Nrf2 went up very quickly by some 5% and its tmax, i.e.

the time at which its highest concentration occurred and the drug's tmax were very similar to each other. This shows shows that the homeostatic system's initiation responds quickly to chemical-induced ROS. The maximum level of Nrf2 and particularly of the proteins that it induces should keep the ROS under balance by maximizing their detoxification (increased Nrf2 triggers the synthesis of antioxidant elements via Nrf2-KEAP1 pathway in our model (Chapter 4); data not shown here. After stopping the administration of drug, the system quickly recovered its initial steady state. This was true for all the response variables shown in figure 10.

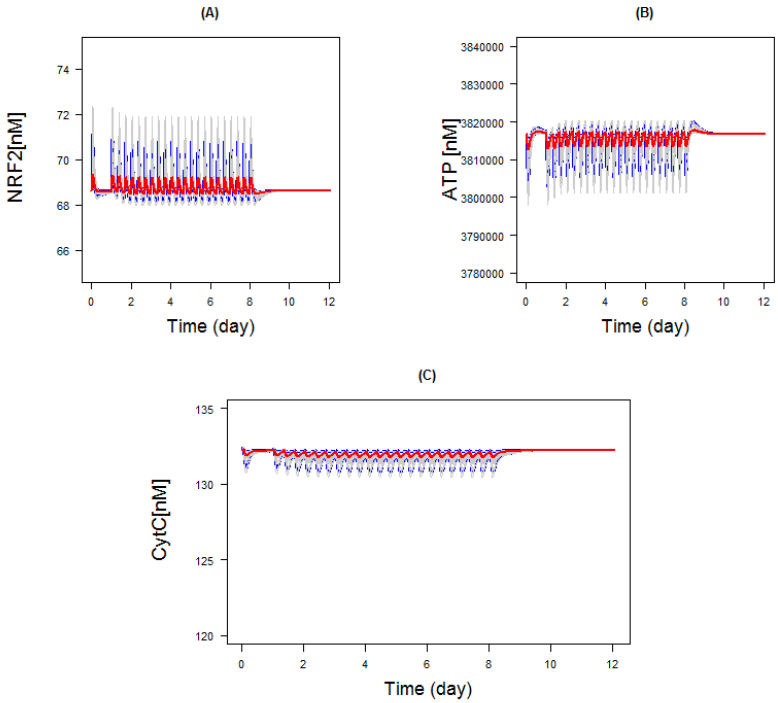

Figure 10: PBPK/ROS SB (Integrative systems toxicology) model predictions of effects of flutamide on the ROS systems biology network; A) NRF2 protein, B) ATP, C) Cytochrome c, in response to administration of a .25 g oral dose of flutamide on a first day and then .25 g three times a day from the 2nd to the 8th day to the humans. Red lines: median predictions; blue lines: 2.5 and 97.5 percentiles; gray lines: 20 random simulations.

Chapter 5

3.4.3. Simulation results for several hypotheses

In this section the results are presented of analyses of the four hypotheses described in section 2.2. The model structure was kept same. Six different submodels were created (A to F) based on these hypotheses. Model A presumes that only the parent compound flutamide is responsible for the generation of ROS in the system. Model B presumes that ROS is generated by both the flutamide and its metabolite flutamide hydroxide. Model C includes the metabolic activation of CYP1A2 in addition to Model B. Furthermore, a SOD mutation was introduced into the ROS SB model in terms of a 50% knockdown of the antioxidant gene (a component of ROS SB). Then the model was run for the steady state and the initial state was updated. This SOD-mutation ROS-SB model was coupled with PBPK (flutamide) to create three more models i.e., D, E and F. Model D includes the two factors functional variation (SOD mutation) SB model and flutamide induced ROS. Model E includes the SOD mutation SB model + both flutamide and flutamide hydroxide induced ROS. Model F includes SOD mutation, metabolic activation of flutamide metabolism by CYP1A2 and Ros induction by both flutamide and flutamide hydroxide.

These models were designed to examine possible flutamide-induced idiosyncratic hepatotoxicity and to identify important contributing factors such as the functional variability in the human population of flutamide metabolism, the underlying mitochondrial functional variability. The simulated levels of healthy mitochondria and ATP subsequent to a usual therapeutic flutamide dose of 0.25 g of flutamide thrice in a day are presented in Figures 11 and 12. If only flutamide induced ROS, its dosing should have no effect on the level of healthy mitochondria and ATP (Fig 11A and 12A respectively). When the effects of flutamide hydroxide were taken into consideration as well (model B), there was a significant drop in both mitochondria and ATP level (Fig 11.B and 12.B). This drop ranged from an approximately 45 % to 2 % fold reduction in healthy mitochondria as compared to control (Fig 11.B). The significant drop was predicted for a 2.5th percentile indicating a low probability hence possible idiosyncrasy. The relative ATP levels for model B ranged from between 55 and 100 % of normal suggesting a somewhat lower ATP sensitivity than mitochondrial damage sensitivity. Adding the metabolic activation factor to the model i.e. flutamide inducing the CYP level which leads to production of more flutamide metabolites (in this case Flu-OH) causing a further increase in ROS production due to high affinity of this metabolite towards ROS production than the affinity of the parent compound. This factor caused a slight further drop in the levels of both the mitochondria and ATP. (Figures 11C and 12C).

By itself the hypotheses of a subpopulation with a mutation in the SOD2 enzyme had little impact on the mitochondrial damage (Fig. 11D) and the ATP depletion (Fig. 12D) caused by the flutamide parent compound. However, also including the metabolite (Flu-OH) and its effects on ROS production, caused a strong drop in both the healthy mitochondria (Fig. 11E) and the ATP level (Fig. 12E), much stronger than in the case of wild type SOD2 enzyme levels. Auto-induction of metabolism of flutamide slightly increased the chances of hepatotoxicity further (Figs 11C, 11F, 12C and 12F). The depletion of both healthy mitochondria and ATP were highly significant in case of both model E and model F. Assuming each random simulation corresponded to a characteristic human individual, it

Chapter 5

becomes important that only a 2.5th percentile of the populations showed signs of hepatotoxicity presuming a threshold of toxicity at 50%. Models E and F (both with SOD knockdown), compromised superoxide inactivation and enhanced the flutamide induced hepatotoxicity. Similar observations have been reported in rat studies with compromised superoxide dismutase activity (Kashimshetty et al., 2009).

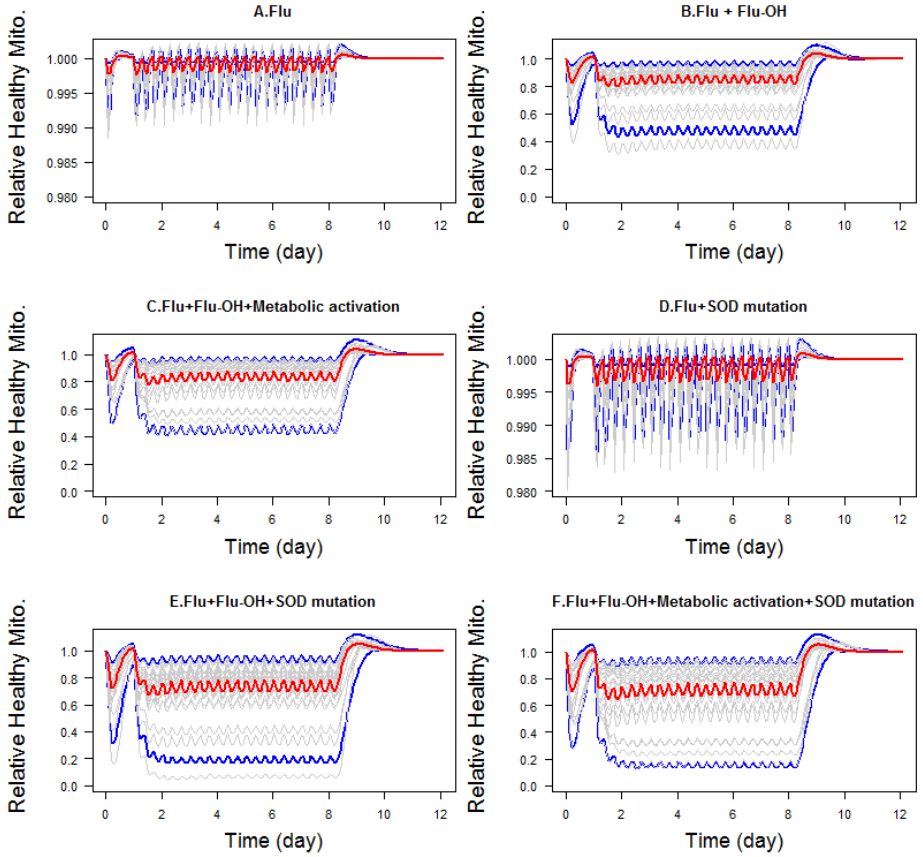

Figure 11: PBPK/ROS SB (Integrative systems toxicology) model predictions of the level of healthy mitochondria ('Mito.') as an effect of flutamide on the ROS systems biology network, following administration of a .25 g oral dose of flutamide on a first day and then .25 g three times a day on the 2nd to 8th day, to humans. Red lines: median predictions; blue lines: 2.5 and 97.5 percentiles; gray lines: 20 random simulations, predictions taken from the ensemble of 50000 instantiations. Predictions are for six submodels such as A) flutamide induced ROS, B) ROS induced by both flutamide and its metabolites, C) Metabolic activation of CYP1A2 + flutamide and flutamide-OH induced ROS, D) Functional variation (SOD mutation) SB model + flutamide induced ROS, E) SOD mutation SB model + both flutamide and flutamide-OH induced ROS, and F) all

Chapter 5

factors, i.e. SOD mutation + Metabolic activation + flutamide and flutamide hydroxide induced ROS.

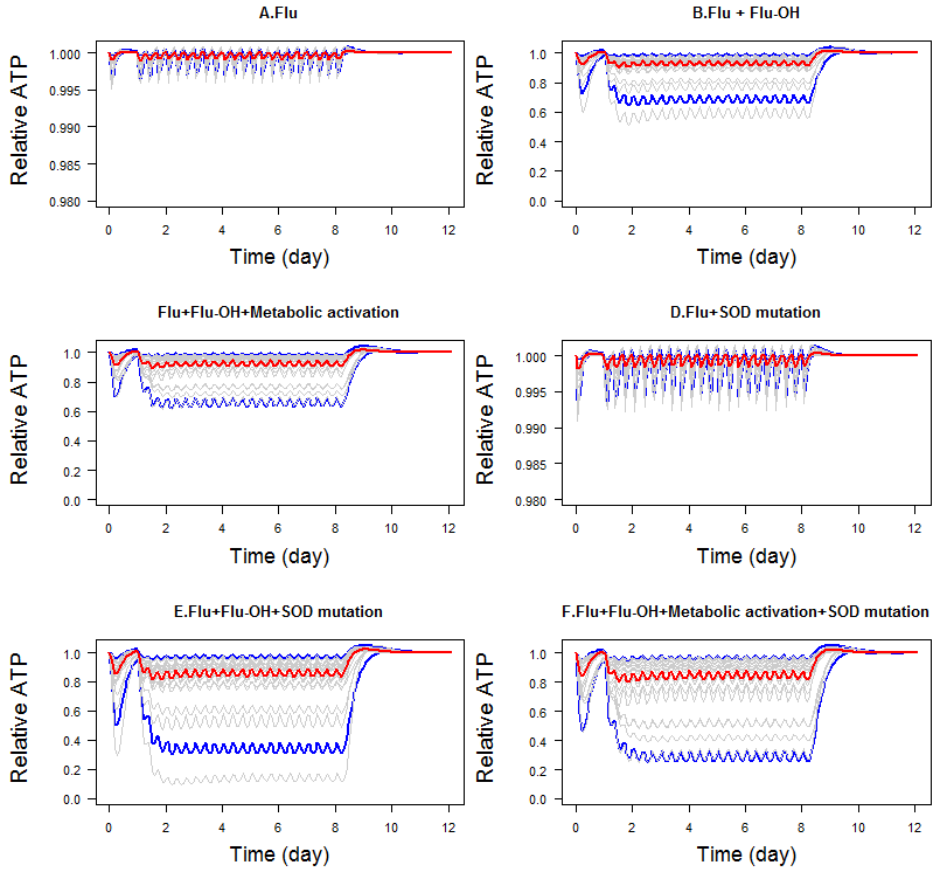

Figure 12: PBPK/ROS SB (Integrative systems toxicology) model predictions of relative ATP level as an effect of flutamide on the ROS systems biology network following administration of a .25 g oral dose of flutamide on the first day followed by .25 g three times a day on the 2nd to 8th day to the humans. Red line: median prediction; blue lines: 2.5 and 97.5 percentiles; gray lines: 20 random simulations, predictions taken from the ensemble of 50000 models (instantiations). It includes several models such as A) flutamide induced ROS, B) flutamide and its metabolites induced ROS, C) Metabolic activation of CYP1A2 + flutamide and flutamide-OH induced ROS, D) Functional variation (SOD mutation) SB model + flutamide induced ROS, E) SOD mutation SB model + both flutamide and flutamide induced ROS, and F) including all factors, i.e. SOD mutation + metabolic activation + flutamide and flutamide hydroxide induced ROS.

Chapter 5

4. Discussion

The framework we developed for a PBPK-integrated systems toxicology of ROS (ROS-IST) included the development and validation of two individual models namely a flutamide PBPK and a ROS-SB model. The integration of both models was then achieved by incorporating drug induced ROS synthesis via a linear pharmacodynamics reaction. We confirmed that the integration could be achieved: our PBPK integrated ROS model enabled us to simulate how perturbations in various components of the ROS-managing network affected cell viability and toxicity as a function of oral flutamide dosing. This demonstrates that this whole framework constitutes a, possibly, first case of integrative systems toxicology.

Integration of an in-vitro pharmacokinetic with a system biology model have been reported to predict the adverse effects of chemical (Leclerc et al., 2014). Similarly integration of genome scale metabolic networks (GSMNs), PBPK and metabolic gene regulation was proposed (Maldonado and Leoncikas, 2017). This approach could link Genetic polymorphism in thousands of metabolic enzyme genes mechanistically. General limitations or challenges of our approach include the use of simple pharmacodynamics rate equations to couple PBPK and ROS Systems biology model and limit extents of validation because several additional experiments are required to confirm the results.

Flutamide toxicity mainly involves a substantial induction of Nrf2- responsive genes, depletion of the ATP level, and mitochondrial dysfunction (Coe et al. 2007). Our model showed a substantial induction of Nrf2 levels in case of both rat and human. However, the modelled level of the ATP did not decrease much and recovered quickly when the drug was eliminated from the body: There was an increase in NRF2 (antioxidant regulator gene) back regulating ROS. As the Nrf2-Keap1 system works as ROS sensor and forms the first contour of defense by activating antioxidant response and mitophagy (Chapter 4). This activation of Nrf2 signaling that accompanies the increase of ROS generation helps to protect against oxidative stress. Our model showed that NRF2 mediated antioxidant defense mechanism is important to protect the systems against the chemical induced ROS. It also showed that an antioxidant defense mechanism compromised in terms of a reduced function of super oxide dismutase, should be expected to cause significant drops in the level of healthy mitochondria and ATP level. The model predicted the trends established under many experimental conditions (Teppner et al., 2016).

It has been observed that patients who develop hepatic toxicity symptoms during treatment, recover once they stop to take the medication (Brahm et al., 2011). This may correspond to our modeling results. There might be other underlying process that the chemical-induced ROS, however. Some of these processes has been discussed and reported in the present study. It seems likely that other processes may be added once their kinetic details become clearer. Already, the model supported the hypotheses of involvement of multiple factors in the flutamide-induced hepatotoxicity.

The results presented in this chapter may be of particular interest to the problem of idiosyncratic toxicity. Because of financial limitations, clinical trials can only involve a limited number of individuals. The statistics thereby are just able to predict average or

median behavior robustly, but not the outliers. We propose that IST may help to fill this gap in the way illustrated here, i.e. by computing families of models, each of the many family members of which correspond to different sets of parameter values. These computations of families of 15 000 members may then yield small subgroups that exhibit extreme, toxicity-related behavior. Figures 9 and 11 may illustrate this best. Where the median showed moderate changes in important cell properties, a 2.5 percentile showed much more drastic changes, drastic enough to lead to cell death. It remains to be seen if in this way we can identify actual cases of idiosyncratic toxicity.

References

Andrade, R., Agundez, J., Lucena, M., Martinez, C., Cueto, R., Garcia-Martin, E., 2009. Pharmacogenomics in Drug Induced Liver Injury. Curr. Drug Metab. 10, 956–970. https://doi.org/10.2174/138920009790711805

Ball, A.L., Kamalian, L., Alfirevic, A., Lyon, J.J., Chadwick, A.E., 2016. Identification of the additional mitochondrial liabilities of 2-hydroxyflutamide when compared with its parent compound, flutamide in HepG2 cells. Toxicol. Sci. 153, 341–351. https://doi.org/10.1093/toxsci/kfw126

Berson, A., Wolf, C., Chachaty, C., Fisch, C., Fau, D., Eugene, D., Loeper, J., Gauthier, J.-C., Beaune, P., Pompon, D., Maurel, P., Pessayre, D., 1993. Metabolic activation of the nitroaromatic antiandrogen flutamide by rat and human cytochromes P-450, including forms belonging to the 3A and 1A subfamilies. J. Pharmacol. Exp. Ther. 265, 366–372.

Boelsterli, U.A., Lim, P.L.K., 2007. Mitochondrial abnormalities—A link to idiosyncratic drug hepatotoxicity? Toxicol. Appl. Pharmacol. 220, 92–107. https://doi.org/10.1016/j.taap.2006.12.013

Coe, K.J., Jia, Y., Han, K.H., Rademacher, P., Bammler, T.K., Beyer, R.P., Farin, F.M., Woodke, L., Plymate, S.R., Fausto, N., Nelson, S.D., 2007. Comparison of the cytotoxicity of the nitroaromatic drug flutamide to its cyano analogue in the hepatocyte cell line TAMH: Evidence for complex I inhibition and mitochondrial dysfunction using toxicogenomic screening. Chem. Res. Toxicol. 20, 1277–1290. https://doi.org/10.1021/tx7001349

Coe, K.J., Nelson, S.D., Ulrich, R.G., He, Y., Dai, X., Cheng, O., Caguyong, M., Roberts, C.J., Slatter, J.G., 2006. Profiling the hepatic effects of flutamide in rats: A microarray comparison with classical aryl hydrocarbon receptor ligands and atypical CYP1A inducers. Drug Metab. Dispos. 34, 1266–1275. https://doi.org/10.1124/dmd.105.009159

Dieckhaus, C.M., Thompson, C.D., Roller, S.G., Macdonald, T.L., 2002. Mechanisms of idiosyncratic drug reactions: the case of felbamate. Chem. Biol. Interact. 142, 99–117. https://doi.org/10.1016/S0009-2797(02)00057-1

Chapter 5

Dinkova-Kostova, A.T., Holtzclaw, W.D., Cole, R.N., Itoh, K., Wakabayashi, N., Katoh, Y., Yamamoto, M., Talalay, P., 2002. Direct evidence that sulfhydryl groups of Keap1 are the sensors regulating induction of phase 2 enzymes that protect against carcinogens and oxidants. Proc. Natl. Acad. Sci. U. S. A. 99, 11908–13. https://doi.org/10.1073/pnas.172398899

Espinosa-Diez, C., Miguel, V., Mennerich, D., Kietzmann, T., Sánchez-Pérez, P., Cadenas, S., Lamas, S., 2015. Antioxidant responses and cellular adjustments to oxidative stress. Redox Biol. 6, 183–197. https://doi.org/10.1016/j.redox.2015.07.008

García Cortés, M., Andrade, R.J., Lucena, M.I., Sánchez Martínez, H., Fernández, M.C., Ferrer, T., Martín-Vivaldi, R., Peláez, G., Suárez, F., Romero-Gómez, M., Montero, J.L., Fraga, E., Camargo, R., Alcántara, R., Pizarro, M.A., García-Ruiz, E., Rosemary-Gómez, M., 2001. Flutamide-induced hepatotoxicity: report of a case series. Rev. Esp. Enferm. Dig. 93, 423–32.

Gautier, L., Cope, L., Bolstad, B.M., Irizarry, R.A., 2004. affy--analysis of Affymetrix GeneChip data at the probe level. Bioinformatics 20, 307–315. https://doi.org/10.1093/bioinformatics/btg405

Generali, J.A., Cada, D.J., 2014. Flutamide: Hirsutism in Women. Hosp. Pharm. 49, 517–520. https://doi.org/10.1310/hpj4906-517

Gomez, J.-L., Dupont, A., Cusan, L., Tremblay, M., Suburu, R., Lemay, M., Labrie, F., 1992. Incidence of liver toxicity associated with the use of flutamide in prostate cancer patients. Am. J. Med. 92, 465–470. https://doi.org/10.1016/0002-9343(92)90741-S

Igarashi, Y., Nakatsu, N., Yamashita, T., Ono, A., Ohno, Y., Urushidani, T., Yamada, H., 2015. Open TG-GATEs: a large-scale toxicogenomics database. Nucleic Acids Res. 43, D921–D927. https://doi.org/10.1093/nar/gku955

Irizarry, R.A., Hobbs, B., Collin, F., Beazer-Barclay, Y.D., Antonellis, K.J., Scherf, U., Speed, T.P., 2003. Exploration, normalization, and summaries of high density oligonucleotide array probe level data. Biostatistics 4, 249–64. https://doi.org/10.1093/biostatistics/4.2.249

Jaeschke, H., McGill, M.R., Ramachandran, A., 2012. Oxidant stress, mitochondria, and cell death mechanisms in drug-induced liver injury: lessons learned from acetaminophen hepatotoxicity. Drug Metab. Rev. 44, 88–106. https://doi.org/10.3109/03602532.2011.602688

Kanda, Y., Hinata, T., Kang, S.W., Watanabe, Y., 2011. Reactive oxygen species mediate adipocyte differentiation in mesenchymal stem cells. Life Sci. 89, 250–258. https://doi.org/10.1016/j.lfs.2011.06.007

Chapter 5

Kaplowitz, N., 2005. Idiosyncratic drug hepatotoxicity. Nat. Rev. Drug Discov. 4, 489.

Kashimshetty, R., Desai, V.G., Kale, V.M., Lee, T., Moland, C.L., Branham, W.S., New, L.S., Chan, E.C.Y., Younis, H., Boelsterli, U.A., 2009. Underlying mitochondrial dysfunction triggers flutamide-induced oxidative liver injury in a mouse model of idiosyncratic drug toxicity. Toxicol. Appl. Pharmacol. 238, 150–159. https://doi.org/10.1016/j.taap.2009.05.007

Katchen, B., Buxbaum, S., 1975. Disposition of a new, nonsteroid, antiandrogen, alpha,alpha,alpha-trifluoro-2-methyl-4'-nitro-m-propionotoluidide (Flutamide), in men following a single oral 200 mg dose. J. Clin. Endocrinol. Metab. 41, 373–9. https://doi.org/10.1210/jcem-41-2-373

Kobayashi, Y., Fukami, T.., Shimizu, M., Nakajima, M., Tsuyoshi., Y., 2012. Short Communication Contributions of Arylacetamide Deacetylase and Carboxylesterase 2 to Flutamide Hydrolysis in Human Liver. Drug Metab. Dispos. 40, 1080–1084.

Leclerc, E., Hamon, J., Legendre, A., Bois, F.Y., 2014. Integration of pharmacokinetic and NRF2 system biology models to describe reactive oxygen species production and subsequent glutathione depletion in liver microfluidic biochips after flutamide exposure. Toxicol. Vitr. 28, 1230–1241. https://doi.org/10.1016/j.tiv.2014.05.003

Li, X., Fang, P., Mai, J., Choi, E.T., Wang, H., Yang, X., 2013. Targeting mitochondrial reactive oxygen species as novel therapy for inflammatory diseases and cancers. J. Hematol. Oncol. 6, 19. https://doi.org/10.1186/1756-8722-6-19

Maldonado, E.M., Leoncikas, V., 2017. Integration of Genome Scale Metabolic Networks and Gene Regulation of Metabolic Enzymes With Physiologically Based Pharmacokinetics 732–746. https://doi.org/10.1002/psp4.12230

Matsuzaki, Y., Nagai, D., Ichimura, E., Goda, R., Tomura, A., Doi, M., Nishikawa, K., 2006. Metabolism and hepatic toxicity of flutamide in cytochrome P450 1A2 knockout SV129 mice. J. Gastroenterol. 41, 231–239. https://doi.org/10.1007/s00535-005-1749-y

Murphy, M.P., 2009. How mitochondria produce reactive oxygen species. Biochem. J. 417, 1–13. https://doi.org/10.1042/BJ20081386

Smyth, G.K., 2004. Linear Models and Empirical Bayes Methods for Assessing Differential Expression in Microarray Experiments. Stat. Appl. Genet. Mol. Biol. 3, 1–25. https://doi.org/10.2202/1544-6115.1027

Teppner, M., Boess, F., Ernst, B., Pähler, A., 2016. Biomarkers of flutamide-bioactivation and oxidative stress in vitro and in vivo. Drug Metab. Dispos. 44, 560–569. https://doi.org/10.1124/dmd.115.066522

Chapter 5

Toyoda, K., Shibutani, M., Tamura, T., Koujitani, T., Uneyama, C., Hirose, M., 2000. Repeated dose (28 days) oral toxicity study of flutamide in rats, based on the draft protocol for the `Enhanced OECD Test Guideline 407' for screening for endocrine-disrupting chemicals. Arch. Toxicol. 74, 127–132. https://doi.org/10.1007/s002040050664

Wen, B., Coe, K.J., Rademacher, P., Fitch, W.L., Monshouwer, M., Nelson, S.D., 2008. Comparison of in vitro bioactivation of flutamide and its cyano analogue: Evidence for reductive activation by human NADPH:cytochrome P450 reductase. Chem. Res. Toxicol. 21, 2393–2406. https://doi.org/10.1021/tx800281h

Wysowski, D.K., Fourcroy, J.L., 1996. Flutamide Hepatotoxicity. J. Urol. 155, 209–212. https://doi.org/10.1016/S0022-5347(01)66596-0

Zamkova, M., Khromova, N., Kopnin, B.P., Kopnin, P., 2013. Ras-induced ROS upregulation affecting cell proliferation is connected with cell type-specific alterations of HSF1/SESN3/p21Cip1/WAF1pathways. Cell Cycle 12, 826–836. https://doi.org/10.4161/cc.23723

Zhang, L., Guo, J., Zhang, Q., Zhou, W., Li, J., Yin, J., Cui, L., 2018. Flutamide induces hepatic cell death and mitochondrial dysfunction via inhibition of Nrf2-mediated heme oxygenase-1. Oxid. Med. Cell. Longev.

General discussion and conclusions

General discussion

Endocrine disrupting chemicals (EDCs) are natural or anthropogenic substances in environment, food, or consumer products that can disrupt hormonal balances in humans and wildlife, and result in adverse health effects even at low dosage. There are several challenges in quantitative prediction of the EDCs-induced adverse effects on human health associated with their complex exposure, non-linear kinetics, metabolite(s), and their complex mechanism or the complex responses of organisms over different life stage or time scales. The ECHA and the EFSA mainly focus on the development of tools, alternative to animal testing, to improve the protection of human health and the environment through the better and earlier identification of the intrinsic properties of chemical substances. These involved development of novel in-vitro assays, in-silico tools and integrated assessment and testing approaches (IATAs) etc.

In-silico techniques have been receiving attention as alternative methods to classical approaches. Emerging high-throughput analysis, OMICS and tools such as PBPK, PD, Systems biology models and AOPs offer an opportunity to understand the chemical fate inside the body, the biological complexities and their multilevel connectivity. The successive use of the PBPK model in the field of toxicology is commendable since it offers the great advantage of predicting internal tissue dose of compounds or metabolites by utilizing the data derived from the in-vitro and in-silico tool such as QSAR, without any animal experiments. The PBPK also allows cross species extrapolation, cross-route dose interpolation, age and population specific without the need of experimental analysis. This is of great advantage to the field of the environmental toxicology enabling to test the large amount of the organic chemicals, reducing the cost and the time of analysis.

Many biological adverse effects emerge from perturbations of multiple signalling pathways. These signalling pathways involve nonlinear interactions consisting of many components which requires more information for their specification than linear interactions do, and it is hard to foresee what comes from nonlinear interactions. Systems biology suggests a solution to this problem – to reconstruct the biological behaviour in an in silico replica of the system. It is possible to reconstruct the biological emergence by translating the information about how components communicate into mathematical equations. By integrating and solving the resulting system of mathematical equations in a computer, one should be able to simulate the biological system's behaviour. Basically, with the use of Systems biology models we could be able to solve the complex biological system. In parallel, the concepts of AOPs has been developed and elaborated as an approach to predict the adverse effects of the chemicals. It presumes that the biological system's behaviour is the result of the events of the sequences of biological components' interactions. This approach was developed to reduce the inherent biological complexity where the knowledge/data are lacking. Integration of a wide range of in silico tools (QSAR, PBPK/PD, AOP, systems biology models etc.), and databases (OMICS,

General discussion

epidemiological and exposure data) can directly tie the results into a predictive adverse outcomes model. This integrative approach would lead to mechanistic understanding of adverse effects vs conventional empirical end points and animal based testing.

The main objective of the thesis was to explore the use of the in-silico models such as PBPK, PD and Systems biology and to elaborate an integrated, harmonized and pragmatic methodology for the human health assessment mostly focusing on endocrine disrupting compounds (EDCs). Our case studies of integrative systems toxicology approaches were presented in 5 subsequent chapters, illustrating the potential of this innovative approach for human health risk assessment.

Chapter 1 explored the possible EDCs and their effects on human health based on their modes of action. Grouping of EDCs was proposed based on their target organs, receptors, and similar adverse outcomes. Chapter I also addressed the challenges in the quantitative risk assessment of such EDCs effects on human health such as multiple mechanisms of action, delayed responses (time lag between exposure to adverse outcomes), dynamic interactions involving crosstalk, and transgenerational effects. The transgenerational effects of EDCs were demonstrated via a case study of female fertility. The potential EDCs targets involved in life stage development from germ cell to zygote have been also identified. A conceptual model of PBPK/PD was proposed. This model involves an integrated risk assessment framework linking exposome-internal exposure-biological effect to the adverse outcome. This chapter showed the need for a dynamic model (AOPs or systems biology) in addition to the PBPK (a kinetic model) to have a complete and wider picture on predicting adverse effects of chemicals on biological systems.

Chapter 2 included the development and validation of a PBPK model for two different chemicals including their metabolite(s). The First part included di (2-ethylhexyl) phthalate (DEHP), and the second part included Flutamide. Both chemicals are categorized as non-persistent Endocrine disruptors' compounds. Two different approaches were used for the development of the PBPK model: 1) a bottom up approach and 2) a cross-species extrapolation.

DEHP is metabolized into a toxic compound, mono-(2-ethylhexyl) phthalate (MEHP) and other metabolites. In this chapter, the DEHP PBPK model including its major metabolites was developed using in-vitro metabolic data. The IVIVE (in-vitro in-vivo extrapolation) approach was used to translate the in-vitro metabolic data into their in-vivo counterpart. The tissue composition QSAR method was used to determine the distribution of the compounds and their metabolites. Both uncertainty and sensitivity analysis were performed. To our knowledge this was the first PBPK model developed with detailed metabolic kinetics. The model was validated against independent experimental data on chemical/metabolite(s) plasma and urine concentrations. The similarity of the model prediction to the experimental data showed that the integration of the data derived from the in-vitro and the in-silico sources was well enough to predict the chemical's kinetics.

General discussion

The currently developed model was applied in both biomonitoring and exposome case studies for human health risk assessment (Martínez et al., 2017, 2018). Both studies were included in two major EU projects: HEALS and EuroMix.

In the second part of the chapter 2, flutamide PBPK model was developed both for the rat and for human. First the rat PBPK model was developed and validated against experimental data on rats. Then the model was extrapolated to the human using human specific data for enzyme activities, organ volumes and blood flow through each organ, keeping the other parameters the same as for the rat PBPK. Parameter uncertainties were handled by running multiple models with various values for each uncertain parameter in parallel. This led to quantitative assessment of uncertainties levels in the predicted dynamic behaviour of flutamide concentrations in the various tissues. The extrapolation of the model for predicting flutamide kinetics in humans were in a good agreement with the observed data. The metabolic data were found to be the most conducive parameters in the model, as they were not only determining the hepatic clearance of the chemicals, but also generating the metabolites. This indicates that metabolic studies are very important and it should be an integral part of a PBPK model.

In general, this chapter showed that integration of an in vitro metabolic and an in silico data into a PBPK using IVIVE (in-vitro in-vivo extrapolation) and QSAR (Quantitative structure activity relationship) approaches could predict the kinetics with minimal or no animal experiments, supporting the 3Rs strategies of minimizing animal use. Since this new whole-body PBPK model can predict chemical's concentrations not only in plasma but also in various organs, the model may have applications for safety assessment of these chemicals. Physiologically specific in nature, the current PBPK models could also be adapted to the context of a large human population by considering their metabolic variations and could be used for analysing the large human biomonitoring data.

The integration of specific dynamic physiological data into the PBPK model enables to predict the chemical kinetics for a special group of a population. Chapter 3 demonstrated this by applying it to a case study on the development of a pregnancy PBPK model for Bisphenol A. Bisphenol A is an EDC which has been associated with the developmental effects on growing fetus, an association that has been experimentally proved in animal studies. In the development of the Pregnancy-PBPK model, pregnancy growth dynamic equations were implemented into the model that mimics the physiology of the pregnant mother. The inclusion of the fetus compartment and its communication with the mother was done via placenta blood flow. The currently developed model is able to predict the concentrations of chemicals in the fetus plasma, in the placenta, the in fetus liver, and in the amniotic fluid. Detailed metabolic kinetics of BPA conjugation and deconjugation was investigated in the fetus liver. Then performance of the model was checked using five different cohort studies. The prediction of higher concentrations of BPA during the mid-gestational period in the amniotic fluid, placenta, and the fetus liver are in accordance with biomonitoring data, indicating that the mid-gestational period might be the critical

window of exposure for the fetus. To our knowledge this was the first Pregnancy PBPK model for BPA.

Chapter 4 demonstrated the complex systems biology model of reconstructing the dynamic network of oxidative stress and its application in personalized therapies for Parkinson's disease. It is based on seven design principles: design principle 1, ROS induces mitophagy and in turn provides stability to the system; design principle 2, Keap1-Nrf2 module provides homeostasis to the system through negative feed-back; design principle 3, NFkB activates recovery of damaged mitochondria and prevents necrosis at high ROS level; design principle 4, DJ-1 coordinates mitochondrial recovery and amplification of NRF2 signalling and helps to bring dynamic homeostasis close to perfect adaptation; design principle 5, strong adaptation runs out with ageing; design principle 6, preconditioning (pre-treatment by NRF2 activation) may play Parkinson's disease protective role; Design principle 7, inter-individual variations cause disease variability between individuals that provide a foundation for the development of personalized medicine. The model demonstrated that fine tuning the balance between mitochondrial recovery and mitophagy is crucial for the systems. The NRF2-KEAP pathway back regulates the ROS level and acts as ROS sensor and as the first important defense mechanism. DJ1 showed to be an additional ROS sensor. DJ1 upregulation increases the cell's robustness, and DJ1 downregulation makes the system more sensitive to oxidative stress. The model was validated against the in-vitro experimental data on antioxidant response, p62, Bclxl and ATP consequent to the addition of menadione in the model. The model showed that chronic exposure to increased ROS generation can exhaust the adaptation so that the system ultimately collapses. The model also showed that mutations in DJ1 and alpha-Synuclein make the defense system weaker, so that the systems collapses more readily with the increased accumulation of ROS. This phenomenon showed that the inter-individual variability can be a susceptibility factor for development or progression of the disease. The current detailed model of ROS management could be very useful in studying the health effects of various types of environmental chemicals/EDCs generating ROS. One case study with flutamide is shown in chapter 5 (part 2).

Chapter 5, illustrated the integrative systems toxicology approach. It included the coupling of a PBPK model to AOPs/ systems biology model. The first part of the chapter included the integration of a PBPK model with a linear mechanistic pathway model (which could be viewed as an AOP) associated with the BDNF link neuronal survivability. The second part of the chapter, included the integration of PBPK (developed in chapter 2) with the ROS System biology model (chapter 4). The first part of this chapter illustrated the ways to systems biology models in the field of toxicology via Pharmacodynamics coupled tissue dosimetry model (PBPK/PD). This was shown by applying a case study on the PFOS-induced neurotoxicity. The integration of the model included three main steps. 1: Development of a PBPK model, 2: Development of a mechanistic system model, and 3: Coupling of the PBPK model with the mechanistic

General discussion

model by using a Pharmacodynamics interaction model. The development of the coupled PBPK/PD-mechanistic model allowed to quantify the dynamics of the endogenous biomolecule concentrations of different species at the different levels of PFOS exposures which perturbed key components of the system (in the miRNA model). The interaction of the PFOS with the given pathway was modelled by implementing an indirect sigmoid response model. This integrated PBPK/PD coupled mechanistic system pathway model can be called a "Systems Toxicology" that describes the kinetics of both -the chemicals and – the biomolecules, helping us to understand the dynamic and steady-state behaviours of molecular pathways under perturbed conditions.

The 2nd part of the chapter included the Integrative Systems Toxicology comprising of PBPK, QIVIVE and Systems Biology (integrating in-vitro, in-vivo and in-silico). This approach was used to evaluate the flutamide induced hepatotoxicity. PBPK was used to describe the time course of drug concentration at the cellular level. Then coupling of the estimated tissue dose of flutamide to consequent perturbation of endogenous ROS was achieved using direct pharmacodynamic response models. These perturbations (changes in the ROS level) were dynamically linked with a systems biology model of ROS. This integrative approach allowed us to predict the behaviour of several components of the ROS management model, such as antioxidant regulated genes, mitochondrial respiration and ATP level as a function of flutamide dosing. The model showed a greater induction in NRF2 levels in case of both rats and humans. However, the level of the ATP did not decrease enough and quickly recovered when drug was eliminated from the body. When flutamide induced ROS, NRF2 was upregulated. The latter activated antioxidant regulator genes and ROS concentration was decreased. This helped the system recover. For individuals with reduced superoxide dismutase activities, the extent of the perturbation was predicted to be a lot higher certainly to the extent of becoming toxic. This led us to suggest relevance of our IST for the issue of idiosyncratic toxicity.

We set out to devise a methodology to predict endocrine disruptive activities of compounds in the environment. One of the issues here is the ultralow concentrations these compounds can have in the human environment. Our results towards this idiosyncrasy plus the possibility to include PBPK-based tissue accumulation of such compounds, suggests that the IST methodology designed here may of use in EDC analyses.

Conclusions

The present work is a systematic study of different building blocks of a new Integrative Systems Toxicology framework aimed at understanding quantitatively the adverse effects of chemicals on a biological system, from its exposure to consequent molecular and physiological alterations, through the integration of exposome-internal exposure-molecular/cellular response with the adverse effect. The integrative systems toxicology models were developed; demonstrated with the example of integrated Science through the integration of multidisciplinary knowledge. We also showed its wider application in predicting adverse effects on human health. Integration of exposure, pharmacokinetics, pharmacodynamics, and systems biology also accomplished under this umbrella under the umbrella of integrative systems toxicology. The PBPK models were developed utilizing a bottom-up, a top-down and middle-out (mixed) approach. Different methodologies such as IVIVE, QSAR and cross-species extrapolation were used for the parametrization of the model. The integration of the in-vitro metabolic data into a PBPK model thorough an IVIVE model has improved the prediction of compound(s) or metabolite(s) time courses plasma concentrations. A population-specific PBPK model was developed with the implementation of dynamic physiological data on mother' organs and fetus growth during pregnancy into the model as a mathematical equation. The Pregnancy-PBPK model credibility was evaluated using five different countries' cohort data for both the mother and the fetus. Further the model was applied to several cohort studies including the one from Tarragona County under several projects (HEALS, EUROMIX and Human Biomonitoring (HBM4EU)) in order to predict the mother and fetus internal target tissue concentrations of chemicals (Martínez et al., 2018, 2017).

We demonstrated how the complexity of the biological system may be addressed via reconstruction of the mode of actions/biological behavior in an in-silico replica in a computer. Moreover, mechanistic understanding of the system as a compendium of interconnected processes has led us to the development of a better integrative in-silico predictive model. Integration of the wide range of in silico tools (QSAR, PBPK/PD, AOP/Systems biology etc.) and databases (OMICS, epidemiological and exposure data) has shown how to improve the prediction power of the model with minimal or no animal experiment data.

Being a very mechanistic, the current models can serve as case studies connecting data-driven biomedical disease maps with systems biological dynamic models. The integrated PBPK coupled ROS systems biology model is able to predict the adverse effects in a population associated with functional variability in enzymes related to defense mechanisms. We demonstrated how inter-individual variations cause toxicity variability between individuals which might provide a foundation for the development of personalised therapy.

Physiology specific and mechanistic in nature, the approach of integrative systems toxicology developed in this thesis could also be adapted to the context of a large human population by considering their metabolic and genetic diversity. In future, research should be more focused on chemical metabolic variability, chemical transport system alteration or inherent functional biological variability, which will improve predictability of Integrative Systems Toxicology models targeting different groups of human population.

Conclusions

Chapter 1

Integrating individual modes of action of each chemical by reconstructing it into mathematical equations and analysing it with advanced tools such as PBPK/PD should enable the simultaneous assessment of EDCs, correlating concentration in various biological matrixes (blood, tissue, urine) to various biological end points (diseases). Timing and duration of exposure are important factors, which need to be considered while assessing the risk. Integrating physiology of the human body at different life stages will help in building life stage dynamic models. Dividing life stage into several phases and incorporating susceptible genes (or receptor) or proteins in those life stages targeted by EDCs and physiological specific data could provide a model able to predict the adverse effects of EDCs in different stages of life.

Chapter 2

A PBPK model was successfully developed and validated for two EDCs, namely DEHP and Flutamide, and their metabolites in the plasma and urine were predicted for the first time in human. This model is also able to predict the concentration of EDCs in several organs of the body. The model fortified with the in-vitro and in-silico data using the IVIVE approach has shown to be as good in predicting the kinetics of compound(s) or metabolites as animal experimental data, supporting the 3Rs strategies of minimizing animal use. The results of this study are promising for application of PBPK modeling in risk assessments of human populations in the context of target tissue concentrations. The current model could be used in a reverse dosimetry context to interpret the available biomonitoring data so as to estimate the degree to which the population is currently being exposed.

Chapter 3

A Pregnancy-PBPK (P-PBPK) model for Bisphenol A was developed for the first time. The advantage of a PBPK mechanistic model was demonstrated by successful development of the P-PBPK model through the integration of the dynamics of growth physiology specific to the pregnant women, into the model. The developed P-PBPK model is able to predict the BPA concentration in the fetus blood and in the target organ by just knowing the amount of the BPA exposed to the mother. Glucuronidation and deglucuronidation in both the mother and the fetus liver and placenta, was found to be an important mechanism altering BPA toxicokinetic profile. The model predicted a higher concentration of BPA during the mid-gestational period in the amniotic fluid, the placenta, and the fetus liver indicating that mid-gestational period might be the critical window of exposure for the fetus.

Chapter 4

A systems biology model of ROS was successfully developed and validated against in-vitro experiments. The current model has demonstrated the role of oxidative stress and its wider application in the understanding of the complex biological systems should help to improve the human health predictions. Being a mechanistic model, the current model can serve as a case study connecting data-driven biomedical disease maps with systems biological dynamic models. We have also illustrated the concept that personalized

Conclusions

medicine may benefit from this connection and that fundamental design principles studies may help address practical biomedical questions.

Chapter 5

The developed integrative model of PBPK/PD coupled with mechanistic systems/AOP (neuronal adverse outcome) demonstrated the wider application of systems toxicology model for the study of PFOS neurotoxicity. The model was able to predict the endogenous molecule concentrations involved in AOP over their time course as a function of chemical exposure. With the combination of the mechanistic biological models and the target tissue dosimetry model (PBPK), the capability of predictions was improved significantly. We have also demonstrated the application of a QIVIVE along with PBPK to reconstruct the in vivo tissue-dose response from the in-vitro dose response. We demonstrated a novel approach to validate the in-vivo mechanistic models based on in-vitro dose response data, presuming linear interpolation of in-vitro response to an in-vivo response.

A PBPK model coupled with a systems biology ROS model was successfully developed. The integrated PBPK-ROS coupled model allows to simulate how perturbations in various components of the ROS-managing network should be expected to affect the system's dynamics. The model was also able to predict the in-vitro dose-response data for several important elements of oxidative stress such as p62, ATP, NQO1 and HOMOX1. The model was able to predict the dynamic behavior of several components of the ROS network underlying from mitochondrial function (ATP level) and antioxidant response to oxidative stress. The model showed no sign of hepatotoxicity with the normal dosage regimen of flutamide. However, model simulations of several hypotheses, e.g. the simulation where population variability was taken into account, identified multiple factors which might be responsible for the flutamide induced idiosyncratic hepatotoxicity. Among them, metabolite induced ROS and functional variability in the antioxidant defense mechanism are the most important factors.

References

Abduljalil, K., Furness, P., Johnson, T.N., Rostami-Hodjegan, A., Soltani, H., 2012. Anatomical, Physiological and Metabolic Changes with Gestational Age during Normal Pregnancy. Clin. Pharmacokinet. 51, 365–396. https://doi.org/10.2165/11597440-000000000-00000

Abdullah, R., Alhusainy, W., Woutersen, J., Rietjens, I.M.C.M., Punt, A., 2016. Predicting points of departure for risk assessment based on in vitro cytotoxicity data and physiologically based kinetic (PBK) modeling: The case of kidney toxicity induced by aristolochic acid I. Food Chem. Toxicol. 92, 104–116. https://doi.org/10.1016/j.fct.2016.03.017

Adachi, K., Suemizu, H., Murayama, N., Shimizu, M., Yamazaki, H., 2015. Human biofluid concentrations of mono(2-ethylhexyl)phthalate extrapolated from pharmacokinetics in chimeric mice with humanized liver administered with di(2-ethylhexyl)phthalate and physiologically based pharmacokinetic modeling. Environ. Toxicol. Pharmacol. https://doi.org/10.1016/j.etap.2015.02.011

Aderem, A., 2005. Systems biology: Its practice and challenges. Cell 121, 511–513. https://doi.org/10.1016/j.cell.2005.04.020

Akingbemi, B.T., Sottas, C.M., Koulova, A.I., Klinefelter, G.R., Hardy, M.P., 2004. Inhibition of Testicular Steroidogenesis by the Xenoestrogen Bisphenol a Is Associated with Reduced Pituitary Luteinizing Hormone Secretion and Decreased Steroidogenic Enzyme Gene Expression in Rat Leydig Cells. Endocrinology 145, 592–603. https://doi.org/10.1210/en.2003-1174

Andersen, M.E., Krewski, D., 2009. Toxicity testing in the 21st century: Bringing the vision to life. Toxicol. Sci. 107, 324–330. https://doi.org/10.1093/toxsci/kfn255

Andersen, M.E., Thomas, R.S., Gaido, K.W., Conolly, R.B., 2005. Dose-response modeling in reproductive toxicology in the systems biology era. Reprod. Toxicol. 19, 327–337. https://doi.org/10.1016/j.reprotox.2004.12.004

Andrade, R., Agundez, J., Lucena, M., Martinez, C., Cueto, R., Garcia-Martin, E., 2009. Pharmacogenomics in Drug Induced Liver Injury. Curr. Drug Metab. 10, 956–970. https://doi.org/10.2174/138920009790711805

Ankley, G.T., Bennett, R.S., Erickson, R.J., Hoff, D.J., Hornung, M.W., Johnson, R.D., Mount, D.R., Nichols, J.W., Russom, C.L., Schmieder, P.K., Serrrano, J.A., Tietge, J.E., Villeneuve, D.L., 2010. Adverse outcome pathways: A conceptual framework to support ecotoxicology research and risk assessment. Environ. Toxicol. Chem. 29, 730–741. https://doi.org/10.1002/etc.34

Ansoumane, K., Duan, P., Quan, C., Yaima, M.L.T., Liu, C., Wang, C., Fu, W., Qi, S., Yu, T., Yang, K., 2014. Bisphenol A induced reactive oxygen species (ROS) in the liver and affect epididymal semen quality in adults Sprague-Dawley rats. J. Toxicol. Environ. Heal. Sci. 6, 103–112. https://doi.org/10.5897/JTEHS2014.0309

References

Aris, A., 2014. Estimation of bisphenol A (BPA) concentrations in pregnant women, fetuses and nonpregnant women in Eastern Townships of Canada. Reprod. Toxicol. 45, 8–13. https://doi.org/10.1016/j.reprotox.2013.12.006

Arrell, D.K., Terzic, a, 2010. Network systems biology for drug discovery. Clin. Pharmacol. Ther. 88, 120–125. https://doi.org/10.1038/clpt.2010.91

Asakawa, N., Koyama, M., Hashimoto, Y., Yamashita, K., 1995. Studies on the Metabolic Fate of Flutamide. (1): Plasma Concentration after Single Administration and Protein Binding in Rats. Drug Metab. Pharmacokinet. 10, 447–453. https://doi.org/10.2133/dmpk.10.447

Atanasov, A.G., Tam, S., Röcken, J.M., Baker, M.E., Odermatt, A., 2003. Inhibition of 11β-hydroxysteroid dehydrogenase type 2 by dithiocarbamates. Biochem. Biophys. Res. Commun. 308, 257–262. https://doi.org/10.1016/S0006-291X(03)01359-7

Auffray, C., Chen, Z., Hood, L., 2009. Systems medicine: the future of medical genomics and healthcare. Genome Med. 1, 2. https://doi.org/10.1186/gm2

Ball, A.L., Kamalian, L., Alfirevic, A., Lyon, J.J., Chadwick, A.E., 2016. Identification of the additional mitochondrial liabilities of 2-hydroxyflutamide when compared with its parent compound, flutamide in HepG2 cells. Toxicol. Sci. 153, 341–351. https://doi.org/10.1093/toxsci/kfw126

Bartel, D.P., 2004. MicroRNAs: Genomics, Biogenesis, Mechanism, and Function. Cell 116, 281–297. https://doi.org/10.1016/S0092-8674(04)00045-5

Bartlett, D.W., Davis, M.E., 2006. Insights into the kinetics of siRNA-mediated gene silencing from live-cell and live-animal bioluminescent imaging. Nucleic Acids Res. 34, 322–333. https://doi.org/10.1093/nar/gkj439

Bell, S.M., Chang, X., Wambaugh, J.F., Allen, D.G., Bartels, M., Brouwer, K.L.R., Casey, W.M., Choksi, N., Ferguson, S.S., Fraczkiewicz, G., Jarabek, A.M., Ke, A., Lumen, A., Lynn, S.G., Paini, A., Price, P.S., Ring, C., Simon, T.W., Sipes, N.S., Sprankle, C.S., Strickland, J., Troutman, J., Wetmore, B.A., Kleinstreuer, N.C., 2018. In vitro to in vivo extrapolation for high throughput prioritization and decision making. Toxicol. Vitr. 47, 213–227. https://doi.org/10.1016/j.tiv.2017.11.016

Berson, A., Wolf, C., Chachaty, C., Fisch, C., Fau, D., Eugene, D., Loeper, J., Gauthier, J.-C., Beaune, P., Pompon, D., Maurel, P., Pessayre, D., 1993. Metabolic activation of the nitroaromatic antiandrogen flutamide by rat and human cytochromes P-450, including forms belonging to the 3A and 1A subfamilies. J. Pharmacol. Exp. Ther. 265, 366–372.

Bessems, J., Coecke, S., Gouliarmou, V., Whelan, M., Worth, A., 2015. EURL ECVAM strategy for achieving 3Rs impact in the assessment of toxicokinetics and systemic toxicity 22. https://doi.org/10.2788/197633

References

Bhattacharya, S., Shoda, L.K.M., Zhang, Q., Woods, C.G., Howell, B.A., Siler, S.Q., Woodhead, J.L., Yang, Y., McMullen, P., Watkins, P.B., Melvin, E.A., 2012. Modeling drug- and chemical-induced hepatotoxicity with systems biology approaches. Front. Physiol. 3 DEC, 1–18. https://doi.org/10.3389/fphys.2012.00462

Birgelen, a Van, Birgelen, a Van, Smit, E., Smit, E., Kampen, I., Kampen, I., 1995. Subchronic effects of 2, 3, 7, 8-TCDD or PCBs on thyroid hormone metabolism: use in risk assessment. Eur. J. Pharmacol. Environ. Toxicol. {…} 293, 77–85.

Bloomingdale, P., Housand, C., Apgar, J.F., Millard, B.L., Mager, D.E., Burke, J.M., Shah, D.K., 2017. Quantitative systems toxicology. Curr. Opin. Toxicol. 4, 79–87. https://doi.org/10.1016/j.cotox.2017.07.003

Boberg, J., Metzdorff, S., Wortziger, R., Axelstad, M., Brokken, L., Vinggaard, A.M., Dalgaard, M., Nellemann, C., 2008. Impact of diisobutyl phthalate and other PPAR agonists on steroidogenesis and plasma insulin and leptin levels in fetal rats. Toxicology 250, 75–81. https://doi.org/10.1016/j.tox.2008.05.020

Boelsterli, U.A., Lim, P.L.K., 2007. Mitochondrial abnormalities—A link to idiosyncratic drug hepatotoxicity? Toxicol. Appl. Pharmacol. 220, 92–107. https://doi.org/10.1016/j.taap.2006.12.013

Bonate, P.L., 2011. Pharmacokinetic-Pharmacodynamic Modeling and Simulation. Springer US, Boston, MA. https://doi.org/10.1007/978-1-4419-9485-1

Boulle, F., van den Hove, D.L. a, Jakob, S.B., Rutten, B.P., Hamon, M., van Os, J., Lesch, K.-P., Lanfumey, L., Steinbusch, H.W., Kenis, G., Hove, D.L.A. Van Den, Jakob, S.B., Rutten, B.P., Hamon, M., Os, J. Van, Lesch, K.-P., van den Hove, D.L. a, Jakob, S.B., Rutten, B.P., Hamon, M., van Os, J., Lesch, K.-P., Lanfumey, L., Steinbusch, H.W., Kenis, G., 2012. Epigenetic regulation of the BDNF gene: implications for psychiatric disorders. Mol. Psychiatry 17, 584–596. https://doi.org/10.1038/mp.2011.107

Bouskine, A., Nebout, M., Brücker-Davis, F., Banahmed, M., Fenichel, P., 2009. Low doses of bisphenol A promote human seminoma cell proliferation by activating PKA and PKG via a membrane G-protein-coupled estrogen receptor. Environ. Health Perspect. 117, 1053–1058. https://doi.org/10.1289/ehp.0800367

Brahm, J., Brahm, M., Segovia, R., Latorre, R., Zapata, R., Poniachik, J., Buckel, E., Contreras, L., 2011. Acute and fulminant hepatitis induced by flutamide: case series report and review of the literature. Ann. Hepatol. 10, 93–8.

Brown, R.P., Delp, M.D., Lindstedt, S.L., Rhomberg, L.R., Beliles, R.P., 1997. Physiological parameter values for physiologically based pharmacokinetic models. Toxicol. Ind. Health 13, 407–484.

Bursac, N., Kirkton, R.D., Mcspadden, L.C., Liau, B., 2010. Circulating levels of brain-derived neurotrophic factor: correlation with mood, cognition and motor function. Biomark. Med. 4, 871–87.

References

Calabrese, E.J., Baldwin, L.A., 2003. Toxicology rethinks its central belief. Nature 421, 691–692. https://doi.org/10.1038/421691a

Cao, X.L., Zhang, J., Goodyer, C.G., Hayward, S., Cooke, G.M., Curran, I.H.A., 2012. Bisphenol A in human placental and fetal liver tissues collected from Greater Montreal area (Quebec) during 1998-2008. Chemosphere 89, 505–511. https://doi.org/10.1016/j.chemosphere.2012.05.003

Caputo, V., Sinibaldi, L., Fiorentino, A., Parisi, C., Catalanotto, C., Pasini, A., Cogoni, C., Pizzuti, A., 2011. Brain derived neurotrophic factor (BDNF) expression is regulated by microRNAs miR-26a and miR-26b allele-specific binding. PLoS One 6. https://doi.org/10.1371/journal.pone.0028656

Carlotti, F., Dower, S.K., Qwarnstrom, E.E., 2000. Dynamic shuttling of nuclear factor ??B between the nucleus and cytoplasm as a consequence of inhibitor dissociation. J. Biol. Chem. 275, 41028–41034. https://doi.org/10.1074/jbc.M006179200

Castillo, B., del Cerro, M., Breakefield, X.O., Frim, D.M., Barnstable, C.J., Dean, D.O., Bohn, M.C., 1994. Retinal ganglion cell survival is promoted by genetically modified astrocytes designed to secrete brain-derived neurotrophic factor (BDNF). Brain Res. 647, 30–36. https://doi.org/10.1016/0006-8993(94)91395-1

Castro, B., Sánchez, P., Torres, J.M., Preda, O., del Moral, R.G., Ortega, E., 2013. Bisphenol A Exposure during Adulthood Alters Expression of Aromatase and 5α-Reductase Isozymes in Rat Prostate. PLoS One 8, 1–7. https://doi.org/10.1371/journal.pone.0055905

Chang, Z., Lu, M., Kim, S.S., Park, J.S., 2014. Potential role of HSP90 in mediating the interactions between estrogen receptor (ER) and aryl hydrocarbon receptor (AhR) signaling pathways. Toxicol. Lett. 226, 6–13. https://doi.org/10.1016/j.toxlet.2014.01.032

Chen, N., Li, J., Li, D., Yang, Y., He, D., 2014. Chronic exposure to perfluorooctane sulfonate induces behavior defects and neurotoxicity through oxidative damages, in Vivo and in Vitro. PLoS One 9, 1–10. https://doi.org/10.1371/journal.pone.0113453

Chitra, K.C., Latchoumycandane, C., Mathur, P.P., 2003. Induction of oxidative stress by bisphenol A in the epididymal sperm of rats. Toxicology 185, 119–127. https://doi.org/10.1016/S0300-483X(02)00597-8

Choi, K., Joo, H., Campbell, J.L., Andersen, M.E., Clewell, H.J., 2013. In vitro intestinal and hepatic metabolism of Di(2-ethylhexyl) phthalate (DEHP) in human and rat. Toxicol. Vitr. 27, 1451–1457. https://doi.org/10.1016/j.tiv.2013.03.012

Clarke, G., Collins, R.A., Leavitt, B.R., Andrews, D.F., Hayden, M.R., Lumsden, C.J., McInnes, R.R., 2000. A one-hit model of cell death in inherited neuronal degenerations. Nature 406, 195–199. https://doi.org/10.1038/35018098

References

Clewell, H.J., Gearhart, J.M., Gentry, P.R., Covington, T.R., VanLandingham, C.B., Crump, K.S., Shipp, A.M., 1999. Evaluation of the uncertainty in an oral reference dose for methylmercury due to interindividual variability in pharmacokinetics. Risk Anal. 19, 547–558. https://doi.org/10.1023/A:1007017116171

Clewell, R. a, Merrill, E. a, Narayanan, L., Gearhart, J.M., Robinson, P.J., 2004. Evidence for competitive inhibition of iodide uptake by perchlorate and translocation of perchlorate into the thyroid. Int. J. Toxicol. 23, 17–23. https://doi.org/10.1080/10915810490275044

Clewell, R.A., Clewell, H.J., 2008. Development and specification of physiologically based pharmacokinetic models for use in risk assessment. Regul. Toxicol. Pharmacol. 50, 129–43. https://doi.org/10.1016/j.yrtph.2007.10.012

Coe, K.J., Jia, Y., Han, K.H., Rademacher, P., Bammler, T.K., Beyer, R.P., Farin, F.M., Woodke, L., Plymate, S.R., Fausto, N., Nelson, S.D., 2007. Comparison of the cytotoxicity of the nitroaromatic drug flutamide to its cyano analogue in the hepatocyte cell line TAMH: Evidence for complex I inhibition and mitochondrial dysfunction using toxicogenomic screening. Chem. Res. Toxicol. 20, 1277–1290. https://doi.org/10.1021/tx7001349

Coe, K.J., Nelson, S.D., Ulrich, R.G., He, Y., Dai, X., Cheng, O., Caguyong, M., Roberts, C.J., Slatter, J.G., 2006. Profiling the hepatic effects of flutamide in rats: A microarray comparison with classical aryl hydrocarbon receptor ligands and atypical CYP1A inducers. Drug Metab. Dispos. 34, 1266–1275. https://doi.org/10.1124/dmd.105.009159

Cooper, R.L., Stoker, T.E., Tyrey, L., Goldman, J.M., McElroy, W.K., 2000. Atrazine disrupts the hypothalamic control of pituitary-ovarian function. Toxicol. Sci. 53, 297–307. https://doi.org/10.1093/toxsci/53.2.297

Coughlin, J.L., Thomas, P.E., Buckley, B., 2012. Inhibition of genistein glucuronidation by bisphenol A in human and rat liver microsomes. Drug Metab. Dispos. 40, 481–485. https://doi.org/10.1124/dmd.111.042366

Csanády, G., Oberste-Frielinghaus, H., Semder, B., Baur, C., Schneider, K., Filser, J., 2002. Distribution and unspecific protein binding of the xenoestrogens bisphenol A and daidzein. Arch. Toxicol. 76, 299–305. https://doi.org/10.1007/s00204-002-0339-5

Cubitt, H.E., Houston, J.B., Galetin, A., 2011. Prediction of human drug clearance by multiple metabolic pathways: Integration of hepatic and intestinal microsomal and cytosolic data. Drug Metab. Dispos. 39, 864–873. https://doi.org/10.1124/dmd.110.036566

Cubitt, H.E., Houston, J.B., Galetin, A., 2009. Relative Importance of Intestinal and Hepatic Glucuronidation—Impact on the Prediction of Drug Clearance. Pharm. Res. 26, 1073–1083. https://doi.org/10.1007/s11095-008-9823-9

References

Davies, B., Morris, T., 1993. No Title. Pharm. Res. 10, 1093–1095. https://doi.org/10.1023/A:1018943613122

Dieckhaus, C.M., Thompson, C.D., Roller, S.G., Macdonald, T.L., 2002. Mechanisms of idiosyncratic drug reactions: the case of felbamate. Chem. Biol. Interact. 142, 99–117. https://doi.org/10.1016/S0009-2797(02)00057-1

Dinkova-Kostova, A.T., Holtzclaw, W.D., Cole, R.N., Itoh, K., Wakabayashi, N., Katoh, Y., Yamamoto, M., Talalay, P., 2002. Direct evidence that sulfhydryl groups of Keap1 are the sensors regulating induction of phase 2 enzymes that protect against carcinogens and oxidants. Proc. Natl. Acad. Sci. U. S. A. 99, 11908–13. https://doi.org/10.1073/pnas.172398899

Djuranovic, S., Nahvi, A., Green, R., 2011. A Parsimonious Model for Gene Regulation by miRNAs. Science (80-.). 331, 550–553. https://doi.org/10.1126/science.1191138

Doerge, D.R., Twaddle, N.C., Vanlandingham, M., Brown, R.P., Fisher, J.W., 2011. Distribution of bisphenol A into tissues of adult, neonatal, and fetal Sprague–Dawley rats. Toxicol. Appl. Pharmacol. 255, 261–270. https://doi.org/10.1016/j.taap.2011.07.009

Doering, D.D., Steckelbroeck, S., Doering, T., Klingmüller, D., 2002. Effects of butyltins on human 5alpha-reductase type 1 and type 2 activity. Steroids 67, 859–867.

El-Masri, H., 2013. Modeling for Regulatory Purposes (Risk and Safety Assessment), in: Reisfeld, B., Mayeno, A.N. (Eds.), . Humana Press, Totowa, NJ, pp. 297–303. https://doi.org/10.1007/978-1-62703-059-5_13

Espinosa-Diez, C., Miguel, V., Mennerich, D., Kietzmann, T., Sánchez-Pérez, P., Cadenas, S., Lamas, S., 2015. Antioxidant responses and cellular adjustments to oxidative stress. Redox Biol. 6, 183–197. https://doi.org/10.1016/j.redox.2015.07.008

Fabrega, F., Kumar, V., Schuhmacher, M., Domingo, J.L., Nadal, M., 2014. PBPK modeling for PFOS and PFOA: Validation with human experimental data. Toxicol. Lett. 230, 244–251. https://doi.org/10.1016/j.toxlet.2014.01.007

Fàbrega, F., Nadal, M., Schuhmacher, M., Domingo, J.L., Kumar, V., 2016. Influence of the uncertainty in the validation of PBPK models: A case-study for PFOS and PFOA. Regul. Toxicol. Pharmacol. 77, 230–239. https://doi.org/10.1016/j.yrtph.2016.03.009

Fang, H., Tong, W., Branham, W.S., Moland, C.L., Dial, S.L., Hong, H., Xie, Q., Perkins, R., Owens, W., Sheehan, D.M., 2003. Study of 202 Natural, Synthetic, and Environmental Chemicals for Binding to the Androgen Receptor. Chem. Res. Toxicol. 16, 1338–1358. https://doi.org/10.1021/tx030011g

Fisher, J.W., Twaddle, N.C., Vanlandingham, M., Doerge, D.R., 2011. Pharmacokinetic

References

modeling: Prediction and evaluation of route dependent dosimetry of bisphenol A in monkeys with extrapolation to humans. Toxicol. Appl. Pharmacol. 257, 122–136. https://doi.org/10.1016/j.taap.2011.08.026

Fletcher, J.M., Morton, C.J., Zwar, R.A., Murray, S.S., O'Leary, P.D., Hughes, R.A., 2008. Design of a conformationally defined and proteolytically stable circular mimetic of brain-derived neurotrophic factor. J. Biol. Chem. 283, 33375–33383. https://doi.org/10.1074/jbc.M802789200

Forsby, A., Blaauboer, B., 2007. Integration of in vitro neurotoxicity data with biokinetic modelling for the estimation of in vivo neurotoxicity. Hum. Exp. Toxicol. 26, 333–338. https://doi.org/10.1177/0960327106072994

Foxenberg, R.J., Ellison, C.A., Knaak, J.B., Ma, C., Olson, J.R., 2011. Cytochrome P450-specific human PBPK/PD models for the organophosphorus pesticides: Chlorpyrifos and parathion. Toxicology 285, 57–66. https://doi.org/10.1016/j.tox.2011.04.002

Friedmann, A.S., 2002. Atrazine inhibition of testosterone production in rat males following peripubertal exposure. Reprod. Toxicol. 16, 275–279. https://doi.org/10.1016/S0890-6238(02)00019-9

Fukumitsu, H., Ohtsuka, M., Murai, R., Nakamura, H., Itoh, K., Furukawa, S., 2006. Brain-Derived Neurotrophic Factor Participates in Determination of Neuronal Laminar Fate in the Developing Mouse Cerebral Cortex. J. Neurosci. 26, 13218–13230. https://doi.org/10.1523/JNEUROSCI.4251-06.2006

Fukuzawa, N.H., Ohsako, S., Wu, Q., Sakaue, M., Fujii-Kuriyama, Y., Baba, T., Tohyama, C., 2004. Testicular cytochrome P450scc and LHR as possible targets of 2,3,7,8-tetrachlorodibenzo-p-dioxin (TCDD) in the mouse. Mol. Cell. Endocrinol. 221, 87–96. https://doi.org/10.1016/j.mce.2004.02.005

Gabrielsson, J., Weiner, D., 2012. Non-compartmental Analysis, in: Reisfeld, B., Mayeno, A.N. (Eds.), Methods in Molecular Biology. Humana Press, Totowa, NJ, pp. 377–389. https://doi.org/10.1007/978-1-62703-050-2_16

García Cortés, M., Andrade, R.J., Lucena, M.I., Sánchez Martínez, H., Fernández, M.C., Ferrer, T., Martín-Vivaldi, R., Peláez, G., Suárez, F., Romero-Gómez, M., Montero, J.L., Fraga, E., Camargo, R., Alcántara, R., Pizarro, M.A., García-Ruiz, E., Rosemary-Gómez, M., 2001. Flutamide-induced hepatotoxicity: report of a case series. Rev. Esp. Enferm. Dig. 93, 423–32.

Generali, J.A., Cada, D.J., 2014. Flutamide: Hirsutism in Women. Hosp. Pharm. 49, 517–520. https://doi.org/10.1310/hpj4906-517

Gentry, P.R., Covington, T.R., Andersen, M.E., Clewell, H.J., 2002. Application of a physiologically based pharmacokinetic model for isopropanol in the derivation of a reference dose and reference concentration. Regul. Toxicol. Pharmacol. 36, 51–68. https://doi.org/S0273230002915400 [pii]

References

Gerona, R.R., Woodruff, T.J., Dickenson, C.A., Pan, J., Jackie, M., Sen, S., Friesen, M.M., Fujimoto, V.Y., Hunt, P.A., 2014. California population 47. https://doi.org/10.1021/es402764d.Bisphenol-A

Gibbs, J.P., Yang, J.S., Slattery, J.T., 1998. Comparison of human liver and small intestinal glutathione S-transferase-catalyzed busulfan conjugation in vitro. Drug Metab. Dispos. 26, 52–55.

Gillespie, L.N., Clark, G.M., Bartlett, P.F., Marzella, P.L., 2003. BDNF-induced survival of auditory neurons in vivo: Cessation of treatment leads to accelerated loss of survival effects. J. Neurosci. Res. 71, 785–790. https://doi.org/10.1002/jnr.10542

Gim, J., Kim, H.S., Kim, J., Choi, M., Kim, J.R., Chung, Y.J., Cho, K.H., 2010. A system-level investigation into the cellular toxic response mechanism mediated by AhR signal transduction pathway. Bioinformatics 26, 2169–2175. https://doi.org/10.1093/bioinformatics/btq400

Godin, S.J., Scollon, E.J., Hughes, M.F., Potter, P.M., DeVito, M.J., Ross, M.K., 2006. Species differences in the in vitro metabolism of deltamethrin and esfenvalerate: Differential oxidative and hydrolytic metabolism by humans and rats. Drug Metab. Dispos. 34, 1764–1771. https://doi.org/10.1124/dmd.106.010058

Gomez, J.-L., Dupont, A., Cusan, L., Tremblay, M., Suburu, R., Lemay, M., Labrie, F., 1992. Incidence of liver toxicity associated with the use of flutamide in prostate cancer patients. Am. J. Med. 92, 465–470. https://doi.org/10.1016/0002-9343(92)90741-S

Goudarzi, H., Nakajima, S., Ikeno, T., Sasaki, S., Kobayashi, S., Miyashita, C., Ito, S., Araki, A., Nakazawa, H., Kishi, R., 2016. Prenatal exposure to perfluorinated chemicals and neurodevelopment in early infancy: The Hokkaido Study. Sci. Total Environ. 541, 1002–1010. https://doi.org/10.1016/j.scitotenv.2015.10.017

Gumy, C., Chandsawangbhuwana, C., Dzyakanchuk, A. a., Kratschmar, D. V., Baker, M.E., Odermatt, A., 2008. Dibutyltin disrupts glucocorticoid receptor function and impairs glucocorticoid-induced suppression of cytokine production. PLoS One 3. https://doi.org/10.1371/journal.pone.0003545

Haley, B., Zamore, P.D., 2004. Kinetic analysis of the RNAi enzyme complex. Nat. Struct. Mol. Biol. 11, 599–606. https://doi.org/10.1038/nsmb780

Hany, J., Lilienthal, H., Sarasin, a, Roth-Härer, a, Fastabend, a, Dunemann, L., Lichtensteiger, W., Winneke, G., 1999. Developmental exposure of rats to a reconstituted PCB mixture or aroclor 1254: effects on organ weights, aromatase activity, sex hormone levels, and sweet preference behavior. Toxicol. Appl. Pharmacol. 158, 231–243. https://doi.org/10.1006/taap.1999.8710

Hayes, T.B., Anderson, L.L., Beasley, V.R., de Solla, S.R., Iguchi, T., Ingraham, H., Kestemont, P., Kniewald, J., Kniewald, Z., Langlois, V.S., Luque, E.H., McCoy, K.A., Muñoz-de-Toro, M., Oka, T., Oliveira, C.A., Orton, F., Ruby, S., Suzawa,

References

M., Tavera-Mendoza, L.E., Trudeau, V.L., Victor-Costa, A.B., Willingham, E., 2011. Demasculinization and feminization of male gonads by atrazine: Consistent effects across vertebrate classes. J. Steroid Biochem. Mol. Biol. 127, 64–73. https://doi.org/10.1016/j.jsbmb.2011.03.015

Heidrich, D.D., Steckelbroeck, S., Klingmuller, D., 2001. Inhibition of human cytochrome P450 aromatase activity by butyltins. Steroids 66, 763–769.

Hood, L., Heath, J.R., Phelps, M.E., Lin, B., 2004. Systems biology and new technologies enable predictive and preventative medicine. Science 306, 640–643. https://doi.org/10.1126/science.1104635

Ikezuki, Y., Tsutsumi, O., Takai, Y., Kamei, Y., Taketani, Y., 2002. Determination of bisphenol A concentrations in human biological fluids reveals significant early prenatal exposure. Hum. Reprod. 17, 2839–2841. https://doi.org/10.1093/humrep/17.11.2839

Jaeschke, H., McGill, M.R., Ramachandran, A., 2012. Oxidant stress, mitochondria, and cell death mechanisms in drug-induced liver injury: lessons learned from acetaminophen hepatotoxicity. Drug Metab. Rev. 44, 88–106. https://doi.org/10.3109/03602532.2011.602688

Johansson, M., Larsson, C., Bergman, a, Lund, B.O., 1998. Structure-activity relationship for inhibition of CYP11B1-dependent glucocorticoid synthesis in Y1 cells by aryl methyl sulfones. Pharmacol. Toxicol. 83, 225–230.

Johansson, N., Fredriksson, A., Eriksson, P., 2008. Neonatal exposure to perfluorooctane sulfonate (PFOS) and perfluorooctanoic acid (PFOA) causes neurobehavioural defects in adult mice. Neurotoxicology 29, 160–169. https://doi.org/10.1016/j.neuro.2007.10.008

Juge-Aubry, C.E., Gorla-Bajszczak, A., Pernin, A., Lemberger, T., Wahli, W., Burger, A.G., Meier, C. a., 1995. Peroxisome proliferator-activated receptor mediates cross-talk with thyroid hormone receptor by competition for retinoid X receptor: Possible role of a leucine zipper-like heptad repeat. J. Biol. Chem. https://doi.org/10.1074/jbc.270.30.18117

Jusko, W.J., 2013. Moving from basic toward systems pharmacodynamic models. J. Pharm. Sci. 102, 2930–2940. https://doi.org/10.1002/jps.23590

Jusko, W.J., Ko, H.C., 1994. Physiologic indirect response models characterize diverse types of pharmacodynamic effects. Clin. Pharmacol. Ther. 56, 406–419. https://doi.org/10.1038/clpt.1994.155

Kanda, Y., Hinata, T., Kang, S.W., Watanabe, Y., 2011. Reactive oxygen species mediate adipocyte differentiation in mesenchymal stem cells. Life Sci. 89, 250–258. https://doi.org/10.1016/j.lfs.2011.06.007

Kaplowitz, N., 2005. Idiosyncratic drug hepatotoxicity. Nat. Rev. Drug Discov. 4, 489.

References

Kashimshetty, R., Desai, V.G., Kale, V.M., Lee, T., Moland, C.L., Branham, W.S., New, L.S., Chan, E.C.Y., Younis, H., Boelsterli, U.A., 2009. Underlying mitochondrial dysfunction triggers flutamide-induced oxidative liver injury in a mouse model of idiosyncratic drug toxicity. Toxicol. Appl. Pharmacol. 238, 150–159. https://doi.org/10.1016/j.taap.2009.05.007

Katchen, B., Buxbaum, S., 1975. Disposition of a new, nonsteroid, antiandrogen, alpha,alpha,alpha-trifluoro-2-methyl-4'-nitro-m-propionotoluidide (Flutamide), in men following a single oral 200 mg dose. J. Clin. Endocrinol. Metab. 41, 373–9. https://doi.org/10.1210/jcem-41-2-373

Kawamoto, Y., Matsuyama, W., Wada, M., Hishikawa, J., Chan, M.P.L., Nakayama, A., Morisawa, S., 2007. Development of a physiologically based pharmacokinetic model for bisphenol A in pregnant mice. Toxicol. Appl. Pharmacol. 224, 182–191. https://doi.org/10.1016/j.taap.2007.06.023

Kell, D.B., 2006. Systems biology, metabolic modelling and metabolomics in drug discovery and development. Drug Discov. Today 11, 1085–1092. https://doi.org/10.1016/j.drudis.2006.10.004

Kester, M.H.A., Bulduk, S., Van Toor, H., Tibboel, D., Meinl, W., Glatt, H., Falany, C.N., Coughtrie, M.W.H., Gerlienke Schuur, A., Brouwer, A., Visser, T.J., 2002. Potent inhibition of estrogen sulfotransferase by hydroxylated metabolites of polyhalogenated aromatic hydrocarbons reveals alternative mechanism for estrogenic activity of endocrine disrupters. J. Clin. Endocrinol. Metab. 87, 1142–1150. https://doi.org/10.1210/jc.87.3.1142

Keys, D.A., Wallace, D.G., Kepler, T.B., Conolly, R.B., 2000. Quantitative evaluation of alternative mechanisms of blood disposition of di(n-butyl) phthalate and mono(n-butyl) phthalate in rats. Toxicol. Sci. 53, 173–184. https://doi.org/10.1093/toxsci/53.2.173

Keys, D.A., Wallace, D.G., Kepler, T.B., Conolly, R.B., 1999. Quantitative evaluation of alternative mechanisms of blood and testes disposition of di(2-ethylhexyl) phthalate and mono(2-ethylhexyl) phthalate in rats. Toxicol. Sci. 49, 172–85. https://doi.org/10.1093/toxsci/49.2.172

Kitano, H., 2002. Systems biology: A brief overview. Sci. (New York, NY) 295, 1662–1664. https://doi.org/10.1126/science.1069492

Kobayashi, Y., Fukami, T.., Shimizu, M., Nakajima, M., Tsuyoshi., Y., 2012. Short Communication Contributions of Arylacetamide Deacetylase and Carboxylesterase 2 to Flutamide Hydrolysis in Human Liver. Drug Metab. Dispos. 40, 1080–1084.

Kohler, J.J., Schepartz, A., 2001. Kinetic Studies of Fos , Jun , DNA Complex Formation : DNA Binding Prior to Dimerization. Biochemistry 40, 130–142. https://doi.org/10.1021/bi001881p

Kortejärvi, H., Urtti, A., Yliperttula, M., 2007. Pharmacokinetic simulation of biowaiver

References

criteria: The effects of gastric emptying, dissolution, absorption and elimination rates. Eur. J. Pharm. Sci. 30, 155–166. https://doi.org/10.1016/j.ejps.2006.10.011

Kuepfer, L., Niederalt, C., Wendl, T., Schlender, J.F., Willmann, S., Lippert, J., Block, M., Eissing, T., Teutonico, D., 2016. Applied Concepts in PBPK Modeling: How to Build a PBPK/PD Model. CPT Pharmacometrics Syst. Pharmacol. 5, 516–531. https://doi.org/10.1002/psp4.12134

Kurebayashi, H., Okudaira, K., Ohno, Y., 2010. Species difference of metabolic clearance of bisphenol A using cryopreserved hepatocytes from rats, monkeys and humans. Toxicol. Lett. 198, 210–215. https://doi.org/10.1016/j.toxlet.2010.06.017

Kuroda, N., Kinoshita, Y., Sun, Y., Wada, M., Kishikawa, N., Nakashima, K., Makino, T., Nakazawa, H., 2003. Measurement of bisphenol A levels in human blood serum and ascitic fluid by HPLC using a fluorescent labeling reagent. J. Pharm. Biomed. Anal. 30, 1743–1749. https://doi.org/10.1016/S0731-7085(02)00516-2

Lai, K.P., Wong, M.H., Wong, C.K.C., 2005a. Inhibition of CYP450scc expression in dioxin-exposed rat Leydig cells. J. Endocrinol. 185, 519–527. https://doi.org/10.1677/joe.1.06054

Lai, K.P., Wong, M.H., Wong, C.K.C., 2005b. Effects of TCDD in modulating the expression of Sertoli cell secretory products and markers for cell-cell interaction. Toxicology 206, 111–123. https://doi.org/10.1016/j.tox.2004.07.002

Lans, M.C., Spiertz, C., Brouwer, a, Koeman, J.H., 1994. Different competition of thyroxine binding to transthyretin and thyroxine-binding globulin by hydroxy-PCBs, PCDDs and PCDFs. Eur. J. Pharmacol. 270, 129–136. https://doi.org/10.1016/0926-6917(94)90054-X

Leclerc, E., Hamon, J., Legendre, A., Bois, F.Y., 2014. Integration of pharmacokinetic and NRF2 system biology models to describe reactive oxygen species production and subsequent glutathione depletion in liver microfluidic biochips after flutamide exposure. Toxicol. Vitr. 28, 1230–1241. https://doi.org/10.1016/j.tiv.2014.05.003

Lee, Y.J., Ryu, H.Y., Kim, H.K., Min, C.S., Lee, J.H., Kim, E., Nam, B.H., Park, J.H., Jung, J.Y., Jang, D.D., Park, E.Y., Lee, K.H., Ma, J.Y., Won, H.S., Im, M.W., Leem, J.H., Hong, Y.C., Yoon, H.S., 2008. Maternal and fetal exposure to bisphenol A in Korea. Reprod. Toxicol. 25, 413–419. https://doi.org/10.1016/j.reprotox.2008.05.058

Lemaire, G., Terouanne, B., Mauvais, P., Michel, S., Rahmani, R., 2004. Effect of organochlorine pesticides on human androgen receptor activation in vitro. Toxicol. Appl. Pharmacol. 196, 235–246. https://doi.org/10.1016/j.taap.2003.12.011

Li, L. a., Wang, P.W., Chang, L.W., 2004. Polychlorinated biphenyl 126 stimulates basal and inducible aldosterone biosynthesis of human adrenocortical H295R cells. Toxicol. Appl. Pharmacol. 195, 92–102. https://doi.org/10.1016/j.taap.2003.11.007

References

Li, M.W.M., Mruk, D.D., Lee, W.M., Cheng, C.Y., 2009. Disruption of the blood-testis barrier integrity by bisphenol A in vitro: Is this a suitable model for studying blood-testis barrier dynamics? Int. J. Biochem. Cell Biol. 41, 2302–2314. https://doi.org/10.1016/j.biocel.2009.05.016

Li, W., He, Q.Z., Wu, C.Q., Pan, X.Y., Wang, J., Tan, Y., Shan, X.Y., Zeng, H.C., 2015. PFOS Disturbs BDNF-ERK-CREB Signalling in Association with Increased MicroRNA-22 in SH-SY5Y Cells. Biomed Res. Int. 2015. https://doi.org/10.1155/2015/302653

Li, X., Fang, P., Mai, J., Choi, E.T., Wang, H., Yang, X., 2013. Targeting mitochondrial reactive oxygen species as novel therapy for inflammatory diseases and cancers. J. Hematol. Oncol. 6, 19. https://doi.org/10.1186/1756-8722-6-19

Li, Y., Ramdhan, D.H., Naito, H., Yamagishi, N., Ito, Y., Hayashi, Y., Yanagiba, Y., Okamura, A., Tamada, H., Gonzalez, F.J., Nakajima, T., 2011. Ammonium perfluorooctanoate may cause testosterone reduction by adversely affecting testis in relation to PPARα. Toxicol. Lett. 205, 265–272. https://doi.org/10.1016/j.toxlet.2011.06.015

Lipsky, R.H., Marini, A.M., 2007. Brain-derived neurotrophic factor in neuronal survival and behavior-related plasticity. Ann. N. Y. Acad. Sci. 1122, 130–143. https://doi.org/10.1196/annals.1403.009

Long, Y., Wang, Y., Ji, G., Yan, L., Hu, F., Gu, A., 2013. Neurotoxicity of Perfluorooctane Sulfonate to Hippocampal Cells in Adult Mice. PLoS One 8, 1–9. https://doi.org/10.1371/journal.pone.0054176

Lorber, M., Angerer, J., Koch, H.M., 2010. A simple pharmacokinetic model to characterize exposure of Americans to Di-2-ethylhexyl phthalate. J. Expo. Sci. Environ. Epidemiol. 20, 38–53. https://doi.org/10.1038/jes.2008.74

Louisse, J., Beekmann, K., Rietjens, I.M.C.M., 2016. Use of physiologically based kinetic modeling-based reverse dosimetry to predict in vivo toxicity from in vitro data. Chem. Res. Toxicol. acs.chemrestox.6b00302. https://doi.org/10.1021/acs.chemrestox.6b00302

Lu, B., 2003. Pro-Region of Neurotrophins. Neuron 39, 735–738. https://doi.org/10.1016/S0896-6273(03)00538-5

Lubin, F.D., Roth, T.L., Sweatt, J.D., 2008. Epigenetic regulation of BDNF gene transcription in the consolidation of fear memory. J. Neurosci. 28, 10576–86. https://doi.org/10.1523/JNEUROSCI.1786-08.2008

Ma, E., MacRae, I.J., Kirsch, J.F., Doudna, J.A., 2008. Autoinhibition of Human Dicer by Its Internal Helicase Domain. J. Mol. Biol. 380, 237–243. https://doi.org/10.1016/j.jmb.2008.05.005

Mager, D.E., Woo, S., Jusko, W.J., 2009. Scaling Pharmacodynamics from In Vitro and Preclinical Animal Studies to Humans. Drug Metab. Pharmacokinet. 24, 16–24.

References

https://doi.org/10.2133/dmpk.24.16

Mager, D.E., Wyska, E., Jusko, W.J., 2003. Diversity of mechanism-based pharmacodynamic models. Drug Metab. Dispos. 31, 510–8. https://doi.org/10.1124/DMD.31.5.510

Martínez, M.A., Rovira, J., Prasad Sharma, R., Nadal, M., Schuhmacher, M., Kumar, V., 2018. Comparing dietary and non-dietary source contribution of BPA and DEHP to prenatal exposure: A Catalonia (Spain) case study. Environ. Res. 166, 25–34. https://doi.org/10.1016/j.envres.2018.05.008

Martínez, M.A., Rovira, J., Sharma, R.P., Nadal, M., Schuhmacher, M., Kumar, V., 2017. Prenatal exposure estimation of BPA and DEHP using integrated external and internal dosimetry: A case study. Environ. Res. 158, 566–575. https://doi.org/10.1016/j.envres.2017.07.016

Masuyama, H., Hiramatsu, Y., Kunitomi, M., Kudo, T., MacDonald, P.N., 2000. Endocrine disrupting chemicals, phthalic acid and nonylphenol, activate Pregnane X receptor-mediated transcription. Mol. Endocrinol. 14, 421–428. https://doi.org/10.1210/mend.14.3.0424

Masuyama, H., Inoshita, H., Hiramatsu, Y., Kudo, T., 2002. Ligands have various potential effects on the degradation of pregnane X receptor by proteasome. Endocrinology 143, 55–61. https://doi.org/10.1210/en.143.1.55

Matsuzaki, Y., Nagai, D., Ichimura, E., Goda, R., Tomura, A., Doi, M., Nishikawa, K., 2006. Metabolism and hepatic toxicity of flutamide in cytochrome P450 1A2 knockout SV129 mice. J. Gastroenterol. 41, 231–239. https://doi.org/10.1007/s00535-005-1749-y

Menei, P., Montero-Menei, C., Whittemore, S.R., Bunge, R.P., Bunge, M.B., 1998. Schwann cells genetically modified to secrete human BDNF promote enhanced axonal regrowth across transected adult rat spinal cord. Eur. J. Neurosci. 10, 607–621. https://doi.org/10.1046/j.1460-9568.1998.00071.x

Michael, G.J., Averill, S., Nitkunan, A., Rattray, M., Bennett, D.L., Yan, Q., Priestley, J. V, 1997. Nerve growth factor treatment increases brain-derived neurotrophic factor selectively in TrkA-expressing dorsal root ganglion cells and in their central terminations within the spinal cord. J. Neurosci. 17, 8476–90.

Mielke, H., Partosch, F., Gundert-Remy, U., 2011. The contribution of dermal exposure to the internal exposure of bisphenol A in man. Toxicol. Lett. 204, 190–198. https://doi.org/10.1016/j.toxlet.2011.04.032

Mikamo, E., Harada, S., Nishikawa, J., Nishihara, T., 2003. Endocrine disruptors induce cytochrome P450 by affecting transcriptional regulation via pregnane X receptor. Toxicol. Appl. Pharmacol. 193, 66–72. https://doi.org/10.1016/j.taap.2003.08.001

Moriyama, K., Tagami, T., Akamizu, T., Usui, T., Saijo, M., Kanamoto, N., Hataya, Y., Shimatsu, A., Kuzuya, H., Nakao, K., 2002. Thyroid hormone action is disrupted

References

by bisphenol A as an antagonist. J. Clin. Endocrinol. Metab. 87, 5185–5190. https://doi.org/10.1210/jc.2002-020209

Mowla, S.J., Pareek, S., Farhadi, H.F., Petrecca, K., Fawcett, J.P., Seidah, N.G., Morris, S.J., Sossin, W.S., Murphy, R. a, 1999. Differential sorting of nerve growth factor and brain-derived neurotrophic factor in hippocampal neurons. J. Neurosci. 19, 2069–2080.

Muiños-Gimeno, M., Espinosa-Parrilla, Y., Guidi, M., Kagerbauer, B., Sipilä, T., Maron, E., Pettai, K., Kananen, L., Navinés, R., Martín-Santos, R., Gratacòs, M., Metspalu, A., Hovatta, I., Estivill, X., 2011. Human microRNAs miR-22, miR-138-2, miR-148a, and miR-488 are associated with panic disorder and regulate several anxiety candidate genes and related pathways. Biol. Psychiatry 69, 526–533. https://doi.org/10.1016/j.biopsych.2010.10.010

Murer, M.., Yan, Q., Raisman-Vozari, R., 2001. Brain-derived neurotrophic factor in the control human brain, and in Alzheimer's disease and Parkinson's disease. Prog. Neurobiol. 63, 71–124. https://doi.org/10.1016/S0301-0082(00)00014-9

Murphy, M.P., 2009. How mitochondria produce reactive oxygen species. Biochem. J. 417, 1–13. https://doi.org/10.1042/BJ20081386

Nestorov, I., 2007. Whole-body physiologically based pharmacokinetic models. Expert Opin. Drug Metab. Toxicol. 3, 235–249. https://doi.org/10.1517/17425255.3.2.235

Nikula, H., Talonpoika, T., Kaleva, M., Toppari, J., 1999. Inhibition of hCG-stimulated steroidogenesis in cultured mouse Leydig tumor cells by bisphenol A and octylphenols. Toxicol. Appl. Pharmacol. 157, 166–173. https://doi.org/10.1006/taap.1999.8674

Niwa, T., Fujimoto, M., Kishimoto, K., Yabusaki, Y., Ishibashi, F., Katagiri, M., 2001. Metabolism and interaction of bisphenol A in human hepatic cytochrome P450 and steroidogenic CYP17. Biol. Pharm. Bull. 24, 1064–1067. https://doi.org/10.1248/bpb.24.1064

O'Leary, P.D., Hughes, R.A., 1998. Structure-activity relationships of conformationally constrained peptide analogues of loop 2 of brain-derived neurotrophic factor. J. Neurochem. 70, 1712–21. https://doi.org/10.1046/j.1471-4159.1998.70041712.x

OECD, 2018. "Users'' Handbook supplement to the Guidance Document for developing and assessing Adverse Outcome Pathways", OECD Series on Adverse Outcome Pathways, No. 1, OECD Publishing, Paris." https://doi.org/10.1787/5jlv1m9d1g32-en

OECD, 2016. "Users'' Handbook supplement to the Guidance Document for developing and assessing Adverse Outcome Pathways", OECD Series on Adverse Outcome Pathways, No. 1, OECD Publishing, Paris" 18. https://doi.org/10.1787/5jlv1m9d1g32-en

References

Ohshima, M., Ohno, S., Nakajin, S., 2005. Inhibitory effects of some possible endocrine-disrupting chemicals on the isozymes of human 11beta-hydroxysteroid dehydrogenase and expression of their mRNA in gonads and adrenal glands. Environ. Sci. 12, 219–230.

Ohtake, F., Takeyama, K., Matsumoto, T., Kitagawa, H., Yamamoto, Y., Nohara, K., Tohyama, C., Krust, A., Mimura, J., Chambon, P., Yanagisawa, J., Fujii-Kuriyama, Y., Kato, S., 2003. Modulation of oestrogen receptor signalling by association with the activated dioxin receptor. Nature 423, 545–550. https://doi.org/10.1038/nature01606

Patisaul, H.B., Todd, K.L., Mickens, J.A., Adewale, H.B., 2009. Impact of neonatal exposure to the ERα agonist PPT, bisphenol-A or phytoestrogens on hypothalamic kisspeptin fiber density in male and female rats. Neurotoxicology 30, 350–357. https://doi.org/10.1016/j.neuro.2009.02.010

Pérez-Ortín, J.E., Alepuz, P.M., Moreno, J., 2007. Genomics and gene transcription kinetics in yeast. Trends Genet. 23, 250–257. https://doi.org/10.1016/j.tig.2007.03.006

Perruisseau-Carrier, C., Jurga, M., Forraz, N., McGuckin, C.P., 2011. MiRNAs stem cell reprogramming for neuronal induction and differentiation. Mol. Neurobiol. 43, 215–227. https://doi.org/10.1007/s12035-011-8179-z

Podratz, P.L., Filho, V.S.D., Lopes, P.F.I., Sena, G.C., Matsumoto, S.T., Samoto, V.Y., Takiya, C.M., Miguel, E.D.C., Silva, I.V., Graceli, J.B., 2012. Tributyltin Impairs the Reproductive Cycle in Female Rats. J. Toxicol. Environ. Heal. Part A 75, 1035–1046. https://doi.org/10.1080/15287394.2012.697826

Poland, a, Knutson, J.C., 1982. 2,3,7,8-Tetrachlorodibenzo-P-Dioxin and Related Halogenated Aromatic Hydrocarbons: Examination of the Mechanism of Toxicity. Annu. Rev. Pharmacol. Toxicol. 22, 517–554. https://doi.org/10.1146/annurev.pa.22.040182.002505

Poulin, P., Krishnan, K., 1996. Molecular Structure-Based Prediction of the Partition Coefficients of Organic Chemicals for Physiological Pharmacokinetic Models. Toxicol. Mech. Methods 6, 117–137. https://doi.org/10.3109/15376519609068458

Poulin, P., Krishnan, K., 1995. A biologically-based algorithm for predicting human tissue: blood partition coefficients of organic chemicals. Hum Exp Toxicol 14, 273–280.

Poulin, P., Theil, F.P., 2000. A priori prediction of tissue: Plasma partition coefficients of drugs to facilitate the use of physiologically-based pharmacokinetic models in drug discovery. J. Pharm. Sci. 89, 16–35. https://doi.org/10.1002/(SICI)1520-6017(200001)89:1<16::AID-JPS3>3.0.CO;2-E

Qatanani, M., Zhang, J., Moore, D.D., 2005. Role of the constitutive androstane receptor in xenobiotic-induced thyroid hormone metabolism. Endocrinology 146, 995–1002. https://doi.org/10.1210/en.2004-1350

References

Qiu, L., Zhang, X., Zhang, X., Zhang, Y., Gu, J., Chen, M., Zhang, Z., Wang, X., Wang, S.L., 2013. Sertoli cell is a potential target for perfluorooctane sulfonate-induced reproductive dysfunction in male mice. Toxicol. Sci. 135, 229–240. https://doi.org/10.1093/toxsci/kft129

Radwanski, E., Perentesis, G., Symchowicz, S., Zampaglione, N., 1989. Single and Multiple Dose Pharmacokinetic Evaluation of Flutamide in Normal Geriatric Volunteers. J. Clin. Pharmacol. 29, 554–558. https://doi.org/10.1002/j.1552-4604.1989.tb03381.x

Raun Andersen, H., Vinggaard, A.M., Høj Rasmussen, T., Gjermandsen, I.M., Cecilie Bonefeld-Jørgensen, E., 2002. Effects of Currently Used Pesticides in Assays for Estrogenicity, Androgenicity, and Aromatase Activity in Vitro. Toxicol. Appl. Pharmacol. 179, 1–12. https://doi.org/10.1006/taap.2001.9347

Rey, R., Lukas-Croisier, C., Lasala, C., Bedecarrás, P., 2003. AMH/MIS: What we know already about the gene, the protein and its regulation. Mol. Cell. Endocrinol. 211, 21–31. https://doi.org/10.1016/j.mce.2003.09.007

Rodríguez-Tébar, A., Dechant, G., Götz, R., Barde, Y.A., 1992. Binding of neurotrophin-3 to its neuronal receptors and interactions with nerve growth factor and brain-derived neurotrophic factor. EMBO J. 11, 917–922.

Rouquié, D., Heneweer, M., Botham, J., Ketelslegers, H., Markell, L., Pfister, T., Steiling, W., Strauss, V., Hennes, C., 2015. Contribution of new technologies to characterization and prediction of adverse effects. Crit. Rev. Toxicol. 45, 172–183. https://doi.org/10.3109/10408444.2014.986054

Saitoh, M., Yanase, T., Morinaga, H., Tanabe, M., Mu, Y.M., Nishi, Y., Nomura, M., Okabe, T., Goto, K., Takayanagi, R., Nawata, H., 2001. Tributyltin or triphenyltin inhibits aromatase activity in the human granulosa-like tumor cell line KGN. Biochem. Biophys. Res. Commun. 289, 198–204. https://doi.org/10.1006/bbrc.2001.5952

Sandhya, V.K., Raju, R., Verma, R., Advani, J., Sharma, R., Radhakrishnan, A., Nanjappa, V., Narayana, J., Somani, B.L., Mukherjee, K.K., Pandey, A., Christopher, R., Keshava Prasad, T.S., 2013. A network map of BDNF/TRKB and BDNF/p75NTR signaling system. J. Cell Commun. Signal. 7, 301–307. https://doi.org/10.1007/s12079-013-0200-z

Sato, I., Kawamoto, K., Nishikawa, Y., Tsuda, S., Yoshida, M., Yaegashi, K., Saito, N., Liu, W., Jin, Y., 2009. Neurotoxicity of perfluorooctane sulfonate (PFOS) in rats and mice after single oral exposure. J. Toxicol. Sci. 34, 569–574. https://doi.org/10.2131/jts.34.569

Saunders, P.T., Majdic, G., Parte, P., Millar, M.R., Fisher, J.S., Turner, K.J., Sharpe, R.M., 1997. Fetal and perinatal influence of xenoestrogens on testis gene expression. Adv. Exp. Med. Biol. 424, 99–110.

Schmitt, W., 2008. General approach for the calculation of tissue to plasma partition

References

coefficients. Toxicol. Vitr. 22, 457–467. https://doi.org/10.1016/j.tiv.2007.09.010

Schönfelder, G., Wittfoht, W., Hopp, H., Talsness, C.E., Paul, M., Chahoud, I., 2002. Parent bisphenol a accumulation in the human maternal-fetal-placental unit. Environ. Health Perspect. 110, 703–707. https://doi.org/10.1289/ehp.021100703

Seo, J.S., Lee, Y.M., Jung, S.O., Kim, I.C., Yoon, Y.D., Lee, J.S., 2006. Nonylphenol modulates expression of androgen receptor and estrogen receptor genes differently in gender types of the hermaphroditic fish Rivulus marmoratus. Biochem. Biophys. Res. Commun. 346, 213–223. https://doi.org/10.1016/j.bbrc.2006.05.123

Shi, Z., Ding, L., Zhang, H., Feng, Y., Xu, M., Dai, J., 2009. Chronic exposure to perfluorododecanoic acid disrupts testicular steroidogenesis and the expression of related genes in male rats. Toxicol. Lett. 188, 192–200. https://doi.org/10.1016/j.toxlet.2009.04.014

Sisson, T.R., Lund, C.J., Whalen, L.E., Telek, A., 1959. The blood volume of infants. I. The full-term infant in the first year of life. J. Pediatr. 55, 163–79. https://doi.org/10.1016/S0022-3476(59)80084-6

Siu, E.R., Mruk, D.D., Porto, C.S., Cheng, C.Y., 2009. Cadmium-induced testicular injury. Toxicol. Appl. Pharmacol. 238, 240–249. https://doi.org/10.1016/j.taap.2009.01.028

Sjo, E., Lennerna, H., Andersson, T.B., Gråsjo, J., Bredberg, U., 2009. Estimates of Intrinsic Clearance (CL int), Maximum Velocity of the Metabolic Reaction (V max), and Michaelis Constant (K m): Accuracy and Robustness Evaluated through Experimental Data and Monte Carlo Simulations ABSTRACT : Pharmacology 37, 47–58. https://doi.org/10.1124/dmd.108.021477.kinetics

Sjögren, E., Tammela, T.L., Lennernäs, B., Taari, K., Isotalo, T., Malmsten, L.-Å., Axén, N., Lennernäs, H., 2014. Pharmacokinetics of an Injectable Modified-Release 2-Hydroxyflutamide Formulation in the Human Prostate Gland Using a Semiphysiologically Based Biopharmaceutical Model. Mol. Pharm. 11, 3097–3111. https://doi.org/10.1021/mp5002813

Sobarzo, C.M., Lustig, L., Ponzio, R., Denduchis, B., 2006. Effect of di-(2-ethylhexyl) phthalate on N-cadherin and catenin protein expression in rat testis. Reprod. Toxicol. 22, 77–86. https://doi.org/10.1016/j.reprotox.2006.02.004

Soetaert, K., Petzoldt, T., 2010. Inverse Modelling, Sensitivity and Monte Carlo Analysis in R Using Package FME. J. Stat. Softw. 33, 2–4. https://doi.org/10.18637/jss.v033.i03

Stasenko, S., Bradford, E.M., Piasek, M., Henson, M.C., Varnai, V.M., Jurasović, J., Kušec, V., 2010. Metals in human placenta: Focus on the effects of cadmium on steroid hormones and leptin. J. Appl. Toxicol. 30, 242–253. https://doi.org/10.1002/jat.1490

Stouder, C., Paoloni-Giacobino, A., 2011. Specific transgenerational imprinting effects

References

of the endocrine disruptor methoxychlor on male gametes. Reproduction 141, 207–216. https://doi.org/10.1530/REP-10-0400

Sturla, S.J., Boobis, A.R., FitzGerald, R.E., Hoeng, J., Kavlock, R.J., Schirmer, K., Whelan, M., Wilks, M.F., Peitsch, M.C., 2014. Systems Toxicology: From Basic Research to Risk Assessment. Chem. Res. Toxicol. 27, 314–329. https://doi.org/10.1021/tx400410s

Teppner, M., Boess, F., Ernst, B., Pähler, A., 2016. Biomarkers of flutamide-bioactivation and oxidative stress in vitro and in vivo. Drug Metab. Dispos. 44, 560–569. https://doi.org/10.1124/dmd.115.066522

Thiel, C., Cordes, H., Conde, I., Castell, J.V., Blank, L.M., Kuepfer, L., 2017. Model-based contextualization of in vitro toxicity data quantitatively predicts in vivo drug response in patients. Arch. Toxicol. 91, 865–883. https://doi.org/10.1007/s00204-016-1723-x

Timchalk, C., Nolan, R.J., Mendrala, A.L., Dittenber, D.A., Brzak, K.A., Mattsson, J.L., 2002. A physiologically based pharmacokinetic and pharmacodynamic (PBPK/PD) model for the organophosphate insecticide chlorpyrifos in rats and humans. Toxicol. Sci. 66, 34–53. https://doi.org/10.1093/toxsci/66.1.34

Toyoda, K., Shibutani, M., Tamura, T., Koujitani, T., Uneyama, C., Hirose, M., 2000. Repeated dose (28 days) oral toxicity study of flutamide in rats, based on the draft protocol for the `Enhanced OECD Test Guideline 407' for screening for endocrine-disrupting chemicals. Arch. Toxicol. 74, 127–132. https://doi.org/10.1007/s002040050664

Trdan Lusin, T., Roskar, R., Mrhar, A., 2012. Evaluation of bisphenol A glucuronidation according to UGT1A1*28 polymorphism by a new LC-MS/MS assay. Toxicology 292, 33–41. https://doi.org/10.1016/j.tox.2011.11.015

Uzumcu, M., Kuhn, P.E., Marano, J.E., Armenti A.E., A.E., Passantino, L., 2006. Early postnatal methoxychlor exposure inhibits folliculogenesis and stimulates anti-Mullerian hormone production in the rat ovary. J. Endocrinol. 191, 549–558. https://doi.org/10.1677/joe.1.06592

Valentin, J., 2002. Basic anatomical and physiological data for use in radiological protection: reference values. Ann. ICRP 32, 1–277. https://doi.org/10.1016/S0146-6453(03)00002-2

Vuong, A.M., Yolton, K., Webster, G.M., Sjödin, A., Calafat, A.M., Braun, J.M., Dietrich, K.N., Lanphear, B.P., Chen, A., 2016. Prenatal polybrominated diphenyl ether and perfluoroalkyl substance exposures and executive function in school-age children. Environ. Res. 147, 556–564. https://doi.org/10.1016/j.envres.2016.01.008

Wambaugh, J.F., Setzer, R.W., Pitruzzello, A.M., Liu, J., Reif, D.M., Kleinstreuer, N.C., Wang, N.C.Y., Sipes, N., Martin, M., Das, K., DeWitt, J.C., Strynar, M., Judson, R., Houck, K.A., Lau, C., 2013. Dosimetric anchoring of In vivo and In

References

vitro studies for perfluorooctanoate and perfluorooctanesulfonate. Toxicol. Sci. 136, 308–327. https://doi.org/10.1093/toxsci/kft204

Wan, H.T., Zhao, Y.G., Wong, M.H., Lee, K.F., Yeung, W.S.B., Giesy, J.P., Wong, C.K.C., 2011. Testicular signaling is the potential target of perfluorooctanesulfonate-mediated subfertility in male mice. Biol. Reprod. 84, 1016–1023. https://doi.org/10.1095/biolreprod.110.089219

Wang, J., Sun, B., Hou, M., Pan, X., Li, X., 2012. The environmental obesogen bisphenol A promotes adipogenesis by increasing the amount of 11β-hydroxysteroid dehydrogenase type 1 in the adipose tissue of children. Int. J. Obes. 999–1005. https://doi.org/10.1038/ijo.2012.173

Wang, X., Li, Y., Xu, X., Wang, Y. hua, 2010. Toward a system-level understanding of microRNA pathway via mathematical modeling. BioSystems 100, 31–38. https://doi.org/10.1016/j.biosystems.2009.12.005

Waters, M.D., Boorman, G., Bushel, P., Cunningham, M., Irwin, R., Merrick, A., Olden, K., Paules, R., Selkirk, J., Stasiewicz, S., Weis, B., Van Houten, B., Walker, N., Tennant, R., 2003. Systems toxicology and the Chemical Effects in Biological Systems (CEBS) knowledge base. Environ. Health Perspect. 111, 811–824. https://doi.org/10.1289/txg.5971

Wen, B., Coe, K.J., Rademacher, P., Fitch, W.L., Monshouwer, M., Nelson, S.D., 2008. Comparison of in vitro bioactivation of flutamide and its cyano analogue: Evidence for reductive activation by human NADPH:cytochrome P450 reductase. Chem. Res. Toxicol. 21, 2393–2406. https://doi.org/10.1021/tx800281h

Wysowski, D.K., Fourcroy, J.L., 1996. Flutamide Hepatotoxicity. J. Urol. 155, 209–212. https://doi.org/10.1016/S0022-5347(01)66596-0

Xi, W., Lee, C.K.F., Yeung, W.S.B., Giesy, J.P., Wong, M.H., Zhang, X., Hecker, M., Wong, C.K.C., 2011. Effect of perinatal and postnatal bisphenol A exposure to the regulatory circuits at the hypothalamus-pituitary-gonadal axis of CD-1 mice. Reprod. Toxicol. 31, 409–417. https://doi.org/10.1016/j.reprotox.2010.12.002

Yang, J., Wang, C., Nie, X., Shi, S., Xiao, J., Ma, X., Dong, X., Zhang, Y., Han, J., Li, T., Mao, J., Liu, X., Zhao, J., Wu, Q., 2015. Perfluorooctane sulfonate mediates microglial activation and secretion of TNF-α through Ca2+-dependent PKC-NF-κB signaling. Int. Immunopharmacol. 28, 52–60. https://doi.org/10.1016/j.intimp.2015.05.019

York, N., 2015. Regulation of Cell Survival by Secreted Proneurotrophins.pdf. Science (80-.). 294, 1945–1949. https://doi.org/10.1126/science.1065057

You, H.J., Park, J.H., Pareja-Galeano, H., Lucia, A., Shin, J. Il, 2016. Targeting MicroRNAs Involved in the BDNF Signaling Impairment in Neurodegenerative Diseases. NeuroMolecular Med. https://doi.org/10.1007/s12017-016-8407-9

Yu, N., Wei, S., Li, M., Yang, J., Li, K., Jin, L., Xie, Y., Giesy, J.P., Zhang, X., Yu, H.,

References

2016. Effects of Perfluorooctanoic Acid on Metabolic Profiles in Brain and Liver of Mouse Revealed by a High-throughput Targeted Metabolomics Approach. Sci. Rep. 6, 23963. https://doi.org/10.1038/srep23963

Yun, Y.E., Cotton, C.A., Edginton, A.N., 2014. Development of a decision tree to classify the most accurate tissue-specific tissue to plasma partition coefficient algorithm for a given compound. J. Pharmacokinet. Pharmacodyn. 41, 1–14. https://doi.org/10.1007/s10928-013-9342-0

Zamkova, M., Khromova, N., Kopnin, B.P., Kopnin, P., 2013. Ras-induced ROS upregulation affecting cell proliferation is connected with cell type-specific alterations of HSF1/SESN3/p21Cip1/WAF1pathways. Cell Cycle 12, 826–836. https://doi.org/10.4161/cc.23723

Zeng, H. cai, Zhang, L., Li, Y. yuan, Wang, Y. jian, Xia, W., Lin, Y., Wei, J., Xu, S. qing, 2011. Inflammation-like glial response in rat brain induced by prenatal PFOS exposure. Neurotoxicology 32, 130–139. https://doi.org/10.1016/j.neuro.2010.10.001

Zhang, J., Cooke, G.M., Curran, I.H.A., Goodyer, C.G., Cao, X.L., 2011. GC-MS analysis of bisphenol A in human placental and fetal liver samples. J. Chromatogr. B Anal. Technol. Biomed. Life Sci. 879, 209–214. https://doi.org/10.1016/j.jchromb.2010.11.031

Zhang, L., Guo, J., Zhang, Q., Zhou, W., Li, J., Yin, J., Cui, L., 2018. Flutamide induces hepatic cell death and mitochondrial dysfunction via inhibition of Nrf2-mediated heme oxygenase-1. Oxid. Med. Cell. Longev.

Zhang, L., Li, Y.-Y., Zeng, H.-C., Wei, J., Wan, Y.-J., Chen, J., Xu, S.-Q., 2011. MicroRNA expression changes during zebrafish development induced by perfluorooctane sulfonate. J. Appl. Toxicol. 31, 210–222. https://doi.org/10.1002/jat.1583

Zhang, T., Sun, H., Kannan, K., 2013. Blood and urinary bisphenol a concentrations in children, adults, and pregnant women from China: Partitioning between blood and urine and maternal and fetal cord blood. Environ. Sci. Technol. 47, 4686–4694. https://doi.org/10.1021/es303808b

Zhao, B., Hu, G.X., Chu, Y., Jin, X., Gong, S., Akingbemi, B.T., Zhang, Z., Zirkin, B.R., Ge, R.S., 2010. Inhibition of human and rat 3β-hydroxysteroid dehydrogenase and 17β-hydroxysteroid dehydrogenase 3 activities by perfluoroalkylated substances. Chem. Biol. Interact. 188, 38–43. https://doi.org/10.1016/j.cbi.2010.07.001

Annex 1

Chapter 1: Supplementary information

EDCs	Glands	Hormones	Biophase action	Risk factor	References
Alachlor	Peripheral	Estrogen and androgen	PXR agonist	Decreased steroid hormone	(Mikamo et al., 2003)
Ammonium Perflurooctane (AMPO)	Steroidogenic gland	Steroid hormone	PPAR agonist, downregulation of PBR and TPSO protein	Affects steriodogenesis	(Li et al., 2011)
Atarazine	Leydig cell HPO axis	Testosterone, estrogen	Inhibits LH induced testosterone production, Inhibits hypothalamus induced production of LH and prolactin	Reduced testosterone level, demasculanizatrion and feminization of male gonads, Premature reproductive senescense	(Cooper et al., 2000; Friedmann, 2002; Hayes et al., 2011)
BPA	Thyroid	T3, T4	Upregulates TRα, TRβ mRNA RXR expression Recruit N-CoR	Inhibit thyroid action Impair TR mediated transcription	(Lans et al., 1994) (Moriyama et al., 2002)

Annex 1

BPA	Adrenal and adipose tissue Gonads	Cortisol Steroid hormones	Increases 11β HSD1, lipoprotein lipase and PPAR-γ mRNA expression Inhibits the CYP17A enzyme	Aceleration of adipogenesis Inhibit steroidogenesis	(Wang et al., 2012) (Niwa et al., 2001)
BPA	Leydig Pituitary	Testosterone and estrogen, LH Testosterone	Inhibits 5α reductase enzyme and aromatase activity Induced pituitary ERβ gene expression	Affect both testosterone and estrogen level Decrease testosterone production	(Castro et al., 2013) (Akingbemi et al., 2004)
BPA, Octyl phenol	Leydig cell	Testosterone	Inhibition of coupling between cAMP and LH receptor	Decreased testosterone level	(Nikula et al., 1999)
BPA	Hypothalamus	GnRH, FSH and LH	Reduced kiss fiber density at prepubertal ERα mRNA during pubertal changing	Decreased level of GnRH Infertility	(Patisaul et al. 2009; Xi et al. 2011)

Annex 1

BPA	Sertoli cell	Testosterone	Redistribution of Occludin, ZO-1 and Cx43 protein	Perturbs the blood testis barrier(BTB) Inhibit spermatogenesis	(Li et al., 2009)
BPA	Sertoli cell Antra follicle	AMH Sex hormone	Proliferation of leydig cell, Inhibited stAR and CYPssc mRNA	Affect SDM Impair sex hormone production	(Rey et al., 2003)
BPA	Epididymis cell	Sex hormone	Induce oxidative stress	Less sperm count	(Ansoumane et al., 2014; Chitra et al., 2003)
BPA	Gonadal cell	Estrogen	Alter CREB, regulator Rb	Alter cell cycle	(Bouskine et al., 2009)
Cadmium and PCB mixture	Gonadal cell	Estrogen	Recruit HSP90 Potentiate the action of PCB	Inhibit estrogenic action	(Chang et al., 2014)
DEHP	Sertoli cell	Germ cell	Upregulation of N-cadherin and catenin	Impairment of spermatogenesi	(Sobarzo et al., 2006)
Dibutyltin	liver	cortisol	Dowregulation of PEPCK and TAT expression	Imbalance in glucose homeostasis	(Gumy et al., 2008)
Dioxin	Leydig cell	Testosterone	Inhibit hCG	Decrease testosteone level	(Lai et al., 2005a)

Annex 1

			Stimulated CYP11A expression		
Dioxin	Ovary	Estrogen	ERE expression, ER degradation	Increase proliferation	(Ohtake et al., 2003)
Dithiocarbmates	Adrenal	Cortisol	Irreversible inhibit 11β HSD2	Increase cortisol level	(Atanasov et al., 2003)
Enodsulfan	Gonadal cell	Andorgen and estrogen	androgen receptor antagonist, ER transactivation, weak CYP19A inhibitor	Altering estrogen and androgen action	(Raun Andersen et al., 2002; Lemaire et al., 2004)
Methoxychlor	Gonadal cell	Estrogen, androgen, AMH	Alter genomic imprinting, stimulates AMH, PXR agonist , androgen receptor antagonist	Affect male and female fertility	(Mikamo et al., 2003; Lemaire et al., 2004; Uzumcu et al., 2006 ; Stouder and Paoloni-Giacobino, 2011)

Annex 1

Nonylphenol	Liver, Gonadal cell	Steroid hormone,	Increase PXR interaction Increase level of coactivator like RIP140, SRC-1, increase CYP3A mRNA expression, Modulation of ER and AR	Alter steroid hormone metabolism. Affecting oogenesis	(Masuyama et al., 2000; Seo et al., 2006)
Octyl phenol	Fetal testis	Steroid hormone	Decreases CYP450, 17α hydroxylase/C17-20 lyase and SF-1 expressions	Chances of Infertility	(Saunders et al., 1997)
-OH PCBs, PCDDs, PCDFs	Thyroid	T3, T4	Increases thyroid hormone available in biophase	Higher metabolic activity	(Lans et al., 1994)
PAH		Estrogen	Sulphotransferase (SULT1E1)	Increase bioavailblity of estrogen	(Kester et al., 2002)
PCBs, PCDDs, PCDFs	Thyroid, ovary, testis	E2,TH,T, GC	Ahr activation	Increase metabolism of hormones	(Poland & Knutson, 1982;Birgelen et al., 1995)

Annex 1

PCB126	Adrenal	Aldosterone	Increases expression of AT1 receptor and CYP11B2	Increase aldosterone level	(Li et al., 2004)
PCB mixture	Fetal (HPOA)	Estrogen	Lowers aromatase activity	Alter hormone homeostasis	(Hany et al., 1999)
Perchlorates	Thyroid	T3, T4	Inhibits iodide transport	Decrease production of thyroid hormone	(Clewell et al., 2004)
PFOA	Liver	Testosterone ,insulin like hormone (IGF)	Inhibits GHR, steriodogenic enzyme inhibition	Decreased production of testosterone	(Shi et al., 2009; Wan et al., 2011)
PFOA	Testis	Testosterone	Lowers 3β HSD and 17β HSD3 expression	Reduction in testosterone synthesis	(Zhao et al., 2010)
PFOS, cadmium	Sertoli cell, BTB	Sex hormone	Activation of p38 MAPK, Affecting TJ and GJ protein	Decrease BTB integrity	(Siu et al. 2009; Qiu et al. 2013)
Phthalates	Thyroid	T3, T4	PPAR and RXR agonist	Disrupting TR-RXR Decrease thyroid action	(Juge-Aubry et al., 1995)
Phthalates, cadmium	HPG axis	FSH and LH	Decreases PPARγ expreesion,	Reduction of anogenital distance	(Boberg et al., 2008;

Annex 1

			Inhibit leptin-kiss –GnRH pathway		Stasenko et al., 2010)
Phthalates	Liver	Steroid hormones	Increases PXR interaction with coactivator like RIP140, SRC-1	Alter steroid hormone metabolism	(Masuyama et al. 2000; 2002)
Sulfone metabolites of PCB	Adrenal	Cortisol	Inhibit Mitochondrial 11 β- hydroxylase Interact with GR	Affecting Glucocorticoidhomeostasis	(Johansson et al., 1998)
TBT, TPT	Granulosa cell	Estrogen and androgen	Decreases aromatase enzyme expression	Decreased E2 level	(Heidrich et al., 2001; Saitoh et al., 2001)
TBT, TPT, PFASs	Placenta	Cortisol	Inhibits 11β HSD2	Increase cortisol level in fetus	(Ohshima et al., 2005)
TCPOBOP	Thyroid	T3, T4	Activation of CAR receptor Increase UGTs and SULTs expression	Increase metabolism of thyroid hormone	(Qatanani et al., 2005)
TCDD	Testis	Androgen and estrogen	Inhibits CYPscc & LHR expression by	Affect sex hormone synthesis	(Fukuzawa et al., 2004)

Annex 1

			interacting with AHR		
TCDD	Sertoli cell		AHR receptor CYP1A1 induction	Produced toxicity in sertoli cell	(Lai et al., 2005b)
Tributyltin chloride	Peripheral, placenta, ovary	Testosterone, estrogen	5α- reductase type I and II irreversible, Aromatase inhibitor, decrease estradiol serum level	Prevent the action of testosterone, Decreased E2 level, Impair reproductive cycle	(Heidrich et al., 2001; Saitoh et al., 2001; Doering et al., 2002; Podratz et al., 2012)
Vincozolin	Gonadal cell	Androgen	PXR agonist, competative inhibitor of androgen, DNA methylation alteration	Increase steroid hormone metabolsim, inhibit androgen action	(Fang et al., 2003; Mikamo et al., 2003)

Annex 2

Chapter 2: Supplementary information

Table A.1: Physiological parameters

Paramter	Symbol	Value	References
Cardiac blood output	QCC	4.8 **(L/h/kg)**	(Brown et al., 1997) (Davies and Morris, 1993)
Fractional liver blood flow	FQliver	0.25	(Brown et al., 1997)
Fractional kidney blood flow	FQkidney	0.177	(Brown et al., 1997)
Fractional fat blood flow	FQfat	0.052	(Brown et al., 1997)
Fractional skin blood flow	FQskin	0.058	(Brown et al., 1997)
Fractional gonads blood flow	FQgonads	0.0002	(Brown et al., 1997)
Constant Fraction of organs volume to body weight			
Fractional liver volume	Fliver	0.026	(Brown et al., 1997)
Fractional fat volume	Ffat	0.187	(Brown et al., 1997)
Fractional gonads volume	Fgonads	0.0027	(Brown et al., 1997)
Fractional plasma volume	Fplasma	0.0428	(Davies and Morris, 1993)
Fractional gut volume	Fgut	0.016	(Brown et al., 1997)
Haematocrit	HCT	0.45	(Davies and Morris, 1993)
Microsomal protein in liver	MSPL	52.5 (mg/g liver)	(Godin et al., 2006)
Microsomal protein in gut	MSPG	20.6 (mg/g gut)	(Cubitt et al., 2009)
Cytosol protein in liver	CYTPL	80.7 (mg/g liver)	(Gibbs et al., 1998)
Cytosol protein in gut	CYTPG	18 (mg/g gut)	(Gibbs et al., 1998)

Table A.2: Metabolites molecular weight

molar mass of DEHP	391	g/mole
Molar mass of MEHP	281	g/mole
molar mass of MEHP-OH	297	g/mole
5-oxo MEHP	295	g/mole
5-cx MEPP	311	g/mole

Table A.3: Subject weight and dose Amount in Koch et al., studies

Annex 2

Body weight	75	kg
Dose	48500	µg
Dose	0.00124	moles

Table A.4: Subject weight and dose amount in Anderson et al., (2011) study

Body weight	60.1–96.6	kg
Dose (low)	310	µg
Dose (high)	2800	µg
Dose (low)	7.92839E-06	moles
Dose (high)	7.16113E-05	moles

Annex 2

Table A.5 Summary statistics of parameters' sensitivities targeting only cplasmaM1					
Parameters	**L1**	**L2**	**Mean**	**Min**	**Max**
k_gut_plasma	0.039453	0.001472	0.039453	0	0.040035
k_liver_plasma	0.051789	0.001977	-0.05179	-0.23862	0
k_gonads_plasma	5.56E-06	2.37E-07	4.51E-06	-1.55E-05	9.96E-06
k_fat_plasma	4.49E-05	2.15E-06	-4.49E-05	-9.78E-05	1.85E-07
k_restbody_plasma	0.001027	4.66E-05	0.00073	-0.0006	0.002011
k_liver_plasmaM1	0.837297	0.031281	-0.8373	-0.99912	0
k_gonads_plasmaM1	0.009357	0.00042	-0.00936	-0.01648	0
k_fat_plasmaM1	0.056833	0.002537	-0.05683	-0.102	0
k_restbody_plasmaM1	0.395788	0.018302	-0.39579	-0.70924	0
vmaxgutM1	0.005837	0.000365	-0.00402	-0.00604	0.13498
vmaxgut_cytM1	0.014574	0.000911	-0.01006	-0.01508	0.335963
vmaxgutM2	5.17E-05	1.94E-06	-5.15E-05	-5.70E-05	1.59E-05
vmaxgutM3	0	0	0	0	0
vmaxgutM4	0	0	0	0	0
vmaxgutM5	0.003274	0.000123	-0.00327	-0.00346	0
kmgutM1	0.002752	0.000186	0.001855	-0.08176	0.002817
kmgut_cytM1	0.006875	0.000465	0.004628	-0.20428	0.007036
kmgutM2	0.000183	6.84E-06	0.000183	0	0.00019
kmgutM3	0	0	0	0	0
kmgutM4	0	0	0	0	0
kmgutM5	0.003229	0.000121	0.003229	0	0.003415
vmaxliverM1	0.000493	6.59E-05	-0.00015	-0.0007	0.038017
vmaxliver_cytM1	0.001253	0.000169	-0.00038	-0.00179	0.098199
vmaxliverM2	0.979128	0.038768	-0.97913	-1.49263	0
vmaxliverM3	0.09024	0.00358	-0.09024	-0.13863	0
vmaxliverM4	0	0	0	0	0
vmaxliverM5	0.028495	0.001128	-0.0285	-0.04339	0
kmliverM1	0.000492	6.53E-05	0.000153	-0.03777	0.000703
kmliver_cytM1	0.001184	0.000161	0.000356	-0.09491	0.001684
kmliverM2	0.971613	0.038483	0.971613	0	1.483151
kmliverM3	0.085736	0.003409	0.085736	0	0.13291
kmliverM4	0	0	0	0	0
kmliverM5	0.028484	0.001127	0.028484	0	0.04337
fracl2	0	0	0	0	0

Annex 2

fracl4	0	0	0	0	0
KgutM2	0	0	0	0	0
vplasmad	0	0	0	0	0
kurineM1	0.352162	0.013983	-0.35216	-0.4713	0
kurineM2	0	0	0	0	0
kurineM3	0	0	0	0	0
kurineM4	0	0	0	0	0

Table A.6 Summary statistics of parameters' sensitivities targeting only cplasmaM2

Parameters	L1	L2	Mean	Min	Max
k_gut_plasma	0.047123	0.001766	0.047123	0	0.051783
k_liver_plasma	0.068659	0.002629	-0.06866	-0.24324	0
k_gonads_plasma	2.41E-05	1.46E-06	2.26E-05	-3.23E-06	9.49E-05
k_fat_plasma	0.000237	1.69E-05	-0.00024	-0.00146	2.98E-06
k_restbody_plasma	0.005842	0.000397	0.005507	-0.00056	0.029542
k_liver_plasmaM1	0.192444	0.007959	0.127031	-0.39701	0.286367
k_gonads_plasmaM1	0.002122	0.000143	-0.00212	-0.01097	1.78E-08
k_fat_plasmaM1	0.013053	0.000866	-0.01305	-0.06432	7.35E-09
k_restbody_plasmaM1	0.086111	0.006066	-0.08611	-0.50726	2.19E-08
vmaxgutM1	0.008849	0.00048	-0.00613	-0.01226	0.1407
vmaxgut_cytM1	0.022085	0.001196	-0.01531	-0.0306	0.350028
vmaxgutM2	7.14E-05	3.28E-06	6.80E-05	-2.67E-05	0.000233
vmaxgutM3	0	0	0	0	0
vmaxgutM4	1.80E-06	7.14E-08	-1.80E-06	-2.87E-06	0
vmaxgutM5	0.00391	0.000148	-0.00391	-0.00443	0
kmgutM1	0.00417	0.000244	0.002813	-0.09142	0.005703
kmgut_cytM1	0.010424	0.00061	0.007024	-0.22819	0.014266
kmgutM2	0.000101	4.14E-06	8.91E-05	-0.00018	0.000171
kmgutM3	0	0	0	0	0

Annex 2

kmgutM4	1.63E-06	6.48E-08	1.63E-06	0	2.85E-06
kmgutM5	0.003857	0.000146	0.003857	0	0.004374
vmaxliverM1	0.001692	0.000114	-0.00114	-0.00493	0.042182
vmaxliver_cytM1	0.004281	0.000291	-0.00289	-0.01247	0.109715
vmaxliverM2	0.575947	0.02403	-0.22911	-0.90994	0.997044
vmaxliverM3	0.132397	0.005447	-0.1324	-0.19792	0
vmaxliverM4	1.934154	0.082937	-1.93415	-3.32217	0
vmaxliverM5	0.041484	0.001701	-0.04148	-0.06145	0
kmliverM1	0.001675	0.000113	0.001136	-0.04198	0.004879
kmliver_cytM1	0.004034	0.000277	0.002717	-0.10695	0.011735
kmliverM2	0.571164	0.023831	0.227702	-0.99675	0.903751
kmliverM3	0.12679	0.005233	0.12679	0	0.191301
kmliverM4	1.734801	0.075526	1.734801	0	3.087483
kmliverM5	0.041469	0.0017	0.041469	0	0.061432
fracl2	0.62405	0.024431	0.62405	0	0.999586
fracl4	0	0	0	0	0
KgutM2	5.00E-05	2.31E-06	-1.52E-05	-5.57E-05	0.000203
vplasmad	0.998613	0.037216	-0.99861	-1	0
kurineM1	0.079033	0.004594	-0.07903	-0.32283	0
kurineM2	1.521062	0.061333	-1.52106	-2.19816	0
kurineM3	0	0	0	0	0
kurineM4	0	0	0	0	0

Table A.7 Summary statistics of parameters' sensitivities targeting only cplasmaM3

Parameters	L1	L2	Mean	Min	Max
k_gut_plasma	0.039169	0.001463	0.039169	0	0.040561
k_liver_plasma	0.071252	0.002799	-0.07125	-0.23786	0
k_gonads_plasma	5.83E-05	2.98E-06	5.72E-05	-1.59E-05	0.00014
k_fat_plasma	0.000617	3.59E-05	-0.00062	-0.00205	2.33E-07
k_restbody_plasma	0.015079	0.000838	0.01476	-0.00073	0.041091
k_liver_plasmaM1	0.293557	0.012871	-0.03568	-0.65568	0.32037

Annex 2

k_gonads_plasmaM1	0.005368	0.000296	-0.00537	-0.01437	8.84E-08
k_fat_plasmaM1	0.032743	0.001785	-0.03274	-0.08577	1.58E-09
k_restbody_plasmaM1	0.223352	0.012786	-0.22335	-0.68659	2.63E-08
vmaxgutM1	0.010665	0.000505	-0.00889	-0.01604	0.134555
vmaxgut_cytM1	0.026612	0.001259	-0.02219	-0.04	0.334906
vmaxgutM2	5.22E-05	1.97E-06	-5.20E-05	-5.83E-05	1.50E-05
vmaxgutM3	0	0	0	0	0
vmaxgutM4	0	0	0	0	0
vmaxgutM5	0.003269	0.000123	-0.00327	-0.00348	0
kmgutM1	0.004988	0.000246	0.004109	-0.08152	0.007447
kmgut_cytM1	0.012479	0.000616	0.010277	-0.20368	0.018641
kmgutM2	0.000182	6.81E-06	0.000182	0	0.00019
kmgutM3	0	0	0	0	0
kmgutM4	0	0	0	0	0
kmgutM5	0.003224	0.000121	0.003224	0	0.003438
vmaxliverM1	0.003584	0.000181	-0.00325	-0.00793	0.037904
vmaxliver_cytM1	0.009062	0.00046	-0.00822	-0.02004	0.09791
vmaxliverM2	1.842867	0.075004	-1.84287	-2.87949	0
vmaxliverM3	0.825822	0.03091	0.825822	0	0.999673
vmaxliverM4	0	0	0	0	0
vmaxliverM5	0.053485	0.002176	-0.05348	-0.08349	0
kmliverM1	0.003546	0.00018	0.003221	-0.03766	0.00784
kmliver_cytM1	0.00853	0.000433	0.007737	-0.09463	0.018855
kmliverM2	1.834113	0.074677	1.834113	0	2.868797
kmliverM3	0.810976	0.030295	-0.81098	-0.99642	0
kmliverM4	0	0	0	0	0
kmliverM5	0.05347	0.002175	0.05347	0	0.08347
fracl2	0	0	0	0	0
fracl4	0	0	0	0	0
KgutM2	0	0	0	0	0
vplasmad	0	0	0	0	0
kurineM1	0.18212	0.009045	-0.18212	-0.39819	0
kurineM2	0	0	0	0	0
kurineM3	1.757363	0.071287	-1.75736	-2.78849	0
kurineM4	0	0	0	0	0

Annex 2

Table A.8 Summary statistics of parameters' sensitivities targeting only cplasmaM4

Parameters	L1	L2	Mean	Min	Max
k_gut_plasma	0.04417	0.001667	0.04417	0	0.051443
k_liver_plasma	0.068276	0.002655	-0.06828	-0.24073	0
k_gonads_plasma	3.37E-05	1.91E-06	3.27E-05	-2.64E-06	0.000103
k_fat_plasma	0.000365	2.41E-05	-0.00036	-0.00178	3.90E-06
k_restbody_plasma	0.008695	0.000544	0.008401	-0.00058	0.032574
k_liver_plasmaM1	0.214529	0.00921	0.070428	-0.53986	0.295537
k_gonads_plasmaM1	0.003148	0.000196	-0.00315	-0.01243	0
k_fat_plasmaM1	0.019177	0.001175	-0.01918	-0.07132	2.24E-09
k_restbody_plasmaM1	0.131367	0.008551	-0.13137	-0.6067	0
vmaxgutM1	0.009332	0.000491	-0.00688	-0.01293	0.141403
vmaxgut_cytM1	0.023287	0.001225	-0.01718	-0.03227	0.351783
vmaxgutM2	0.000107	1.79E-05	9.72E-05	-3.88E-05	0.010168
vmaxgutM3	0	0	0	0	0
vmaxgutM4	5.21E-05	1.70E-05	5.04E-05	-1.76E-06	0.009991
vmaxgutM5	0.003679	0.00014	-0.00368	-0.00441	0
kmgutM1	0.004391	0.000249	0.003161	-0.09171	0.006012
kmgut_cytM1	0.010981	0.000622	0.007899	-0.22893	0.015042
kmgutM2	0.00016	1.81E-05	5.02E-05	-0.01016	0.000177
kmgutM3	0	0	0	0	0
kmgutM4	5.20E-05	1.70E-05	-5.06E-05	-0.00999	1.56E-06
kmgutM5	0.003629	0.000138	0.003629	0	0.004351
vmaxliverM1	0.00218	0.000131	-0.00172	-0.00542	0.041706
vmaxliver_cytM1	0.005517	0.000333	-0.00435	-0.01371	0.108469
vmaxliverM2	0.620667	0.025837	-0.39684	-1.00276	0.988154
vmaxliverM3	0.141021	0.005787	-0.14102	-0.20717	0
vmaxliverM4	1.386633	0.059874	-1.09269	-2.61153	0.990101
vmaxliverM5	0.044021	0.001802	-0.04402	-0.06426	0
kmliverM1	0.002159	0.00013	0.001707	-0.0415	0.005365
kmliver_cytM1	0.005198	0.000316	0.004092	-0.10572	0.012904
kmliverM2	0.615761	0.025639	0.394001	-0.98668	0.996369
kmliverM3	0.13556	0.005577	0.13556	0	0.200423
kmliverM4	1.215283	0.053406	0.972995	-0.98908	2.380021
kmliverM5	0.044006	0.001801	0.044006	0	0.064243

Annex 2

fracl2	0.398382	0.016858	-0.39838	-0.67029	0
fracl4	0.998561	0.037214	0.998561	0	1
KgutM2	4.03E-05	1.68E-06	-3.22E-05	-5.95E-05	0.000115
vplasmad	0	0	0	0	0
kurineM1	0.109411	0.00603	-0.10941	-0.36501	1.34E-09
kurineM2	0	0	0	0	0
kurineM3	0	0	0	0	0
kurineM4	1.044303	0.039388	-1.0443	-1.13376	0

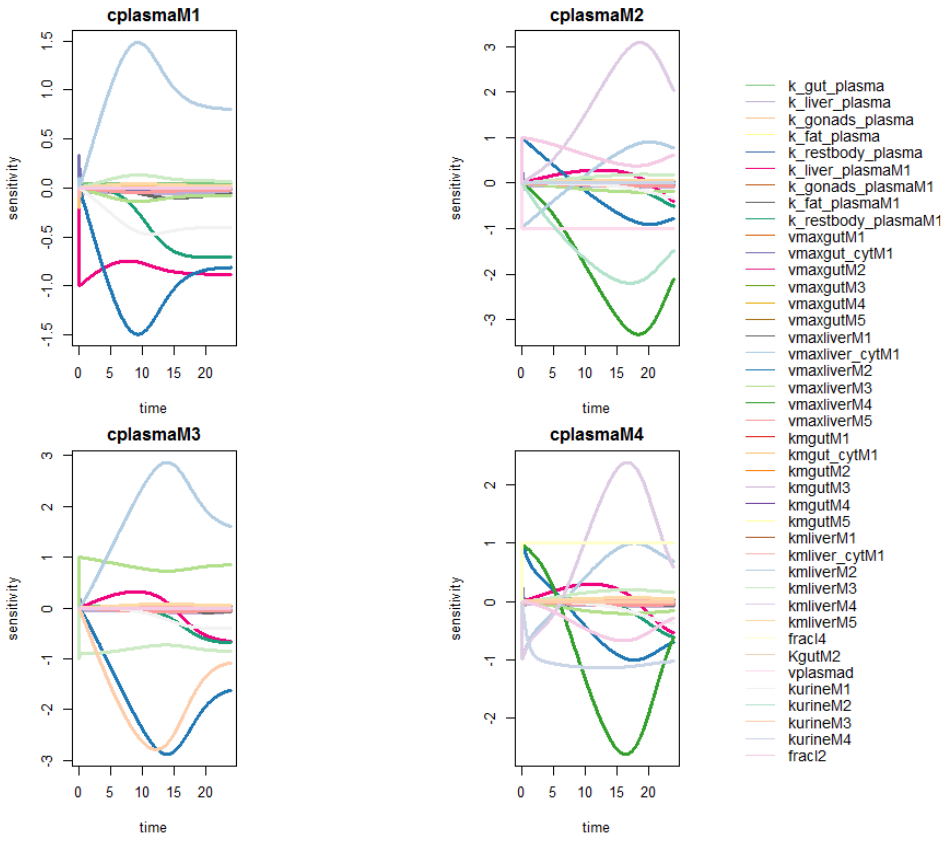

Figure A.1 Sensitivity plot for all the parameters with target output of metabolites concentration in plasma

Annex 2

Standard ordinary differential equations used in tissue dosimetry model (DEHP)

$$\frac{d}{dt}(Agut) = Qgut * (cplasma * fu - cgut * fu/k\_gut\_plasma) - RAMG1 - RAMG1\_cyt$$

- $Agut$ is the amount of DEHP in gut
- $Qgut$ is the blood flow to the gut
- $cgut$ is the concentration of chemical in gut
- fu is the plasma fractional unbound for DEHP
- k_gut_plasma is the gut plasma partition coefficient
- $RAMG1$ is metabolism of DEHP into MEHP in microsomal fraction of gut
- $RAMG1\_cyt$ is metabolism of DEHP into MEHP in cytosol fraction of gut

$$\frac{d}{dt}(ALiver) = Qliver * cplasma * fu + (Qgut * cgut * (fu/\ k\_liver\_plasma)) - (Qliver + Qgut) * cliver * (fu/\ k\_liver\_plasma) - RAML1 - RAML1\_cyt$$

- $ALiver$ is the amount of DEHP in liver
- $Qliver$ is the cardiac blood flow to liver
- $Cplasma$ is the plasma concentration of DEHP
- $Cliver$ is the concentration of DEHP in liver
- $K_{liver_{plasma}}$ is the liver plasma partition coefficient

$$\frac{d}{dt}(Afat) = Qfat * (cplasma * fu - cfat * (fu/k\_fat\_plasma))$$

- $Afat$ is the amount of chemical in fat
- $Qfat$ is the blood flow to fat
- $K_{fat_{plasma}}$ fat plasma partition coefficient

$$\frac{d}{dt}(Agonads) = Qgonads * \left(Cplasma * fu - Cgonads * \left(\frac{fu}{K_{gonads_{plasma}}}\right)\right)$$

- $Agonads$ is the amount of chemical in fat
- $Qkidney$ blood flow to gonads
- $K_{gonads_{plasma}}$ gonads plasma partition coefficient

$$\frac{d}{dt}(Arestbody) = Qrestbody * \left(Cplasma * fu - Crestbody * \left(\frac{fu}{K_{restbody_{plasma}}}\right)\right)$$

- $Arestbody$ is the amount of chemical in rest of the body
- $Qrestbody$ is the blood flow to rest of the body
- $K_{restbody_{plasma}}$ restbody plasma partition coefficient

Annex 2

$$\frac{d}{dt}(Aplasma) = Qfat * cfat * \left(\frac{fu}{k_{fat_{plasma}}}\right) + \left((Qliver + Qgut) * cliver * \left(\frac{fu}{k_{liver_{plasma}}}\right)\right) + \left(Qgonads * cgonads * \left(\frac{fu}{k_{gonads_{plasma}}}\right)\right) + \left(Qrestbody * crestbody * \left(\frac{fu}{k_{restbody_{plasma}}}\right)\right) - (QCplasma * cplasma * fu)$$

- $Aplasma$ is the amount of chemical in plasma
- $Qplasma$ is the blood flow to plasma
- $QCplasma$ cardiac output for plasma flow

$$\frac{d}{dt}(AgutM1) = -kgut * AgutM1 + RAMG1 + RAMG1\_cyt - RAMG2 - RAMG5$$

$$\frac{d}{dt}(AgutM2) = RAMG2 - KgutM2 * AgutM2 - RAMG4$$

$$\frac{d}{dt}(AliverM1) = kgut * AgutM1 + Qliver * \left(cplasmaM1 * fum - cliverM1 * \left(\frac{fum}{k_{liver_{plasmaM1}}}\right)\right) + RAML1 + RAML1_{cyt} - RAML2 - RAML3 - RAML5$$

$$\frac{d}{dt}(AliverM2) = RAML2 + KgutM2 * AgutM2 - fracl2 * AliverM2 - RAML4$$

$$\frac{d}{dt}(AfatM1) = Qfat * \left(cplasmaM1 * fum - cfatM1 * \left(\frac{fum}{k_{fat_{plasmaM1}}}\right)\right)$$

$$\frac{d}{dt}(ArestbodyM1) = Qrestbody * \left(cplasmaM1 * fum - crestbodyM1 * \left(\frac{fum}{k_{restbody_{plasmaM1}}}\right)\right)$$

Annex 2

$$\frac{d}{dt}(AplasmaM1) = Qfat * cfatM1 * \left(\frac{fum}{k_{fat_{plasmaM1}}}\right) + Qliver * cliverM1 * \left(\frac{fum}{k_{liver_{plasmaM1}}}\right) + Qgonads * cgonadsM1 * \left(\frac{fum}{k_{gonads_{plasmaM1}}}\right) + \left(Qrestbody * crestbodyM1 * \left(\frac{fum}{k_{restbody_{plasmaM1}}}\right)\right) - QCplasma * cplasmaM1 * fum - kurineM1 * AplasmaM1$$

$$\frac{d}{dt}(AurineM1) = kurineM1 * AplasmaM1$$

$$\frac{d}{dt}(AM2) = fracl2 * AliverM2 - kurineM2 * AM2$$

$$\frac{d}{dt}(AM3) = RAML3 - kurineM3 * AM3$$

$$\frac{d}{dt}(AM4) = fracl4 * RAML4 + RAMG4 - kurineM4 * AM4$$

$$\frac{d}{dt}(AurineM2) = kurineM2 * AM2$$

$$\frac{d}{dt}(AurineM3) = kurineM3 * AM3$$

$$\frac{d}{dt}(AurineM4) = kurineM4 * AM4$$

$$RAMG1 = vmaxgutM1 * cgut * fu/(cgut * fu + kmgutM1)$$
$$RAMG1\_cyt = vmaxgut\_cytM1 * cgut * fu/(cgut * fu + kmgut\_cytM1)$$
$$RAMG2 = vmaxgutM2 * cgutM1 * fumi/(cgutM1 * fumi + kmgutM2)$$
$$RAMG3 = vmaxgutM3 * cgutM1 * fumi/(cgutM1 * fumi + kmgutM3)$$
$$RAMG4 = vmaxgutM4 * cgutM2/(cgutM2 + kmgutM4)$$
$$RAMG5 = vmaxgutM5 * cgutM1 * fumi/(cgutM1 * fumi + kmgutM5)$$
$$RAML1 = vmaxliverM1 * cliver * fu/(cliver * fu + kmliverM1)$$
$$RAML1\_cyt = vmaxliver\_cytM1 * cliver * fu/(cliver * fu + kmliver\_cytM1)$$
$$RAML2 = vmaxliverM2 * cliverM1 * fumi/(cliverM1 * fumi + kmliverM2)$$
$$RAML3 = vmaxliverM3 * cliverM1 * fumi/(cliverM1 * fumi + kmliverM3)$$
$$RAML4 = vmaxliverM4 * cliverM2/(cliverM2 + kmliverM4)$$
$$RAML5 = vmaxliverM5 * cliverM1 * fumi/(cliverM1 * fumi + kmliverM5)$$

- $RAMG1$ is metabolism of DEHP into MEHP in microsomal fraction of gut

Annex 2

- $RAMG1\_cyt$ is metabolism of DEHP into MEHP in cytosol fraction of gut
- $RAMG2$ is metabolism of MEHP into MEHP-OH in microsomal fraction of gut
- $RAMG3$ is metabolism of MEHP into 5-carboxy MEPP
- $RAMG4$ is metabolism of MEHP-OH into 5-oxo MEPP
- $RAMG5$ is metabolism of MEHP into phthalic acid
- $RAML1$ is metabolism of DEHP into MEHP in microsomal fraction of liver
- $RAML1$_is metabolism of DEHP into MEHP in cytosol fraction of liver
- $RAML2$ is metabolism of MEHP into MEHP-OH
- $RAML3$ is metabolism of MEHP into 5-carboxy MEPP
- $RAML4$ is metabolism of MEHP-OH into 5-oxo MEPP
- $RAML5$ is metabolism of MEHP into phthalic acid
- $vmaxgutM1$ is the maximum metabolic rate of reaction in gut microsomes (DEHP to MEHP)
- $vmaxgut\_cytM1$ is the maximum metabolic rate of reaction in gut cytosol (DEHP to MEHP)
- $kmgutM1$ is the concentration at which half maximum reaction occur (microsomal fraction)
- $kmgutM1\_cytM1$ is the concentration at which half maximum reaction occur (cytosol fraction)
- $vmaxgutM2$ is the maximum metabolic rate of reaction for MEHP to MEHP-OH
- $kmgutM2$ is the concentration at which half maximum reaction occur (MEHP to MEHP-OH)
- $vmaxgutM3$ is the maximum metabolic rate of reaction for MEHP to 5-carboxy MEPP
- $kmgutM3$ is the concentration at which half maximum reaction occur (MEHP to 5-carboxy MEPP)
- $vmaxgutM4$ is the maximum metabolic rate of reaction for MEHP-OH to 5-oxo MEPP
- $kmgutM4$ is the concentration at which half maximum reaction occur (MEHP-OH to 5-oxo MEPP)
- $vmaxgutM5$ is the maximum metabolic rate of reaction for MEHP to phthalic acid
- $kmgutM5$ is the concentration at which half maximum reaction occur (MEHP to phthalic acid)
- $vmaxliverM1$ is the maximum metabolic rate of reaction in liver microsomes (DEHP to MEHP)
- $vmaxliver\_cytM1$ is the maximum metabolic rate of reaction in liver cytosol (DEHP to MEHP)
- $kmliverM1$ is the concentration at which half maximum reaction occur (microsomal fraction)

Annex 2

- $kmliver\_cytM1$ is the concentration at which half maximum reaction occur (cytosol fraction)
- $vmaxliverM2$ is the maximum metabolic rate of reaction for MEHP to MEHP-OH
- $kmliverM2$ is the concentration at which half maximum reaction occur (MEHP to MEHP-OH)
- $vmaxliverM3$ is the maximum metabolic rate of reaction for MEHP to 5-carboxy MEPP
- $kmliverM3$ is the concentration at which half maximum reaction occur (MEHP to 5-carboxy MEPP)
- $vmaxliverM4$ is the maximum metabolic rate of reaction for MEHP-OH to 5-oxo MEPP
- $kmliverM4$ is the concentration at which half maximum reaction occur (MEHP-OH to 5-oxo MEPP)
- $vmaxliverM5$ is the maximum metabolic rate of reaction for MEHP to phthalic acid
- $kmliverM5$ is the concentration at which half maximum reaction occur (MEHP to phthalic acid)
- $fumi/fum$ is the fractional unbound for the MEHP in plasma and microsomes are assume to be same

Note:

M1, M2, M3 and M4 corresponds to MEHP, 5-OH MEHP, 5-cx MEPP and 5-oxo MEHP, respectively.
Kurine = urine elimination rate constant.
A corresponds to amount.
Amounts are converted to concentration by dividing with the respective volume of organs.
Vmax has a unit of µg/hr/whole BW weight

Annex 3

Chapter 3: Supplementary information

Standard ordinary differential equations used in tissue dosimetry model for the development of P-PBPK model of BPA

$$\frac{d}{dt}(stomach) = input1 - K * Astomach - GE * Astomach$$

- $\frac{d}{dt}(stomach)$ is the rate of change of chemical amount in Stomach (nmol)
- $input1$is the oral dose exposure (nmol/day) ;3 equal divided dose per day
- K is the absorption rate constant in the stomach (1/hr),
- GE is the gastric emptying time

$$\frac{d}{dt}(gut) = GE * Astomach - Vmaxgut_{glu} * Cgut * fu/(Cgut * fu + Kmgut\_glu) - K1 * AGut$$

- $Vmaxgut\_glu$ is the scaled maximum rate of glucuronidation in gut (nM/hr)
- $cgut$ is the concentration of chemical in gut
- fu is the plasma fractional unbound
- $Kmgut\_glu$ is the concentration in nmol/liter to produce half maximum reaction
- $K1$ is uptake rate of chemical from oral to liver

$$\frac{d}{dt}(Liver) = Qliver * \left(Cplasma * fu - Cliver * \left(\frac{fu}{K_{liver_{plasma}}} \right) \right) + K1 * AGut - Vmaxliver_{glu} * Cliver * \frac{fu}{Cliver * fu + Kmliver_{glu}} - Vmaxliver\_sulf * Cliver * fu/(Cliver * fu + Kmliver\_sulf)$$

- $Qliver$ is the cardiac blood flow to liver
- $Cplasma$ is the plasma concentration of chemical
- $Cliver$ is the concentration of chemical in liver
- $K_{liver_{plasma}}$ is the liver plasma partition coefficient
- $Vmaxliver_{glu}$ is the maximal glucuronidation rate of chemical in liver
- $Kmliver_{glu}$ is the concentration at which half maximal reaction occurs for glucuronidation in liver
- $Vmaxliver\_sulf$ is the maximal sulfation rate of chemical in liver
- $Kmliver\_sulf$ is the concentration at which half maximal reaction sulfation occurs in liver

Annex 3

$$\frac{d}{dt}(Brain) = Qbrain * \left(Cplasma * fu - \ Cbrain * \left(\frac{fu}{K_{brain_{plasma}}} \right) \right)$$

- $Qbrain$ is the blood flow to brain
- $K_{brain_{plasma}}$ brain plasma partition coefficient

$$\frac{d}{dt}(Kidney) = QKidney * \left(Cplasma * fu - \ Ckidney * \left(\frac{fu}{K_{kidney_{plasma}}} \right) \right) -$$

$$Kurine * Ckidney$$

- $Qkidney$ blood flow to kidney
- $K_{kidney_{plasma}}$ kidney plasma partition coefficient
- $Kurine$ is the excretion rate of chemical to urine

$$\frac{d}{dt}(fat) = Qfat * \left(Cplasma * fu - \ Cfat * \left(\frac{fu}{K_{fat_{plasma}}} \right) \right)$$

- $Qfat$ blood flow to the fat
- $K_{fat_{plasma}}$ fat plasma partition coefficient

$$\frac{d}{dt} skin = Qskin * (Cplasma * fu - Cskin * \frac{fu}{K\_skin\_plasma})$$

- $QSkin$ blood flow to the skin
- K_skin_plasma is the skin plasma partition coefficient
- Cskin is the concentration of BPA in skin

$$\frac{d}{dt}(restbody) = Qrestbody * \left(Cplasma * fu - \ Crestbody * \left(\frac{fu}{K_{restbody_{plasma}}} \right) \right)$$

- $Qrestbody$ is the blood flow to rest of the body
- $K_{restbody_{plasma}}$ restbody plasma partition coefficient

Annex 3

$$\frac{d}{dt}(placenta) = \left(Qplacenta * \left(Cplasma * fu - Cplacenta * \left(\frac{fu}{K_{placenta_{plasma}}} \right) \right) \right) - K_{t1} * Cplacenta * \left(\frac{fu}{K_{placenta_{plasma}}} \right) + K_{t2} * Cplasma_{fetus} * fu - Vmaxplacenta_{glu} * Cplacenta * \frac{fu}{Cplacenta * fu + Kmplacenta_{glu}} + kde * Cplacenta$$

- $Qplacenta$ is the blood flow to placenta
- $Cplacenta$ is the concentration of chemical in placenta
- $K\_placenta\_plasma$ placenta plasma partition coefficient
- K_t1 is the transfer rate of chemical to the fetus from placenta
- K_t2 is the transfer of chemical to placenta from fetus
- $Vmaxplacenta\_glu$ is the glucuronidation of chemical in the placenta (similar with liver scaled assuming 10 percent of microsomal protein (MSP) in comparison to liver MSP)
- $Kmplacenta\_glu$ is the concentration of chemical producing half maximal reaction
- Kde is the chemical deconjugation rate (BPAG to BPA)

$$\frac{d}{dt}(plasma) = Qfat * Cfat * \left(\frac{fu}{K_{fat_{plasma}}} \right) + Qliver * Cliver * \left(\frac{fu}{K_{liver_{plasma}}} \right) + \left(Qbrain * Cbrain * \left(\frac{fu}{K_{brain_{plasma}}} \right) \right) + \left(Qkidney * Ckidney * \left(\frac{fu}{K_{kidney_{plasma}}} \right) \right) + \left(Qrestbody * Crestbody * \left(\frac{fu}{K_{restbody_{plasma}}} \right) \right) - (QCplasma * Cplasma * fu) + \left(QSkin * Cskin * \left(\frac{fu}{K_{skin_{plasma}}} \right) \right) + Qplacenta * Cplacenta * (fu/K\_placenta\_plasma)$$

- $Qplasma$ is the blood flow to plasma

Annex 3

Fetus model equation

$$\frac{d}{dt}liver_{fetus} = Qliver_{fetus} * \left(Cplasma_{fetus} * fu - Cliver_{fetus} * \left(\frac{fu}{K_{liver_{fetus_{plasma}}}} \right) \right) - Vmaxliver_{glu_{fetus}} * \frac{Cliver_{fetus}}{Cliver_{fetus} + Kmliver_{glu}} + kde * Cliver_{fetus}$$

- $Qliver\_fetus$ is the blood flow to the fetal liver
- $Cplasma_{fetus}$ is the chemical fetus plasma concentration
- $Cliver_fetus$is the liver chemical concentration
- $K_{liverfetus}: plasma$ is the fetus liver plasma concentration
- $Vmaxliver\_glu\_fetus$ is the scaled maximum rate of reaction for chemical metabolism from in-vitro data considering fetal liver volume and fetus liver microsomal protein content
- $Kmliver$_glu is the concentration of substrate (chemical) producing half maximal reaction
- Kde is the chemical deconjugation rate

$$\frac{d}{dt}fetus\_brain = Qbrain\_fetus * (Cplasma\_fetus * fu - Cbrain\_fetus * \left(\frac{fu}{K_{brain_{fetus_{plasma}}}} \right)$$

- Qbrain_fetus is the blood flow to the fetal brain
- Cbrain_fetusis the brain chemical concentration

$$\frac{d}{dt}restbody\_fetus = Qrestbody\_fetus * (Cplasma\_fetus * fu - Crestbody\_fetus * \left(\frac{fu}{K_{restbody\_fetus\_plasma}} \right)$$

- Qrestbody_fetus is the blood flow to the rest of the body
- $Crestbody\_fetus$ is the concentration in rest of the body of fetus

$$\frac{d}{dt}amnioticfluid = K\_t3 * Cliver\_fetus * fu - Camnioticfluid * K\_t4$$

- K_t3 is chemical transfer rate from fetus to amniotic fluid
- k_t4 is the chemical transfer rate from amniotic fluid to fetus
- Camnioticfluidis the concentration of BPA in amniotic fluid

Annex 3

$$\frac{d}{dt}plasma\_fetus = (Qliver\_fetus * (Cliver\_fetus * (fu/K\_liver\_fetus\_plasma))) + (Qbrain\_fetus * (Cbrain\_fetus * (fu/K\_brain\_fetus\_plasma))) + Qrestbody\_fetus * (Crestbody\_fetus * (fu/K\_restbody\_fetus\_plasma)) - (QCplasma\_fetus * Cplasma\_fetus * fu) + (K\_t1 * Cplacenta * (fu/K\_placenta\_plasma)) - K\_t2 * Cplasma\_fetus * fu + Kde * Cplasma\_fetusBPAG$$

Equations for scaling physiological parameter for the fetus

1. $\mathbf{V\_fetus} = 3.779 * \left(e^{-16.08*e^{-5.67*e^{-4}*GD*24}}\right) + \left(e^{-140.78*e^{-7.01*e^{-4}*24*GD}}\right)$
   - **V_fetus = fetal volume**
   - GD= Gestational day (T/24)

2. $\mathbf{V\_Aminiotic\ fluid} = 0 + 1.9648 * GA - 1.2056 * GA^2 + 0.2064 * GA^3 - 0.0061 * GA^4 + 0.00005 * GA^5$

3. $\mathbf{Vbldfet} = \mathbf{F_{vldfet}} * \mathbf{Vfet}$
   - **Vbldfet = fetal blood volume in L**
   - F_{vldfet} = fetal blood volume as a fraction of body weight, L/kg = 0.085
   - Vfet = fetal body weight in kg
4. $\mathbf{Vliverfet} = \mathbf{F_{liverfet}} * \mathbf{Vfet}$
   - **Vliverfet = fetal liver volume in L**
   - $F_{liverfet}$ = fetal liver volume as a fraction of body weight = 0.04 (Valentin, 2002)
   - Vfet = fetal body weight in kg
5. $\mathbf{Vkidneyfet} = \mathbf{F_{kidneyfet}} * \mathbf{Vfet}$
   - **Vkidneyfet = fetal kidney volume in L**
   - $F_{kidneyfet}$ = fetal kidney volume as a fraction of body weight = 0.0072
   - Vfet = fetal body weight in kg
6. $\mathbf{Vbrainfet} = \mathbf{F_{brainfet}} * \mathbf{Vfet}$
   - **Vbrainfet = fetal brain volume in L**
   - $F_{brainfet}$ = fetal brain volume as a fraction of body weight = 0.11
   - Vfet = fetal body weight

7. $\mathbf{Qfet} = \mathbf{F_{Qfet}} * \mathbf{Vbldfet}$
   - **Qfet = fetal cardiac output L/h**

Annex 3

- F_{Qfet} = fetal cardiac output as fraction of blood weight in kg (L/h/Kg) = 54
- Vbldfet = fetal blood volume in kg

8. $\mathbf{QLiv\ fet = F_{Qlive_m} * Qfet}$
   - **QLiv fet = fetal liver flood flow in L/h**
   - F_{Qlive_m} = maternal liver blood flow as fraction of cardiac output
   - Qfet = fetal cardiac output in L/h
9. $\mathbf{Qkidney\ fet = F_{Qkidney_m} * Qfet}$
   - **Qkidney fet = fetal kidney flood flow in L/h**
   - $F_{Qkidney_m}$ = maternal kidney blood flow as fraction of cardia output
   - Qfet = fetal cardiac output in L/h
10. $\mathbf{Qbrain\ fet = F_{Qbrain_m} * Qfet}$
    - **Qbrain fet = fetal brain blood flow in L/h**
    - F_{Qbrain_m} = maternal brain blood flow as fraction of cardiac output
    - Qfet = fetal cardiac output

Table A.1: General physiology parameters for PBPK model

Parameter	Symbol	Value	References
Cardiac blood output	QCC [a]	20 (L/h/kg$^{0.75}$)	(Clewell et al., 1999) (Clewell and Clewell, 2008)
Fractional liver blood flow	FQliver	0.25	(Brown et al., 1997)
Fractional brain blood flow	FQbrain	0.117	(Brown et al., 1997)
Fractional kidney blood flow	FQkidney	0.177	(Brown et al., 1997)
Fractional fat blood flow	FQfat	0.052	(Brown et al., 1997)
Fractional skin blood flow	FQskin	0.058	(Brown et al., 1997)
Constant Fraction of organs volume to body weight			
Fractional liver volume	Fliver	0.026	(Brown et al., 1997)
Fractional brain volume	Fbrain	0.021	(Brown et al., 1997)
Fractional kidney volume	Fkidney	0.004	(Brown et al., 1997)
Fractional fat volume	Ffat	0.187	(Brown et al., 1997)
Fractional skin volume	Fskin	0.0371	(Brown et al., 1997)

Annex 3

Fractional plasma volume	Fplasma	0.0428	(Davies and Morris, 1993)
Fractional gut volume	Fgut	0.016	(Brown et al., 1997)
Haematocrit	HCT	0.45	(Davies and Morris, 1993)
Fetal Blood flow as fraction of blood weight in kg	FQblood_fetus	54(L/h/$Kg^{0.75}$)	(Clewell et al., 1999)
Fetal haematocrit	HCT_fetus	0.5	(Sisson et al., 1959)
Fraction liver volume of fetus BW	Fliver_fetus	0.04*	(Valentin, 2002)
Fraction kidney volume of fetus BW	Fkidney_fetus	0.0072*	(Valentin, 2002)
Fraction brain volume of fetus BW	Fbrain_fetus	0.11*	(Valentin, 2002)

[a] parameter depends on body weight and on physical activity can be vary from 15-25 (Clewell and Clewell, 2008) .

*Fractional organ weight for the fetus was estimated from ICRP (2002) data. Blood flow is scaled by multiplying fractional blood flow to tissue in a mother with the volume of fetus tissue.

Table A.2 Pharmacokinetic parameters of BPA used for the P-PBPK

Parameters	Symbol/Unit	Mean value	References
Gastric emptying time	GE (L/h/kg-0.25)	3.5	(Kortejärvi et al., 2007)
Oral absorption rate	K_oral (L/h/kg-0.25)	9	Optimize
BPAG uptake to the liver	KGlin_BPAG (L/h/kg-0.25)	50	(Fisher et al., 2011)
Fraction of BPAS transferred to plasma from liver	Fbpasliver	1	(Fisher et al., 2011)
Enterohepatic recirculation of BPAG	Kentero_BPAG (L/h/kg-0.25)	0.2	(Fisher et al. 2011)

Annex 3

BPA urinary excretion rate	Kurine_BPA (L/h/kg0.75)	0.1	Optimize
BPAG urinary excretion rate	Kurine_bpag (L/h/kg0.75)	0.40	Optimize
BPAS urinary excretion rate	Kurine_bpas (L/h/kg0.75)	0.025	Optimize
BPAG fraction volume of distribution	Vdbpag a (L)	0.0435	set equal to plasm fraction volume
BPAS fraction volume of distribution	Vdbpasa (L)	0.0435	set equal to plasm fraction volume
fractional constant placental transfer from mother to fetus	FK_t1 b	5.2e-05	(Kawamoto et al., 2007)
fractional constant for placental transfer from fetus to mother	FK_t2b	2.0e-05	(Kawamoto et al., 2007)
fractional constant for chemical transfer from fetus to amniotic fluid	FK_t3b	0.008	Visually fit against (Ikezuki et al., 2002) data
fractional constant for chemical from amniotic fluid to fetus	FK_t4b	0.001	Visually fit against (Ikezuki et al., 2002) data
fractional constant for placental transfer from mother to fetus	FK_t1_BPAGb	3.3e-6	(Kawamoto et al., 2007)
fractional constant for placental transfer from fetus to mother	FK_t2_BPAGb	6.6e-14	(Kawamoto et al., 2007)
Deconjugation rate in placenta and fetus	Kde	0.35	Estimated
Glucuronidation of BPA in liver c			

Annex 3

Vmax nmol/min/mg of protein	Km (µmole)	Vmax (nmol/hr/ kg BW.75)	Reference
4.71	45.8	680,095. 6	(Coughlin et al., 2012)
Glucuronidation of BPA in gut c			
1.4	58	22750	(Trdan Lusin et al., 2012)
Sulfation of BPA in liver c			
149 nmol/h/g liver	10.1	11657	(Kurebayashi et al., 2010)
Partition coefficient			
Liver/blood PC	k_liver_plasma	0.73	(Doerge et al., 2011)
Brain/blood PC	k_brain_plasma	2.8	(Doerge et al., 2011)
Kidney/blood PC	k_kidney_plasma	0.858	(Kawamoto et al., 2007)
Fat/blood PC	k_fat_plasma	5.0	(Doerge et al., 2011)
Skin/blood PC	k_skin_plasma	5.7	(Mielke et al., 2011)
Rest of the PC body/blood	k_restbody_plasm a	2.7	Assumed similar to brain
Placenta/blood PC	k_placenta_plasm a	1.43	(Csanády et al., 2002)
Placenta/blood BPAG PC	k_placentaBPAG _plasma	0.680	(Kawamoto et al., 2007)
Fetus Liver/blood PC	k_liver_fetus_plas ma	0.73	set equal to mother
Fetus rest of the PC body/blood	k_restbody_fetus_ plasma	2.7	set equal to mother

Annex 3

a = parameter set to plasma volume, **b**= value need to scale ($Vfetus^{0.75}$) to use in P-PBPK modeling, c = mean experimental value has used for scaling to in-vivo

Table A.3. Subject Anthropometries

Cohort	BW (mean) Kg	Age (mean) year	Height (mean) meter
(Schönfelder et al., 2002) (Aris, 2014), (Zhang et al., 2013)	78	33	1.6
(Kuroda et al., 2003), (Ikezuki et al., 2002	53	33	1.58

Table A.4. Human biomonitoring data collected from literature from different pregnancy cohort studies

References	**Mother Plasma (nM)**	**Fetal Plasma (nM)**	**Placenta (nM)**	**Fetal liver (nM)**	**Fetal amniotic fluid conc. (nM)**	**Cohort**
(Zhang et al., 2013) (at delivery)	15.7±18.73	0.57±0.52	NA	NA	NA	China
(Schönfelder et al., 2002) (at delivery)	19.3±2.8	12.7±1.8	49±6.63	NA	NA	Germany
(Lee et al., 2008) (at delivery)	11.97[b] (13.6±4.8)[c]	2.74[b] (2.85±4.6)[c]	NA	NA	NA	Korean

Annex 3

(Ikezuki et al., 2002) (at early pregnancy)	6.6±0.86	NA	NA	NA	36.4±6.9	Japan
(Ikezuki et al., 2002 (at delivery)	6.1±0.65	9.6±1.4	NA	NA	4.8±0.71	Japan
(Kuroda et al., 2003)	2.0±0.3	2.8±0.19	NA	NA	NA	Japan
BPA(Cao et al., 2012) (early to mid-gestational)	NA	NA	55.3[b] (2.41-723)[d]	39.56[b] (4.50-165)[d]	NA	Canada (1998-2008)
(J. Zhang et al., 2011) (at early pregnancy)	NA	NA	41.6±70	37.28±42	NA	Canada
(Aris, 2014) (at delivery)	(0-19.5)[d] 5.96±5.17	(0-20.17)[d] 5.39±4.56	NA	NA	NA	Canada eastern township
(Gerona et al., 2014) (mid-gestational)	NA	0.219[b] (LOD-229)[d]	NA	NA	NA	North California

Annex 3

b = median value, c = geometric mean, d= range value, LOD= limit of detection (0.220nM)

NA = not available

Note: all units are converted into nM for this study.

Annex 4

Chapter 4: Supplementary information

dt(KEAP1) = -(((kf_re2*KEAP1*NRF2_cyt)/(kinh_re2* PARK7Act + 1)) - kb_re2*(KEAP1_NRF2_cyt)) - (kf_re3*KEAP1*ROS -kb_re3*KEAP1_ROSmod)+ KEAP1synt*S + ((k1_re4*KEAP1_NRF2_cyt - k2_re4*KEAP1*NRF2cytUB))- k1_re31*KEAP1 - ((k1_re6*KEAP1*P62_cyt - k2_re6*KEAP1_P62));

dt(KEAP1_ROSmod) = (kf_re3*KEAP1*ROS - kb_re3*KEAP1_ROSmod) - k1_re33 *KEAP1_ROSmod;

dt(VDAC1) = -(kf_re1*VDAC1*(0.01 + PINK1_PARK2) - kb_re1*VDAC1UB);

dt(PARK2) = -(((kf_re26*PINK1*PARK2*ROS)/(kinh_re26*PARK7Act +1))- kb_r26*PINK1_PARK2);

dt(ATP) = ((kf_re8*RE*O2*Mit_H*ADP)/(1 + kup_re8*UPp)) - k1_re14*S*ATP - k1_re29*ATP;

dt(ADP) = -((kf_re8*RE*O2*Mit_H*ADP)/(1 + kup_re8*UPp)) + k1_re14*S*ATP + k1_re29*ATP;

dt(Antioxidant_p) = kf_re12*Antioxidant_m *S - k1_re13*Antioxidant_p - k1_re40*ROS*Antioxidant_p;

dt(NRF2_cyt) = -(((kf_re2 * KEAP1*NRF2_cyt)/(kinh_re2* PARK7Act + 1)) - kb_re2*(KEAP1_NRF2_cyt)) + NRF2_synt*S - (k1_re17*NRF2_cyt - k2_re17*NRF2_nucleus) - k1_re30*NRF2_cyt;

dt(PARK7Act) = kf_re46*PARK7InAct_DJ1*(0.01 +ROS)-kb_re46*PARK7Act;

dt(PARK7InAct_DJ1) = kb_re46*PARK7Act - kf_re46*PARK7InAct_DJ1*(0.01 +ROS);

dt(UPp) = kf_re24*UPm*S -k1_re25*UPp;

dt(PINK1) = -(((kf_re26*PINK1*PARK2*ROS)/(kinh_re26*PARK7Act +1))- kb_r26*PINK1_PARK2);

dt(Mit_H) = k1_re14*S*ATP - kf_re34*Mit_H*(ROS +1) + kf_MitR*BCLxL*Mit_D;

dt(Mit_D) = kf_re34*Mit_H*(ROS +1)- kf_re35*AP*Mit_D - kf_MitR*BCLxL*Mit_D;

dt(AP) = -k1_re38*AP + kf_apoptosis*S;

dt(Aggr) = kf_re36*Alfa_synuclein*ROS -kb_re36*Aggr - (k1_re37*Aggr*P62_cyt - k2_re37*P62_im);

Annex 4

dt(P62_im) = (k1_re37*Aggr*P62_cyt - k2_re37*P62_im) - k1_re50*P62_im;

dt(P62_cyt) = -((k1_re16*P62_cyt*VDAC1UB - k2_re16*VDAC_P62))-
k1_re32*P62_cyt - ((k1_re37*Aggr*P62_cyt -k2_re37*P62_im))
-((k1_re6*KEAP1*P62_cyt- k2_re6*KEAP1_P62)) + kf_re7*P62_m*S;

dt(ROS) = -k1_re40*ROS*Antioxidant_p + ((ROS_synt*O2*RE*Mit_D -
kb_re41*ROS)/(1+ kUPp_re41*UPp;

dt(KEAP1_P62) = -kf_re28*KEAP1_P62*(ROS+1) + k1_re6*KEAP1*P62_cyt -
k2_re6*KEAP1_P62 ;

dt(PINK1_PARK2) = (((kf_re26*PINK1*PARK2*ROS)/(kinh_re26*PARK7Act +1))-
kb_r26*PINK1_PARK2);

dt(VDAC1UB) = (kf_re1*VDAC1*(0.01+ PINK1_PARK2)- kb_re1*VDAC1UB) -
((k1_re16*P62_cyt*VDAC1UB - k2_re16*VDAC_P62));

dt(VDAC_P62) = k1_re16*P62_cyt*VDAC1UB - k2_re16*VDAC_P62;

dt(KEAP1_NRF2_cyt) = (((kf_re2 * KEAP1*NRF2_cyt)/(kinh_re2* PARK7Act + 1)) -
kb_re2*KEAP1_NRF2_cyt) -(k1_re4*KEAP1_NRF2_cyt -
k2_re4*KEAP1*NRF2cytUB);

dt(NRF2cytUB) = k1_re4*KEAP1_NRF2_cyt - k2_re4*KEAP1*NRF2cytUB -
k1_re5*NRF2cytUB;

dt(NFkB) = k1_re42*IKK - ((kf_re43*NFkB)/(1 + kinh_re43*PARK7Act));

dt(BCLxL) = kf_re44*NFkB*S - k1_re45*BCLxL;

dt(CytC) = kf_re49*S*Mit_D/(1+kinh_re49*BCLxL)-k1_re48*CytC;

dt(Ncells) = -Ncells*k1_re59*celldeathcoeficient*CytC;

dt(AntioxidantInActGene) = -(k1_re9*AntioxidantInActGene*NRF2_nucleus -
k2_re9*AntioxidantActGene);

dt(AntioxidantActGene) = k1_re9*AntioxidantInActGene*NRF2_nucleus -
k2_re9*AntioxidantActGene;

dt(Antioxidant_m) = -k1_re11*Antioxidant_m + kf_re10*AntioxidantActGene*Snuc;

dt(P62_m) = kf_re19*P62ActGene*Snuc -k1_re20*P62_m;

dt(P62ActGene) = (kf_re18*P62InActGene*NRF2_nucleus*NFkB -
kb_re18*P62ActGene/1);

Annex 4

dt(P62InActGene) = -(kf_re18*P62InActGene*NRF2_nucleus*NFkB - kb_re18*P62ActGene/1);

dt(UPActGene) = kf_re21*UPInActGene*PARK7Act - kb_re21*UPActGene;

dt(UPm) = kf_re22*UPActGene*Snuc - k1_re23*UPm;

dt(UPInActGene) = -(kf_re21*UPInActGene*PARK7Act - kb_re21*UPActGene);

dt(NRF2_nucleus) = (k1_re17*NRF2_cyt - k2_re17*NRF2_nucleus) - (kf_re18*P62InActGene*NRF2_nucleus*NFkB-kb_re18*P62ActGene/1) - ((k1_re9*AntioxidantInActGene*NRF2_nucleus -k2_re9*AntioxidantActGene));

dt(UPActGene) = kf_re21*UPInActGene*PARK7Act - kb_re21*UPActGene;

dt(UPm) = kf_re22*UPActGene*Snuc - k1_re23*UPm;

dt(UPInActGene) = -(kf_re21*UPInActGene*PARK7Act - kb_re21*UPActGene);

dt(NRF2_nucleus) = (k1_re17*NRF2_cyt - k2_re17*NRF2_nucleus) - (kf_re18*P62InActGene*NRF2_nucleus*NFkB-kb_re18*P62ActGene/1) - ((k1_re9*AntioxidantInActGene*NRF2_nucleus -k2_re9*AntioxidantActGene));

Parmeters value for ROS systems biology model

ROS_synt_coefficient = 1;
ROS_synt_corrected = 8e-14;
kf_re2= 0.5;
kinh_re2= 0.1;
kb_re2= 100;
kf_re3= 1;
kb_re3= 1;
KEAP1synt= 1;
k1_re4= 500;
k2_re4= 0.01;
k1_re31= 0.0001;
k1_re6= 60;
k2_re6= 6000;
k1_re33= 0.1;
kf_re1= 1;
kb_re1= 100;
kf_re26= 1;
kinh_re26= 0.1;
kb_r26= 10;
kf_re8= 8e-14;
RE= 5000000;
O2= 250000;
kup_re8= 0.0001;
kf_re28 = 0.002;
k1_re14= 2e-07;
S= 1;
k1_re29= 4;
kf_re12= 100000;
k1_re13= 50;
k1_re40= 0.05;
NRF2_synt= 100;
k1_re17= 1;
k2_re17=1;
k1_re30= 0.0002;
kf_re46= 1;
kb_re46=1 ;
kf_re24= 192;
k1_re25= 0.1;
kf_re34= 0.01;
kf_MitR= 0.0001;
kf_re35=0.1;
k1_re38= 0.1;
kf_re36= 0.1;
Alfa_synuclein= 3;

Annex 4

kb_re36= 0.1;
k1_re37=0.1;
k2_re37=0.1;
k1_re50= 0.1;
k1_re16= 6;
k2_re16=600;
k1_re32= 0.001;
kf_re7=20;
kb_re41= 0;
kUPp_re41= 0.0001;
k1_re5= 1000;
k1_re42= 0.005;
kf_re43=0.001;
kinh_re43=0.001;
kf_re44= 1;
k1_re45= 0.5;
kf_re49= 0.5;
kinh_re49= 0.001;
k1_re48= 0.1;
k1_re59= 2.5e-06;
k1_re9=0.022;
k2_re9= 2.1;
k1_re11=0.0011;
kf_re10= 0.1;
Snuc= 1;
kf_re19= 0.1;
k1_re20= 0.002;
kf_re18= 0.03;
kb_re18= 25;
kf_re21= 1;
kb_re21=200;
kf_re22=50;
k1_re23=0.8;
IKK = 1

Annex 5

Chapter 5A: Supplementary information

Model equations for PBPK/PD coupled mechanistic model

#%%#
Model equations for PFOS

$$\frac{d}{dt}(Agut) = \mathrm{Qgut} * \left(\mathrm{cplasma} * \mathrm{fu} - \mathrm{cgut} * \left(\frac{\mathrm{fu}}{\mathrm{k_{gutplasma}}}\right)\right)$$

$$\frac{d}{dt}(Aliver) = \mathrm{Qliver} * \mathrm{cplasma} * \mathrm{fu} + \mathrm{Qgut} * \mathrm{cgut} * \left(\frac{\mathrm{fu}}{\mathrm{k_{gut_{plasma}}}}\right) - \left((\mathrm{Qliver} + \mathrm{Qgut}) * \mathrm{cliver} * \left(\frac{\mathrm{fu}}{\mathrm{k_{liver_{plasma}}}}\right)\right)$$

$$\frac{d}{dt}(Abrain) = \mathrm{Qbrain} * \left(\mathrm{cplasma} * \mathrm{fu} - \mathrm{cbrain} * \left(\frac{\mathrm{fu}}{\mathrm{k_{brain_{plasma}}}}\right)\right)$$

$$\frac{d}{dt}(Afat) = \mathrm{Qfat} * \left(\mathrm{cplasma} * \mathrm{fu} - \mathrm{cfat} * \left(\frac{\mathrm{fu}}{\mathrm{k_{fat_{plasma}}}}\right)\right)$$

$$\frac{d}{dt}(Akidney) = \mathrm{Qkidney} * \left(\mathrm{cplasma} * \mathrm{fu} - \mathrm{ckidney} * \left(\frac{\mathrm{fu}}{\mathrm{k_{kidney_{plasma}}}}\right)\right) + \left(\frac{\mathrm{Tm} * \mathrm{cfilterate}}{\mathrm{kt} + \mathrm{cfilterate}}\right)$$

$$\frac{d}{dt}(Afilterate) = \mathrm{Qfilterate} * (\mathrm{cplasma} * \mathrm{fu} - \mathrm{cfilterate}) - \left(\frac{\mathrm{Tm} * \mathrm{cfilterate}}{\mathrm{kt} + \mathrm{cfilterate}}\right)$$

$$\frac{d}{dt}(Adelay) = \mathrm{Qfilterate} * \mathrm{cfilterate} - \mathrm{kurine} * \mathrm{Adelay}$$

$$\frac{d}{dt}(Alung) = \mathrm{Qlung} * \left(\mathrm{cplasma} * \mathrm{fu} - \mathrm{clung} * \left(\frac{\mathrm{fu}}{\mathrm{k_{lung_{plasma}}}}\right)\right)$$

$$\frac{d}{dt}(Abm) = \mathrm{Qbm} * \left(\mathrm{cplasma} * \mathrm{fu} - \mathrm{cbm} * \left(\frac{\mathrm{fu}}{\mathrm{k_{bm_{plasma}}}}\right)\right)$$

$$\frac{d}{dt}(Arestbody) = \mathrm{Qrestbody} * \left(\mathrm{cplasma} * \mathrm{fu} - \mathrm{crestbody} * \left(\frac{\mathrm{fu}}{\mathrm{k_{restbody_{plasma}}}}\right)\right)$$

$$\frac{d}{dt}(Aurine) = \mathrm{Kurine} * \mathrm{Adelay}$$

Annex 5

$$\frac{d}{dt}(Aplasma) = \text{Qfat} * \text{cfat} * \left(\frac{\text{fu}}{\text{k}_{\text{fat}_{\text{plasma}}}}\right) + (\text{Qliver} + \text{Qgut}) * \text{cliver} * \left(\frac{\text{fu}}{\text{k}_{\text{liver}_{\text{plasma}}}}\right) + \left(\text{Qbrain} * \text{cbrain} * \left(\frac{\text{fu}}{\text{k}_{\text{brain}_{\text{plasma}}}}\right)\right) + \text{Qlung} * \text{clung} * \left(\frac{\text{fu}}{\text{k}_{\text{lung}_{\text{plasma}}}}\right) + \text{Qbm} * \text{cbm} * \left(\frac{\text{fu}}{\text{k}_{\text{bm}_{\text{plasma}}}}\right) + \left(\text{Qkidney} * \text{ckidney} * \left(\frac{\text{fu}}{\text{k}_{\text{kidney}_{\text{plasma}}}}\right)\right) + \text{cfilterate} * \text{fu} + \left(\text{Qrestbody} * \text{crestbody} * \left(\frac{\text{fu}}{\text{k}_{\text{restbody}_{\text{plasma}}}}\right)\right) - (\text{QCplasma} * \text{cplasma} * \text{fu})$$

##
#Mechanistic base model equations
##

$$\frac{d}{dt}(\text{pri}_{\text{miRNA}}) = \text{k1} - \text{k2} * \text{pri}_{\text{miRNA}} - \text{k} * \text{R} - \text{d1} * \text{pri}_{\text{miRNA}}$$

$$\frac{d}{dt}(pre_{miRNA_n}) = k2 * pri_{miRNA} + k * R - d2 * pre_{miRNA_n} - k3 * pre_{miRNA_n} * \left(\frac{vp}{vn}\right)$$

$$\frac{d}{dt}(pre_{miRNA_c}) = \left(\frac{vp}{vn}\right) * k3 * pre_{miRNA_n} - d3 * pre_{miRNA_c} - k4 * pre_{miRNA_c}$$

$$\frac{d}{dt}(dsRNA) = k4 * pre_{miRNA_c} - d4 * dsRNA - k5 * dsRNA$$

$$\frac{d}{dt}(miRNA) = k5 * dsRNA + k11 * RISC - d5 * miRNA - k6 * miRNA$$

$$\frac{d}{dt}(mRNA) = km + k8 * RISCm - k7 * RISC * mRNA - d8 * mRNA$$

$$\frac{d}{dt}(RISC) = k9 * RISCm + k8 * RISCm + k6 * miRNA - d6 * RISC - k7 * RISC * mRNA - k11 * RISC$$

$$\frac{d}{dt}(RISCm) = k7 * RISC * mRNA - k9 * RISCm - k8 * RISCm - d7 * RISCm$$

$$\frac{d}{dt}(BDNF) = k10 * mRNA - d9 * BDNF$$

$$\frac{d}{dt}(cellsurvivability) = d9 * BDNF * \left(1 + \left(\frac{Emax_{cell} * BDNF}{EC50_{BDNF} + BDNF}\right)\right) - kd_{cell} * cell$$

Annex 5

##
PBPK/PD Model coupled mechanistic signalling pathway Model
##

$$\frac{d}{dt}(\mathrm{pri_{miRNA\_change}}) = \mathrm{k1} - \mathrm{k2} * \mathrm{pri_{miRNA_{change}}} - \mathrm{k} * \mathrm{R} - \mathrm{d1} * \mathrm{pri_{miRNA\_change}}$$

$$\frac{d}{dt}\left(pre_{miRNA_{change_n}}\right) = k2 * pri_{miRNA_{change}} + k * R - d2 * pre_{miRNA_{change_n}} - k3 * pre_{miRNA_{change_n}} * \left(\frac{vp}{vn}\right)$$

$$\frac{d}{dt}\left(pre_{miRN_{change_c}}\right) = \left(\frac{vp}{vn}\right) * k3 * pri_{miRNA_{change}} - d3 * re_{miRN_{change_c}} - k4 * pre_{miRN_{change_c}}$$

$$\frac{d}{dt}(dsRNA_{change}) = k4 * pre_{miRNA_{change_c}} - d4 * dsRNA_{change} - k5 * dsRNA_{change}$$

$$\frac{d}{dt}(miRNA_{change}) = k5 * dsRNA * \left(1 + \left(\frac{Emax_{miRNA} * cbrain}{EC50_{miRNA} + cbrain}\right)\right) + k11 * RISC_{change} - d5 * miRNA_{change} - k6 * miRNA_{change}$$

$$\frac{d}{dt}(mRNA_{change}) = km + k8 * RISCm_{change} - k7 * RISC_{change} * mRNA_{change} - d8 * mRNA_{change}$$

$$\frac{d}{dt}(RISC_{change}) = k9 * RISCm_{change} + k8 * RISCm_{change} + k6 * miRNA_{change} - d6 * RISC_{change} - k7 * RISC_{change} * mRNA_{change} - k11 * RISC_{change}$$

$$\frac{d}{dt}(RISCm_{change}) = k7 * RISC_{change} * mRNA_{change} - k9 * RISCm_{change} - k8 * RISCm_{change} - d7 * RISCm_{change}$$

$$\frac{d}{dt}(BDNF_{change}) = k10 * mRNA_{change} - d9 * BDNF_{change}$$

$$\frac{d}{dt}(cell\ survivability_{change}) = d9 * BDNF_{change} * \left(1 + \left(\frac{Emax_{cell} * BDNF_{change}}{EC50_{BDNF} + BDNF_{change}}\right)\right) - kd_{cell} * cell_{change}$$

Annex 5

Table 1. Physiological parameters used for PBPK model

QCC = 16.6	**Cardiac blood output (L/h/kg^0.75)**
FQliver = 0.25	Fraction cardiac output going to liver
FQbrain = 0.117	Fraction cardiac output going to brain
FQkidney = 0.177	Fraction cardiac output going to kidney
FQfilterate = 0.035	Fraction cardiac output to the filtrate compartment
FQgut = 0.181	Fraction cardiac output going to gut
FQbm = 0.1	Fraction cardiac output going to bone marrow
FQfat = 0.052	Fraction cardiac output going to fat
FQlung = 0.034	Fraction cardiac output going to lung
Fraction tissue volume of BW	
Fliver = 0.026	Fraction liver volume
Fbrain = 0.021	Fraction brain volume
Fkidney = 0.004	Fraction kidney volume
Ffilterate = 0.0004	Fraction filtrate compartment volume
Ffat = 0.187	Fraction fat compartment volume
Flung = 0.014	Fraction of lung volume
Fbm = 0.05	Fraction bone marrow volume
Fplasma = 0.0428	fraction volume of plasma
Fgut = 0.0171	Fraction gut

Annex 5

Table 2. Physicochemical parameter For PFOS

fu = 0.025	Free fraction of PFOS in plasma
k_liver_plasma = 2.2	Liver/blood partition coefficient
k_gut_plasma = 0.05	Gut/blood partition coeffcient
k_brain_plasma = 0.37	brain/blood partition coefficient
k_kidney_plasma = 1.05	Kidney/blood partition coefficient
k_fat_plasma = 0.04	Fat/blood partition coefficient
k_lung_plasma = 9.08	Skin/blood partition coefficient
k_bm_plasma = 18.73	bone marrow/blood partition coefficient
k_restbody_plasma = 0.120	Rest of the body/blood partition coefficient
Tmc = 7.0	resorption maximum (nmole/h/kg^0.75); from adult human model
kt = 0.023	affinity constant; from monkey model
kurinec = 0.1	urinary elimination rate constant (1/h)
kurine = kurinec*BW^(-0.25)	urine elimination
Tm = Tmc*BW^0.75	transporter maximum (scaled as BW^0.75)